Electrical Breakdown and Discharges in Gases

Part A
Fundamental Processes and Breakdown

NATO Advanced Science Institutes Series

A series of edited volumes comprising multifaceted studies of contemporary scientific issues by some of the best scientific minds in the world, assembled in cooperation with NATO Scientific Affairs Division.

This series is published by an international board of publishers in conjunction with NATO Scientific Affairs Division

A Life Sciences **B Physics**	Plenum Publishing Corporation New York and London
C Mathematical and Physical Sciences	D. Reidel Publishing Company Dordrecht, Boston, and London
D Behavioral and Social Sciences **E Applied Sciences**	Martinus Nijhoff Publishers The Hague, London, and Boston
F Computer and Systems Sciences **G Ecological Sciences**	Springer Verlag Heidelberg

Recent Volumes in Series B: Physics

Volume 84— Physical Processes in Laser–Materials Interactions
edited by M. Bertolotti

Volume 85— Fundamental Interactions: *Cargèse 1981*
edited by Maurice Lēvy, Jean-Louis Basdevant, David Speiser, Jacques Weyers, Maurice Jacob, and Raymond Gastmans

Volume 86— Surface Mobilities on Solid Materials: Fundamental Concepts and Applications
edited by Vu Thien Binh

Volume 87— Relativistic Effects in Atoms, Molecules, and Solids
edited by G. L. Malli

Volume 88— Collective Excitations in Solids
edited by Baldassare Di Bartolo

Volume 89a— Electrical Breakdown and Discharges in Gases: Fundamental Processes and Breakdown
edited by Erich E. Kunhardt and Lawrence H. Luessen

Volume 89b— Electrical Breakdown and Discharges in Gases: Macroscopic Processes and Discharges
edited by Erich E. Kunhardt and Lawrence H. Luessen

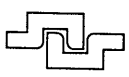

Electrical Breakdown and Discharges in Gases

Part A
Fundamental Processes and Breakdown

Edited by

Erich E. Kunhardt

Texas Tech University
Lubbock, Texas

and

Lawrence H. Luessen

Naval Surface Weapons Center
Dahlgren, Virginia

Plenum Press
New York and London
Published in cooperation with NATO Scientific Affairs Division

Proceedings of a NATO Advanced Study Institute on
Electrical Breakdown and Discharges in Gases,
held June 28 – July 10, 1981,
in Les Arcs, France

83 E 435-A

Library of Congress Cataloging in Publication Data

NATO Advanced Study Institute on Electrical Breakdown and Discharges in Gases (1981: Les Arcs, France)
Electrical breakdown and discharges in gases.

(NATO ASI series. Series B, Physics; v. 89)
"Proceedings of a NATO Advanced Study Institute on Electrical Breakdown and Discharges in Gases, held June 28 – July 10, 1981, in Les Arcs, France"—T.p. verso.
Includes bibliographical references and indexes.
Contents: pt. a. Fundamental processes and breakdown—pt. b. Macroscopic processes and discharges.
1. Electric discharges through gases—Congresses. 2. Breakdown (Electricity)—Congresses. 3. Plasma (Ionized gases)—Congresses. I. Kunhardt, Erich E. II. Luessen, Lawrence H. III. North Atlantic Treaty Organization. Scientific Affairs Division. IV. Title. V. Series.
QC710.N37 1981 537.5'2 82-19006
ISBN 0-306-41194-6 (v. 1)
ISBN 0-306-41195-4 (v. 2)

© 1983 Plenum Press, New York
A Division of Plenum Publishing Corporation
233 Spring Street, New York, N.Y. 10013

All rights reserved. No part of this book may be reproduced, stored in a retrieval system, or transmitted in any form or by any means, electronic, mechanical, photocopying, microfilming, recording, or otherwise, without written permission from the Publisher

Printed in the United States of America

PREFACE

The Advanced Study Institute on Breakdown and Discharges in Gases was held in Les Arcs, France, June 28 to July 10, 1981.

The object of the Institute was to provide a broad but comprehensive presentation of the various topics in the field of Gaseous electronics. To achieve this goal, a number of lectures, seminars, and panel discussions were scheduled. Each topic was developed by two tutorial and/or review lectures, and brought to the present state of the topic by seminars and panel discussions. The program of topics and speakers was selected with the assistance of the advisory committee composed of: J. A. Rees, European Coordinator, England; M. Goldman, French Coordinator, France; A. H. Guenther, USA; M. Kristiansen, USA; and A. V. Phelps, USA.

The most memorable aspect of the Institute was the sustained high interest of the faculty and participants for the two week period. The daily schedule was demanding: five hours of lectures, two hours of seminars and one of discussion. These sessions were often extended because of presentation by the participants of impromptu seminars. The discussions were intense. Majestic Mont Blanc provided the backdrop for the lecture hall, and these surroundings and the weather contributed to the overall positive mood. It was a wonderful occasion.

The lectures and seminars have been collected into two volumes. The sequence of topics in these volumes is very much the same as that of the Institute, although some lectures were rearranged to balance the size of the two volumes. The subjects are divided as follows: in Part A: Basic Discharge Processes, Kinetic Theory and Gas Breakdown; in Part B: Coronas, Gas Discharges, Diagnostics, Plasma Chemistry and Applications.

This collection is both tutorial and representative of the state of the field. We hope it will be useful both to beginners and experienced researchers.

We are grateful to a number of organizations for providing financial assistance. The Scientific Affairs Division of NATO provided the major contribution for the Institute. The Office of Naval Research, the Naval Surface Weapons Center at Dahlgren, the Air Force Office of Scientific Research and the Air Force Weapons Laboratory provided additional support. The National Science Foundation financed the travel of one student.

We would like to acknowledge the many people who helped us organize and carry the Institute to its successful completion. Our thanks to the organizing committee, lecturers, and participants for their support; to Dr. H. Davidson of the Army Research Office for his guidance, to W. P. Allis, A. V. Phelps and A. Rees' whose initial interest in the Institute encouraged us to pursue its organization; to Dr. Mario di Lullo, and Dr. T. Kester of the Scientific Affairs Division of NATO for their personal interest and advice, to J. P. Boeuf for reviewing manuscripts and indexing, to our wives Christine K. and Lynn L. and to Marie Byrd for their assistance in Les Arcs.

A special thanks to Elizabeth Orem of Associated Editors & Authors, whose editorial assistance was invaluable to the preparation of these proceedings.

E. E. Kunhardt
Texas Tech University
Lubbock, Texas

L. H. Luessen
U.S. Naval Surface Weapons Center
Dahlgren, Virginia

July 26, 1982

CONTENTS

BASIC DISCHARGE PROCESSES

The Development of Theories of the Electrical Breakdown of Gases. 1
F. Llewellyn-Jones

Basic Processes of Electrical Discharges. 73
J. A. Rees

Transport Data for the Modeling of Electrical Breakdown and Discharges. 109
A. V. Phelps

Electronegative Gases 133
L. G. Christophorou

KINETIC THEORY

Kinetic Theory of Ion Transport in Gases. 177
H. R. Skullerud

On the Divergence of the Legendre Expansion of the Electron Velocity Distribution 187
W. P. Allis

BREAKDOWN IN UNIFORM FIELDS

Prebreakdown Ionization in Gases Under Steady-State and Pulsed Conditions in Uniform Fields 207
J. Dutton

Nanosecond Pulse Breakdown of Gas Insulated Gaps. 241
E. E. Kunhardt

BREAKDOWN IN NONUNIFORM FIELDS

Physical Models of Long Air Gap Breakdown Processes. 265
I. Gallimberti

Spark-Over Characteristics of Long Gaps 291
G. Baldo

SEMINARS

A Numerical Solution of the Boltzmann Equation 313
L. C. Pitchford

The Microscopic Treatment of Nonequilibrium Regions in a Weakly Ionized Gas. 331
P. Segur, M. Yousfi, J. P. Boeuf, E. Marode, A. J. Davies, and J. G. Evans

Current Research Topics in Low-Pressure Glow Discharges in Rare Gases and in Pure Nitrogen 395
C. M. Ferreira

Contributions to Continuous Leader Channel Development. 419
M. M. Kekez and P. Savic

PARTICIPANTS 455

INDEX 463

THE DEVELOPMENT OF THEORIES OF THE ELECTRICAL BREAKDOWN OF GASES

F. Llewellyn-Jones

University of Wales

Swansea, United Kingdom

SCOPE OF INVESTIGATION

Range of the Phenomena

In its normal state a gas is almost a perfect insulator and in everyday life is used as such. Under certain conditions, however, when an electric field is established between two electrodes, of intensity dependent upon their geometry and the gas properties, the gas can become an almost perfect conductor. The transition from insulating to conducting states is an electrical discharge known as the electrical breakdown of the gas or spark. An outstanding feature of this process is that for most geometries the interelectrode potential difference at which this transition occurs can be highly critical, and electrical technology as we know it is dependent on this fact. This critical potential difference is known as the breakdown potential V_s of the gas for that particular electrode system. In practice, it is the lowest potential difference at which breakdown can occur providing initiating electrons are present.

The nature of this electrical discharge can be extremely varied and can involve applied potential differences over a great range from some tens of volts (as in contact-relay gaps $\sim 10^{-4}$ cm in communication circuits) to many millions of volts (as in lightning flashes over paths of some miles). Similarly, the range of gas pressure in which breakdown phenomena are important is equally wide, extending from almost vacuum conditions (as in various switches, circuit breakers, space equipment, or large nuclear particle accelerators) to very high pressure in gas-insulated high-power machines or power transmissions systems. In underground cables the two electrodes are the insulated interior cable and its outer earthed casing,

while with overhead transmission systems in the atmosphere, the two electrodes are usually the cable and bodies at ground level; in certain flash-over peak safety devices the electrodes are provided by two points (ends of wires). With the cylindrical system the breakdown is sometimes known as "corona breakdown". Another form of technical interest which concerns certain physical problems is the "point-to-plane" type, and the precise nature of the surface of the "point" or the cable is of great importance owing to the concentration of field there. All these problems are important in the operation of all gas-insulated, high-voltage equipment installed in confined spaces, and the risk of breakdown is the subject of much modern study.

The breakdown process itself, or the electric spark, occurs in very short times varying from milliseconds to nanoseconds, depending upon the gas density and forms of applied electronic field. The rapidity of the transition from the insulating state to the highly conducting state, as well as the ability of the gas medium to pass heavy currents during the spark and then recover its original insulating state after the applied e.m.f. is removed, all constitute the characteristics of a good switch. Indeed, the spark discharge has a wide application in modern technology and electronics, as in flash tubes, thyratrons, high-energy particle-counting apparatus, gas laser technology, and timing devices.

Forms of Breakdown

The actual physical form of the luminous tracks at breakdown depends upon the nature of the applied e.m.f. as well as upon the electrode geometry. At the lower gas pressures < 50 torr and with a steady applied e.m.f., the initial discharge has the form of a uniform glow, but at higher pressures, the discharge narrows and can become a thin track between the electrodes. With high impulse fields ($V > V_S$), however, a final continuous track may be preceded by luminous streaks which, in some cases, appear to be cathode-directed and in others anode-directed, but apparently originating in the gas itself rather than at the electrodes.

Breakdown of gases can also be produced by alternating electric fields over a wide range from power oscillation frequencies ($\sim$50 Hz) to optical frequencies ($\sim 10^{15}$ Hz), and at the higher frequencies, including radio- and microwave frequency, this "high-frequency" breakdown can be electrode-less. A different form of gaseous breakdown can be obtained in a small localized volume of gas at the focus of a high-intensity laser beam. This form is of particular interest because the energy of the laser light photon ($\lesssim 2$ eV) may be much lower than the ionization potential ($\gtrsim 17$ eV) of the gas atoms themselves and with extremely short duration laser flashes over certain pressure ranges different processes of photon ionization have to be considered.

Still another form of breakdown takes place on the microscale ($\sim 10^{-4}$ cm) such as that found at the closing and the opening of the contact surfaces of a relay in low-voltage communication circuits; with circuit voltages ~10 V, breakdown of the gap can occur resulting in transient microplasmas. These have been extensively studied because the plasmas produce deleterious electrode erosion and matter transfer, which are of considerable technological importance.

The atomic, molecular, electronic, ionic, and photon collision processes in the gas and at electrodes, which can be involved in the various mechanisms of breakdown, are themselves of fundamental physical interest, and much information about these processes has been gained from the scientific study of breakdown phenomena. Elucidation of mechanisms has lead to effective control of the initiation and lifetime of spark discharges in their varied applications in modern electrotechnology. This paper reviews the systematic development of the understanding of breakdown phenomena from the early work to the recent application of modern techniques of experimental and mathematical procedure.

RANGE OF INVESTIGATION IN STATIC UNIFORM FIELDS

Sparking Potentials

The simplest and original case investigated was that of large parallel plates, distance d apart in a permanent gas at pressure p, in an enclosed glass envelope, at constant temperature, when steady electrical potential differences V (say from a battery) were applied. It was assumed that the electrode surfaces were clean, smooth, and electrically inactive at room temperature (i.e., there was no thermionic or field emission). It was found that for any given values of p and d, the gas remained almost a perfect insulator for all values of V up to a certain value V_s at which electrical breakdown occurred, and a high current could pass practically limited only by the external circuit. To fix ideas, in the atmosphere with d = 1 cm, V_s was about 30,000 V, while when p was only ~1 torr, V_s was only ~300 V. Two important results should be noted: (i) the value of V_s is critical within the experimental error of measuring, and (ii) the breakdown only occurs in the presence of initial ionization whether by deliberate irradiation of the cathode by ultraviolet light, for example, or "naturally" by local radioactivity or cosmic rays. In the atmosphere, chance electrons or ions and cosmic rays eventually supply the required initiatory electrons, but in laboratory measurements of V_s, it is usual to provide a steady source of photoelectrons by irradiating the cathode with ultraviolet light. The first significant studies of breakdown properties were carried out by de la Rue and Muller (1880) and by Paschen (1889) with CO_2 and H_2 and establish the relationship, known as Paschen's Law,

$$V_s = \psi\ (pd) \qquad (1)$$

where ψ is a function of the parameter pd only. This is a particular instance of a Similarity Principle which is of considerable importance in the diagnostics of electrical discharges in general. Typical forms of (1) are shown in Figs. 1 and 2 (Llewellyn-Jones, 1957) of which the main characteristics are that when pd is very low, V_s is high, then passes through a minimum V_m (at pdm) as pd increases, and afterwards V_s continues to increase with pd; experiment also shows that the ratio V_s/pd (= E_s/p) asymtotically diminishes as pd increases.

Early work (Carr, 1903) with numerous but unprepared electrode surfaces indicated that V_s was independent of the nature of the cathode, but later work with clear out-gassed and smooth surfaces showed that V_s was strongly dependent on the nature of the cathode surface, the effect being greatest and considerable in the neighborhood of the Paschen minimum. At high values of pd the change in V_s due to change in cathode surface could lie within the experimental error measurement of V_s.

Spatial Growth of Ionization

The next step forward in the investigation of breakdown took place in the years 1901-1905 which saw the study of current growth in uniform fields in gases at pressures $\lesssim$ 100 torr. The potentials were $\lesssim$ 2000 V provided by secondary batteries and were certainly

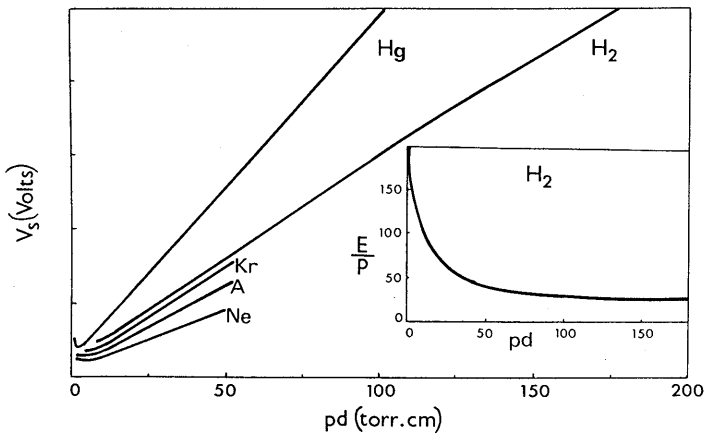

Fig. 1. Paschen curves for gases with nickel electrodes (lower Hg curve with steel cathode). Inset: asymtotic decrease of E/p as pd increases. (Reproduced by permission of the Institute of Physics and of the Philosophical Magazine.)

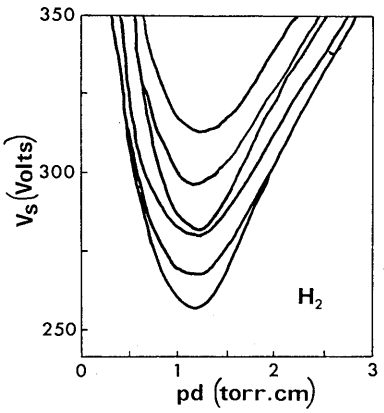

Fig. 2. Dependence of the minimum sparking potential of hydrogen on cathode surfaces. Cathodes, from top to bottom: Staybrite steel; copper; oxidized Staybrite; nickel; pure aluminum; commercial aluminum. (Reproduced by permission of the Philosophical Magazine.)

quite steady — a most fortunate feature as it turned out. The cathode surface was irradiated by rays from an adjacent spark gap, so as to produce a small initial current $I_o 10^{-13}$A of photoelectrons, which was collected at the anode at low applied voltages. Currents up to about 10^{-6}A were measured with an electrometer and inductive balance (Townsend, 1910).

It was found that at fixed gap d, increase of V produced an increase of current I(V) as a function of V until a spark was produced at V_s corresponding to pd. However, when V was maintained constant, it was found that the current then depended on d, sometimes falling as d increased, but with higher values of V sometimes increasing with d. Clearly I was a function of V and d. Experiments with a wire and coaxial cylinder showed that an initial photoelectric current was considerably amplified when the wire was positive but not when negative, so that the high field at the wire through which nearly all the electrons passed when the wire was positive was significant. Results such as these led Townsend (1902, 1910, 1915) to consider that electrons could generate others in collisions with neutral gas molecules, and he postulated a certain critical energy eV_i, characteristic of each molecule or atom, which had to be supplied in order to release one of its electrons in a collision. Clearly, momentum considerations require that the colliding electron has to possess energy greater than the critical energy eV_i necessary to produce ionization, and its magnitude depends on the energy gained in travelling a free path ℓ along the field E, i.e., on $E\ell$ or on E/p since ℓ is proportional to 1/p.

Thus, to investigate the spatial growth of current due to this process of ionization by collision by electrons, it was necessary to maintain the mean energy of agitation of all the electrons constant, and vary only the amount of gas traversed, i.e., just vary d. This is a fundamental requirement for investigation of spatial growth of current: namely E/p must be constant; otherwise misleading results are obtained. There was, of course, no difficulty in fulfilling this when V was provided by a battery of secondary cells, but difficulties and misleading conclusions were, in fact, drawn when, in later years, the potentials were provided by a rectifier-transformer A.C. generator inadequately smoothed and so providing insufficiently stable potentials V.

In these conditions extensive experiments in many gases established that over a limited range of d from d = 0, the ionization current I(d) in the gas was given by

$$I(d) = C_1 \exp(C_2 d) \tag{2}$$

where C_1 was constant proportional to and usually taken to be the initiatory photoelectric current I_o, and C_2, a constant which varied with the gas but satisfied

$$C_{2/p} = f(E/p) = f(V/pd) \tag{3}$$

and obtained from the semilog plots of I

$$\ell n\{I(d)/I_o\} = C_2 d \ ,$$

since in many permanent gases these plots were practically linear over a considerable range of d. At the time this early work was done, experiments with clean out-gassed electrodes and pure monatomic gases were not possible.

When d was further increased and V correspondingly raised so as to maintain E/p constant, the currents increased at a rate faster than exponential; i.e., the apparently linear semilog plot of $\ell n(I/I_o)$ curved up. Experiment showed that they very accurately followed a relationship of the form

$$I(d) = \frac{C_1 \exp[C_2(d - C_3)]}{1 - C_4\{\exp[C_2 (d - C_3)] - 1\}} \tag{4}$$

in which C_3 and C_4 also were constants when E/p was constant. Again, C_1 at the lower pressures investigated, say 50 torr, E/p was not too low, and the constant C_1 was practically the same as I_o. The physical significance of the relation (4) follows elucidation of the constants C_3 and C_4, which clearly relate to collisional phenomena, since with a given gas and electrode system

$$C_4 = \phi(E/p) \quad . \tag{5}$$

Typical spatial growth curves at these lower values of pd < 150 torr cm are given in Fig. 3 (Llewellyn-Jones, 1957).

Theory of Spatial Growth

As electrons move from cathode to anode at sufficiently high values of E/p, their number grows, resulting from ionizing and exciting gas collisions, to form an avalanche according to Eq. (2) consisting of more electrons, positive ions, excited (possibly metastable) molecules with resultant photons. Positive ions drift back in the field towards the cathode, excited and metastable atoms diffuse in all directions, while photons may be scattered, absorbed or degraded in the gas, reflected or absorbed at electrodes. These secondary products of the initial ionization themselves can produce more electrons: photons, possibly by direct photoionization of the gas(if of sufficient energy), but more likely by photoelectric effect at the cathode. Similarly, ions may act by direct collision (when of high enough energy) with gas molecules or, more probably, by secondary emission on incidence at the cathode; excited atoms are only incident if not previously destroyed during their diffusion.

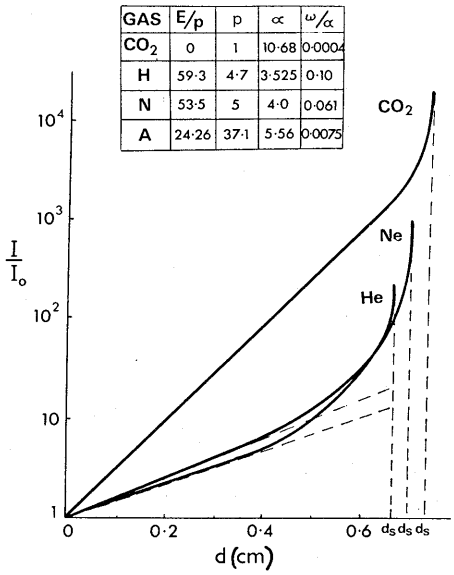

Fig. 3. Ionization growth curves in different gases, showing how the shape depends on the value of ω/α. (Reproduced by permission of Methuen & Co., Ltd.)

Consider first ionization by collision by electrons. Let n(x) electrons be at distance x from the cathode travelling along the field a distance dx and generating $\alpha n_x dx$ new electrons, so that

$$dn_x = \alpha n_x dx$$

giving

$$n(d)/n(o) = \alpha d$$

or in terms of currents, I(= e n W_), where W_ is their drift velocity,

$$I(d)/I(o) = d \ , \qquad (6)$$

which agrees with (2) when $\alpha = C_2$. This coefficient, α, is known as the Townsend primary coefficient (2), and the cloud of total amplified number of electrons is called an avalanche which also contains positive ions and excited molecules radiating photons in all directions. As this cloud, limited in size mainly by its self-diffusion, proceeds, it leaves a trail of excited molecules and positive ions originally filling all the gap, diminishing in size towards the cathode where the ions are all collected. Here, more electrons are released and themselves initiate another avalanche, and so the processes continue until the number of secondary electrons produced from all the remnants of avalanche ionization eventually falls to zero. The operation then ceases, unless external irradiation maintains an initial current from the cathode. The cycle of operation from original electrons emanating from the cathode to the next emission of all secondary electrons by these secondary processes is known as a generation. Possible secondary processes may be described by analogue coefficients defined in relation to α as follows (Townsend, 1915, 1923):

$\beta n_x dx$ is the number of electrons produced by collision by n_x positive ions travelling dx along the field;

γn_x is the number of electrons produced when n_x positive ions are incident on the cathode;

$\delta n_x dx$ is the number of photoelectrons emitted from the cathode on incidence of the fraction of all photons generated when n_x electrons travel dx along the field;

ε_{ex}, ε_m are similarly defined coefficients for the action on the cathode on diffusion of excited or metastable atoms; and

η is a similar coefficient which in certain conditions can represent electrons produced by photoionization of the gas

by any high-energy photons which may also be produced when n_x electrons travel dx.

From the equation of continuity of electrons in the gas, it can then be shown that (Llewellyn-Jones, 1957)

$$I(d) = \frac{I_o(1 - \beta/\alpha)\exp \alpha d}{\exp(\beta d)\left[(1 - \frac{\beta}{\alpha} + \beta\frac{\delta d}{\alpha}) - \{\exp(\alpha - \beta)d - 1\}\{\gamma + \frac{\delta}{\alpha - \beta} + \frac{\beta}{\alpha}(1 - \delta d)\}\right]} \quad (7)$$

When β, δ and γ are all small compared with α, this reduces to the simpler well-known form

$$I = I_o \exp(\alpha d)/[1 - (\omega/\alpha)\{\exp \alpha d - 1\}] \quad (8)$$

where

$$\omega/\alpha = \beta/\alpha + \delta/\alpha + \gamma ,$$

or more generally

$$\omega = \beta + \alpha\gamma + \delta + \varepsilon_m + \varepsilon_{ex} + \eta \quad (9)$$

in which the individual coefficients are known as Townsend secondary ionization coefficients, and ω/α the generalized Townsend secondary coefficient representing the combined action of all the individual processes.

It follows that the same form of growth Eq. (8) is obtained if any of the above secondary processes act alone.

Evaluation of Ionization Coefficients

In the earlier work Townsend (1910) considered only the β and γ processes with positive ions, but later (1923) showed that a δ type process also conformed to (8), while more recent work (Dutton et al., 1952; Davidson, 1953) incorporated the coefficients representing the influence of the slow diffusion of excited and metastable atoms as well as photoionization in the additional coefficients ε_{ex}, ε_m and η of relation (9).

It is clear that the theoretical relation (8) is similar to the experimental relation (4) when $C_1 = I_o$, $C_2 = \alpha$, and $C_4 = \omega/\alpha$.

Consider now the constant C_3 in (4). This equation was based on the assumption that α was constant and finite and independent of gap width d even for very small values. In fact, this cannot be the case for small distances of a few free paths, because the electrons will require a number of gas collisions before attaining a mean energy of agitation determined by the parameter E/p. Since α

depends upon the mean energy, $\alpha(x)$ will be a function of x, the distance travelled from the cathode until $x = d_o$ when the steady state is reached. Thus a distance d_o can be defined such that

$$\alpha d_o = \int_c^{d_1} \alpha(x)dx$$

so giving

$$I/I_o = \exp[\alpha(d - d_o)] . \qquad (10)$$

In many gases, d_o may be neglected especially for measurements at the larger distances and higher pressures, but important exceptions are the monatomic gases at values of pd not greatly exceeding that near the Paschen minimum. However, for accurate interpretation of the experimental growth data according to (8) in order to evaluate the Townsend coefficients α and ω/α, determination of values I_o and d_o can be avoided by suitable analytical methods (Grosseries, 1939; Crompton et al., 1956; Jones and Llewellyn-Jones, 1958).

Further complications in the interpretation of (4) arise from the back-scattering collisions with gas molecules of electrons emitted from the cathode whether by the external irradiation or by secondary effects of the current. This effect was observed in the earliest Townsend experiments. The electron current which finally leaves the cathode to traverse the gap constitutes a fraction c of the number originally given by J. J. Thomson (1928)

$$I/I_o = 1/\{1 + u/W_- \sqrt{6\pi}\} \qquad (11)$$

where u is the most probable electron velocity of ejection and W_- the drift velocity of electrons along the field. This phenomenon is often studied in the type of gap considered above by measuring its (I,V) characteristic curves at a given value of d. When no ionization occurs (E/p and p low), I increases with V up to the saturation value I_o; but at higher pressures and E/p, no saturation value is attained because ionization sets in before saturation and I continues to increase, although dI/dV may have a minimum value > 0. In this case, a current I is measured which is a certain fraction $c[= f(E/p)]$ of I_o when V is near the value at which dI/dV is a minimum and amplifications negligible. With suitable analysis, knowledge of the value of c is not required in an interpretation of growth curves to evaluate α and ω/α from experimental growth data. The Townsend coefficients α and ω/α have been measured over wide ranges of E/p and for most permanent gases and published in reference works (Dutton, 1975).

Interpretation of the Coefficients

The earliest work showed that experimental curves for $\alpha/p = f(E/p)$ over large ranges for various gases satisfied the empirical relationship

$$\alpha/p = A \exp\{- B/(E/p)\} \qquad (12)$$

which is of considerable use in modern numerical calculations of current growth or particle concentration. In hydrogen, for example, when A = 5 and B = 13, this expression agrees well with measurements of α for $100 < E/p < 600$ V $cm^{-1}torr^{-1}$, (Townsend, 1915). A theoretical interpretation of this empirical expression for α was also given by Townsend from simple consideration of those free paths traversed in the direction of the field E. The proportion of these which exceed length x is $\exp(-N\sigma x)$ where $N(= ap)$ is the molecular concentration of the gas and σ is the molecular cross-sectional area for ionization. Putting $x = V_i/E$, the fraction of collisions which ionize is then $\exp\{- N\sigma V_i/E\}$, and since there are $N\sigma$ collisions per cm, it follows that the average number of ionizations per electron per cm (α) is given by

$$\alpha/p = N_o\sigma \exp\{- \sigma N_o V_i/(E/p)\} ,$$

which has the same form as the empirical relation (12) above when $A = \sigma N_o$ and $B = N_o\sigma V_i$. Thus approximate estimates of molecular and atomic cross sections for ionization, as well as estimates of ionization potentials for many gases were made in this way from evaluation of the constant B some years before the more explicit and correct values deduced from the Bohr atomic model. However, they did not widely differ, considering the impure state of the gases (especially monatomic gases) for which estimates were made. For example, V_i for air was given as 25 V and for impure helium, 12.3 V. Another interesting, but correct conclusion was also reached concerning atomic cross sections by comparing σ in the constant A with gas kinetic values which were greater. This implied that the cross section for ionization at a given electron energy was lower than the gas-kinetic value, in accordance with later atomic theory.

However, the coefficient α can be accurately calculated in terms of atomic constants by solving the Boltzmann equation and using data on cross sections for excitation, ionization and elastic energy losses in deriving the energy distribution function (Massen and Burhop, 1952), as well as by using Monte Carlo methods (Thomas and Thomas, 1969). The relationship (10) generally conforms to the expressions deduced theoretically since the mean electron energy is usually nearly proportional to (E/p) if not too high.

In general (ω/α) is small compared with α and Fig. 3 shows how the relative magnitude of (ω/α) and α determines the shape of the

$\{\ell n(I/I_o),d\}$ curves. When (ω/α) is very small, the initial stages, indeed most of the curve, is practically linear and the upcurving takes place over a very small range of d, and α may be calculated with negligible error from the slopes. However, in the hydrocarbon gases, such as n-pentane, (ω/α) can be extremely small $\lesssim 4.10^{-7}$. In such cases the growth curve is found to be almost completely linear; this is in accordance with (8) which shows that any upcurving can then only take place over a very small range of d, which requires very careful and accurate experimental technique to measure (Morgan, 1965). On the other hand, when (ω/α) is relatively larger, say ~ 0.1, as in the case in monatomic gases, no section of the growth curve is linear enough for α to be derived from a slope, and correct values of α can only be derived when the analytical procedures are based on Eq. (8) and not on Eq. (2). Misleading values of ionization coefficients can be obtained if the essential requirement of the use of a uniform field is not satisfied. Lateral diffusion of electrons and ions and scattering of photons are of little consequence when the field everywhere is uniform because their ionizing properties are unaffected. However, if charged particles diffuse into regions of different field intensity (e.g., at edges of the gap) the spatial rate of ionization will be affected and this alters the growth curve of the whole gap, which will not then satisfy (8) exactly, and false values of α and ω/α can be obtained by still using (8). Hence the ratio of electrode diameter to gap distance must always be sufficiently high, and electrodes should preferably have a Rogowski-Bruce profile. Further, the area of cathode irradiation should be confined to the central region in order to restrict any diffusion from the central current stream to regions of uniform field. Some lateral loss of photons is unavoidable, in addition to loss at the anode. Electron diffusion is particularly high in argon, so that special care should be exercised in measuring growth curves or sparking potentials in that gas. Electron diffusion along the electric field can also affect the value of α deduced from (8), but in steady fields the effect is not serious (Crompton, 1967).

Finally, it should be emphasized that accurate experimental determination of ionization coefficients depends not only on the observation of the experimental conditions indicated above, such as constant uniform fields, inactive and smooth electrode surfaces, stable irradiation and gas constitution, and accurate measuring techniques, but reliable values also depend upon the use of effective techniques of analysis when the experimental data are obtained from the spatial $\{\ell n(I/I_o),d\}$ growth curves.

An important modification of (8) is required when electron attachment processes occur in electronegative gases, such as oxygen or nitrous oxide. Four attachment processes have been shown by Massey (1952) to be important:

(1) Radiative attachment, when an electron collides with a neutral molecule AB, to form an excited negative ion AB^-_{ex} which itself emits a photon $h\nu$ on deexcitation to become a stable negative ion AB^- as follows

$$e + AB \rightarrow AB^-_{ex} \rightarrow AB^- + h\nu \ .$$

(2) Dissociative attachment, when an excited negative ion dissociates

$$e + AB \rightarrow AB^-_{ex} \rightarrow A_{ex} + B^- \ .$$

(3) Three-body attachment in which an excited ion is stabilized in collision with a slow neutral molecule which carries off excess energy

$$e + AB \rightarrow AB^-_{ex} \ ; \quad AB^-_{ex} + AB \rightarrow AB^- + AB(\text{fast}) \ .$$

(4) Positive and negative ion formation by electron impact on a neutral molecule. This process, unlike the previous processes, does not reduce the concentration of free electrons, generally requiring a higher electron energy; it is neglected at the lower values of E/p.

Thus, electron attachment not only reduces electron density but also changes the constituents of the gas by forming stable and unstable negative ions. A change of conditions can also take place by a conversion of one kind of positive ion such as N_4^+ in nitrogen being converted in collision with a molecule into a molecular positive ion N_2^+; but this has insignificant influence on current growth. Further complication is introduced when an electron detachment process also occurs, thus restoring free electrons. The expressions for spatial growth in these circumstances have been given by Davidson (Llewellyn-Jones, 1967) and by Thomas (1965); and for the case of only one stable negative ion with attachment coefficient, a (defined in a way analogous to α), the expression reduces to the simpler expression given previously by Penning (1938) and by Geballe and Reeves (1953).

$$I = \frac{I_o(\alpha/\alpha') \cdot \exp(\alpha' d) - (a/\alpha')}{1 - (\omega/\alpha')\{\exp(\alpha' d) - 1\}} \ , \qquad (13)$$

where $\alpha' = \alpha - a$, is the apparent ionization coefficient and deducible from the slope of $\ell n(I/I_o), d$ curves.

These effects are naturally more evident at the lower values of E/p and higher gas pressures, but there are considerable difficulties in attempting to deduce accurate values of a for the $\{\ell n(I/I_o), d\}$ curves from Eqs. (8) and (13) so that published data are not all in close agreement. However, at the higher values of

E/p in permanent gases, the effect may be taken into consideration by just using the apparent ionization coefficient α' instead of the real α.

Evaluation of Secondary Processes

The total regeneration inherent in the coefficient (ω/α) incorporates a number of possible processes of very differing characteristics, involving their different rates of operation. In the steady-state measurements the time factor is of little consequence, as practically every possible process can operate and be incorporated in expressions for α and ω/α. Hence, steady-state experiments cannot make a definitive diagnosis of all their separate processes, and time-resolved techniques must be employed to do this. Nevertheless, considerable information can still be obtained from experimental data on ω/α and its dependence on E/p and on the nature of the cathode surface. Detailed studies have been made of processes of electron ejection by positive ions, and estimates have been made of possible values of γ in Auger neutralization and deexcitation processes (Jones and Llewellyn-Jones, 1962). Work on surface states and cold electron emission has shown the importance of cleanliness and microscopic uniformity of cathode surface in ionization phenomena. Thin (10^{-7}cm) oxide or tarnish films, for example, alter the work function and emission processes; enhanced emission can be produced by a layer of positive ions on a thin tarnish film (Llewellyn-Jones and Morgan, 1953). Values of γ and of δ can thus be greatly influenced. Microscopic asperities, as well as small areas of low work function, create nonuniformity of high field intensity, and so contribute to concentration of ionization current and lead to instability of local electron emission, and then of the whole discharge. In general terms, γ should increase with E/p especially in the highest range, when the positive ions can acquire increased energies. Theoretical calculations concerning the process have been made for hydrogen (Davies et al., 1958), and results indicate a dependence on p as well as upon E/p. This is due to absorption especially at high pressure. In general, (δ/α) should increase as pd increases and E/p diminishes, in contrast to the dependence of γ which increases as E/p increases. Thus, at lower pressures and high E/p, the γ effect generally predominates over the δ effect as components of ω/α; while at higher pressure and lower E/p, δ tends to become predominant.

Taking into account possible absorption as well as backscattering given by expression (11), (δ/α) can be expressed by the relationship, neglecting resonance fluorescence,

$$\delta/\alpha = \frac{1}{\{1 + u/(\sqrt{6\pi}\, W_{-})\}} \cdot \frac{kg\theta}{(\alpha - \mu)}$$

where

k is photoelectric efficiency of photons at cathode,
g is a geometrical factor,
θ is the number of electrons produced at the cathode on the average per electron per cm along the field,
μ is absorption coefficient of photons in the gas,
$\omega = \delta = kg\theta$ when $\mu = 0$, as when E/p is not very low.

When μ is finite, (δ/α) should depend on p, with correspondingly small dependence of V_s on p and departure from Paschen's law. Further, when diffusion of metastable is involved in the (ε/α) process, the gap distance d becomes important, and the effect can be significant at high pressures. Here the Similarity Principle (Llewellyn-Jones, 1957) can be a useful diagnostic tool.

The Breakdown Criterion and Sparking Potential

It can be seen from Eq. (8) that d can be increased to a value d_s satisfying the relation

$$1 - (\omega/\alpha)\{\exp(\alpha d_s) - 1\} = 0 \qquad (14)$$

which determines the gap width when the $\{\ell n(I/I_o), d\}$ curves asymptotically approach the vertical. Here the applied potential is V_s, and it would seem that the current $I(d_s)$ would increase without limit or be limited only by the external circuit. At least the insulation of the gap would apparently cease, so that V_s could be described as the sparking potential for the gap characterized by the particular parameter pd_s. The coefficients α and (ω/α) for the particular value of E/p for any gap then determine a value of d_s which satisfies (8) and so determine the corresponding value of $V_s (= Ed_s)$, i.e., predict the value of the static sparking potential, which could then be compared with the values obtained experimentally.

Townsend (1910) obtained values of V_s for all gases with which growth of current measurements had been made, and Table 1 gives typical results. Pure monatomic gases have been carefully investigated

Table 1. Values of V_s (Townsend, 1910).

Gas	E ($V\,cm^{-1}$)	p (torr)	α	ω/α	d_s cm	V_s calc. (Volts)	V_s obs. (Volts)
Air	1400	8	16.47	0.013	0.431	603	603
CO_2	1400	2	21.24	0.0084	0.369	516	517

in later years and comprehensive data are now available (Dutton, 1975). In the large number of gases investigated, the values of sparking potentials with a parallel-plate gap calculated from data on α and ω/α obtained on the spatial growth of photoelectric currents were, within experimental error, equal to the values obtained by experiment. Further, in conditions when relations (3) and (4) strictly hold both α and (ω/α) are functions of E/p so that Eq. (8) can be rewritten in terms of E/p, i.e., of V_s/pd_s

$$1 - (V_s/pd_s)\ \{\exp f(V_s/pd_s) \cdot pd_s - 1\} = 0 \quad , \tag{15}$$

indicating that for a given gas V_s is a function of pd_s only, thus accounting for Paschen's Law in those conditions. However, when (3) or (4) do not strictly hold, then Paschen's Law fails.

In considering gas-collisional ionization processes, it follows that as p is progressively reduced, the electrons in traversing a gap undergo a diminishing number of gas collisions. Thus, in order to maintain the magnitudes of α and (ω/α) large enough to satisfy (8), the chance of any collision producing ionization must be increased; hence E_s, and so V_s, must be raised progressively as p, when in the lower range, is progressively reduced. On the other hand, as p is progressively increased, the number of gas collisions encountered per cm of drift is increased, reducing the free paths and so the rate of acquisition of energy per path. Hence, E and so V must eventually be progressively raised as the pressure is increased. It follows that the Paschen curve must pass through a minimum V_m in accordance with observation. This conclusion can be seen to follow formally from (14). Consider, for simplicity, the case then $\gamma(=\omega/\alpha)$ is practically constant, as is the case of air or neon at the higher values of E/p, 70 V/cm torr, with Ni cathodes. Using (11) it follows that

$$V_s = \frac{B(pd_s)}{Z + \ln(pd_s)} \tag{16}$$

where $Z = \ln\{A/\ln\ (1 + 1/\gamma)\}$ and $B = AV_i$. γ varies greatly for different cathode surfaces and different gases. V_m and (pd_m) are found from (16) by differentiation which gives

$$V_m = A \cdot V_i(pd_m); \quad (pd_m) = (2.72/A) \cdot \ln(1 + 1/\gamma) \ .$$

When pd is large (16), V_s increases with pd; and when pd is low, V_s still increases as pd decreases, in general agreement with experiment. Equation (16) also indicates that V_m should be low for gases for which V_i is low and γ large, which generally agrees with observation.

It is interesting to note that the Paschen minimum determines the properties of the cathode fall of potential in a cold cathode glow discharge (Llewellyn-Jones, 1966). In the transition from breakdown to the glow, the current increases to form a space charge and a uniform positive column extending from the anode to near the cathode, the remaining distance being occupied by the cathode fall. This region is, in effect, a parallel plate gap operating at the minimum sparking potential.

When cathode processes predominate, Eq. (14) also shows how the breakdown potential changes with change of cathode. The proportional dependence of V_s on proportional changes in $(\omega/\alpha)_s$ is obtained by differentiating (15) to give

$$\frac{\Delta V_s}{V_s} = \frac{\Delta(\omega/\alpha)_s}{(\omega/\alpha)_s} \Big/ \{V_s \, f'(E/p)_s\} \, . \qquad (17)$$

Thus, the change in V_s due to a change in (ω/α) depends upon (E/p). At high values of pd, and therefore of V_s, E/p is practically constant, and the proportional change in V_s is then practically inversely proportional to V_s; so that at high values of V_s, the change in V_s can be small enough to fall within experimental error. Hence, high breakdown potentials would appear to be practically independent of cathode material even when cathode processes dominate secondary ionization, as is found experimentally.

The relationships (12) and (14) also explain the Stoletov constant which was derived in early researches on ionization currents. In a parallel plate gap d, with a given potential difference V, Stoletov (1890) found that the current increased as the gap pressure was reduced and that at a certain pressure p_m, the current attained a maximum value, after which the current diminishes as p was further reduced; also p_m was proportional to the field E but independent of d. Thus, Stoletov found for air; V cm^{-1}

$$E/p_m = 372 \text{ (Stoletov constant)}.$$

The current is a maximum where α is greatest, and so by differentiating (3) and equating to zero, it follows that E/p_m is a constant depending upon the form of $f(E/p)$. Also

$$f(E/p)/(E/p) = df(E/p)/d(E/p)$$

so that the tangent to the $\{(\alpha/p), (E/p)\}$ curve at (E/p_m) passes through the origin. In the case of air experimental curves, this occurs when $(E/p) = 370$ and $(\alpha/p) = 5.3$, in agreement with Stoletov. The same result naturally follows analytically from the particular form of the function $f(E/p)$ in (11), since this agrees with experiment. Thus differentiation gives

$$d\alpha/dp = A \exp(- Bp/E) - (p/E)\, AB \exp(- Bp/E) = 0$$

and

$$p_m = E/B = E/AV_i; \text{ and } \alpha_m = E/V_i e$$

where e is the base of Naperian logarithms. Experiment shows that $AV_i = 365$ in fair agreement with Stoletov (d_o of (10) was here neglected).

These explanations over a wide range of ionization and breakdown phenomena at gas pressures such that pd < 200 torr cm are generally regarded as conclusive evidence of the validity of the Townsend mechanism of ionization growth and breakdown over this range.

Physical Significance of the Breakdown Criterion

Clearly the passage of a large current introduces a space charge which distorts the field invalidating (8), and the criterion (14) must relate to a certain condition produced by the small ionization current in the gap in which the field is still undistorted by the current. This view is supported by the fact that (14) is found to hold over a considerable range of values of the initiating current I_o indicating that all significant ionization processes are proportional to the current; i.e., they are single-impact processes. It is important that the relation (8) should be correctly interpreted. The apparent formal condition that $I \to \infty$ as the denominator approaches zero in (14) can have no physical meaning, since any current which is large enough to distort the field also invalidates the derivation of (14). This relation expresses a replacement condition that as the denominator approaches zero, then I_o can also approach zero and still allow I to be finite. Further, V_s would be independent of I when I is small. In physical terms, when (4) is satisfied, a finite small current can be maintained in the gap without any initial cathode current produced by external radiation, V_s being independent of the current. This is a conclusion which can be, and has been, fully tested by experiment as shown in Fig. 4 which gives a typical curve obtained by Jones and Morgan (Llewellyn-Jones, 1957) for breakdown in hydrogen near the minimum sparking potential.

A (V, I) characteristic of a gap is taken by using an external circuit which can accurately control the current with, say, a diode. This shows that when $V = V_s$ this value is independent of the small current passing, in the absence of external radiation. This small self-maintained current is sometimes known as Townsend discharge.

This interpretation can be justified formally by consideration of the conditions required for the self-maintenance of a small ionization current in a gas (Townsend, 1910). In the steady state

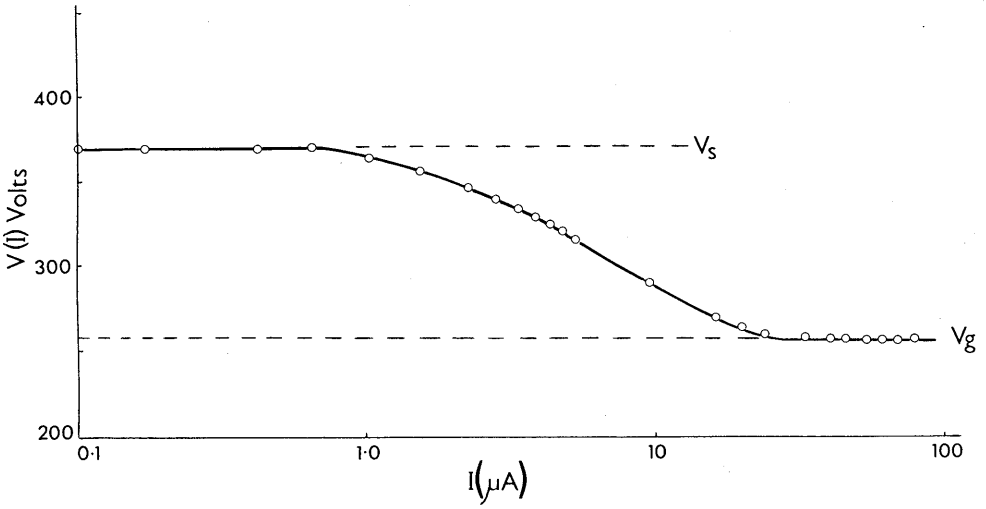

Fig. 4. Current-voltage characteristic at breakdown, showing attainment of a stable state when a glow discharge is set up. Copper electrodes in hydrogen, p = 11.8 torr, d = 0.2 cm. (Reproduced by permission of Methuen & Co. Ltd.)

$$\frac{dn_-}{dt} = -\frac{d}{dx}(n_-W_-) + \alpha n_-W_- \ ,$$

$$\frac{dn_+}{dt} = \frac{d}{dx}(n_+W_+) + \alpha n_-W_- \ ,$$

$$I = n_+W_+ + n_-W_- \ .$$

At the cathode, $x = 0$, and

$$(n_-W_-)_{x=0} = \gamma(n_+W_+)_{x=0} \ .$$

Also

$$(n_-W_-)_x = A \exp \int_0^x \alpha dx \ ,$$

giving

$$A = \gamma(n_+W_+)_{x=0} \ ,$$

and

$$(n_-W_-)_x = \gamma(n_+W_+)_{x=0} \exp \int_0^x \alpha dx$$

$$= I - (n_+W_+)_x ,$$

Hence

$$\gamma \exp \int_0^x \alpha dx = [I - (n_+W_+)_x]/(n_+W_+)_{x=0} .$$

when $x = d$, $n_+ = 0$, so that

$$\gamma \exp \int_0^d \alpha dx = \frac{I}{(n_+W_+)_{x=0}} = \left[\frac{(n_+W_+) + \gamma(n_+W_+)}{(n_+W_+)}\right]_{x=0} = 1 + \gamma$$

giving

$$1 - \gamma\{\exp \int_0^d \alpha dx - 1\} = 0$$

which is the criterion (14) for setting the static sparking potential.

It is now readily seen why breakdown apparently does not occur in a gap when $V < V_s$. When initiatory electrons n_o leave the cathode, they produce an avalanche $n_o \exp(\alpha d)$ at the anode and throughout the gap the secondary product of $n_o[\exp(\alpha d) - 1]$ positive ions, together with excited atoms and resulting photons. The arrival of all these products at the cathode generates a total of $n_o(\omega/\alpha)[\exp(\alpha d) - 1]$ new electrons. When criterion (14) is satisfied, at $V = V_s$, this total is n_o; thus the initial number after removal at the anode is on the average replaced by the regenerative process; and so the whole operation repeats itself indefinitely. On the other hand, when $V < V_s$ and $(E/p) < (E_s/p)$, α and ω/α are then lower, criterion (14) is no longer satisfied since $(\omega/\alpha)[\exp(\alpha d) - 1] < 1$ and the number of n new electrons then less than n_o. Hence, the next avalanche $n \exp(\alpha d)$ is smaller than its predecessor, and a succession of diminishing avalanches is set up, until eventually no replacement of electrons at the cathode occurs, and the discharge ceases. Since the time factor is a multiple of $\sim 10^{-5}$s for a γ process, or $\sim 10^{-7}$s for undelayed photons, in practice the extinction appears instantaneous, but modern high-speed and time-resolving experimental techniques can disclose the whole procedure, as well as the relative importance of the various secondary processes acting in any given case.

The static sparking or breakdown potential of a gap can thus be defined precisely as that potential difference which, independent of the current, supports a small self-maintained current in a uniform static field. In such cases the criterion which determines the value of V_s is set by (14) and shows that the electric field at this stage is undistorted by the space charge of the small ionization

currents which produced the condition (14). These currents are thus known as the prebreakdown currents.

Statistics of Avalanches and Breakdown Potentials

In the above discussion, ionization coefficients were treated as precise quantities, but this is only true on a macroscopic scale since physical quantities have a discrete structure. Currents and avalanches were regarded as continuous, while in reality they consist of a finite number of discrete atomic particles. Consider, for example, a Townsend discharge in which only α and γ processes occur; experiment shows that γ is a fraction, seldom exceeding 0.1, but can be as low as $\sim 10^{-7}$. In fact, γ is precisely defined only for a statistically large number n_+ of positive ions in order to make γn_+ still a finite number. Generally, while the vast majority of ions produce no secondary electrons, nevertheless some ions may produce one, two, or possibly three, electrons (depending upon the surface, the ion, and its velocity). Similar considerations apply to I_o or the number n_o of initiatory electrons. With weak cathode irradiation, there will be a statistical distribution of electrons, sometimes singly emitted and sometimes (more rarely) emitted in close pairs. Thus, with a very small number of initiatory electrons in a gap, the resulting avalanches, will reflect the statistical nature both of n_o and of γ, as well as the effects of gas-kinetic fluctuations in the values of collisional coefficients such as α and δ/α; such fluctuations will then produce consequent fluctuations in (ω/α). Consequently, when n_o is small, there is a finite chance of a self-maintained Townsend discharge still quickly extinguishing itself although $V = V_s$, and the discharge is steady macroscopically.

Similarly, because of the statistical nature of γ and of avalanches, fluctuations may produce a value of γn_+ favorably high enough to satisfy (14) even with V slightly below V_s. In practice, stability of a gap is obtained by inserting a resistor R in the external circuit, so that as I increases, V is reduced by RI, so reducing I (Evans, 1967).

It is now necessary to consider why, in practice, V has such a critical value. Davies and Evans (1965) investigated the statistical properties of a Townsend discharge in the neighborhood $V = V_s$ with $(\omega/\alpha = \gamma)$. The probability distribution of the current at any time after the removal of an initiatory current I_o depends only on the charges and excited atoms present in the gap at time zero, all of which had originated during a previous generation interval $\tau_o = \{1 - (1/\alpha d)\}d/W_+$. Let $\gamma[\exp(\alpha d) - 1] = \mu$, so that criterion (14) becomes $\mu = 1$; and let m be the number of electrons released in the gap at $t = 0$. The probability P(k) that a single electron produces a series of avalanches of at least k generations, i.e., a current still flows after a time $k\tau_o$, is given by (Legler, 1955):

$$P(k) = \frac{(1 - 1/\mu)}{(1 - 1/\mu^k)} \qquad \mu \neq 1$$

$$P(k) = 1/k; \qquad \mu = 1 .$$

The probability P(m,k) that a current still flows after k generations when a single electron is replaced at time zero by a pulse in electrons is given by

$$P(m,k) = 1 - \left\{ \frac{\mu^{(k-1)} - 1}{\mu^k - 1} \right\}^m ; \qquad \mu \neq 1$$

$$P(m,k) = 1 - (1 - 1/k)^m ; \qquad \mu = 1 .$$

To fix ideas, take hydrogen at E/p = 140 V cm^{-1} $torr^{-1}$, V_s = 350 V, d = 1.55 cm, and p = 1.6 torr, when experimental values of α/p are given empirically by 3.3 exp(- 88.9 p/E). At t = 0, the cathode current lies between 10^{-11}A and 10^{-7}A, while $\tau_o \sim 10^{-6}$s, so that m lies between 10^2 and 10^6. Experimental measurement of sparking potentials as defined above requires a small current flowing for some seconds (to enable measurements to be made), so that k is then $\sim 10^6$. At large values of k, P(m,k) is a rapidly varying function of μ in the region $V = V_s$ when $\mu = 1$. This fact is illustrated by calculating the values of μ which result in two values of P(m,k), say 0.001 and 0.999, for various values of m; and these are given in Table 2. Thus, for m = 1, μ = 1000, showing that when the number of initiatory electrons is small, μ must be large in order to maintain a small current even for times only $\sim$ 1s. To obtain a μ of this magnitude, V must considerably exceed V_s. This result is of technological significance when a breakdown spark is specifically required in a given gap as, for example, in switching or timing devices. Consequently, it is thus advisable to provide high external irradiation,

Table 2. Values of μ for various m and P.

m	for P = 0.001	for P = 0.899	P for μ = 1
1	1.001	1000.000	10^{-6}
10	1.0002	1.996	10^{-5}
10^2	1.00002	1.072	10^{-4}
10^3	1.0	1.007	10^{-3}
10^4	0.999 9992	1.0007	10^{-2}

or a sufficiently high overvoltage to produce certain breakdown in any given short interval.

Suppose, however, the number of initiatory electrons is raised to 10^4 and the applied voltage to the 1.55 cm gap in H_2, is raised by only 0.88 V above V_s, thus making $\mu = 1.0007$. Even then, in only one experiment in a thousand will it be found that the self-maintained Townsend current will cease after one second. On the contrary, when V is reduced by an extremely small amount, from 350 V to 349.9999 V, when $\mu = 0.999\ 999\ 2$, then in only one case in a thousand will any current be maintained for one second. When the operative secondary process is the fast photoelectric process (δ/α), τ_o is then ~ 10^{-8}s, and the corresponding k is 10^8, while m ranges from 1 to 10^4. The figures in Table 2 relating to the γ process, then apply also to the faster δ process, provided the current measurement is made in the shorter time of 0.01s instead of 1s.

Conclusion

In the range of the parameter pd $\lesssim$ 200 torr cm and with the lower pressures $\lesssim$ 100 torr, the generalized Townsend mechanism of spatial growth of ionization is able to give an explanation in considerable quantitative detail of the characteristics and related phenomena of the breakdown of gases in uniform fields in agreement with observation.

STATIC BREAKDOWN IN UNIFORM FIELDS AT HIGH VALUES OF pd AND VOLTAGES

First Difficulties with pd > 200 Torr cm

In the absence of evidence to the contrary, it was assumed at first that the Townsend mechanism of spatial growth of prebreakdown current leading to the criterion setting the value of the static sparking potential, which experiment showed was valid when pd > 200 torr cm, applied also at higher values of pd. Of special technological interest was the case of breakdown of a 1 cm gap in the atmosphere, with pd ~750 torr cm, requiring V_s ~30,000 V. Thus when suitable high-voltage generators (whether impulse or smoothed rectified transformed A.C.) became available, investigations of high-voltage breakdown were carried out.

Rogowski (1924) applied an impulse ~30 kV to a 1 cm gap in air and found that the voltage collapsed in times ~ 10^{-6} or 10^{-7}s. Clearly, these short times appeared to exclude the feasibility of a Townsend mechanism based on the action of slow positive ions (γ process) requiring times ~10^{-5}s, the faster photoelectric δ-effect apparently being ignored. Further, photographs of the narrow bright spark tracks gave rise to the impression that some constricted process operated along such tracks, and this view was also

supported by the extensive cloud chamber photographs of ionization tracks obtained in necessarily damp gas (alcohol and air) by Raether (1936, 1937, 1964). Some of these were interpreted as single Townsend electron avalanches, $n = \exp(\alpha d)$. Other photographic records of breakdown in gases showed luminous tracks which appeared even to originate in the gas itself, almost mid-gap, rather than always at the cathode or anode; in some conditions the luminous streak would rapidly proceed to the anode, while in others it would travel towards the cathode. Such results appeared to be consistent with the view that a single Townsend avalanche would proceed until it suddenly developed at its head into a luminous high-current track which would rapidly complete transit of the gap, thus closing the circuit. About the same time experiments were carried out in highly nonuniform gaps between spheres or points and a plane. Breakdown in these cases was even more characterized by transient, luminous, narrow streaks which were termed streamers, in contrast to broad discharges which were assumed, without any quantitative calculation, to be characteristic of a Townsend mechanism.

Such results were taken to indicate that final breakdown was produced by a new, as yet undisclosed, extremely rapid process of ionization which required only a single large avalanche, rather than the cumulative action of primary and secondary processes involving repeated electron, ion or photon transits of the gap. These new gas processes were independent of the cathode surface and were likely to have been initiated by high electron density at the head of the original avalanche (Raether, 1939; Loeb, 1939; Loeb and Meek, 1941).

At that time, this conclusion also appeared to be consistent with measurement of the spatial growth curves obtained at these higher pressures when pd exceeded 200 torr cm in that these did not conform to the Townsend Eq. (8), based on the combination of various secondary processes with the primary ionization process α. With parallel plates in air, the semilog plots obtained appeared to be straight lines for all values of d until a spark occurred to limit further investigation, the plots showing no curvature which would indicate a (ω/α) process, even for conditions when there was no field distortion due to the initial ionization currents. Conclusions were then drawn (Loeb, 1939) that the mechanism leading to (8) no longer held when pd > 200 torr cm and that breakdown was due to some mechanism, independent of the cathode and initiated by an electron avalanche alone.

Kanal and Streamer Theories

Raether (1939, 1955, 1964) and Kohrmann (1955) considered that the essential factor for introducing any very rapid process, such as intense local photoionization of the gas in a Kanal, is the actual numerical size N of the electron avalanche in conditions when the path is concentrated on account of the low lateral diffusion of

electrons at high pressures. Consequently, the criterion for Kanal formation, assuming undistorted fields, with a single initiating electron producing an avalanche in an undistorted field is

$$\exp(\alpha d) = N \sim 10^9 \quad ,$$

or $$(\alpha d)_c = \text{constant } C. \qquad (18)$$

This constant can be found empirically for any given case when d_s and V_s are known, since the parameter (V/pd) then determines the value of α/p. The value 18 was originally suggested but later changed to about 20 (Kohrmann and Raether, 1954). No quantitative analysis had been made of the precise field distortion produced by the avalanche, but it was noted qualitatively that the general effect of the field set up by the positive ions created behind the avalanche head, together with the field set up by the electrons at the actual head of the avalanche, and facing the anode, is mainly axial to the primary avalanche. This enhanced field in the cathode half of the gap can act on any electrons produced there by photoionization to create more electron avalanches; thus, this axial field would appear to be more effective than a radial or forward field for enhancing the current.

The number of any photoionizations would be proportional to the number of excited molecules producing the required photons in the primary avalanche and so proportional approximately to the total number of ionizations, i.e., to $\exp(\alpha d)$. Hence, some physical significance can be attached to the importance of the term $\exp(\alpha d)$ in a breakdown mechanism. In fact, it was known for some time (Schumann, 1923) that an empirical expression of this form could give sparking potentials in agreement with observation and that the criterion (14) can be reduced to this approximate form. For example, when E/p is low as at higher pressures and in gases when the γ process predominates and varies slowly with E/p, then γ would appear almost constant over a wide range of pressure, since E/p varies slowly at high values of pd. Since $\gamma \exp(\alpha d) = 1$, criterion (14) would then become $\exp(\alpha d) = \gamma^{-1}$ constant. Another interesting deduction can be made from the Kanal theory standpoint. If the applied field is so high that this critical value of N is reached at a distance $x < d$, i.e., before the primary avalanche $\exp(\alpha x)$ reaches the anode at d, then the Kanal process should initiate at x after a lapse of time $x/W_- < d/W_-$, and a mid-gap Kanal and a very short formative time (less than electron transit time) become feasible.

Another view on similar lines, but directing more emphasis to the nature of the positive space charge and its radial field at the head of an avalanche, was proposed by Loeb and Meek (1941) and known as Streamer theory. On this view, the density of a positive ion space charge was estimated from the total number in the avalanche, and an expression for a radial field E was derived. This radial

field was assumed to be strong enough to draw into the avalanche head any electrons produced in the gas in the vicinity by high-energy photons created in the high field at the avalanche head. These electrons themselves initiate small avalanches in this radial field attracting them into the head and so increase the number of positive ions and, possibly, the radial field also. The result is a rapidly developing plasma to form a streamer extending first to one and then to the other electrode. The arrival of this plasma at the cathode might also release a burst of electrons to give a high field running back along the track.

The criterion proposed by Meek (1940) for initiations of this process is that the radial space charge field E_r should be proportional to the undistorted field $E = V/d$ in the gap; i.e.,

$$E_r = kE = kV/d \ . \tag{19}$$

Originally k was put = 1, but other values have been attributed empirically to k for different ranges for agreement with experiment. However, analysis by Zeleny (1942) of a radial field so calculated indicated that the field was unlikely to act in that way, and Fisher (1943) pointed out other difficulties relating to large avalanches. Nevertheless, regarded as empirical relationships, the two new criteria (18) and (19) have in common that they give values of V_s over certain ranges of pressure or gap distances on assumptions of suitable values for the constants which accord with those measured.

Both Kanal and Streamer theories have similar basic concepts and lead to similar conclusions: both emphasize the critical importance of expression $\exp(\alpha d)$ when d is large > 18. The Raether Kanal theory laid stress in the axial distortion of the original field both ahead and at the rear of the avalanche and on the efficiency of any electrons created (by photoionization) on the cathode side as far as reinforcement of the original avalanche is concerned. Both theories of breakdown mechanism practically satisfy the experimental requirement to obey Paschen's Law and have the following properties, whether the applied field is static or impulsive, uniform or nonuniform:

(a) There is no cathode or gas secondary ionization process, apart from photoionization, in a Townsend-type mechanism, so that semilog plots of the prebreakdown ionization currents are straight lines with no upcurving at larger values of d; these curves proceed until a critical value of $\exp(\alpha d) \sim 10^9$ is reached, when space charge suddenly distorts the field and breakdown suddenly occurs.

(b) The sparking potential is independent of the nature of the cathode surface.

(c) High field distortion, due to space charge at the avalanche head, is essential to produce secondary avalanches and a plasma from electrons produced in the vicinity, so that the criterion which sets the value of the breakdown potential is uniquely determined by space-charge distortion of the field.

(d) The transition from a Townsend mechanism, which operates at the lower pressures, to a Streamer mechanism takes place when pd > 200 torr cm.

(e) The resulting spark tracks can be narrow filamentary streamers of cross section ~ that of the avalanche space charge.

(f) It is feasible that breakdown could take place in very short times $\lesssim 10^{-7}$ for a 1 cm gap and that luminous streamers can cross the gap in less than an electron transit time.

(g) The generation of high-energy photons is essential in order to produce adequate photoionization of the neutral gas molecules.

At the time these theories were put forward (1939-40), no detailed quantitative theoretical or experimental treatment of the spatiotemporal growth of ionization had been given, so that no knowledge of how space charges precisely do, in fact, develop in a gap and ion distributions develop for any specified mechanism of generation existed; in other words, the continuity equations and Poisson's equations had not been analytically solved. Further, there were no available reliable experimental data on the formative times, from appearance of the necessary initiatory electron to occurrence of a specifically defined breakdown of the gap, other than observations of the apparent fast rates of propagation of luminosity in long gaps and lightening flashes and short breakdown times of gaps overvolted with impulsive, short-duration, applied potentials (Loeb, 1939). This "streamer" luminosity represented the final stage of current growth, and apparent propagation time of the flash was not strictly relevant to the times that the originally invisible prebreakdown ionization currents required to grow into luminous tracks (Llewellyn-Jones, 1957). In either theory, no detailed account of the process of creation and subsequent action of the necessary high-energy photons was given for simple gases.

Photoionization in gases had long been known to occur given photons of adequate energy usually from an external source. Its importance as a secondary process in ionization growth lies in the fact that it is similar to the positive ion β process because it takes place entirely in the gas and is independent of the electrodes. It had long been considered that both processes were only likely to become important in the presence of high electric fields and were consequently not significant at values of E/p in prebreakdown

discharge conditions. However, over a limited range of absorption coefficients, photoionization, like the β process, can approximately be represented by a spatial rate coefficient (η/α), however small, as a component of the generalized Townsend secondary ionization coefficient ω/α; but η/α would be of negligible significance in comparison with the (ω/α) coefficient at the lower pressure when pd $\lesssim$ 200 torr cm. Photoionization would be more effective at the higher pressures which inhibit penetration of the gas and in which lateral diffusion of the avalanche would be reduced leading to higher space charge density. The η process, like the β process, might possibly have application in discharges such as those from a positive point at atmospheric pressure in conditions when no other secondary process may be effective. However, in the absence of specification of gas-collisional process of production of the required photons as well as of reliable data on their absorption cross sections, no quantitative calculation of current growth due to photoionization can be made or of containment of the photons within the avalanche itself. In simple molecular gases or the monatomic gases under normal fields, no mechanism of creation of photons capable of ionizing these gases was specified in the original streamer, and no evidence of multiple ionization was produced. On the other hand, in gas mixtures such as air, a photon creation process is feasible in that photons emitted by excited nitrogen molecules (>15 eV) could, in principle, ionize oxygen atoms ($V_i \sim 15$ eV); even so, reliable data on absorption coefficients were scanty.

Nevertheless, the importance attributed to the behavior of single avalanches encouraged theoretical and experimental investigation of the statistics of single avalanches, notably by Wisjman (1949), Legler (1955), Frommhold (1958), Schlumbohm (1959), and Davidson (1964). The next step in the investigation of these proposed new mechanisms for setting the criterion for static breakdown in uniform fields was to test experimentally the specific conclusions (a), (b), (c) and (d) above over the range of pd exceeding 200 torr cm, using high voltage ionization chambers, larger distances, and gas pressures up to atmospheric and higher.

Prebreakdown Currents, 200 Torr cm < pd < 4000 Torr cm

The first requirement for accurate measurement of the ratio I/I_o is that the parameter E/p must be maintained so steady that resolution of separate semilog plots of I/I_o is possible for small changes ($\lesssim$ 3%) in E/p; i.e., the conditions specified previously should be stringently followed, particularly for measurements of p and d and uniformity of field. Typical results obtained in air (Llewellyn-Jones and Parker, 1950, 1952) are shown in Fig. 5 from which it is seen that the spatial growth curves followed Eq. (8), disclosing an upcurving and yielding values of α/p and (ω/α). Sparking potentials were calculated from the criterion (14) to give values equal to those observed, thus confirming the validity

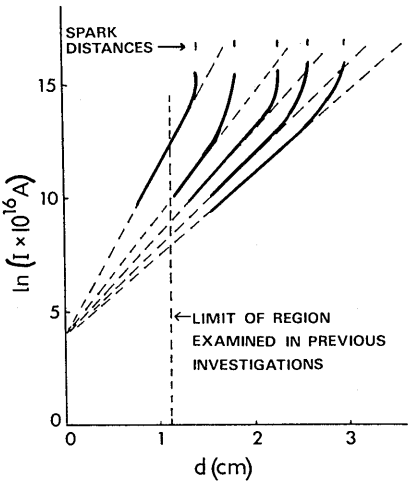

Fig. 5. Growth of photoelectric currents in dry, mercury-free air at 200 torr. (From Nature, Vol. 165, p. 964. Copyright (c) 1950, Macmillan Journals Limited.)

of the derivation of that relationship throughout the ranges 12 kV $< V_s <$ 30 kV and 300 torr cm $<$ pd $<$ 760 torr cm (Fig. 6).

Thus in a gas mixture in which a process of photoionization was conceivably possible, the spatial growth of prebreakdown current in

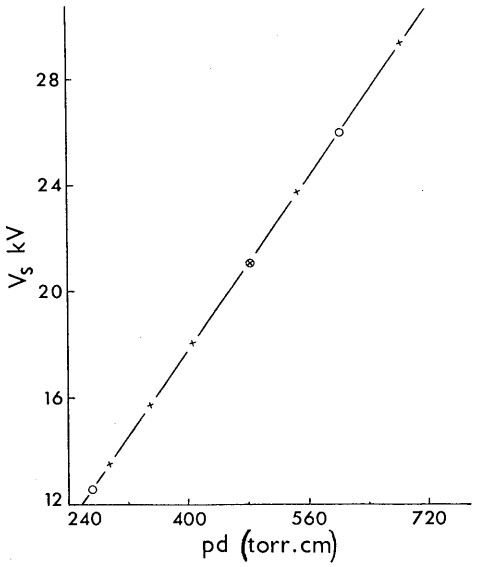

Fig. 6. Calculated (x) and observed (o) sparking potentials in dry, mercury-free air. (From The Royal Society.)

air, followed the Townsend relationship (8) or (13). The early experimental $\{\ell n(I/I_o),d\}$ curves, which were apparently linear up to the point of instability and sparking and which had been taken to demonstrate absence of upcurving and characteristic of any secondary ionization, had been obtained with gap voltages insufficiently steady to provide the required constant electric field for discrimination of the $\ell n(I/I_o),d$ curves.

In all gases investigated changes in cathode surface had readily observable effects on the slope of the upcurving of the $\ell n(I/I_o),d$ plots, indicating a change in (ω/α), although the effect on V_s was understandably very small.

In any Kanal-Streamer mechanism, initial field distortion in an avalanche is an essential feature, and the attainment of critical space charge must be dependent upon the current and therefore upon the initiatory electron current. Hence, if the sparking potential at static breakdown were space-charge dependent, the sparking process and the prebreakdown currents should depend upon I_o. This was tested in nitrogen by measuring prebreakdown currents and sparking potentials over a range of I_o from 10^{-15}A to 10^{-12}A from the same small area of cathode surface. All the curves obtained led to the same value of d_s and V_s, thus indicating that the criterion could be set in the absence of any significant field distortion because of space charge of prebreakdown currents.

Because concentration of current due to elimination of lateral diffusion increases with gas pressure, space charge effects are more likely to occur at the higher gas pressures. It was later proposed (Kohrmann, 1959; Schröder, 1961) that a transition from Townsend-type mechanism in uniform-field static breakdown to a Kanal-Streamer mechanism would occur at values of pd ~5000 torr cm rather than at 200 torr cm, as below this higher limit the value of αd was thought to be too low to produce a large enough initial avalanche. However, the experiments in air with pd up to 12,200 torr cm (Dutton and Morris, 1967) and in nitrogen (Daniel and Harris, 1970) up to 13,000 (V_s 0.5 MV), and in highly electronegative gases (Dutton, 1977) like SF_6 all showed that the Townsend mechanism sets the criterion for the static breakdown potential in uniform fields at least up to pd_s = 13,000 torr cm, and no evidence was found for transition to another mechanism. Thus, the properties of a Kanal-Streamer mechanism given in (a), (b), (c) and (d) above have no relevance to static breakdown, at least throughout the range $0.1 < pd < 13{,}000$ torr cm. The properties (e) and (f) refer to the later stages of current development after the condition has been attained for which the criterion (14) is set; i.e. the replacement condition has been passed, and the current, should the external circuit permit, can increase in time sufficiently to distort the field and change the values of α and (ω/α). At this stage the relationships (8), (13) and (14) have no relevance. Quantitative assessment of

the mechanism of the spatio-temporal development of ionization in the gas then requires time-resolving techniques of impulse voltages and corresponding current measuring devices, together with diagnosis of experimental data on the basis of the solution of the continuity and Poissons' equations. The results of such developments will be discussed later.

Photons in Secondary Ionization at High Pressures

At the higher (~200 V/cm torr) values of E/p obtaining at the lower gas pressures near the minimum sparking potential, a pronounced dependence of V_m on the cathode was found, thus demonstrating that the two gas-collisional processes of ionization by positive ions (β) and photoionization of the gas were of minor significance in comparison with cathode processes, if they occurred at all in these conditions. Atomic momentum considerations alone would appear to rule out β, and the sparse cross-sectional data available on appropriate photon-absorption coefficients would appear to eliminate photionization in these conditions, although ionizing photons have been detected from spark discharges (Thomson and Thomson, 1933). The situation would, however, be possibly different when very high fields are available, as in the case of discharges from sharp positive points, or in highly overvolted gaps ($V > V_s$) when exp (αx) could attain much higher values than is possible in the steady state.

With static breakdown, accurate determination of (α/p) and (ω/α) can be obtained by appropriate analysis of the $\ell n(I/I_o)$,d curves, but such determinations themselves do not quantitatively distinguish between the different components γ, (δ/α), (ε_{ex}/α), (ε_m/α) which can constitute the generalized coefficient (ω/α). Nevertheless, considerable information can still be obtained from analysis of the dependence of (ω/α) upon (E/p), pd, p, d and the work function of the cathode. Marked dependence of (ω/α) on the cathode has been found for gases: air, N_2, O_2 and H_2 over a wide range of pd up to the highest value attained, and it follows that the significant components are the γ and (δ/α) processes. Results for hydrogen indicated that (ω/α) is almost inversely proportional to the work function of the cathode. Further, at a given (E/p), a marked decrease of (ω/α) was produced by increase in pressure, thus indicating a departure from Paschen's law but not necessarily to an extent observable from measurements of V_s.

It has been shown that the proportional change in V_s due to a proportional change in (ω/α) is almost inversely proportional to V_s at high values of pd_s, so V_s becomes practically independent of the cathode. Conversely, observed independence of V_s of the cathode is no evidence for absence of cathode effects. At high values of pd, any cathode effects are more readily disclosed by measuring the change in d_s due to a change in (ω/α) caused by a change of cathode at a given value of E/p.

Back diffusion of emitted electrons and dependence on cathode work function apply to both processes, but as pointed out consideration of the electron energy distribution functions and ionization and excitation processes shows that the relative importance of (δ/α) to γ should increase as (E/p) falls, i.e., as pd increases, so that it is likely that in the above cases, (δ/α) is the predominating process. Further, analysis (Jones and Llewellyn-Jones, 1963) of emission processes due to impact of positive ions indicates that γ should be independent of p, so that (δ/α) must be the dominant process in these conditions.

Taking into account absorption of photons, and further loss of photons due to destruction of excited molecules in molecular collisions, it can be shown (Davies et al., 1958) that (13) is modified to give

$$(\omega/\alpha) = \frac{Kg\theta}{(\alpha - \mu)} \cdot \frac{\{\exp[pd(\alpha - \mu)/p]-1\}(1 - \nu\tau P)}{\{1 + u/(W\sqrt{6\pi})\}\{\exp(pd\ \alpha/p)-1\}}$$

where ν is the collision frequency (= Kp) with neutral molecules of an excited molecule of lifetime τ, and P is the probability of destruction of that state in a radiation-less collision of the second kind. Thus

$$(\omega/\alpha)_p = (\omega/\alpha)(1 - \nu\tau PK_p) \ , \qquad (20)$$

and when (E/p) is constant, $(\omega/\alpha)_p$ should be linearly dependent upon p, in agreement with experiment for hydrogen for E/p = 20 V/cm torr.

In helium, at atmospheric pressure, on the other hand, (ω/α) was neither pressure- nor distance-dependent, but satisfied similarity as a function of E/p. This is consistent with the predominance of the (δ/α) process due to destruction of helium metastable atoms in collision with neutral gas atoms resulting in production of nonresonance photons which penetrate the gas to produce a photoelectric effect at the cathode. In nitrogen, no significant pressure-dependence was found.

It is of interest to consider on general grounds some characteristics of a photoionization process in the gas, assuming that some process of single-impact excitation can produce ionizing photons, proportional to the current, as when the photons ionize a gas component of a mixture, seemingly feasible in air. Again, let θ be the spatial rate of excitation, proportional to α, so that the number of photons produced by single-impact excitations in an avalanche is $(\theta/\alpha)\ I_o \exp(\alpha d)$. Assuming, for simplicity, that these are produced mostly near the anode and are absorbed in traversing the gas, it can be seen that the total ionization produced, when μ

is caused by photoionization, is

$$I = I_o \exp(\alpha d)/\{1 - \phi \exp(\alpha - \mu)d - 1\} \qquad (21)$$

where $\phi = \theta f g \mu/(\alpha - \mu)$. This expression illustrates the importance of the absorption coefficient in determining the spatial growth. When μ is a small fraction of α, (21) is of the same general form as (8) with growth approximately satisfying (13), so that breakdown is possible at the appropriate d_s. On the other hand, if μ is high, as is possible with resonance photons at high pressure, this reduces to

$$I = M.\ I_o \exp(\alpha d) \quad .$$

where M is a multiplier independent of d. In this case, the result of photoionization is practically the same as enhancement of α, giving a linear $\{\ell n/I/I_o, d\}$ plot and breakdown not possible for finite values of d, and there would be no agreement with Eq. (8). Further, when $\mu \sim 0$, or at the lower gas pressures, relation (21) again becomes a single exponential. More detailed mathematical analysis by Davidson determined the restrictions on values of μ for which breakdown is possible in the special case of the gas mixture air; even so, the form of the $\ell n(I/I_o), d$ plot was not in agreement with that measured. For single gases, the problems of specifying a suitable process of photon creation proportional to the current still remains for single-impact processes, and the case of very high fields and high current densities when multiple-impact processes occur have yet to be quantitatively investigated. The production of high-energy photons by further excitation of already excited atoms in an avalanche has been considered by Lozanskii (1976), who concluded that in helium the process could be significant in reinforcing ahead of the electron avalanche. However, as far as this is a multiple-impact process dependent on the current, it would therefore have little significance in setting a criterion for the static breakdown potential, which is independent of the prebreakdown current when this is small; but it might have application in any high current phases of complete breakdown of a gap.

BREAKDOWN IN NONUNIFORM STATIC FIELDS

Electrode Asymmetry

Nonuniformity of field can be produced by changes in the gas as well as by electrode geometry, but here it is of interest to consider only the second case with small currents. Since (α/p) and (ω/α) are functions of E/p, both these coefficients will be functions of position, and the product (αd) for uniform fields is replaced by

$$\int_0^d \alpha(s) \cdot ds \ .$$

In a parallel-plate Townsend gap, the mechanism and processes involved in breakdown under static fields have been fully investigated, and an infinitesimal change of geometry of, say, one electrode involves only an infinitesimal change in field distribution and so in the various ionization coefficients; hence, no significant departure from the original mechanism is to be expected until a considerable nonuniformity of field is set up. The criterion (8) at least for pd < 200 cm torr, is replaced by

$$1 - (\omega/\alpha)\{\exp \int_0^d \alpha ds - 1\} = 0 \ , \qquad (22)$$

and Paschen's law should still hold, provided no very high fields are set up at an electrode, a condition which is also necessary for uniform fields.

Another condition of the extent of nonuniformity is that the field should not be such a rapid function of position that the coefficient α would lose its significance. In fact, E(s) at position s, although varying with s, should still be sensibly constant over a few electron free paths and equal to E(s) in a uniform field when space charges are negligible. The value of $\alpha(s)$ at s can then be taken as $f(E_s/p)$ as given by (3) and (2). Clearly, this condition is not satisfied for the highly divergent field set up at a very sharp point. Quantitative treatment of breakdown in nonuinform fields thus requires knowledge of the spatial distribution of field; known values of (α/p) and of (ω/α) as functions of (E/p) may then be used in the absence of highly divergent fields. Otherwise (α/p) must be calculated using, say, Monte Carlo methods.

Polarity Effects

Geometrical asymmetry of electrodes introduces another difference from the uniform field case by producing a polarity effect. This is due to the large difference of field intensity at the electrodes which can affect the primary and electrode secondary processes.

An electron avalanche proceeding outwards from a negative small electrode moves under a weakening field towards the anode, but when the smaller electrode is the anode, the electron avalanche moves under an increasing field. Similarly, all positive ions formed in the gap proceed to the cathode, but when this is the smaller electrode the ions move under a stronger field, so that in gases at pressures when $\gamma = \phi(E/p)$, then γ should be higher at the smaller

electrode than at the larger. In the system, for example, of a thin wire, radius a, and coaxial cylinder, radius b, the field E_r at a radial distance r at breakdown is related to the breakdown potential V_s by the expression

$$E_r = V_r/r\ell n(b/a) \ , \tag{23}$$

so that

$$\gamma = \exp\left[- \frac{V_s}{\ell n(b/a)} \int_{E_b/p}^{E_a/p} \frac{(\alpha_r/p)}{(E_r/p)^2} \, d(E_r/p) \right] \tag{24}$$

giving the dependence of V_s on γ. Hence the higher is γ, the lower is V_s, so that V_s for the wire negative could be lower than that for a positive wire. In the case of nitrogen ($\bar{}$) (Huxley, 1928) and for hydrogen (Bruce, 1931) V_s is lower than V_s^-, but in air the Paschen curves intersect (Boulind, 1934), V_3^- exceeding V_s^+ when pa = 0.7 mm torr. Clearly, the γ-process cannot be the predominant secondary process in air, and the (δ/α) process must also be considered.

The interception of photons generated in prebreakdown currents depends upon the area of the electrode, so that practically all photons are reflected and or absorbed by an outer cylinder, for example; but only a small fraction is intercepted by a thin wire or point. Clearly, polarity effect can be produced in this way, since (δ/α) could be larger for a negative cylinder than for a negative wire.

In pure monatomic gases no intersection of the Paschen curves for a positive and negative discharge is found, V_s^- always being lower than V_s^+. Traces of impurity, however, can produce a lowering of V_s^+, and intersection of the curves occurs at the higher values of pa, an effect due to collisions of the second kind between metastable atoms and molecules of impurity (Penning, 1931). Exchange processes can affect the value of the energy acquired by positive ions under high electric fields. Thus, it is not possible to postulate a general conclusion concerning the nature and magnitude of the polarity effect for all gases. In general, this polarity effect will depend upon the relative significance of the various possible secondary ionization processes. Each gas type must be considered separately for the specified gap and field geometry for which the values of (α/p) and (ω/α) are known as functions of (E/p) from parallel-plate spatial growth experiments, together with further knowledge, where possible, of the separate components: γ, (δ/α), (ε/α) and η of the generalized coefficient (ω/α). Further, if E exceeds values 10^5 V/cm at the smaller electrode when negative, then field-dependent electron emission can occur; this is highly

dependent upon surface films and the micronature of the cathode surface (Llewellyn-Jones and de la Perrelle, 1953) and would produce a departure from similarity. Electron attachment and detachment processes can have considerable significance. This polarity effect is generally accentuated by increasing the nonuniformity of field, and a point-to-plane system can be used as a rectifier.

Corona Relationship at Low Pressures

The glow discharge in a wire-coaxial cylinder system is often referred to as a corona discharge and is one of the earliest forms studied. Gaugain (1866) first established that with a wire of radius a and coaxial cylinder of radius b, V_s varied with b in such a way as just to maintain the field E_a at the wire constant, where E_a is given by (23). Hence Paschen curves

$$V_s = aE_a \ln(b/a) = F(pa) \tag{25}$$

are sometimes plotted as aE_s versus pa. Consider two systems with same wire radius a, but different cylinder radii b_1 and b_2, with corresponding breakdown potentials V_1 and V_2. From Eq. (25)

$$\frac{V_1}{V_s} = \frac{\ln(b_1/a)}{\ln(b_2/a)} \quad . \tag{26}$$

This corona relationship is confirmed experimentally in air for negative discharges and for pure hydrogen with out-gassed electrodes (Llewellyn-Jones and Williams, 1953). The relationship (26) is also confirmed in pure helium with positive discharges only, but not with impure helium, a result attributed to effects of collisions of the second kind. If $\bar{E}_1$ is defined as the average field V_1/b_1 in the gap, it can be seen that this average value decreases as b_1 is increased.

In the wire-cylinder system, the region of ionization by collision by electrons is confined to a single coaxial volume around the wire where the field is adequate; the thinner the wire, the narrower is this volume. The space outside this narrow volume and extending to the outer cylinder is a region of low E/p, where there is no ionization by collision, and diffusion and drift are the significant processes in the absence of negative ions. In electronegative gases the effect of negative ions can be considerable, since attachment can readily occur at these low values of E/p, while detachment may be produced later in regions of high E/p, effectively providing another source of ionization. In general, the results of experiments on breakdown in nonuniform fields at low pressures are consistent with a breakdown mechanism involving primary and secondary processes of the same general nature as for uniform fields.

Higher Pressures and Nonuniform Fields

At high gas pressures, ~ 760 torr, breakdown phenomena in nonuniform fields are more complicated than at low pressures; this is especially the case in long gaps between points or between point and plane. The simpler cases of very pure diatomic or monatomic gases in fields with precisely known spatial distribution have not yet been completely investigated in the laboratory in order to diagnose the possible gas and electrode ionization processes. The case of locally highly divergent fields near thin wires or sharply pointed electrodes in long gaps in the atmosphere can be extremely complicated, especially in the presence of electronegative gas, dust, or air turbulence between the electrodes. Further, two important complications can occur in polluted atmospheres by producing thin tarnish films or microscopic ($\sim 10^{-4}$ cm) execrescences on the electrodes. At negative points, or wires when the field attains values $\gtrsim 10^5$, considerable field-induced electron emission occurs. This phenomenon causes loss of power from high-tension cables in industrial atmosphere. However, recent collaborative investigations have made considerable progress in elucidating general properties of breakdown in long gaps, and this area is discussed in these A.S.I. proceedings. The case of a small sphere (or point-to-plane) gap in air in laboratory conditions has recently been considered by Goldman and Sigmond (Sigmond, 1978), who confirmed that the action of negative ions can be very important in the region of low E/p.

In all cases, the form of the final breakdown appears to change from the glows occurring at low pressure and become more filamentary or Streamer-type. It appears clear that in the prebreakdown currents a space charge builds up and completely changes the field distribution so as to reduce the field near the wire or point and enhance the field at the cylinder or plane, effectively shortening the gap. In fact, the field distribution may even approximate to a parallel-plate gap between two cylinders which then breaks down when the potential difference becomes sufficient (Wright, 1964).

The interesting case of a very sharp point has not yet been quantitatively investigated. In the very high local fields, attainable photoionization, or even ionization by collision by positive ions, cannot be ruled out in the absence of evidence to the contrary.

THE NONSTEADY STATE OF BREAKDOWN

Spatio-Temporal Growth of Current in Uniform Fields

The next stage in the elucidations of complete breakdown phenomena was the investigation of the spatio-temporal growth of current in parallel-plate gaps when V just exceeds V_s. Then $(\omega/\alpha)\{\exp(\alpha d - 1)\} > 1$, and cathode-emitted initiatory electrons are replaced by a

greater number at each generation, and the current $I(x,t)$ increases with time. Clearly, the growth rate must depend upon the electron gap transit time $t_d (= d/W_-)$ and upon the generation period of the processes involved in (ω/α); for a simple γ process this is $d/W_+ \sim 10^{-5}$s, while for an undelayed photon (δ/α) process the delay $d/W_- 10^{-7}$s. Although at first the field may be undistorted by space charge, if the current increase continues, its space charge must eventually distort the original field V/d. As soon as this occurs, steady state conditions no longer apply, and the arguments above concerning spatial growth become no longer relevant. Since the experiment had shown that no significant space charge distortion occurred up to the setting of the breakdown criterion at $V = V_s$, it was important to find at what stage in the subsequent current growth that significant field distortion does, in fact, appear. Thereafter, precise knowledge of the field distribution in the gap as a function of time is essential before any quantitative assessment of all the significant ionization processes is to be undertaken. Expressions for the spatio-temporal growth of ionization are obtained by solving the general basic equation of continuity, but formal solutions are only possible in steady uniform fields, since the coefficients α and (ω/α) depend upon the field. However, since the field is uniform just when the static breakdown criterion is satisfied and before the current begins its rapid increase, it is of interest to consider the case when the field still remains constant (for a certain limited time) and the formal solution of the continuity equations is still possible. Diagnosis of the full growth mechanism depends upon the interpretation of experimental data on current temporal growth in terms of all possible secondary processes incorporated in the theoretical growth equations with their characteristic delays.

Delay Processes and Growth

In contrast to the case of steady-state spatial growth, each different possible secondary process has its own characteristic generation period (composed of particle transit time plus any other delay times) and the contribution of any process depends upon the time available; in the steady state all the processes contribute. Thus, statement of the basic equations of continuity must contain the characteristic times associated with each contributing secondary process. These are usually significantly different in different gases, and no general statement is possible and quantitatively applicable to all cases. Two main groups, however, are of interest: the simpler class of diatomic gases such as hydrogen, and less so, nitrogen, and the more complicated class of noble gases, the contrast being mainly due to the action of metastable atoms. These can be destroyed in various ways leading to emission of nonresonance photons, which traverse the gas without absorption, and involving a delay time τ, the lifetime of the metastable atom. The following processes involving the delays can be significant in the temporal

growth of ionization, in addition to the γ and (δ/α) processes, and can slow down the rate of growth:

(a) Electron attachment and detachment in electronegative gases:

(b) Cathode electron emission due to diffusion there of excited molecules, but as diffusion is slow ($\tau_d \sim 10^{-2}$s) and lifetimes of excited species short ($\tau_{ex} \sim 10^{-8}$s), only metastables need be considered;

(c) Lifetimes τ_{ex} can be significant in very rapid ionization growth and conversion of atomic-positive ions to molecular ions in collision with ground state atoms at rates $\sim p^2$, reducing secondary emission efficiency by about 40%;

(d) Nonresonance photon production from metastables (Biondi, 1952; Burhop, 1954) by following processes can be important;

(e) Excitation at some time in the life of a metastable to a nearby radiating level in 3-body collisions with ground-state gas atoms when the energy difference is small;

(f) Perturbation of a metastable in collision-induced emission of nonresonance photons in transition from 2^1S singlet state to the ground state in 2- and 3-body collision with gas atoms breaking selection rules; these photons traverse the gap unimpeded so that the time delay involved is equal to the lifetime of the metastable state. In helium this state can be generated both by electron impact and by transitions from the higher 2^1P resonance state with liberation of nonresonance photons;

(g) Production of a short-lived excited molecule in 3-body collisions with two ground-state gas atoms, which dissociates on emission of a nonresonance photon;

(h) Resonance photons themselves are delayed in transmission through the gas by repeated absorption, re-emission and consequent broadening until they become nonresonance and thereafter travel unimpeded through the gas; the time delay involved is then average time required for sufficient broadening to occur taking into account dipole-dipole interaction and spectral line broadening. Holstein (1947) and Biberman (1947) showed that

$$n = 0.8y(3\pi^2 d/\lambda_o)^{1/2}$$

where n is the number of absorbing collisions and λ_o is the wavelength at the center of the broadened line; and the total delay is then $n\tau_x$ where τ_x is the average lifetime of the excited atoms.

Considerable experimental data on the rates and cross section of

Considerable data on the rates and cross section of these processes in noble gases have been published. Biondi (1952) studied He and Ne and concluded that the 2^1S(He) metastable could be perturbed by neutral atom collision to emit a nonresonance photon with cross section $8.9 \times 10^{-20} cm^2$. In Ne deexcitation occurred by further excitation to a nearby radiating state. Phelps and Molnar (1953) studied He, Ne and A and concluded that 2^3S(He) metastables are destroyed in 3-body collisions with two gas atoms at a rate $0.2\ s^{-1}mm^{-2}$ at 300°K; the $^3P_2$ (Ne) metastables are destroyed in 2-body collisions at the rate $50\ s^{-1}mm^{-1}$ at 300°K; and $^3P_2$(A) metastable was destroyed both by 2-body collisions with a neutral atom at the rate $40\ s^{-1}mm^{-1}$ and in 3-body collision with two gas atoms at the rate $9\ s^{-1}mm^{-2}$. Colli (1954) measured lifetimes of photons emitted by excited states of argon produced in a Townsend discharge and concluded that the $^3P_2$ states are destroyed in 3-body collisions with two atoms forming a metastable molecule which decayed releasing a photon, in agreement with Phelps and Molnar.

In a study of helium, Phelps (1955) showed that the 2^1S(He) metastable was destroyed in a 2-body collision, producing nonresonance photons, and also by conversion to 2^3S(He) metastable state with thermal atoms; this latter state was completely converted into the 2^3(He) metastable molecule in a 3-body collision with two gas atoms after a lifetime ~0.05 s. Helium is a suitable gas for detailed diagnosis of the ionization processes in producing current growth coefficients, so that the theoretical growth curves can be directly tested by experiment. Phelps (1960) considered the contribution rates of likely secondary collision processes relevant in temporal growth in that gas by setting up the continuity equations and boundary conditions for each process, expressing the solutions on which all terms increase through a factor $\exp(\lambda_n t)$, (as indicated by the theory below). The resulting expression gives the current at large times in terms of the factor $\exp(\lambda t)$, in which the growth constant λ is related to all the various delay processes. An expression of similar form had been obtained by Menes (1959) on the basis of a delayed nonresonance (δ/α) process, the photons being emitted from an excited state with a lifetime sufficient to cause the delay. To apply these results to the nonsteady state temporal growth of ionization, it is necessary to obtain detailed expressions for $I(x,t)$ incorporating the various secondary processes, and then to compare the theoretical $\{I(x,t)$ vs. $t\}$ curves with those found experimentally; agreement would then indicate the particular secondary processes acting.

Spatio-Temporal Growth Equations in Static Uniform Fields

The equations of continuity-controlling generation and drift of charged particles in a gas are:

$$\frac{\partial}{\partial t}\left\{\frac{I_+(x,t)}{W_+}\right\} = \alpha I_-(x,t) + \frac{\partial}{\partial x} I_+(x,t) \qquad (27)$$

$$\frac{\partial}{\partial t}\left\{\frac{I_-(x,t)}{W_-}\right\} = \alpha I_-(x,t) - \frac{\partial}{\partial x} I_-(x,t) \qquad (28)$$

and are subject to the electrode boundary conditions, which for a gas in which the γ and undelayed (δ/α) process act at the cathode, are

$$I_-(0,t) = I_o + \gamma I_+(0,t) + (\delta/\alpha) \int_0^d \alpha I_-(x,t)\,dx \qquad (29)$$

$$I_+(d,t) = 0 \quad . \qquad (30)$$

In static uniform fields, the drift velocities W_+ and W_- are constants, and exact solutions of (27) and (28) subject to (29) and (30) were derived by Davidson (1953, 1954, 1955, 1956) at Swansea for the case when there are arbitrary distributions of charge at time zero in the gap. He also gave an approximate solution in the form

$$I_-(0,t) = A - B \exp(\lambda t) \qquad (31)$$

which approaches the exact solution when $t \gtrsim 3d/W_+$. The exponential factor is the one considered above.

Here, the growth constant λ is the real root of

$$F(\lambda) = 0$$

where

$$F(\lambda) = 1 - (\alpha\gamma/\phi)\{\exp(\phi d) - 1\} - (\delta/\alpha)\{\exp(\psi d) - 1\} \qquad (32)$$

and

$$\phi = \alpha - \lambda/W_j \qquad \psi = \alpha - \lambda/W_-$$

$$\frac{1}{W} = \frac{1}{W_-} + \frac{1}{W_+}$$

$$A = I_o/\{1 - (\omega/\alpha)\{\exp(\alpha d) - 1\} \quad .$$

B was not specified, but can be chosen to give approximate agreement with conditions at time zero. Thus, if there is no initial charge in the gap, putting B = A gives

$$I_-(0,t) = I_o\{1 - \exp(\lambda t)\}/[1 - (\omega/a)\exp(\alpha d) - 1] \quad . \qquad (33)$$

Hence, generally,

$$I_-(x,t) = \exp(\alpha x)\{I_-(0,t - x/W_-)\}; \quad t \gtrsim x/W_- \qquad (34)$$

and

$$I_+(x,t) = \int_o^d \alpha I_-(0,t - x'/W + x/W_+)\exp(\alpha x')dx \qquad (35)$$

for

$$t \gtrsim x'/W - x/W_+ \quad .$$

Earlier treatments of temporal growth by Steenbeck (1930), for only a γ process, and by Bartholomeycz (1940) and von Gugelberg (1947) for both γ and (δ/α) processes gave approximate solutions similar to (31) which did not satisfy boundary and initial conditions. Davidson (1955, 1957, 1962), however, derived an exact general solution in several different algebraic forms suitable for different time ranges. The general expression for $I_-(x,t)$ can be considered in two parts: (a) the value it would have when I_o and V are applied simultaneously when there is no charge distribution in the gap, and (b) the value it would have when an initial charge distribution was present but there was no maintained I_o. Hence, the current will then be the sum of these two parts.

Using Laplace contour integration in a complex plane for the case of a maintained I_o but no charge distribution, it is shown that

$$I_-(0,t) = \frac{I_o}{2\pi i} \int_c \frac{\exp(qt)dq}{q(F(q)}$$

where counter-clockwise integration is taken around the infinite semicircle to the right of the imaginary axis and F(q) is given by (32). This expression also leads to other albegraic forms of the exact solution for part (a) by expansion in a way suitable for the required time range. For example, for large t, a convenient form, valid for all times when $\omega = \alpha\gamma + \delta$ is:

$$\frac{I_-(0,t)}{I_o} = \frac{1}{F(0)} + \sum_\lambda \left\{\frac{\exp(\lambda t)}{\frac{F(q)}{q}}\right\}_{q=\lambda}, \qquad (36)$$

which is of the form

$$\frac{I_-(0,t)}{I_o} = A - \Sigma B_\lambda \exp(\lambda t). \qquad (37)$$

summation being taken over all real and complex values of λ which are roots of (32). $F(\lambda)$ has to be expressed in terms of the ionization processes occurring.

Although Eq. (32) has one real root λ_o and an infinite number of complex roots, the real part of these complex roots is smaller than λ_o and so becomes damped out at large t; the oscillating component is only discernable at a small t. Thus at large t the coefficient of the exponential growth term becomes

$$B_o = \frac{I_o}{\lambda_o} \left\{ \frac{\partial}{\partial \lambda} F(\lambda) \right\}_{\lambda=\lambda_o} .$$

This is the form of the coefficient of the exponential growth terms which is of most general interest experimentally, when there are no initial charges present; the part (b) forms for $I_-(x,t)$ and $I_+(x,t)$ were also calculated by using four Green's functions. Davidson further adapted solutions of the form (36) to take into account the photon delay processes discussed above and diffusion of metastables to the cathode, as well as attachment and detachment processes. From these solutions, it is now possible to calculate the electron, ion, and excited atom densities at any point at any time in the gap, after the initial current I_o, or the field V/d is established, as long as the field remains undistorted by their space charge.

Application to Experimental Studies of Growth

The next developments involved experimental investigation of (a) the secondary processes which operate during the initial stage of temporal growth and incorporated in the growth constant λ, when V exceeds V_s, and the field might well remain undistorted, and (b) the times t_f required to reach the stage of ionization growth when field distortion sets in and the current then rises rapidly and the gap voltage collapses; the magnitude of this current can be monitored in the external circuit.

In these two techniques, ("breakdown" is monitored by electrical methods, but there is another way of specifying the occurrence of breakdown: the optical technique of using the intensity of the luminosity, i.e., the visible light "spark". Now, luminosity appears in this way when the density of photons from the gas activates the eye, and this usually means attainments of currents ~1μA. The use of modern photomultipliers and image intensifiers now enables radiation to be detected at much earlier stages of

ionization growth, so that whether radiation is observed or not depends upon the sensitivity of the detecting apparatus. Some photons are, of course, being emitted right from the initial movement of the electron avalanche away from the cathode. Thus the question arises as to what constitutes breakdown of the gap in these circumstances. We have seen that in the static case mentioned earlier attainment of V_s for static breakdown can be specifically defined, theoretically and practically, before the current is allowed to grow in time, and some equivalent criterion for complete breakdown of the gap is desirable for the case of temporal growth, if exact meanings are to be given to expressions like the "formative time lag t_f", or to the apparent rapid "traverse of the gap" by a flash of light. This aspect is of particular importance in all studies involving impulse and step-function fields, for the assumed instant of time, $t = 0$, must coincide either with the appearance of initiatory electrons in an existing field $E > E_s$ or with the application of the field when an initial electron density already exists. Neither ideal condition is very easy to attain experimentally, particularly with high voltages. The criterion for resulting final breakdown must also then be equally carefully defined. Diagnosis of the ionization processes involved thus requires comparison of experimentally observed t_f with the times calculated, using the same time criteria, in formal solutions of the growth equations for uniform fields (such as those given above by Davidson); otherwise, misleading conclusions can be drawn. The current $I(x,t)$ depends upon the value of the initiatory current I_o, which must be sufficient to permit detection if $I(x,t)$.

When a step-function voltage $V(t)$ is applied to a gap in many experiments, the almost constant voltage trace is found to terminate sharply at $t = t_f$ as the voltage rapidly collapses to the value for maintenance of a glow discharge. In successive recordings of numerous times t_f to voltage collapse, the equal lengths of the horizontal CRO traces of voltage demonstrate very high consistency, thus enabling t_f to be accurately specified experimentally, provided only that experimental conditions are all carefully controlled and constant. This requires employment of adequate outgassing and surface preparation of electrodes, gas purification and ultra-high vacuum techniques with steady and accurate step-function voltage sources.

It now remains to relate the theoretical expressions for the ionization currents $I_-(x,t)$ and $I_+(x,t)$ in the gap and used in the growth equations (34) and (35) to observable quantities such as a gap voltage $V(t)$ or the current $I_c(t)$ in the external circuit containing the e.m.f. source and oscilloscope. When the circuit is regarded as a series capacitance C and resistor R in parallel with the gap of capacitance C_g, the relevant relations are

$$V(0) - V(t) = \frac{1}{C_g} \int_0^t \{\bar{I}(t) - I_c(t)\}dt \qquad (38)$$

where

$$I(t) = \frac{1}{d} \int_0^d \{I_+(x,t) + I_-(x,t)\}dx \ ,$$

$$I_c(t) = \frac{\exp(-Bt)}{C_g R} \int_0^t \bar{I}(t)\exp(Gt)dt$$

and

$$G = \frac{1}{R}\{\frac{1}{C_g} + \frac{1}{C}\} \ .$$

Using these equations for V(t) and $\bar{I}(t)$, two electrical techniques are thus available for diagnosing ionization growth:

(a) by directly measuring the time lag t_f to the sharply defined gap voltage collapse; and

(b) by measuring the current $\bar{I}(t)$ as a function of time to give the growth constant λ;

and then comparing those values obtained with those deduced from the growth equations assuming various ionization and delay processes. Comparison must be made over as wide a range of E/p as possible to obtain definitive conclusions.

Experimental Results at Low Pressures (pd 200 Torr)

Early work (Llewellyn-Jones, 1957) using approximate growth theory with experimental measurements of current by means of a register in the external circuit was carried out in H_2, N_2, He, Ne, A and Kr by Tank and Graf (1929), von Gugelberg (1947) and by Schmidt-Tiedemann (1958) assuming a γ and undelayed δ processes. In view of the fairly complete knowledge of the ionization processes in hydrogen, and of the photon-delaying atomic collisional processes in helium, studies in some detail of ionization growth using the appropriately accurate theoretical growth equations have been carried out at Swansea. Typical results for these two contrasting cases of high and low E/p are given in Fig. 7 for hydrogen, from which it is seen that for low values of E/p, ~50 V $cm^{-1}torr^{-1}$, t_f was ~μs with overvoltages as low as 1%, while at higher values of E/p ~300 V $cm^{-1}torr^{-1}$, t_f was ~ms (Morgan, 1957). This was in general agreement with previous work. Comparison of these times with those calculated as a family of curves for different proportions of the γ and (δ/α) coefficients in the measured values of (ω/α) (from static spatial growth measurements) enabled values of the individual coefficients to be found for a regime of still uniform field when V exceeded V_s by values < 10 %.

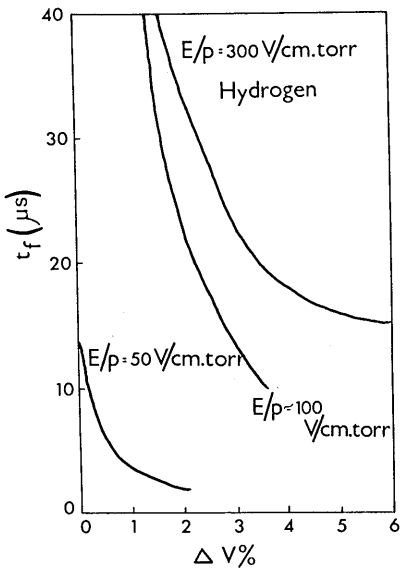

Fig. 7. Formative time lags in hydrogen at low pressures. (Reproduced by permission of Methuen & Co. Ltd.).

Using an energy balance equation for the (δ/α) process, and estimates of γ from the theory of resonance neutralization and Auger neutralization (Jones and Llewellyn-Jones, 1962) magnitudes of the γ and (δ/α) coefficients were obtained. These results lead to information concerning Auger processes at the cathode for different values of electrode work function, over the range $15 < E/P < 250$ V cm^{-1} (Llewellyn-Jones and Jones, 1960). For example γ_N for Auger neutralization in hydrogen was 0.044 electrons per ion, and γ_D for Auger deexcitation was 0.067 electrons per ion. This procedure of investigating secondary processes from measurements of ionization growth are also applied to the case of helium over the range $5 < E/p < 38.5$ torr. The first significant result obtained was that values of t_f, as given in Fig. 8, were many orders of magnitude (~100 ms) larger than those found in hydrogen (Davies et al., 1963). From the consideration of the section "Delay Processes and Growth," times were still too fast to be accounted for by diffusion of metastables to the cathode, yet too slow to be accounted for by positive ion drift, or, indeed, any combination of these two processes alone and simultaneously to satisfy the essential test over a wide range of E/P. Consequently, it must be concluded that these secondary processes involving photon delay and discussed above in the mentioned section could well be operative in helium, as was to be expected. For example, at pressures exceeding about 19 torr, the dominant secondary process was that of delayed photoelectric cathode emission (δ'/α) due to incidence of nonresonant collision-induced photons

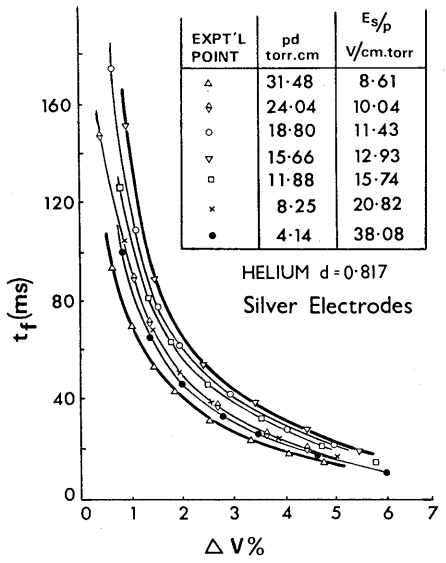

Fig. 8. Dependence of t_f on percentage overvoltage at different values of E/p. (Reproduced by permission of the Institute of Physics, London).

produced in the volume destruction of singlet 2^1S metastable atoms in 2-body collisions in the gap. The computed cross section for these processes was about $3.10^{-20}cm^2$ in agreement with Phelps (1960). At lower pressures the γ process becomes more important and with $E/p > 38, \gamma \rightarrow 0.75(\omega/\alpha)$. Also, the photons $\lambda = 584$ Å emitted in the spontaneous decay of resonance 2^1P atoms, which suffer the Holstein-Bibermann process, do not contribute to (ω/α). During this process it appears that the majority of these 2^1P excited atoms ultimately form 2^1S metastables in spontaneous transitions emitting infrared photons. Detailed application of exact Davidson solutions produced data on the photoelectric yield from silver and the cross section for conversion of atomic positive ions to the molecular form on collision with gas atoms (Llewllyn-Jones et al., 1965).

Using the method of measuring growth rates, McClure (1962) investigated neon with molybdenum electrodes at the pressure of 40 torr and interpreted his results on the basis of the γ and (ε_m/α) processes including diffusion of metastable atoms; γ was considered to predominate. This gas was also investigated using the voltage collapse technique (Davies and Llewellyn-Jones, 1960). Argon, with copper electrodes, was studied by Menes (1959) using a similar method and finding λ from:

$$\lambda = \frac{d}{dt}\{\ell n\ I(t)\}$$

for large t's. It was concluded that the slow growth rates found were possibly due to the two different photon-delaying processes. At high pressures the delay is due simply to the long (3.3 ms) lifetime of the excited molecule, while at lower pressures, two different photon-electric (δ'/α) processes occur: a dominant one with time constant of 6 μs and another (20%) with time constant 2.2 μs, due to trapped resonance radiation. Further theoretical analysis of the transport of resonance radiations in neon and argon indicates that some inconsistencies are still unexplained in argon data related to apparent variations of current with d (Thomas, 1966), and some further work is required. Nevertheless, the amount of information obtained on collisional process cross sections and photoelectric efficiencies illustrates the power and scope of these "swarm" methods of investigating atomic and molecular properties.

It next remains to consider the important use of formative time lags obtained at the higher pressure ~ 760 torr.

Formative Time Lags at High Pressures ~ 760 Torr

Values of t_f for air in uniform fields and E/p = 41.6 V cm^{-1} $torr^{-1}$ were measured by Fisher and Bederson (1951) and illustrated in Fig. 9. When the overvoltage was low $\lesssim$ 0.5%, long time lags ~10^{-5}s were found, but t_f rapidly diminished as $\Delta V/V$ was increased. They consequently concluded that the breakdown mechanism at and just above the static potential V_s was set by Townsend primary and secondary processes, the latter being almost entirely the (δ/α) photoelectric process. Their results are compared in Fig. 9 with theoretical {t_f vs. $\Delta V/V$} curves computed from Davidson's equations (37) above (Dutton et al., 1953). The degree of agreement is influenced by the lack of accurate data on α/p, ω/α, W_+ and W_- for air at atmospheric pressure. Fisher et al. have made similar studies of t_f for positive point corona in air (1951), and for uniform fields in oxygen, nitrogen (1952), argon (1953) and hydrogen (1954), with similar general results as for air, except that in oxygen and argon, t_f was usually larger than for air and depended upon the gas pressure. Measurements of t_f have also been made in uniform fields using a standard 1/50 impulse, rather than an exact step function, for high voltages ~150 kV (Aked et al, 1955); and at low overvoltages, results agreeing with Fisher and Bederson were obtained. Thus, the general result with impulse fields is that at low impulse overvoltages, both at low and at high gas pressure, breakdown is brought about by a generalized Townsend mechanism, a conclusion consistent with that found for static breakdown at all pressures.

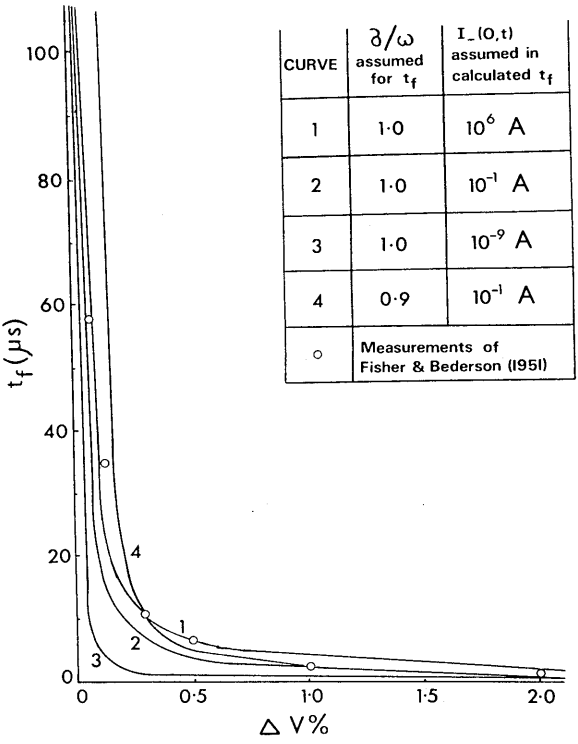

CURVE	δ/ω assumed for t_f	$I_-(0,t)$ assumed in calculated t_f
1	1·0	10^6 A
2	1·0	10^{-1} A
3	1·0	10^{-9} A
4	0·9	10^{-1} A
○	Measurements of Fisher & Bederson (1951)	

Fig. 9. Theoretical curves for formative times t_f vs. percentage overvoltage in air, for various assumed values of $I_-(0,t)$ and of (δ/ω), and comparison with the measured values of Fisher and Bederson (1951). (Reproduced by permission of the Institute of Physics, London).

BREAKDOWN AVALANCHES AT HIGH OVERVOLTAGES

Techniques of Avalanche Studies

In the decade of the 1930's, considerable experimental work based on the luminosity of the current was done on the shape of avalanches and their temporal progression across the gap. Using a Kerr cell shutter, photographs of luminous streaks (later referred to as "streamers") were obtained by Dunnington, by White and others (see Loeb, 1939 for references) together with estimates of the time required to progress in a 1 cm gap at pressures ~40 torr. Raether (1937) obtained similar photographs of the progress of single avalanches by using a cloud chamber technique by which the positive ions acted as nuclei for condensation of water droplets. This work, together with measurements of the apparent formative time lags t_f, between application of the field and the appearance of a bright spark, by von Laue, Zuber, White and Wilson, led to the general

conclusions: a) luminous streamers could appear from a mid-gap region as well as from near the cathode, when the overvoltage was sufficient; b) the formative time lag t_f diminished as $\Delta V/V$ increased to ~100% when times ~10^{-8}s were obtained; and c) values of t_f in this definition of breakdown as a bright flash were so short that electrons could not possibly have crossed the gap in that time, i.e., $t_f < d/W_-$.

Apart from the fact that this optical technique was such that small currents, and therefore low light intensities, could not be recorded, these luminous streaks were tacitly equated with the actual ionization current streams in that the apparent measurement of a region of luminosity was regarded as the actual path of ionization current in the direction of the field across the gap; no quantitative theory of ionization growth was available at that time. The development of modern sensitive high-speed oscillography, image converters and intensifiers in electron "streak" cameras gave new impetus to experimental investigation of single avalanches during the last two decades, especially by the Hamburg school, which employed both optical and electrical methods of approach.

In the electrical methods, the currents in the external circuit were recorded by high-speed C.R.O.'s and estimates of avalanche size N_e, as well as of W_- and W_+ were obtained from current pulse-time records, from which α was found (Frommhold, 1959). It is important to note the magnitude of the statistical spread of N_e in an avalanche when dealing with experiments involving initiation by a single or even a small number of electrons, because fluctuations of N about $\bar{N}$ can be large. Photon intensity vs. time records were also obtained, and these showed that photon intensity was proportional to ionization density. This technique was also used to demonstrate the succession of avalanches produced by secondary processes in the Townsend prebreakdown mechanism (Schröder, 1961; Schmidt-Tiedmann, 1958) in which the statistical spread of avalanche size was significant for small values of N_e, γ, or δ/α.

It is recognized that with avalanche sizes ~10^8 electrons, their space charge significantly distorts the original field in the gap, and it had been postulated that in those conditions a new fast streamer-Kanal photoionization process rapidly took over; for smaller avalanches the Townsend mechanism operated to produce growth. The search for demonstration of a sudden transition from one mechanism to another always attracted considerable interest, and these optical and electrical pulse techniques were used for such investigation. Elementary quantitative considerations indicate that the positive ion space charge immediately behind the avalanche front would tend at first to retard electron progress, while the enhanced field at the rear would tend to accelerate electrons and increase ionization (Richter, 1960).

It was considered, for example, that in methylol at pd = 230 torr cm, breakdown defined as a high luminosity current, takes place after the transit of a single avalanche without any cathode process and almost as soon as the critical avalanche size ~10^8 was created, even near static breakdown (Franke, 1960). These short times appeared to be characteristic only of organic vapors, in which (ω/α) is very small. Köhrman (1963) measured t_f in humid air at pd = 1000 torr cm in terms of $\Delta V/V$ and found a small "step" at overvoltages about 5% which he regarded as a transition from a Townsend to a Streamer-Kanal mechanism.

All these results, especially the appearance of current in its final stage of growth as a filamentary streak of luminosity flashing across the gap at high speed, were taken as fundamental characteristics of breakdown, inexplicable on any view other than a Streamer-Kanal process involving photoionization effective in the high field set up ahead of an advancing avalanche. One difficulty which this view has encountered ever since its introduction in the 1940's is to explain quantitatively the mechanism of production of photons with energies sufficiently high to ionize the gas molecules in a single impact process of electron collision. In an earlier section it was shown how such a process could take place in a suitable gas mixture like air, but the problem still remained with pure gases. However, Przybylski (1962) reported the production of high-energy photons in O_2 with μ values 550, 250, 30 and 2.5 cm^{-1}, but as discussed, a photon process necessary for streamer theory has to take place at some restricted distance ahead of the electron avalanche. If absorbed too strongly near points of emission, the only effect is to produce an apparently enhanced value of α, and if absorbed too weakly, photons will penetrate the gas as far as electrodes and then enhance the (δ/α) photoelectric effect. Again, in dynamic studies of overvolted gap in gases, in which α and ω/α increase with the field, electrical methods of measuring avalanche size actually measure the total charge moving in the gap and require careful interpretation. Let $n(x,t)$ electrons moving through dx at x at time t create $\alpha n(x,t)W_dt$ electrons at dx and almost simultaneously by undelayed photons $\delta n(x,t)W_dt$ at the cathode, so that the number of new electrons created in the gap is

$$dn(t) = (\alpha + \delta)n(x,t)W_dt.$$

When the original avalanche first reaches the anode at time $t = t_d = d/W_$, the number of electrons moving in the gap is

$$dn(t_d) = n(0,t)\exp(\alpha + \delta)W_dt$$

which is the same as that generated in an avalanche with enhanced α process. More recently, further study has been given to processes of photon production by Lozanskii (1969, 1970), who considered an atom A*, already excited by a single electron collision in the

avalanche, ionized in collision with a ground state gas atom A in forming an ionized molecule, according to the relation

$$A^* + A \rightarrow A_2^+ + e,$$

and calculations for helium to give a cross section = 10^{-15}cm^2. Further work is required to establish the actual occurrence of this process with appropriate cross section and absorption coefficients to account quantitatively for observed spatial and spatio-temporal growths of currents.

Formative Time Lags with High Overvoltage

Developments in measuring techniques of high step-voltage have led to renewed interest in formative time lags with high overvoltages, especially in the search for a transition phase from a Townsend mechanism to a self-propogating Kanal breakdown process. Early work with impulse voltages (probably departing in shape from exact step functions) had seemed to indicate that gap voltage collapse could take place in very short times ~10^{-7}s and even less than in electron transit times. Early consideration of this work did not seem to take into account the great enhancing effect on the coefficients α and ω/α or even the short growth times even to be expected with a Townsend δ/α process. Calculations using Davidson's equation showed that, with low overvoltages $\lesssim$ 2% when the field was still initially uniform, growth times to high currents at atmospheric pressure could still be as low as 10^{-6}s or 10^{-7}s with moderate overvoltages (Dutton et al., 1953). However, a different situation seemed at first to be the case with very high overvoltages > 100%.

With 100 $\Delta V/V$ ~300%, Fletcher (1949) obtained times to voltage collapse in uniform fields as low as 0.57 ns for a 1 mm gap in air, and much shorter than those found earlier by White or Wilson. This short time is almost an order of magnitude lower than the electron gap transit time, assuming reasonable electron mobility values ~2.10^7cm s^{-1}. Here again, breakdown of the gas was taken as indicated by voltage collapse, and t_f was then given by

$$t_f = \ell n\ N_e/\alpha W_-.$$

This result was interpreted by assuming that the original field V/d remained undisturbed while the avalanche grew to the value $\exp(\alpha W_- t_f)$, at which point $N_e \rightarrow 10^8$ electrons considerable field distortion set in, and suddenly (<< 10 ns) introduced a photoionization streamer process. On this view, t_f would then depend upon E(= V/d) rather than upon d; the dependence of t_f upon N_e was not critical. All time lags were found to increase as $\Delta V/V$ diminished, and this dependence was later investigated experimentally by Kohrman (1956), by Allen and Phillips (1964), and by Chalmers and Tedford (1972). Dickey (1952) pointed out, however, that observance of voltage

collapse was no indication of a high electronic and ionic breakdown current passing from cathode to anode, because a rapid voltage collapse can be produced just by movement of charges inside the gap, whether they reached electrodes or not. Application of Eq. 38 above to the cases recorded by Fletcher (1949) yielded theoretical times in good agreement with those observed. Hence, voltage collapse within very short times does not necessitate introduction of a new rapid ionization process.

Considerable work in this general area is now being undertaken by Kunhardt in the U.S. and Mesyats in the USSR. Mesyats (1972) suggests a chain model consisting of successive avalanches, while Kunhardt and Byszewski (1980) have proposed that the component containing the fastest electron in an avalanche rapidly grows under very high overvoltages. This theory describes a continuous transition to a Townsend mechanism as the overvoltage is reduced.

For measurements involving such short times, very careful experimental specification and control are required in the establishment of a step-function field, as well as in the liberation of an initiatory electron (or electrons) at time zero; i.e., the statistical time lag must be eliminated. Measurement of the actual electron and ionic currents in the gas is not easy when voltage collapse and the current in the external circuit are the observables; further precision work in this field is desirable, especially on the magnitude and location of any "step" in the $\{t_s$ vs. $\Delta V/V\}$ curves, which has previously been taken to indicate a transition from one type of breakdown mechanism to another. Also, application of spatio-temporal growth equations in the theoretical calculations, necessary for the interpretation of experimental data, requires accurate evaluation of the electric field, taking into account relevant images in the electrodes.

Electron-Streak Photography Analysis

Other developments have taken place in the general application of modern sophisticated optical techniques and their interpretation in the light of solutions of the growth equations, well into the regime of electric fields highly distorted by currents having grown from a few electrons up to currents of the order of 100A. A survey of such experimental methods has been given by Haydon (1968).

Wagner (1966) obtained successions of electron-streak photographs at intervals throughout the growth time range of 100 to 15 in nitrogen (with small mixtures of CH_4) with overvoltages ~25% which were generally similar to Raether's cloud chamber photographs. Mid-gap, anode-directed and cathode-directed luminous streamers were recorded on a sufficiently accurate time scale, with a sensitivity high enough to illustrate avalanches growing in a field as yet undistorted. After some initial travel, the light emitted becomes sufficient to record on photographic film as the avalanche moves in

a uniform field, spreading in all directions by self-diffusion as it moves, and the luminosity spreading accordingly. As a population $\sim 10^8$ is being approached and field distortion occurs the leading edges of luminosity show increased velocity to form an anode-directed streamer. The rear of the luminous head sometimes also shows enhanced velocity in the reverse direction to form the cathode-directed streamer. Qualitative assessment of the extremely rapid extension of luminous filaments (faster than an electron avalanche) across the gap was taken to illustrate the appearance of a new rapid streamer-ionization process as soon as sufficient field distortion occurred when $\alpha d \rightarrow 18$. However, it had been pointed out (Llewellyn-Jones, 1957) that the spatio-temporal development of luminosity represented rather the spatio-temporal development of the concentration of photon-emitting excited gas molecules (proportional to the ionization), and so was not necessarily an indication of an entirely new ionization process. Movement of regions of high luminosity across the gap is not necessarily a representation of physical movement of the photon-emitting particles along the electric field. In fact, almost any speed of luminosity movement can be obtained by choosing a suitable spatial distribution of electrons and ions in a gap for subsequent spatio-temporal development. Consequently, for quantitative diagnosis of given streak photographs, these have to be sufficiently accurately detailed in specified and controlled experimental conditions and then compared with correspondingly accurate solutions of the growth equations applicable to these experimental conditions.

Wagner's streak photographs, together with later examples by Chalmers et al. (1972) are suitable for use in such analysis, and we must now consider solving the growth equations for those conditions.

CALCULATIONS OF GROWTH TIMES TO HIGH CURRENTS

Fundamental Considerations

The continuity equations which govern the generation and velocities of electrons and ions in a gas in a parallel-plate gap have been given above as equations (27) to (30). The general coefficient $\omega/\alpha (= \gamma + \delta/\alpha)$ can be readily measured directly in steady-state experiments over a range of E/p, and α/p, W_- and W_+ have been measured as functions of E/p, so that numerical values of all these quantities over a wide range of E/p are available for various gases.

Formal solutions of these continuity equations have been given above — valid, of course, only in uniform fields, but these solutions cannot be used when the field is continuously affected by growing space charges. Changes in the field produce corresponding changes in field-dependent quantities like ionization coefficients and in electron and ion drift speeds. Numerical integration must

therefore be used, and by this means the development of electron and ion densities and their resultant electric field can be followed from the initiatory electron up to high currents ~10^2A. However, for expressions for the resultant field at x, t must first be obtained.

Accurate calculation of the space charge field is not without considerable difficulty. An avalanche moves in three dimensions by diffusion in traveling along the electric field, and the resulting field distortion is also 3-dimensional. Thus, complete evaluation of space charge field must be found from

$$\nabla^2 V = -4\pi\rho \tag{39}$$

where ρ is the resultant charge density of electrons and ions. But this is not easy. Early calculations in solving the growth equations (Ward, 1958, 1962, and 1965; Ward and Jones, 1961; Lucas, 1961; Borsch-Supan and Oser, 1963) considered the one-dimensional form of Eq. (39)

$$\frac{\partial E(x,t)}{\partial x} = 4\pi\rho(x) = 4\pi e\{n_+(x,t) - n_-(x,t)\} \tag{40}$$

which should apply only to a wide discharge, such as the form produced by Koppitz (1973). Nevertheless, fairly good agreement was obtained between Ward's calculations of {I(t) vs. t} current growth and Bandel's (1954) measurements of growth in air at 722 torr. The more realistic case of a discharge in the form of a long thin cylinder in a uniform field was considered by Davies et al. (1964) in introducing the "cylindrical method" of calculating the field distortion to avoid some of the errors inherent in a one-dimensional treatment. In this method, the axial field is calculated by dividing a long cylindrical discharge path into discs and summing the contribution of the charge on each disc to the field at any point. The discharge is bounded by electrodes, and an infinite series of discs of images in the electrodes of the disc charges should be taken into account; but in many cases a small number (about three) suffice. Some error is also introduced by assuming that the discs of discharge have uniform charge densities over their cross section, as is also done in one-dimensional calculations. Davies, Evans and colleagues (Davies and Evans, 1967; Davies et al., 1975; Davies et al., 1977) at Swansea have given considerable attention to such problems using relaxation methods and conclude that in some cases the cylindrical method can give a good approximation to 3-dimensional cases, but unrealistic growth curves can be obtained by inadequate treatment of Poisson's equations.

Expressions for the field distortion involve the discharge radius r, and reasonable values must be considered. For example, an upper limit may be taken as the electrode radius, but smaller

values are relevant for narrow discharges. The numerical calculations also involve particular values of γ and δ/α. When the number of exciting collisions is the same as that of ionizing collisions, (δ/α) is field independent; but γ varies strongly with the field. Hence, assumptions have to be made about the nature of all secondary processes introduced into the calculations, but considerable guidance can be obtained from the results of measurements of (ω/α) in steady-state experiments, as discussed earlier. For numerical simulation, the charge continuity equations are put into their finite difference form and integrated with the method of characteristics, using the cylindrical method for solving Eq. (39).

Curves of {I(t) vs. t} of ionization growth calculated in this way (Davies et al., 1964) are generally similar to oscillograms obtained by Bandel (1954) with argon and Menes (1959) with air. As the current grows, the space charge diminishes the field near the anode but increases the field at the cathode, and this can have a marked effect on the γ emission itself as well as on the total amplified cathode emission due to γ and δ/α effects. Calculations of curves of iso-density of electrons and the resultant axial electric field have produced interesting results (Davies et al., 1971). The higher fields at the head and tail of an advancing avalanche produce enhanced ionization there, and the consequent higher excitation in those regions can lead to the apparent rapid development of luminosity both forward and backwards, producing the so-called anode- and cathode-directed streamers. Iso-density curves at succeeding time intervals make this clear. The field, being such a determining factor for ionization and excitation rates, must be calculated as accurately as possible; otherwise misleading conclusions can be drawn.

Applications to Single Avalanches for High Overvoltage

For cases involving very rapid growth, numerical integration becomes more complicated as the minimum time intervals involved in the method of characteristics $\tau_e/50$ are $\sim 10^2$ smaller than those adequate for slower growth at low overvoltages. Nevertheless, Davies et al. (1971) derived a method which also took into account the appreciable lifetime of excited atoms, by introducing a delay in electron cathode emission, and was applicable to the cases of constant, externally maintained cathode current and time-dependent initiatory pulse of electrons. These initial conditions should be carefully specified, as they can significantly influence the computed particle iso-density contours in detail. They must therefore be also carefully controlled in experiments if comparison is to be valid. By taking an arbitrary photograph-sensitivity constant, such calculated iso-density curves were converted into simulated streak photographs, which could then be compared directly with actual electron streak photographs for the same experimental conditions. These computer-simulated photographs for an initial pulse of electrons in nitrogen at 91 torr at various overvoltages gave striking agreement

with the actual photographs of Wagner (1966) for overvoltages between 15% and 50%. Results such as these show that the phenomena of mid-gap, anode- and cathode-directed narrow streamers, traversing the gap with great rapidity, are consistent with ionization development in terms of the basic Townsend mechanism involving primary and secondary cathode processes, provided that the distortion of the field produced by the growing current is correctly allowed for. Hence, the existence of rapid luminous Streamer-Kanal phenomena is not necessarily conclusive evidence for introducing a new fast ionization process on the grounds that a primary-secondary buildup process is inherently too slow.

It may here be noted that, since all amplification is produced by the α process, these simulations do not in themselves uniquely determine the nature of the secondary process, whether photoelectric cathode emission or photoionization. At high overvoltages, the amplification factor $\exp(\alpha x)$ can be very high, and the rate of production of secondary electrons by whatsoever means need only be comparatively low because the high speed of resultant ionization current development is mainly controlled by the α process enhanced in high distorted fields. In fact, computations of ionization development have been carried out by Kline (1974) in which cathode processes were ignored in favor of photoionization gas process (without the necessity of specifying any particular photon-generation mechanism), and again a good general agreement with Wagner's results was obtained. Production of more fine detail in the numerical computations at present requires more accurate methods using a finer grid, and work in this area is proceeding. A similar improvement on the detail of the experimental electron-streak photographs is also desirable before definitive conclusions can be reached concerning the fine detail difference in ionization development based on the various secondary processes assumed.

As pointed out above, another factor involved in the calculation does require specification; this is the assumed discharge radius. The cross section of the discharge affects the efficiency of a δ/α process, since photons can fall over all the electrode surface; whereas the α process takes place only over the relatively smaller area where the positive ion current strikes the cathode thereby producing a narrower discharge. On the other hand, the rate of temporal growth is, in fact, not highly dependent upon the magnitude of the (δ/α) process (Bayle and Bayle, 1974), so that this effect is not too great.

The growth of currents of high values has been studied (Davies et al., 1975) using improved numerical methods which allow the later stages of growth to be followed up to currents of 100A. The results give good agreement with the experimental data of Chalmers et al. (1972) and of Doran (1968) for nitrogen. The influence of negative ions was also considered. The apparent radius of the luminous

streamer had been observed by Doran to vary rapidly with time for the larger currents, and in order to investigate this effect theoretically, Davies et al. (1975) and Davies with Townsend (1976) have introduced a method for consideration of axially symmetrical discharges. The simulated photographs predict an apparent decrease in radius as the streamer approaches the cathode because of the enhanced ionization there. Plates 1 and 2 (Davies, 1981) illustrate computer-simulated streak photographs and show the different forms of streamers to be expected at various stages of the space-charge distortion of the applied field using a 2-dimensional solution of Poisson's equation (39). Good agreement with the experimental electron-streak photographs of Doran (1968) is obtained on the basis of assuming only the γ and (δ/α) cathode secondary process in the growth equations.

An outstanding problem still remains, as discussed earlier, namely, that of finding a detailed explanation of the necessary secondary process for ionization growth in the case of highly nonuniform fields, and especially that of a positive point and distant plane cathode. Presumptive evidence indicates a gas-collisional process such as photoionization or possibly fast positive ions in the high local field at the point. In fields of such high nonuniformity, quasi-equilibrium between electrons energies and the field in elements cannot be assumed; further, the phenomena are greatly influenced by electron attachment and detachment processes. Calculations on the lines of those successful for parallel-plates represent considerable difficulty, although some progress is being made in considering suitable methods, with the eventual aims of calculating the field contour and consequent ionization contours, for such cases of highly nonuniform fields from points or in long gaps.

BREAKDOWN IN EXTREME CONDITIONS

Range of Parameters

It is of interest to conclude this account of the development of our understanding of breakdown mechanisms by referring to phenomena occurring in conditions very different from those specified in the earlier sections of this paper. These phenomena may be considered in relation to extreme values of the basic parameters: electric field, electrode separation, and pressure of ambient gas; further, the temperature and the time available for operation of the ionization processes must also be taken into account. Experiment shows that extreme ranges of the parameters may be conveniently classified as follows: a) high gas pressures $>10^2$ atmospheres for normal gap ~ 1 cm; b) low pressures $<10^{-5}$ torr, including so-called vacuum breakdown; c) very short gaps $d \sim 10^{-4}$ cm; d) very high fields $E \gtrsim 10^5$ V cm^{-1}; and e) very high field oscillation frequencies $\gtrsim 10^{15}$ hertz, as in laser-induced breakdown.

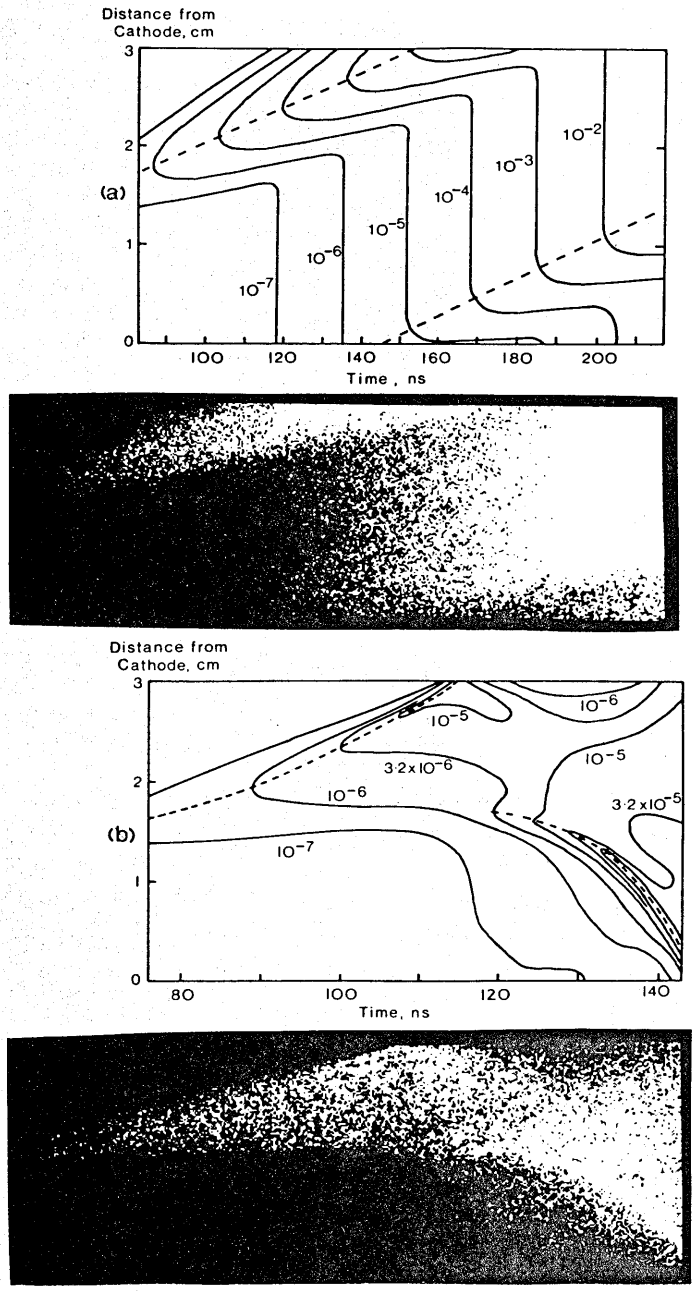

Plate 1. Computed 180-density contours as a function of time and corresponding simulated streak photograph for nitrogen (a) when the effect of space charge distortion is neglected; (b) when space charge distortion is taken into account. (Davies, 1981).

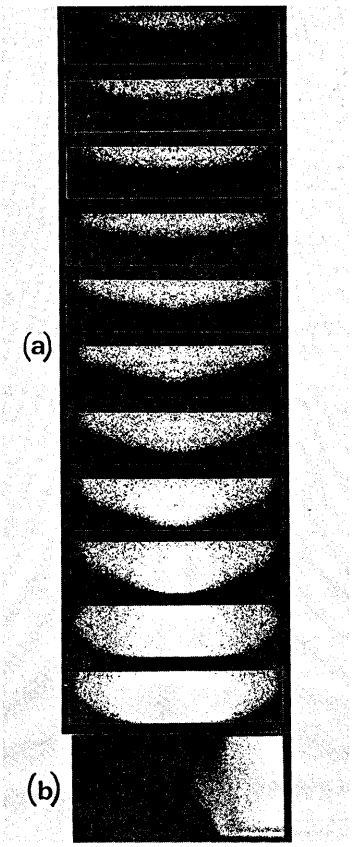

Plate 2. Simulated (Davies, 1981) shutter (a) and streak photographs (b) of light output for conditions of Doran (1968).

Gap breakdowns in these conditions apparently differ in character so much from those considered earlier that it is necessary to analyze the basic ionization processes involved. Restrictive conditions imposed in "Range of Investigation in Static Uniform Fields" required that the temperature and field intensity should not be high enough as to produce cathode electron emission independent of the gas ionization, and the electrode surfaces should be microscopically plane so that the applied field is not locally enhanced by microscopic asperities. Further, any geometrical nonuniformity of applied field should not be so high that regional equilibrium between electron energies and the local field does not occur.

Extremes of Pressure

As discussed earlier, from Paschen's law, V_s should be unaltered as d_s is decreased, always provided that p_s is increased to maintain $(pd)_s$ constant even though the average gap field $E_s = (V_s/d_s)$ is also increased. In practice, this is not the case for very high values of p ($pd > 10^4$ cm torr), and Paschen's law breaks down. The breakdown potential becomes lower than that predicted from Paschen's law, a fact recorded by Van de Graaff et al. (1946) in connection with high-voltage insulation of pressurized electrostatic generators and X-ray tubes. More recent work (Chalmers and Thom, 1972; Coates et al., 1976) confirms extensive previous work (Trump et al., 1941) that at the highest pressures where $E(= V/d)$ exceeded about 10^5V cm^{-1}, V_s fell below the Paschen value, became more ill defined, and almost completely cathode-dominated when the gas amplification fell to < 10 and the breakdown current was nearly all produced at the cathode surface. Further, surface finish became extremely important, as also was the degree of humidity of the gas. On the contrary, in well-controlled conditions, the drier the gas and the more microscopically smooth the cathode surface, then the higher became the breakdown potential. In fact, in pure gases and with single crystal electrode surfaces, the Paschen value of V_s could be practically restored (Stankevitch and Kalinin, 1967). In general, with unprepared or "industrial" surfaces, no specific breakdown criterion is obtainable with these high gas pressures; V_s becomes vague and progressively changes with electrode conditioning.

At the extreme of pressure << 10^{-5} torr, the region of so-called vacuum breakdown, the problems concern the nature of the source of initiatory electrons and the processes of interelectrode gas amplification, which could not be provided by the initial low pressure gas ambient. Here again, the influence of the microscopic constitution of the electrode surface and the local magnitude there of applied fields are of paramount importance. With macroscopic applied fields ~ 10^5V cm^{-1}, cold emission of initiatory electrons is found which sometimes leads to bursts, local metal evaporation, and then final gaseous breakdown. This series of processes is implemented by the presence of microscopic surface asperities or even dust particles, which readily produce local field enhancement by factors ~ 10^2. Micro-optical examination of cathode surfaces suggests the presence of active sites, and considerable research is now being undertaken on their nature and on the sequences of ionization events at the electrodes which may ultimately lead to gas production and breakdown. For example, cold-field electron emission, under greatly enhanced field at the tip of an asperity, may produce Joule heating which finally melts and evaporates the metal tip, thus providing gas molecules in which ionization can occur in the high field. Thus, cathode phenomena in the case of vacuum breakdown have much in common with phenomena of breakdown at very high pressures and high cathode fields.

Extremes of Distances

Large distances have been referred to earlier and will also be discussed in detail in other papers. However, the case of small gaps $\lesssim 10^{-4}$ cm introduces interesting problems. Consider a gap d being reduced, at a given gas pressure, below the value corresponding to the minimum sparking potential V_{min}(~ 300V) at $(pd)_{min}$. At first V_s increases, but when $d \to 10^{-4}$ cm, V_s drops to about 30V, as recorded by Earhart (1901). Plate 3 (a) illustrates the minute discharge produced in a relay as the contacts approach to within 10^{-4} cm with a circuit voltage of 40V. The influence of surface tarnish films on this phenomenon has been examined by Germer and Haworth (1949). It will be noted that the breakdown occurs when the average field becomes $\gtrsim 10^5$ V cm^{-1}, and the surface field can be further enhanced by local roughness, so that the ionization processes have much in common with those considered in the previous section. In all these apparently different cases of breakdown, however, the outstanding problem is the same, namely, the quantitative evaluation of the actual cold field-dependent cathode current when neither the precise value of the local applied field, nor the area and nature of the actual electron emitting sites, are known with certainty.

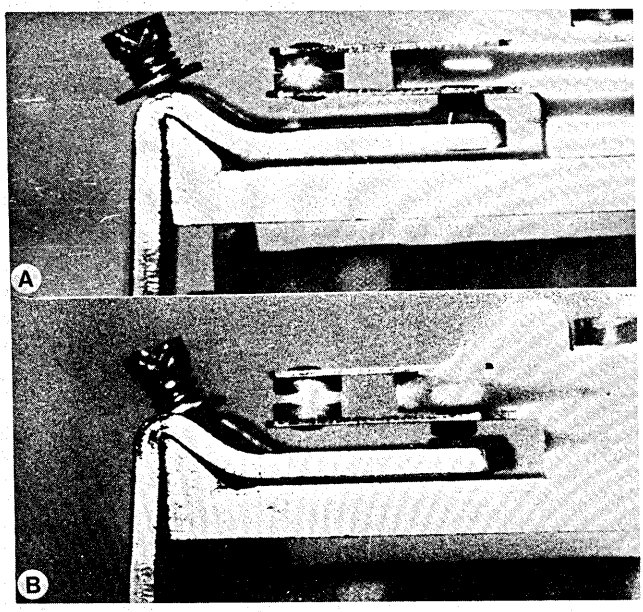

Plate 3. Transient microplasma produced at short distances ~ 10^{-4} cm at contacts of a relay (a) on approach before contact V = 40 volts; (b) on opening just after contact V = 4 volts.

Another form of transient gaseous microdischarge is obtained when the closed contacts in a current-carrying circuit are opened. This example is illustrated in Plate 3(b) when a plasma is produced with d $\sim 10^{-4}$ cm as the same relay contacts are separated with a circuit voltage of 4V. This phenomenon has been investigated in some detail, and a satisfactory explanation is obtained based on the application of contact physics. The phenomenon is independent of the presence of any ambient gas because the microplasma take place in the metal vapor produced by the explosive vaporization of the microscopic molten contact bridge formed as the electrodes start to separate (Llewellyn-Jones, 1957a, 1980). This form of breakdown is completely cathode-temperature dominated, as areas of the cathode ($\sim 10^{-7}$ cm^2) attain the metal boiling point by contact processes, thus producing both initiatory and maintenance electrons and also copious vapor molecules.

Mechanism of Cold Cathode Field-Dependent Emission

The mechanisms of cold cathode emission, relevant to the above cases of breakdown, have been investigated at Swansea using two techniques: one based on measurements of statistical time lags (Llewellyn-Jones and de la Perrelle, 1953) and the other on direct measurement of electron emission (Kerner and Raether, 1954). In the time-lag technique the cathode surface under examination forms part of a small parallel-plate small gap d($\sim$0.3 mm) in a gas and is subject to a step function e.m.f. V $\sim 1.25\ V_s$, so that the formative time lag $t_f \sim 10^{-7}$s of spark breakdown is negligible compared with the statistical time lag $t_s \sim 10^{-5}$ s of electron emission from the cathode under the macroscopic field E = V/d. A large number N of times t are recorded electronically to yield the average time $\bar{t}$, and the average electron emission is then given by (Llewellyn-Jones and Nicholas, 1962),

$$I(E) = 1/\bar{t} \quad . \tag{41}$$

Numerous {I(E), E} curves were obtained corresponding to a variety of electrode surfaces in various ambient gases. Results with the metals nickel, iron, gold, tungsten and al-alloy of different finishes from ground, rolled, turned, oxidized to highly polished and conditioned surfaces — all showed that considerable electron emission rates $\sim 10^6$ s^{-1} were obtainable with macroscopic-applied fields as low as 10^5 V cm^{-1}. This rate was highly dependent upon the nature of the surface, its former history, and presence of dust or tarnish layers. The cleaner, more polished and out-gassed the surface, then the lower was the emission at a given field; with the most plane and clean surfaces, the emission only became measurable with high fields $\gtrsim 10^7$ V cm^{-1}. The time-lag results were also consistent with those obtained from direct measurements of field currents with electrometers.

Over considerable ranges, experimental data satisfy the relationship

$$I(E) = AE^2 \exp(- B/E) \tag{42}$$

which has the Fowler-Nordheim form for cold field emission, as well as the relation

$$I(E) = C \exp(- D\sqrt{E}) \tag{43}$$

of the Schottky-Richardson form for thermionic emission. The mechanisms involved, however, are very different; the S-R mechanism does not readily account for the high variation of I with the presence of electronegative gases, but predicts a very high dependence on temperature which is not observed. In fact, the experimental measured temperature dependence is in more agreement with the generalized Murphy and Good (1956) temperature modification of F-N theory and is orders of magnitude different from that predicted by the S-R theory.

Nevertheless, the F-N form (42) is only satisfied quantitatively for certain magnitudes of the basic constants: emitting area S, its work function ϕ, and local field-enhancing factor β; and typical values are $\phi = 10^{-1}$ eV, $S = 10^{-20}$ cm^2, $\beta = 10$. These are consistent with the presence of asperities at sites of, say, negative ion clusters, and such sites of emission could play an important part in initiating vacuum breakdown, as well as in the reduction of sparking potential in gaps at very high gas pressures discussed above. For example, at high local fields, the cold emission current could produce Joule heating of the tips of microscopic asperities sufficient to evaporate them, thus not only providing initiatory electrons, but also providing a vapor atmosphere in which gas ionization could occur. Much research is being undertaken in this area, and reference might be made to the discussion of such cathode processes at the Novosibirsk meeting in 1976 of the VIIth International Symposium in Insulation and Electrical Discharges in Vacuum (USSR Academy of Sciences, Siberian Branch).

Another cathode process can also operate in the presence of thin, insulating surface films. In such cases, it is found that the initial time lag when a series of step-function potentials are applied is often very long, while succeeding lags are statistically distributed and consistently much lower ($\sim 10^{-5}$ s), even with fields as low as 10^4 V cm^{-1}. Such results are explicable in a process by which positive ions (formed by the very first spark) drift to the cathode and settle upon the thin film (d $\sim 10^{-8}$ cm), so setting a very high field $\sim 10^8$ V cm^{-1} at the metal surface. Quantitative agreement with experimental data can be obtained on this view (Llewellyn-Jones and Morgan, 1953).

The relation between the cold electron cathode emission found by the two methods: time lag for lower fields and direct electrometer for high fields and leading ultimately to vacuum breakdown is such that the {ℓn I, E} curves for the high fields appear to be practically continuations of the curves for the lower fields (Llewellyn-Jones and Owen, 1964). An experimental examination of this higher range was made by Calvert (1956), who observed current bursts, some of which led to breakdown; work on vacuum breakdown has been reviewed by Chatterton (1978).

High Frequency Discharges

With unidirectional fields, the electron avalanche is removed from the gap on reaching the anode. If with remote electrodes, the field is reversed before this happens, the motion of the avalanche is reversed, there is no loss of electrons, and the avalanche continues to grow until the rate of generation exceeds the rate of loss (usually by lateral diffusion to boundaries). This state can be regarded as breakdown, and is dependent on suitable values of d and the ratio of oscillation frequency f to gas density. The restricting conditions are that the electron mean free path ℓ should be small compared with the linear dimensions of any containing vessel, and $f < \nu$, where ν is the electron-gas collision frequency (Townsend and Williams, 1958). In this range, given that classically all directions of electron motion are equally probable after a molecule collision, the actual direction of the applied field is of little consequence in the process of building up the mean electron energy. Indeed, this consideration applies to a uniform positive column plasma, in which the mean electron energy under an oscillating field of amplitude E is the same as that in a plasma under a steady unidirectional field $E/\sqrt{2}$ (Llewellyn-Jones, 1931). When the gas pressure is so low that electrons reach the electrodes or containing walls at each oscillation, then secondary effects occur with ensuing complications, which can limit breakdown, depending upon ambient gas pressure, linear dimensions, and oscillation frequency. In these cases, when d and f/p are such that electrodes do not interact with electrons or ions, the electrodes themselves can be dispensed with by using an induction field.

An interesting case of an electrode-less discharge, which at first seemed to raise problems of gas-discharge mechanism, is that produced in the atmosphere at the focus of a high-energy laser beam. Such cases are illustrated in Plate 4 and are typical of those studied by Morgan (1978) at Swansea. In (a) the exciting field was produced by a 40 ns ruby laser flash (λ = 6943 Å; $h\nu$ = 1.78 eV) focussed by a 3 cm glass lens to a flux of 10^{11} W. cm^{-2} in the atmosphere. The two small plasmas were caused by highly aberrated optics. In the other photograph (b), the brighter glow shows considerable structure and extended plasma caused by a 100 ns CO_s laser flash (λ = 106,000 Å; $h\nu$ = 0.12 eV) focussed by a 5 cm rock salt lens in

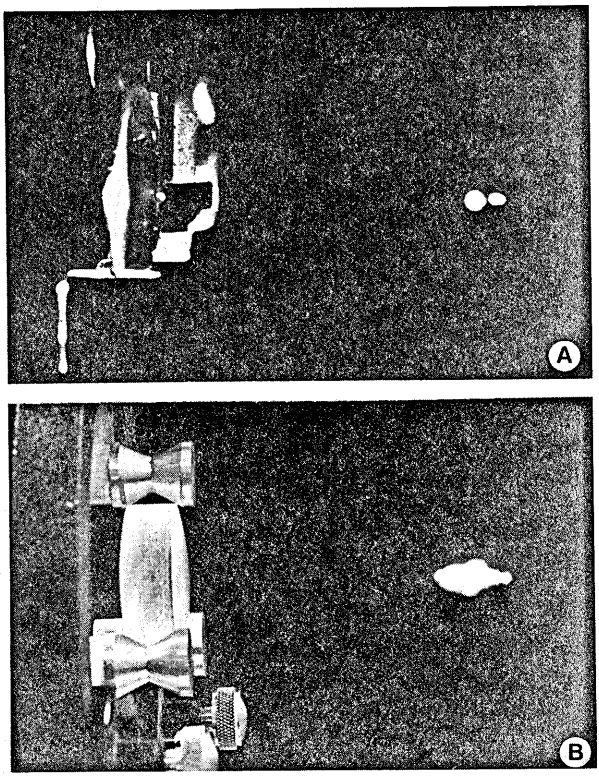

Plate 4. (a) Laser-induced breakdown plasma produced in air by 40 ns Ruby flash with highly aberrated optics. (b) Breakdown plasma produced by 100 ns Ruby laser flash in air, showing coalescence with lower aberration.

the atmosphere to a flux ~5.10^9 W.cm^{-2}; the aberration is lower and coalescence has occurred. Even with these optical oscillation frequencies ~10^{14} h, the cumulative ionization by collision is of the same kind as that with the more familiar radio-frequency breakdown. However, it is at the higher optical frequencies > 10^{15} hertz and still higher power fluxes that the laser-beam induced breakdown poses a fundamental problem of ionization process. With gas molecules of ionization potential ~20 eV and photon energy ~2.0 eV, single photon excitation or ionization is not possible, and the explanation lies with multiphoton interaction with a molecule. With a sufficiently high photon flux, a succession of unstable excited molecular states can almost simultaneously be produced, in steps of ~2.0 eV, by the presence of a sufficiently large number of photons, until the final excitation or ionization is produced. This process provides the essential initiatory electrons to start an avalanche buildup. It is interesting to note that because the time involved for this

multiphoton ionization to occur is $\lesssim 10^{-8}$ s, no radiation is emitted by the gas molecules, so that the transient breakdown plasma produced is only rendered visible later by recombination radiation.

REFERENCES

Abdelnabi, L. and Massey, H. S. W., 1953, Proc. Phys. Soc., 66:288.
Allen, K. R. and Phillips, K., 1964, Proc. R. Soc. London, A, 278:188.
Bandel, H. W., 1954, Phys. Rev., 95:1117.
Bartholeyczyk, W., 1940, Z. Phys., 116:235.
Bayle, P. and Bayle, M., 1974, J. Phys., 266:275.
Biberman, L. M., 1947, Zh. Eksp. Teor. Fiz., 17:416.
Biondi, M. A., 1952, Phys. Rev., 88:660.
Borsch-Supan, W. and Oser, H., 1963, J. Res. Nat. Bur. Stand., Sect. B, 67:41.
Boulind, M. F., 1934, Philos. Mag., 18:909.
Bruce, J. H., 1931, Philos. Mag., 10:476.
Calvert, W. J. B., 1956, Proc. Phys. Soc. London, Sect. B, 69:651.
Carr, W. R., 1963, Phil. Trans. R. Soc. London, Ser. A, 201:403.
Chalmers, I. D., Duffy, H., and Tedford, D. J., 1972, Proc. R. Soc. London, A, 329:171.
Chalmers, I. D. and Tedford, D. J., 1972, in: "Proceedings, 2nd International Conference on Gas Discharges, London," IEE Conf. Publ. No. 90, Vol. 1, p. 288.
Chalmers, I. D. and Thom, J., 1972, in: "Proceedings, 2nd International Conference on Gas Discharges," IEE Conf. Publ. No. 90, Vol. 1, p. 276.
Chatterton, P. A., 1978, in: "Electrical Breakdown of Gases," 2nd Ed., J. M. Meek and J. D. Craggs, eds., Wiley, New York and Chichester, Chap. 2.
Coates, R., Dutton, J., and Harris, F. M., 1974, in: "Proceedings, 3rd International Conference on Gas Discharges, London," IEE Conf. Publ. No. 118, p. 403.
Coates, R., Dutton, J., and Harris, F. M., 1976, in: "Proceedings, 4th International Conference on Gas Discharges, Swansea," IEE Conf. Publ. No. 143, Vol. 1, p. 133.
Colli, P. R., 1954, Phys. Rev., 95:892.
Crompton, R. W., 1967, Br. J. Appl. Phys., 38:4093.
Crompton, R. W., Dutton, J., and Haydon, S. C., 1956, Proc. Phys. Soc., 2:369.
Daniel, T. N. and Harris, F. M., 1970, J. Phys. B, 3:363.
Davidson, P. M., 1953a, Br. J. Appl. Phys., 4:170.
Davidson, P. M., 1953b, Proc. R. Soc. London, Sect. A, 218:206.
Davidson, P. M., 1954b, Proc. Phys. Soc. London, Sec. B, 67:159.
Davidson, P. M., 1955, Phys. Rev., 99:1072.
Davidson, P. M., 1956, Phys. Rev., 103:1897.
Davidson, P. M., 1957, Phys. Rev., 106:1.
Davidson, P. M., 1958, Proc. R. Soc. London, A, 249:237.
Davidson, P. M., 1962, Proc. Phys. Soc., 80:143.

Davidson, P. M., 1964, Proc. Phys. Soc., 83:259.
Davies, A. J., 1981, in: "Proceedings, 15th International Conference on Phenomena in Ionized Gases, Minsk."
Davies, A. J., Davies, C. S., and Evans, C. J., 1971, Proc. IEE, 118:816.
Davies, A. J. and Evans, C. J., 1965, Br. J. Appl. Phys., 16:57.
Davies, A. J. and Evans, C. J., 1967, Proc. IEE, 114:1547.
Davies, A. J., Evans, C. J., and Llewellyn-Jones, F., 1964, Proc. R. Soc. London, A, 281:164.
Davies, A. J., Evans, C. J., and Woodison, P. M., 1975, Proc. IEE, 122:765.
Davies, A. J., Townsend, P., and Woodison, P. M., 1977, Proc. IEE, 124:179.
Davies, D. K., Dutton, J., and Llewellyn-Jones, F., 1958, Proc. Phys. Soc., 72:(1)1061.
Davies, D. K., Llewellyn-Jones, F., and Morgan, C. G., 1963, Proc. Phys. Soc., 81:677.
Davies, R. D. and Llewellyn-Jones, F., 1966, in: "Proceedings, 7th International Conference on Phenomena in Ionized Gases, Beograd," Vol. 1, p. 275.
Dickey, F. R., 1952, J. Appl. Phys., 23:1336.
Doran, A. A., 1968, Z. Phys., 208:427.
Dutton, J., 1975, J. of Phys. and Chem. Ref. Data, 4:(3)577.
Dutton, J., 1977, W. E. L. K., Moscow, USSR Academy of Sciences, Sect. 2, Paper 68.
Dutton, J., 1978, in: "Electrical Breakdown of Gases," 2nd Ed., J. M. Meek and J. D. Craggs, eds., Wiley, New York and Chichester, Chap. 3.
Dutton, J., Evans, N. B., and Morgan, G. B., 1967, Br. J. Appl. Phys., 18:1387.
Dutton, J., Haydon, S. C., and Llewellyn-Jones, F., 1952, Proc. R. Soc. London, A, 213:203.
Dutton, J., Llewellyn-Jones, F., and Palmer, R. W., 1961, Proc. Phys. Soc., 78:569.
Dutton, J. and Morris, W. T., 1967, Br. J. Appl. Phys., 18:1115.
Dutton, J. and Rees, D. B., 1967, Br. J. Appl. Phys., 18:309.
Earhart, R. F., 1901, Philos. Mag., 1:147.
Engelhardt, A. G. and Phelps, A. V., 1963, Phys. Rev., 131:2115.
Evans, C. J., 1967, Br. J. Appl. Phys., 18:777.
Fisher, L. H. and Bederson, B., 1951, Phys. Rev., 81:109.
Fisher, L. H. and Kachitas, G., 1953, Phys. Rev., 91:775.
Fisher, L. H. and Menes, H., 1951, Phys. Rev., 86:134.
Fisher, L. H. and Lessin, I., 1954, Phys. Rev., 93:649.
Franke, W., 1960, Z. Phys., 158:96.
Fletcher, R. C., 1949, Phys. Rev., 76:1501.
Frommhold, L., 1959, Z. Phys., 150:172.
Gaugain, J. M., 1966, Ann. Ch. Phys., 8:(4)75.
Geballe, R. and Reeves, M. L., 1953, Phys. Rev., 92:867.
Von Gugelberg, H. L., 1940, Helv. Phys. Acta, 20:350,307.
Gosseries, A., 1939, Physica, Utrecht, 6:453.

Germer, L. H. and Haworth, F. E., 1949, J. Appl. Phys., 20:1085.
Haydon, S. C., 1968, Int. Atomic Energy Agency, Vienna.
Holstein, T., 1947, Phys. Rev., 72:1212.
Huxley, L. G. H., 1930, Phil. Mag., 10:185.
Jones, E. and Llewellyn-Jones, F., 1958, Proc. Phys. Soc., 72:363.
Jones, E. and Llewellyn-Jones, F., 1962, Proc. Phys. Soc., 80:450.
Kerner, K., 1956, Z. Angew Phys., 8:1.
Kohrman, W., 1956, Ann. Phys., 18:379.
Kohrman, W., 1963, Z. Angew Phys., 7:183.
Kohrman, W. and Reather, H., 1954, Naturwissenschaften, 17:400.
Kunhardt, E. E. and Byszewski, W. W., 1980, Phys. Rev. A, 21:2069.
Legler, W., 1955, Z. Phys., 140:221.
Legler, W., 1956, Ann. Phys. (Leipzig), 18:5.
Llewellyn-Jones, F., 1957a, "Ionization and Breakdown in Gases," Methuen, London.
Llewellyn-Jones, F., 1957b, "Physics of Electrical Contacts," Clarendon, Oxford.
Llewellyn-Jones, F., 1966, "The Glow Discharge," Methuen, London.
Llewellyn-Jones, F., 1967, "Ionization Avalanches and Breakdown," Methuen, London.
Llewellyn-Jones, F., 1979, J. de Phys., 40:C7-47, Part 1.
Llewellyn-Jones, F. and Jones, E., 1960, Proc. Phys. Soc., 75:762.
Llewellyn-Jones, F. and Parker, A. B., 1950, Nature, 165:1960.
Llewellyn-Jones, F. and Parker, A. B., 1952, Proc. R. Soc. London, A, 213:185.
Llewellyn-Jones, F. and de la Perrele, E. T., 1953, Proc. R. Soc. London, A, 216:267.
Llewellyn-Jones, F. and Morgan, C. G., 1953, Proc. R. Soc. London, A, 218:88.
Llewellyn-Jones, F. and Morgan, C. G., 1965, Proc. Phys. Soc., 85:351.
Llewellyn-Jones, F. and Nicholas, D. J., 1961, in: "Proceedings, 5th International Conference on Phenomena in Ionized Gases, Munich," North Holland, Amsterdam, p. 1179.
Llewellyn-Jones, F. and Williams, G. C., 1953, Proc. Phys. Soc. London, Sect. B, 66:345.
Loeb, L. B., 1939, "Fundamental Processes of Electrical Discharges In Gases," Wiley, New York, Chaps. 9 and 10, p. 407.
Loeb, L. B. and Meek, J. M., 1947, "Mechanism of the Electric Spark," Stanford Univ. Press, Stanford.
Lozinskii, E. D., 1969, Sov. Phys. Tech. Phys., 13:1269.
Lozinskii, E. D., 1976, Sov. Phys.-Usp., 18:893.
Lucas, J., 1961, in: "Proceedings, 5th International Conference on Phenomena in Ionized Gases, Munich," North Holland, Amsterdam, Vol. 1, p. 693.
Massey, H. S. W. and Burhop, E. H. S., 1952, "Electronic and Ionic Impact Phenomena," Clarendon, Oxford.
McClure, B. T., 1962, Phys. Rev., 125:11.
Meek, J. M., 1940, Phys. Rev., 57:722.

Meek, J. M. and Craggs, J. D., eds., 1953, "Electrical Breakdown of Gases," Clarendon, Oxford.
Menes, M., 1959, Phys. Rev., 116:481.
Mesyats, G. A., Bychkov, Y. I., and Kremmer, V. V., 1972, Sov. Phys.-Usp., 15:282.
Morgan, C. G., 1956, Phys. Rev., 104:566.
Morgan, C. G., 1965, "Handbook of Vacuum Physics: Physical Electronics," Vol. 2, Part 1, Pergamon, London, Sect. 4.8.1.
Morgan, C. G., 1978, Sci. Prog., Oxford, 65:31.
Murphy, E. L. and Good, R. H., 1956, Phys. Rev., 102:1464.
Paschen, F., 1889, Wied. Ann., 37:69.
Penning, F. M., 1931, Phil. Mag., 11:961.
Penning, F. M., 1938, Ned. T. Natuurkde, 5:33.
Phelps, A. V., 1955, Phys. Rev., 99:1307.
Phelps, A. V., 1960, Phys. Rev., 117:619.
Phelps, A. V. and Molnar, J. P., 1953, Phys. Rev., 89:1202.
Przybylski, T. A., 1962, Z. Phys., 168:504.
Raether, H., 1937, Z. Phys., 107:91.
Raether, H., 1938, Z. Phys., 110:611.
Raether, H., 1939, Z. Phys., 112:464.
Raether, H., 1955, Z. Angew. Phys., 7:50.
Raether, H., 1964, "Electron Avalanches and Breakdown in Gases," Butterworth, London.
Richter, K., 1960, Z. Phys., 158:312.
Rogowski, W., 1928, Arch. Electrotech., 20:99.
De la Rue, W. and Muller, H. W., 1880, Phil. Trans. R. Soc. London, 171:109.
Schade, R., 1937, Z. Phys., 104:487.
Schlumböhm, H., 1959, Z. Angew, Phys., 11:56.
Schmid-Tiedemann, K. J., 1958, Z. Phys., 150:299.
Schröder, G. A., 1961, Z. Angew. Phys., 13:206 and 367.
Schumann, W. O., 1923, "Elektrishe Darchbruckestarke von Gasen," Springer, Berlin.
Sigmond, R. S., 1978, in: "Electrical Breakdown in Gases," J. M. Meek and J. D. Craggs, eds., Wiley, New York, Chap. 4.
Stankevitch, Y. L. and Kalinin, V. G., 1967, Sov. Phys. Tech. Phys., 1:270.
Steenbeck, M., 1930, "Wiss Z. Siemens-Konzern," 9:42.
Tank, F. and Graf, K., 1929, Helv. Phys. Acta, 2:33.
Thomas, W. R. L., 1966, in: "Proceedings, 7th International Conference on Phenomena in Ionized Gases," Beograd, Vol. 1, p. 366.
Thomas, W. R. L., 1968, Ph. D. Thesis, University of Wales.
Thomas, W. R. L. and Thomas, R. W. L., 1969, J. Phys. B, 2:551.
Thomson, J. J. and Thomson, G. P., 1928, "Conduction of Electricity Through Gases," Vol. 1, Cambridge Univ. Press, Cambridge.
Thomson, J. J. and Thomson, G. P., 1933, "Conduction of Electricity Through Gases," Vol. 2, Cambridge Univ. Press, Cambridge.
Townsend, J. S., 1902, Phil. Mag., June.

Townsend, J. S., 1910, "The Theory of the Ionization of Gases by Collision," Constable, London.
Townsend, J. S., 1915, "Electricity in Gases," Clarendon, Oxford.
Townsend, J. S., 1923, Phil. Mag., 45:444.
Townsend, J. S. and Llewellyn-Jones, F., 1931, Phil. Mag., 11:679 and 12:815.
Townsend, J. S. and McCallum, S. P., 1928, Phil. Mag., 6:857.
Townsend, W. G. and Williams, G. C., 1958, Proc. Phys. Soc., 72:823.
Trump, J. G., Safford, F. J., and Cloud, R. W., 1941, Trans. Amer. Inst. Electr. Engs., 60:132.
Van de Graaf, R. J., Trump, J. G., and Beuchner, J., 1946, Rep. Prog. Phys., 11:1 (London: Physical Society).
Wagner, K. H., 1966, Z. Phys., 189:465.
Ward, A. L., 1958, Phys. Rev., 112:1852.
Ward, A. L., 1962, J. Appl. Phys., 33:2789.
Ward, A. L., 1965, Phys. Rev. A, 138:1357.
Ward, A. L. and Jones, E., 1961, Phys. Rev., 122:376.
Wisjman, R. A., 1949, Phys. Rev., 75:833.
Wright, J. K., 1964, Proc. R. Soc. A, 278:23.
Zeleny, J., 1942, J. Appl. Phys., 13:442.

BASIC PROCESSES OF ELECTRICAL DISCHARGES

J. A. Rees

University of Liverpool

INTRODUCTION

Eighty years ago Townsend observed that the current flowing between parallel plate electrodes, when a potential difference was applied between them and when a small number of electrons were released from the cathode, varied with the applied electric field E as shown in Fig. 1. He recognized that an important parameter was the ratio E/p of the field strength and gas pressure, p, and introduced the parameter α which became known as the "Townsend primary ionization coefficient." α describes the production of electron-positive ion pairs by collisions between electrons and molecules in the discharge gap. If this is the only collision process operating, then the electron current in the gap increases with distance ℓ from the cathode according to the equation

$$i_\ell = i_o \exp(\alpha\ell) \ . \qquad (1)$$

In practice, the increase in current is often greater than that predicted in Eq. (1) and is better described by an equation of the form

$$i_\ell = \frac{i_o \exp(\alpha\ell)}{1 - (\omega/\alpha)\{\exp(\alpha\ell) - 1\}} \qquad (2)$$

where ω/α is the so-called "generalized secondary ionization coefficient." This secondary coefficient represents the net effect of a number of possible collision processes occurring either in the discharge gap or at the cathode.

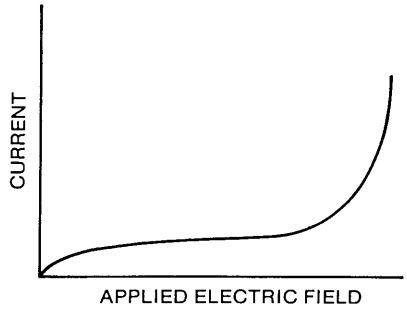

Fig. 1. Typical variation of current with applied field for a parallel-plate discharge gap of fixed plate-separation.

From 1900 to 1950 studies of prebreakdown discharges in gases gave little attention to the different behavior of electronegative and electropositive gases, although Penning (1938) discussed the possible effects of electron attachment, as well as of electronic and vibrational excitation and space charge, on the growth of a discharge between parallel plates. Penning gave an equation equivalent to

$$i_\ell = i_o \{(\frac{\alpha}{\alpha - \eta}) [\exp(\alpha - \eta)\ell - (\frac{\eta}{\alpha - \eta})]\} \qquad (3)$$

where η is the attachment coefficient. Equation (3) was reviewed by Geballe and Harrison (1952 and 1953, a and b) and extended to include secondary ionization effects. There has been much subsequent investigation of the role of electron attachment in discharges.

Since the early 1950's the additional possibility of the reverse process of electron detachment has been recognized (e.g., Prasad and Craggs, 1965), and more recently the role of other ion-molecule collision processes in breakdown phenomena has received considerable attention (e.g., Moruzzi, 1968 and Wagner, 1971).

It is clear, therefore, that the establishment of a discharge through the development of a breakdown process is largely controlled by the relative effectiveness of a large number of possible electron-molecule and ion-molecule collision processes. Similarly, the decay of any discharge is dependent on a number of processes, particularly recombination processes. It is also necessary to consider the transport properties of the electrons and ions — their drift velocities, diffusion and energy distributions. The present paper deals briefly with a selection of the collision processes involved in the establishment or decay of a discharge. The processes are discussed in more detail, together with other related processes, elsewhere in these ASI proceedings (for example, by Christophorou, Phelps, and Vriens). Transport features are discussed by Skullerud,

Phelps, Allis and Pitchford, while the application of the basic data to discharges is considered in other papers.

COLLISION CROSS SECTIONS AND REACTION RATES

Any collision process between two particles can be characterized in terms of a "collision cross section," i.e., in terms of the effective cross sectional area, σ, the target particle presents for the type of collision process considered. The product $(n\,\sigma)$ is the sum of the effective cross sections of all the n target particles in a volume of 1 cm^3 and is called the total effective cross section, absorption coefficient, or macroscopic cross section. For electrons moving through a gas, $n\,\sigma$ is often quoted for standard conditions of 273 K and a pressure of 1 torr, i.e., for $n = 3.53 \times 10^{16}$ cm^{-3}. For a stream of N_o particles per second per cm^3 passing through a target gas of number density n, the number of incident particles which have not made a collision after a distance x is N where

$$N = N_o \exp\{-n\,\sigma\,x\}\,, \tag{4}$$

or

$$N = N_o \exp\{-(x/\lambda)\} \tag{5}$$

where λ is the so-called "free path" between two collisions of the type under consideration.

For the swarm conditions normally encountered in discharge situations, it is often more usual to state the probability of occurrence of a particular kind of collision process in terms of a rate coefficient rather than as a cross section. For a 2-body process between particles of concentrations n and n_1, the rate of change of the concentrations is given by

$$\frac{\partial n}{\partial t} = \frac{\partial n_1}{\partial t} = k^1\, n\, n_1 \tag{6}$$

where k^1 is the rate constant and has dimensions cm^3 sec^{-1}. For a 3-body process k^1 has the dimensions cm^6 sec^{-1}. The rate constant k^1 and the corresponding cross section are related through an expression of the form

$$k^1 = \int_o^\infty \sigma(v_r) \cdot v_r \cdot f(v_r)\, dv_r \tag{7}$$

where v_r is the relative speed of the colliding particles and $f(v_r)$ is the fraction of the collisions in which v_r lies between v_r and

$(v_r + dv_r)$. When the cross section $\sigma(v_r)$ is independent of v_r, Eq. (7) reduces to

$$k^1 = \sigma\bar{v}_r \ , \tag{8}$$

where $\bar{v}_r$ is the mean relative speed.

In many discharge situations, as we saw earlier, it is usual to talk in terms of swarm coefficients (such as α, the primary ionization coefficient), defined by an equation of the form

$$\frac{\partial n_1}{\partial x} = \alpha n_1 \ , \tag{9}$$

where a swarm of the particles of concentration n_1 drifts in the x - direction with a mean velocity W under the influence of the applied field E through particles of concentration n. It follows from Eqs. (6) and (9) that

$$\alpha = \frac{k^1 n}{W}$$

or

$$\frac{\alpha}{n} = \frac{k^1}{W} \ , \tag{10}$$

and hence from Eq. (7)

$$\alpha/n = \frac{1}{W} \int_0^\infty \sigma(v_r) \cdot v_r \cdot f(v_r) \cdot dv_r \ . \tag{11}$$

As an example, for ionization by electron impact, α is the primary ionization coefficient, W is the mean electron drift velocity, $\sigma(v_r)$ is the ionization cross section and $f(v_r)$ is the speed distribution for the appropriate values of the gas number density n and the field strength E. Equation (11) applies, with appropriate changes in the definition of the quantities concerned, to other electron-molecule collision processes and to ion-molecule reactions.

ELECTRON-MOLECULE COLLISION PROCESSES

Elastic Collisions

Differential Cross Sections. When an electron collides with a gas molecule, the most likely outcome of the collision is that the electron is elastically scattered, i.e., that there is no change in the internal energy of the target molecule. It is important, therefore, in the modeling of any electrical discharge situation that the

characteristics of elastic scattering be well understood. While it is sometimes sufficient to know the energy dependence of the momentum transfer cross section and/or that of the total elastic cross sections there are other situations — particularly where these concern low-pressure, high-field conditions — where it is necessary to have available differential cross section data, i.e., to know the explicit dependence of the scattering probability on scattering angle as well as on electron energy.

Existing differential scattering data have been obtained for gases and vapors by experimental methods which fall into two main groups: those involving the passage of an electron beam through a gas-filled cell, and a second group involving a "crossed beam" geometry. Among the factors which control the accuracy of the data are the specification of the collision volume from which the elastically scattered electrons are collected, the target gas number density, the electron beam characteristics (energy, energy spread, geometry, etc.), the performance of the detector system(s), background effects, and the electron energy scale calibrations. Much of the early work employed relatively simple electron guns and retarding potential analyzers with Faraday cup detectors. When the early 1960's brought a resurgence of interest in electron scattering, the electron guns and energy analyzers were much improved. The greatly improved energy resolution of 127° of hemispherical analyzers was particularly useful in examining the resonance effects observed as a result of the scattering event being effectively a 2-stage process

$$e + X \rightarrow (X^-)^* \rightarrow X + e \qquad (12)$$

involving the temporary excited negative ion $(X^-)^*$.

For the determination of nonresonant cross sections, typical examples of static target and crossed-beam systems are shown in Fig. 2 and 3. The system in Fig. 2 was used by two of my research students, Sethuraman and Gupta, to study elastic scattering by the inert gases. One major uncertainty concerns the change of collision volume with scattering angle, θ, particularly at values of $\theta < 30°$ and $> 150°$. The system in Fig. 3 is typical of the earlier systems used by the group at the Jet Propulsion Laboratory, California Institute of Technology, and features a crossed-beam geometry, with the beam energy-selected using the first of the two hemispherical selectors and the scattered electrons analyzed using the second hemispherical system. The gas target was a beam produced from either a single capillary tube or a capillary array. The most useful configuration is that in which the electron beam is narrow and wholly contained within the spread of the atomic beam, with the acceptor angle of the detector system being large enough to include the whole of the collision volume.

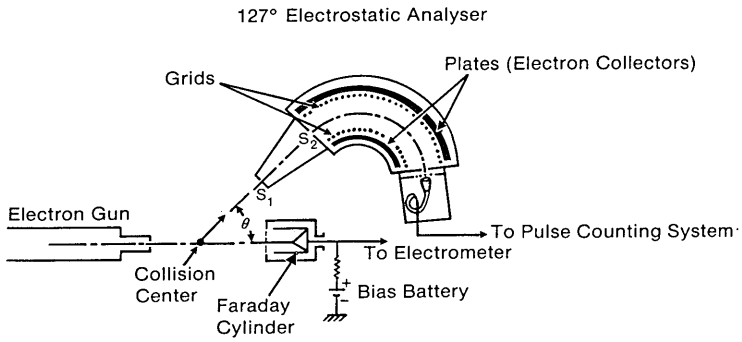

Fig. 2. Schematic diagram of apparatus used at Liverpool University to investigate differential elastic scattering (see Gupta and Rees, 1975, for example).

Typical forms of a variation of cross section with scattering angle are sketched in Fig. 4. The variation shown in Fig. 4a is typical of scattering by simple targets such as helium and atomic hydrogen. Figure 4b is typical of targets such as sodium and neon at low energy while Fig. 4c is typical of heavier targets such as xenon and mercury. The minima observed can be very pronounced, as shown, for example, in Fig. 5 (Menendez et al., unpublished) for 64 eV electrons in neon.

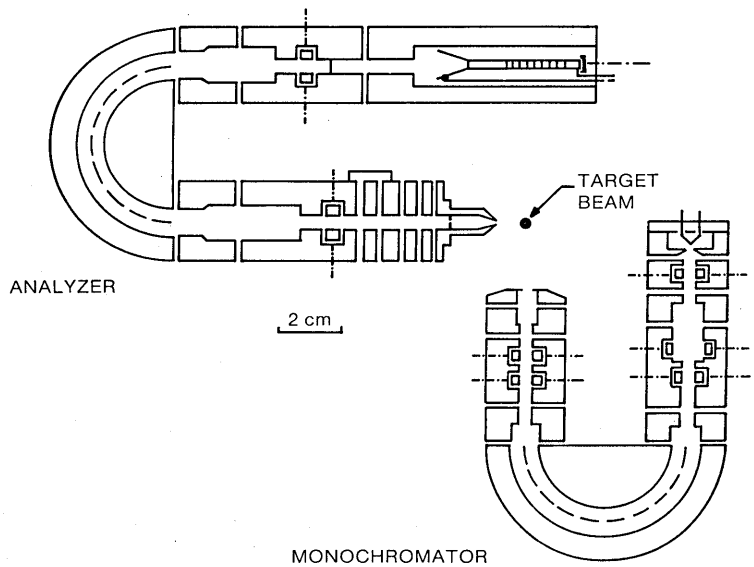

Fig. 3. Typical early crossed-beam system used at J. P. L., Pasadena, California to investigate differential elastic scattering (see Chutjian, 1974).

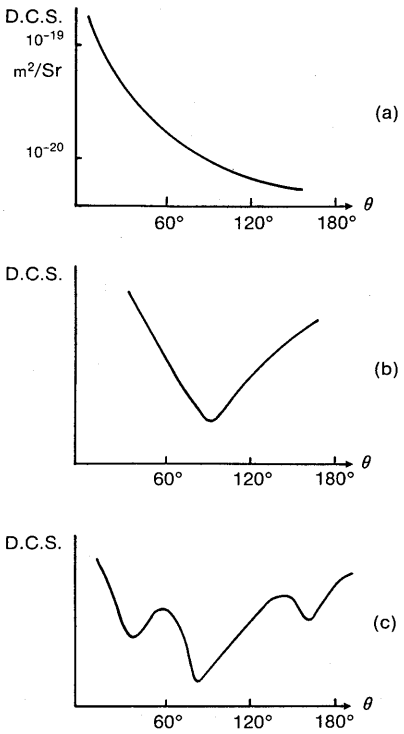

Fig. 4. Typical variations of cross section with scattering angle. 4a: typical of simple targets such as H, He; 4b: typical of targets such as sodium and neon at low energy; 4c: typical of heavy targets such as xenon and mercury.

Few determinations of differential cross sections have yielded absolute cross-section data directly, and a number of methods have been used to transfer the relative data usually obtained to an absolute scale. Normalization to an absolute determination made in an earlier investigation is a popular approach, and recent work has addressed the problem of providing a comprehensive set of reference data for helium. At low energies it is arguable that the most reliable data set for helium is still that obtained by Andrick and Bitsch (1975) who normalized their data using a phase-shift analysis. If we write the differential cross section as $d\sigma/d\Omega$ where

$$\frac{d\sigma}{d\Omega} = |f(\theta)|^2 , \qquad (13)$$

$f(\theta)$, the scattering amplitude being given by

$$f(\theta) = \frac{1}{2ik} \sum_{\ell=0}^{\infty} (2\ell + 1) [\exp (2 i \eta_\ell) - 1] P_\ell(\cos \theta) \qquad (14)$$

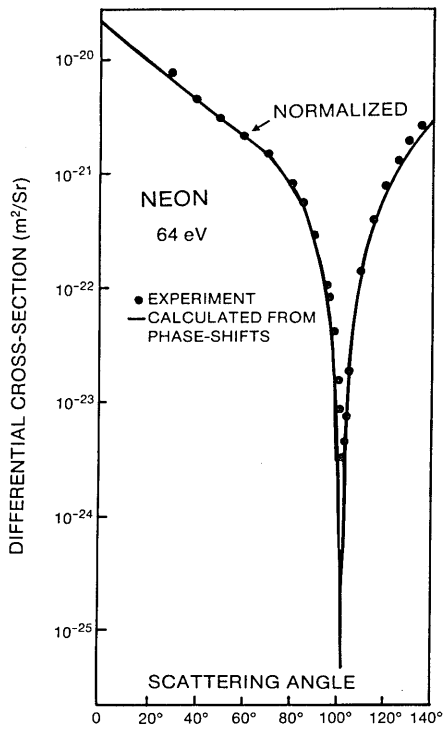

Fig. 5. Differential cross sections for elastic scattering of 64 eV electrons by neon (Menendez, Rees, and Beaty, 1980).

where k is the wave number of the free electron (i.e., $k^2 = E(eV)/13.6$), $P_\ell(\cos\theta)$ are Legendre polynomials, and η_ℓ are the scattering phase-shifts; then for purely elastic scattering with no spin effects, the scattering phase-shifts η_ℓ are real. And at low electron energies, the first few partial waves, i.e., the first few values of ℓ, are the only important ones and largely determine the "shape" of the differential cross-section curves. In fact, if the angular dependence is well enough determined, it may be analyzed to find η_o, η_1, η_2 ... and the scaling factor necessary to establish the absolute scale of the cross-section data. It is very important that the angular dependence of the cross section be very accurately known. This does not appear always to have been the case even in very recent investigations for helium [e.g., Shyn (1980) and Newell et. al., (1980)].

Momentum Transfer Cross Sections and Total Elastic Cross Sections. It is of course possible to integrate the differential elastic cross sections considered above to obtain either the total cross section for elastic scattering, σ_{el}, or the momentum transfer cross section, σ_m, using the relationships

$$\sigma_{el} = 2\pi \int_0^{\pi} \sigma(\theta) \cdot \sin\theta \cdot d\theta \qquad (15)$$

and

$$\sigma_m = 2\pi \int_0^{\pi} \sigma(\theta) \cdot \sin\theta (1 - \cos\theta) \cdot d\theta \ . \qquad (16)$$

These values of σ_{el} and σ_m may then be used in calculations of discharge properties such as the electron mobility and diffusion coefficients and the conductivity. In calculating σ_{el} and σ_m from differential cross sections, care is needed with regard to the contribution to the integrated cross sections of scattering at angles of less than say, 20° and greater than 150° because there are few reliable measurements of $\sigma(\theta)$ at these extreme angles, and the choice of extrapolation from angles in the range 20° to 150° is important. Typical calculations for electron energies of $\geq$ 20 eV are described by de Heer et al. (1979) using various sets of experimental data for $\sigma(\theta)$. The results may be compared with those obtained using a number of theoretical models. If it is possible to represent the differential cross-section data by a reliable set of phase-shifts, as discussed above, then it may be preferable to use these phase-shifts to calculate σ_m and σ_{el} rather than the raw cross-section data because this method overcomes to some extent the influence of the low-and high-angle data.

Momentum transfer cross sections have been deduced by a number of authors from analyses of swarm data using methods pioneered by Phelps and his co-workers. Huxley and Crompton (1974) have summarized the methods and some of the data obtained. The methods are most usefully employed at low electron energies and become less reliable as the electrons participate in an increasing number of inelastic collision processes. It is always necessary for the swarm data analyzed to be of high quality.

An interesting set of targets for laser, MHD and other discharge applications are provided by vapors. Nakamura and Lucas (1978 a and b) described the measurement in a heat-pipe system of electron drift velocities in mercury, sodium and thallium vapors. Elford (1980) (see Fig. 6) has also investigated the case of mercury with somewhat different results. It is possible that the data of Nakamura and Lucas were affected by traces of argon in the mercury vapor. In both investigations the swarm data were fitted to obtain values of σ_m (see Fig. 7) which could then be used in calculations of the variation with E/n of other parameters such as electron mean energies and fractional energy loss through excitation.

For molecules with a large dipole moment, it is clear from the work of Christophorou and Christodoulides (1969), Spencer and Phelps

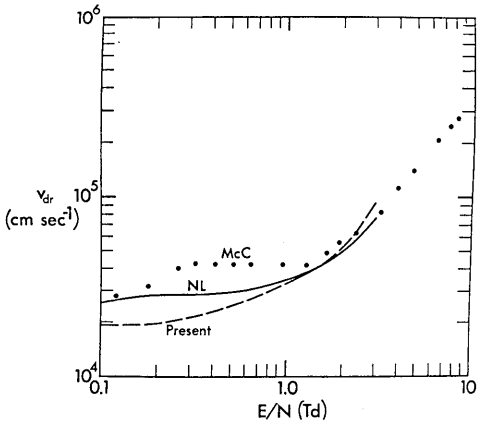

Fig. 6. Drift velocity of electrons in mercury vapor. Curve labelled "present" is that of Elford (1980); curve labelled "NL" shows data of Nakamura and Lucas (1978a); data points labelled "McC" are from McCutcheon (1958).

(1976) and others that when better estimates are not available, reasonable approximations to σ_m may be obtained by taking roughly 60% of the values calculated from Altschuler's formula

$$\sigma_m = \frac{8\pi}{3} \frac{(2\pi De)^2}{h\,v}, \qquad (17)$$

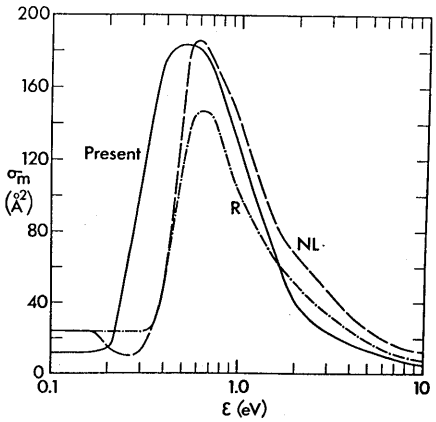

Fig. 7. Momentum transfer cross section for electrons in mercury vapor. Curve labelled "present" is that of Elford (1980). Curve labelled R is that of Rockwood (1973). Curve labelled NL is that of Nakamura and Lucas (1978b).

where D is the dipole moment of the target, h is Planck's constant and v is the electron speed. Equation (17) follows from the application of the plane-wave Born approximation and assumes that the only significant interaction is that between the electron and the permanent dipole moment of the molecule. Some of the gases considered by Spencer and Phelps are of considerable interest in work on MHD generators.

For some gases there are, of course, direct experimental measurements of σ_{el} and σ_m at low energies. Data obtained prior to 1971 were reviewed by Bederson and Kieffer (1971), while Itikawa (1978) has reviewed more recent data. For helium, which has been of particular interest as a reference set of data, I have recently calculated σ_{el} and σ_m from phase shift data available either from theory (Nesbet, 1979) or from analyses of differential cross sections and have compared the results with Crompton et al.'s (1970) analysis of swarm data and the direct measurements of Kauppila et al. (1977) and Kennerly and Bonham (1978). The comparison is shown in Table 1 for electron energies between 0.6 and 12 eV. The agreement is clearly good. This is less true if the phase-shifts obtained from analyses of other differential cross-section data are included. Recent data for σ_{el} for electron energies of between 0.02 and 2 eV were reported by Ferch et al. (1980) who used a time-of-flight spectrometer for their experiments. Their results agree with those of Kennerly and Bonham for energies between 0.5 and 1.0 eV. Other data were taken for H_2, D_2, and HD with no significant differences between the data for these three gases. Dalba et al. (1980) have also measured σ_{el} for hydrogen in the range 0.2 to 100 eV. Their results included the first absolute cross sections for resonances in the energy range 11 to 15 eV. Figure 8 shows data for 20 eV.

Inelastic Collisions

Differential Cross Sections. For a number of atomic targets, such as the alkali and other metals, differential cross sections for excitation of particular states of the target have been measured in the same experiments as elastic cross sections. The electron energies have often been too high to be of much interest in the present context but, in other cases, are relevant to discussions of metal vapor laser systems. Figure 9, for example, shows a typical set of data for electrons of 40 eV in zinc (Trajmar and Williams, 1976).

For discharge applications the differential scattering of electrons in ionizing collisions is of particular interest — for example, in discussing breakdown at low pressures — and there has been an increasing number of such investigations in the last decade. An extensive set of data was obtained by Beaty and his co-workers at J.I.L.A. (Peterson et al., 1972; Opal et al., 1972). More recent investigations are those of Beaty et al. (1977); Stefani et al.

Table 1. Momentum Transfer and Total Elastic Cross Section for Helium, 0.58 to 12 eV.

$\sigma_m(10^{-20}m^2)$					$\sigma_{el}(10^{-20}m^2)$					
Nesbet	Andrick and Bitsch	Register et al.	Williams	Crompton et al.	Nesbet	Andrick and Bitsch	Register et al.	Williams	Kauppila et al.	Kennerley and Bonham
(theory)	*(differential scattering)*			*(swarm)*	*(theory)*	*(differential scattering)*			*(direct expt.)*	
6.700			6.713	6.646	6.106			6.078		6.24
6.977			6.924	6.96	6.080			5.918		6.18
6.994	7.44		6.896	6.98	5.983	6.39		5.823	5.91	6.01
6.320	6.39	6.451	6.575	6.31	5.379	5.41	5.482	5.576	5.39	5.25
4.213	4.238	4.27	4.278	4.15	4.059	4.085	4.127	4.112	4.07	3.96

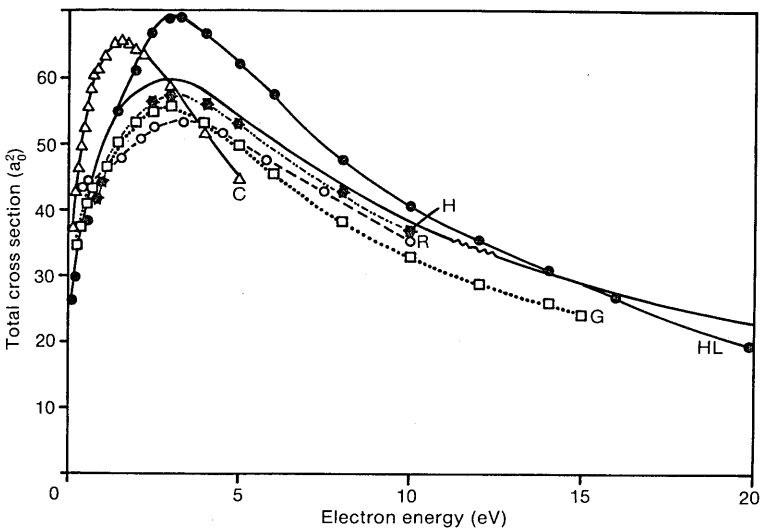

Fig. 8. Total cross sections for molecular hydrogen. Full curve, Dalba et al. (1980); full circles, Henry and Lane (1969); asterisks, Hasa (1969); open circles, Ramsauer and Kollath (1930); squares, Golden, Bandel and Salerno (1966); triangles, Crompton, Gibson and McIntosh (1969) (data are for momentum transfer in this case).

(1978); van Wingerden et al. (1979) and others. The ranges of primary electron energy studied have often been rather too high for usual discharge situations. The data are largely for so-called double differential cross sections, but there are also limited data for the triple differential cross sections obtained from co-incidence experiments in which the angular distribution of both the primary and secondary electrons are measured (see Ehrhardt et al., 1974 and Schubert et al., 1979, for example). Figure 10 shows typical data for helium, where both outgoing electrons have the same energy (5.3 eV). The arrow from the bottom to the center of the plots shows the direction of the incident electron. One outgoing electron is detected at angle θ_a, and the dots show the net true co-incidences measures at various θ_b, the scattering angle for the 2nd ejected electron. The curves are theoretical predictions.

Electron Impact Ionization – Total Cross Sections. Total cross sections for electron impact ionization have perhaps attracted more than their fair share of interest from gas discharge physicists when compared to cross sections for other inelastic collision processes. Even so, for many targets the data available are not extensive or are of limited accuracy. Kieffer and Dunn (1966) reviewed the data then available and concluded that cross sections reliable to better than 20% were hard to find. In the intervening years the situation

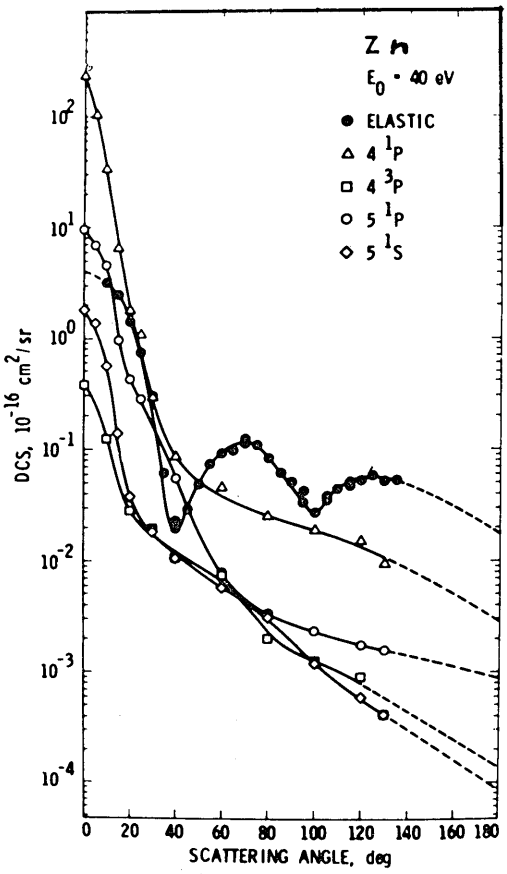

Fig. 9. Differential cross sections for 40 eV electrons in zinc vapor (Trajmar and Williams, 1976).

has improved somewhat; but Dunn (1976), in discussing the range of targets which have been examined, including ionized targets, concluded that there was room for much further work. For unexamined targets, empirical relationships such as those given by Lotz (1968 and 1971) have to be relied upon. The relationships developed by Lotz and others (Dunn, 1976) amount to prescribing a recipe for giving the function $f(E/V_i)$ in the general expression for the ionization cross section σ_i,

$$\sigma_i = \sum_i \xi \frac{n_i}{EV_i} f(E/V_i) \qquad (18)$$

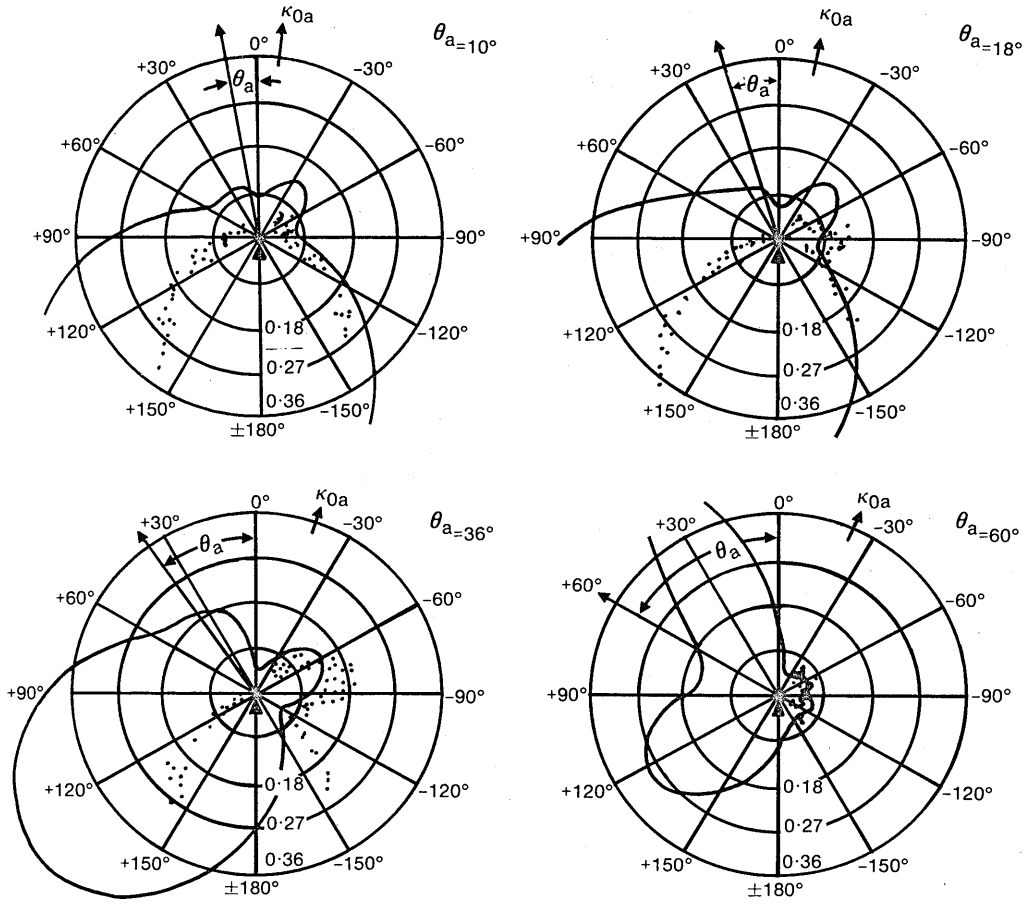

Fig. 10. Polar plots of the angular dependence of the triple differential cross sections as a function of the scattering angle θ_b. θ_a is given on the upper right side of each diagram. $E_a = E_b = 5.3$ eV. The measured data are shown as dots. The curve is a theoretical calculation using the Coulomb-projected Born approximation.

where

n_i = number of electrons in the i^{th} shell
V_i = ionization energy
E = electron energy
ξ = a constant.

Dunn emphasized that care is needed in using such empirical relationships when processes such as

$$X^{+n} + e \rightarrow X^{+(n+1)*} + 2e \rightarrow X^{+(n+1+m)} + (m+2)e \qquad (19)$$

or $$X^{+n} + e \rightarrow X^{+n*} + e \rightarrow X^{+(n+m)} + (m+1)e \qquad (20)$$

are expected to occur. Process (19) includes, for example, the ejection of an inner shell electron followed by Auger ejection of m other electrons.

In recent years, crossed-beam methods of studying ionization cross sections have largely been preferred to experiments using "static" gas targets, particularly for metal targets and for studies of the ionization of ions. A typical investigation is that described by Peart and Dolder (1975) for Ca^+, Sr^+, Mg^+ and Ba^+. Figure 11 shows some of their data. The occurrence of process (20) above — excitation followed by autoionization — with its infinite slope characteristic at threshold contrasting strongly with the near-linear behavior at threshold of the direct ionization process, may be noted (Dunn, 1976).

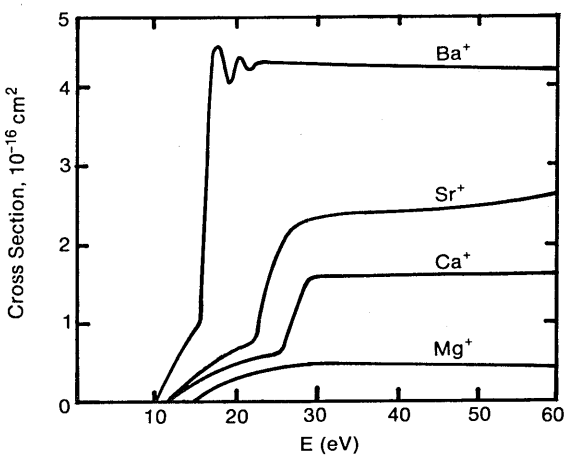

Fig. 11. Ionization cross sections for Ba^+, Sr^+, Ca^+ and Mg^+ (Peart and Dolder, 1975).

An important example of ionization of multicharged ions is provided by thermonuclear-type plasmas, such as those in tokamak machines. Barnett (1977) has summarized some of the atomic physics involved in the cooling of the plasma by impurities such as oxygen and molybdenum; see also Bengtson and Benesch in these proceedings. Figure 12 shows the increase in abundance of Mo^{31+}, Mo^{32+} and Mo^{14+} with time observed in the French tokamak, while Fig. 13 shows calculated radial profiles for Fe ions in a 750 eV hydrogen plasma (Hogan, 1974). Such calculations and the corresponding estimates of power losses are limited in accuracy by the available cross-section data.

Vibrational Excitation. For molecular targets, an important interaction between electrons and the target molecules, particularly for those discharges involved in gas discharge lasers, is that in which the molecules are vibrationally excited as a result of the interaction. The carbon dioxide laser, for example, relies on vibrational excitation for its operation. In other discharges, also, the interaction of the vibrationally excited molecules with other molecular species can be of great importance. There has been much work in recent years on the vibrational excitation process, pioneered to a large extent by Schulz, whose excellent review (1976) considered the cross sections for vibrational excitation in two categories — resonant and nonresonant processes. For the resonant processes, the projectile electron spends an appreciable amount of time in the neighborhood of the target molecule — a much larger amount than the transit time expected from its velocity — and hence it produces a more effective distortion of the molecule and an increased cross section. The resonance cross sections produced can vary considerably in character (Schulz, 1976). If the resonance lifetime is much less than a typical

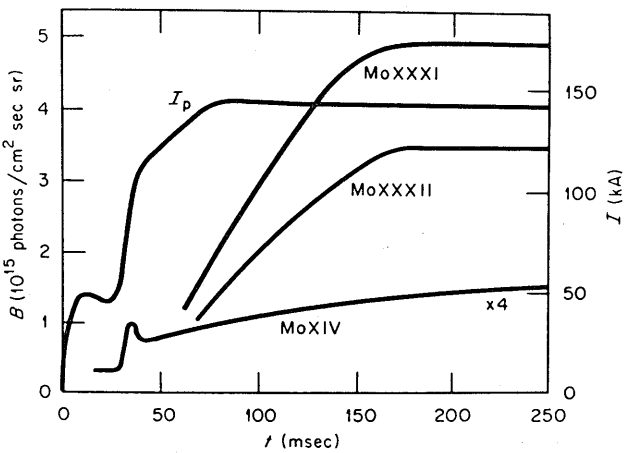

Fig. 12. Time evolution of highly excited states of molybdenum. I_p is the plasma current (Barnet, 1977).

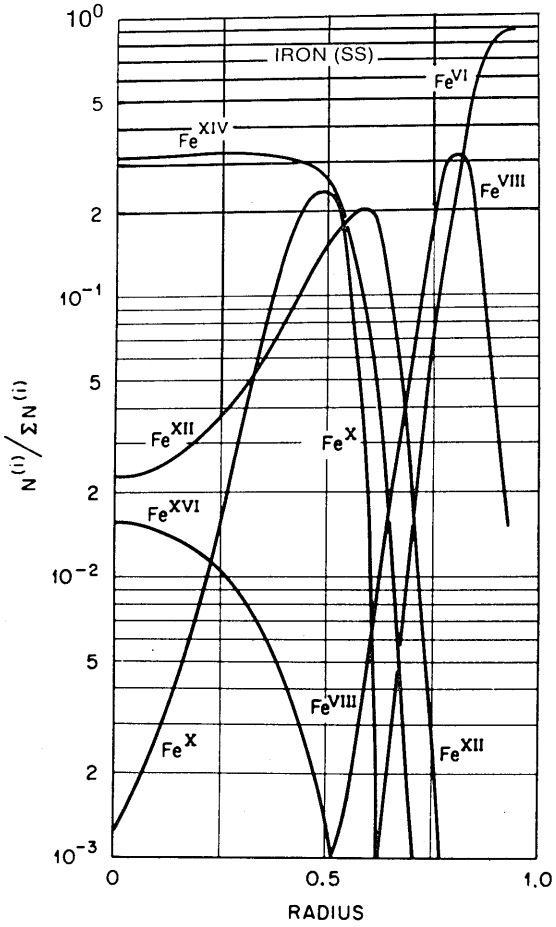

Fig. 13. Radial profiles of iron ions in a 750 eV plasma (Hogan, 1974).

vibrational period ($\tau << 10^{-14}$ sec), the nuclei do not vibrate during the resonance lifetime. The incident electron attaches itself to the molecule to give a temporary intermediate state which when it decays by emission of the attached electron leaves the molecule vibrationally excited. The intermediate state has a large energy width, $\Gamma \approx \hbar/\tau$, which gives a broad hump in the vibrational cross section. Figure 14 for N_2O (Azria et al. 1975) is an example. If the lifetime is significantly greater than the transit time of the incident electron across the molecular diameter and comparable to the vibrational period ($\tau \approx 10^{-14}$ sec), the so-called "boomerang model" (Herzenberg, 1968) may be applied. Figure 15 shows the basic ideas as applied to ($e - N_2$) near 2.3 eV. The incident electron

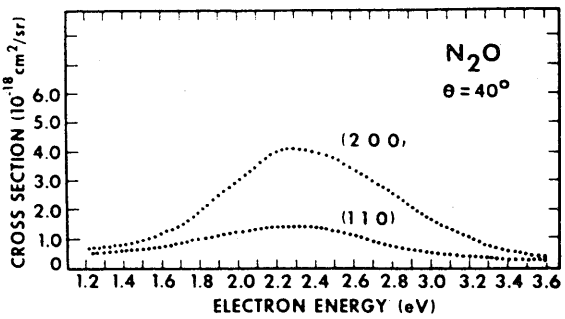

Fig. 14. Differential cross sections for 200 and 110 modes in N_2O (Azria et al., 1975).

attaches itself to the N_2 molecule, and the outgoing nuclear wave packet propagates across the N_2^- potential well, reflected as shown in the figure due to the molecular bond stretching and contracting. During this process the resonant state decays by emitting an electron; i.e., the wavepacket is annihilated by auto-detachment when the end of the first cycle is reached. The two waves, outgoing and reflected, give a standing wave whose nodes change in position as the electron's incident energy is varied. The resulting vibrational cross section shows peaks as the nodes coincide, or otherwise, with particular vibrational states of the neutral molecule.

When the lifetime τ increases further, there is the possibility of many vibrations of the nuclei during the period τ, i.e., of the excitation of vibrational levels of the compound state which give sharp spikes in the vibrational cross sections at the energies of the vibrational levels of the compound state when the latter decay by ejection of the attached electron to vibrational levels of the neutral molecule. Figure 16 shows the positions of the spikes in the energy-integrated cross section for oxygen found in the well-known investigation by Linder and Schmidt (1971).

We may look briefly at three examples of the effects of vibrational excitation on electrical discharge behavior. Firstly, as an example of the effect of vibrational excitation on the total collisional cross section, the behavior of low energy electrons in sulphur hexafluoride may be considered. Rohr (1977) showed the integrated total vibrational cross section to be about 10^{-15} cm^2, i.e., about 1.5 times the elastic cross section. The cross section was dominated by excitation of the V_1, and V_3 modes, involving energy losses of 95.4 and 117.5 meV respectively, the angular dependence of the cross sections for the two modes being quite different (see Fig. 17).

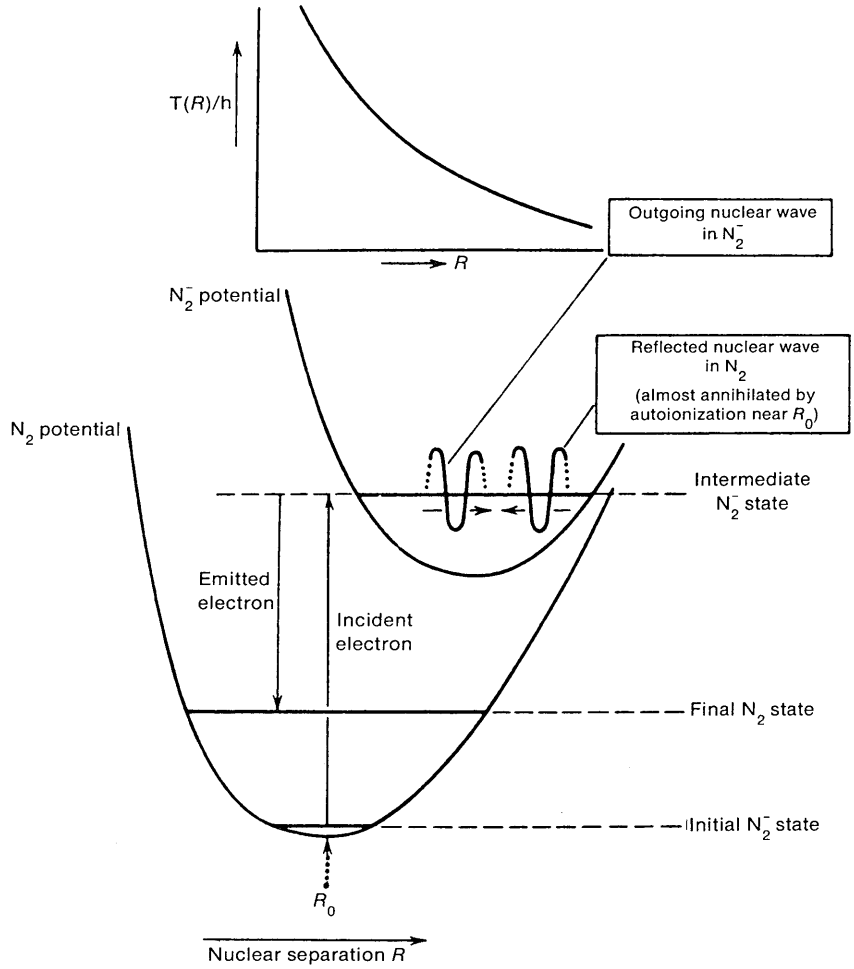

Fig. 15. Boomerang model for (e - N_2) system (from Birtwistle and Herzenberg, 1971).

Secondly, the strong influence of vibrational excitation on electron energy distributions is illustrated in Fig. 18 for electron swarms in nitrogen, the electron energies being limited to energies below $\simeq$ 2.5 eV for low vibrational temperatures, T_V, while at high T_V super elastic collisions lead to the high energy tail of the distribution. Even for E/n $\simeq$ 1.5 x 10^{-15}V cm^2, the sharp cut-off is obtained.

Finally, as an example of the effect of vibrational energy on ion-molecule reaction rates, we may refer to the work of Alge et al., (1979) on the reactions between O_2^+ and CH_4. For low vibrational energy of the O_2^+, the forward reaction is

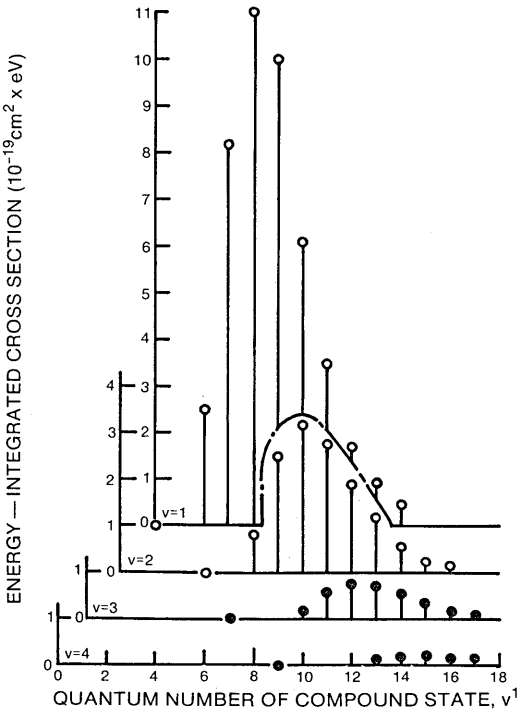

Fig. 16. Energy-integrated, vibrational excitation cross section for oxygen (Linder and Schmidt, 1971). The positions of the narrow peaks in the cross section correspond to those of the vibrational levels of the compound state.

$$O_2^+ + CH_4 \rightarrow O_2\ CH_3^+ \text{ (exothermic)} \qquad (21)$$

whereas as the vibrational energy increases the reactions

$$O_2^+ + CH_4 \rightarrow CH_3^+ \text{ (endothermic)} \qquad (22)$$

and $$O_2^+ + CH_4 \rightarrow CH_4^+ \text{ (endothermic)} \qquad (23)$$

become possible. Reaction rates may also be reduced as the vibrational energy of the ion increases, as is the case, for example, in the reaction of CO_2^+ with D_2. A recent discussion of molecular-beam experiments in which the effects of vibrational and rotational excitation are evident was given by Gentry (1979).

Dissociative Attachment, Associative Detachment. When an electron collides with a molecule XY and forms a temporary complex, an

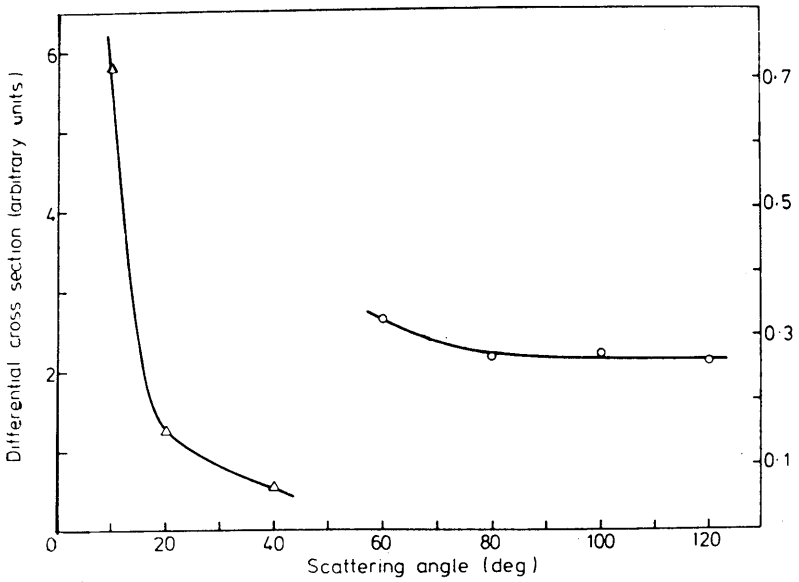

Fig. 17. Angular dependence of scattering cross section for ν_1 and ν_3 excitation in SF_6. Collision energy = 1 eV. The triangles and circles are for the ν_3 and ν_1 modes respectively. The left hand ordinate is for ν_3 and the right hand ordinate for ν_1.

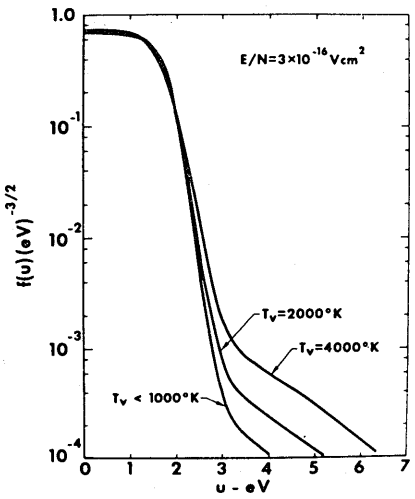

Fig. 18. Distribution function for electrons in Nitrogen at E/n = 3 x 10^{-16} Vcm^2 (Nighan, 1970).

alternative outcome to that of vibrational excitation accompanied by ejection of the extra electron is that of dissociative attachment. For the model shown in Fig. 19, the electron is attached at point (E, R_0), and the XY^- ion starts to dissociate along its repulsive potential curve. Until the crossing point of the XY^- and XY curves, the system decays into a free electron and a vibrationally excited molecule. Beyond this crossing point the decay channel is closed, and the dissociation is into X and Y^-. It often makes sense, therefore, to study dissociative attachment and vibrational excitation in a common investigation. A typical example is the investigation of Hall et al. (1977) for the (e,H_2) systems, discussed in some detail by Linder (1980). Figure 20 shows the energy dependence of the H^- production for electron energies between 10 and 13 eV. The similarity between the form of Fig. 20 and earlier figures for vibrational excitation is obvious.

The effects of the vibrational states of the target molecules and the intermediate negative ion states, and their rotational states, in some cases, on the cross section observed for dissociative attachment leads to a temperature-dependence of the cross section. This was demonstrated clearly some years ago for oxygen by Spence and Schulz (1969) and for N_2O by Chantry (1969). In the latter case Chantry was able to show that existing discrepancies in the cross sections reported by earlier authors could be explained by arguing that below 2 eV, attachment was via the ground state of the linear intermediate N_2O^- whereas for energies above 2 eV, the temperature-

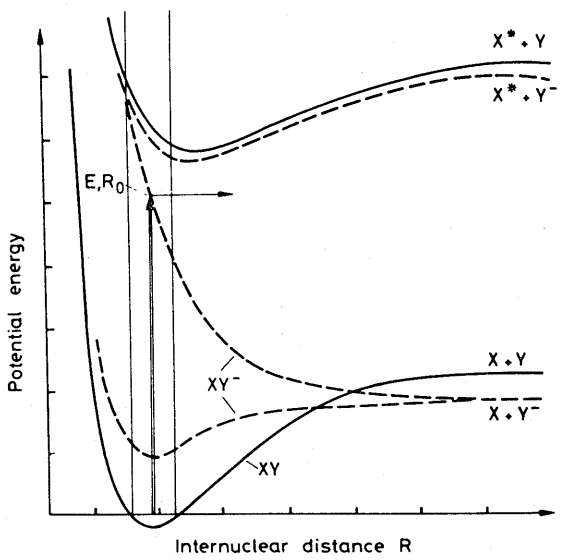

Fig. 19. Dissociative attachment/vibrational excitation model (Linder, 1980).

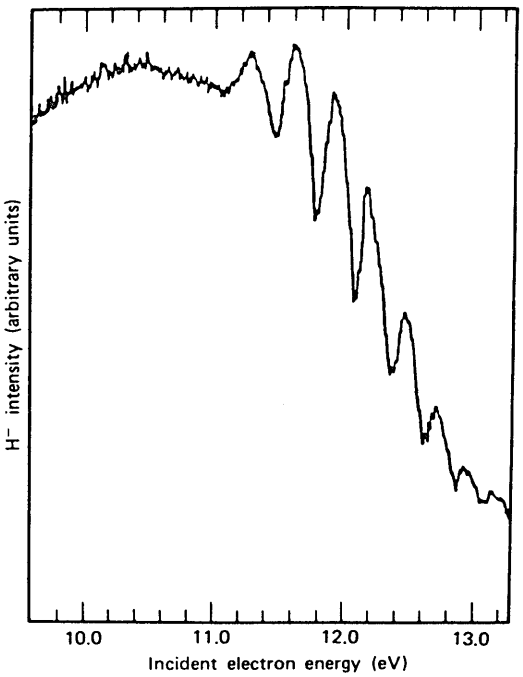

Fig. 20. H^- formation at energies between 10 and 13 eV observed at scattering angle of 50° (Tronc et al., 1977).

insensitive cross sections were due to attachment via the highest energy N_2O^- state connected to electronic ground state N_2 and O^-. More recent work by Spence and Schulz and by Chen and Chantry and others on attachment in gases such as CH_3Br, CH_3I, and SF_6 is discussed by Christophorou (these proceedings). For the fusion program an interesting case is that of dissociative attachment to vibrationally excited H_2. Allan and Wong (1978) showed the process

$$e + H_2(v = 0,1,2....) \rightarrow H_2^- \rightarrow H^- + H \qquad (24)$$

to have a cross section which increases by about an order of magnitude for successive vibrational states for v = 0 to 4. Calculations by Wadehra and Bardsley (1978) showed this increase to continue for higher values of v. For D_2 the increase is dramatic — 8 orders of magnitude as v increases from 0 to between 9 and 13. Hiskes (1979) has discussed the process in connection with the interpretation of experiments on hydrogen discharges by Bacal et al. (1979) which showed unexpectedly high negative ion densities.

The reverse process to dissociative attachment, namely, associative detachment

$$X^- + Y \rightarrow XY + e, \tag{25}$$

was predicted many years ago but was not studied experimentally until the mid 1960's. It can be of considerable importance in discharge work since for appropriate conditions (the electron affinity of X^- < the dissociation energy of XY), the reaction proceeds for zero relative kinetic energy of the X^- and Y. Typical processes are

$$O^- + O \rightarrow O_2 + e \tag{26}$$

$$O^- + CO \rightarrow CO_2 + e \tag{27}$$

$$O_2^- + C_2H_2 \rightarrow 2CHO + e. \tag{28}$$

The reaction rates can be large ($\simeq 5 \times 10^{-10}$ cm^3 sec^{-1}). As the ion energy is increased, the associative detachment process is sometimes replaced in importance by competing ion-molecule reactions, e.g., in the case of O_2^-, and acetylene reaction (28) has to compete with

$$O_2^- + C_2H_2 \rightarrow C_2H^- + O_2 + H \tag{29}$$

and $$O_2^- + C_2H_2 \rightarrow C_2OH^- + OH. \tag{30}$$

Ion-Molecule Reactions. Reactions such as (26) to (30) above, and many others, have been widely studied at energies of interest in discharge work in flowing afterglow experiments and in drift-tube/mass spectrometer systems. There is also a limited amount of data from merging-beams and ion cyclotron resonance and other experiments. Albritton (1979) estimated the number of reactions for which reaction rates have now been determined, at least at thermal energies, as being thousands. While the flowing afterglow technique is well-suited to the measurement of such thermal reaction rates, for temperatures up to say 900 K, and the merging beams technique allows the benefits of normal beam techniques to be utilized at collision energies of 1 eV or less, drift-tube investigations are still difficult to better for data which are of direct interest to discharge problems. The drift-tube technique is well known and need not be described here. It is worth, however, emphasizing that the primary data from drift-tube experiments are reaction coefficients and that the comparison of these measurements with flowing afterglow or single collision experiments relies fairly heavily on the Wannier equation

$$\langle KE_{lab} \rangle = \frac{1}{2} m \langle v^2 \rangle = 3/2\ kT + \frac{1}{2} m W^2 + \frac{1}{2} M W^2 \tag{31}$$

for the kinetic energy of the drifting ions, m and M being the masses of the ions and neutral molecules respectively, and W the ion drift velocity. Albritton (1979) has discussed the reasons why (31) appears to give reliable values of $\langle KE_{lab} \rangle$ for many drift-tube experiments provided the values used for W are the experimental values appropriate to the experimental conditions (E/n in particular) and not the values calculated from the same polarization model theory which leads to (31). He reasons that using the experimental drift velocity in (31) corrects for almost all the deficiencies of the polarization-model and that available comparisons between drift-tube data and other data, such as that shown in Fig. 21, suggest that (31) is accurate to a few percent. In Fig. 21 the broken curve shows drift-tube data; the solid curve shows flow-drift tube data, whereas the open circles are crossed-beam data. The curves are plotted using the upper E/n scale while the open circles are plotted using the lower energy scale.

To compare reaction coefficient data with cross-section data, it is necessary to know not only the mean energy of the ions in the drift-tube situation but also their speed distribution, f(v), [see Eqs. (7) and (11)]. This is particularly important, as Albritton discusses, if the drift-tube experiments in which the reaction coefficients are determined involve using a "buffer" gas which largely controls f(v). Figure 22 shows speed distributions found

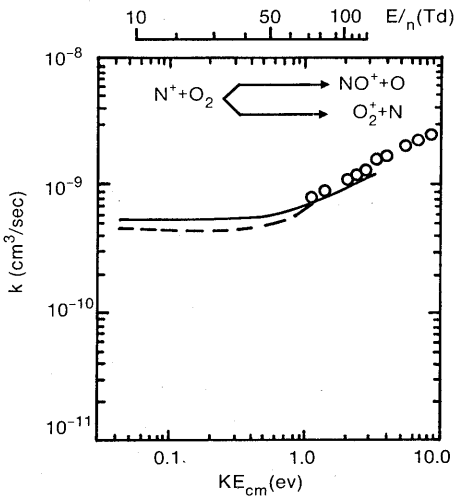

Fig. 21. Rate constants for the $N^+ + O_2 \rightarrow NO^+$ or O_2^+ reaction. Full curve, flow-drift tube data; broken curve, static drift-tube data; open circles, crossed-beam data. The relationship between the upper E/n and lower kinetic energy scales was established via Eq. 31 and experimental drift velocity data. (Based on Fig. 3, Albritton, 1979.)

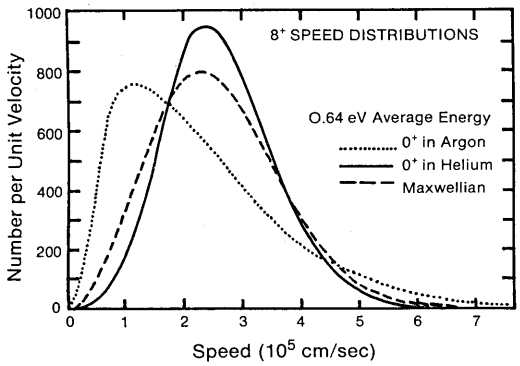

Fig. 22. Speed distributions for O^+ ions in helium and argon calculated by Lin and Bardsley (1977). The Maxwellian speed distribution for the same mean energy (0.64 eV) is shown for comparisons.

by Lin and Bardsley (1977) using a Monte Carlo calculation for O^+ ions in helium and argon for an average energy in each case of 0.64 eV. The effects of such different distributions on measured reaction rates are shown clearly in Fig. 23 which shows data for the reaction

$$O^+ + N_2 \rightarrow NO^+ + N + 1.1 \text{ eV}. \qquad (32)$$

The solid lines in Fig. 23 were calculated by unfolding from the helium-buffered data the reaction cross section for reaction (32), using Lin and Bardsley's O^+ in He data for f(v) and then combining the reaction cross section with Lin and Bardsley's O^+ in Ar data for f(v). The agreement for the argon-buffered data is clearly good. Similar work for the charge transfer reaction of O^- and O_2 has been reported by Lin et al. (1980).

Recombination. It is convenient to consider electron-ion and ion-ion recombination separately. For electron-ion recombination, the simplest processes are those of 2-body and 3-body radiative recombination. The processes are important in the decay of highly ionized spark channels. The 2-body process is simply

$$e + X^+ \rightarrow X^* + h\nu \qquad (33)$$

where X* is in general an excited state of X, but may be the ground state. The efficiency of the process can be described in terms of a swarm recombination rate coefficient, α_R, where as usual the rate coefficient is related to the cross section σ_R by an expression of the form of Eq. (11). In some cases it is adequate to write $\alpha_R = \bar{v}_r \cdot \sigma_R(v_r)$ where $\bar{v}_r$ is the mean relative velocity. At higher electron densities, 3-body recombination

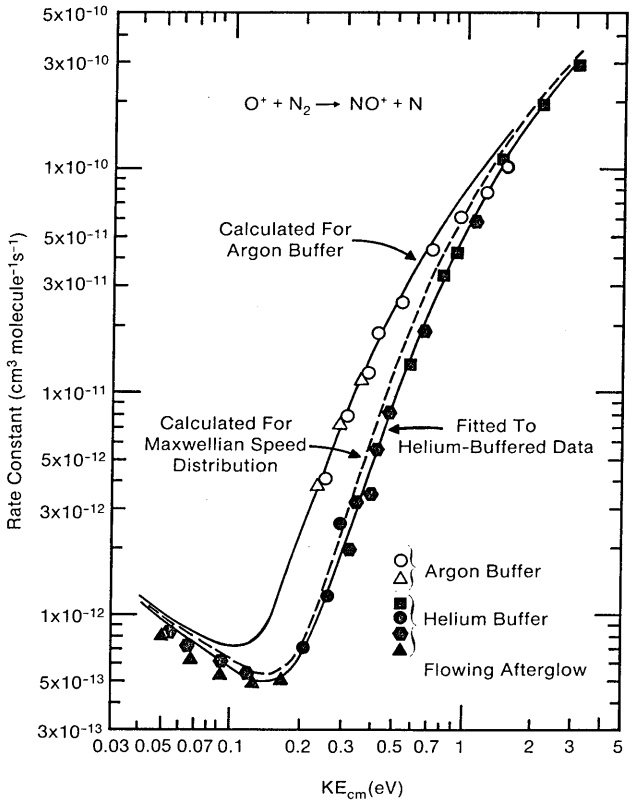

Fig. 23. Rate constants for the $O^+ + N_2 \rightarrow NO^+ + N$ reaction observed using helium and argon as alternative buffer gases. The rate constants calculated for a Maxwellian distribution are shown for comparison (From Albritton, 1979).

$$X^+ + 2e \rightarrow X + e \qquad (34)$$

becomes important and cannot be ignored in spark-channel decay. For the complete modeling of such situations, a whole complex of other processes needs to be considered — collisional excitation and de-excitation, free-free transitions and so on.

A further electron-ion recombination process is that known as di-electronic recombination. Whereas in the case of 2-body radiative recombination, the cross section falls off fairly rapidly with increasing electron energy, this is not necessarily the case for di-electronic recombination where some of the excess energy can be dissipated in exciting the bound electrons. The process may be written

$$e + X^+ \rightarrow X^{**} \rightarrow X^* + h\nu \qquad (35)$$

where the intermediate state X** is unstable and may autoionize to $X^+ + e$. The radiative lifetime is $\simeq 10^{-10}$ sec, so that it is quite possible for establization to occur rather than autoionization (see Botcher, 1980). In favorable cases, the recombination rate α_R is $\simeq 10^{-12}$ cm^3 sec^{-1}. The process was first considered in terms of a single autoionizing state but is now known to involve a whole Rydberg series. A recent review by Seaton and Storey (1976) should be consulted for further details. In a plasma at small particle and radiation densities, reaction (35) is followed by radiative decay of the X* to lower states and finally the ground state. For higher densities the particles interact with the surrounding plasma, and Seaton and Storey point out that in principle all the collisional and radiative processes connecting all the states of the intermediate and final X** and X* should be considered; for example, collisionally induced stabilization, stimulated stabilization, and photoexcitation might occur.

For many discharge situations the recombination processes considered above are relatively slow. Much faster processes are those of dissociative recombination

$$e + AB^+ \rightarrow (A\ B^*)_r \rightarrow A^* + B + K.E. \qquad (36)$$

involving molecular positive ions. It follows that in discharge systems any processes converting atomic ions to molecular ions may well be the controlling processes as far as recombination is concerned. Dissociative recombination rates of 10^{-7} cm^3 sec^{-1} or greater are commonly encountered. Much of the data for dissociative recombination is due to Biondi and his co-workers. The process may be understood by reference to Fig. 24 (Biondi, 1980). The ion is approached by an electron of energy ε, resonant capture giving an intermediate excited state, the probability of capture being high. If nothing else happens the electron is released after a short time. Much more probable, however, is that the repulsive intermediate state breaks up into A* + B, stabilizing the recombination. The rate coefficient can be high if the dissociating state of AB crosses the ionic state in the Franck Condon region of the ground vibrational state, as shown in the figure. The atoms A* and B share the dissociation energy ε_D as kinetic energy, and the line radiation emitted by the excited A* is Doppler-shifted as a result. Connor and Biondi (1965) observed this.

Biondi and his co-workers have measured recombination rates for many molecular ion species, atmospheric ions such as O_2^+, NO^+, N_2^+ and others, and for cluster complexes such as $H_3O^+(H_2O)_n$ (see Biondi, 1973). For the latter hydrated H_3O^+ ions, the recombination coefficient increases significantly as n increases, becoming $\simeq 10^{-5}$ cm^3 sec^{-1}, which is remarkably large. H_3O^+ ions are more common than might be expected in discharge systems; for example, Fleming et al.

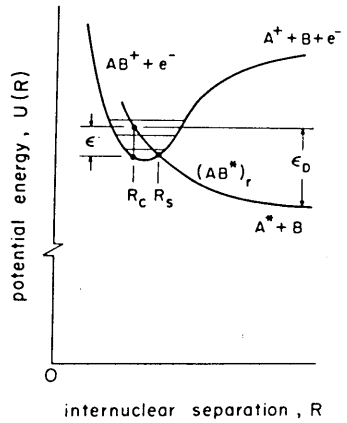

Fig. 24. Dissociative recombination (Biondi, 1979).

(1969) observed H_3O^+ ions to dominate over the expected H_3^+ or other hydrogen ions in a prebreakdown discharge in a comparatively pure sample of hydrogen and were led to postulate that much of the data then existing for the decay of hydrogen afterglows was probably controlled by recombination between H_3O^+ ions and electrons other than between hydrogen ions and electrons.

Where clusters such as H_3O^+. $(H_2O)_n$ exist in plasmas, a further fast recombination process is that of ionic recombination, also referred to as ion-ion neutralization. For example, Smith et al. (1976) have studied reactions such as

$$H_3O^+(H_2O)_3 + NO_3^-(HNO_3) \rightarrow \text{products} \qquad (37)$$

at thermal energies and have observed rate coefficients $\simeq 10^{-8}$ cm^3 sec^{-1}. The process occurs widely and for both atomic and molecular ions and deserves further study in view of its relevance to the decay of spark channels in electronegative gases. A useful review is that by Flannery (1980). At high pressures, 3-body processes predominate, the 3rd-body helping to dispose of the excess energy either as kinetic energy or perhaps as rotational/vibrational excitation energy.

CONCLUSIONS

It is very evident from the above that there is no shortage of reaction processes in which the species present in an electrical discharge may participate. I am conscious that more possibilities have been omitted than have been considered. For example, it was my original intention to discuss in more detail ion-molecule reactions,

particularly those involving negative ions, and to consider ion-production processes such as Penning ionization and the production of negative ions at surfaces when the latter are bombarded by beams of positive ions — processes which are important for fusion systems (Hiskes, 1979). To emphasize the complexity and interdependence of the collision processes occurring in discharge situations, one may consider Figs. 25 and 26. Figure 25 was not developed for discharge situations but for the D-region of the ionosphere. Nevertheless for discharges in air, many of the species mentioned in the figure, O_4^-, NO_2^-, CO_3^-, etc., will certainly be present, and the reaction scheme needed to describe and model the discharge situation will be equally complex. Figure 26 shows by way of contrast the reaction sequence used by Laudenslager (1979) in discussing the operation of a gas discharge N_2^+ laser. I leave it to others to discuss in more detail the setting up and testing of such models as those of Figs. 25 and 26 for particular discharge situations — corona discharges, for example.

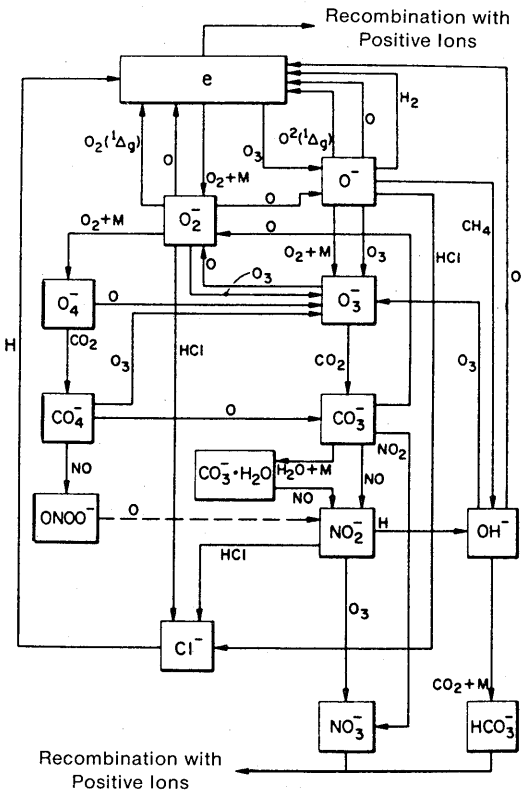

Fig. 25. Negative ion reaction scheme for the D-region of the Earth's ionosphere (Ferguson, 1979).

Reaction	
$He^+ + e$	$\rightarrow He^+ + 2e$
$He + e$	$\rightarrow He^* + e$
$N_2 + e$	$\rightarrow N_2^+ + 2e$
	$\rightarrow N^+ + N + 2e$
	$\rightarrow N_2^* + e$
$He^+ + N_2$	$\rightarrow N_2^+ + He$
	$\rightarrow N^+ + N + He$
$He^+ + 2He$	$\rightarrow He_2^+ + He$
$He_2 + 2He$	$\underset{3}{\overset{2}{\rightleftharpoons}} He_3^+ + He$
$He_2^+ + e$	$\rightarrow He_2^*$
$He_3^+ + e$	$\rightarrow 3He$
$He_2^+ + N_2$	$\rightarrow N_2^+(B) + 2He$
$He_2^+ + N_2 + He$	$\rightarrow N_2^+(B) + 3He$
$He_3^+ + N_2$	$\rightarrow N_2^+(B) + 3He$
$N_2^+(B) + e$	$\rightarrow 2N$
$N_2^+(B) + He$	$\rightarrow$ Products
$N_2^+ + N_2 + He$	$\rightarrow N_4^+ + He$
$N_2^+(B)$	$\rightarrow N_2^+(X) + h\nu$
$h\nu + N_2^+(B)$	$\rightarrow N_2^+(X) + 2\ h\nu$
$N_2^+(X),\ v'' = 1 + e$	$\rightarrow N_2^+(X),\ v'' = 0 + e$
$He^* + N_2$	$\rightarrow N_2^+(X)$
	$\rightarrow N_2^+(B)$

Fig. 26. Kinetic sequence of reactions controlling the behavior of the N_2^+ laser (Laudenslager, 1979).

REFERENCES

Albritton, D. L., 1979, in: "Kinetics of Ion Molecule Reactions," NATO ASI B40, P. Ausloos, ed., Plenum, New York, p. 119.
Alge, E., Villinger, H., Pesca, K., Ramler, H., Storitt, H., and Lindinger, W., 1979, in: "Proceedings, 14th International Conference on Phenomena in Ionized Gases, Grenoble," Contrib. Papers, p. 67.
Allan, M. and Wong, S. F., 1978, Phys. Rev. Lett, 41:1791.
Andrick, D. and Bitsch, A., 1975, J. Phys. B., 8: 393.
Azria, R., Wong, S. F., and Schulz, G. J., 1975, Phys. Rev. A, 11:1309.
Bacal, M. and Hamilton, G. W., 1979, Phys. Rev. Lett., 42:1538.
Barnett, C. F., 1977, in: "Atomic Physics, No. 5," R. Marrus, M. Prior, and H. Shugart, eds., Plenum, New York, p. 375.
Beaty, E. C., Hesselbacher, K. H., Hong, S. P., and Moore, J. H., 1977, J. Phys. B, 10:611.
Bederson, B. and Kieffer, L. J., 1971, Rev. Mod. Phys., 43:601.
Biondi, M. A., 1980, in: "Electron-Molecule Scattering," S. C. Brown, ed., Wiley, New York.
Biondi, M. A., 1973, University of Pittsburg SRCC Report 192.
Birtwistle, D. T. and Herzenberg, A., 1971, J. Phys. B., 4:53.
Bottcher, C., 1980, in: "Atomic and Molecular Physics in Controlled Thermonuclear Fusion," NATO ASI B53, M. R. C. McDowell and A. M. Ferendeci, eds., Plenum, New York.
Chantry, P. J., 1969, J. Chem. Phys., 51:3369.
Christophorou, L. G. and Christodoulides, A. A., 1969, J. Phys. B., 2:71.
Chutjian, A., 1974, J. Chem. Phys., 61:4279.
Connor, T. R., and Biondi, M. A., 1965, Phys. Rev. A., 140:778.
Crompton, R. W., Gibson, D. K., and McIntosh, A. I., 1969, Aust. J. Phys., 22:715.
Crompton, R. W., Gibson, D. K., and Robertson, A. G., 1970, Phys. Rev. A., 2:1386.
Dalba, G., Fornasini, P., Lazzizzera, I., Ranieri, G., and Zecca, A., 1980, J. Phys. B., 13:2839.
Dunn, G. H., 1976, IEEE Trans. Nucl. Sci., 23:929.
Ehrhardt, H., Hesselbacher, K. H., Jung, K., Schubert, E., and Willman, K., 1974, J. Phys. B., 7:69.
Elford, M. T., 1980, Aust. J. Phys., 33:251.
Ferch, J., Raith, W., and Schroder, K., 1980, J. Phys. B., 13:1481.
Ferguson, E. E., 1979, in: "Kinetics of Ion Molecule Reactions," NATO ASI B40, D. Ausloos, ed., Plenum, New York, p. 392.
Flannery, M. R., 1980, in: "Atomic Processes & Applications," P. E. Burke and B. L. Moiseiwitsch, eds., North Holland, Amsterdam.
Fleming, I. A., Tunnicliffe, R. J., and Rees, J. A., 1969, J. Phys. D., 2:551.
Gaballe, R. and Harrison, M. A., 1952, Phys. Rev., 85:372.
Geballe, R. and Harrison, M. A., 1953a, Phys. Rev., 91:1.

Geballe, R. and Harrison, M. A., 1953b, Phys. Rev., 92:867.
Gentry, W. R., 1979, in: "Kinetics of Ion Molecule Reactions," NATO ASI B40, P. Ausloos, ed., Plenum, New York, p. 82.
Golden, D. E., Bandel, H. W. and Salerno, J. A., 1966, Phys. Rev., 146:40.
Gupta, S. C. and Rees, J. A., 1975, J. Phys. B., 8:1267.
Hall, R. I., Cadez, I., Schermann, C., and Tronc, M., 1977, Phys. Rev. A., 15:599.
Hara, S., 1969, J. Phys. Japan, 27:1009.
De Heer, F. J., Jansen, R. H. J., Van der Kagg, W., 1979, J. Phys. B., 12:979.
Henry, R. J. W. and Lane, N. F., 1969, Phys. Rev., 183:221.
Herzenberg, A., 1968, J. Phys. B., 1:548.
Hiskes, J. R., 1979, in: "Proceedings, 14th International Conference on Phenomena in Ionized Gases, Grenoble," Invited Papers, p. 179.
Hogan, J. T., 1974, Oak Ridge National Laboratory Report ORNL-5035, p. 43.
Huxley, L. G. H. and Crompton, R. W., 1974, "The Diffusion and Drift of Electrons in Gases," Wiley, New York.
Itikawa, Y., 1978, At. Data Nucl. Data Tables, 21:69.
Kauppila, W. E., Stein, T. S., Jesion, G., and Pol, V., 1977, in: "Proceedings, 10th International Conference on the Physics of Electronic and Atomic Collisions, Paris," p. 802.
Kennerly, R. E. and Bonham, R. A., 1978, Phys. Rev. A., 17:1844.
Kieffer, L. J. and Dunn, G. H., 1966, Rev. Mod. Phys., 38:1.
Laudenslager, J. B., 1979, in: "Kinetics of Ion Molecule Reactions," NATO ASI B40, P. Ausloos, ed., p. 405.
Lin, S. L. and Bardsley, J. N., 1977, J. Chem. Phys., 66:435.
Lin, S. L., Bardsley, J. N., Dotan, I., Fehsenfeld, F. C., and Albritton, D. L., 1980, Int. J. Mass. Spec. Ion Phys. 34:113.
Linder, F., 1980, in: "Electron-Molecule Scattering," S. C. Brown, ed., Wiley, New York.
Linder, F. and Schmidt, H., 1971, Z. Naturforsch
Lotz, W., 1968, Z. Phys., 216:241.
Menendez, M., Rees, J. A., and Beaty, E. C., 1980, unpublished.
Moruzzi, J. L., 1968, J. Phys. D., 1:1587.
Nakamura, Y. and Lucas, J., 1978a, J. Phys. D., 11:325.
Nakamura, Y. and Lucas, J., 1978b, J. Phys. D., 11:337.
Nesbet, R. K., 1979, Phys. Rev. A., 20:58.
Newell, W. R., Brewer, D. S. C., and Smith, S. C. H., 1981, J. Phys. B., 14:3209.
Nighan, W. L., 1970, Phys. Rev. A., 2:1989.
Opal, C. B., Beaty, E. C., and Peterson, W. K., 1972, Atomic Data, 4:209.
Peart, B. and Dolder, K. T., 1975, J. Phys. B., 8:56.
Penning, F. M., 1938, Ned T. Natuukde, 5:33.
Peterson, W. K., Beaty, E. C., and Opal, C. B., 1972, Phys. Rev. A., 5:712.
Prasad, A. N. and Craggs, J. D., 1965, Electron. Lett., 1:118.

Ramsauer, von C. and Kollath, R., 1930, Ann. Phys. (Leipzig), 4:91.
Rockwood, S. D., 1973, Phys. Rev. A., 8:2348.
Rohr, K., 1977, J. Phys. B., 10:1175.
Schubert, E., Schuck, A., Jung, K., and Geltman, S., 1979, J. Phys. B., 12:967.
Schulz, G. J., 1976, in: "Principles of Laser Plasmas," G. Bekefi, ed., Wiley, New York.
Seaton, M. J. and Storey, P. J., 1976, in: "Atomic Processes and Applications," P. G. Burke and B. L. Moiseiwitsch, North Holland, Amsterdam.
Shyn, T. W., 1980, Phys. Rev. A., 22:916.
Smith, D., Adams, N. G. and Church, M. J., 1976, Planet. and Space Sci., 24:697.
Spence, D. and Schulz, G., 1969, Phys. Rev., 188:280.
Spender, F. E. and Phelps, A. V., 1976, in: "Proceedings, 15th Symposium on Engineering Aspectc of Magnetohydrodynamics," Philadelphia, PA: Univ. of Pennsylvania.
Stefani, F., Camilloni, R. and Giardini, G. A., 1978, Phys. Lett. A., 64:364.
Trajmar, S. and Williams, W., 1976, in: "Physics of Ionized Gases," B. Navinsek, ed., Univ. of Ljubljana, Ljubljana, Yugoslavia, p. 199, (see also Williams, W. and Bozinis, D. E., 1975, Phys. Rev. A., 12:57.
Tronc, M., Fiquet-Fayard, F., Schermann, C., and Hall, R. I., 1977, J. Phys. B., 10:325.
Wadehra, J. M. and Bardsley, J. N., 1978, Phys. Rev. Lett., 41, 1795.
Wagner, K. H., 1971, Z. Phys., 241:258.
Van Wingerden, B., Kimman, J. T., van Tilburg, M., Weigold, E., Jaachain, C. J., Piraux, B., and de Heer, F. J., 1979, J. Phys. B., 12:L627.

TRANSPORT DATA FOR THE MODELING OF ELECTRICAL BREAKDOWN AND DISCHARGES

A. V. Phelps

Joint Institute for Laboratory Astrophysics
National Bureau of Standards and University of Colorado
Boulder, CO 80309

INTRODUCTION

In recent years the modeling of electrical breakdown and electrical discharges has rapidly grown because of the availability of high speed computers. Modeling activity has created considerable demand for reliable transport and rate coefficient data describing the behavior of electrons, ions, excited atoms and molecules, and radiation in gaseous systems. Since a wide range of particle energies, gas mixtures, degrees of excitation ionization and time scales are encountered in these models, the ideal approach is to combine the cross-section data, such as discussed at this meeting by Rees (1982), with transport theories, such as discussed by Allis (1982), by Skullerud (1982), and by Pitchford (1982) in order to calculate the transport coefficients and the reaction rate coefficients for a particular problem. As pointed out by these authors there are many cases where this approach is practical. However, there are many cases for which there are insufficient cross-section data or for which verification of the calculated transport and rate coefficients is desired. One then turns to direct experimental measurements of the coefficients.

The measurement and analyses of electron and ion transport coefficients in gases were among the earliest techniques used to study electron and ion collision processes (Townsend, 1915, Huxley and Crompton, 1974). Even today transport coefficient measurements

---

Contribution of the National Bureau of Standards, not subject to copyright in the United States.

and their subsequent analyses provide the best methods for the accurate determination of low energy collision cross sections, i.e., elastic collisions of electrons with He atoms (Miloy and Crompton, 1977). In this discussion we will not be concerned with the determination of cross sections from electron transport data, but rather we will review the available experimental transport data. The next section contains the discussion of electron transport and reaction rate coefficient data. Ion transport and reaction rates are considered next, followed by a discussion of radiation transport and photoionization. Finally, we summarize data concerned with excited atoms and molecules. Note that we have attempted to provide the reader with an initial reference list and have not attempted to list all of the important, relevant papers.

ELECTRON TRANSPORT AND REACTION

The behavior of electrons in models of electrical discharges is of particular importance because most of the energy transferred from the electrical fields is acquired by fast-moving electrons. Most models make use of the hydrodynamic approximation (Kumar et al., 1980) in which electron behavior is described by Eq. (1):

$$\frac{\partial n}{\partial t} = D_L \frac{\partial^2 n}{\partial z^2} + D_T\left(\frac{\partial^2 n}{\partial x^2} + \frac{\partial^2 n}{\partial y^2}\right) - w\frac{\partial n}{\partial z} + kn \quad , \tag{1}$$

where D_L and D_T are the electron diffusion coefficients (Huxley and Crompton, 1974) parallel (longitudinal) and transverse to the z direction, w is the electron drift velocity in the z direction, and kn is the net rate of electron production due to ionization and attachment. Here the electric field E is in the negative z direction, so that the electrons are accelerated in the positive z direction. Equation (1) is also known as the continuity equation for the electron density. Note that D_L, D_T, w, and k are assumed to be independent of time. In many models one is also interested in the production of excited atoms or molecules either for diagnostics or as an end product, as in an electrically excited laser (Bekefi, 1976). Recent work has shown the utility of free-free radiation excited in electron-atom or electron-molecule collisions as a diagnostic (Rutscher and Pfau, 1976; Winkler et al., 1978). Finally, one needs to consider the available information regarding the range of applicability of the hydrodynamic model. That is, we need to consider the information available on nonequilibrium effects for electrons in gases.

Electron Transport

Since much of the available electron transport data for atomic and simple molecular gases has been reviewed by Dutton (1975) or is

cited in recent bibliographies (Dutton, 1975; Beaty et al., 1979), we will be concerned only with citing examples of various types of data. Thus, Fig. 1 shows what we believe to be representative of the more reliable electron transport data for hydrogen. The upper set of points shows the measured values of electron drift velocity (Dutton, 1979) as a function of the electric field to gas density ratio, E/N. The lower set of points shows values (Dutton, 1975) of the quantity known as the characteristic energy (Frost and Phelps, 1962) which is equal to the ratio of the transverse diffusion coefficient to the mobility coefficient for the electrons. The smooth curves show the results of calculations (Phelps, 1980) of the electron-drift velocity and characteristic energy which were made using cross-section data taken from the literature. These cross sections have been reviewed by Michel and Winkler (1976), Brunet and Vincent (1979), and Hayashi (1979). One notes that the agreement between calculated and measured values of electron transport coefficients is quite good for these data. The mean electron energy in this figure varies from about 0.01 eV to about 12 eV. The experimental data and calculated values shown in Fig. 1 represent the best results that have been obtained for electrons in a molecular gas.

Recent theoretical work (Tagashira et al., 1977; Skullerud, 1977; Pitchford, 1982) has shown that when electron production or loss is significant, the drift velocity and diffusion coefficients of Eq. (1) are modified. Furthermore, the drift velocities inferred from various experimental arrangements may differ significantly

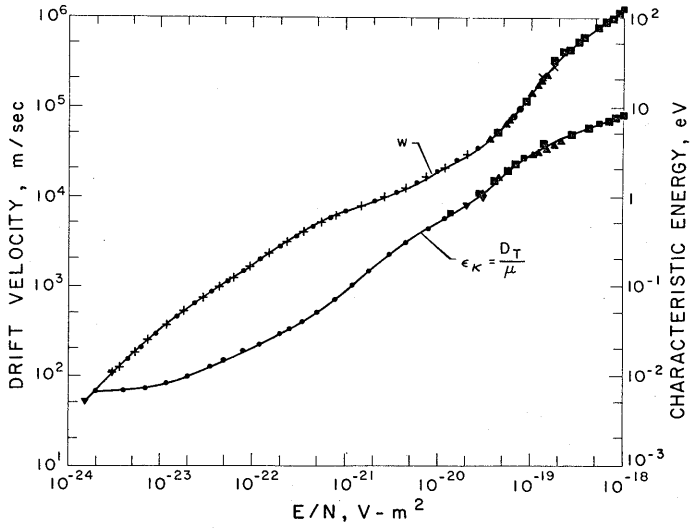

Fig. 1. Measured and calculated electron drift velocities w and characteristic energies ε_K for electrons in H_2.

(Thomas, 1969; Tagashira et al., 1977; Skullerud, 1977). The result has been the theoretical specification of as many as four different drift velocities differing by as much as 30 percent in nitrogen at high E/N. Hopefully, this situation can be simplified in the near future.

As an example of the difference between longitudinal and transverse diffusion coefficients, we show in Fig. 2 the measured and calculated values for electrons in argon as given by Lowke and Parker (1969). One notes that at high E/N, the values of D_T/μ (marked D /μ in this figure) are about 7 times those for the D_L/μ. This large ratio of the transverse diffusion coefficient D_T to the longitudinal diffusion coefficient D_L has been shown to be the result of the rapid increase with energy in the cross section for momentum transfer collisions between electron and argon atoms (Lowke and Parker, 1969). In this case the agreement between the calculated curves and the experimental points is only fair.

The examples that we have shown for electron transport in Figs. 1 and 2 are among the better understood cases. In many gases of technical interest, for example the halogens, there are essentially no reliable drift velocity and diffusion coefficient data available

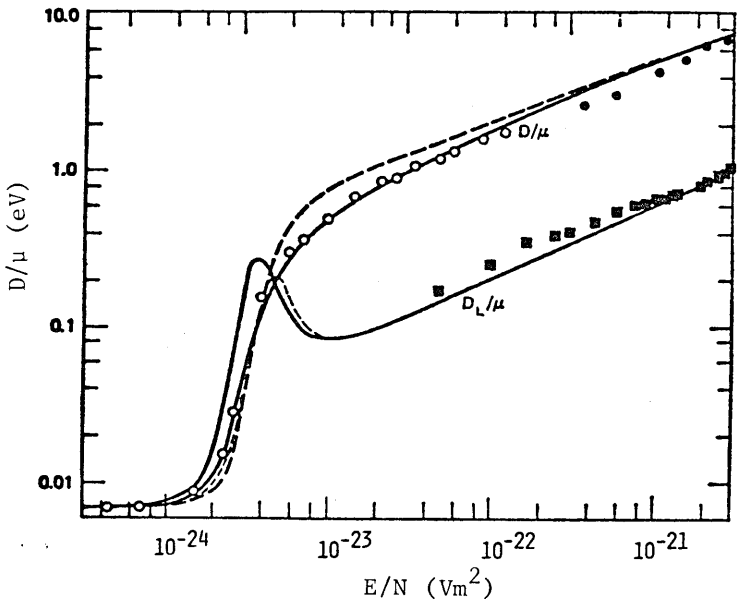

Fig. 2. Calculated and measured values of ratios of diffusion coefficients to mobilities for electrons in Ar. In this figure, D is the transverse diffusion coefficient. From Lowke and Parker (1969).

(Beaty et al., 1979). Very recently theoretical techniques have been developed which allow the accurate calculation of electron transport coefficients for gases with large ratios of inelastic to elastic collision cross sections (Lin et al., 1979; Reid, 1979; Braglia et al., 1979; Pitchford et al., 1981). Thus far, the techniques have been applied to only a few gases, i.e., N_2, CO, CO_2, and CH_4.

Electron Production and Loss

Dutton (1975) has reviewed experimental measurements and theoretical calculations of the coefficients describing production of electrons by ionization of atoms and simple molecules. Bibliographies are available (Beaty et al., 1979) covering the results of measurements for complicated molecules and for the more recent data on simple atoms and molecules. As an example of recent results, Fig. 3 shows the ionization coefficient data obtained by Haydon and

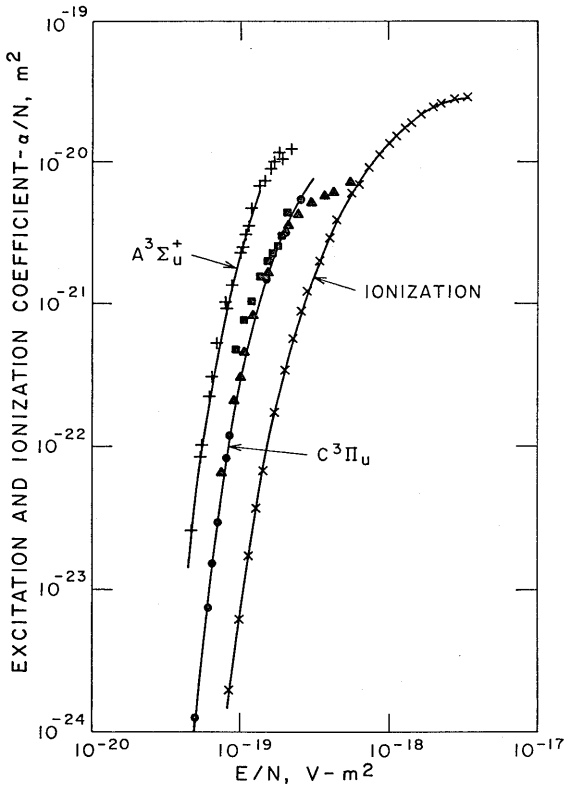

Fig. 3. Measured excitation and ionization coefficients for electrons in N_2.

Williams (1976) for electrons in nitrogen. These authors showed the importance of taking into account secondary electron emission due to the metastable nitrogen molecules when analyzing the experimental data.

Figure 4 shows the results of measurements (Dutton, 1975) and calculations (Lawton and Phelps, 1978) of electron attachment coefficients for oxygen as low E/N, i.e., for electron energies below about one electron volt. The points in the dashed curve are the results of experiment while the smoothed curve is the calculation based on our current understanding of electron behavior in oxygen. This three-body electron attachment process is the dominant loss mechanism for electrons in weakly ionized oxygen and air at low electron energies (Christophorou, 1978; Shimamori and Fessenden, 1981). Unfortunately, these attachment coefficients are so large that measurements of electron transport in oxygen at low E/N are extremely difficult, if not impossible.

Electron-positive ion recombination has been the subject of several reviews (Bates, 1973; Biondi, 1976). As with other processes involving positive ions, it is essential to know the identity of positive ions present in the gas discharge. In most high-pressure gas discharges, the dominant recombination process is the dissociative recombination of electrons and molecular ions. When the degree of ionization is high and the electron temperature is moderately low, collisional-radiative recombination in which an electron serves as the third body is often important.

Recent measurements (Bates, 1973; Biondi, 1976; Warman et al., 1979) and theory have shown the importance of collisional-radiative recombination in which the third body is a neutral atom or molecule. The results of these investigations are summarized in Fig. 5. Here we have attempted to correlate these three-body recombination coef-

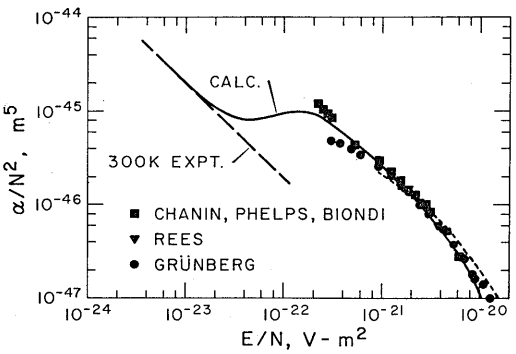

Fig. 4. Measured and calculated apparent three-body attachment coefficients for electrons in O_2.

ficients by plotting the magnitude of the recombination coefficient as a function of the parameter which is a measure of the frequency of energy loss collisions between electrons and the neutral third-body atom or molecule ν_u/N (Frost and Phelps, 1962; Warman et al., 1979). The points are the results of experimental measurements or of specific theoretical calculations (Bates et al., 1971; Bates, 1976). The solid, straight line is the theoretical prediction by Pitaevskii (1962) expressed in terms of ν_u/N while the dashed straight line is the earlier prediction given by Massey and Burhop (1952). One sees that there is an approximately linear correlation between the three-body recombination coefficients and the energy loss per collision parameter over many orders of magnitude (Warman et al., 1979). The horizontal chained line is a prediction for electrons, hydrogenic ions and a representative rare gas atom based on a simple model of collisional excitation and deexcitation of the excited hydrogenic atom (See Excitation and Deexcitation of Excited Atoms).

Electron Excitation

The older measurements of electron excitation coefficients are reviewed by Dutton (1975). Figure 3 shows the results of recent measurements for electrons in nitrogen. The upper set of points shows results of measurements of excitation coefficients for the $A^3\Sigma_u^+$ state of nitrogen by Levron and Phelps (1979). The middle set of points shows the results of various measurements (Legler, 1963; Tachibana and Phelps, 1979; Urosević et al., 1980) for the $C^3\Pi_u$ state of nitrogen. Excitation coefficient data such as shown in Fig. 3 have proven very useful in determining electron collision cross section sets for nitrogen (Tachibana and Phelps, 1979). Similar results have been obtained and used in determining cross sections

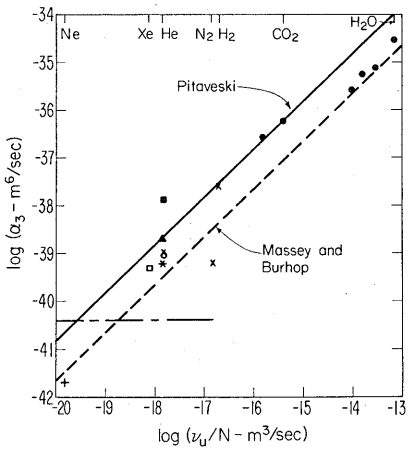

Fig. 5. Experimental and theoretical electron-positive ion-neutral recombination coefficients vs. energy-exchange, collision-rate coefficients.

for electrons in oxygen (Lawton and Phelps, 1978) and in hydrogen (Michel and Winkler, 1976). However, excitation coefficient data are very scarce for other gases (Dutton, 1975).

Recently measurements have been made of electron excitation coefficients for the production of free-free radiation in collisions between electrons and rare gas atoms (Rutscher and Pfau, 1976; Winkler et al., 1978; Yamabe and Phelps, 1981). The observation of free-free radiation by electrons in rare gases has been shown to be a useful discharge diagnostic (Rutscher and Pfau, 1976; Winkler et al., 1978).

Nonequilibrium Effects

In this section we are concerned with the question of when it is proper to use the hydrodynamic approximation as represented by Eq. (1). We will limit our discussion to situations in which the electric field is independent of position. Thus, we will not consider the cathode fall region (Druyvesteyn and Penning, 1940) or the highly nonuniform field region at the head of the streamer occurring during electrical breakdown (Llewellyn-Jones, 1982). Nonequilibrium effects were observed many years ago as fluctuations in the light output near the cathode of Townsend discharges in the rare gases (Druyvesteyn and Penning, 1940) and as a reduction in the apparent Townsend ionization coefficient near the cathode in experiments measuring the growth of ionization between parallel plane electrodes (Druyvesteyn and Penning, 1940). These experiments led to the introduction of a distance d_i through which electrons leaving the cathode must travel before producing significant ionization. In this discussion we will express these results in terms of the voltage difference d_iE through which the electrons must travel in order for the ionization coefficient to reach about half of its final value. The values of this inoization relaxation voltage for electrons in nitrogen (Haydon and Williams, 1976) are shown by the upper set of points in Fig. 6. The upper dashed lines shows the ionization potential for the nitrogen molecules. Observation of experimental data below this line may indicate the effects of the energy with which electrons are released from the cathode of the drift tube.

Calculations (Pitchford and Phelps, 1982) of the distance d_A required for the excitation coefficient for the $A^3\Sigma_u^+$ state of nitrogen to reach one half its equilibrium value are expressed as a voltage and are shown by the middle curve in Fig. 6. Again the dashed line indicates the excitation energy for this state of nitrogen.

The lower solid curve of Fig. 6 shows the voltage difference through which electrons must travel in order for the bulk of the electrons to reach equilibrium with the electric field (Frost and Phelps, 1962; Lowke and Davies, 1977). The corresponding energy relaxation distance is equal to the electron drift velocity divided

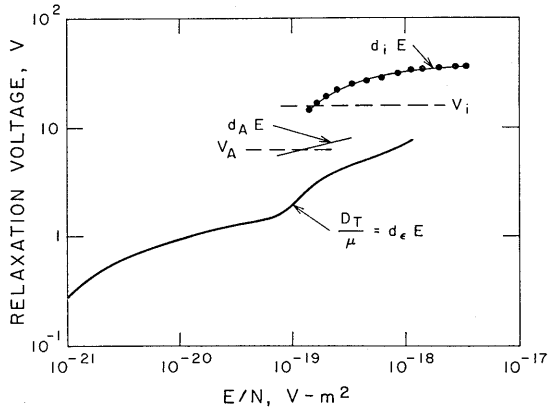

Fig. 6. Ionization and excitation relaxation voltages and characteristic energy vs. E/N for electrons in N_2.

by the frequency of energy exchange collisions. Here we have assumed that the electron mean energies are well above their thermal values. An important conclusion to be drawn from the examination of Fig. 6 is that different parts of the electron energy distribution require different voltages for relaxation to the steady-state or equilibrium distribution. In particular, a much larger relaxation voltage is required for the high energy portion of the distribution function responsible for ionization. Application of criteria represented by the lower curve for the bulk of the electrons has led to erroneous conclusions about the validity of Eq. (1) in nonuniform field situations.

The second type of nonequilibrium effect is illustrated by the results of the simulation calculation shown in Fig. 7. These curves are a replot of Monte Carlo calculations by Hayashi (1976) of the growth of electron current in a Townsend drift experiment for electrons in helium. For our purposes the important result of this calculation is that for E/N of 565 x 10^{-21} Vm^2 and below, the growth in the number of electrons with voltage is exponential for voltages above about 50 V. This result implies that, as for N_2 in Fig. 6, about one half the final ionization coefficient is reached after the electrons have fallen through the ionization relaxation voltage. However, for higher E/N the growth in the number of electrons with voltage is no longer exponential at any voltage. This behavior has been interpreted as the result of the runaway of a portion of the electrons, i.e., the electron energy distribution never reaching an equilibrium in which the rate of gain of energy from the electric field is balanced by the rate of loss of energy in collisions (Golant et al., 1980). This behavior has been observed experimentally by Folkhard and Haydon (1971). For nitrogen (Folkhard and

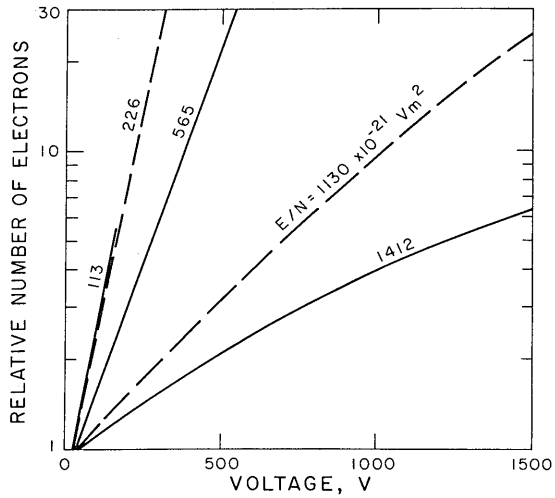

Fig. 7. Simulated current growth in helium vs. applied voltage for various E/N. Based on Hayashi (1976).

Haydon, 1973), this condition occurs just above the highest E/N values for which ionization relaxation voltages are shown in Fig. 6.

In summary the results cited in this section show that a great deal of useful data is available regarding the electron behavior in the more common gases. However, there are many gases for which few if any electron transport or reaction rate data are available. Particularly important for modeling real systems is the lack of agreement among measurements of diffusion and attachment coefficients in water vapor and air at moderate E/N. Similarly, although much progress has been made in the calculation of electron transport and reaction rate coefficients, there is a great deal to be done, particularly for gases with large inelastic collision cross sections, such as water vapor, and for high E/N situations.

ION TRANSPORT AND REACTIONS

In this section we will be concerned with the transport of ions in the presence of a uniform electric field and of the nonuniform electric fields characteristic of ambipolar diffusion. We will also consider briefly ion-molecule reactions of importance in electrical breakdown.

Transport in Uniform Electric Fields

Because of the large number of different positive and negative ions which may be produced in a given gas or gas mixture, it is essential in both experiments and in modeling to identify the positive ions that are present and to take into account the differences in their behavior. For this reason we will consider as reliable only the experimental transport data for ions that have been identified using a mass spectrometer (McDaniel and Mason, 1973) or for which unambiguous models predict a dominant type of ion. Ellis et al. (1976, 1978) have summarized the reliable ion mobility and ion diffusion coefficient data available prior to August, 1976. The ion mobility data for the more common ions found in nitrogen are shown as a function of E/N in Fig. 8 from the results of Moseley et al. (1969). Note that the more complex and less stable ions N_3^+ and N_4^+ are observed only at the lower E/N. Much of the recent experimental work concerns the properties of ions formed by the reactions of parent gas ions with polar gases, such as water vapor (Dotan et al., 1976). These ions can, in turn, form large relatively stable clusters. Experiment and theory have shown that over much of the range of available E/N, there is a close correlation of the ion mobility and the ion diffusion coefficients through what is known as the Wannier formula (McDaniel and Mason, 1973; Pai et al., 1975).

The negative ions formed by electron attachment to gases such as oxygen often play an important role in electrical breakdown (Goldman, 1982) and in the stability of gas discharges (Nighan and Wiegand, 1974; Kline, 1975).

Ambipolar Diffusion

In many steady-state electrical discharges and in some relatively slowly developing discharges, the effects of space charge in electric fields at right angles to the applied electrical fields can be accounted for by replacing the transverse diffusion coefficient of Eq. (1) by an effective ambipolar coefficient for electrons D_{se}. This coefficient depends upon such discharge parameters as the electron density and "temperature" and the electron and ion mobilities (Allis and Rose, 1954; Ingold, 1972; Muller and Phelps, 1980). As the electron density increases, the effective transverse diffusion coefficient for electrons will be reduced from the value for free electrons and will approach the limiting ambipolar diffusion coefficient (Druyvesteyn and Penning, 1940). For ions (Gusinow and Gerber, 1972) the effective transverse diffusion coefficient will increase from the value for ions in the absence of a space charge field, pass through a maximum, and then decrease toward the limiting ambipolar diffusion coefficient.

Figure 9 shows a recent comparison (Muller and Phelps, 1980) of various theoretical calculations of the ratio of the effective

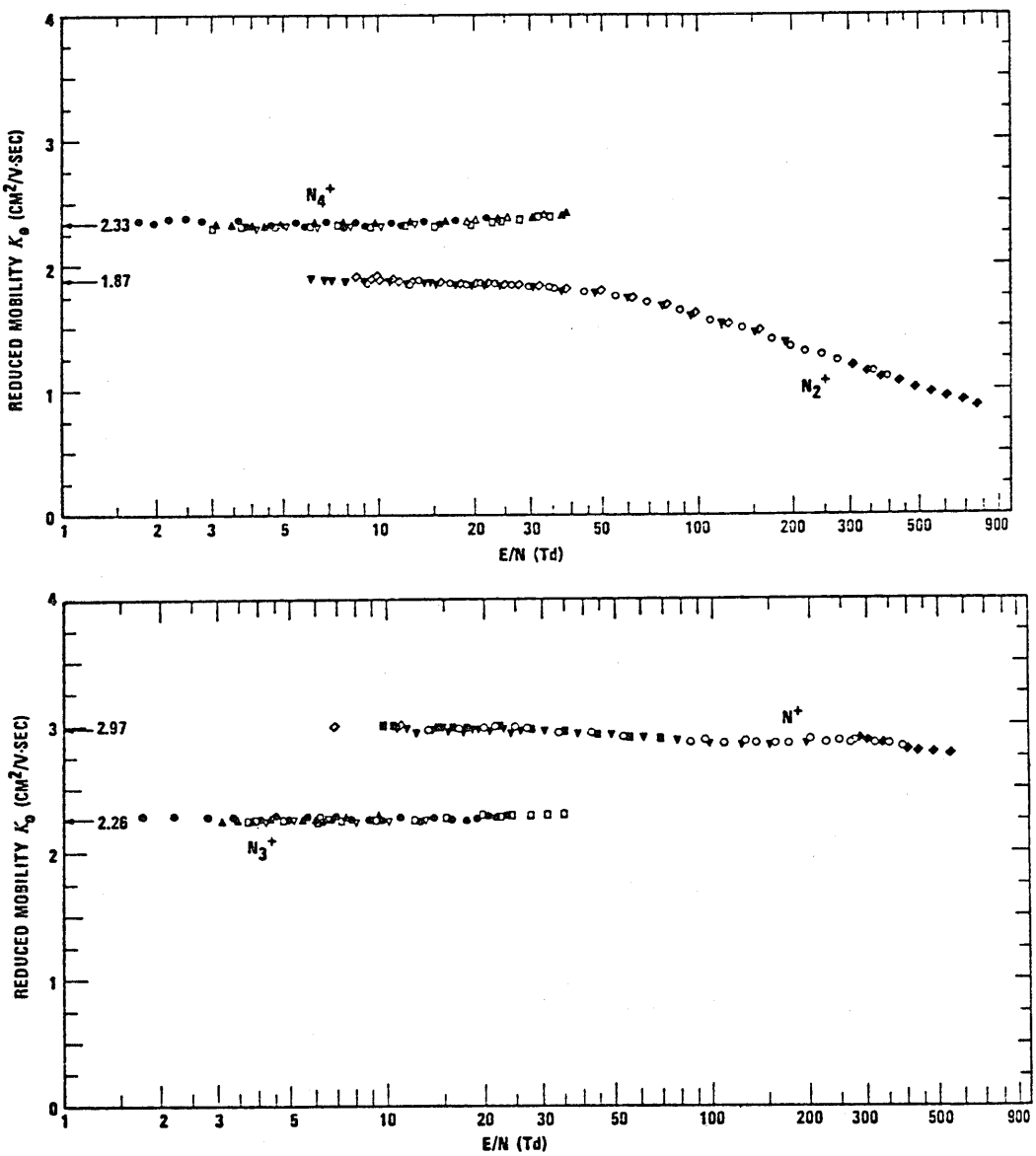

Fig. 8. Experimental values of the reduced mobility K_o for the dominant positive ions in pure N_2 vs. E/N. Here $K_oN_o = \mu N$ where $N_o = 2.69 \times 10^{25}$ atoms/m^3. From Moseley et al. (1969). Here 1 Td = 10^{-21} V m^2.

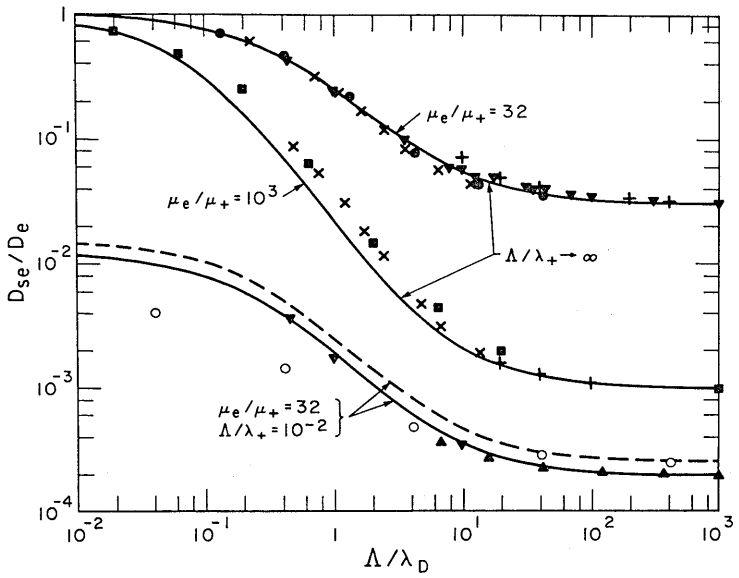

Fig. 9. Theoretical values of the ratio of the effective diffusion coefficient for electrons to the free diffusion coefficient for electrons vs. the ratio of the diffusion length to the Debye length for various ratios of the electron to ion mobilities and for various ratios of the diffusion length to the ion-mean-free path.

diffusion coefficient for electrons to that for free electrons as a function of ratio of the diffusion length to the Debye length for various values of the ratio of the electron mobility to the ion mobility and of the ratio of the diffusion length to the ion mean-free path. The diffusion length is equal to the tube radius divided by 2.4. The smooth curves show the values of an empirical expression for the effective electron diffusion coefficient given by Muller and Phelps (1980). The usefulness of these steady-state results for transient discharges has been evaluated for an afterglow plasma (Gusinow and Gerber, 1972).

Ion Molecule Reactions

Since the general topic of ion molecule reactions has been covered by Rees (1982), we will cite only one of the ion molecule reactions of particular importance in electrical breakdown. This reaction is the collisional detachment of electrons when O^- ions collide with oxygen molecules. Parkas (1974) has summarized the available data and shows that there is an uncertainty in the rate coefficient for detachment of at least an order of magnitude over the whole range of E/N of interest in electrical breakdown problems. Only

recently techniques for the measurement of ion molecule reactions using the injection of mass identified ions have become reliable (Smith and Adams, 1979). Hopefully, these techniques will be applied to this very important problem and to similar problems involving electron detachment from other negative ions and in other gases.

RADIATION TRANSPORT

In this section we will first be concerned with radiative and nonradiative transport of resonance excitation energy. Then we will consider the data available regarding ionizing radiation produced by electrical discharges.

Resonance Excitation Transport

The transport of resonance excitation energy is important in the modeling of electrical discharges because of the possibility of ionization of the resonance states by electrons and by collisions with other excited atoms (Druyvesteyn and Penning, 1940). The radiation from these states is often used as a diagnostic for electrical discharges. Theory and experiment have shown that the transport of resonance radiation is governed by optical depth considerations rather than by usual diffusion or random walk models (Holstein, 1947, 1951; Biberman, 1947, 1948). The diffusion of the excited atoms does occur, but because of the very large cross sections for the excitation transfer scattering of the excited atoms, the diffusion coefficients for resonance states are very small (Phelps and McCoubrey, 1960). Diffusion effects are observed most easily when the excited states are produced by incident laser radiation tuned to the center of the resonance line (Zajonc and Phelps, 1981).

The results of theory and experiment are often expressed in terms of the decay constant for the density of resonance atoms following the sudden turnoff of the excitations. Representative results are those shown in Fig. 10 for the resonant state of argon which emits radiation at 104.8 nm. These data are taken from the results of Payne et al. (1974) and show the transition from the low argon density region in which the transport of the resonant radiation is dominated by the Doppler portion of the line profile, to the high argon density region. There the transport of resonance excitation is dominated by the collision-broadened Lorentzian portion of the line profile. In these limits the agreement between theory (Holstein, 1947, 1951; Biberman, 1947, 1948) and experiment (Payne et al., 1974) is good. At intermediate densities, where the transport excitation is affected by the Lorentzian shaped, natural-broadened portion of the line profile, the agreement between theory and experiment is much less satisfactory. At the low densities the scaling of the decay constant is approximately equal to the inverse of the product of density of the ground state atoms and the radius of the container.

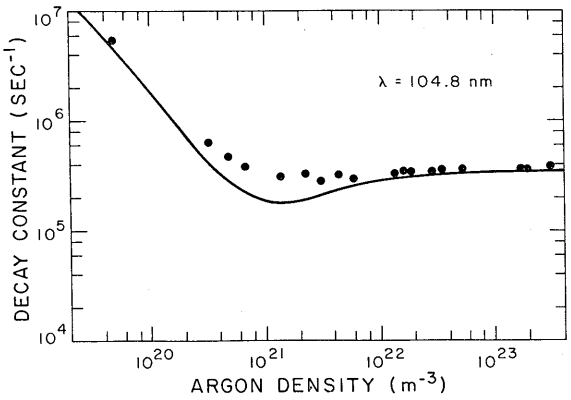

Fig. 10. Experimental and theoretical decay constants for argon resonance radiation (104.8 nm) vs. argon density. Based on Payne et al. (1974).

At high densities the experimental data show that the decay constant is independent of gas density and varies inversely as the square root of the radius of the container. It is to be noted that these same scaling laws apply to the transport of resonance radiation in electrical breakdown problems (Phelps, 1960).

Ionizing Radiation

The role of radiation in producing ionization during breakdown and during steady state discharges has been subject to a great deal of controversy (Llewellyn-Jones, 1982). Effective attenuation coefficients and ionization coefficients have been measured for many years (Penney and Hummert, 1970). Studies related to laser discharges have been summarized by Kline and Denes (1982). Only recently have measurements been made of wavelengths of the radiation responsible for gas ionization under discharge conditions, and most of these measurements have been concerned with gas mixtures of interest in the development of high power lasers. In these laser mixtures it is often impurity species which are ionized by the radiation. As a result, our knowledge of the role of ionization in pure gases - for example, nitrogen - is poor.

METASTABLE AND EXCITED ATOMS

The importance of metastable atoms in rare gas and metal vapor discharges is well known and the effects of these atoms must be included in models of these systems. In this section we discuss representative data for the transport and reaction rate coefficients for metastable atoms and for metastable molecules. We also consider the process of ionization of atoms or molecules by these metastables.

Finally we discuss the excitation and deexcitation of highly excited atoms by electrons and by other atoms.

Metastable Transport and Kinetics

As an example of currently available data, the transport and collision kinetics for the metastable and nearby radiating states of argon are shown in Fig. 11. These data are compiled from a number of experimental papers and in some cases represent averages of occasionally divergent data (Ellis and Twiddy, 1969; Thonnard and Hurst, 1972; Hurst et al., 1974; Payne et al., 1974; Boxall et al., 1975; Firestone et al., 1979). At low argon densities the metastable states $^3P_2$ and $^3P_0$ are lost by diffusion to the walls of the container. The curves shown are for parallel plane electrodes separated by 20 mm. At low densities the radiating states $^3P_1$ and $^1P_1$ are lost by radiative transport to the walls of the container. At very high densities all of these excited atoms appear to be destroyed in three-body collisions with neutral atoms. Only the metastable $^3P_0$ state shows evidence of destruction in two-body collisions with argon. Presumably this process is collisional deexcitation to the $^3P_1$ radiating state. The metastable molecules produced by the three-body destruction of the metastable atoms have been of considerable

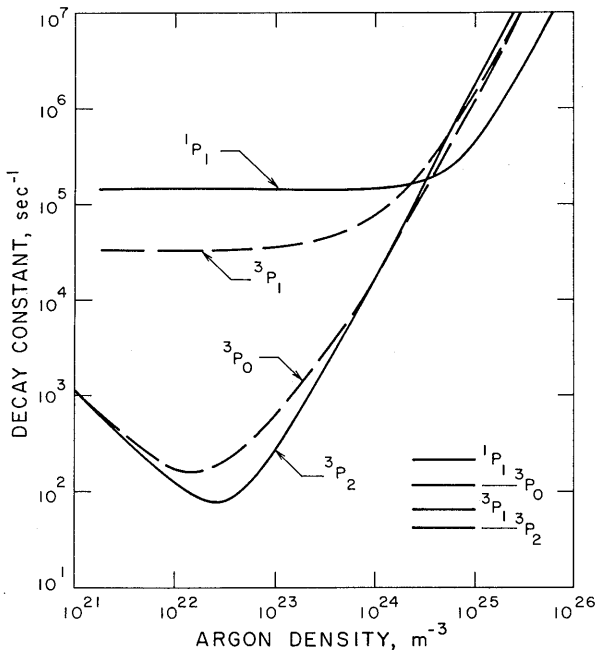

Fig. 11. Summary of experimental decay constant data for the first four excited states of argon.

interest in connection with the operation of ultraviolet lasers (McCusker, 1979).

An example of the data now available for a few molecular gases is shown in Fig. 12. Here we have shown decay constants for some of the more important metastable and radiating states of the nitrogen molecule as a function of nitrogen density. At low nitrogen densities, the loss of nitrogen metastables in the $A\ ^3\Sigma_u^+$ state is governed by diffusion, as observed by Brömer and Spiewick (1967) for a large spherical chamber. This curve shows that on the basis of data available at present, the metastable decay at high densities of extremely pure nitrogen would be governed by radiative decay (Shemansky and Carleton, 1969), i.e., collisional deexcitation by N_2 has yet to be observed. The curve labelled $a\ ^1\Pi_g$ actually represents the behavior of the collisionally coupled a and a' states (Dreyer and Perner, 1972; Freund, 1972). The dashed portion of this curve indicates our

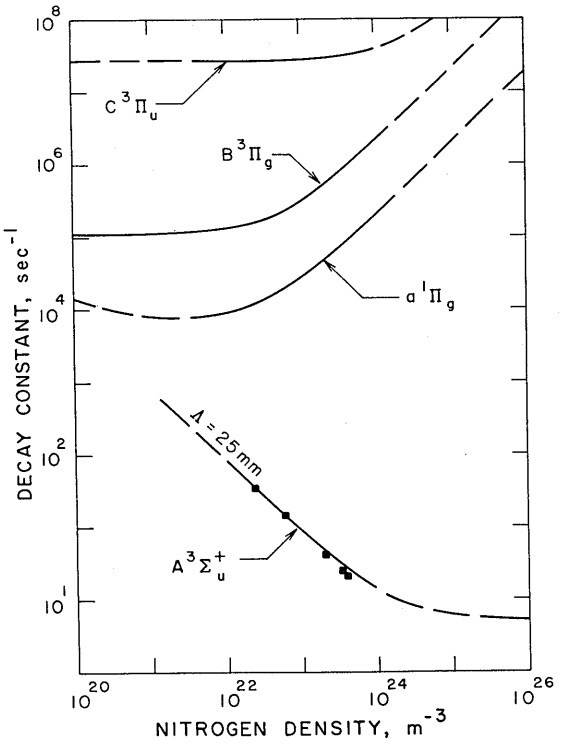

Fig. 12. Summary of experimental decay constant data for some of the more important excited states of N_2.

estimate of the expected effect of diffusion at low nitrogen densities. The dashed portion at high densities indicates an uncertainty because of our lack of experimental data. Here three-body collisions could be important. The curves marked $B^3\Pi_g$ and $C^3\Pi_u$ represent the expected behavior of these well-known levels (Dreyer and Perner, 1972; Freund, 1972, Gartner and Thrush, 1975; Cartwright, 1978). The available data on many other metastable molecules have been reviewed by McGowan et al. (1975). Note, however, that this is a rapidly changing field as shown by the changes (Lawton et al., 1977) in the rate coefficient for the collisional destruction of the $b^1\Sigma_g$ state O_2 by O_2.

Ionization by Metastables and Exciting Atoms

In recent years the area of the ionization of atoms and molecules by metastables and other excited atoms has been one of the more active fields in atomic physics. The available data have been discussed by a number of authors (Delcoix et al., 1976; Vagner et al., 1977; Hotop, 1980; Niehaus, 1981). It is convenient to classify as Penning ionization those reactions in which the products are a free electron, an ion and an atom or molecule and, as associative ionization, those reactions in which the products are a free electron and a molecular ion formed from the colliding atoms or molecules. It is important that these ionization processes be incorporated in models (Druyvesteyn and Penning, 1974; Delcroix et al., 1976; Vagner et al., 1977; Muller and Phelps, 1980) of ionization growth and of electrical discharges.

Excitation and Deexcitation of Excited Atoms

In order to quantitatively model the ionization and recombination processes in high power density discharges, we must take into account the collisional excitation and deexcitation of the highly excited atoms caused by electrons and by heavy particles (Biberman et al., 1979). In the past few years considerable progress has been made by theoreticians in the calculations of cross sections for the excitation and deexcitation of highly excited atoms by electrons (Percival and Richards, 1975; Vriens and Smeets, 1981). In a few cases it has been possible to test these theories by experiment (Devos et al., 1979). Some of these theoretical values for excitation and deexcitation rate coefficients have been incorporated into models of electrical discharges (Golubovskii et al., 1976; Bacri et al., 1976; Biberman et al., 1979; Fujimoto, 1979; Shuker et al., 1980) and have shown that the highly excited states can be very important in providing ionization.

More recently, experiment (Gounand et al., 1977; Devos et al., 1979; Gallagher and Cooke, 1979; Gallagher, 1979, private communication) and theory (Flannery, 1970; de Prunelé and Pascale, 1979) have yielded data for the rate coefficients for excitation and

deexcitation of highly excited atoms, i.e., Rydberg states of atoms, as the result of collisions with neutral atoms and molecules. Figure 13 shows collisional deexcitation rate coefficients for the highly excited states of the alkali metals. These data can be very roughly approximated by the solid smooth curve. This curve has the general shape of that calculated for collisional deexcitation. It is this curve that was used to calculate the three-body recombination coefficient indicated by the horizontal chain line in Fig. 5. The measured rate coefficients for collisional deexcitation by H atoms and H_2 molecules are significantly larger (Devos et al., 1979) than the values shown in Fig. 13. Other arguments in favor of larger rate coefficients for the deexcitation of highly excited atoms have been given (Drawin et al., 1971; Bacri and Gomes, 1978) and criticized (Fleschmann and Dehmel, 1971). Obviously further work on this subject is essential.

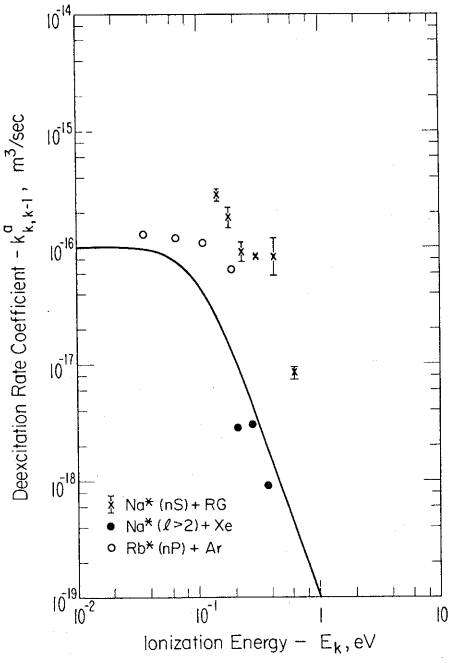

Fig. 13. Deexcitation rate coefficient data (points) for excited alkali atoms in rate gases vs. ionization energy of the excited atom. The smooth curve is an approximate empirical fit to these data having a shape based on theory. The symbols and the associated references are: x - Gallagher and Cooke (1979); o - Gallagher (1979, private communication); o - Gounand et al. (1977).

SUMMARY

In this paper we have presented some of the more important data sources for the behavior of electrons, ions, resonance atoms, metastable states, and other excited states appropriate to the modeling of electrical discharges. We have also cited some examples of the data that are now available. In our effort to cite examples of reliable data for a wide range of experimental conditions, we have most certainly painted too optimistic a picture. Thus, while accurate data are available for electron drift velocities and characteristic energies for diffusion coefficients for hydrogen over a very wide range of E/N, there are uncertainties of an order of magnitude in the electron attachment coefficient for air at the average E/N values typical of long spark electrical breakdown. Similarly there are factors of three uncertainty in the rate coefficients for the dissociation of molecular oxygen by electron impact. In the case of more exotic gases, such as the SiH_4 currently being used in the preparation of hydrogenated amorphous silicon, there are no data available on the electron impact dissociation rate coefficients. Even in the case of water vapor too little data are available at mean electron energies on the order of 0.1 to 0.5 eV for us to determine the effective cross sections for vibrational excitation and for momentum transfer collisions. Because of this there is considerable uncertainty in the electron transport coefficients for electrons with energies on the order of 0.1 eV in moist air, such as is found at sea level. This H_2O case is one in which we do not really know what is necessary to obtain reliable experimental data; thus far, data obtained by conventional techniques have not been self-consistent.

ACKNOWLEDGMENT

The author wishes to acknowledge helpful discussions and correspondence concerning the nonequilibrium phenomena discussed in this paper with S. C. Haydon, L. C. Pitchford and H. R. Skullerud. This work was supported in part by the Army Research Office and by the Air Force Wright Aeronautical Laboratories.

REFERENCES

Allis, W. P., 1982, in this volume.

Allis, W. P. and Rose, D. J., 1954, Phys. Rev., 93:84.

Bacri, J. and Gomes, A. M., 1978, J. Phys. D., 11:2185.

Bacri, J., Gomes, A. M. and Benzaid, S., 1976, J. Phys., D., 9: 1743.

Bates, D. R., 1973 in: "Case Studies in Atomic Physics," M. R. C. McDowell and E. W. McDaniel, eds., North Holland, Amsterdam, p. 57.

Bates, D. R., 1976, Proc. Roy. Soc. London, A, 348:427.
Bates, D. R., Malaviya, V., and Young, N. A., 1971, Proc. Roy. Soc. London, A, 320:437.
Beaty, E. C., Dutton, J., and Pitchford, L. C., 1979, JILA Information Center Report No. 20.
Bekefi, G., 1976, "Principles of Laser Plasmas," Wiley, New York.
Biberman, L., 1947, Zh. Eksp. Teor. Fiz., 17:416.
Biberman, L., 1948, Dokl. Akad. Nauk SSSR, 59:659.
Biberman, L. M., Vorob'ev, V. S., and Yakubov, I. T., 1979, Usp. Fiz. Nauk, 128:233 (1979, Sov. Phys.-Usp., 22:411).
Biondi, M. A., 1976, in: "Principles of Laser Plasmas, " G. Bekefi, ed., Wiley, New York, p. 125.
Boxall, M. J., Chapman, C. J., and Wayne, R. P., 1975, J. Photochem., 4:281.
Braglia, G. L., Bruzzese, R., and Caraffini, G. L., 1979, Lettre al Nuovo Cimento, 25:139.
Brömer, H. H., and Spiewick, F., 1967, Planet. Space Sci., 15:689.
Brunet, H. and Vincet, P. J., 1979, J. Appl. Phys., 50:4700.
Cartwright, D. C., 1978, J. Geophys. Res., 83:517.
Christophorou, L. G., 1978, Radiat. Phys. Chem., 12:19.
Delcroix, J. L., Ferreira, C. M., and Ricard, A., 1976, in: "Principles of Laser Plasma," G. Bekefi, ed., Wiley, New York, Chap. 5.
De Prunelé, E. and Pascale, J., 1979, J. Phys. B, 12:2511.
Devos, E., Boulmer, J., and Delpech, J-F., 1979, J. de Phys., 40:215.
Dotan, I., Albriton, D. L., Lindinger, W., and Pahal, M., 1976, J. Chem. Phys., 65:5028.
Drawin, H. W., Klan, F., and Ringler, H., 1971, Z. Naturforsch., 26a:186.
Dreyer, J. W. and Perner, D., 1972, Chem. Phys. Letters, 16:169.
Druyvesteyn, M. J. and Penning, F. M., 1940, Rev. Mod. Phys., 12:87.
Dutton, J., 1975, J. Phys. Chem. Ref. Data, 4:577.
Ellis, E. and Twiddy, N. D., 1969, J. Phys. B, 2:1366.
Ellis, H. W., McDaniel, E. W., Albritton, D. L., Viehland, L. A., Lin, S. L., and Mason, E. A., 1978, At. Data Nucl. Tables, 22:179.
Ellis, H. W., Pai, R. Y., McDaniel, E. W., Mason, E. A., and Vieland, L. A., 1976, At. Data Nucl. Data Tables, 17:177.
Firestone, R. F., Oka, T., and Takao, S., 1979, J. Chem. Phys., 70:123.
Flannery, M. R., 1970, Ann. Phys., 61:465.
Fleischmann, H. H. and Dehmel, R. C., 1972, Z. Physik, 252:435.
Folkhard, M. A. and Haydon, S. C., 1971, Aust. J. Phys. 24:519.
Folkhard, M. A. and Haydon, S. C., 1973, J. Phys. B, 6:214.
Freund, R. S., 1972, J. Chem. Phys., 56:4344.
Frost, L. S. and Phelps, A. V., 1962, Phys. Rev., 127:1621.
Fujimoto, T., 1979, J. Quant. Spectrosc. Radiat. Transfer, 21:439.
Gallagher, T. F. and Cooke, W. E., 1979, Phys. Rev. A, 19:2161.
Gartner, E. M. and Thrush, B. A., 1975, Proc. Roy. Soc. London, A, 346:121.

Golant, V. E., Zhilinsky, A. P., Sakharov, I. E., and Brown, S. C., 1980, "Fundamentals of Plasma Physics," Wiley, New York, p. 234.
Goldman, M. and Sigmond, R. S., 1982, this volume.
Golubovskii, Yu B., Zakharova, V. M., Kagan, Yu M., and Lyagushchenko, R. I., 1976, Opt. Spektrosk., 40:971.
Gounand, F., Fournier, P. R., and Berlande, J., 1977, Phys. Rev. A, 15:2212.
Gusinow, M. A. and Gerber, R. A., 1972, Phys. Rev. A, 5:1802.
Hayashi, M., 1976, in: "Proceedings, 4th International Conference on Gas Discharges, Swansea," IEE Conf. Publ. No. 143, p. 195.
Hayashi, M., 1979, J. Physique, C7:45.
Haydon, S. C. and Williams, O. M., 1976, J. Phys. D, 9:523.
Holstein, T., 1947, Phys. Rev., 72:1212.
Holstein, T., 1951, Phys. Rev., 83:1159.
Hotop, H., 1980, in: "Electronic and Atomic Collisions," N. Oda and K. Takayanagi, eds., North Holland, Amsterdam, p. 271.
Hurst, G. S., Wagner, E. B., and Payne, M. G., 1974, J. Chem. Phys., 61:3680.
Huxley, L. G. H., and Crompton, R. W., 1974, "The Diffusion and Drift of Electrons in Gases," Wiley, New York, Chap. 1.
Ingold, J. H., 1972, Phys. Fluids, 15:75.
Kline, L. E., 1975, J. Appl. Phys., 46:1994.
Kline, L. E. and Denes, L. J., 1982, in: "Gas Lasers," "Applied Atomic Collision Physics," Vol. 3, W. L. Nighan, ed., Academic, New York, Chap. 3.
Kumar, K., Skullerud, H. R., and Robson, R. E., 1980, Aust. J. Phys., 33:343.
Lawton, S. A., Novick, S. E., Broida, H. P., and Phelps, A. V., 1977, J. Chem. Phys., 66:1381.
Lawton, S. A. and Phelps, A. V., 1978, J. Chem. Phys., 69:1055.
Legler, W., 1963, Z. Physik, 173:169.
Levron, D. and Phelps, A. V., 1979, Bull. Am. Phys. Soc., 24:129.
Lin, S. L., Robson, R. E., and Mason, E. A., 1979, J. Chem. Phys., 71:3483.
Llewellyn-Jones, F., 1982, in this volume.
Lowke, J. J. and Davies, D. K., 1977, J. Appl. Phys., 48:4991.
Lowke, J. J. and Parker, J. H., Jr., 1969, Phys. Rev., 181:302.
Massey, H. S. W. and Burhop, E. H. S., 1952, in: "Electronic and Ionic Impact Phenomena," Oxford, England, p. 633.
McCursker, M., 1979, in: "Excimer Lasers," "Topics in Applied Physics," Vol. 30, C. K. Rhodes, ed., Springer, Berlin, Chap. 3.
McDaniel, E. W. and Mason, E. A., 1973, "The Mobility and Diffusion of Ions in Gases," Wiley, New York, Chap. 5.
McGowan, J. Wm., Kummler, R. H., and Gilmore, F. R., 1975, in: "The Excited State in Chemical Physics," "Advances in Chemical Physics," Vol. 28, J. Wm. McGowan, ed., Wiley, New York, Chap. 6.
Michel, P. and Winkler, R., 1976, Beit. Plasmaphysik, 16:233.
Miloy, H. B. and Crompton, R. B., 1977, Phys. Rev. A, 15:1847.

Moseley, J. T., Snuggs, R. M., Martin, D. W., and McDaniel, E. W., 1969, Phys. Rev., 178:240.
Muller, C. H. III and Phelps, A. V., 1980, J. Appl. Phys., 51:6141.
Niehaus, A., 1981, in: "The Excited State in Chemical Physics," "Advances in Chemical Physics," Vol. 45, Part 2, Wm. McGowan, ed., Wiley, New York, p. 399.
Nighan, W. L. and Wiegan, W. J., 1974, Phys. Rev., 10:922.
Pai, R. Y., Ellis, H. W., Akridge, G. R., and McDaniel, E. W., 1975, Phys. Rev. A, 12:1781.
Parkes, D. A., 1974, Vacuum, 24:561.
Payne, M. G., Talmage, J. E., Hurst, G. S., and Wagner, E. B., 1974, Phys. Rev. A, 9:1050.
Penney, G. W. and Hummert, G. T., 1970, J. Appl. Phys., 41:572.
Percival, I. C. and Richard, D., 1975, in: "Advances in Atomic and Molecular Physics," D. R. Bates and B. Bederson, eds., Academic, New York, p. 1.
Phelps, A. V., 1960, Phys. Rev., 117:619.
Phelps, A. V., 1980, unpublished.
Phelps, A. V. and McCoubrey, A. O., 1960, Phys. Rev., 118:1561.
Pitaevskii, L. P., 1962, Zh. Eksp. Teor. Fiz.-JETP, 42:1326 (1962, Sov. Phys.-JETP, 15:919).
Pitchford, L. C., 1982, in this volume.
Pitchford, L. C., O'Neil, S. V., and Rumble, J. R., Jr., 1981, Phys. Rev. A, 23:294.
Pitchford, L. C. and Phelps, A. V., 1982, Phys. Rev. A, 25:540.
Rees, A., 1982, in this volume.
Reid, I. D., 1979, Aust. J. Phys., 32:231.
Rutscher, A. and Pfau, S., 1976, Physica, 81C:395.
Shemansky, D. E. and Carleton, N. P., 1969, J. Chem. Phys., 51:689.
Shimamori, H. and Fessenden, R. W., 1981, J. Chem. Phys., 74:453.
Shuker, R., Gallagher, A., and Phelps, A. V., 1980, J. Appl. Phys., 51:1306.
Skullerud, H. R., 1977, in: "Proceedings, 13th International Conference on Phenomena in Ionized Gases, Berlin," VEB Export-Import, Leipzig, p. 303.
Skullerud, H. R., 1982, in this volume.
Smith, D. and Adams, N. G., 1979, in: "Gas Phase Ion Chemistry," Vol. 1, M. T. Bowers, ed., Academic, New York, Chap. 1.
Tachibana, K. and Phelps, A. V., 1979, J. Chem. Phys., 71:3544.
Tagashira, H., Sakai, Y., and Sakamoto, 1977, J. Phys. D, 10:1051.
Thomas, W. R. L., 1969, J. Phys. B, 2:551.
Thonnard, N. and Hurst, G. S., 1972, Phys. Rev. A, 5:1110.
Townsend, J. S., 1915, "Electricity in Gases," Clarendon, Oxford.
Urošević, V. V., Petrović, A. Lj., Bozin, J. V. and Zeković, Lj. D., 1980, in: "Proceedings, Symposium on the Physics of Ionized Gases," B. Čobić, ed., Boris Kidric Institute, Beograd, p. 88.
Vagner, S. D., Kagan, Yu. M., and Niskonen, I. S., 1977, Zh. Tekh. Fiz., 47:772 (1977, Sov. Phys. Tech. Phys., 22:465).
Vriens, L. and Smeets, A. H. M., 1980, Phys. Rev., 22:940.

Warman, J. M., Sennhauser, E. S., and Armstrong, D. A., 1979, J. Chem. Phys., 70:995.
Winker, R., Michel, P., and Wilhelm, J., 1978, Beit. Plasmaphysik, 18:31.
Yamabe, C. and Phelps, A. V., 1981, in: "Proceedings, 34th Gaseous Electronics Conference, Boston."
Zajonc, A. G., and Phelps, A. V., 1981, Phys. Rev. A, 23:2479.

ELECTRONEGATIVE GASES[†]

L. G. Christophorou[‡]

Atomic, Molecular, and High Voltage Physics Group
Health and Safety Research Division
Oak Ridge National Laboratory
Oak Ridge, Tennessee 37830

A DEFINITION

An electronegative gas is an electron attaching gas in which long-lived negative ions (parent and/or fragment) are produced. The electron attaching species must have a positive (>0 eV) electron affinity; metastable anions may require (collisional) stabilization for their detection.

BASIC ELECTRON ATTACHMENT PROCESSES

The basic processes via which negative ions are formed in electron-molecule collisions at low energies ($\gtrsim$15 eV) -- neglecting those at higher energies (e.g., ion-pair processes) and those involving collisions of molecules with electronically-excited species (e.g., metastable atoms, Rydbert states) -- may be classified as follows:

(1) Electron attachment to ground-state molecules predominantly in their lowest state(s) of internal excitation:

[†]Research sponsored by the Division of Electrical Energy Systems, U.S. Department of Energy, under contract W-7405-eng-26 with the Union Carbide Corporation.

[‡]Also Department of Physics, University of Tennessee, Knoxville, Tennessee 37916.

$$e(\varepsilon) + AB...CD(G;\ \nu \simeq 0) \xrightarrow{\sigma_o(\varepsilon)} AB...CD^{-*}(G \text{ or } E) \begin{cases} \rightarrow AB...CD^{(*)} + e(\varepsilon') & (1) \\ \Longrightarrow AB^{(*)} + CD^- \\ \quad\quad [AB + C]^{(*)} + D^- & (2a) \\ \text{or} \\ \Longrightarrow AB^{(*)} + CD^{-*} \begin{cases} \rightarrow CD^{(*)} + e \\ \rightarrow C^{(*)} + D^- \end{cases} & (2b) \\ \rightarrow AX^- + \text{energy} & (3) \end{cases}$$

where $e(\varepsilon)$ is the impacting electron of energy ε; $AB...CD(G;\ \nu \simeq 0)$ is a neutral ground-state polyatomic molecule predominantly in its lowest vibrational, ν, state of excitation; $AB...CD^{-*}(G \text{ or } E)$ is a transient negative ion formed in either the field of the ground (G) or excited (E) electronic state with a capture cross section $\sigma_o(\varepsilon)$; and $\varepsilon'(\leq\varepsilon)$ is the energy of the scattered electron. The asterisk indicates excess internal energy, and the asterisk in parenthesis indicates possible increase in the internal energy of the corresponding species. Reaction (1) is indirect elastic and inelastic electron scattering. Reaction (2a) is dissociative attachment leading to stable fragment negative ions (for a polyatomic molecule this process can lead to simultaneous multiple fragmentation). Reaction (2b) is dissociative attachment leading to metastable negative ion fragment(s) which are subject to autodetachment and/or autodecomposition. Reaction (3) is parent negative ion formation which is possible when the electron affinity, EA, of AB...CD is positive (>0 eV), and the excess internal energy is removed, principally by collision with another body. All three reactions have been studied extensively, especially over the last decade. At room temperature the preponderance of AB...CD molecules are in the $\nu = 0$ level. However, depending on the molecule, even a small population of higher vibrational and/or rotational levels can affect significantly the cross sections and the onsets, especially for reaction(s) (2) (see later section "Dissociative Electron Attachment...").

(2) Electron attachment to "hot" molecules:

$$e(\varepsilon) + AB...CD^*(G;\ \nu > 0;\ j > 0) \xrightarrow{\sigma_{o,\nu,j}(\varepsilon)} AB...CD^{-*}(G \text{ or } E) \rightleftarrows \text{decay}. \quad (4)$$

Here the molecule $AB...CD^*$ is in the ground electronic state but in higher rotational, j, and/or vibrational, ν, states. In this case, the cross section for formation $\sigma_{o,\nu,j}(\varepsilon)$ and the probability of

the ensuing decomposition(s) depend on the vibrational and/or rotational quantum states. Reaction (4) is appropriate to "hot" gases, and it has been investigated recently.

(3) Electron attachment to electronically excited molecules:

$$e(\varepsilon) + AB...CD^{*}(E) \xrightarrow{\sigma_E(\varepsilon)} AB...CD^{*-}(E) \rightleftarrows \text{decay}. \qquad (5)$$

Here the electron is captured by an electronically excited molecule with a cross section $\sigma_E(\varepsilon)$ forming $AB...CD^{*-}(E)$ in the field of an excited electronic state. Very little is known about this process.

MODES OF ELECTRON CAPTURE BY MOLECULES

The various ways by which slow electrons attach to molecules have been well reviewed (see, for example, Bardsley and Mandl, 1968; Christophorou, 1971, 1978a, 1980a; Schulz, 1973; Massey, 1976; Christophorou et al., 1977). In general, four such mechanisms leading to the formation of a transient negative ion [negative ion resonance (NIR)] can be distinguished:

(1) Shape resonances

(2) Nuclear-excited Feshbach resonances

(3) Core-excited resonances (type I)

(4) Core-excited resonances (type II).

In Fig. 1a we illustrate schematically (1). Here, the electron affinity, EA, of the molecule is negative (<0 eV), and the incident electron is trapped in the potential well which arises from the interaction between the electron and the neutral molecule in its ground electronic state. This potential barrier is the combined effect ($V_{effective}$ in Fig. 1a) of the attractive polarization potential between the neutral molecule and the incident electron ($V_{attractive}$ in Fig. 1a) and the repulsive centrifugal potential which arises from the relative motion of the two bodies ($V_{repulsive}$ in Fig. 1a; this varies as $\ell(\ell+1)/2\rho^2$ where ℓ is the angular momentum quantum number and ρ is the electron-molecule separation). Since the negative ion potential energy curve/surface for a shape resonance lies above that of the neutral molecule, the transient negative ion is subject to autodetachment, decaying back to the neutral molecule in its ground electronic state plus a free electron, leaving the neutral molecule with or without vibrational and/or rotational energy. The lifetime, τ_a, for this autodetachment process is a function of both the size of the barrier and the energy of the anion (i.e., the relative height and thickness of the barrier through which the electron has to penetrate). The former is strongly

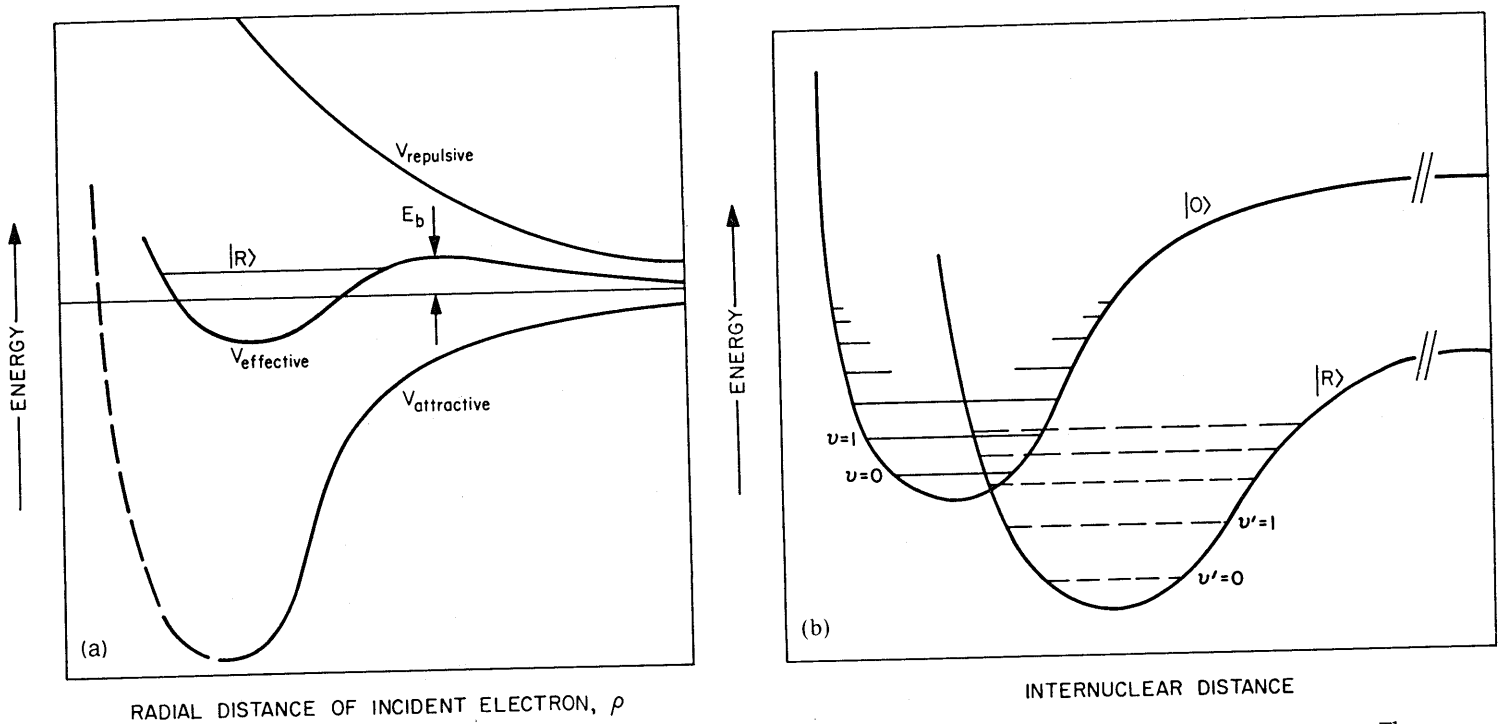

Fig. 1. Schematic illustration of (a) shape and (b) nuclear-excited Feshbach resonances. The symbols |0> and |R> designate, respectively, the electronic ground state of the neutral molecule and the NIS (Christophorou et al., 1977).

dependent on the ℓ of the state occupied by the captured electron, and the latter largely on the attractive portion of the potential. If energetically possible, the NIR can undergo dissociative attachment. Such NIRs may involve an excited electronic state of the neutral molecule, and in this case, they are called core-excited (type II) resonances.

In Fig. 1b we illustrate schematically the nuclear-excited Feshbach resonance. Here EA is positive (>0 eV), and the NIR lies energetically below the ground state of the neutral. Thus, unless the anion is in vibrational levels ν' higher than the lowest vibrational level $\nu = 0$ of the parent neutral state, the NIR cannot decay into the parent state. This mode of electron capture can involve an electronically excited neutral molecule, in which case the NIR is called core-excited (type I).

Molecular NIR states are abundant (e.g., Schulz, 1973; Christophorou, 1978b, 1980a, 1981a). Often they can be described [and their energies (positions) approximated] in terms of the unoccupied molecular orbitals of the neutral molecule. At times, also, molecular geometrical changes concomitant with electron impact and strong electrophore sites in a polyatomic molecule can constitute effective modes of electron trapping (Christophorou, 1978a).*

THE BINDING OF ATTACHED ELECTRONS TO MOLECULES ("ELECTRON AFFINITY")

The electron affinity (EA) of a molecule is normally defined as the difference in energy between the neutral molecule plus an electron at rest at infinity and the molecular negative ion when both, neutral molecule and negative ion, are in their ground electronic, vibrational and rotational states (Christophrou, 1971). The electron affinity can be positive (>0 eV) or negative (<0 eV) (see Fig. 2). Two other quantities, the vertical-detachment energy (VDE) and the vertical-attachment energy (VAE), are closely related to EA, the former when EA is positive and the latter when EA is negative. The VDE is defined (Christophorou, 1971) as the minimum energy required to eject the electron from the negative ion in its ground electronic and nuclear state without changing the internuclear separation, and the VAE is defined (Christophorou, 1971) as the difference in energy between the neutral molecule in its ground electronic, vibrational and rotational states plus the electron at rest at infinity, and the molecular negative ion formed by addition of the electron to the neutral molecule without allowing a change in the internuclear separation of the constituent nuclei. The schematic

---

*Electron attachment to molecular clusters and van der Waals dimers is not considered in the present discussion.

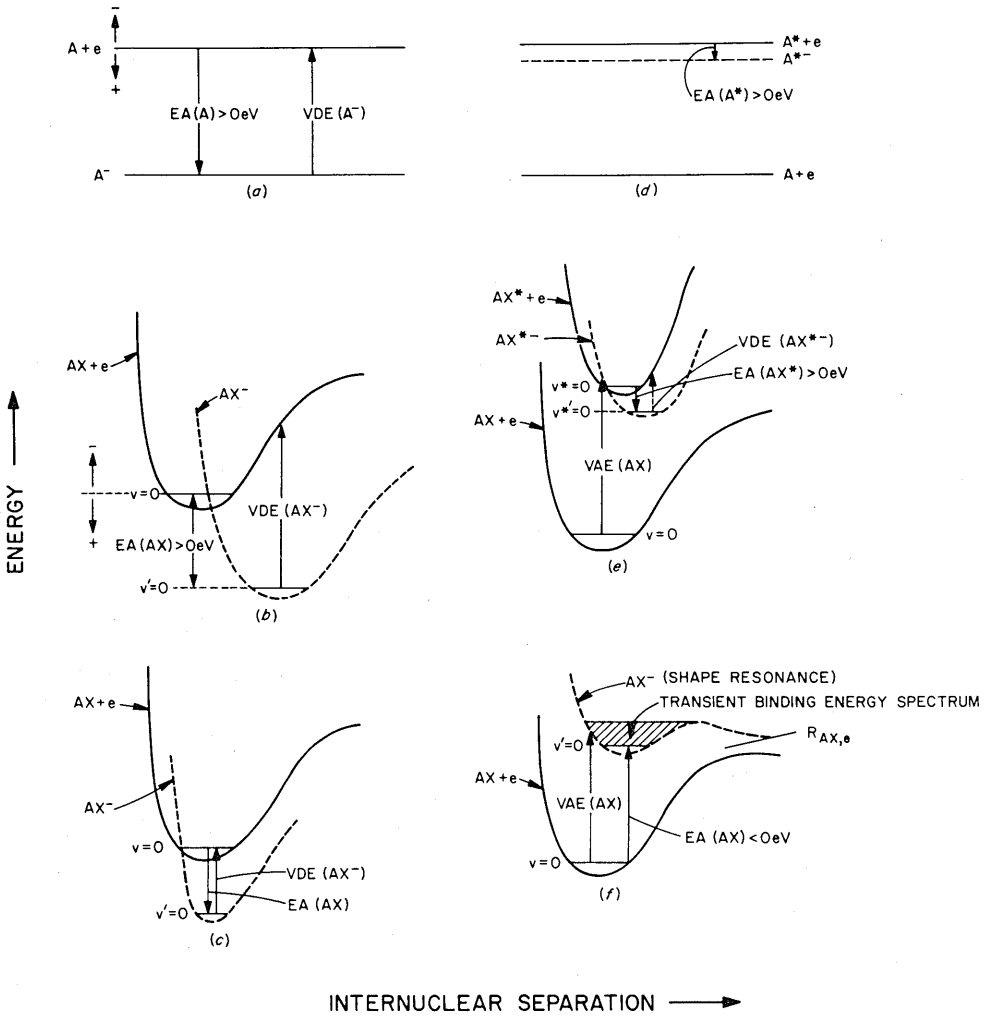

Fig. 2. Schematic diagrams illustrating the positive and negative values of EA and the relation of EA to VAE and VDE and the modes of electron capture (Christophorou, 1980a).

diagrams in Fig. 2 clarify the physical significance of these quantities and their relation to the various modes of electron capture discussed in the previous section.

Figures 2a, b, c refer to an electron captured in the field of the ground electronic state of an atom (Fig. 2a) and a diatomic molecule (Fig. 2b and c). In all three cases, the EA is positive and the traditional measurements of EA are typical of these cases.

In Fig. 2a EA(A) = $|VDE(A^-)|$; this is always the case for atoms. For molecules, however, EA(AX) = $|VDE(AX^-)|$ only if the equilibrium internuclear separation for AX and AX^- are the same (as shown in Fig. 2c). Although for some small molecular species, this is the case (see, e.g., Christophorou, 1971; Hotop and Lineberger, 1975), in the majority of molecular species a situation similar to that in Fig. 2b prevails for which $|VDE(AX^-)| > EA(AX)$. Cases b and c are, of course, typical examples of nuclear-excited Feshbach resonances (see previous section).

Figures 2d and 2e illustrate the case of electron-excited Feshbach resonances (core-excited type I) for atoms and molecules, respectively. Here the electron is captured in the field of an excited atom A^* or an electronically excited molecule AX^*, forming, respectively, A^{*-} and AX^{*-}. Note our nomenclature: A^{*-} and AX^{*-} indicate, respectively, a negative ion formed by electron capture by an electronically excited atom or molecule; while A^{-*} and AX^{-*} indicate, respectively, an atomic and molecular negative ion with excess internal energy. The $EA(A^*)$ and $EA(AX^*)$ now refer to the electron affinity of the excited atom A^* and the electronically excited molecule AX^*; they are both positive and can be greater than those of the corresponding ground-state species. Actually the electron affinity of the ground state atom or molecule can be negative while that for the corresponding excited species positive.

In Fig. 2f, a case is depicted which is appropriate for a shape resonance. It should be noted that although in this case $VAE(AX) \leq -EA(AX)$, the electron is temporarily bound to the molecule with a "transient binding energy spectrum" shown by the shaded area in Fig. 2f. The coordinate system depicting the potential well is indicated in the figure by $R_{AX,e}$, the radial distance of the electron which is different from that of the internuclear separation.

The electron affinities of atoms and molecules and the methods used for their determination have been reviewed by many authors (e.g., Christophorou, 1971; Hotop and Lineberger, 1975; Blaunstein and Christophorou, 1971; Franklin and Harland, 1974; Rosenstock et al., 1977).

SHORT-LIVED TRANSIENT NEGATIVE IONS

Short-lived ($\lesssim 10^{-12}$ s) transient negative ions are common phenomena in low-energy electron-molecule collisions. In the incident electron energy range in which the temporal trapping of the electron occurs, the magnitude of the electron-scattering cross section changes profoundly, and the "resonance" signifies the existence and gives the position of the negative ion state. Such short-lived negative ion states--lying above the ground state of the neutral molecule--are abundant and decay by autodetachment (indirect electron scattering) and/or by dissociative attachment. This indirect

electron scattering is a most efficient way of slowing-down subexcitation electrons in electrically stressed gases. As an example, representative data are shown in Fig. 3 for H_2 and N_2 whose main features elucidate a number of points directly relevant to breakdown.

(1) Rotational excitation cross sections are substantial to electron energies $\geq$ 10 eV.

(2) Vibrational excitation cross sections are also substantial to high energies; these decrease with increasing vibrational quantum number.

(3) The total cross sections are much larger than the overall inelastic scattering cross section, dramatizing the large probability for elastic electron scattering in the subexcitation energy range.

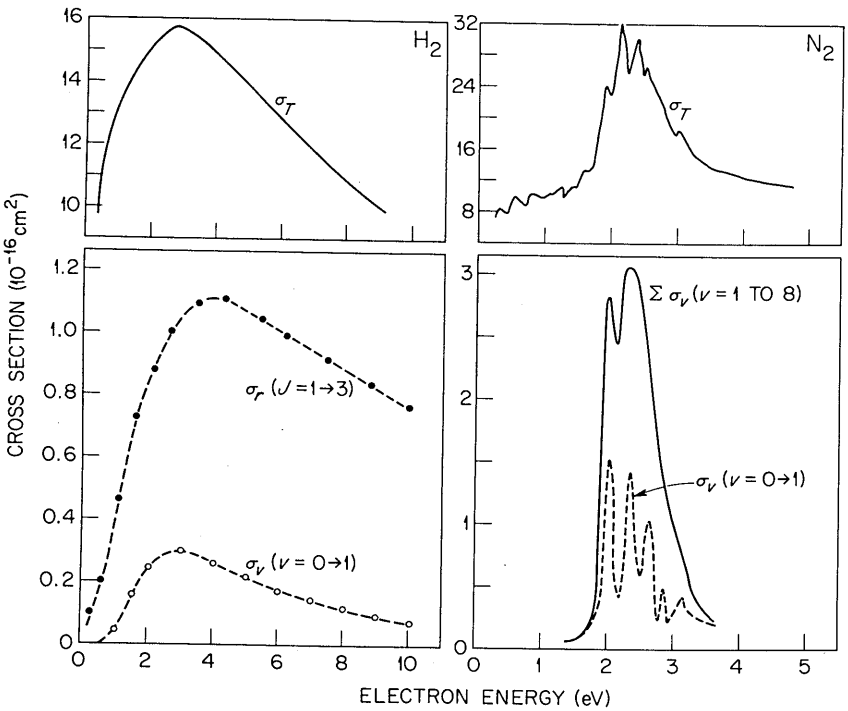

Fig. 3. Energy dependence of electron scattering cross sections for H_2 and N_2: total electron scattering cross section, σ_T, for H_2 (Golden et al., 1966) and N_2 (Golden, 1966), vibrational excitation cross section for $\nu = 0 \rightarrow \nu = 1$ transition, $\sigma_\nu(\nu = 0 \rightarrow 1)$, for H_2 (Linder and Schmidt, 1971) and N_2 (Schulz, 1964); rotational excitation cross section for the $J = 1 \rightarrow J = 3$ transition, $\sigma_r(J = 1 \rightarrow 3)$, for H_2 (Linder and Schmidt, 1971). $\Sigma\sigma_\nu(\nu = 1$ to 8) (from Christophorou, 1978b).

(4) The cross sections for elastic, rotational, and vibrational excitation are all strongly affected by NIRs, indicating that a large fraction of these are indirect, via the decay of such resonances. This is particularly dramatized by the N_2 data where $\Sigma\sigma_\nu(\nu = 1 \text{ to } 8)$ is the sum of the vibrational excitation cross sections for the first eight ($\nu = 1$ to $\nu = 8$) vibrational levels of N_2 via the decay of the $N_2^{-*}(2\Pi_g)$ shape resonance.

At low energies, polyatomic molecules which are good electron scavengers can be simultaneously good electron thermalizers owing to their complex structure and the availability of a multiplicity of rotational, vibrational, and low-lying NIR states. Through a combination of gases, NIR states can be positioned over the entire subexcitation energy range, keeping in this way the electron energies low (e.g., see Christophorou, 1978b, 1981a; Christophorou et al., 1979a, 1981a).

DISSOCIATIVE ELECTRON ATTACHMENT TO GROUND-STATE MOLECULES

As indicated in an earlier section, resonant dissociative electron attachment is visualized proceeding through a negative ion intermediate--formed by capture of an electron in a restricted energy range defined by a Franck-Condon transition between the initial (neutral molecule and electron at infinite separation) and the final state representing the transient negative ion--which dissociates into (often multiple) neutral and negative-ion fragments. The reaction has been studied extensively in recent years both experimentally and theoretically.

The cross section, $\sigma_{da}(\varepsilon)$, for dissociative attachment as a function of electron energy, ε, is equal to the product of the cross section, $\sigma_o(\varepsilon)$, for capture of the electron by the molecule to form the metastable negative ion intermediate and the probability, $p(\varepsilon)$, that the transient negative ion will decay via dissociative attachment (rather than autodetachment or the other possible decay channels); see earlier section, namely

$$\sigma_{da}(\varepsilon) = \sigma_o(\varepsilon)p(\varepsilon). \tag{6}$$

Expressions for $\sigma_o(\varepsilon)$ and $p(\varepsilon)$ have been given for diatomic molecules. Following O'Malley (1966), we write for $\sigma_{da}(\varepsilon)$ for a diatomic molecule AX initially in its lowest vibrational level ($\nu = 0$) and with a purely repulsive negative ion state (Fig. 4):

$$\sigma_{da}(\varepsilon)_{\nu=0} = \frac{4\pi^{3/2}}{(2m/\hbar^2)\varepsilon}\frac{g}{}\frac{\Gamma_a}{\Gamma_d}\underbrace{\exp\left[\frac{\Gamma_a^2 - 4(\bar{\varepsilon}_o - \varepsilon)^2}{\Gamma_d^2}\right]}_{\sigma_o(\varepsilon)}\underbrace{e^{-\rho(\varepsilon)}}_{p(\varepsilon)} . \tag{7}$$

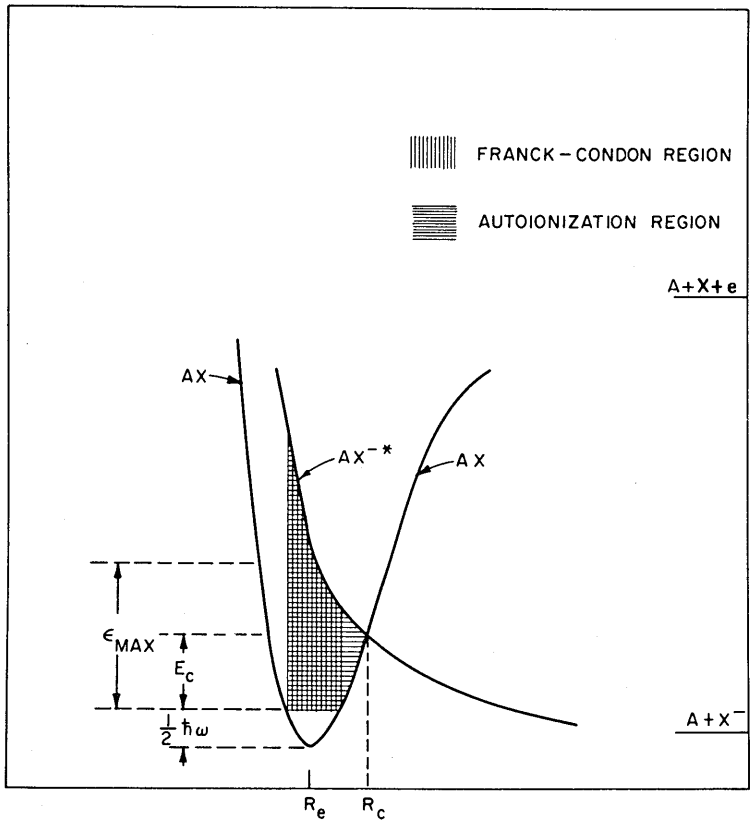

Fig. 4. Schematic potential energy diagram illustrating the process of dissociative electron attachment for a diatomic molecule.

In Eq. (7) m is the electron mass; $\hbar$ is Planck's constant divided by 2π; $\bar{g}$ is a statistical factor; Γ_a is the total autodetachment width; $\Gamma_{\bar{a}}$ is the partial autodetachment width; Γ_d is the dissociative attachment resonance width, $\bar{\varepsilon}_o = \varepsilon_o + \frac{1}{2}\hbar\omega$ (see Fig. 4); ε_o is the electron energy at the peak of $\sigma_{da}(\varepsilon)$; $1/2\,\hbar\omega$ is the zero-point energy; and $e^{-\rho(\bar{\varepsilon})}$, referred to as the survival probability, is now explicitly defined as

$$e^{-\rho(\varepsilon)} = \exp\left(-\int_{R_\varepsilon}^{R_c} \frac{\Gamma_a(R)}{\hbar v(R)}\, dR\right) \simeq \exp(-\bar{\tau}_s/\bar{\tau}_a) \quad . \tag{8}$$

In Eq. (8), R_ε is the interatomic separation at which electrons of energy ε reach the negative ion state [within the Franck-Condon region (see Fig. 4)]; R_c is the value of R at the crossing point between the negative ion AX^{-*} and the neutral molecule AX potential energy curves (for $R > R_c$, $p = 1$); v(R) is the relative velocity of separation

of separation of A and X^-;

$$\bar{\tau}_s = \int_{R_\varepsilon}^{R_c} \frac{dR}{v(R)} \quad \text{and} \quad \bar{\tau}_a = \frac{\bar{n}}{\bar{\Gamma}_a} \ .$$

Although Eq. (7) is limited, strictly speaking, to situations as pictured in Fig. 4, it relates in a general way σ_{da} to σ_o, ε, τ_s, τ_a and the reduced mass, M_r, of the A - X^- system. It explains nicely the various isotope effects observed in dissociative attachment studies (see Chap. 6 in Christophorou, 1971).

Negative ion potential energy curves/surfaces have a variety of shapes, and $\sigma_{da}(\varepsilon)$ is affected by these and the competitive decay channels. This limits the applicability of Eq. (7), especially in the case of polyatomic molecules. However, in certain cases of dissociative attachment to polyatomic molecules such as $n\text{-}C_NH_{2N+1}Br$, where the formation of Br^- involves a direct fast cleavage of Br^- along the C-Br coordinate, and the complex molecule may be visualized, as far as this process is concerned, as a diatomic-like $R(n\text{-}C_NH_{2N+1})^-$ Br system, Eq. (7) may describe the process satisfactorily (Christophorou et al., 1971a).

In the case of polyatomic molecules, many types of fragment ions can be produced and dissociative attachment processes may not be fast; the dissociation time would depend on the distribution of the internal energy in the transient intermediate, the structural rearrangements following electron capture, and the orbital in which the electron is captured. The modes of decomposition and the nature of the fragment negative ions, thus, strongly depend on the details of molecular structure. We may identify four types of dissociate attachment fragment negative ions (see Christophorou, 1980a and Fig. 15):

(1) Directly cleaved,

(2) Complementary,

(3) Multiple,

(4) Rearrangement.

The multiplicity of negative ion states and the production of a variety of negative ion fragments with large cross sections clearly show the fragility of metastable polyatomic negative ions and the effectiveness of slow (including thermal) electrons to cause extensive and often multiple molecular decompositions tantamount to a molecular "explosion." This and the delicate dependence of the type and abundance of negative ions on the details of molecular

structure can, perhaps, be illustrated by the work of Johnson et al. (1977) on the negative ions produced in collisions of slow ($\lesssim$3 eV) electrons with chlorethanes and chlorethylenes. For these chlorocarbons, the transient anions, M^{-*}, fragment, even when they are formed by the capture of electrons with virtually zero energy, through a multiplicity of channels. Depending on M^{-*}, all or part of the decomposition channels are shown below were found (Johnson et al., 1977) to be possible:

$$e + M \longrightarrow M^{-*} \begin{cases} \longrightarrow M^{(*)} + e^{(')} \\ \longrightarrow (M - Cl) + Cl^- \\ \longrightarrow Cl + (M - Cl)^- \\ \longrightarrow (M - 2Cl) + Cl_2^- \\ \longrightarrow M^{-*} \text{(long-lived; } > 10^{-6} \text{ s)}. \end{cases}$$

The cross section for Cl^- production (Fig. 5) indicates the existence of five maxima below ~2.0 eV for the chloroethylenes (and also for the chloroethanes). It seems that these are not due to vibrational

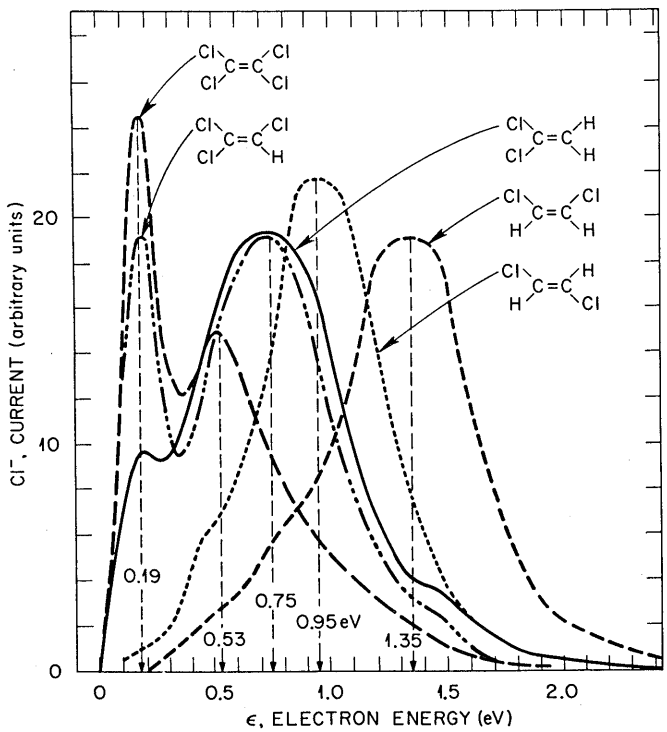

Fig. 5. Comparison of the energy dependence of the Cl^- yield for the chloroethylenes (Johnson et al., 1977).

excitation, but rather to separate NIR states associated (Johnson et al., 1977) with orbitals dominated by the p-orbitals of the Cl atom. Their positions are relatively insensitive, and their cross sections very sensitive to the details of the molecular structure. A similar behavior is exhibited by a number of freons and perfluorocarbons (e.g., see Christophorou 1978b, 1980a, 1981a; Christodoulides et al., 1979; Pai et al., 1979; McCorkle et al., 1980a; Sauers et al., 1979).

Although for the molecules in Fig. 5, dissociative attachment processes are expected to be fast ($<<10^{-6}$s), for $C_2Cl_4^{-*}$ at ~0.0 eV (and for a number of other autodissociating long-lived parent negative ions), both the autodissociation and the autodetachment processes are slow, as a result of vibrational redistribution of internal energy (Christophorou, 1978a).

An extensive study of electronegative gases using the swarm and also mass spectrometric methods has been undertaken in recent years at the author's laboratory at Oak Ridge National Laboratory and the University of Tennessee. In these studies, the electron attachment rate constant k_a is measured as a function of E/N (ratio of electric field strength to number density) for molecules mixed in minute amounts with a buffer gas such as N_2 or Ar for which the electron energy distribution functions can be determined as a function of E/N since it is then possible to quantify the dependence of k_a on the mean energy $\langle\varepsilon\rangle$ and to calculate the total electron attachment cross section function, $\sigma_a(\varepsilon)$, from the measured $k_a(E/N)$ and the calculated $f(\varepsilon,E/N)$. The measured rate constant, k_a, is related to $\sigma_a(\varepsilon)$ by

$$k_a = (2/m)^{\frac{1}{2}} \int_0^\infty \sigma_a(\varepsilon)\varepsilon^{\frac{1}{2}} f(\varepsilon,E/N)d \ , \qquad (9)$$

where m is the electron mass. A deconvolution procedure has been developed (Christophorou et al., 1971b) whereby $\sigma_a(\varepsilon)$ is determined from an integral solution to Eq. (9) from the measured $k_a(\langle\varepsilon\rangle)$ and $f(\varepsilon,E/N)$. Examples of $k_a(\langle\varepsilon\rangle)$ are shown in Figs. 6 and 7 and swarm-unfolded $\sigma_a(\varepsilon)$ in Fig. 7 (see also Figs. 14 and 16). The data in Figs. 6 and 7 show the effect of F substitution as well as the effect of the number and relative positions of the Cl atoms in the molecule on the energies and corresponding cross sections of the negative ion states of these compounds. For a given number of Cl atoms in these molecules, replacement of H by F lowers the positions of the resonance maxima and increases the magnitude of $\sigma_a(\varepsilon)$; the magnitude of $\sigma_a(\varepsilon)$ increases with increasing number of Cl atoms in the molecule. The 1,1,1- or 1,1-isomers capture electrons much more efficiently than the 1,1,2- or 1,2-isomers, and the positions of the resonance maxima lie in the lower energies for the former than for the latter.

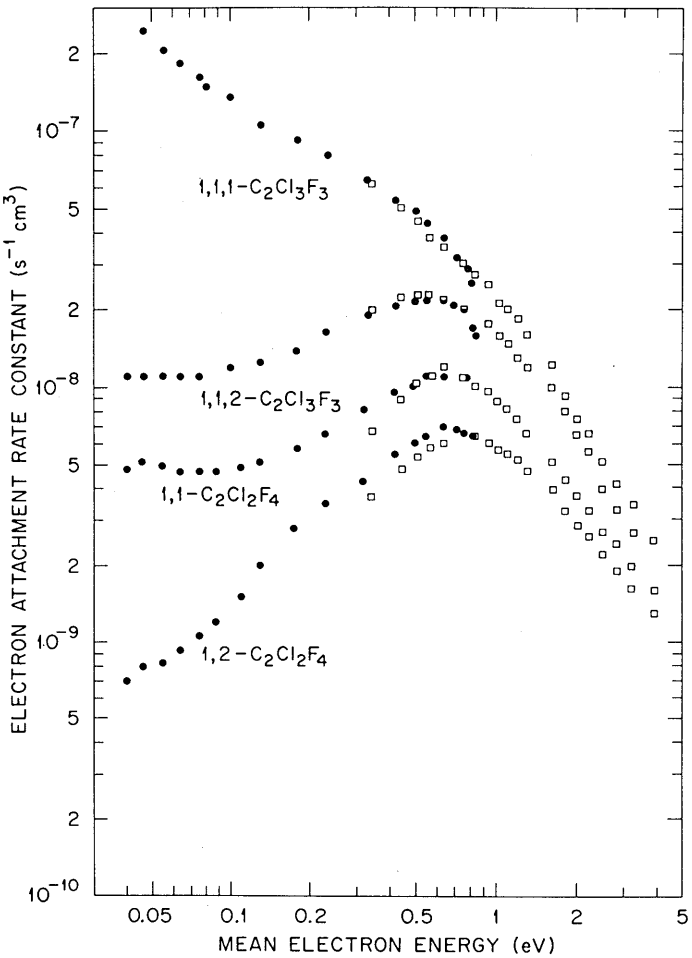

Fig. 6. Total electron attachment rate constants vs. mean electron energy for the chlorofluoroethanes measured in N_2(•) and Ar(□) (McCorkle et al., 1980b).

Although the attachment cross sections reported here are "total" (i.e., for all negative ions produced), mass spectrometric studies show that the predominant ion is Cl^- (other fragment anions are produced but with much lower yields). This is shown in Fig. 8 for 1,1,1-$C_2Cl_3F_3$. In general, aliphatic halocarbons have large cross sections for electron attachment, and molecular decomposition via electron attachment proceeds through a multiplicity of negative ion states. This molecular decomposition needs to be considered when such compounds are used as dielectrics in view of its possible effect on the long-range stability of the dielectric.

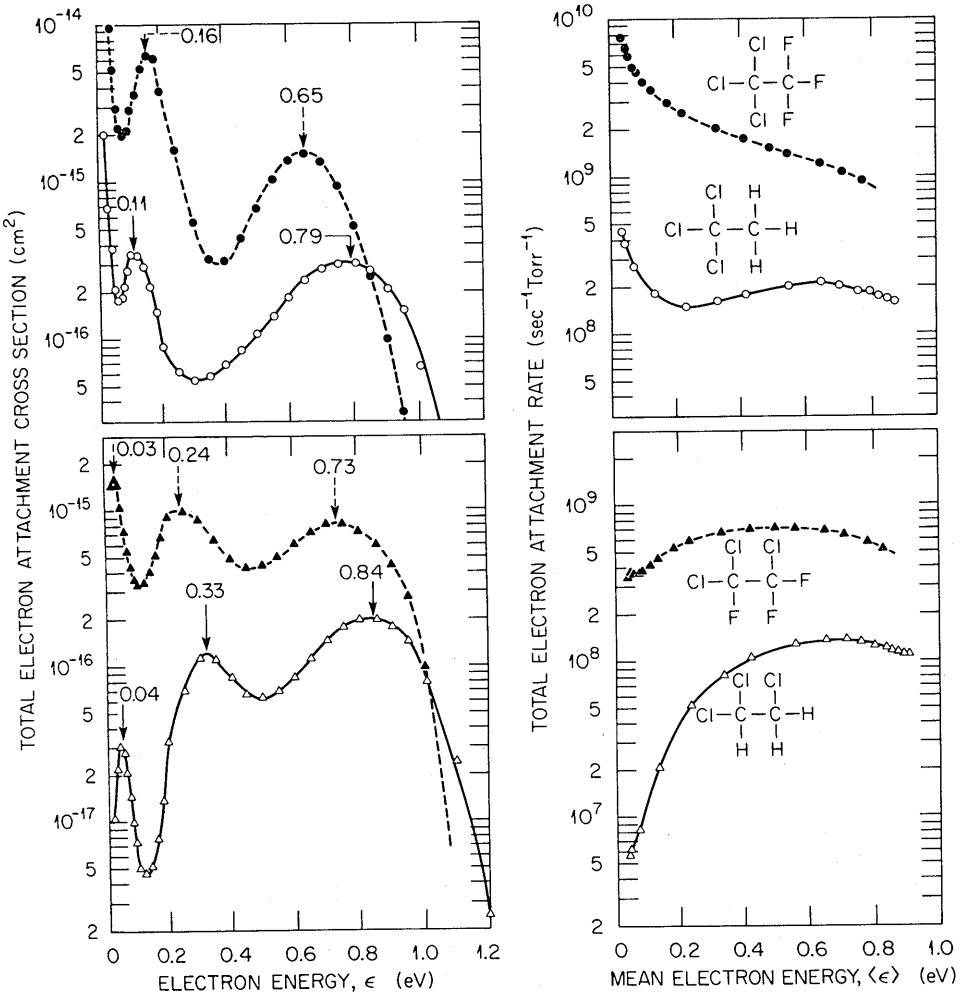

Fig. 7. Total electron attachment rates as a function of mean electron energy, and swarm-unfolded electron attachment cross sections as a function of electron energy for chlorofluoroethanes (McCorkle et al., 1980b). Note that the electron attachment rates are in units of s^{-1} $torr^{-1}$. To change to s^{-1} cm^3 units, divide by 3.25×10^{16}.

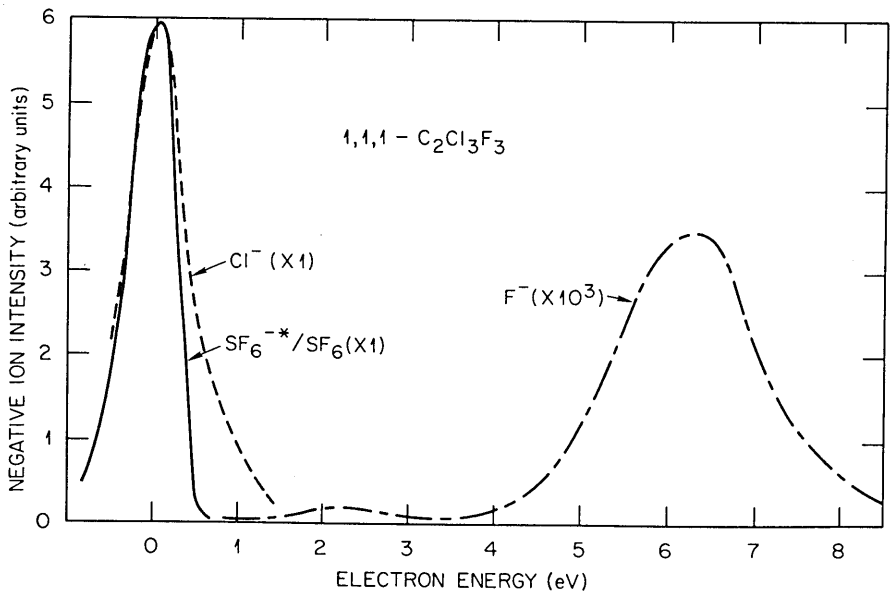

Fig. 8. Negative ion intensity as a function of electron energy for Cl^- and F^- from 1,1,1-$C_2Cl_3F_3$ compared with SF_6^{-*} from SF_6 (Christophorou et al., 1979b).

Finally, in Fig. 9, $\sigma_{da}(\varepsilon)$ are represented for a number of molecules in the energy range from 0 to ~16 eV. We point out three of the salient features of the behavior of σ_{da}:

(1) The magnitude of σ_{da}--varying by more than seven orders of magniture--depends on the position, ε_{max}, of the NIR state; the higher the ε_{max} the smaller the σ_{da}.

(2) As $\varepsilon_{max} \rightarrow$ thermal, $\sigma_{da} \rightarrow \pi\lambda\!\!\!^{-2}$ [where $\pi\lambda\!\!\!^{-2}$ is the s-wave capture across section (see later section)].

(3) Many molecules possess a multiplicity of NIRs in the subexcitation energy region.

DISSOCIATIVE ELECTRON ATTACHMENT TO "HOT" MOLECULES (EFFECTS OF TEMPERATURE ON ELECTRON ATTACHMENT)

Electron attachment processes are often affected by the gas temperature, T. The effects of temperature on the various electron attachment processes are of intrinsic value, of basic significance to determinations of thermodynamic data from electron attachment studies, and of interest to many applied areas (employing temperatures higher than ambient) where electron densities are crucially affected by negative ion formation. The effects of temperature on

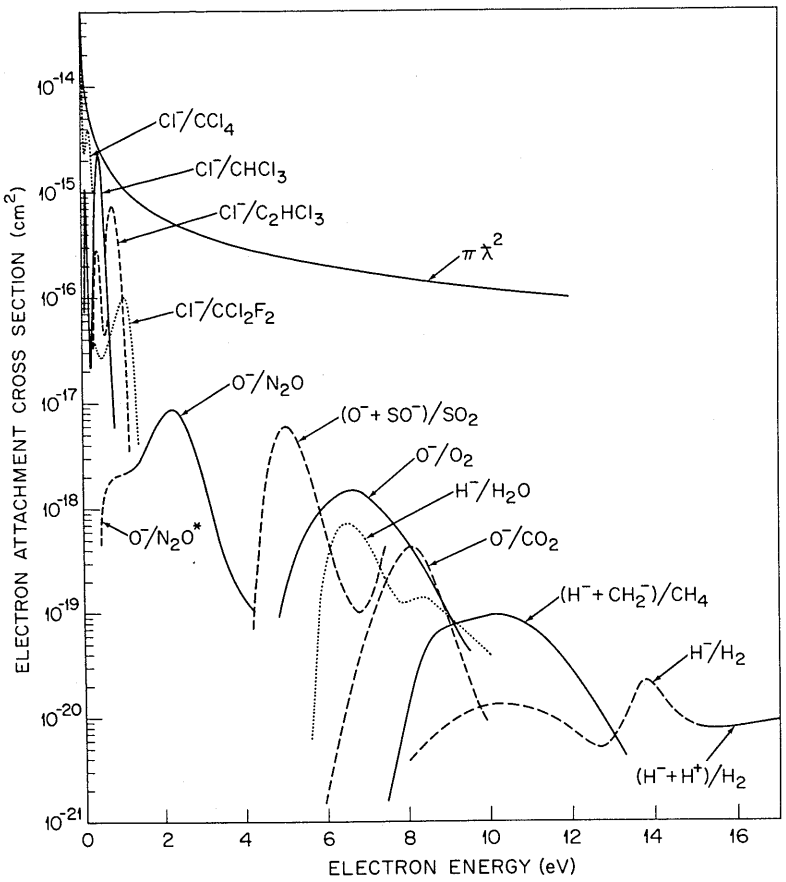

Fig. 9. Dissociative attachment cross sections as a function of electron energy for a number of molecules. Some of the plotted $\sigma_{da}(\varepsilon)$ were deduced from swarm experiments and are thus "total" cross sections. They are identified with the specific ions as shown because these were the most abundant in mass spectrometric studies. Some of the molecules shown have other resonances which were not plotted for convenience of display. O^-/N_2O^* denotes dissociative attachment from vibrationally excited N_2O molecules, and $(H^- + H^+)/H_2$ denotes ion-pair formation from H_2 (Christophorou, 1978b).

the magnitude and energy dependence of the cross section for specific and total negative ion production have been investigated by both the electron beam (Hickam and Berg, 1958; Fite and Brackmann, 1963; Fite et al., 1965; Henderson et al., 1969; Spence and Schulz, 1969, 1973; Chantry, 1969; Chen and Chantry, 1970, 1971, 1979; Allan and Wong, 1978, 1981) and the electron swarm (Compton et al., 1966; Wentworth et al., 1967, 1969; Chaney and Christophorou, 1969;

Fehsenfeld, 1970; Warman and Sauer, 1971) methods; the latter have been restricted to $T \lesssim 500^{\circ}K$.

Let us, then, first refer to the experimental results of Fite and coworkers in Fig. 10 on the temperature dependence of dissociative attachment to O_2 producing O^-. It is seen from Fig. 10 that as T increases, the threshold energy decreases (it actually shifts from ~4 eV at ~300°K to ~1.2 eV at 1970°K), the energy position of the resonance maximum decreases, and the magnitude of the cross section and the resonance width increases. These data have been explained theoretically by O'Malley (1967) who assumed that the direct effect of T on O_2 is to produce a Maxwellian distribution of vibrational (ν) and rotational (j) states. The effective cross section $\sigma_{da}(T, \varepsilon)$ for dissociative attachment, then, is the Boltzmann average of the cross section $\sigma_{da}^{\nu,j}(\varepsilon)$ from each of the individual states, i.e.,

$$\sigma_{da}(T, \varepsilon) = \sum_{\nu=\nu_{min}}^{\infty} \sum_{j=j_{min}}^{\infty} N e^{-(E_\nu + E_j)/kT} \sigma_{da}^{\nu,j}(\varepsilon) \qquad (10)$$

where

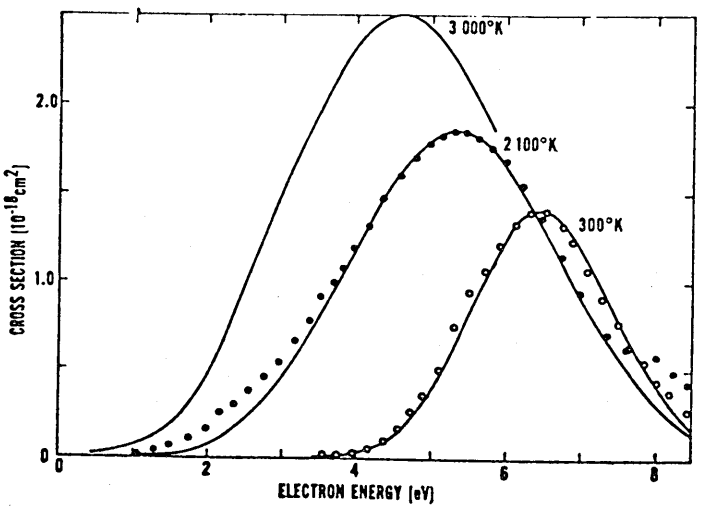

Fig. 10. Total cross section for dissociative attachment of electrons to O_2 as a function of electron energy at the indicated temperatures. (oooooooo) experimental results (Fite and Brackmann, 1963; Henderson et al., 1969); (——) theoretical results (O'Malley, 1967).

$$N = \left[\sum_{\nu=\nu_{min}}^{\infty} \sum_{j=j_{min}}^{\infty} e^{-(E_\nu + E_j)/kT} \right]^{-1}$$

and ν_{min} and j_{min} are subject to the energy threshold requirement:

$$\varepsilon + E_\nu + E_j \geq E_{threshold} = D(O-O) - EA(O) = 5.08 - 1.46 = 3.62 \text{ eV}.$$

The cross section $\sigma_{da}^{\nu,J}(\varepsilon)$ is (O'Malley 1966, 1967)

$$\sigma_{da}^{\nu,j}(\varepsilon) = \frac{4\pi^2 g}{k^2} \frac{\Gamma_{a,X}}{\Gamma_d} \left| \tilde{\chi}_\nu \left(R_\varepsilon - i \frac{\Gamma_a}{\Gamma_d} \right) \right|^2 e^{-\rho} \tag{11}$$

where $\tilde{\chi}_\nu$ is the vibrational wave function, $\Gamma_{a,X}$ is the partial autodetachment width for the state X and the rest of the symbols are as defined earlier. In his treatment, O'Malley considered the effect of rotational states to be negligible, and the excellent agreement of his predictions on the threshold, magnitude, width, and energy position of the O^-/O_2 resonance with the experimental results justifies this assumption. As T increases, higher vibrational levels are populated, the internuclear distances increase (and hence the Franck-Condon region broadens) significantly, and although even at 2000°K there is only a limited amount of vibrational excitation, there is a profound change in the survival factor $e^{-\rho}$ in Eq. (11) which dominates the temperature dependence of the cross section.

The insignificance of rotational excitation seems to be at variance with earlier theoretical predictions (Chen and Peacher, 1967) of a strong effect of rotational excitation on the yield of H^-/H_2. In this regard, recent experimental (Allan and Wong, 1978) and theoretical work (Wadehra and Bardsley, 1978a, b; Bardsley and Wadehra, 1979) on H^-/H_2 in the 3.75 eV H_2^- resonance region are quite relevant. Thus, the threshold cross section for the 3.75 eV H^-/H_2 resonance was reported to have shown (Allan and Wong, 1978) an increase by a factor $\geq$10 with each increase in vibrational quantum and a three-fold increase for rotational level increase from j = 0 to j = 7. The results of a recent calculation employing resonance scattering theory with semiempirical parameters (Wadehra and Bardsley, 1978a, b; Bardsley and Wadehra, 1979) indicated that although the effect of rotational excitation is not as high as that of vibrational excitation and not as significant as suggested earlier (Chen and Peacher, 1967), it is, nonetheless, considerable.

Additional examples of the effects of T on dissociative attachment processes are the recent work of Allan and Wong (1981) on the formation of Cl^- from HCl and F^- from HF and the work of Chen and Chantry (1979) on the formation of SF_5^- from SF_6. The results of the latter investigators are shown in Fig. 11. Two peaks in the

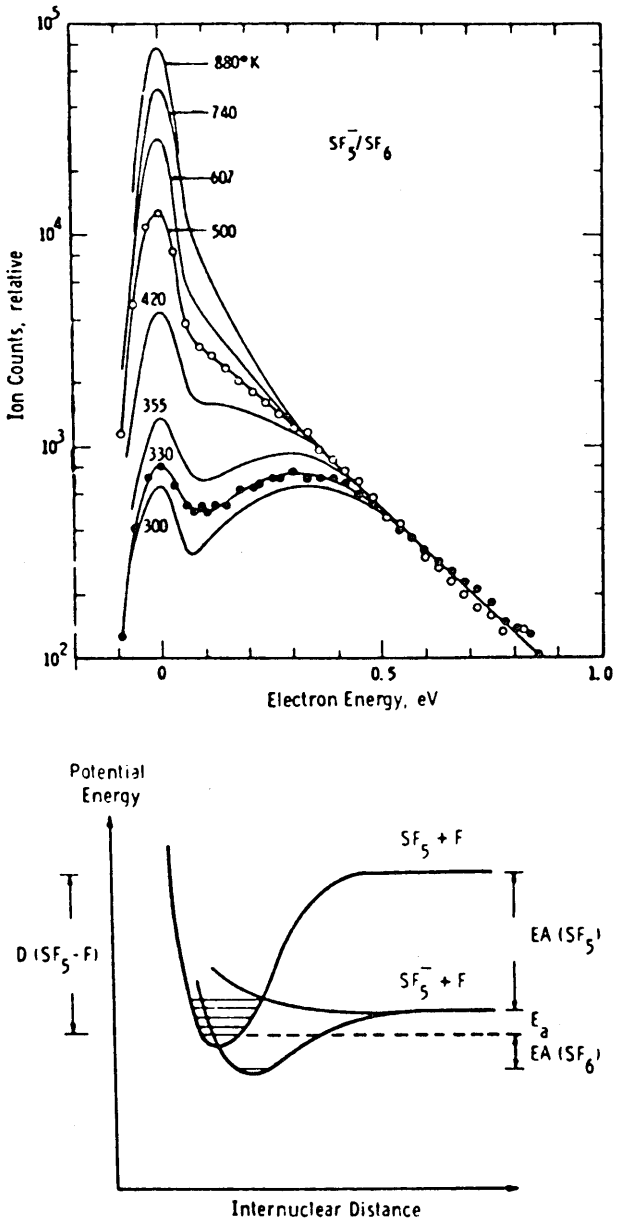

Fig. 11. Upper portion: SF_5^- from SF_6 vs ε at various T. Lower Portion: Schematic potential energy diagram illustrating the origin of the two peaks in the SF_5^-/SF_6 current (Chen and Chantry, 1979).

SF_5^- vs ε are seen: one at ~0.0 eV and the other at ~0.38 eV. The ~0.38 eV peak is rather broad and temperature insensitive. The ~0.0 eV peak is extremely sensitive to T. A semilogarithmic plot of the relative SF_5^- signal at the zero-energy peak vs T^{-1} yielded an activation energy of 0.2 eV. The two peaks can be understood on the basis of the lower portion of Fig. 11. The zero-energy peak is the result of attachment of near-zero energy electrons to those vibrational-rotational states of SF_6 at energies $\geq$0.2 eV above the ground state, and the 0.38 eV peak is the result of vertical Franck-Condon transitions of SF_6 to the repulsive negative ion curve after capturing a ~0.38 eV electron.

In Fig. 12 is shown the variation with T of the energy integrated total attachment cross section for various polyatomics studied by Spence and Schulz (1973). Three observations can be made with respect to Fig. 12:

(1) The spread in the magnitude of the total attachment cross section seen at room temperature decreases as the temperature increases.

(2) The smaller the magnitude of the attachment cross section at room temperature, the larger seems to be its temperature dependence.

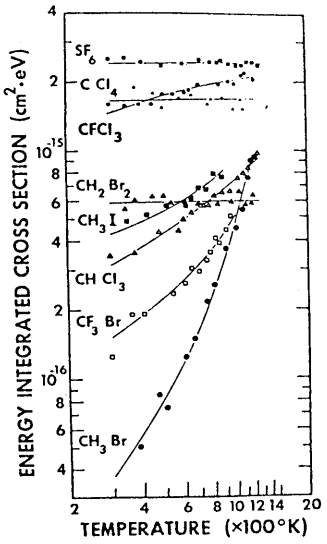

Fig. 12. Energy-integrated attachment cross sections as a function of temperature for various halocarbons and SF_6 (Spence and Schulz, 1973).

(3) The attachment cross section for certain polyatomics approaches the theoretical maximum value (see Fig. 14 and next section) as the temperature increases.

Finally, in Fig. 13 are shown recent results (McCorkle et al., 1980b; Christophorou et al., 1980a) on the T-dependence of the total electron attachment rate constant as a function of $\langle\varepsilon\rangle$ for 1,1,-$C_2Cl_2H_4$. When the $\sigma_a(\varepsilon, T)$ were deconvoluted from these data, structure was indicated which could arise from vertical transitions to a repulsive negative ion state from the $\nu = 0$ and $\nu = 1$ levels of the neutral molecule.

PARENT NEGATIVE IONS

For a parent negative ion to form (Reaction 3), the electron affinity of the molecule must be positive. If the excess energy of the ion is not removed rapidly enough, however, it will be destroyed by autodetachment within an average time τ_a, even though its EA is positive. If the autodetachment lifetime, τ_a, of the transient

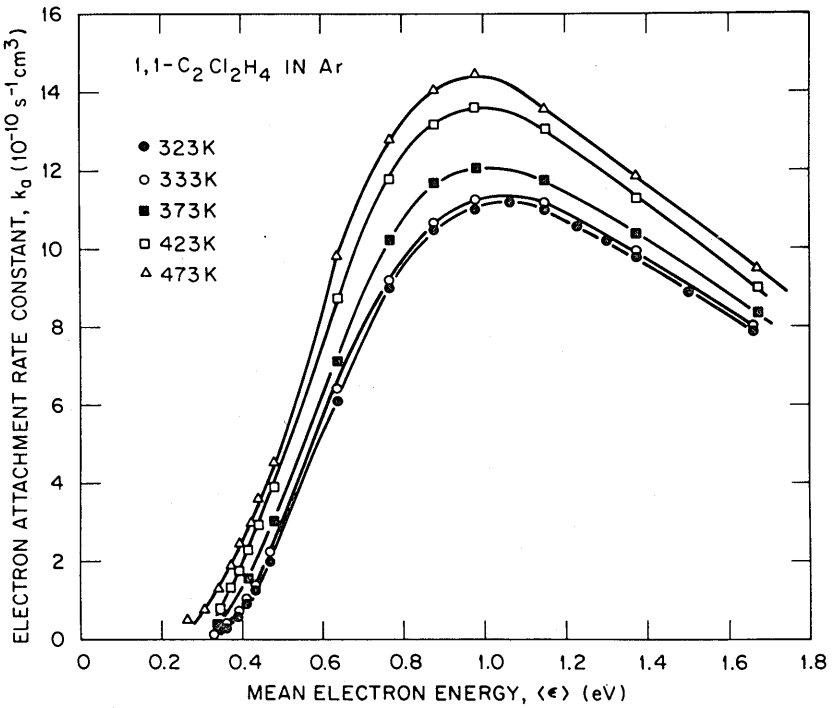

Fig. 13. Total electron attachment rate constant as a function of mean electron energy for 1,1-$C_2Cl_2H_4$ in Ar at several temperatures (McCorkle et al., 1980b; Christophorou et al., 1980a).

parent negative ion is $\gtrsim 10^{-6}$ s, it can be detected directly (e.g., by using conventional time-of-flight mass spectrometers) and its τ_a can be measured. On the other hand, for the total pressures normally employed in swarm experiments (Christophorou, 1971, 1978a, 1976) the time, τ_{coll}, between collisions of the transient parent negative ion and a stabilizing body (usually a buffer gas molecule) is much smaller than τ_a, and thus such ions are completely stabilized; swarm studies then conveniently provide $\sigma_a(\varepsilon)$ for these ions. If the transient parent negative ion is moderately long-lived ($10^{-12} \lesssim \tau_a < 10^{-6}$ s), its complete stabilization by collision requires high pressure swarm experiments. Long-lived parent negative ions are usually formed via a nuclear-excited Feshbach resonance mechanism, and their cross sections are very large at thermal and epithermal electron energies (see, for example, Christophorou, 1971, 1978a). Many polyatomic molecules have been found to exhibit this property. Two examples are shown in Fig. 14 where $k_a(\langle\varepsilon\rangle)$ and $\sigma_a(\varepsilon)$ are shown for the perfluorocarbons 1,3-C_4F_6 and c-C_6F_{10}. The $k_a(\langle\varepsilon\rangle)$ were pressure independent, and they are taken to give a true measure of the rate of formation of the lowest negative ion states of these molecules. The attachment cross sections and rate constants approach their maximum values for s-wave capture. These maximum values are shown in Fig. 14 and are defined as:

$$(\sigma_a)_{max} = \pi\lambda\!\!\!^{-2} \tag{12}$$

and

$$[k_a(\langle\varepsilon\rangle)]_{max} = \left(\frac{\pi^2\hbar^4}{2m^3}\right)^{1/2} \int_0^\infty \varepsilon^{-1/2} f_{N_2}(\varepsilon, \langle\varepsilon\rangle)\, d\varepsilon \tag{13}$$

where $f_{N_2}(\varepsilon, \langle\varepsilon\rangle)$ is the electron energy distribution function at $\langle\varepsilon\rangle$, $\lambda\!\!\!^{-}$ is the electron de Broglie wavelength divided by 2π, and the rest of the symbols are as defined earlier. The cross sections and the attachment rates in Fig. 14 are <u>total</u> (i.e., for <u>all</u> ions produced). At thermal and near-thermal energies, they are mostly due to parent ions, but at higher energies they may contain varying degrees of contributions from dissociative attachment processes (depending on the molecule) as indicated by the electron beam studies.

Studies of these and other perfluorocarbons indicated that the number and energy positions of the negative ion states of these molecules do not vary considerably, contrary to the large variations in the respective $\sigma_a(\varepsilon)$. The cross sections, the lifetimes, and the dependence of these two quantities on the energy of the captured electron depend strongly on the details of molecular

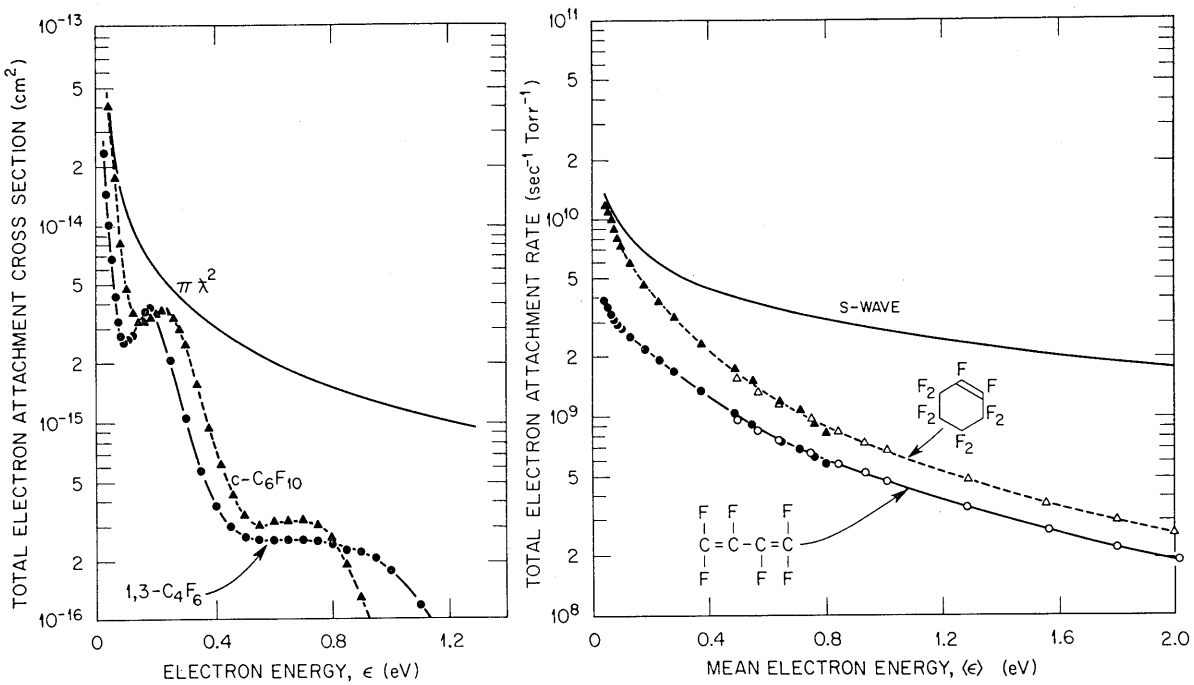

Fig. 14. Left-hand side: Total electron attachment cross section as a function of electron energy for 1,3-C_4F_6 and c-C_6F_{10}. These were unfolded by McCorkle et al. (1980a) from the k_a vs E/d data of Christodoulides et al. (1979) on 1,3-C_4F_6 and Pai et al. (1979) on c-C_6F_{10}. Right-hand side: Total electron attachment rate (in units of s^{-1} $torr^{-1}$) as a function of mean electron energy (Christodoulides et al., 1979, Pai et al., 1979). Solid lines are, respectively, the maximum s-wave capture cross section and capture rate.

structure (for a comprehensive review of the lifetimes of negative ions, (see Christophorou, 1978a). Thus, the replacement of the H-atoms in the molecule by fluorines which, for the two perfluorocarbons in Table 1 and for other similar structures with four or more carbon atoms (Christophorou, 1980a), lowers the lowest negative ion state such that the EA attains a positive value. This, in turn, has a profound effect on the magnitude of the attachment cross section and the autodetachment lifetime of the parent anions. Thus, although the nonfluorinated forms do not attach low-energy electrons, the perfluorinated molecules have very large electron attachment cross sections (close to the maximum s-wave capture cross section; see Fig. 14), and the lifetimes of the parent ions are $>10^{-6}$ s; i.e., orders of magnitude longer than those ($<10^{-12}$ s) of the negative ion states of the nonfluorinated analogues.

As will be seen, these and similar strongly electron attaching perfluorocarbon gases have excellent properties to be used either as unitary gas dielectrics or as electronegative components of dielectric gas mixtures. Though they form parent anions at thermal electron energies, they also--depending on their structure--can decompose readily by low-energy electron impact. This is clearly shown in Fig. 15 where the fragment and parent anions are shown for the two isomers 1,3-C_4F_6 and 2-C_4F_6.

Unavoidably, I should refer here to another system known to form long-lived (Christophorou, 1978a) parent negative ions at thermal energies, namely SF_6, since this is the most commonly used gas dielectric to date. The electron attachment rate constant as a function of $\langle\varepsilon\rangle$ measured (Christophorou et al., 1971c, 1972; Gant

Table 1. Effect of perfluorination on the energies and lifetimes of NISs (from Christophorou, 1980a).

Molecule	Formula	Position of observed NIS (eV)	EA (eV)	Auto-detachment lifetime (μs)
1,3-butadiene	$H_2C{=}CH{-}CH{=}CH_2$	-0.62	-	<<1
1,3-perfluoro-butadiene	$F_2C{=}CF{-}CF{=}CF_2$	†	>0	7
Cyclohexene	c-C_6H_{10}	-2.07	-	<<1
Perfluoro-cyclohexene	c-C_6F_{10}	†	$\geq 1.4 \pm 0.3$	106;113

†The $\sigma_a(\varepsilon)$ shows at least three resonances below ~1 eV (see Fig. 14).

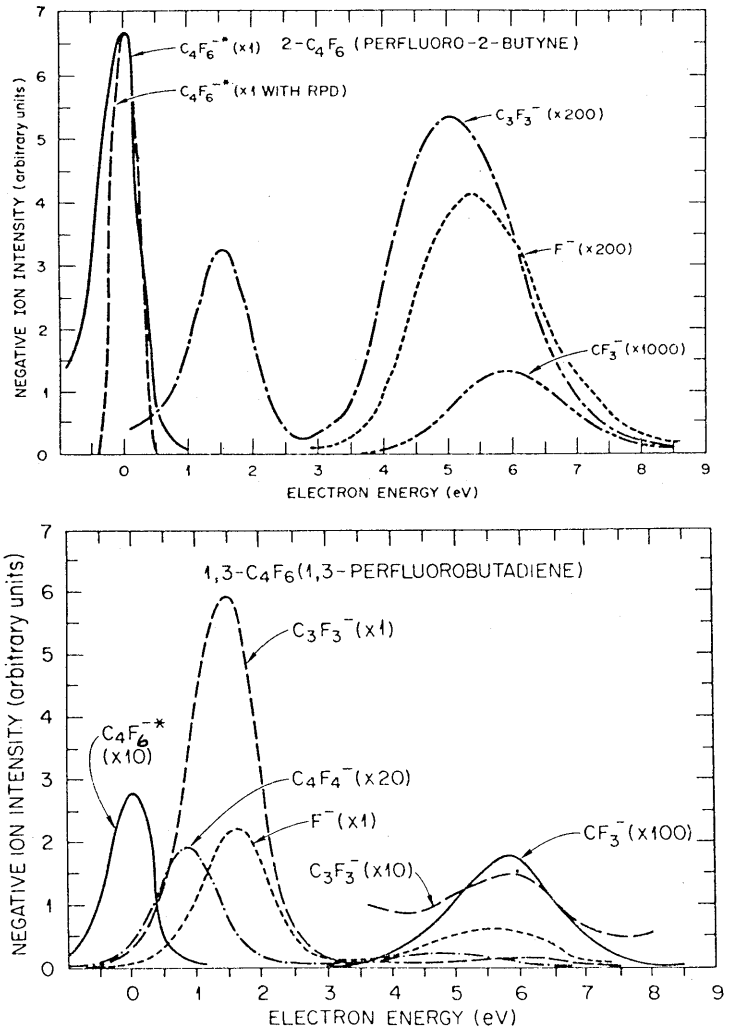

Fig. 15. Parent and fragment negative ion intensity as a function of electron energy for 1,3-C_4F_6 and 2-C_4F_6 (note the multiplication factors for the various ions). The lifetimes of 1,3-$C_4F_6^{-*}$ and 2-$C_4F_6^{-*}$ at thermal energies are 7 and 6 μs, respectively (Sauers et al., 1979).

and Christophorou, 1976) in the buffer gases N_2 and Ar is shown in the inset of Fig. 16. Cross sections unfolded from these along with other data are compared in the figure. The sharp peak at thermal energy is due to SF_6^- and that at ~0.35 eV due to SF_5^-. There is considerable uncertainty in the cross section around 0.3 eV. McCorkle et al. (1980a) indicated that in the swarm unfolding

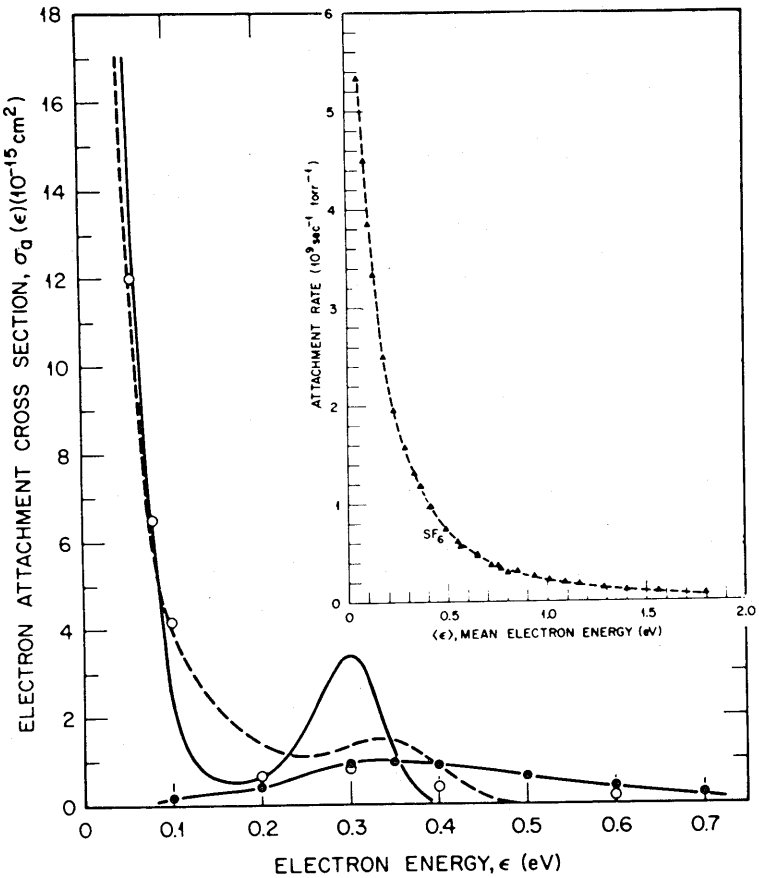

Fig. 16. Electron attachment cross section for SF_6 as a function of ε obtained by McCorkle et al (1980a) from swarm data (——, — — — —) using two sets of electron energy distributions for N_2. The open circles are $\sigma_a(\varepsilon)$ for the production of SF_6^- and SF_5^- (Kline et al., 1978) and a dash-dot curve is $\sigma_a(\varepsilon)$ for the production of SF_5^- (Christophorou et al., 1971c, 1972). Note the considerable uncertainty around the SF_5^- peak (at ~0.35 eV). The inset is a plot of the total attachment rate (in units of 10^9 s^{-1} $torr^{-1}$) vs $\langle\varepsilon\rangle$ (Gant and Christophorou, 1976 and Christophorou et al., 1971c, 1972).

technique the magnitude of a weak resonance (in this case the SF_5^- peak) in $\sigma_a(\varepsilon)$ near a very strong resonance (in this case the SF_6^- peak) may be affected by small differences in the $f(\varepsilon, E/N)$ used in the unfolding procedure. The thermal value of electron attachment rate constant to SF_6 is (Christophorou et al., 1981b)

24.9×10^{-8} s^{-1} cm^3 (see data on other species in Christodoulides et al., 1979; Pai et al., 1979, McCorkle et al., 1980a, b, Christophorou et al., 1981b).

Nondissociative electron attachment processes involving a transient ion $AB...CD^{-*}$ which requires collisional stabilization, show a strong dependence on both the nature and the density of the medium in which the anion is embedded. Figures 17 and 18 exemplify this for O_2 (Christophorou, 1976; Goans and Christophorou, 1974). Similar behavior has been exhibited by other systems (Christophorou, 1976); the understanding of these dependences of k_a on the density and nature of the medium is of intense current interest (e.g., see Christophorou 1976, 1981b).

ELECTRON ATTACHMENT TO ELECTRONICALLY-EXCITED MOLECULES

There is virtually no information on this process [Process (5)]. To our knowledge the only existing measurements are those on the dissociative attachment to the O_2 molecule excited in the lowest (metastable) $a^1\Delta_g$ state which lies 0.98 eV above the ground state, $X^3\Sigma_g^-$, of O_2. Burrow (1973) found the dissociative attachment cross section (at its maximum; located 5.5 eV above $a^1\Delta_g$ or 6.5 eV above $X^3\Sigma_g^-$) for the reaction

$$e + O_2(a^1\Delta_g) \rightarrow O_2^-(^2\Pi_u) \rightarrow O^-(^2P) + O(^3P)[3.64 \text{ eV limit}] . \qquad (14)$$

to be 4.6×10^{-18} cm^2, i.e., 3.5 ± 1 times larger than the peak cross section value of 1.3×10^{-18} cm^2 (at 6.5 eV) from the ground state $X^3\Sigma_g^-$, viz.

$$e + O_2(X^3\Sigma_g^-) \rightarrow O_2^-(^2\Pi_u) \rightarrow O^-(^2P) + O(^3P)[3.64 \text{ eV limit}] . \qquad (15)$$

Recently Belić and Hall (1981) reported for Eq. (14) a peak cross section of 3.8×10^{-18} cm^2. These authors also reported peak cross section values of 1.8×10^{-18} cm^2 and $<10^{-20}$ cm^2 at 7.5 eV and 8.5 eV above $a^1\Delta_g$, respectively, for the dissociative attachment reactions

$$e + O_2(a^1\Delta_g) \rightarrow O_2^-(^2\Sigma_g^+) \rightarrow O^-(^2P) + O(^1D)[5.61 \text{ eV limit}] , \qquad (16)$$

$$e + O_2(a^1\Delta_g) \rightarrow O_2^-(^2\Sigma_g^+?) \quad O^-(^2P) + O(^1S)[7.89 \text{ eV limit}] . \qquad (17)$$

Dissociative attachment to electronically excited molecules naturally have lower energy onsets and should be significant in cases where the population of low-lying metastable states is high.

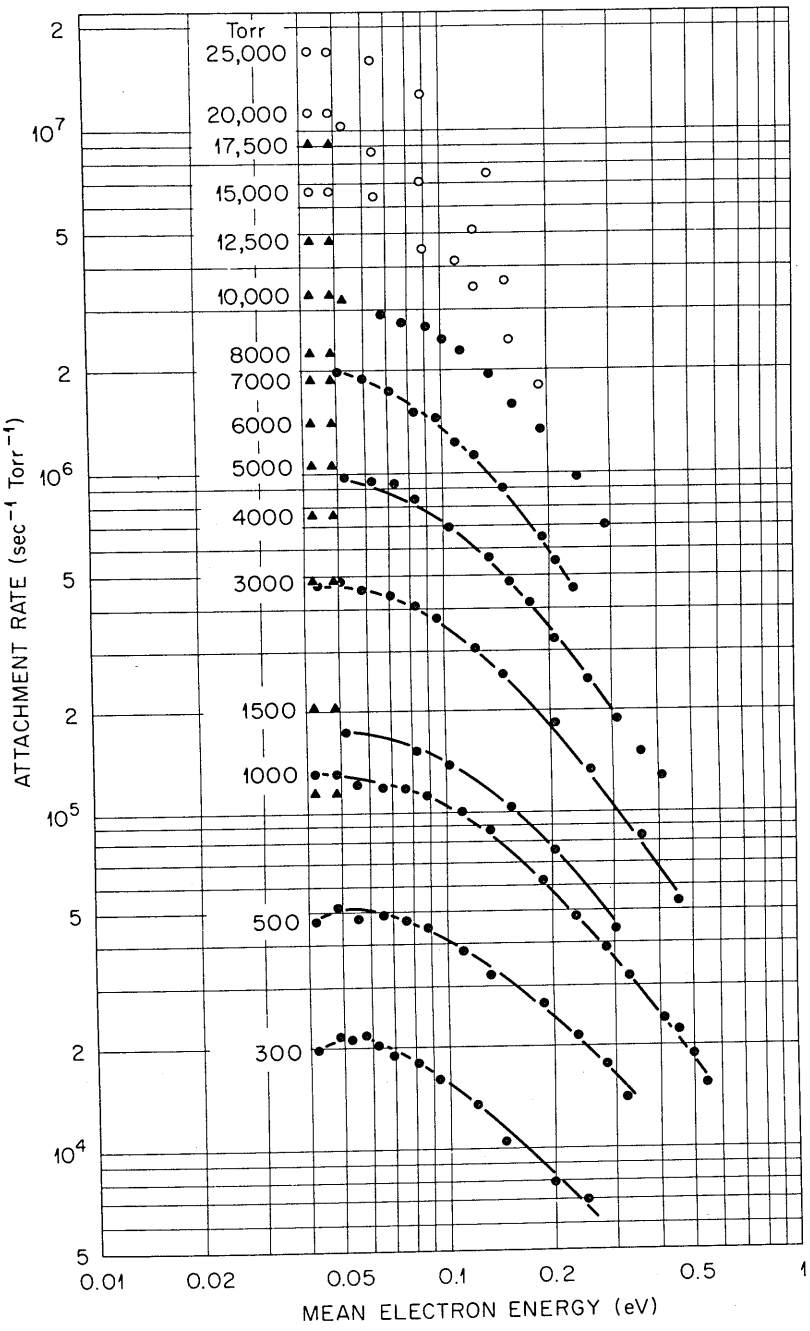

Fig. 17. Attachment rate (in units of s^{-1} $torr^{-1}$) as a function of mean electron energy, $\langle\varepsilon\rangle$, for O_2 in N_2, for N_2 pressures between 300 and 25,000 torr. The attachment rates plotted are for $P_{O_2} \to 0$. ($T = 298^{o}K$; Goans and Christophorou, 1974).

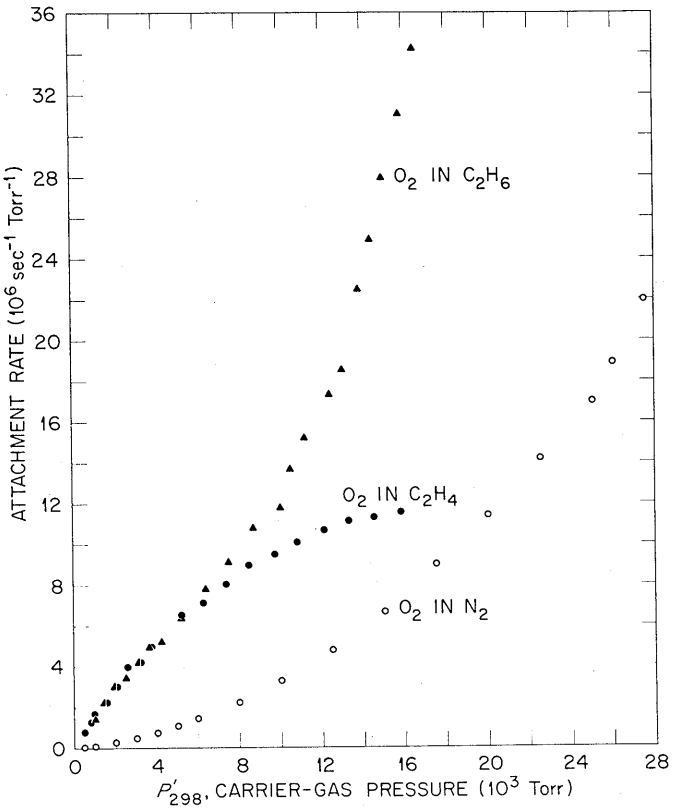

Fig. 18. Attachment rate (in units of s^{-1} $torr^{-1}$) for O_2 in the gaseous media N_2 (o), C_2H_4 (●), and C_2H_6 (▲) as a function of their respective pressures corrected for compressibility. The data plotted are for $\langle\varepsilon\rangle \simeq 0.05$ eV and for $P_{O_2} \to 0$ (Goans and Christophorou, 1974).

FROM BASIC RESEARCH TO APPLICATION

What Makes a Good Dielectric?

In a gas under an applied electric field, as the voltage is increased, the ever-present free electrons gain energy and their $f(\varepsilon, E/N)$ shifts to higher ε. When a sufficient fraction of the electrons can induce ionization, gas breakdown occurs.

The most effective way to prevent electrons from initiating breakdown is the removal of the electrons from the dielectric. An effective way of achieving this is to attach the electrons to the gas molecules forming negative ions. The unattached electrons

must be slowed down and be prevented from ionizing the gas and triggering breakdown.

The gas dielectric strength, therefore, can be optimized by effective control of the energies and number densities of the free electrons present, i.e., by maximizing the quantity

$$\int_0^\infty \sigma_a(\varepsilon)\, f(\varepsilon, E/N)\, d\varepsilon \ , \tag{18}$$

and by minimizing the quantity

$$\int_0^\infty \sigma_i(\varepsilon)\, f(\varepsilon, E/N)\, d\varepsilon \ . \tag{19}$$

To maximize (18), $\sigma_a(\varepsilon)$ should be as large as possible over as wide an energy range as possible, and since $\sigma_a(\varepsilon)$ increases with decreasing ε (see earlier sections), to optimize (18) $f(\varepsilon, E/N)$ must be shifted to as low energies as possible. To minimize (19), $\sigma_i(\varepsilon)$ must be as small as possible, especially close to I, which itself must be as high as possible. For a given $\sigma_i(\varepsilon)$, $f(\varepsilon, E/N)$ must again be shifted to low ε to minimize (19). Thus, the reduction of the electron energies is of paramount significance because a lower $f(\varepsilon, E/N)$ minimizes (19) but also maximizes (18). Such a reduction in electron energies requires large cross sections for elastic and inelastic electron scattering, especially in the subexcitation energy range.

The Concept of the Multicomponent Gaseous Insulator; Tailoring Gas Dielectrics

From (18) and (19) it is apparent that the optimum gaseous dielectric is not a single (unitary) gas but rather a combination of gases (a multicomponent gas mixture) designed as to components to provide the best effective combination of electron-attaching and electron-slowing-down properties to optimize (18) and (19). The art of designing multicomponent gaseous insulators is complicated but also enriched by the many processes entering (18) and (19). Basic knowledge on these processes offers several ways to the systematic development of dielectric gas mixtures (Christophorou, 1978b).

The Coefficients α and η and the Formulation of the Breakdown Criteria

Electron swarm and electron beam studies provided valuable information on the total electron attachment cross section $\sigma_a(\varepsilon)$,

especially at subexcitation energies. The former also provided information on the primary ionization coefficient, α, and the effective electron attachment coefficient, η, as a function of E/N. These latter coefficients are related to the respective attachment, $\sigma_a(\varepsilon)$, and ionization, $\sigma_i(\varepsilon)$, cross sections and $f(\varepsilon, E/N)$ by

$$\alpha/N = (2/m)^{1/2} w^{-1} \int_I^\infty f(\varepsilon, E/N)\varepsilon^{1/2} \sigma_i(\varepsilon)d\varepsilon , \tag{20}$$

$$\eta/N_a = (2/m)^{1/2} w^{-1} \int_o^\infty f(\varepsilon, E/N)\varepsilon^{1/2} \sigma_a(\varepsilon)d\varepsilon , \tag{21}$$

where I is the ionization onset energy, N is the total number density, N_a is the electron-attaching gas number density, and w the electron drift velocity.

The coefficients α and η have been measured for a number of gas dielectrics (e.g., see Fig. 19) and have been used to predict the breakdown voltage of gases/mixtures in both uniform and nonuniform fields. In the uniform-field case the limiting, $(E/N)_{lim}$, value of E/N at which breakdown occurs is defined as that for which

$$\frac{\alpha-\eta}{N} \equiv \frac{\bar{\alpha}}{N} = 0. \tag{22}$$

Figure 20 illustrates this for SF_6 (Kline et al., 1978). The "net ionization coefficient," $\bar{\alpha}/N$, is plotted against E/N; $(E/N)_{lim} = 3.62 \times 10^{-15}$ V cm^2. Similar studies have been performed for other gases and gas mixtures (Christophorou, 1980b, Kline et al., 1978).

For nonuniform fields, $\bar{\alpha}$ is a function of the position between the electrodes, and the breakdown voltage can be calculated using the Townsend criterion for a self-sustaining avalanche or the Meek criterion for streamer growth (Waters, 1978); the latter can be expressed as

$$\int_o^{x_o} \bar{\alpha}(x)dx = k, \tag{23}$$

where x_o is the length at which the electron avalanche reaches a critical number of electrons in the avalanche tip to cause a streamer formation, and k is a constant characteristic of the gas.

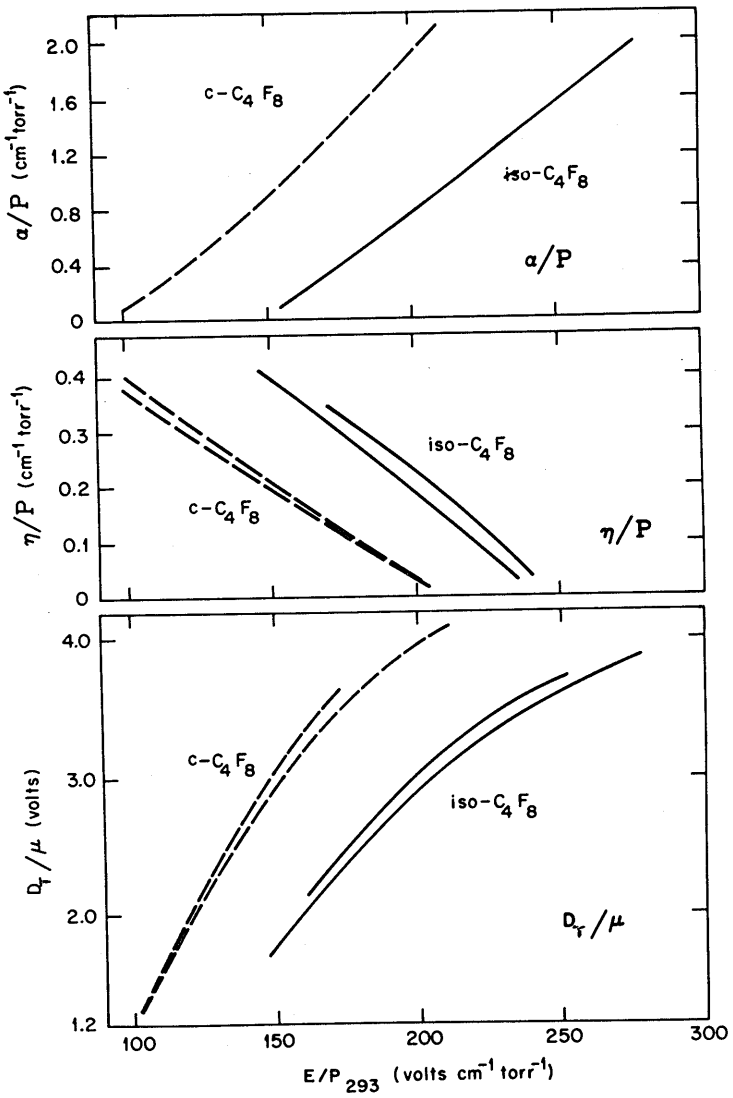

Fig. 19. α/P, η/P, and D_T/μ vs E/P_{293} for electrons in $c\text{-}C_4F_8$ and $2\text{-}C_4F_8$ (iso-C_4F_8) (Naidu and Prasad, 1972a, b; Naidu et al., 1972). The double lines in the η/P and D_T/μ vs E/P_{293} data refer to different values of P.

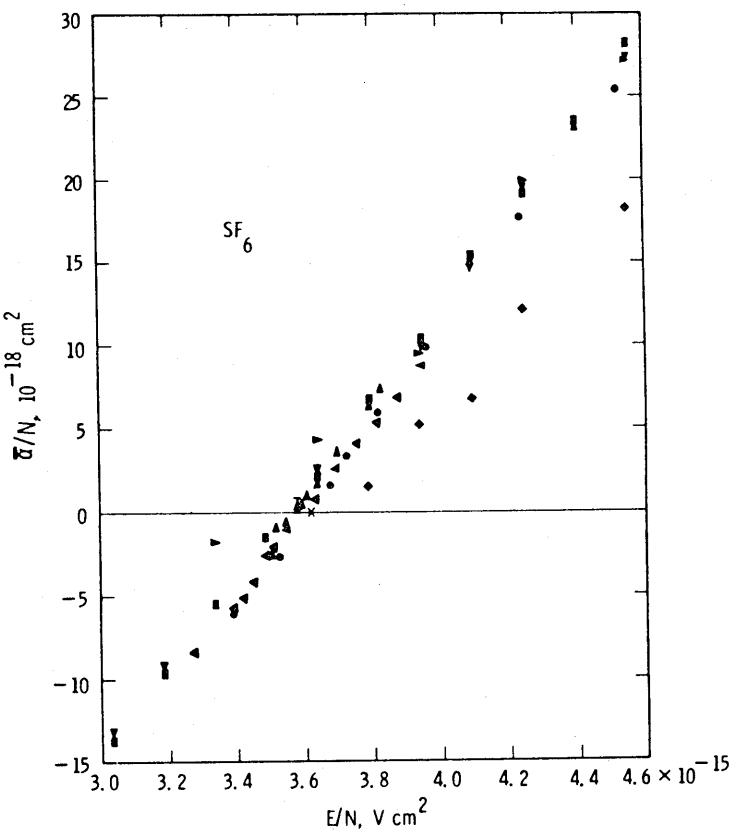

Fig. 20. $\bar{\alpha}/N$ vs E/N for SF_6 in uniform fields; data of Kline et al. (1978) and earlier investigators (Kline et al., 1978) in the vicinity of $(E/N)_{lim}$.

The Electron Attachment Cross Section and The Choice of Unitary Gas Dielectrics or Electronegative Components of Mixtures

Though the role of electronegative gases in dielectrics has long been recognized (Meek and Craggs, 1978), it is only recently that the dominant effect of both the magnitude and energy dependence of $\sigma_a(\varepsilon)$ on the breakdown strength and other dielectric gas properties has been investigated and effectively used to develop new gaseous dielectric materials (e.g., see Christophorou et al., 1981a; Christophorou, 1978b, 1980b).

The highest known dielectric strengths are exhibited by those gases (e.g., SF_6, perfluorocarbons) which possess the largest electron attachment cross sections as can be seen from the data in Table 2 (see also Fig. 14 and 16) and Fig. 21. For the

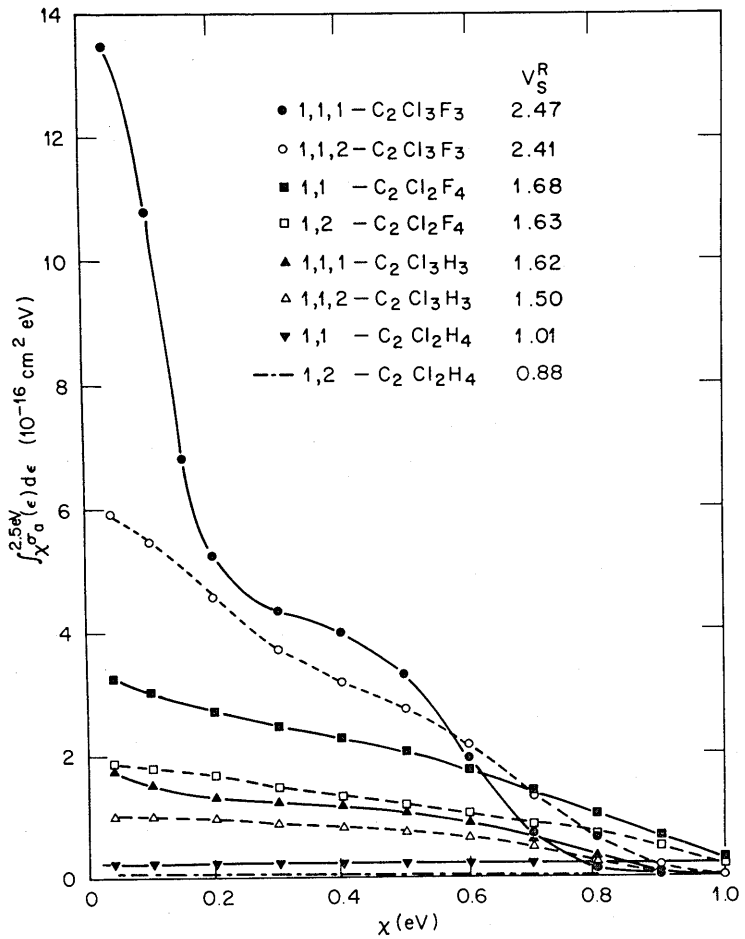

Fig. 21. $\int_{\chi}^{2.5\ eV} \sigma_a(\varepsilon)\, d\varepsilon$ vs χ for chlorofluoro and hydrochloroethanes[a] (Christophorou et al., 1981b).

perfluorocarbons in Table 2 (Groups A and B) which capture strongly thermal and near-thermal energy electrons forming mainly long-lived (>10^{-5} s) parent negative ions, the DC uniform-field breakdown voltage, V_s, (relative to SF_6 of 1), shows a general increase with the energy-integrated attachment cross section*

*Due to the general lack of knowledge of $f(\varepsilon, E/N)$ for polyatomic gas dielectrics, determination of (18) is not possible, and use is made of (24).

Table 2. Electron Attachment Data and Relative DC Uniform Field Breakdown Strengths of Some Gaseous Dielectrics*

Gas	$\int_{0.04}^{2.5\ eV} \sigma_a(\varepsilon)d\varepsilon$ = IA (10^{-16} cm^2 eV)	kth† (10^{-8} cm^3 s^{-1})	EA (eV)	$V_s R$§	Comments
SF_6	11.1	24.9	>0.46	1	
1-C_7F_{14}	4.4	0.38		1.2	Group A: Anions mostly parent at low energies and long lived ($\tau_a > 10^{-5}$ s); (IA) = 6.6 x 10^{-16} cm^{2}eV.
c-C_4F_6	5.1	14.3		1.7	
2-C_4F_8	7.2	4.7	>0.7	1.7	
c-C_4F_8	9.7	1.3	>0.4	1.2-1.3	
1,3-C_4F_6	10.5	12.6		∿1.5	
2-C_4F_6	12.9	5.4	0.7-1.45	2.2-2.4	Group B: Anions mostly parent at low energies and long lived ($\tau_a > 10^{-5}$ s); (IA) = 19 x 10^{-16} cm^{2}eV.
c-C_8F_{16}	17.4	7.4		∿2.4	
c-C_5F_8	18.1	38.9		∿2.1-2.2	
c-C_6F_{12}	18.1	15.0		2.3-2.4	
c-C_6F_{10}	19.1	39.2		1.9-2.2	
C_7F_8	20.3	27.4	>1.7	∿2.4	
c-C_7F_{14}	26.6	5.2		2.1	
1,1,1-$C_2Cl_3F_3$	13.5	28.0		2.47	Group C: Anions are dissociative attachment fragments; mostly Cl^-. The electron affinity of Cl is 3.61 eV.
1,1,2-$C_2Cl_3F_3$	5.94	1.1		2.41	
1,1-$C_2Cl_2F_4$	3.23	0.5		1.68	
1,2-$C_2Cl_2F_4$	1.85	0.07		1.63	
1,1,1-$C_2Cl_3H_3$	1.74	1.5		1.62	
1,1,2-$C_2Cl_3H_3$	1.02‡	0.02		1.50	
1,1-$C_2Cl_2H_4$	0.23‡	0.002		1.01	
1,2-$C_2Cl_2H_4$	0.07‡	0.003		0.88§§	
CCl_4	24.9 ‡	23.7		2.36	
CCl_3F	6.4 ‡	1.2		1.84	
CCl_3H	4.4 ‡	0.38		1.77	
CCl_2F_2	0.66‡	0.012		1.08	
CF_4	§			0.39	Group D: Weak dissociative attachment.
C_2F_6	§			0.80	
C_3F_8	§			0.90	
CO	§			0.40	
CO_2	§			0.30	
N_2O	§			0.44	
Ne	§			0.006	Group E: Nonelectron attaching.
Ar	§			0.07	
H_2	§			0.18	
N_2	§			0.36	

* All data from Christophorou et al. (1981b) unless otherwise indicated. See Christophorou et al. (1981b) for references to original data.
† Thermal electron attachment rate constant.
‡ IA upper limit = 1.8 eV.
§ From Christophorou et al. (1981c).
§§ Christophorou et al. (1981e).

$$\int_{0.04\ eV}^{x} \sigma_a(\varepsilon)d\varepsilon = IA. \qquad (24)$$

A one-to-one correspondence between V_s and IA is rather difficult to expect since other factors (Christophorou et al., 1981b) which change from one compound to another also affect V_s. When the variation of the unknowns from one gas to another is minimized--as in the case of the haloethanes and halomethanes in Table 2 (Group C) (these freons capture slow electrons, dissociatively forming principally Cl^- whose large [=3.61 eV] electron affinity would preclude detachment)--a rather quantitative relationship between V_s and IA is observed (Fig. 21 and Christophorou et al., 1981b). Interestingly, the data in Table 2 (see also Christophorou et al., 1981b) indicate that as IA increases, V_s saturates, suggesting an upper limit to V_s^R of ~2.5. Additionally, studies by Christophorou and coworkers suggest that the higher the energy range over which $\sigma_a(\varepsilon)$ is large, the higher is V_s. Extension of $\sigma_a(\varepsilon)$ to high energies can increase considerably (18) since it allows for a larger overlap between $\sigma_a(\varepsilon)$ and $f(\varepsilon, E/N)$.

Weakly electron-attaching or nonelectron-attaching gases (Table 2) have low V_s. Some weakly electron attaching polyatomic gases, however, have reasonably high V_s compared to, say, the rare gases, and this reflects the role of electron scattering processes on V_s.

Certain perfluorocarbons in Table 2, SF_6, and mixtures of these are suitable for industrial use. Of great practical potential, also, are mixtures of the strongly electron attaching gases in Table 2 with abundant, inert, and cheap buffer gases (e.g., N_2 and CHF_3) with which they act synergistically, the buffer gas scattering electrons into the region where the electronegative gas captures electrons most efficiently (see next section).

Electron Scattering at Low Energies and the Choice of Buffer Gases for Mixtures Containing Electronegative Gases

Although the role of $f(\varepsilon, E/N)$ is crucial in efforts to understand and to tailor gas dielectrics, there is, in spite of recent progress, a general lack of knowledge of $f(\varepsilon, E/N)$ for practical situations. Independently of the state of our knowledge of $f(\varepsilon, E/N)$, however, a larger scattering cross section shifts $f(\varepsilon, E/N)$ to lower ε and causes fast electron relaxation. In this way the number of electrons in the electrically stressed dielectric can be substantially reduced even by narrow but strong low-lying electron attachment resonances.

Examples of the use of basic knowledge on electron scattering processes to assess the effects of molecular structure and electron

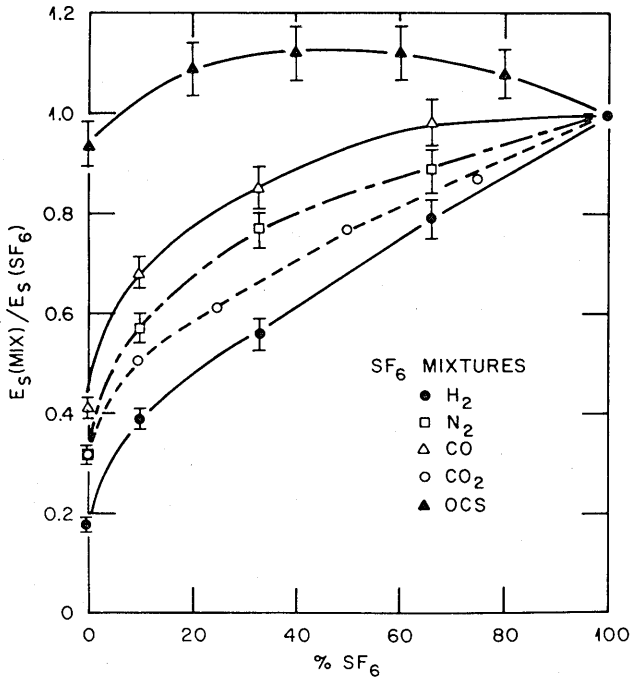

Fig. 22. $E_s(Mix)/E_s(SF_6)$ for mixtures of SF_6 with: H_2, N_2, CO, CO_2, and OCS (Christophorou et al., 1981a; see this reference for sources to original data).

energy-loss processes on the V_s of gases and the tailoring of dielectric gas mixtures containing electronegative gases can be found in--among others--Christophorou (1978b, 1980b, 1981b) and Christophorou et al. (1979a, 1981a, b, c, d).* In Fig. 22 $E_s(Mix)/E_s(SF_6)$ is shown for mixtures of SF_6 with each of the gases H_2, N_2, CO, CO_2 and OCS which at subexcitation energies scatter electrons efficiently via NIR states. When each of these nonelectron attaching gases is mixed with an electronegative gas (SF_6 for the data in Fig. 22), the mixtures exhibit distinct synergism.† The synergistic effects and the values

*Defined here as the difference between the measured V_s of the mixture and the sum of the partial-pressure-weighted V_s of the mixture components.

†The reader is referred also to Oak Ridge National Laboratory's reorts on Gaseous Dielectrics (e.g., Christophorou et al., 1979b, 1980a, b, 1981c). See these reports, also, as to the effects of other processes on the performance of gaseous dielectrics and the practical and engineering aspects of dielectric gases.

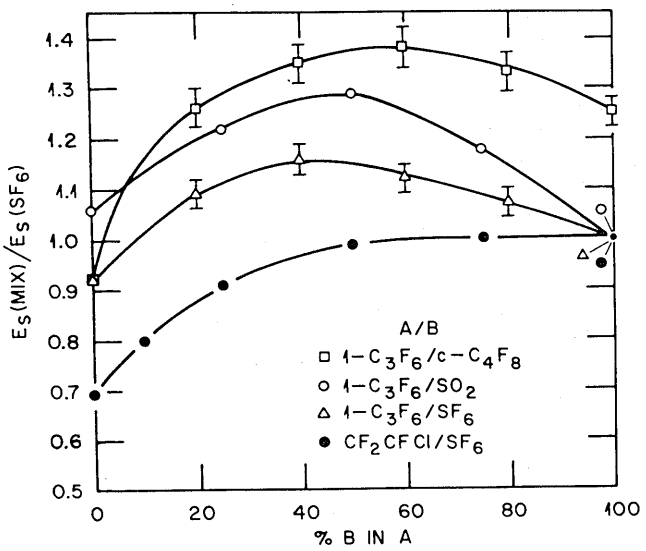

Fig. 23. $E_s(Mix)/E_s(SF_6)$ for mixtures containing double-bonded compounds (□) 1-C_3F_6/c-C_4F_8 (James et al., 1980); (○) 1-C_3F_6/SO_2 (Wootton et al., 1980); (△) 1-C_3F_6/SF_6 (James et al., 1980); (●) CF_2CFCl/SF_6 (Wootton et al., 1980) (From Christophorou et al., 1981a).

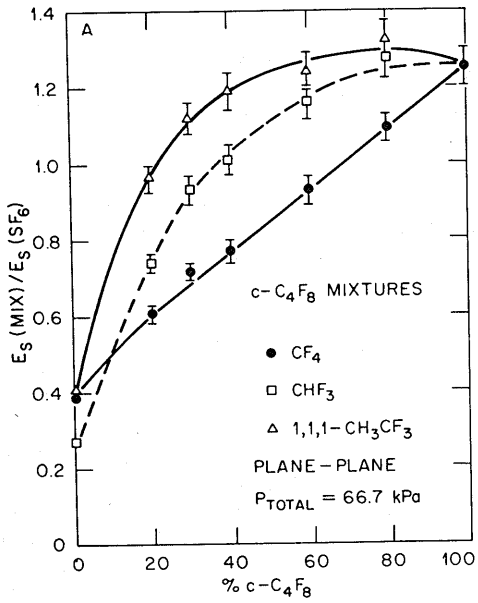

Fig. 24. $E_s(Mix)/E_s(SF_6)$ vs percent of c-C_4F_8 in CF_4, CHF_3, 1,1,1-CH_3CF_3 (Christophorou et al., 1981a).

of the V_s of the unitary gases increase in the order of increasing scattering cross section via the respective low-lying NIRS (i.e., $COS > CO > N_2 > CO_2 > H_2$).

Figure 23 shows the significant synergism exhibited by mixtures containing double-bonded compounds and electronegative gases. Electron swarm studies have shown (e.g., see Fig. 13 in Christophorou, 1978b) that the electron scattering cross section increases significantly, and, for a fixed E/N, the $\langle\varepsilon\rangle$ is appreciably lower for compounds with double bonds. Although these data are for the low-energy range ($\lesssim$2 eV), they suggest that one would expect double-bonded compounds to slow down electrons efficiently in gas mixtures.

Additionally, it has been found (Christophorou et al., 1981d) that polar electron slowing-down components effect a sharp increase in the V_s of mixtures with small percentages of electron attaching additives. This is seen from the data in Fig. 24 where mixtures of the polar buffer gases CHF_3 (D = 1.65 debye) and 1,1,1-CH_3CF_3 (D = 2.32 debye) with the electron attaching gas c-C_4F_8 exhibit strong synergism while the nonpolar gas CF_4 (D = 0) shows no such synergism. Stronger synergism was observed in mixtures of c-C_4F_8 with the highly polar CH_3CH (D = 3.92 debye) (see Christophorou et al., 1981d for more details and a complete discussion).

These and other findings (Christophorou et al., 1981a) suggest that a careful combination of electron-attaching gases with gases slowing down electrons via dipole scattering and via NIRs can effect large V_s. They indicate that a number of dielectric gas mixtures containing one or two electron attaching components from c-C_4F_8, 2-C_4F_8, SF_6, and a dipolar component from CHF_3, CH_2F_2, 1,1,-CH_3CF_3 with or without N_2 are excellent candidates for large-scale testing for possible eventual industrial adoption. Expecially since recent studies (Sauers et al., 1980, Frees et al., 1981, Christophorou et al., 1981c) show that proper tailoring of dielectric gas mixtures containing fluorocarbon(s) and SF_6 can alleviate (or greatly reduce) both the problems of carbonization and SF_6 toxic product formation and since small amounts of strongly electron-attaching perfluorocarbons in SF_6 or $SF_6 + N_2$ can improve the impulse and nonuniform field breakdown characteristics of the dielectric (Christophorou et al., 1981e).

REFERENCES

Allan, M. and Wong, S. F., 1978, in: "Abstracts of the 31st Annual Gaseous Electronics Conference, Buffalo, New York," Paper

MA-2, p. 125.
Allan, M. and Wong, S. F., 1981, J. Chem. Phys., 74:1687.
Bardsley, J. N. and Mandl, F., 1968, Rep. Prog. Phys. 31(2):471.
Bardsley, J. N. and Wadehra, J. M., 1979, Phys. Rev., 20:1398.
Belić, D. S. and Hall, R. I., 1981, J. Phys. B , 14:365.
Blaustein, R. P. and Christophorou, L. G., 1971, Rad. Res. Revs., 3:69.
Burrow, P. D., 1973, J. Chem. Phys., 59:4922.
Chaney, E. L. and Christophorou, L. G., 1969, J. Chem. Phys., 51: 883.
Chantry, P. J., 1969, J. Chem. Phys., 51:3369.
Chen, C. L. and Chantry, P. J., 1970, Bull. Am. Phys. Soc., 15:418.
Chen, C. L. and Chantry, P. J., 1971, Bull. Am. Phys. Soc., 17:1133.
Chen, C. L. and Chantry, P. J., 1979, J. Chem. Phys., 71:3897.
Chen, J. C. Y. and Peacher, J. L., 1967, Phys. Rev., 163:103.
Christodoulides, A. A., Christophorou, L. G., Pai, R. Y., and Tung, C. M., 1979, J. Chem. Phys., 70:1156.
Christophorou, L. G., 1971, "Atomic and Molecular Radiation Physics," Wiley-Interscience, New York.
Christophorou, L. G., 1976, Chem. Revs., 76:409.
Christophorou, L. G., 1978a, in: "Advances in Electronics and Electron Physics," Vol. 46, Academic, New York, p. 55.
Christophorou, L. G., 1978b, in: "Proceedings, 13th International Conference on Phenomena in Ionized Gases, Berlin," Invited Lectures, VEB Export-Import, Leipzig, p. 51.
Christophorou, L. G., 1980a, Environ. Health Perspect., 36:3.
Christophorou, L. G., ed., 1980b, "Gaseous Dielectrics II," Pergamon, New York.
Christophorou, L. G., 1981a, in: "Photon Electron and Ion Probes of Polymer Structure and Properties," D. W. Dwight, T. J. Fabish and H. R. Thomas, eds., ACS Symposium Series 162, Washington, p. 11.
Christophorou, L. G., ed., 1981b, "Electron and Ion Swarms," Pergamon, New York.
Christophorou, L. G., Carter, J. G., Collins, P. M., and Christodoulides, A. A., 1971a, J. Chem. Phys., 54:4706.
Christophorou, L. G., Grant, M. W., and McCorkle, D. L., 1977, "Advances in Chemical Physics," Vol. 36, Wiley-Interscience, New York, p. 413.
Christophorou, L. G., James, D. R., and Mathis, R. A., 1979a, J. Phys. D., 12:1223.
Christophorou, L. G., James, D. R., Pai, R. Y., 1981a, in: "Applied Atomic Collision Physics," H. S. W. Massey, E. W. McDaniel, and B. Bederson, eds., Vol. II, in press.

Christophorou, L. G., James, D. R., Pai, R. Y., Mathis, R. A., Sauers, I., Frees, L. C., Pace, M. O., Bouldin, D. W., Chan, C. C., and Kent, E. J., 1979b, Oak Ridge National Laboratory Report ORNL/TM-6902.

Christophorou, L. G., James, D. R., Pai, R. Y., Mathis, R. A., Sauers, I., Frees, L. C., Pace, M. O., Bouldin, D. W., and Chan, C. C., 1980b, Oak Ridge National Laboratory Report ORNL/TM-7173.

Christophorou, L. G., James, D. R., Pai, R. Y., Mathis, R. A., Sauers, I., Hunter, S. R., Pace, M. O., Bouldin, D. W., Spyrou, S. M., Fatheddin, A., 1981e, Oak Ridge National Laboratory Report ORNL/TM-7862.

Christophorou, L. G., James, D. R., Pai, R. Y., Mathis, R. A., Sauers, I., Smith, D. H., Frees, L. C. Pace, M. O., Bouldin, D. W., Chan, C. C., Fatheddin, A., and Hunter, S. R., 1981c, Oak Ridge National Laboratory Report ORNL/TM-7624.

Christophorou, L. G., James, D. R., Pai, R. Y., Mathis, R. A., Sauers, I., Smith, D. H., Frees, L. C., Pace, M. O., Bouldin, D. W., Chan, C. C., Fatheddin, A., and Maughan, D., 1980a, Oak Ridge National Laboratory Report ORNL/TM-7405.

Christophorou, L. G., James, D. R., and Mathis, R. A., 1981b, J. Phys. D , 14:675.

Christophorou, L. G., McCorkle, D. L., and Anderson, V. E., 1971b, J. Phys. B , 4:1163.

Christophorou, L. G., McCorkle, D. L., and Carter, J. G., 1971c, J. Chem. Phys., 54:253.

Christophorou, L. G., McCorkle, D. L., and Carter, J. G., 1972, J. Chem. Phys., 57:2228.

Compton, R. N., Christophorou, L. G., Hurst, G. S., and Reinhardt, P. W., 1966, J. Chem. Phys., 45:4634.

Fehsenfeld, F. C., 1970, J. Chem. Phys., 53:2000.

Fite, W. L. and Brackmann, R. T., 1963, in: "Proceedings, 6th International Conference on Phenomena in Ionized Gases, Paris," Vol. 1, p. 21.

Fite, W. L., Brackmann, R. T., and Henderson, W. R., 1965, in: "Proceedings, 4th International Conference on the Physics of Electronic and Atomic Collisions, Quebec," Science Bookcrafters, Hastings-on-Hudson, New York, p. 100.

Franklin, J. L. and Harland, P. W., 1974, Ann. Rev. Phys. Chem., 25:485.

Frees, L. C., Sauers, I., Ellis, H. W., and Christophorou, L. G., 1981, J. Phys. D., 14:1629.

Gant, K. S. and Christophorou, L. G., 1976, J. Chem. Phys., 65: 2977.

Goans, R. E. and Christophorou, L. G., 1974, J. Chem. Phys., 60: 1036.

Golden, D. S., 1966, Phys. Rev. Lett., 17:847.

Golden, D. E., Bandel, H. W., and Salerno, J. A., 1966, Phys. Rev., 146:40.

Henderson, W. R., Fite, W. L., and Brackmann, R. T., 1969, Phys. Rev., 183:157.
Hickam, W. M. and Berg, D., 1958, J. Chem. Phys., 29:517.
Hotop, H. and Lineberger, W. C., 1975, J. Phys. Chem. Ref. Data, 4:539.
James, D. R., Christophorou, L. G., and Mathis, R. A., 1980, in: "Gaseous Dielectrics II," L. G. Christophorou, ed., Pergamon, New York, p. 115.
James, D. R., Christophorou, L. G., Pai, R. Y., Pace, M. O., Mathis, R. A., Sauers, I., and Chan, C. C., 1978, in: "Gaseous Dielectrics," L. G. Christophorou, ed., Oak Ridge National Laboratory Report CONF-780301, p. 224.
Johnson, J. P., Christophorou, L. G., and Carter, J. G., 1977, J. Chem. Phys., 67:2196.
Kline, L. E., Davies, D. K., Chen, C. L., and Chantry, P. J., 1978, in: "Proceedings, International Conference on Gaseous Dielectrics," L. G. Christophorou, ed., Oak Ridge National Laboratory Report, CONF-780301, p. 258.
Linder, F. and Schmidt, H., 1971, Z. Naturforsch, 26a:1603.
Massey, H. S. W., 1976, "Negative Ions," 3rd E-., Cambridge University, Cambridge.
McCorkle, D. L., Christodoulides, A. A., Christophorou, L. G., and Szamrej, I., 1980b, J. Chem. Phys., 72:4049.
Meek, J. M. and Craggs, J. D., eds., "Electrical Breakdown of Gases," 2nd Ed., Wiley, New York and Chichester.
Naidu, M. S., and Prasad, A. N., 1972a, J. Phys. D., 5:983.
Naidu, M. S., and Prasad, A. N., 1972b, J. Phys. D., 5:1090.
Naidu, M. S., Prasad, A. N., and Craggs, J. D., 1972, J. Phys. D., 5:741.
O'Malley, T. F., 1966, Phys. Rev., 150:14.
O'Malley, T. F., 1967, Phys. Rev., 155:59.
Pai, R. Y., Christophorou, L. G., and Christodoulides, A. A., 1979, J. Chem. Phys., 70:1169.
Rosenstock, H. M., Draxl, K., Steiner, B. W., and Herron, J. T., 1977, J. Phys. Chem. Ref. Data, 6, Suppl. 1.
Sauers, I., Christophorou, L. G., and Carter, J. G., 1979, J. Chem. Phys., 71:3016.
Sauers, I., Christophorou, L. G., Frees, L. C., and Ellis, H. W., 1980, in: "Gaseous Dielectrics II," L. G. Christophorou, ed., Pergamon, New York, p. 429.
Schulz, G. J., 1964, Phys. Rev. A, 135:988.
Schulz, G. J., 1973, Rev. Mod. Phys., 45(3):378.
Spence, D. and Schulz, G. J., 1969, Phys. Rev., 188:280.
Spence, D. and Schulz, G. J., 1973, J. Chem. Phys., 58:1800.
Wadehra, J. M. and Bardsley, J. N., 1978a in: "Abstracts of the 31st Annual Gaseous Electronics Conference, Buffalo," Paper MA-3, p. 123.
Wadehra, J. M. and Bardsley, J. N., 1978b, Phys. Rev. Lett., 41: 1795.

Warman, J. M. and Sauer, M. C., Jr., 1971, Int. J. Rad. Phys. Chem., 3:273.

Waters, R. T , 1978, in: "Electrical Breakdown of Gases," 2nd Ed., J. M. Meek and J. D. Craggs, eds., Wiley, New York and Chichester, p. 392.

Wentworth, W. E., Becker, R. S., and Tung, R., 1967, J. Phys. Chem., 71:1562.

Wentworth, W. E., George, R., and Keith, H., 1969, J. Chem. Phys., 51:1791.

Wootton, R. E., Dale, S. J., and Zimmerman, N. J., 1980, in: "Gaseous Dielectrics II," L. G. Christophorou, ed., Pergamon, New York, p. 137.

KINETIC THEORY OF ION TRANSPORT IN GASES

H. R. Skullerud

Physics Department
Norwegian Institute of Technology
Trondheim, Norway

INTRODUCTION

Ion swarm experiments are extensively used to obtain information about low-energy ion-molecule collision processes. The activity in this field has resulted in a large number of sophisticated drift-tube experiments (Kaneko, 1980), and in the development of kinetic theories which enable accurate calculations of transport properties to be made assuming a given set of collision cross sections (Kumar et al., 1980). For the simplest ion-atom systems, it has even been shown how an interaction potential V(r) can be determined by direct inversion of transport coefficient data (Viehland et al., 1976).

For the purpose of this paper, which closely follows the presentation of Kumar et al. (1980), we define a swarm as an ensemble of independent charged test particles (ions) moving in a neutral background gas. The motion of the particles is determined by the forces exerted by external electric and magnetic fields and by collisions with the gas molecules. These collisions may in some cases lead to reactions, i.e., to a change in the number of test particles.

The swarm can be described in detail by its phase-space distribution function $f(\vec{r},\vec{v},t)$, but this function is seldom measured directly. What is actually measured is usually the current incident on some electrode. However, it is often more convenient to think that the measured quantity is the ion number density

$$n(\vec{r},t) = \int f(\vec{r},\vec{v},t)\,d\vec{v} \quad . \tag{1}$$

In swarm experiments, one can usually identify a state of steady or stationary random transport, the so-called hydrodynamic regime, in which the number density $n(\vec{r},t)$ satisfies a linear partial differential equation. The coefficients of this equation are the transport coefficients.

We shall now first present a formal phenomenological description of the hydrodynamic regime, and then proceed to show how the transport coefficients can be obtained from the solution of kinetic equations.

HYDRODYNAMIC EQUATIONS

The hydrodynamic description is a phenomenological description of the time development of the number density $n(\vec{r},t)$. The description is applicable when the memory of the initial distribution in velocity space has disappeared, and the distribution function has become a functional of $n(\vec{r},t)$ as far as its space-time dependence is concerned.

In our discussions, we will assume for the sake of simplicity that the fields and neutral gas parameters are time independent and homogeneous.

The starting point for the hydrodynamic description is the continuity equation for the number density

$$\partial_t n(\vec{r},t) + \nabla \cdot (n\vec{u}(\vec{r},t)) = (\partial_t n(\vec{r},t))_{coll} \cdot \tag{2}$$

This equation describes the changes in $n(\vec{r},t)$ due to a convective particle current density $n\vec{u}(\vec{r},t)$ and a production term $(\partial_t n)_{coll}$.

One now assumes that both $n\vec{u}(\vec{r},t)$ and $(\partial_t n)_{coll}$ can be expressed formally as power series in the gradient operator. This is equivalent to a Fourier expansion of the quantities in Eq. (2) followed by a power series expansion in the wavenumber (Kumar and Robson, 1973), and gives rise to a transport equation of the form

$$(\partial_t - \sum_{k=0}^{\infty} \underset{\sim}{\omega}^{(k)} \circledcirc (-\nabla)^k) n(\vec{r},t) = 0 \ . \tag{3}$$

The symbol $\circledcirc$ indicates a k-fold scalar multiplication, and the constants $\underset{\sim}{\omega}^{(k)}$ are tensorial transport coefficients of order k. They can be taken to be symmetrical under permutation of space indices, since their antisymmetrical parts are lost in the scalar multiplication.

The transport coefficients can be interpreted physically as time derivatives of moments of the density. Let $\psi(\vec{r})$ be any function of $\vec{r}$ and

$$N(t) = \int n(\vec{r},t)d\vec{r} \tag{4}$$

$$\langle\psi(r)\rangle = \int\psi(\vec{r})\ n(\vec{r},t)d\vec{r}\ . \tag{5}$$

Assuming that $n(\vec{r},t)$ and its derivatives vanish at the boundaries of the domain of integration, one obtains from Eq. (3) the following equations for the time development of the averages $\langle\psi(\vec{r})\rangle$

$$dN/dt - \omega^{(o)}N = 0 \tag{6}$$

$$d\langle\psi(\vec{r})\rangle/dt - \sum_{k=1}^{\infty} \underset{\sim}{\omega}^{(k)} \circledcirc \langle(\nabla)^k\psi(\vec{r})\rangle = 0\ . \tag{7}$$

If $\psi(\vec{r})$ is a polynomial of order j in $\vec{r}$, only transport coefficients of order $k \leq j$ occur. Taking successive moments, we thus get, with $\vec{r}^* = \vec{r} - \langle r\rangle$,

$$\omega^{(o)} \equiv -\alpha = d(\log N)/dt \tag{8a}$$

$$\underset{\sim}{\omega}^{(1)} \equiv \vec{v}_{dr} = d\langle\vec{r}\rangle/dt \tag{8b}$$

$$\underset{\sim}{\omega}^{(2)} \equiv \vec{\vec{D}} = (1/2!)d\langle\vec{r}^*\vec{r}^*\rangle/dt \tag{8c}$$

$$\underset{\sim}{\omega}^{(3)} = (1/3!)d\langle\vec{r}^*\vec{r}^*\vec{r}^*\rangle/dt \tag{8d}$$

where α is the reaction rate, $\vec{v}_{dr}$ the drift velocity, $\vec{\vec{D}}$ the diffusion tensor, and $\underset{\sim}{\omega}^{(3)}$ a coefficient describing the evolution of the skewness of the swarm. Note that $\vec{v}_{dr}$ may differ from the mean velocity of the ions, if reactions occur.

In most cases, the summation in Eq. (3) is truncated at k=2, to yield the usual diffusion equation

$$(\partial_t + \vec{v}_{dr}\cdot\nabla - \vec{\vec{D}} : \nabla\nabla)n(\vec{r},t) = -\alpha n(\vec{r},t) \tag{9}$$

with the fundamental solution

$$P(\vec{r},t) = \{\det(4\pi Dt)\}^{-\frac{1}{2}}\exp\{-(\vec{r}-\vec{v}_{dr}t)\cdot(4\vec{\vec{D}}t)\cdot(\vec{r}-\vec{v}_{dr}t)\}\exp(-\alpha t). \tag{10}$$

In cases of inhomogeneous field or neutral gas temperature, Eq. (9) has to be modified to take into account also the gradients of the background parameters. New transport coefficients then appear, describing e.g., nonlocal electric field effects (Rohlena,

1980, private communication) and thermal diffusion effects (Weinert, 1980).

THE BOLTZMANN EQUATION

The Boltzmann equation is a continuity equation in phase space for the distribution function $f(\vec{r},\vec{v},t)$. It is the starting point for most quantitative theories of transport processes in dilute gases, and there is a vast literature on its properties and use in that context (see e.g., Ferziger and Kaper (1972). We shall here only discuss the equation as it appears in test particle problems.

In the absence of reactions, $f(\vec{r},\vec{v},t)$ must fulfill a continuity equation

$$\partial_t f + \nabla \cdot (f\, d\vec{r}/dt) + \nabla_v \cdot (f\, d\vec{v}/dt) = 0 \tag{11}$$

where $d\vec{r}/dt$ and $d\vec{v}/dt$ are time derivatives taken along an ion trajectory. The acceleration $d\vec{v}/dt$ is composed of an external field term $\vec{a} = (q/m)(\vec{E} + \vec{v} \times \vec{B})$ and a term representing interactions with the neutrals. Separating out the interaction term gives

$$(\partial_t + \vec{v} \cdot \nabla + \vec{a} \cdot \nabla_{\underline{v}} + J) f(\vec{r},\vec{v},t) = 0 \tag{12}$$

where J is a collision operator. The acceleration a could be taken outside the ∇_v - operator because its velocity-dependent part is perpendicular to $\vec{v}$.

The collisions are now treated as local processes, where the velocities are changed discontinuously, $(\vec{r},\vec{v}) \rightarrow (\vec{r},\vec{v}')$. Further, the colliding particles are assumed totally uncorrelated <u>before</u> a collision. The collision frequency per particle, ν, is then uniquely determined by the angular cross section σ_Ω and the distribution function of the collision partners $f_1(\vec{r}_1,\vec{v}_1,t)$;

$$\nu(\vec{r},t;\vec{v}) = \int f_1(\vec{r}_1,\vec{v}_1,t) g \sigma_\Omega(g,\chi)\, d\hat{g}'\, d\vec{v}_1 \tag{13}$$

where $\vec{g} = \vec{v} - \vec{v}_1$ is the relative velocity, $d\hat{g}'$ is the solid angle element described by the relative velocity after collision, and χ is the scattering angle.

The net loss of particles, per unit time, from a volume element $d\vec{r}d\vec{v}$, is the difference between the number scattered out of the volume element and the number scattered into the volume element from other areas $d\vec{v}'$ in velocity space;

$$Jf(\vec{r},\vec{v},t)d\vec{r}d\vec{v} = f(\vec{r},\vec{v},t)\,\nu(\vec{r},t;\vec{v})d\vec{r}d\vec{v}$$

$$- \int f(\vec{r},\vec{v}'t)f_1(\vec{r},\vec{v}_1',t)g'\sigma_\Omega(g;\chi)d\hat{g}d\vec{v}';d\vec{r}d\vec{v}' \ . \qquad (14)$$

Introducing the Jacobian

$$\Delta_J = \partial(\hat{g},\vec{v}',\vec{v}_1')/\partial(\hat{g}',\vec{v},\vec{v}_1) = g'/g \qquad (15)$$

Eq. (14) may be rewritten to give (we omit r and t for convenience)

$$Jf(\vec{v}) = \int\{g\sigma_\Omega(g,\chi)f(\vec{v})f_1(\vec{v}_1) - \Delta_J g'\sigma_\Omega(g',\chi)f(\vec{v}')f(\vec{v}_1')\}d\hat{g}'d\vec{v}_1 \qquad (16)$$

which for elastic collisions reduces to Boltzmann's form

$$J^{el}f(\vec{v}) = \int\{ff_1 - f'f_1'\}g\sigma_\Omega(g,\chi)d\hat{g}'dv_1 \ . \qquad (17)$$

In the test particle problems, the distribution function $f_1(r,v,t)$ is assumed known, and independent of f. The Boltzmann equation then becomes a <u>linear</u> intergro-differential equation for $f(\vec{r},\vec{v},t)$, while the equation as it appears in most fluid problems is basically nonlinear.

KINETIC EQUATIONS FOR THE TRANSPORT COEFFICIENTS

The transport Eq. (3) assumes the time derivative of the density $\partial_t n$ to be uniquely determined by the spatial derivatives of $n(\vec{r},t)$. Making the same assumption about the distribution function $f(\vec{r},\vec{v},t)$ leads to a set of equations from which the transport coefficients $\underset{\sim}{\omega}^{(k)}$ can be determined. We thus insert in the Boltzmann equation the expansions

$$\partial_t n(\vec{r},t) = \sum_{k=0}^{\infty} \underset{\sim}{\omega}^{(k)} \circledcirc (-\nabla)^k n(\vec{r},t) \qquad (3)$$

$$f(\vec{r},\vec{v},t) = \sum_{k=0}^{\infty} \underset{\sim}{f}^{(k)}(\vec{v}) \circledcirc (-\nabla)^k n(\vec{r},t) \qquad (18)$$

with the normalization necessary for self-consistency

$$\int \underset{\sim}{f}^{(k)}(\vec{v})d\vec{v} = \delta_{ok} \ . \qquad (19)$$

By equating the coefficients of $(-\nabla)^k n(\vec{r},t)$ individually to zero, we then obtain the hierarchy of kinetic equations

$$(\vec{a}\cdot\nabla_{\underline{v}} + J)\underset{\sim}{f}^{(k)}(\vec{v}) = \vec{v}\underset{\sim}{f}^{(k-1)} - \sum_{j=0}^{k} \underset{\sim}{\omega}^{(j)}\underset{\sim}{f}^{(k-j)} \ . \qquad (20)$$

These can be solved by starting with the equation for the spatially averaged velocity distribution $f^{(o)}(\vec{v})$,

$$(a\cdot\nabla_{\underline{v}} + J)f^{(o)}(\vec{v}) = -\omega^{(o)}f^{(o)}(\vec{v}), \tag{21}$$

and proceeding successively to higher values of k.

Eq. (21) defines an eigenvalue problem and, corresponding to the assumption that the hydrodynamic regime is the longtime limit, one associates the lowest eigenvalue $\omega^{(o)}$ with the reaction rate $\alpha = -\omega^{(o)}$. In the absence of reactions this eigenvalue is trivially zero. The equations for $k > 0$ are inhomogeneous and do not represent any eigenvalue problem.

Expressions for $\underset{\sim}{\omega}^{(k)}$'s in terms of the $\underset{\sim}{f}^{(k)}$'s are found by integrating Eq. (20) over $d\vec{v}$, noting that only the reactive part $J^{(R)}$ of the collision operator contributes to this integral, and using Eq. (19);

$$\omega^{(o)} = -\int J^{(R)}\underset{\sim}{f}^{(o)}(\vec{v})d\vec{v} \tag{22a}$$

$$\underset{\sim}{\omega}^{(k)} = -\int\vec{v}\,\underset{\sim}{f}^{(k-1)}(\vec{v})d\vec{v} - \int J^{(R)}\underset{\sim}{f}^{(k)}(\vec{v})d\vec{v}\ . \tag{22b}$$

Note that when reactions are present, the calculation of a transport coefficient of rank k requires solutions of the equations up to order k. In the absence of reactions, solutions to the order k-1 suffice for the same purpose.

CALCULATION OF DRIFT AND DIFFUSION

We now turn to the problem of actually solving the kinetic equations. For the sake of simplicity, we will restrict the discussion to the problem of calculating drift and diffusion of ions moving in homogeneous, electrostatic fields, in the absence of magnetic fields and reactions. The possible presence of several internal states of the ions will be ignored. Those interested can find discussions of systems with internal states in the papers of Viehland et al. (1981) and Kumar et al. (1980, Chap. 26).

The only preferred direction in our problem is now the one provided by the electric field $\vec{E}$, that is, by the acceleration $\vec{a} = q\vec{E}/m$ suffered by the ions. The kinetic equations and the transport coefficients therefore have cylindrical symmetry about this direction $\hat{a}$., and the drift velocity $\vec{v}_{dr}$ and the diffusion tensor $\vec{\vec{D}}$ have the form

$$\vec{v}_{dr} = v_{dr}\,\hat{a}\ , \quad \vec{\vec{D}} = D_L\,\hat{a}\hat{a} + D_T(1 - \hat{a}\hat{a})\ . \tag{23}$$

The kinetic equations needed for the present problem are simplified versions of Eqs. (19-22);

$$Lf^{(o)}(\vec{v}) = 0 \quad \text{with} \quad \int f^{(o)}(\vec{v})d\vec{v} = 1 \tag{24a}$$

$$\text{and} \quad \vec{v}_{dr} = \langle\vec{v}\rangle \equiv \int \vec{v} f^{(o)}(\vec{v})d\vec{v} \tag{24b}$$

$$L\underset{\sim}{f}^{(1)}(\vec{v}) = (\vec{v} - \vec{v}_{dr})f^{(o)}(\vec{v}) \quad \text{with} \quad \int \underset{\sim}{f}^{(1)}(\vec{v})d\vec{v} = 0 \tag{25a}$$

$$\text{and} \quad \overleftrightarrow{D} = \langle\vec{v}\rangle^{(1)} \equiv \int \vec{v}\underset{\sim}{f}^{(1)}(\vec{v})d\vec{v} \tag{25b}$$

where

$$L = \vec{a}\cdot\nabla_{\underline{v}} + J \ . \tag{26}$$

The equations may be transformed to integral equations, which may be solved by iteration, path integral, or computer simulation methods (see, e.g., Braglia (1980) and Kuhn (1981)), and this may ultimately be the most preferable way of proceeding. The main progress the last years has however been in the use of Galerkin methods (i.e., generalized moment methods), and especially in methods using orthogonal polynomial expansions with Gaussian weight functions.

When the ion velocity distribution — or, more critically, the distribution of relative veolocities — is not too anisotropic, it seems reasonable to attempt an expansion around an <u>isotropic</u> Gaussian

$$\omega(\alpha;\vec{v}) = (\alpha^2/2\pi)^{3/2} \exp(-\tfrac{1}{2}\alpha^2 v^2) \ ; \tag{27}$$

α is here a free parameter. It has in general no connection with the gas temperature, but may or may not be related to the kinetic temperature of the ions.

Polynomials orthogonal with $\omega(\alpha;\vec{v})$ are the Burnett functions

$$\phi^{(\underline{\nu})}(\vec{x}) = \phi^{(\underline{\nu})}(\alpha\vec{v}) = R_{\nu\ell}(x)Y_m^{(\ell)}(\hat{x}) \tag{28a}$$

$$R_{\nu\ell}(x) = N_{\nu\ell}(x/\sqrt{2})^{\ell} \, S^{(\nu)}_{\ell+\frac{1}{2}}(\tfrac{1}{2}x^2) \tag{28b}$$

where $Y_m^{(\ell)}$ are spherical harmonics, $S^{(\nu)}_{\ell+\frac{1}{2}}$ the Sonine polynomials, $N_{\nu\ell}$ a normalization factor, and $\underline{\nu} = (\nu,\ell,m)$. We insert for $\underset{\sim}{f}^{(k)}(v)$ expansions of form

$$f(\vec{v}) = \sum_{\ell,\nu} \xi_{\nu}^{(\ell)} \omega(\alpha;\vec{v})\phi_{\ell m}^{(\nu)}(\vec{v}) \tag{29}$$

and transform the Boltzmann equation (with normalization conditions) to a set of linear algebraic equations for the expansion coefficients $\xi_\nu^{(\ell)}$ by using projection operators

$$P^{\nu'}_{\ell' m} = \int d\vec{v}\ \phi^{(\nu')}_{\ell' m}(\vec{v}) \ \ldots . \tag{30}$$

These equations are then solved by standard methods. In the drift and longitudinal diffusion calculations, the index $m \cdot 0$, while in lateral diffusion calculations $m = \pm 1$.

The main problem is in practice the calculation of matrix elements of the collision operator J,

$$J^{(\underline{\nu}\underline{\nu}')} = \int \phi^{(\underline{\nu})}(\vec{v}) J(\omega\phi^{(\underline{\nu}')}(\vec{v}))\, d\vec{v} \tag{31}$$

as this involves the evaluation of an eightfold integral. The spherical symmetry of J makes $J^{(\underline{\nu}\underline{\nu}')}$ diagonal in the ℓ and m indices and also simplifies the calculation of the nonvanishing matrix elements. Nevertheless, the matrix element evaluation becomes unfeasible for large ν and ℓ-values, and this sets limits to basis size and obtainable accuracy in the transport coefficient calculation.

If high accuracies and consequently large basis sets are needed, the choice of basis set parameter $\alpha = (m/2kT_b)^{1/2}$ is not critical, as shown in Fig. 1 (from Kumar et al., 1980). For a rough (5-10%) estimate of the drift velocity, the lowest order approximation of Viehland and Mason (1978) may be used,

$$\vec{v}_{dr} \approx \frac{3}{8} q \frac{E}{n_o} \left(\frac{\pi}{2mkT_{eff}} \frac{m + m_o}{m_o}\right)^{1/2} / \Omega^{(1,1)}(T_{eff}) \tag{32}$$

$$kT_{eff} = kT_o + \frac{1}{3} m_o v_{dr}^2 \ . \tag{33}$$

Here $\Omega^{(1,1)}$ is one of the usual "Ω-integrals" in transport theory (see e.g., Ferziger and Kaper (1972)).

When the velocity distribution is very anisotropic, as for heavy ions in a light gas, expansions around isotropic gaussians do not converge satisfactorily. Lin et al. (1979) introduced instead of polynomial expansion around an anisotropic drifted gaussian. The collision operator matrix elements are more difficult to evaluate in this case, but this difficulty is compensated for by a much faster convergence. Especially is the diffusion calculation drastically bettered.

Considerations over the asymptotic behavior of velocity distribution show the high energy tail to be of form (Wannier, (1953).

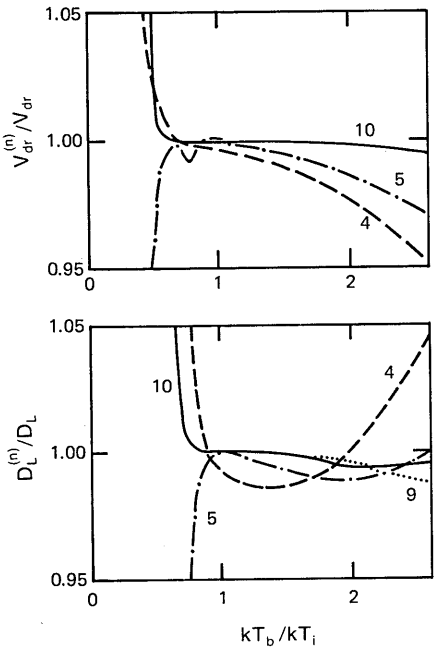

Fig. 1. Successive approximations in a Burnett function basis with isotropic weight function as a function of basis temperature T_b, for a hard sphere, cold gas, unit mass ratio model. Numbers on the graph indicate $n = \ell_{max} = \nu_{max}$; $(kT_i = 1/2\ m(\langle v^2\rangle - v_{dr}^2)$; $v_{dr} = 1.1467\ (a\lambda)^{1/2}$; $D_L = 0.2202\ (a\lambda^3)^{1/2}$, with λ the mean free path) .

$$f(\vec{v}) \sim \exp(-\int^{v} \nu(v')dv'/a) \qquad (34)$$

where v is a characteristic collision frequency. For realistic interactions, the tail Eq. (34) falls off slower than any gaussian. Despite their success in transport coefficient calculations, the Gaussian polynomial expansions can therefore not be absolutely convergent, and for "difficult" cases, one may have to resort to other techniques.

REFERENCES

Braglia, G. L., 1980, Beitr. Plasmaphys. 20:147.
Ferziger, J. H. and Kaper, H. G., 1972, "Mathematical Theory of Transport Process in Gases," North Holland, Amsterdam.

Kaneko, Y., 1980, in "Proceedings, 11th International Conference on the Physics of Electronic and Atomic Collisions, Kyoto," Invited Papers and Progress Reports, North Holland, Amsterdam, p. 109.
Kuhn, S., 1980, Phys. Rev. A, 22:2460.
Kumar, K. and Robson, R.E., 1973, Aust. J. Phys. 26:157.
Kumar, K., Skullerud, H. R., and Robson, R. E., 1980, Aust. J. Phys., 33:343.
Lin, S. L., Viehland, L. A. and Mason, E. A., 1979, Chem. Phys. 37:411.
Viehland, L. A., Harrington, M. M., and Mason, E. A., 1976, J. Chem. Phys., 17:433.
Wannier, G. G., 1953, Bell Sys. Tech. J., 32:170.
Weinert, U., 1980, Phys. Fluids, 23:1518.

ON THE DIVERGENCE OF THE LEGENDRE EXPANSION OF THE ELECTRON VELOCITY DISTRIBUTION

W. P. Allis

Joint Institute for Laboratory Astrophysics
Boulder, Colorado
and
Laboratoire de Physique des Gas et des Plasmas
Orsay, France

INTRODUCTION

In this chapter, we consider the velocity distribution of free electrons in a gas of stationary molecules subjected to an electric field $E = - ma/e$ but with no density gradients. We first discuss the distribution $\phi(\vec{v})$ when the electrons disappear, by attachment or recombination, at each collision, and then introduce the scattered-in electrons as a separate source function $S(v,f)$ to evaluate the full distribution $f(\vec{v})$. It will be seen that the functions ϕ are a recognizable part of the function f. They describe the collision-less "streaming" of the fast electrons in front of the swarm which gain energy from the field and effectively disappear on collision, whereas the bulk of the distribution is determined by the balance between energy gained from the field and lost to recoil or inelastic collisions.

SCATTERING-OUT-ONLY

Cylindrical Coordinates

The Boltzmann equation with no scattering-in term or gradients is

$$\frac{\partial \phi}{\partial t} + a \frac{\partial \phi}{\partial v_z} + \nu_c \phi = 0 \qquad (1)$$

where $\nu_c(v) = NQ_c v$ is the total collision frequency. The charac-

teristics of Eq. (1)

$$dt = dv_z/a = -d\phi/\nu_c\phi \ , \ dv_r = 0 \tag{2}$$

are the dynamical trajectories, and the stationary solution is determined by the trajectory integral

$$\zeta(v_r,v_z) = \int_o^{\nu_z} \frac{\nu_c}{a}\, dv_z \tag{3}$$

with v_r constant; and

$$\phi = R(v_r^2)e^{-\zeta}. \tag{4}$$

$R(v_r^2)$ is a completely arbitrary function in the plane $v_z = 0$, but we are assuming cylindrical symmetry. The function $\zeta(v_r v_z)$ is defined for all v_z, but in general $\zeta \to -\infty$ as $v_z \to -\infty$; hence $\phi \to \infty$, which is physically not acceptable. There is no finite static solution for the electron distribution in an attaching gas, and the infinity represents a source of electrons at $v_z = -\infty$. Equation (4) shows how the density decays as the electrons drift downfield.

The integral (3) is to be computed from exact total cross sections $Q_c(v)$, but in the analysis, it is often convenient to assume a power law dependence;

$$\nu_c = N_c\, v^{h-1} = Nqu^{(h-1)/2} \tag{5}$$

$$u = mv^2/2e \ ,$$

and in this case a simple dimensional argument shows that the function $\zeta(v,\theta)$ is separable,

$$\zeta(v,\theta) = w(v)\psi(\theta)$$

$$w = \int \frac{\nu_c}{a}\, dv = \int \frac{NQ_c}{E}\, du \to \frac{\nu_c v}{ah} = \frac{2NQu}{Eh} \ , \tag{6}$$

and the corresponding angle functions are given by the table

$h =$	-1	0	1	2
$\psi_h =$	$\frac{2\theta-\Pi}{2\sigma}$	$\frac{1}{2}\,\ell n\,\frac{1+\mu}{1-\mu}$	μ	$\mu + \frac{\sigma^2}{2}\,\ell n\,\frac{1+\mu}{1-\mu}$

(7a)

$\mu = \cos\theta$ $\qquad$ $\sigma = \sin\theta$

and the recursion relation

$$\psi_{h+2} = \mu + (1 + 1/h)\sigma^2\psi_h \quad . \tag{7b}$$

The constant collision frequency $h = 1$, $w = \nu_c\, v/a$ and constant cross section $h = 2$, $w = NQ_c u/E$ are, respectively, the mathematically simplest and most commonly used assumptions.

Spherical Coordinates

When we introduce scattering-in, the artificial source at $v_z = -\infty$ will be redistributed with nearly spherical symmetry, and the boundary condition will be that $f \to 0$ as $v \to \infty$, also spherically symmetrical. This constrains us to convert the differential equation (1) to spherical coordinates

$$\mu \frac{\partial \phi}{\partial v} + \frac{\sigma^2}{v} \frac{\partial \phi}{\partial \mu} + \frac{\nu_c}{a} \phi = 0 \quad . \tag{8}$$

This does not change the characteristics (2), and the broken symmetry between characteristics and boundaries is the source of the mathematical difficulties we will encounter.

If we substitute $\phi = R(v_r^2)$ in (8), the derivatives of R cancel, and the function R divides out.

If we substitute

$$\phi = e^{-w(v)\psi(\mu)}, \tag{9}$$

$w(v)$ and $\psi(\mu)$ being arbitrary functions, we obtain

$$\mu\, w'\, \psi + \frac{\sigma^2}{v}\, w\, \psi' = \frac{\nu_c}{a} \quad , \tag{10}$$

and the variables separate only if

$$\frac{aw'}{\nu_c} = h \frac{aw}{\nu_c v} = \text{const} = 1 \tag{11}$$

where h is an arbitrary constant, and the constant to the right would divide out in ψ if it were not incorporated in w. But (11) leads precisely back to (6), so the power law is not only sufficient but necessary for the form (9) to hold.

Substituting from (11) into (10) we obtain for ψ

$$\psi = h\sigma^h \int_o^\mu \frac{d\mu}{\sigma^{2+h}} \tag{12}$$

which is an alternative to (7) for evaluating ψ.

Legendre Expansion

We shall define an unconventional Legendre coefficient by

$$\phi_\ell = \frac{1}{2}(-)^\ell \int_{-1}^{1} \phi\ (v,\mu)\ P_\ell(\mu)\ d\mu \tag{13}$$

in which the factor $(-)^\ell$ has replaced the usual $(2\ell+1)$. Applying this transformation to Eq. (8) and using the formulae for the derivative of P_ℓ, we obtain the recursion relation for the ϕ_ℓ:

$$(\ell+1)\left(\frac{d}{dv} + \frac{\ell+2}{v}\right)\phi_{\ell+1} + \ell\left(\frac{d}{dv} - \frac{\ell-1}{v}\right)\phi_{\ell-1} = \frac{\nu_c}{a}(2\ell+1)\phi_\ell . \tag{14}$$

The parameter ν_c/a, or NQ_c/E, can be eliminated by using w as independent variable and using the power law

$$(\ell+1)\left(\frac{d}{dw} + \frac{\ell+2}{hw}\right)\phi_{\ell+1} + \ell\left(\frac{d}{dw} - \frac{\ell-1}{hw}\right)\phi_{\ell-1} = (2\ell+1)\phi_\ell . \tag{15}$$

Solutions of these equations will be called "scattering-out-only" functions, or SOO-functions. They are in general Legendre components of the functions (4), but these are usually difficult to calculate because of the awkward functions $\psi(\mu)$. In the case h = 1, a constant collision frequency ν_c, $w = \nu_c v/a$, $\psi = \mu$, and the integrals are easy. Chosing R = 1, $\phi = e^{-w\mu}$, we find

$$\phi_o = \frac{\sinh w}{w} = 1 + \frac{w^2}{3!} + \frac{w^4}{5!} + \frac{w^6}{7!} + \text{--}$$

$$\phi_1 = \frac{\cosh w}{w} - \frac{\sinh w}{w^2} = 2w\left(\frac{1}{3!} + \frac{2w^2}{5!} + \frac{3w^4}{7!} + \text{--}\right) \tag{16}$$

$$\phi_2 = \frac{\sinh w}{w} - \frac{3\cosh w}{w^2} + \frac{3\sinh w}{w^3} = 8w\left(\frac{1}{5!} + \frac{3w^2}{7!} + \text{--}\right)$$

and in general a power series starting with

$$w^\ell/1\cdot3\cdot5\cdot\text{---}\ (2\ell+1) .$$

Using the relation $(2\ell+1)\ P_\ell = P'_{\ell+1} - P'_{\ell-1}$, one finds that

$$\frac{2\ell+1}{w}\phi_\ell = \phi_{\ell-1} - \phi_{\ell+1} . \tag{17}$$

The functions (16) are recognized (Abramowitz and Stegun, 1965, p. 443) as modified spherical Bessel functions of the first kind:

$$\phi_\ell = \sqrt{\frac{\pi}{2w}}\ I_{\ell+1/2}^{(w)}\ , \tag{18}$$

These Bessell functions also have the step-down and step-up operators

$$\left(\frac{d}{dw} + \frac{\ell+2}{w}\right)\ \phi_{\ell+1} = \phi_\ell \quad \text{and}$$

$$\left(\frac{d}{dw} - \frac{\ell-1}{w}\right)\ \phi_{\ell-1} = \phi_\ell\ , \tag{19}$$

and these make it obvious that these functions satisfy (15) for $h = 1$. The corresponding functions satisfying (15) (S00-functions) for $h \neq 1$ have not been found, and we know that operators similar to (19) with $h \neq 1$ do not commute so that it is not easy to find a second order differential equation for them. But nevertheless they exist and must have similar properties.

The modified spherical Bessel functions (MSBF) of the third kind with alternating sign

$$\sqrt{\frac{\pi}{2w}}\ K_{1/2} = \frac{\pi}{2w}\ e^{-w} \qquad \phi_\ell = (-)^\ell \sqrt{\frac{\pi}{2w}}\ K_{\ell+1/2} \tag{20}$$

$$\sqrt{\frac{\pi}{2w}}\ K_{3/2} = \frac{\pi}{2w}\ e^{-w}\ (1+1/w)$$

$$\sqrt{\frac{\pi}{2w}}\ K_{5/2} = \frac{\pi}{2w}\ e^{-w}\ (1+3/w+3/w^2)$$

also satisfy (19) and hence (15), are S00 functions, and can be derived from (4) by integrating as in (13) but with limits 1 to ∞ for μ. The MSBF of the first kind diverge at $w \to \infty$ which corresponds to $v_z \to -\infty$ in (4) and injection at that boundary. The MSBF of the third kind diverge at the origin, $w \to o$, which is a boundary in spherical coordinates.

Converting to normal Legendre coefficients

$$f_\ell = (-)^\ell\ (2\ell + 1)\ \phi_e = (2\ell+1)\ \sqrt{\frac{\pi}{2w}}\ K_{\ell+1/2}^{(\omega)}\ , \quad (h=1) \tag{21}$$

The high energy limit of all the $K^{(\omega)}_{\ell+1/2}$ are the same, and in this limit the Legendre series can be summed

$$f \to \sum (2\ell+1)\, \frac{\pi}{2w}\, e^{-w}\, P_\ell(\mu) = \frac{\pi}{w}\, e^{-w}\, \delta(\mu-1). \tag{22}$$

This represents a parallel beam of electrons in the direction of $\vec{a}$ whose current-density $vf \approx \pi a/\nu_c$ decays exponentially as e^{-w}. For $h \neq 1$, $w^{1/h}$ is in the denominator. This is the "maximum anisotropy" of Baraff and the distributions calculated by Baraff and Buchsbaum (1963) were S00 functions when the electrons were all returned with zero energy.

There is also a particular integral of Eq. (14) valid for all h

$$\phi_\ell = (-)^\ell\, e^{-w}/u \tag{23}$$

which sums to $f = \pi e^{-w}\delta(\mu-1)/u$ and corresponds to injection at $u = 0$.

If we consider the parenthesis in (15) to be first order Taylor series of $\phi_{\ell\pm1}(w + a)$, these equations become

$$(\ell+1)(\ell+2)\phi_{\ell+1}\left(w + \frac{hw}{\ell+2}\right) - \ell(\ell-1)\phi_{\ell-1}\left(w - \frac{hw}{\ell-1}\right) = (2\ell\pm1)hw\ \phi_\ell,$$

which indicates that $\phi_\ell(w)$ is "related" to the neighboring $\phi_{\ell\pm1}$ along the approximate lines

$$\frac{\Delta w}{\Delta \ell} \approx \frac{2hw}{2\ell+1\pm3}\ . \tag{24}$$

For instance, if two neighboring $\phi_\ell = 0$ lie along such a line, all ϕ_ℓ will be zero along this line, and maxima or minima will follow the same approximate rule. These "tracks" of similarities across energy-index printouts from computers are quite striking and follow (24) except for factors of the order 2.

SCATTERING-IN-ALSO

Near the Origin Inelastic Scattering-In

We have seen that injection at the origin leads to a pole at the origin and MSBF of the third kind for $h = 1$ or similar functions for $h \neq 1$. We will now consider a distributed "injection" due to inelastic collisions at higher energies u^+. Collisions at v^+ which excite levels of critical potentials $V_k = mv_k^2/2e$ produce secondary electrons of velocity v such that

$$v^2 = v^{+2} - v_k^2 \quad . \tag{25}$$

Symbols without superscripts represent post-collision quantities whereas $(\ )^+$ indicates that the quantities in the parentheses are those before the collision. The total excitation frequency density is given by

$$d\nu_x = \sum_k (\nu_k f_o)^+ 4\pi v^{+2} dv^+ = \sum_k (\nu_k f_o)^+ 2\pi v^+ dv^{+2} = S_x 2\pi v dv^2 \tag{26}$$

in which it has been assumed that the inelastic scattering is isotropic and hence depends only on f_o^+. Because of energy conservation (25), $dv^{+2} = dv^2$ and hence

$$S_x = \frac{1}{v} \sum_k (\nu_k v f_o)^+ = \frac{N}{v} \sum_k (Q_k v^2 f_o)^+ . \tag{27}$$

We will assume that all inelastic cross sections Q_k^+ vary with the same power of the post-collision velocity v

$$Q_k^+ = q_k v^j , \tag{28}$$

so that the inelastic scattering-in is

$$S_x = v^{j-1} N \Sigma q_k (v_k^2 + v^2) f_o^+ = s v^{j-1} \tag{29}$$

and

$$S_{el} = v^{h-1} c f_o \quad .$$

The Boltzmann equation can then be written

$$a \frac{\partial f}{\partial v_z} + \nu_c f = S_{el} + S_x = S \ , \tag{30}$$

which does not explicitly contain the inelastic scattering-out because we are now considering energies below the lowest excitation potential. The formal solution of (30) is

$$f = e^{-\zeta} \int_{-\infty}^{v_z} e^{\zeta} \frac{S}{a} dv_z = e^{-\zeta} \int_{-\infty}^{\zeta} \frac{S}{\nu_c} e^{\zeta} d\zeta \ ; \tag{31}$$

and it is convenient to split the integral into two parts

$$R(v_r^2) = \int_{-\infty}^{0} e^{\zeta} \frac{S}{a}\, dv_z \qquad Q(v_r,v_z) = \int_{0}^{v_z} e^{\zeta} \frac{S}{a}\, dv_z \tag{32}$$

where $R(v_r^2)$ is the same function as written in Eq. (4) but is now expressed as the electron density drifting onto the plane $v_z = 0$ from the lower half-space.

In order to evaluate these integrals, we shall make several assumptions. First we assume $h > j$ so that $S_x > S_{el}$ at small velocities, and next we assume $h = 1$, ν_c constant because integral $R(v_r^2)$ is then found in the tables in terms of gamma, Struve, and Newmann functions (Abramowitz and Stegun, 1965, 12.1.8) $v_d = a/\nu_c$,

$$R_j = \frac{s\sqrt{\pi}}{a} \frac{1}{2^{\Gamma}} \left(\frac{j+1}{2}\right) (2\, v_r)^j \left[H_{j/2}\,(v_r/v_d) - N_{j/2}(v_r/v_d)\right], \tag{33}$$

$Q(v_r,v_z)$ can be found for any h by expanding e^{ζ} in power series. The results are

$$h - j = 2 \quad R + Q = \frac{s}{a}\left[\frac{\Pi-\theta}{v_r} + \frac{1}{v_d}\left(\ln \frac{\gamma v}{v_d} - 1\right)\right],$$

$$h - j = 1 \quad R + Q = \frac{s}{a}\left[\ln \frac{2v_d/\gamma}{v-v_z} + \frac{v}{v_d}\right], \text{ and} \tag{34}$$

$$h = j \qquad R + Q = \frac{s}{\nu_c} e^{\zeta}, \quad \gamma = 1.7811 .$$

In the three cases, R and Q contribute about equally to the answer, and they have been indexed by the value of h-j because this is the power of the singularity in the integral of (31), and it is expected that the results are not sensitive to the value of h separately. In the first two, only the inelastic scattering-in enters. In the third, elastic and inelastic combine and the solution is exact. For $h < j$, elastic scattering-in dominates.

The singularity of $h - j = 2$ is the same as that found by Baraff and Buchsbaum (1963) in their "maximum loss approximation," and the assumption $h - j = 1$ corresponds to assuming a step function at V_k for $Q_k(v)$.

The $\ell = 0$ Equation

If we introduce the full scattering-in formula, including recoil loss but assuming isotropic scattering and neglecting gas temperature, the Boltzmann equation becomes

$$a \frac{\partial f}{\partial v_z} + \nu_c (f-f_o) =$$

$$= \frac{1}{v^2} \frac{d}{dv} \frac{m}{M+m} \nu_d v^3 f_o + \frac{(\nu_k v f_o)^+}{v} - \nu_c f_o = \qquad (35)$$

$$= \frac{v}{u} [\frac{d}{du} \frac{m}{M+m} Ne_{el} u^2 f_o + (NQ_k uf_o)^+ - NQ_k uf_o],$$

where summations over k are to be understood. Making a conventional (not as in Eq. (13)) Legendre transformation, we obtain the set of equations

$$\frac{\ell + 1}{2\ell+ 3} (\frac{d}{du} + \frac{\ell+2}{2 u}) f_{\ell+1} + \frac{\ell}{2\ell-1} (\frac{d}{du} - \frac{\ell-1}{2u}) f_{\ell-1} = - \frac{NQ_c}{E} f_\ell \qquad (36)$$

for $\ell \neq 0$. This set corresponds exactly to (14) and is satisfied by the functions $(-)^\ell (2\ell+1)\phi_\ell$. But the zero-order equation is different as it contains the scattering-in. It is

$$\frac{E}{3} \frac{d}{du} uf_1 = N [\frac{d}{du} \frac{2 m}{M+m} Q_{e\ell} u^2 f_o + (Q_k uf_o)^+ - Q_k uf_o]. \qquad (37)$$

The left side and the recoil term integrate directly. The integrals of the two inelastic terms cancel each other above $u + u_k$, and the second term is zero for $u < u_k$. Consequently

$$\int_0^u [(Q_k uf_o)^+ - Q_k uf_o] du = \int_{u(k)}^{u+u_k} Q_k uf_o du \qquad (38)$$

where $u_{(k)} = u$ or u_k, whichever is larger. Equation (38) represents the total rate of ionization between $u_{(k)}$ and $u + u_k$, or equivalently the downflux of electrons crossing the energy level u.

It is convenient to define the total effective inelastic loss cross section between $u_{(k)}$ and $u + u_k$ by the weighted average

$$Q_x(u) = \frac{1}{u^2 f_o(u)} \sum_k \int_{u_{(k)}}^{u+u_k} Q_k uf_o(u) du, \qquad (39)$$

and we note that it is referred to the post-collision energy u. The general behavior of this cross section is illustrated by assuming that near threshold

$$Q_k = q_k\ (u-u_k) \text{ and } f_o^+ = f_o(u_k)\ .$$

We then find for $u < u_k$

$$Q_x = \frac{1}{2}\, Q_k(2u_k)\quad (1 + \frac{2u}{3u_k})\quad \frac{f_o(u_k)}{f_o(u)}\ , \tag{40}$$

and at high energies, we assume that

$$Q_k = q_k/u \qquad f_o = e^{-w}$$

$$Q_x = \sum q_k(u)\, \frac{E}{NQ_c\, u}\ (\ 1 - e^{-w_k})\ . \tag{41}$$

In between, Q_x has a maximum near where inelastic scattering-in = scattering-out

$$(u + u_k)\ f_o(u+u_k) = (u-u_k)\ f_o(u) \tag{42}$$

which is necessarily above the excitation potential. $Q_x(u)$ is a relatively smooth function, but, of course, cannot be calculated until we know f_o.

Integrating Eq. (37) and introducing the effective inelastic loss cross section $Q_x(u)$ yields the ratio

$$\frac{f_1}{f_o} = \frac{3N}{E}\ [\frac{2m}{M+m}\, Q_{e\ell} + Q_x(u)]\ u\ . \tag{43}$$

This is nearly always a monotonously increasing function of u, and the equation

$$[\frac{2m}{M+m}\, Q_{e\ell} + Q_x(u_1)]\ u_1 = E/3N \tag{44}$$

determines a crossing energy u_1 at which $f_1 = f_o$. Below u_1, $f_1 < f_o$, and the distribution is fairly isotropic because the scattering-in dominates Eq. (35). But above u_1, $f_1 > f_o$, and the distribution is dominantly in the forward direction, that of the acceleration a. Expressed in units of the variable w, Eq. (44) becomes

$$w_1 = \frac{2Q_{c/3h}}{\frac{2m}{M+m}\, Q_{e\ell} + Q_x} \tag{45}$$

so that 2/3 hw is simply the ratio of the loss cross section to the

total cross section and depends upon E/p only implicitly as it enters in the definition of Q_x.

The P_1 Approximation

The ratio f_1/f_o expressed by Eq. (43) is the complete equivalent of the $\ell = 0$ equation (37) and acts as a "boundary condition" to the infinite set of equations (36) whose solutions apart from this are the known S00 functions. Physically Eq. (43) must replace the infinite boundary sources of the S00 functions by a distributed source which conserves electrons. For energies below w_1, $f_1 < f_o$, and one may expect that $f_2 < f_1$ and that it is therefore a good approximation to neglect f_2 in the $\ell = 1$ equation. This uncouples the remaining equations and gives the P_1 approximation:

$$f_1 = \frac{-E}{NQ_c} \frac{df_o}{du} = - \frac{df_o}{dw} , \qquad (46)$$

Inserting this in (37) gives a second order differential equation which may be directly solved numerically, but for discussion it is better to use the first integral (43), which integrates a second time to

$$f_o = A\, e^{-g}$$

$$g = \int_o^u 3 \frac{N^2}{E^2} Q_c \left(\frac{2m}{M+m} Q_{e\ell} + Q_x \right) udu = \int_o^w \frac{3h}{2} \frac{\frac{2m}{M+m} Q_{e\ell}+Q_x}{Q_c} wdw = \beta w^2 \qquad (47)$$

where $\beta(u)$ will in general vary slowly compared to w^2. Setting $Q_x = 0$, $Q_c = Q_{e\ell}$, and $h = 2$, we obtain the Druyvesteyn distribution; so (47) is a generalization of the Druyvesteyn distribution, and it can be set into (39) with an estimated β to obtain $Q_x(u)$ and hence an improved $\beta(u)$. If the cross section ratios are all constant, $\beta = 1/2\, w_1$.

For energies above u_1, the neglect of f_2 is not only a priori unjustified, but the P_1 approximation

$$f = f_o + f_1 \cos\theta = \left(1 + \frac{3h}{2} \frac{\frac{2m}{M+m} Q_{e\ell}+Q_x}{Q_c} w \cos\theta\right) f_o \qquad (48)$$

shows it by becoming negative in the backward direction for

$$w \cos\theta < - \frac{2Q_c/3h}{\frac{2m}{M+m} Q_{e\ell}+Q_x(w)} . \qquad (49)$$

This situation requires the appearance of an appreciable f_2 above $u = u_1$. But f_2/f_1 will also increase with u and eventually f_2 will become too big and produce negative areas which will require an appreciable f_3, and so on. Thus the set of f_ℓ's will change progressively with increasing energy from a decreasing to an increasing sequence resembling the set of MSBF. This happens because we have assumed that the electrons removed at u^+ were returned at a lower energy u, and hence scattering-out-only dominates the higher energies. With superelastic collisions this might not hold.

COMPUTATIONS

The Component Distributions

The convergence of the Legendre expansion was tested on the simple model of constant cross sections and recoil loss only, hence the Druyvesteyn model. The following mass-ratios were used:

$$M/m = 1.4, \quad 11, \quad 59;$$

$$\text{hence, } w_1 = \frac{M+m}{6m} = 0.4, \; 2, \quad 10. \tag{50}$$

The small mass-ratios were used to simulate inelastic losses Q_x according to the equivalence indicated by Eq. (43). The computations were carried out by Dr. Leanne Pitchford on the Cray computer at NCAR. The expansion was carried to $\ell=7$ and tuncated ($f_8=0$), and the results are shown in the following figures.

Figure 1 compares computed curves of f_o and shows that they approach the Druyvesteyn distribution for large w_1, even for $w > w_1$ when $w_1 = 10$, but for $w_1 = 0.4$ the comparison is poor everywhere. However, if we compare average energies $\bar{u}$ with that of the Druyvesteyn $\bar{u}_D$ we find

$$w_1 = 0.4, \quad 2, \quad 10$$

$$\bar{u}/\bar{u}_D \quad .915, \quad .978, \quad .995 \; . \tag{51}$$

Even for $w_1 = 0.4$ the error is only 10%.

Computed values of the f_ℓ's extend over eleven decades, and semilog plots show only the exponential decay. Multiplying throughout by e^w, they fall within one decade. Figure 2 shows $e^w f_\ell(w)$ for $w_1 = 2$ and $u \leq \ell \leq 4$. Curves for $w_1 = 0.4$ or 10 are quite similar. Curves for $\ell = 5,6,7$ are not shown because they confuse the figure. The high energy parts of these f_ℓ are clearly pulled down by setting $f_8 = 0$ and cut across the others. All distributions for $\ell > 1$ start

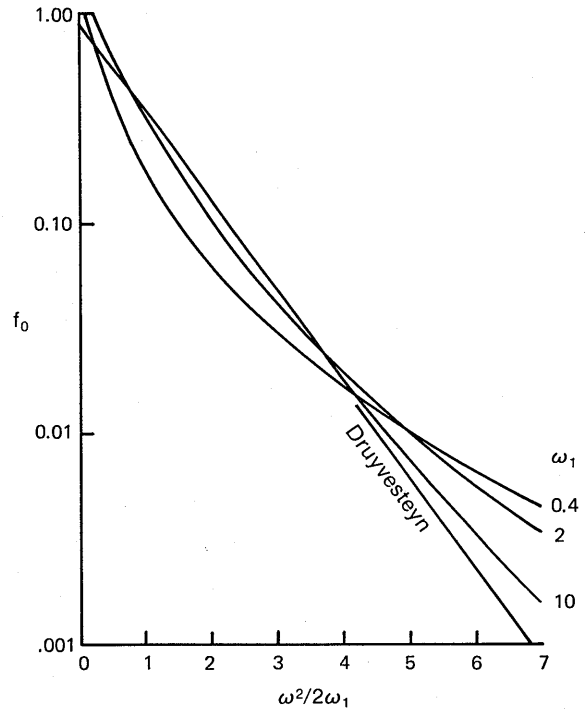

Fig. 1. f_o plotted against $w^2/2w_1$ for $w_1 = 0.4, 2, 10$. +10 shows the progressive deviations from the Druyvesteyn function as w_1 decreases.

out negative, turn up and cross zero, cross $f_{\ell-1}$, pass a maximum and decay as $1/w^{\alpha}$ with $\alpha \geq 1$. f_ℓ crosses $f_{\ell-1}$ at approximately ℓw_1; i.e., the crossings are about evenly spaced in w. Clearly f_2 cannot be neglected after it crosses f_o at about 1.5 w_1. Except at low energies, the f_ℓ are all positives, which means that they add in the forward direction producing a "tongue" of fast electrons and tend to cancel each other in the backward direction, as anticipated. The errors in the higher ℓ's would be greatly reduced if the Baraff truncation

$$\frac{f_\ell}{2\ell+1} + \frac{f_{\ell-1}}{2\ell-1} \tag{52}$$

were used when $w > \ell\, w_1$ and the ratio scaled down to zero at lower energies.

Figure 3 shows the "tracks" in a computer printout (energy increases downwards). The steps show the crossovers: $f_{\ell-1} < f_\ell$ (divergence) on the left of this line and $f_{\ell-1} > f_\ell$ (convergence) in the

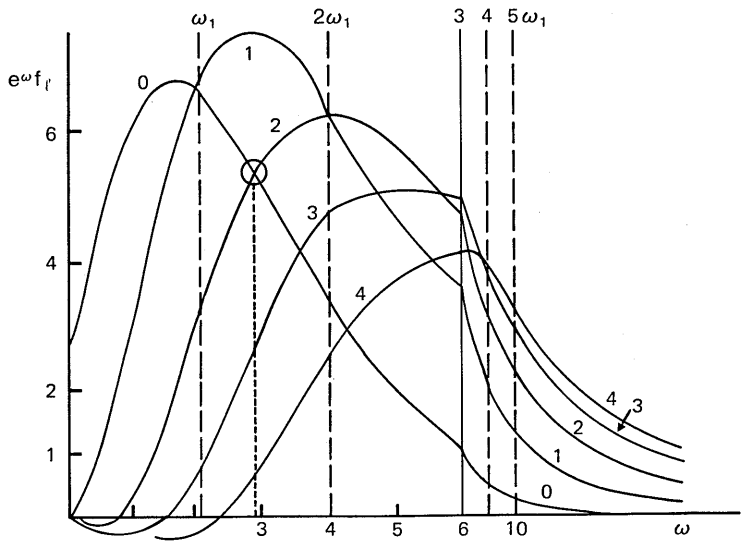

Fig. 2. Plots of $e^{w} f_{\ell}(w)$ for $w_1 = 2$ and $\ell = 0$ to 4. Note the change of scale at $w = 6$.

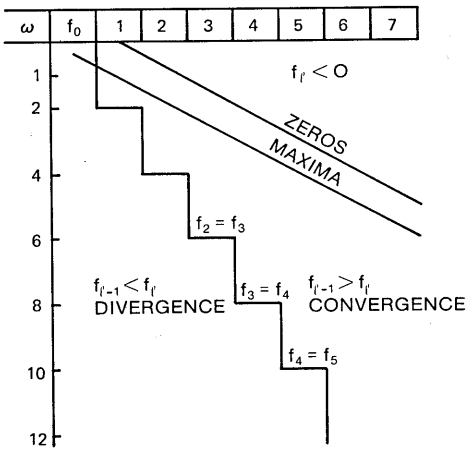

Fig. 3. Tracks on a computer printout.

right. The tracks of the maxima and zeroes are lines which agree very roughly with the prediction of Eq. (24).

The Partial Sums

We are particularly interested in the convergence, or rather the lack of it, which is exhibited by the partial sums in the backward direction:

$$F_L(w) = \sum_0^L e^w f_\ell(w)\ P_\ell(-1) = \sum_0^L (-)^\ell e^w f_\ell \ . \qquad (53)$$

These are shown for $w_1 = 2$ in the sequence of Figures 4a, 4b, and 4c, which covers successive ranges of energy, each at a different scale.

These show that odd sums (even L) remain positive whereas even sums (odd L) cross the axis once at w_L and remain negative, confirming our earlier statement that each f_ℓ overcorrects the error of $f_{\ell-1}$. w_1 is, as previously defined, the zero of the P_1 approximation, but the w_L are not evenly spaced as were the crossovers w_x; they crowd together as L increases. The curves also show that shortly after each w_L, F_{L+1} turns up — again, the overcorrection — and this bend gets sharper and closer to the axis as L increases. Below w_L the functions F_L and F_{L+1} are close to each other and probably give a reasonable approximation to F. Beyond w_L there is no convergence, and nowhere is there any preference for even over odd sums. The only advantage of even sums is that the divergence becomes obvious by the negative sign.

That all was not well with the P_1 approximation has been evident for a long time. The exponent g of Eq. (47) varies as $(p/E)^2$ is modified by $Q_x(u)$ which itself depends upon $f_o(u)$ and hence on $(p/E)^2$. There is no easy way to get an exponent linear in p/E. Yet Stoletow (1890) showed that the ionization coefficient α/p varied as $e^{-Bp/E}$ for high, but reasonable, E/p, and this has been well confirmed. Now the S00 functions all vary as $Re^{-\zeta}$ and $\zeta = 2NQu/hE\ \psi(\theta)$ so that any S00 function will give the Stoletow formula directly, and the value of p/E at which the log plot of α/p vs. p/E becomes straight, should correspond approximately to

$$N/E \leq w_1/Q_c\ V_i .$$

It is difficult to extend the convergence of the Legendre expansion beyond the P_1 approximation. In this case by extending the sum from 2 to 8 terms, the range of convergence has been extended from w = 2 to $2 = 4 = 2w_1$. Figure 4b shows that for $w_1 = 2$ the range is extended from 2 to $4 = 2w_1$. Perhaps we can generalize and say that the range is extended by a factor $\sqrt{(L+1)/2}$. Thus it is

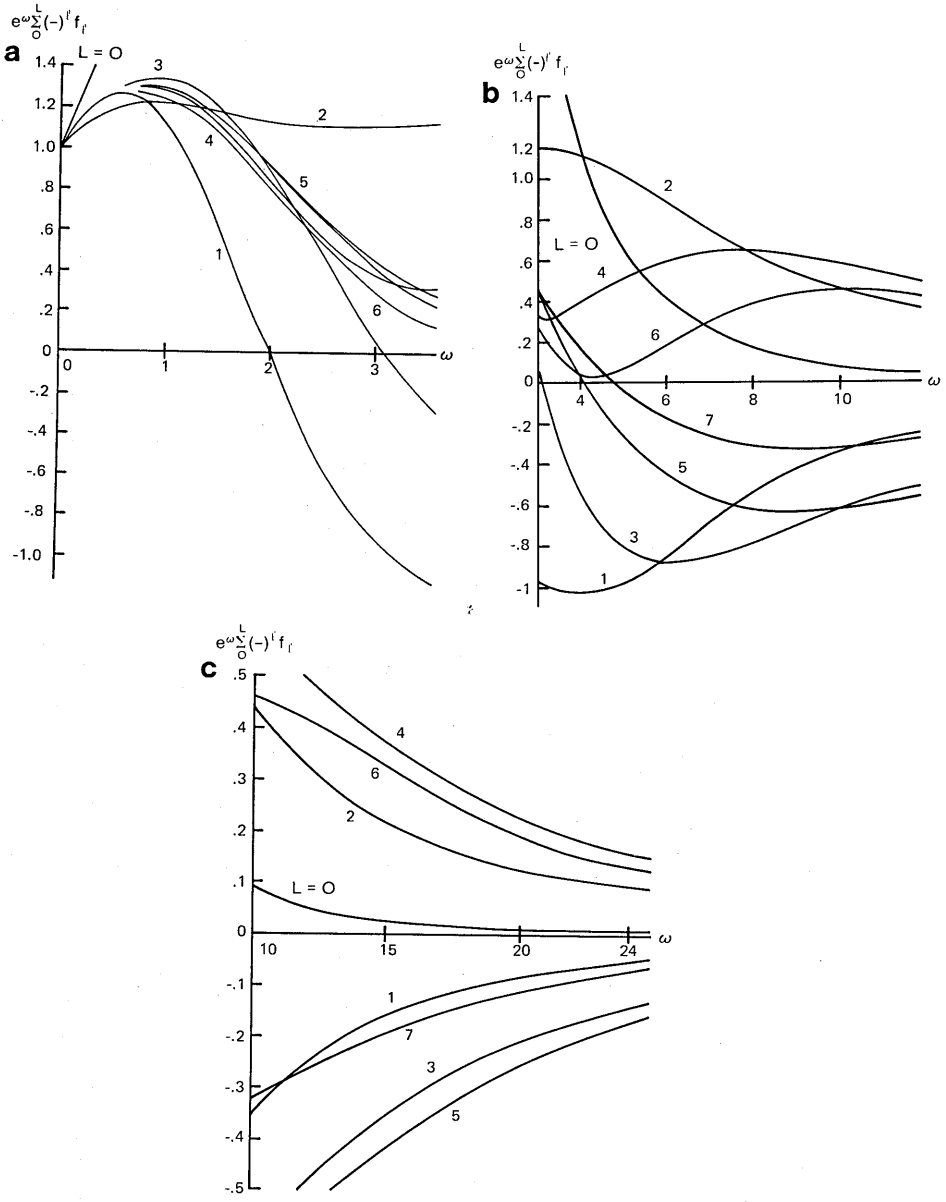

Fig. 4. Partial sums of $e^{w} f(w) P(-1)$ for $w_1 = 2$. 4a) $0 \leq w \leq 3.5$-convergence, 4b) $3 < w < 16$-confusion! 4c) $10 < w < 25$-divergence.

necessary to extend the expansion from L = 1 to L = 7 in order to double the range of w for which the computations are valid.

Granting that the P_1 approximation is invalid above w_1, how bad is this? At $w = w_1$, $f_o = e^{-w1/2}$. For $w_1 = 2$, 1/e of the distribution is invalid. For $w_1 = 2$, $f_o(w_1) = e^{-5} = 1/150$ which might give 1% accuracy.

ITERATION IN CYLINDRICAL COORDINATES

To obtain the limiting forms of the distribution function, it is necessary to go back to the trajectory integral equation (31) and solve it by iteration. [This was done for hydrogens by Baraff and Bucksbaum (1963).] We start with the P_1 approximation

$$f_o = e^{-w^2/2w_1} \tag{54}$$

where $w_1(w)$ may be a slow variable which at least varies less rapidly than w and also write

$$S/\nu_c = s\, f_o \tag{55}$$

where s(w) may also vary but more slowly than f_o. Its weighted average must be one because total scattering-in must equal scattering-out.

The integral equation is then

$$f = e^{-\zeta} \int_{-\infty}^{\zeta} s e^{\zeta - w^2/2w_1}\, d\,\zeta. \tag{56}$$

The exponent has a maximum, where

$$w_1\, d\,\zeta = wdw$$

$$\text{or} \quad w_1 dv_z = wdv = w(v_z/v)dv_z \tag{57}$$

$$w_1 = \mu w \quad .$$

This defines a surface, a plane, if w_1 is constant, which cuts the v_z-axis at $w = w_1$ — precisely where the P_1 approximation gets into trouble. This surface is a line of saddle-points in the complex ζ-plane, and saddle-point integration may be used to evaluate (56). Also the function f may be expected to have a different form on the two sides of the saddle-surface (57).

This will be illustrated by assuming a constant collision frequency. The functions w and ζ are then linear in v and v_z so that they separate

$$\begin{cases} \zeta = v_z \nu_c/a \\ \\ \rho = v_r \nu_c/a \end{cases} \qquad w^2 = \zeta^2 + \rho^2$$

$$f = se^{-\zeta} \int_{-\infty}^{\zeta} e^{\zeta - w^2/2w_1} \, d\zeta$$

$$= s\sqrt{\frac{\pi w_1}{2}} \; e^{(w_1^2 - \rho^2 - 2w_1\zeta)/2w_1} \left[1 + \operatorname{erf} \frac{\zeta - w_1}{\sqrt{2w_1}}\right] .$$

It is convenient to introduce these symbols:

$$A = 1 - \frac{w_1}{(\zeta - w_1)^2} + \frac{3w_1^2}{(\zeta - w_1)^4} + \cdots$$

$$B = 1 - \frac{(\zeta - w_1)^2}{6w_1} + \frac{(\zeta - w_1)^4}{40w_1^2} + \cdots$$

for the asymptotic and convergent series for the error function, and

$$P = e^{-w^2/2w_1} , \qquad R = \sqrt{\frac{\pi w_1}{2}} \; e^{(w_1^2 - \rho^2)/2w_1}$$

to characterize the P_1 approximation and the S00 functions. The function (59) then has three limiting forms.

$$\zeta \to -\infty, \; \cos\theta < 0 \qquad f = \frac{w_1}{w_1 - w\cos\theta} \; PA$$

$$\zeta \to w_1 \qquad f = Re^{-\zeta} \left[1 + \frac{\zeta - w_1}{\sqrt{\pi w_1/2}} \, B\right]$$

$$\zeta \to -\infty, \; \cos\theta > 0 \qquad f = 2Re^{-\zeta} + \frac{w_1}{w_1 - w\cos\theta} \; PA .$$

These equations illustrate the transition from the P_1 exponent to a S00 function as ζ increases. For large negative ζ the angular dependence is mainly in the denominator which has the form proposed by Long (1978), but the exponent is P_1 which is generally quadratic in u. Provided the cross sections are relatively constant, Eqs. (43) and (45) show that

$$w/w_1 = f_1/f_o, \tag{63}$$

and as soon as $w \cos\theta < w_1$ one can write

$$\frac{w_1}{w_1 - w\cos\theta} = \frac{f_o}{f_o - f_1\cos\theta} \sim \frac{f_o + f_1\cos\theta}{f_o} . \tag{64}$$

Thus Eq. (62a) confirms the validity of the P_1 solution for small w. The series A and B overlap of course, and the above argument gives preferences to the asymptotic series near w = 0, provided w_1 is large.

For $\zeta \geq w_1$ the S00 form takes over, and the angular dependence is mainly that of the exponent $(w_1 - 2w_1\zeta - \rho^2)/2w_1$ so that the surfaces of constant density are paraboloids projecting in front of the quasi-spherical body of the distribution (see Fig. 5). The tongue decays in the forward direction as $e^{-\zeta}$ whereas the distribution decays much faster, as $e^{-\zeta^2/2w_1}$, in the backward direction. Scatter-

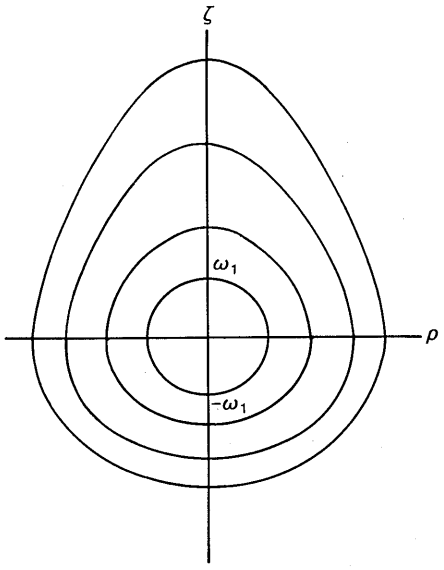

Fig. 5. Density contours for $w_1 = 2$.

in is negligible in this region, partly because energy losses take them out of the region, but mainly because the tongue is narrow and the scattering-in distributed over the whole sphere. The next iteration takes these into account.

REFERENCES

Abramowitz, M. and Stegun, I. R., eds., 1965, "Handbook of Mathematical Functions with Formulas, Graphs, and Mathematical Tables," Dover, New York.

Baraff, G. A. and Buchsbaum, S. J., 1963, Phys. Rev., 120:1007.

Stoletow, A., 1890, J. de Phys., 9:468.

Long, W. H., Jr., 1978, "Plasma Sheath Processes," Northrop Corp. Quarterly, R&D Status Report, April, 1978.

PREBREAKDOWN IONIZATION IN GASES UNDER STEADY-STATE AND PULSED CONDITIONS IN UNIFORM FIELDS

J. Dutton

Department of Physics
University College of Swansea
University of Wales
Swansea, United Kingdom

INTRODUCTION

The electrical breakdown of a gas is a dramatic event in which the electrical conductivity of the gas between a pair of electrodes with an applied voltage changes by many orders of magnitude on a time scale dependent on the conditions, but typically in the range of nanoseconds to milliseconds. The breakdown results from a series of atomic and molecular collision processes following the release of one or more charged particles which gain energy in the electric field E existing between the electrodes. The number of free charges increases rapidly as a result of the collision processes which effectively transfer energy from the field to the gas.

Thus, in principle, the phenomena associated with breakdown should be quantitatively predictable given a knowledge of the cross sections and their energy dependence for all the possible collision processes, together with the efficiency with which electrons are emitted from the electrode surfaces when bombarded with various particles possessing kinetic and/or potential energy. With the Boltzmann equation, a knowledge of the cross sections allows an energy balance to be set up, which in turn leads to an energy distribution. The cross sections can then be integrated over the energy distribution and used together with the appropriate charge conservation equations to determine the development of the current in the gas.

In practice, the main difficulties in proceeding in this way are two-fold. Firstly, there are often a large number of types of collision processes to be considered, and the cross-section data

for all of them over the required energy ranges are frequently not available. Secondly, the procedure itself is relatively difficult involving numerical integration which has only become possible in recent years with the advent of high speed digital computers.

This second difficulty does not arise if, instead of using cross sections, measured values of the so-called electron swarm coefficients are used as the starting point, because these coefficients represent averages of various cross sections over the energy distribution of the charged particle swarm. The swarm coefficients include the drift velocity W and the diffusion coefficient D related to the cross section for momentum transfer, together with the coefficients of excitation ε, primary ionization α, electron attachment a, detachment d and ion molecule reaction c, each related to the corresponding collision cross section. The swarm coefficients are dependent on the gas number density n and on the mean energy, which is determined by the ratio E/n.

There is thus considerable interest in obtaining accurate experimental values of the electron swarm coefficients. On the one hand, they enable predictions of discharge development to be made in the way we have just been discussing. On the other hand, as we have seen, they can also be used together with the Boltzmann equation to go in the reverse direction and give information about cross sections, particularly at low energies where there is a lack of data.

TOWNSEND THEORY

The usefulness of dealing in terms of swarm coefficients for the first of these purposes was demonstrated, as Professor Llewellyn-Jones indicates in his survey, in the early work of Townsend on ionization and breakdown in uniform fields. In this work he showed experimentally that at pressures of a few torr in gases in which the only significant ionization processes were primary electron ionization in the gas and secondary ionization by one of a variety of processes in the gas or at the cathode, the spatial growth of prebreakdown ionization current resulting from an initial externally maintained current I_o from the cathode at a constant value of E/n was given by

$$I = I_o e^{\alpha d} \left[1 - (\omega/\alpha)(e^{\alpha d} - 1) \right]^{-1} , \qquad (1)$$

where α and ω/α were constants.

The constant α was interpreted as the number of new electrons on the average produced per electron per unit drift distance in the field direction and designated the primary ionization coefficient.

The coefficient ω/α was interpreted as the number of secondary electrons produced per primary electron and called the secondary ionization coefficient. The basis for this interpretation was that Eq. (1) is the steady-state solution of the continuity equation established on the basis of these definitions and neglecting diffusion.

It follows from Eq. (1) that there is a certain $d = d_s$, say, such that

$$(\omega/\alpha)(e^{\alpha d_s} - 1) = 1. \qquad (2)$$

At this d_s, which corresponds to a voltage $V = V_s = (E/n)(nd_s)$, the current becomes just self-sustaining. For any $V < V_s$ the current depends on the initial current I_o, dying out if I_o ceases to be maintained by some external source, but for $V > V_s$ even a short burst of electrons at the cathode gives rise to a current which (ignoring statistical fluctuations) increases with time. V_s is the static breakdown voltage, i.e., the lowest voltage at which breakdown can occur for the system and is predictable from a knowledge of the ionization coefficients.

The early experiments of Townsend were carried out at relatively low gas pressures and for voltages < 1000 V, corresponding to low values of nd_s. The interpretation is valid when the only significant processes are primary ionization by electrons, together with the consequent processes of secondary ionization.

Since the time when the theory was first postulated, considerable effort has been devoted, firstly, to examining how it can be generalized to take into account a range of other processes which are recognized as important; secondly, to considering the temporal, as well as spatial, development of the current; and thirdly, to investigating the range of validity of the theory. I should like to examine briefly each of these aspects in turn. For more detailed discussions concerning these aspects of breakdown, see Dutton (1978), Llewellyn-Jones (1966 and 1967) and Raether (1964).

GENERALIZED TOWNSEND THEORY

As far as the processes involved are concerned, those that have to be considered are 1) secondary ionization processes in the gas such as ionization by positive ions, or photoionization, together with secondary processes at the cathode such as emission electrons by the incidence of ions, photons and metastables; 2) processes of electron attachment, which occur in electronegative gases, whereby relatively light mobile electrons become relatively heavy sluggish negative ions; 3) processes of electron detachment, whereby electrons are removed from the negative ions; and 4) ion conversion processes or ion molecule reactions which are particularly

important in the case of negative ions, because changes in the ion species can significantly influence the rate at which electrons are released from the ions by processes of detachment.

The solution of the continuity equations taking all these processes into account can lead to involved expressions containing a large number of coefficients, but fortunately it is often possible in a given case to make simplifying assumptions by assessing the relative significance of the various processes.

As an example of the procedure, let us consider a relatively involved case and then see how the solution can be simplified under certain circumstances. The case I want to consider is that of an electronegative gas in which two negative ion species A^- and B^- are formed in two-body processes. Let us also assume that species A^- which readily undergoes detachment is converted in an ion-molecule reaction to species B^- for which detachment and ion conversion reactions are negligible.

At any distance x from the cathode of a uniform field electrode system, the currents of electrons, positive ions and negative ions of species A and B may be represented by i_-, I_+, I_-^A and I_-^B, respectively, and are all functions of x. The continuity or charge conversion equations may be written as

$$\begin{aligned}
\frac{di_-}{dx} &= \alpha i_- + \Delta I_-^A(x) - a_1 i_- - a_2 i_- \\
\frac{dI_+}{dx} &= \alpha i_- \\
\frac{dI_-^A}{dx} &= a_1 i_- - \Delta I_-^A - c I_-^A \\
\frac{dI_-^B}{dx} &= a_2 i_- + c I_-^A \quad ,
\end{aligned} \tag{3}$$

where α is the primary ionization coefficient, a_1 and a_2 the electron attachment coefficients to form species A^- and B^- respectively. Δ is the detachment coefficient from A^-, and c, the ion conversion coefficient for the reaction in which A^- is converted into B^-.

These have to be solved subject to the boundary conditions that the electron and negative ion currents at the anode are all zero and that the electron current at the cathode is

$$i_-(0) = I_o + (\omega/\alpha) I_+(0) \quad . \tag{4}$$

The solution is

$$I = \frac{\left[I_o \frac{\alpha(\lambda_1 + c + \Delta)}{\lambda_1(\lambda_1 - \lambda_2)} e^{\lambda_1 d} - \frac{\alpha(\lambda_2 + c + \Delta)}{\lambda_2(\lambda_1 - \lambda_2)} e^{\lambda_2 d} + \frac{(a_1 + a_2)c + a_1\Delta}{\lambda_2\lambda_2} \right]}{\left[1 - \left(\frac{\omega}{\lambda_1 - \lambda_2} \right) \frac{\lambda_1 + c + \Delta}{\lambda_1} (e^{\lambda_1 d} - 1) - \frac{\lambda_2 + c + \Delta}{\lambda_2} (e^{\lambda_2 d} - 1) \right]} \quad (5)$$

where λ_1 and λ_2 are the roots of

$$\lambda^2 - (\alpha - a_1 - a_2 - c - \Delta)\lambda - (\alpha - a_1 - a_2)(c + \Delta) - a_2\Delta = 0. \quad (6)$$

If this were the end of the matter, this would not be a very useful expression since it contains seven unknown coefficients, but if, as in many cases, detachment and ion conversion can be neglected, we get

$$I = I_o \frac{\frac{\alpha}{\lambda_1} e^{\lambda_1 d} - \frac{a}{\lambda_1}}{1 - \frac{\omega}{\lambda_1} (e^{\lambda_1 d} - 1)} \quad (7)$$

where the effective attachment coefficient $a = a_1 + a_2$ and the effective ionization coefficient $\lambda_1 = \alpha - a$.

In each case, there is a sparking criterion given by $V_s = Ed_s$, where d_s is the value of d_s at which the denominator vanishes, i.e., in the case represented by Eq. (7) where

$$(\omega/\lambda_1)/(e^{\lambda_1 d_s} - 1) = 1 \quad . \quad (8)$$

Thus, V_s can be predicted from a knowledge of the coefficients and essential tests of the correctness of these ideas are 1) that the prebreakdown growth follows the form predicted and 2) that calculated and experimental V_s agree. Results of prebreakdown ionization current measurements are conveniently represented as log I,d curves. The shape of these curves depends on the values of the coefficients, but when $a < \alpha$ and $\omega/\alpha << \alpha$, as is the case in molecular gases, the curves take the form shown in Fig. 1, with a linear middle section, a so-called upcurving at larger d's, which represents the increasing significance of secondary ionization as d increases and a so-called downcurving at low d which shows clearly the influence of attachment. Such curves can be analyzed to obtain the effective ionization coefficient λ_1 and the secondary ionization coefficient ω/λ_1 from the section of the curve beyond the downcurving portion and to obtain λ_1 and the effective attachment coefficient from the section below the upcurving portion.

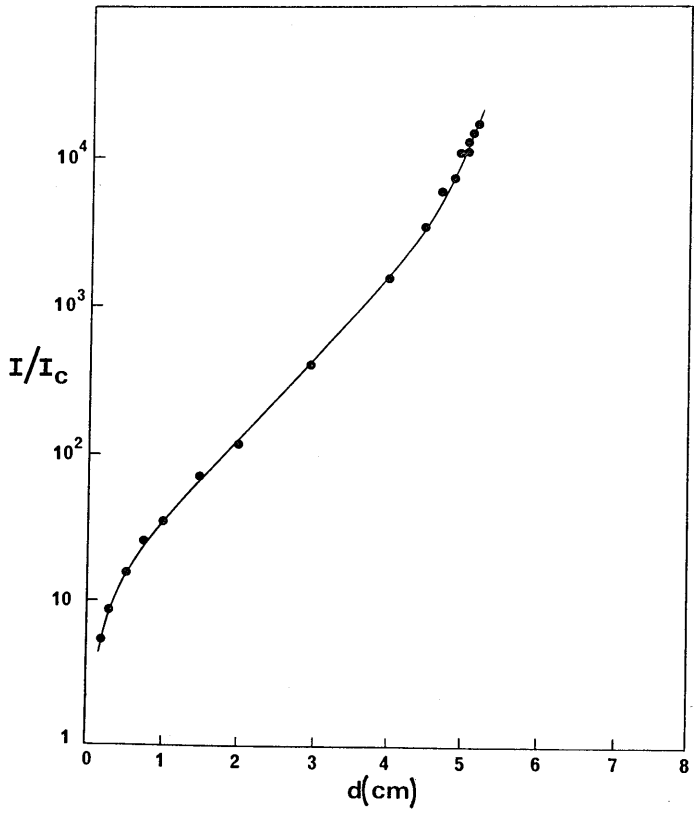

Fig. 1. A typical $\ell n\ I/I_c$,d curve for N_2O. ($I_c = cI_o$ where c is a constant) (Hughes, 1973. Reproduced by permission of the author).

ELECTRON AVALANCHES

So far we have considered the interpretation of the spatial growth of ionization for $V < V_s$ which was the condition for which the Townsend theory was first developed, because this was the region amenable to experimental study. With the advent of fast pulse techniques, however, it became possible to determine the temporal growth of prebreakdown ionization experimentally and hence, by extending the theory to this case, to obtain useful additional information on electron swarm coefficients supplementing that obtained from steady-state measurements.

In general, in order to obtain swarm coefficients from the observed characteristics of pulses, it is necessary to set up and solve the appropriate continuity equation, but in order to gain

some physical insight, let us first consider some simple cases in which we release N_o electrons from the cathode in a very short period, compared with the transit time of the electrons across the gap.

The charge density of any species present with a number density $n(x,t)$ in the gap is $en(x,t)$, where e is the electronic charge. Assuming no diffusion out of the gap, the current across any plane at distance x from the cathode at time t is given by

$$i(x,t) = en(x,t)WA(x),$$

where $A(x)$ is the area through which particles pass, and W is the drift velocity.

The current in the external circuit at any time t_1 is given by the spatial average of the current at t_1, i.e.,

$$I_{t=t_1} = \frac{\int_0^d en(x)_{t=t_1} WA(x)\,dx}{\int_0^d dx} = \frac{1}{d}\int_0^d en(x)_{t=t_1} A(x)W\,dx . \quad (9)$$

If there is no primary ionization, then the last integral is constant and equal to N_o for $0 < t < t_-$ where t_- is the electron transit time $= d/W_-$. Thus, the current in the external circuit has the constant value

$$I_o' = N_o eW_-/d \qquad \text{for } 0 < t < t_- . \quad (10)$$

If primary ionization occurs, the total electronic charge in the gap at time t when the electrons have reached a plane x is given by

$$Q = eN_o \exp(\alpha W_- t) \qquad \text{for } 0 < t < t_- . \quad (11)$$

At the same time, there is a current arising from the positive ions produced which is given by

$$I_+(t) = I_+' \left[\exp(\alpha W_- t) - \exp(\alpha W' t)\right] \qquad \text{for } 0 < t < t_- \quad (12)$$

and by

$$I_+(t) = I_+' \left[\exp(\alpha W_- t_-) - \exp(\alpha W' t)\right] \qquad \text{for } t_- < t < t_- + t_+ \quad (13)$$

where

$$W' = \frac{W_+ W_-}{W_+ + W_-} \quad \text{and} \quad I'_+ = eN_o W_+/d.$$

Since $W_+ << W_-$, the ion current is of smaller magnitude than the electron current during the electron transit time but persists for much longer. Thus, the resultant pulse takes the form of an exponential growth, resulting from the electron component with a time constant $(\alpha W_-)^{-1}$ for a duration $t_- = d/W_-$, followed by a drop to the lower steady value corresponding to the ion current for a duration $t_+ = d/W_+$, after which the pulse ceases. Measurements on the length of the electron and ion components give values of W_- and W_+ respectively; the value of W_-, together with measurements of the exponential growth of the electron component can be used to obtain α.

Clearly, other cases involving different processes such as attachment and detachment can be dealt with in the same way, although in the more complicated cases it is preferable to set up the continuity equations and solve them, using for example, Laplace transform techniques.

If secondary processes are not negligible, then, of course, we get a succession of avalanches which decrease in size because $(\omega/\alpha)(e^{\alpha d} - 1) < 1$ for $V < V_s$. A study of the succession of pulses resulting from these avalanches can be used to obtain useful information about the secondary processes. This can be seen by considering two simple cases, in which the secondary ionization is due 1) to electron emission by positive ion bombardment at the cathode and 2) to photoelectric effect.

Using the approximation that the avalanches can be considered as discreet, there will be an initial electron avalanche which would typically have a duration of about 10^{-7} sec in a 1 cm gap followed by a much smaller ion current which, when the bulk of the ions reach the cathode after about 10^{-5} sec, produces a second electron avalanche after which the process is repeated. In the second case, the repetition frequency of the avalanches is much greater ($\sim 10^7$/ sec cf $\sim 10^5$/sec) because the photons take a negligible time to cross the gap and the dominant time is thus the electron transit time.

More exact treatments lead to good quantitative agreement between theory and experiment (Schlumbohm, 1960).

So far, then, we have used the Townsend theory to relate the spatial and temporal growth of ionization at $V < V_s$ to ionization coefficients. Thus experimental measurements of the growth serve two purposes. They allow us both to test the model and to obtain values of the ionization coefficients in the range over which the

model applies; so I should just like to consider briefly the experimental methods used for such measurements.

EXPERIMENTAL METHODS

Both steady state and pulse methods are available and I will consider them in turn.

Steady-State Methods

Still probably the most widely used and, in general, most accurate method of determining ionization coefficients is the original method of Townsend in which the spatial growth of ionization at constant E/n is measured.

In this method, a potential difference from a highly stabilized source of static voltage, which is continuously variable, is applied across a pair of electrodes specially profiled to ensure that the field in the central region is uniform and higher than elsewhere in the system. The electrodes, the separation of which can be varied, are contained in an ionization chamber which can be evacuated and filled with the gas under investigation. The ionization currents, resulting from an externally generated current from the cathode of about 10^{-12} A, are measured by using an electrometer to measure the potential drop developed across a high resistance (10^6 to 10^{12} Ω) in series with the electrode system. The potential difference across the electrodes is determined by a resistive potential divider. For significant results, it is desirable to limit the error in setting E/n = V/dn to about 0.1% which requires that the electrode separation, voltage and gas pressure be determined with similar accuracy. In addition, in order to be able to measure the small ionization currents involved to 1 or 2%, it is necessary for the fluctuations in the voltage during the period of measurement to be controlled to better than about 1 part in about 10^4.

The dimensions of the electrode system depend on the range being investigated, but a system which has been widely used for work at high voltages (~100 to 600 kV) and high pressures (~100 to 7,000 torr) in our laboratory is shown in Fig. 2.

In this case the voltage supply was a high stability SAMES electrostatic generator, the output of which was measured by a high precision, wire-wound potential divider. Typical results for the measured ionization currents are shown in Fig. 3.

A second method is based on the measurement of the photon flux as a function of distance from the cathode. The photon flux arises from the radiation produced when atoms and molecules excited by the electrons return to the ground state.

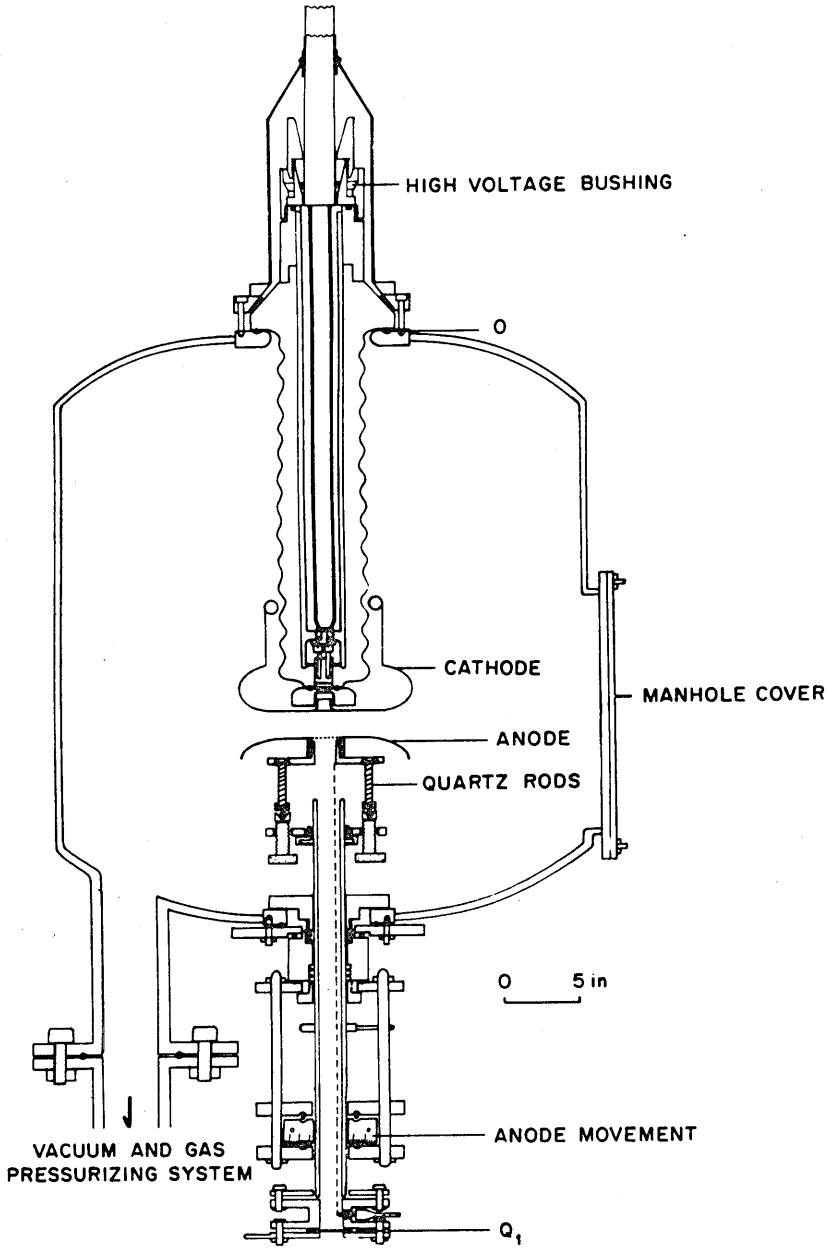

Fig. 2. Ionization chamber for use in steady-state method of determining ionization coefficients at high values of nd_s. (Davies, Dutton and Harris, 1966. Reproduced by permission of The Institute of Physics).

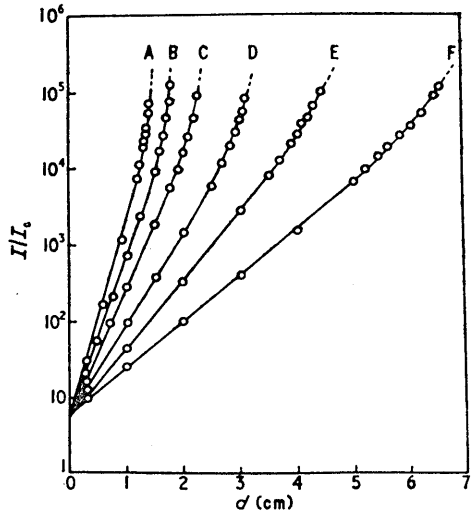

Fig. 3. A set of $(\ell n(I/I_o),d)$ curves for nitrogen using silver electrodes for N = 8.25 x 10^{-19} cm^{-2};
O experimental points
——— curves computed from the generalized Townsend equation (1) using values of α and ω/α given below:

Curve	A	B	C	D	E	F
$E/N(10^{-16}$ V $cm^2)$	10.0	9.79	9.39	9.09	8.79	8.48
α (cm^{-1})	6.05	4.81	3.73	2.79	2.06	1.42
$\omega/\alpha(x\ 10^{-4})$	1.19	1.56	1.48	1.12	0.57	0.32

(Daniel & Harris, 1970. Reproduced by permission of The Institute of Physics).

The flux between x and x + dx may be written as

$$d\phi(x) = \varepsilon i_-(x)dx, \quad \text{where } \varepsilon \text{ is the excitation coefficient.} \tag{14}$$

$$\text{But } i_-(x) = i_-(0)e^{\alpha x} = I_o e^{\alpha x}/\left[1 - (\omega/\alpha)(e^{\alpha d} - 1)\right] \tag{15}$$

$$\text{Thus, } d\phi(x) = \frac{\varepsilon I_o e^{\alpha x}}{\left[1 - (\omega/\alpha)(e^{\alpha d} - 1)\right]} dx = Ke^{\alpha x}dx\ . \tag{16}$$

The photon fluxes are extremely small and so far the method has only been applied to hydrogen, first by Corrigan and von Engel (1958) and later by Blasberg and de Hoog (1971). Attempts by de Hoog and Kasdorp (1967), Jones and Grey Morgan (1969), Buursen,

de Hoog, and van Montford (1974) to use the greater light output from self-sustained discharges have given problematical results.

Pulse Methods

If we turn now to pulse methods, there are, in general, again two measurements which can be made, those of current and of light output, both of which have been exploited, especially by Raether (1964) and his group in Hamburg.

Current Pulses. There are a number of pulsed current techniques which have been developed. The method which has been used to obtain the most data, involves the measurement of the pulse in the external circuit resulting from the release of a short nanosecond pulse of electrons from the cathode. This requires the same circuit as for the steady state current measurements, except that the resistance in series with the gap has to be reduced to a value consistent with the time constant required, and the electrometer is replaced by a broad band amplifier and fast oscilloscope in order to measure the transient voltage V(t). This voltage is related to the transient current I(t) given by Eq. (9) by

$$V(t) = I(t)R_s + R_s C_g \frac{dV_g}{dt} \quad , \tag{17}$$

in which the second term represents the contribution of the displacement current.

The solution of this equation is given by

$$V(t) = \frac{1}{C_g} e^{-t/R_s C_g} \left[\int_0^t I(t) \exp(t/R_s C_g) dt + C_g V_g(0) \right]. \tag{18}$$

If electron attachment and detachment are negligible, inserting the appropriate expressions $I_-(t)$ and $I_+(t)$ gives

$$V(t) = \frac{e}{C_g} \left(\frac{1}{t_-} + \frac{1}{t_+} \right) \frac{1}{\alpha W_- + (1/R_s C_g)} (e^{\alpha W_- t} - e^{-t/R_s C_g}) \text{ for } 0<t<t_- \tag{19}$$

which gives

$$V(t_-) \approx \frac{e}{C_g} \frac{1}{\alpha d} e^{\alpha d} \tag{20}$$

if $R_s C_g \alpha W_+ = \rho$, say, $\gtrsim 0.1$. (21)

Thus, the voltage pulse rises exponentially with time constant $(\alpha W_-)^{-1}$ for the electron transit time to $V(t_-)$ and this provides one method of abtaining α.

Another technique using the same equipment depends on measurements on the subsequent ion pulse. The shape of this pulse depends on the time constant of the circuit and that corresponding to $\rho = R_s C_g \alpha W_+ = 1$ can readily be recognized. Thus, by changing R_s until this characteristic shape is obtained, a value of αW_+ is obtained. The duration of the pulse $t_+ = d/W_+$ is also determined and hence α can be obtained.

An alternative approach is to use a very weak, continuous illumination so that the statistics of a succession of avalanches resulting from single electrons can be studied. The primary ionization coefficient α may then be obtained from the mean of the distribution because $\overline{N} = e^{\alpha x}$.

Both these methods require a total of about 10^5 electrons to give an adequate signal to noise ratio. Consequently, they have mostly been used for hydrocarbon vapors for which $\omega/\alpha << 10^{-5}$, and sufficiently large avalanches can be obtained without $(\omega/\alpha)(e^{\alpha d} - 1)$ becoming unity and giving rise to breakdown.

Recently Lakshminarasimha, Snelson and Lucas (1975) have developed a method in which the anode is screened from induced charges and measurements of the arrival of electrons at the anode have yielded values of α for a number of gases. This technique is particularly useful for separating the effect of primary ionization from Penning ionization which occurs for example with helium containing molecular impurities.

Light Pulses. By replacing αx by $\alpha W_- t$, the expressions for the light flux emitted as a function of distance can be used to obtain α from measurements of the flux from transient avalanches, and this method has recently been developed, again for H_2, by Blevin et al. (1978).

Alternatively, the total light photon flux $d\phi$ in time interval dt from an avalanche may be used. In this case,

$$d\phi = \varepsilon N W_- dt \tag{22}$$

and

$$\frac{dN}{dt} = \alpha N W_- \tag{23}$$

so that the photomultiplier current

$$I_p(t) = \kappa \left(\frac{\varepsilon}{\alpha}\right) \frac{dN}{dt} \text{ , where } \kappa \text{ is a constant,} \tag{24}$$

and the resulting voltage pulse is

$$V(t) = \frac{1}{C}\int_0^t I_p(t)dt \qquad \text{if } RC_s >> (\alpha W_-)^{-1} \quad . \tag{25}$$

The sensitivity depends on ε/α and is about the same as the method based on current pulses for hydrocarbon gases but considerably higher for common molecular gases.

These, then, are the methods of obtaining the ionization coefficients and, in general, where two methods have been used for a particular gas, there is reasonable agreement. It is not profitable to discuss the values obtained here, but for calculations, there are two recent bibliographies, Dutton (1967) and Beaty, Dutton and Pitchford (1979) and a review available (Dutton, 1975). A further review on electronegative gases is nearing completion and will be published shortly.

THE RANGE OF VALIDITY OF THE GENERALIZED THEORY

Let me now turn to the third point I raised near the beginning—the range of validity of the generalized Townsend theory. This is most readily discussed in terms of the similarity relation,

$$V_s = f(Nd_s), \tag{26}$$

usually known as Paschen's law, which was first observed experimentally and which follows directly from Townsend's theory if the gas processes are two-body processes. It is usually represented in the form of a graph of V_s, Nd_s or equally well, since $V_s/Nd_s = E_s/N$ as a graph of E_s/N, Nd_s. These graphs have the general form shown in Fig. 4. The two regions of interest are low Nd_s (i.e., high E_s/N) and high Nd_s (i.e., low E/N) since the theory has long been established at intermediate values of these parameters.

Low Nd_s. As Nd_s is decreased below that corresponding to the minimum V_s, it is to be expected that a region will be reached where the Townsend theory will no longer be applicable, because it corresponds to a region in which the number of collisions of electrons with gas atoms become fewer and fewer as they cross the gap. Eventually, there are insufficient collisions for a steady state to be reached. A theory based on the concept of steady-state swarm coefficients will then clearly not be appropriate. It is of interest to investigate at what value of Nd_s or E/N this transition occurs.

The beginning of the transition is marked by the fact that the distance d_o required by the electrons to come into steady state after being released from the cathode becomes significant with

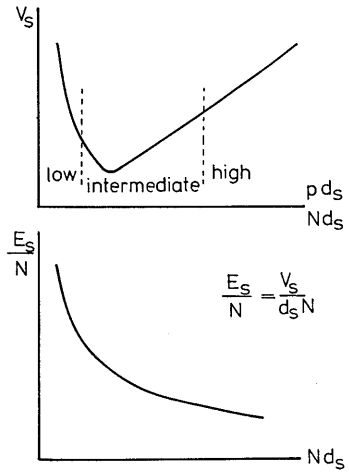

Fig. 4. General form of Paschen's Law represented as the variation of V_s with pd_s (or Nd_s) and the corresponding variation of E_s/N with Nd_s.

respect to d so that the current at a constant E/n can be represented by

$$I(d) = \frac{I(d_o)e^{\alpha(d-d_o)}}{1-(\omega/\alpha)'(e^{\alpha(d-d_o)}-1)} \quad \text{where} \quad (\omega/\alpha)' = (\omega/\alpha)I(d_o')/I_o. \qquad (27)$$

In order to explore experimentally, when d_o becomes a significant fraction of d, it is found convenient to use the so-called Gosseries plot, i.e., to take measurements at d_1, $d_1 + \Delta d$, $d_1 + 2\Delta d$, and to plot Y_d versus $Y_{d+\Delta d}$, where Y_d and $Y_{d+\Delta d}$ are the reciprocals of the currents at those distances. Some results (Folkard and Haydon, 1971) obtained for H_2 are shown in Fig. 5 and clearly show the way in which the departures from the steady state (indicated by departure from linearity) occur over more and more of the gap as E/p (i.e., E/N) increases. The limiting value of E/N above which a steady state is not achieved experimentally has so far been obtained for four gases, viz., H_2, N_2, Ne and Ar, for which the values are 705, 3,100, 280 and 330 Td respectively.

In the non-steady-state region, the appropriate method for calculating the current and determining the breakdown potential is a Monte Carlo method using collision cross sections, and this has proved successful in experiments on ionization growth and breakdown

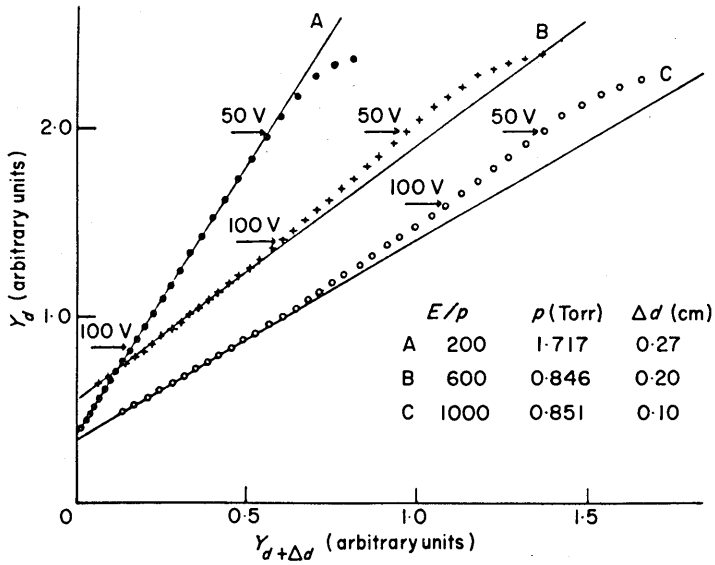

Fig. 5. Gosseries plots of prebreakdown ionization current in H_2 at high values of E/p (Folkard and Haydon, 1971. Reproduced by permission of CSIRO, Australia).

in this region by Parker and Johnson (1971), Johnson and Parker (1971), Pace and Parker (1973) and Raina and Parker (1972).

High Nd_S. At the other end of the Nd_S scale, there was for a number of years, considerable question as to whether the Townsend theory was still applicable, but there is now ample evidence to show that prebreakdown ionization and the static breakdown criterion are applicable up to $V_S \sim 500$ kV (which is the highest voltage so far investigated in this way) for a range of gases. Some of the evidence, in the form of the agreement between measured sparking potentials and those predicted from ionization coefficients obtained by measuring prebreakdown currents, is given in Table 1 and Figs. 6 and 7.

It thus looks as if we have solved all our problems, until we take a closer look at Fig. 7 for SF_6. In this figure it can be seen that one set of results shows a marked departure from Paschen's law within the region where we expect the theory to hold, and moreover the departure is large. If we ask ourselves what the conditions were in which these results were obtained, we find that we are in a region which has been known for a long time now to pose particular problems — the region of high fields.

Table 1. Comparison of the Measured and Calculated Values of the Electrical Breakdown Voltage in Nitrogen for a Range of Values of E/N and N. (Daniel & Harris, 1970).

E/N (10^{-6}V cm^2)	N (10^{19}cm^{-3})	(10^{19}cm^{-2})	V_s (meas.) (kV)	V_s(calc.) (kV)
8.48	8.21	59.9	500.3 ± 2.3	508.6 ± 9.8
8.79	6.60	39.1	342.7 ± 1.1	343.9 ± 2.1
9.39	4.92	20.45	194.0 ± 0.9	192.1 ± 2.9
9.39	4.95	20.34	193.9 ± 0.9	191.2 ± 2.2
10.00	3.29	12.06	121.3 ± 0.7	120.6 ± 1.1

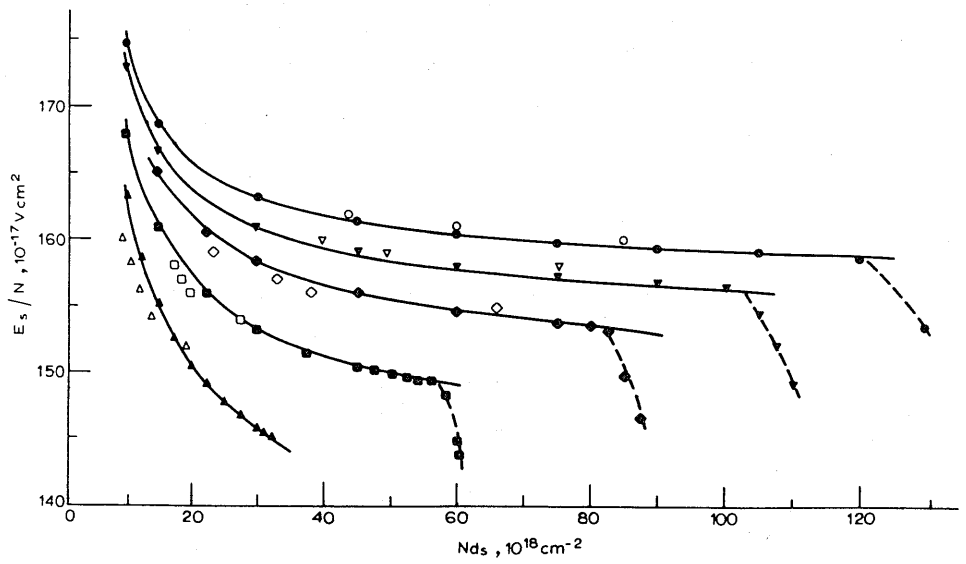

Fig. 6. Comparison of results for E_s/N vs. Nd_s at various N obtained from the measurements of sparking potentials (filled-in symbols) and of prebreakdown ionization (open symbols) for nitrous oxide.

○, ● N = 16.19 x 10^{18}cm^{-3} □, ■ N = 6.47 x 10^{18} cm^{-3}

▽, ▼ N = 13.12 x 10^{18}cm^{-3} △, ▲ N = 3.26 x 10^{18} cm^{-3}

◇, ◆ N = 10.00 x 10^{18}cm^{-3}

(Dutton, Harris & Hughes, 1972. Reproduced by permission of The Institution of Electrical Engineers).

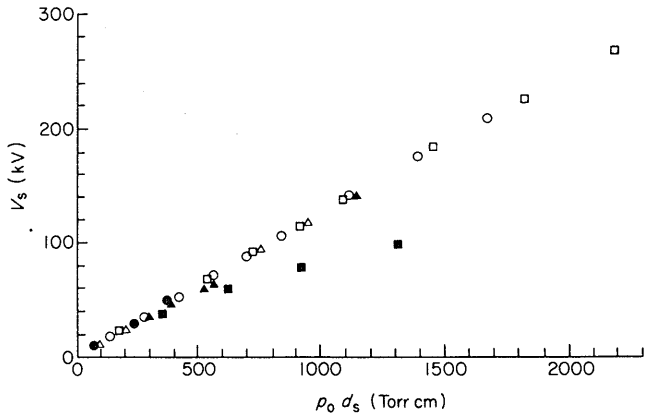

Fig. 7. Experimental values of V_s for uniform fields at low values of E/n in SF_6 (Dutton, Harris and Jones, 1970. Reproduced by permission of Macmillan (Journals) Ltd.) Experimental: □ , ○ , △ (Dutton, Harris and Jones, 1970); ■ (Cohen, 1956). ● (Bhalla and Craggs, 1962). ▲ (George and Richards, 1969).

HIGH FIELD BREAKDOWN

The results I have presented to this point have been at high voltages but low p and large d, so that $E_s = V_s/d$ is relatively low $\lesssim 10^7 V\ m^{-1}$. As p is increased, however, d decreases at the same pd_s so that E_s increases and at values of E_s in excess of about 10^7 $V\ m^{-1}$, the breakdown phenomena become quite different in the following ways:

(i) there are marked departures from Paschen's law (see Fig. 8),

(ii) there is a very much greater dependence of the sparking potential on the cathode material than at low fields (see Fig. 9), and

(iii) there is much greater scatter in the values of V_s obtained at a given value of pd_s (see Fig. 10).

There is little doubt that these changes are brought about by the introduction of dominant, field-dependent cathode processes. In some circumstances it seems possible to predict breakdown on the basis of semiempirical theories based on the enhancement of the

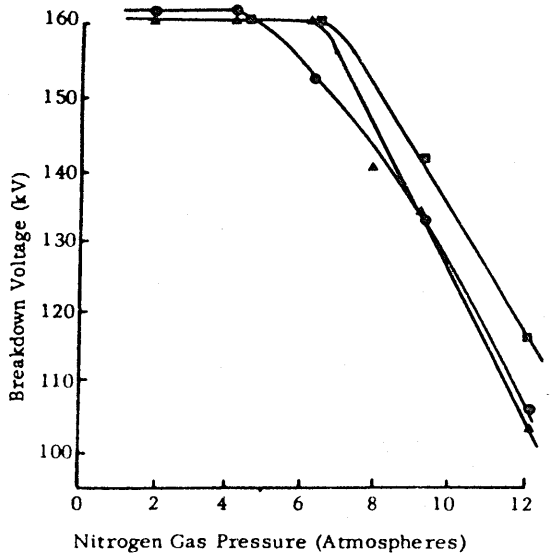

Fig. 8. Mean-conditioned breakdown voltages for titanium electrodes as a function of nitrogen pressure. (Coates, Dutton & Harris, 1976. Reproduced by permission of The Institution of Electrical Engineers).
● as machined surface ▲ medium-polish surface
■ diamond polished surface.

field at cathode protrusions (Pederson, 1975), but there is still considerable doubt about the basic processes occurring. These are extremely difficult to investigate directly because there is evidence that the process which triggers breakdown develops in a short time scale (Muller, 1966) at microscopic sites on the cathode in the presence of the high field and high gas pressure. In these circumstances, we are at present carrying out some experiments on breakdown using single crystal electrodes in order to try to investigate whether any factors other than surface topography are important, e.g., the presence of grain boundaries, dislocations or inclusions. Some of the recent results are shown in Figs. 11 and 12. The first shows that in SF_6 there is no very marked difference in the breakdown voltages, at a given Nd_s and field, between single crystal and polycrystalline electrodes in contrast to earlier Russian work in N_2, which showed that a breakdown voltage as high as that of the Paschen curve obtained at low fields, could be reached with single crystals at fields of $2 \times 10^8 V\ m^{-1}$. We, ourselves, are unable to investigate to a maximum of about 10 atmospheres and the gap separation to a maximum of about 5 mm. As part of the work

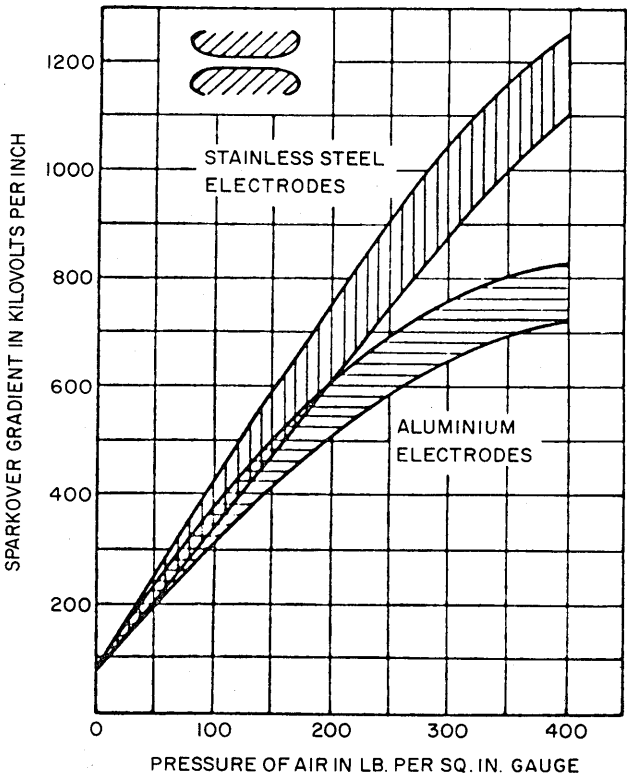

Fig. 9. Influence of electrode material on high field breakdown in air (Trump, Cloud, Mann and Hansen, 1950). Reproduced by permission of The Institute of Electrical and Electronics Engineers, Inc.).

of the Franco-British Group on Gas Discharges, however, we are collaborating with Professor Boulloud's group at the University of Nantes, where they have an ionization chamber which can be pressurized to much higher pressures ~ 200 atmospheres and similar studies in N_2 are being made there.

Fig. 12 shows that in SF_6 the cathode surface finish makes a significant difference even for single crystal cathodes. We plan shortly to introduce a grain boundary to see the effect of this on breakdown.

TEMPORAL GROWTH OF IONIZATION FOR $V > V_s$.

So far we have been concerned with the static breakdown V_s and the information which can be gained from steady-state and pulse experiments for $V < V_s$.

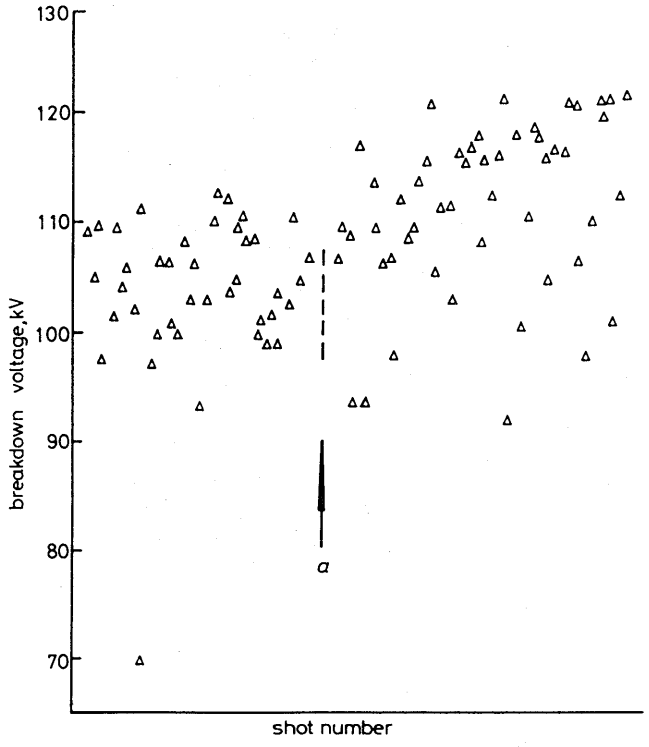

Fig. 10. Typical scatter of breakdown potentials at a given Nd_s in nitrogen in the high-field region using Aluminum electrodes; [pressure 1.2 x 10^6Pa; $Nd_s = h.69 \times 10^{24} m^{-2}$.] At α damping resistance was increased from zero to 50 KΩ. (Coates, Dutton and Harris, 1978. Reproduced by permission of The Institution of Electrical Engineers).

No discontinuous change is expected in the processes or the coefficients representing them as the voltage is increased above V_s so that it is of interest to consider the solution of the same continuity equations that we had previously, recognizing, however, that we are now in a non-steady-state in which the current increases with time.

Temporal Growth in the Absence of Space Charge

Qualitatively we can see that the rate of growth will depend on the secondary processes operative, because the regeneration time for the emission of electrons from the cathode by ions will be a hundred times longer than that for photoelectric emission, for example.

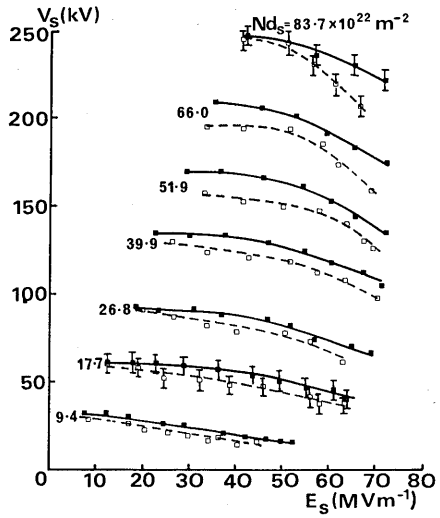

Fig. 11. Breakdown voltages at constant Nd_s for polished single crystal (—■—) and polycrystalline (--□--) electrodes. (Dutton & Williams, 1981).

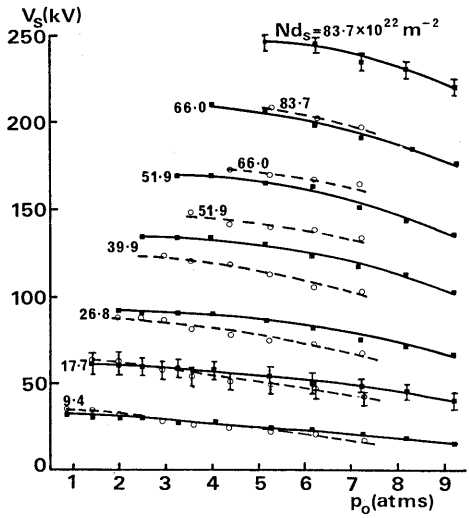

Fig. 12. Breakdown voltages at constant Nd_s for electro-polished (——) and unpolished (----) single crystal electrodes in SF_6. (Dutton & Williams, 1981).

Quantitatively, the continuity equations can be solved analytically for $I(x,t)$ if the current is sufficiently low that there are no space charge effects, because the coefficients are then constant, depending only on the applied value of E and the gas number density.

For the simplest case of primary ionization and secondary ionization due to photoelectric effect and positive ion incidence on the cathode, the continuity equations may be written

$$\frac{\partial}{\partial t}\left(\frac{I_+(x,t)}{W_+}\right) = \alpha i_-(x,t) + \frac{\partial I_+(x,t)}{\partial x} \tag{28}$$

$$\frac{\partial}{\partial t}\left(\frac{i_-(x,t)}{W_-}\right) = \alpha i_-(x,t) - \frac{\partial i_-(x,t)}{\partial x} \tag{29}$$

with boundary conditions

$$i_-(0,t) = I_o + \gamma I_+(0,t) + \frac{\delta}{\alpha}\int_0^d \alpha i_-(x,t)dx$$

$$I_+(d,t) = 0. \tag{30}$$

The approximate solution is (Davidson, 1953)

$$i_-(0,t) = A - Be^{\lambda t}, \tag{31}$$

where λ is the growth constant, given by the real root of

$$f(p) = 1 - (\alpha\gamma/\phi)(e^{\phi d}-1) - \left(\frac{\delta}{\psi}\right)(e^{\psi d}-1) = 0 \tag{32}$$

where $\phi = \alpha - \lambda/W, \psi = \alpha - \lambda/W_-$, $1/W = 1/W_+ + 1/W_+ + 1/W_-$, and $A = I_o/[\,1 - (\omega/\alpha)(e^{\alpha d}-1)\,]$. B depends on the initial conditions, e.g., if there is no charge in gap at time zero B = A, giving

$$i_-(0,t) = I_o(1 - e^{\lambda t})/[1 - (\omega/\alpha)(e^{\alpha d} - 1)]$$

and $$i_-(x,t) = e^{\alpha x}\, i_-(0, t - \tfrac{x}{W_-}) \quad \text{for } t \geq \tfrac{x}{W_-}\ . \tag{33}$$

To see how good an approximation this is to the exact solution obtained by Davidson (1958), we can look at a typical case for hydrogen shown in Fig. 13 for typical values of $\alpha = 2.8\ cm^{-1}$ and $\omega/\alpha = 0.12$, $\delta/\alpha = 0.087$.

The exact solution was generalized by Davidson (1955, 1956, 1962, 1958), to take into account other cathode secondary processes

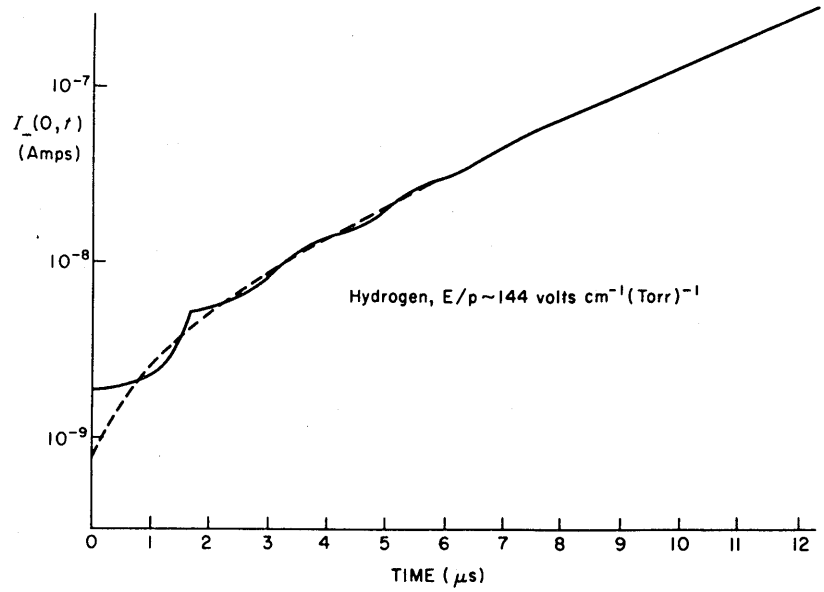

Fig. 13. Comparison of Davidson's exact (———) and approximate (------) solution for current growth in H_2 at 1.6 Torr (α = 2.845 cm^{-1}; ω/α = 0.124; δ/α = 0.087 (Davies, 1964. Reproduced by permission of the author).

and attachment and detachment, there being a different expression for f(p) involving the appropriate coefficients in each case.

Since the analytical treatment neglects space charge, the question arises: "Are there any conditions under which this analytical theory can be useful in the analysis of experimental data?" It turns out that where a low overvoltage of a few percent is applied to a gas at low pressure, the formative time lag, i.e., the time between the application of the voltage in the presence of an adequate supply of electrons and the collapse of voltage across the gap is of the shape shown in Fig. 14.

The voltage remains approximately constant for most of the period and then collapses very rapidly. During the time when the voltage is almost constant, the current is growing exponentially indicating that it is growing in a relatively space-charge-free environment. It is only in the very last stages of the growth that the space charge becomes significant and the growth becomes super-exponential.

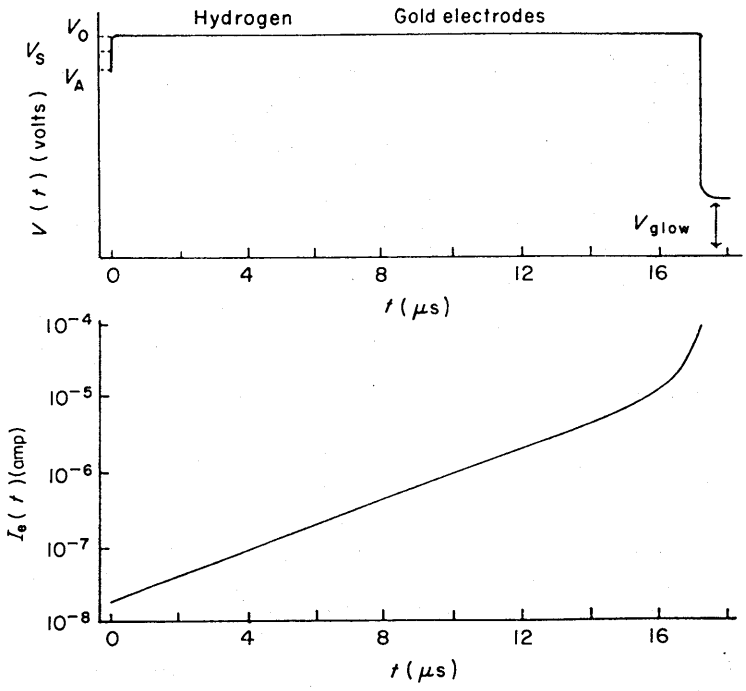

Fig. 14. Simultaneous temporal variation of gap voltage V(t) and current in external circuit $I_c(t)$; p_o = 14.05 Torr, d = 1.167 cm, V_o = 918.5 volts, E/p_o = 56.0 V $cm^{-1}Torr^{-1}$. ΔV = 0.50% (Morgan & Williams, 1965. Reproduced by permission of The Institute of Physics).

This is useful because if measurements are made of the current as a function of time in these conditions a value of the growth constant λ can be obtained and since λ involves the individual secondary ionization coefficients, this gives a method of determining the proportion of the secondary ionization processes contributing to the total secondary ionization coefficient.

The Influence of Space Charge on the Temporal Growth

Once space charge becomes significant the analytical theory is no longer applicable, because although the continuity equations remain the same, the coefficients vary continuously as the applied field is modified by the space charge field. In these circumstances, we need to resort to numerical integration of the equations.

In a uniform field, it is natural to attempt a one-dimensional simulation. However, it soon becomes clear that unless the radius of the discharge is large compared with the gap separation, which is unusual, the use of the one-dimensional form of Poisson's equation to calculate the space charge field could give rise to considerable error. Consequently, Davies, Evans, and Llewellyn-Jones (1964) developed an approach in which they used the one-dimensional continuity equations but chose a radius for the discharge and considered the space charge distributed uniformly over a series of rings as shown in Fig. 15. This has sometimes been called the one-and-a-half dimensional approach. The necessity for it is demonstrated in Fig. 16 which gives the results of a calculation of the field distortion on axis calculated by a number of different methods. Using this approach, the continuity equations were integrated using the so-called method of characteristics, i.e., by rewriting the equations for the electron density in the form

$$\frac{Dn_e}{Dt} = (\alpha W_- - \frac{\partial W_-}{\partial x})n_e, \tag{34}$$

where D/Dt represents the derivative evaluated in the frame of reference moving with the electrons, i.e., along curves $x - W_- t =$ constant — the so-called characteristic direction.

In this way it is possible to obtain computer simulations of the growth of the electron and ion densities and the electric field as functions of space and time.

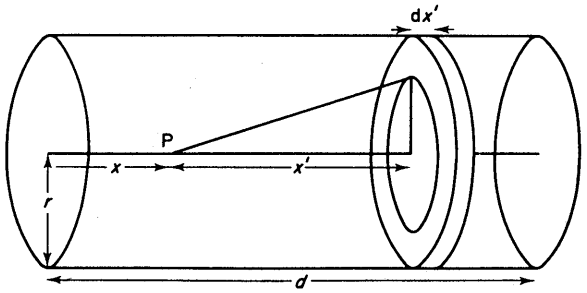

Fig. 15. Diagram for the method of calculating the field distortion due to a cylinder of charge (Davies, Evans and Llewellyn-Jones, 1964. Reproduced by permission of The Royal Society).

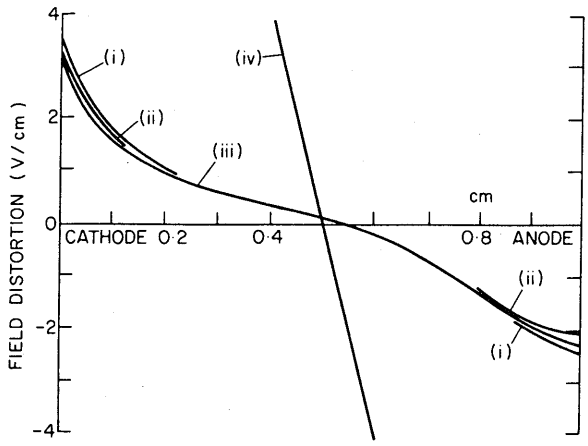

Fig. 16. Field distortion along the axis of a discharge gap (Davies and Evans, 1967. Reproduced by permission of The Institution of Electrical Engineers). Discharge radius/electrode separation = 0.12.
(i) cylindrical method with images up to a distance d of the point under consideration.
(ii) cylindrical method with images up to a distance 20d or 2½d outside both electrodes.
(iii) three dimensional relaxation method.
(iv) Poisson's equation in one dimension.

Application to Low Pressures and Low Over-Voltages. The first conditions to which the numerical simulation was applied were the later stages of the growth at low pressures discussed earlier. In this case, the times of interest are several ion transit times, and a minimum time step of about $d/50W_+$ was used to enable the computation to be made in a reasonable time. Effectively, the assumption is made that for the chosen time interval $\partial n_e/\partial t = 0$, which is valid because the ion space charge has the dominant influence on the space charge distortion. Some results showing the agreement obtained between results obtained in this way and later experimental data in hydrogen are shown in Fig. 17.

High Pressures and High Over-Voltages. The study of the temporal growth at high pressures is a much more difficult problem both experimentally and theoretically because in these circumstances space-charge distortion of the applied field becomes significant much earlier in the growth, and the growth itself is much more rapid.

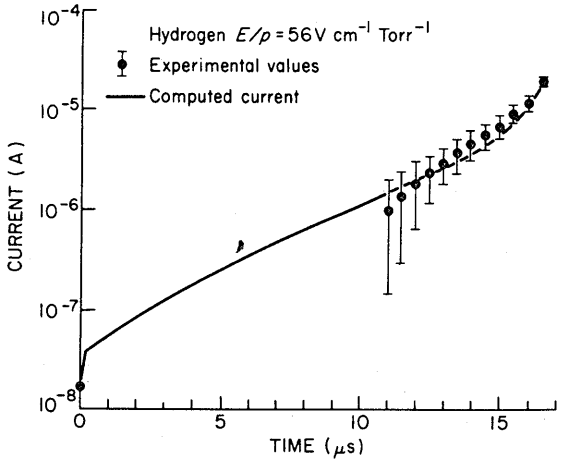

Fig. 17. Comparison of measured temporal growth of current in H_2 at E/p = 56 V $cm^{-1}Torr^{-1}$ with the curve computed by numerical integration of continuity equations taking into account space charge (Morgan, Evans, Williams and Davies, 1965. Reproduced by permission of The Institute of Physics).

(a) Experiment. Experimentally, current measurements are difficult and consequently much of the evidence comes from measurements on light output from discharges and photographs of the condensation on ions produced in discharges in cloud chambers (Raether, 1964). The type of results obtained is shown in Fig. 18, which shows image converter records obtained for breakdown in N_2 at Strathclyde (Chambers, Duffy and Tedford, 1972). We see the, by now familiar, development of the light from the discharge. It is first detected in mid-gap, and then one light front moves towards the anode and another towards the cathode. These have come to be referred to as the anode- and cathode-directed streamers.

The early cloud chamber results and approximate calculations of the space charge indicated that these streamers were detectable when the number of charge carriers was about 10^8. For an avalanche started from a single electron, this corresponds to a value of αd of about 20 in the undistorted applied field. This empirical criterion of $\alpha d \sim 20$, often known as the streamer criterion for breakdown, is thus a criterion for the development of significant space charge in a single avalanche. As such, it has been found to be useful in fast impulse breakdown for which, if a discharge is to occur, the space charge controlled phase of development has to be reached before the applied voltage decays.

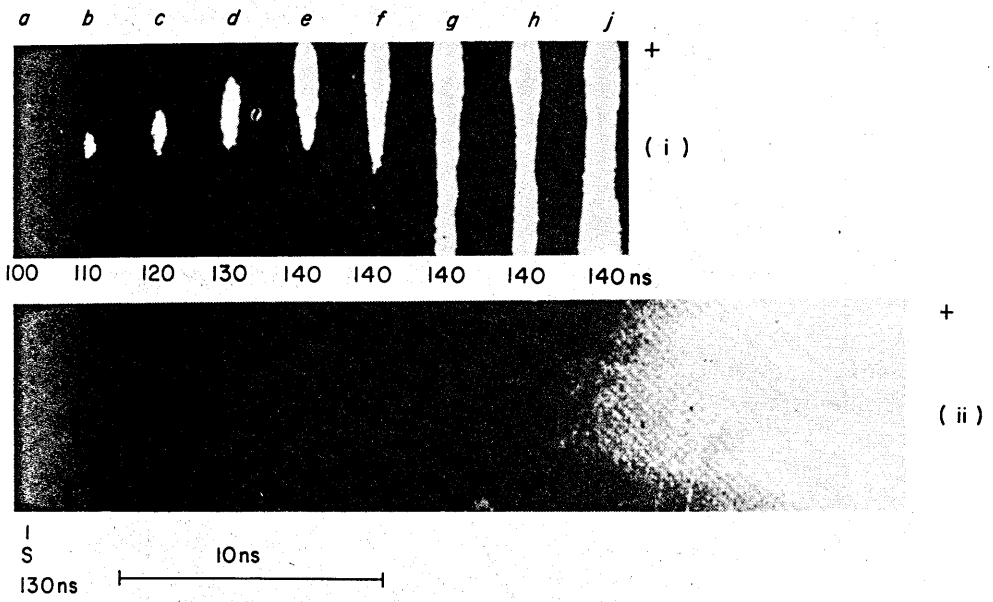

Fig. 18. High speed photographs of the development of ionization in nitrogen at a pressure of 200 Torr and for 25% overvoltage (Chalmers, Duffy and Tedford, 1972. Reproduced by permission of The Royal Society).

(b) Computer simulation. As far as accurate computations of the temporal growth in these conditions are concerned, the difficulty lies in the fact that the electron space charge now becomes as important as the positive ion space charge. The quasi-equilibrium assumption used at low pressures can no longer be made and the time steps taken have to be ~ $d/50W_-$. Computations under these conditions have, however, now been carried out to obtain $n_e(x,t)$, $n_+(x,t)$ and $E(x,t)$ for a number of different conditions and assumptions about the processes involved (Davies, Davies & Evans, 1971; Kline, 1974; Bayle and Bayle, 1974). Since most of the experimental results are in the form of light output measurements, it is also of interest to obtain the photon output as a function of time which can, of course, be obtained given $n_e(x,t)$ and $E(x,t)$. A typical result for N_2 is shown in Fig. 19 which shows the light output curves for N_2, from which simulated streak photographs were obtained. Professor Llewellyn-Jones shows the detailed agreement obtained between these simulated streak photographs and those obtained by experiment.

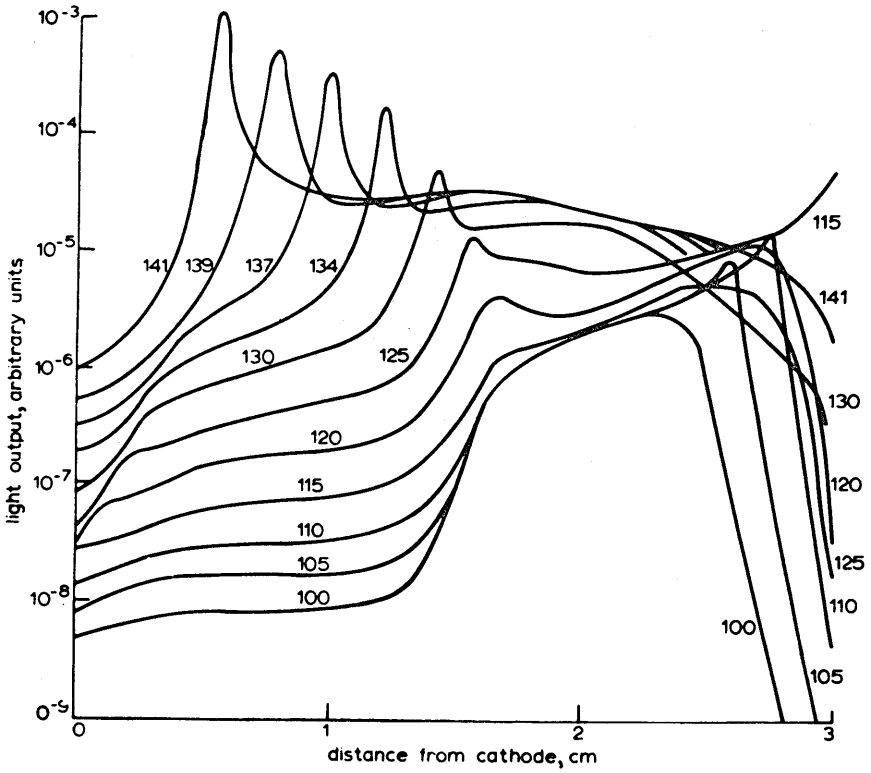

Fig. 19. Computed light output from a discharge in N_2 at p = 91 Torr and E/p = 62 V $cm^{-1}Torr^{-1}$, allowing for distortion of field. Number of initiatory electrons ~ 400; Diameter of spark ~ 0.5 mm. The time, in ns, is indicated on the curves (Davies, Davies and Evans, 1971. Reproduced by permission of The Institution of Electrical Engineers).

Despite the experimental difficulties in obtaining such data, there are also a few experimental results (Doran, 1968) available for current growth in N_2 under the conditions now being considered. Computer simulations of the current growth under identical conditions have been made, and Fig. 20 shows the good agreement obtained between the experimental and calculated values.

I should, perhaps, add that a full two-dimensional simulation has now also been carried through (Davies, Evans, Towsend and Woodison, 1977), and although it does not significantly change the picture, this treatment is clearly more satisfactory, because it does not need the assumption of a radius for the discharge (as the

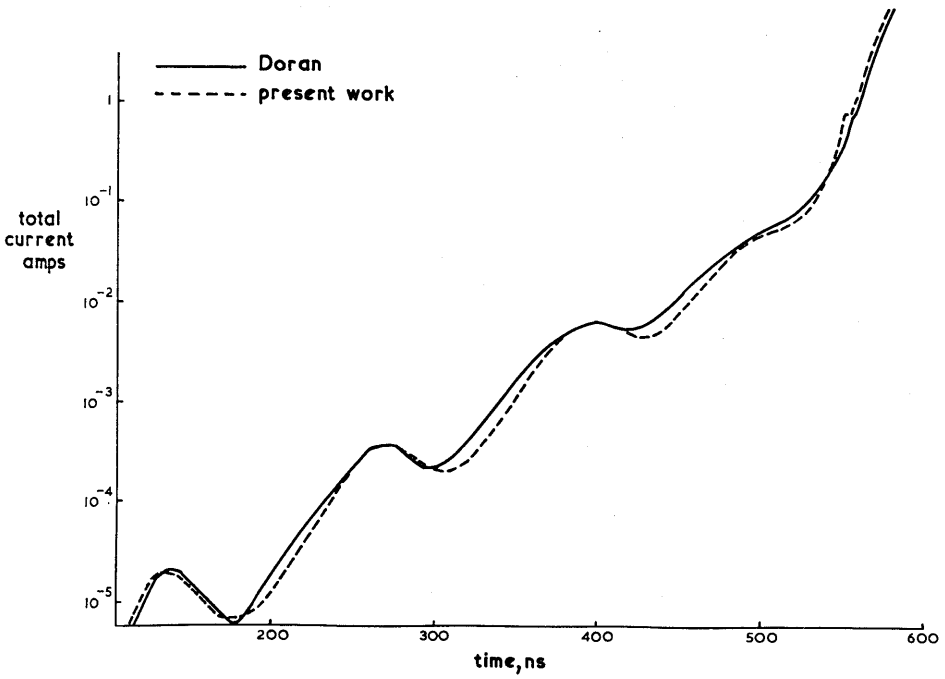

Fig. 20. Calculated (-----) and experimentally measured (———) growth of total current against time for nitrogen (Davies, Evans and Woodison, 1975. Reproduced by permission of The Institution of Electrical Engineers). p = 300 torr, d = 2 cm and overvoltage = 7.56%.

one-and-a half dimension simulation does) and it can be extended to nonuniform field electrode systems provided they are axially symmetric (Davies et al., 1978).

CONCLUSIONS

The general conclusion, as far as uniform-field breakdown is concerned, is that, over a wide range of parameters, the observed spatio-temporal growth of ionization at voltages both above and below the static breakdown voltage can be quantitatively explained in terms of the generalized Townsend theory. Thus, within this range, a knowledge of the appropriate swarm coefficients enables the theory to be used with confidence to predict quantitatively (i) the growth of prebreakdown ionization currents, (ii) the static breakdown potential and (iii) the development of the current and light output from the discharges which develop when voltages greater than the sparking potential are applied. I have already indicated what I see as the limitations to the range in which the prebreakdown

growth of current and V_s can be calculated on the basis of the generalized Townsend model. As far as the calculation of I(x,t) and light output from developing discharges is concerned, the limitations on the applicability of the theory will be related to the same kind of considerations and will occur in regions where the field is varying so rapidly that the electrons do not come into equilibrium with the field. Examples of situations in which such conditions occur are (i) in the development of the cathode fall region of the glow discharge (Davies, Evans, Marode and Segur, 1980) and (ii) in current growth at very high over-voltages (Abbas and Bayle, 1981a and b). The methods for dealing with these situations are a matter for active current research and some of the experimental results at high over-voltages will be discussed in a later paper by Dr. Kunhardt.

REFERENCES

Abbas, I. and Bayle, P., 1981, J. Phys. D , 14:649.
Abbas, I. and Bayle, P., 1981, J. Phys. D , 14:661.
Bayle, P. and Bayle, M., 1972, Z. Phys., 266:275.
Beaty, E. C., Dutton, J. and Pitchford, L. C., 1979, JILA Information Center Report No. 20.
Bhalla, M. S. and Craggs, J. D., 1962, Proc. Phys. Soc., 80:151.
Blasberg, H. A. M. and de Hoog, F. J., 1971, Physica, 54:468.
Blevin, H. A., Fletcher, J. and Hunter, S. R., 1978, J. Phys. D, 11:2295.
Buursen, C. G. J., de Hoog, F. J., and Van Mountford, L. H., 1974, Physica, 60:244.
Chalmers, I. D., Duffy, H. and Tedford, D. J., 1972, Proc. Roy. Soc. London A, 329:171.
Coates, R., Dutton, J. and Harris, F. M., 1976, in: "Proceedings, 4th International Conference on Gas Discharges, Swansea," IEE Conf. Publ. No. 143, Vol. 1, p. 133.
Coates, R., Dutton, J. and Harris, F. M., 1978, Proc. IEE, 125: 558-562.
Cohen, E. H., 1956, Proc. IEE, 103A:57.
Corrigan, S. J. B. and Von Engel, A., 1958, Proc. Roy. Soc. London A, 245:335.
Daniel, T. N. and Harris, F. M., 1970, J. Phys. B , 3:363.
Davidson, P. M., 1953, Br. J. Appl. Phys., 4:170.
Davidson, P. M., 1955, Phys. Rev., 99:1072.
Davidson, P. M., 1956, Phys. Rev., 103:1897.
Davidson, P. M., 1958, Proc. Roy. Soc. London A, 249:237.
Davidson, P. M., 1962, Proc. Phys. Soc., 80:143.
Davies, A. J., 1964, Ph.D. Thesis, University of Wales.
Davies, A. J., Davies, C. A. and Evans, C. J., 1971, Proc. IEE, 118:816.
Davies, A. J. and Evans, C. J., 1967, Proc. IEE, 114:1547.
Davies, A. J., Evans, C. J. and Llewellyn-Jones, F., 1964, Proc. Roy. Soc. London A, 281:164.

Davies, A. J., Evans, J. G., Marode, E. and Segur, P., 1980, in: "Proceedings, 6th International Conference on Gas Discharges, Edinburgh," IEE Conf. Publ. No. 189, Vol. 2, p. 59.
Davies, A. J., Evans, C. J., Townsend, P. and Woodison, P. M., 1977, Proc. IEE, 124:179.
Davies, A. J., Evans, C. J. and Woodison, P. M., 1975, Proc. IEE, 122:765.
Davies, A. J., Evans, C. J. and Woodison, P. M., 1978, in: "Proceedings, International Symposium on Gaseous Dielectrics, Knoxville, Tennessee," L. G. Christophorou, ed., NTIS, Springfield, VA, p. 84.
Davies, W. E. V. J., Dutton, J. and Harris, F. M., 1966, J. Sci. Instr., 43:457.
De Hoog, F. J. and Kasdorp, J., 1967, Physica, 34:63.
Doran, A. A., 1968, Z. Phys., 208:427.
Dutton, J., 1967, JILA Information Center Report No. 4.
Dutton, J., 1975, J. Chem. Phys. and Chem. Ref. Data, 4:577.
Dutton, J., 1978, in: "Electrical Breakdown of Gases," 2nd Ed., J. M. Meek and J. D. Craggs, eds., Wiley, New York, Chap. 3.
Dutton, J., Harris, F. M. and Hughes, D. B., 1973, Proc. IEE, 120:941.
Dutton, J., Harris, F. M. and Jones, G. J., 1970, Nature, 227:702.
Dutton, J. and Williams, W. T., 1981, in: "Proceedings, 15th International Conference on Phenomena in Ionized Gases, Minsk," p. 593.
Folkard, M. A. and Haydon, S. C., 1971, Aust. J. Phys., 24:527.
George, D. W. and Richards, P. H., 1969, Brit. J. Appl. Phys., 2:1470.
Hughes, D. B., 1973, Ph.D. Thesis, University of Wales.
Johnson, P. C. and Parker, A. B., 1971, Proc. Roy. Soc. London A, 325:529.
Jones, G. H. and Morgan, C. G., 1969, in: "Proceedings, 9th International Conference on Phenomena in Ionized Gases, Bucharest," Vol. 1, p. 135
Kline, L. E., 1974, J. Appl. Phys., 45:2046.
Lakshminarasimha, C. S., Lucas, J., and Snelson, R. A., 1975, Proc. IEE, 122:1162.
Llewellyn-Jones, F., 1966, "Ionization and Breakdown in Gases," 2nd Ed., Methuen, London.
Llewellyn-Jones, F., 1967, "Ionization Avalanches and Breakdown," Methuen, London.
Morgan, C. G., Evans, C. J., Williams, W. T. and Davies, A. J., 1965, Brit. J. Appl. Phys., 16:1797.
Morgan, C. G. and Williams, W. T., 1965, Proc. Phys. Soc., 85:443.
Muller, E. K., 1966, Z. Angew. Math. and Phys., 21:219.
Pace, J. D. and Parker, A. B., 1973, J. Phys. D , 6:1525.
Parker, A. B. and Johnson, P. C., 1971, Proc. Roy. Soc. London A, 325:511.
Pedersen, A., 1975, IEEE Trans. Power and Apparatus Systems, PAS-94:1749.

Raether, H., 1964, "Electron Avalanches and Breakdown in Gases," Butterworth, London.

Raina, R. K. and Parker, A. B., 1972, in: "Proceedings, 2nd International Conference on Gas Discharges, London," IEE Conf. Publ. No. 90, Vol. 1, p. 291.

Schlumbohm, H., 1960, Z. Phys., 159:212.

Trump, J. G., Cloud, R. W., Mann, J. G. and Hansen, E. P., 1950, Elec. Eng., 69:961.

NANOSECOND PULSE BREAKDOWN OF GAS INSULATED GAPS

E. E. Kunhardt

Ionized Gas Laboratory
Texas Tech University
Lubbock, Texas

INTRODUCTION

Over the last few decades there has been and continues to be an interest in elucidating those processes which have a major influence on the spatial-temporal development of the space charge in a gas insulated gap, leading to the collapse of the voltage applied across it. The various processes which must be considered have been discussed by Rees and by Dutton (this ASI). The gap parameters (i.e., pressure, p; applied external fields, E_o; gap dimensions, d; and gas type) and the time scales associated with the current growth serve in narrowing down the number of processes that need to be considered for any particular situation. There has been considerable controversy as to what processes play a role in the various regions of gap parameter space. A discussion of these issues has been given by Professor Llewellyn-Jones at this ASI.

The processes are in general divided into two catagories: those involving the cathode (i.e., "cathode processes") and those occurring in the interelectrode space (i.e., "gas processes"). The cathode processes have been discussed by Dutton (this ASI). The gas process over which there has been the most clamor is gas photoionization. However, there are a number of processes, besides photoionization, which may be occurring in the gas (depending again on the gap parameters), and it is very difficult to assess which of them, if any, is dominant. This is specially true at the higher values of E/N where space charge effects due to gas ionization cannot be ignored. Dutton discussed the evolution of current in a gap when this effect need not be considered. The Townsend model discussed by him gives very good agreement with experiments. Its

physical and quantitative foundations, however, separate it from other models (to be discussed later) and should be referred to as the Townsend Theory.

The physical phenomenon I will be discussing is the growth of the ionization of a gas leading to the collapse of the voltage across a gap for values of E_o/p such that the space charge generated by an electron avalanche cannot be ignored. These values of E_o/p are achieved when the applied voltages are significantly higher than the static breakdown voltage, V_s (i.e., for V greater than 25% above V_s).

This regime is in general very diffcult to investigate. The difficulty stems from, first, the broad range of electron densities through which the avalanche progresses; second, the large spatial variations associated with the various field variables; and third, the time scales involved in the transition. As an illustration of the problem, the electron avalanche first behaves as a swarm (Debye length, $\tau_D >>$ avalanche dimensions, ℓ_a), then as a nonideal plasma ($\tau_D \sim \ell_a$); and finally as a plasma ($\tau_D << \ell_a$); so that no single analytical framework can be used to model this progression. Experimental investigations have also been thwarted by the speed and sensitivity required of the diagnostic apparatus in order to observe the above progression. For $V >> V_s$, the development occurs in times of the order of nanoseconds.

In the subsequent section, I will first describe a typical experimental arrangement that has been used in the investigations of voltage collapse for the large overvoltage regime. Such a description will help to create a physical picture for subsequent discussion. A standard terminology will then be established. The results obtained with the experimental set-up depend, of course, on the initial conditions in the gap. These conditions and the diagnostic techniques used to obtain information on the processes will serve to classify the experiments. After this classification is described, the experimental results and the models proposed to explain them will then be discussed.

EXPERIMENTAL BACKGROUND

The coaxial arangement shown in Fig. 1 is normally used in the investigations of breakdown for the conditions described in the previous section. This arrangement assures that the electrical circuit can react, with sufficient speed, to the events occurring in the gap. The sequence of events during the experiment is as follows: A voltage pulse of magnitude greater than the static breakdown voltage, V_s, is launched in a coaxial line, and it appears across the electrodes formed by an interruption in the center

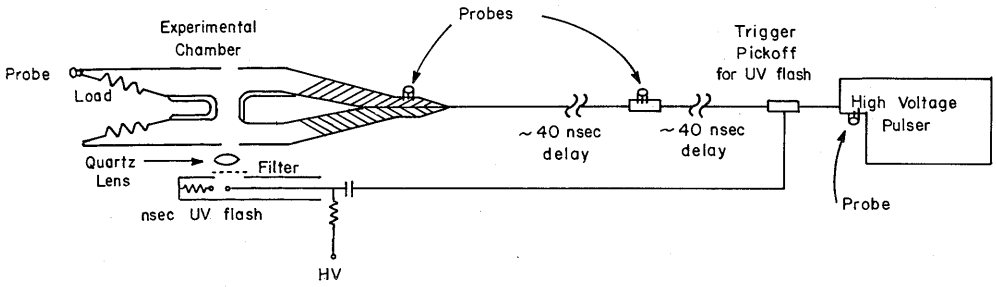

Fig. 1. Diagram of coaxial experimental arrangement.

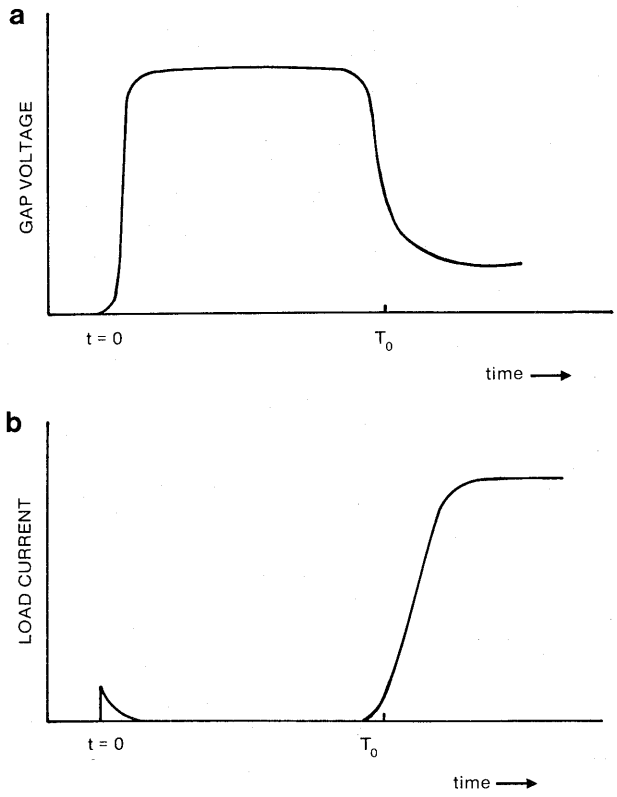

Fig. 2. a) Sketch of voltage waveform across the gap. b) Sketch of current waveform at the load.

conductor of the coaxial test chamber. The chamber is terminated with its characteristic impedance to avoid any unwanted reflections. A schematic indication of the evolution of the gap voltage as a function of time is shown in Fig. 2a while Fig. 2b shows the evolution of the current at the terminating load. The time elapsed from the application of the voltage to the gap to the observed time for the collapse of voltage across the gap, i.e., T_o in Fig. 2, is called the observational time lag. This time is in the nanosecond range. The collapse of the voltage, under these conditions, constitutes the breakdown of the insulating properties of the gap. This definition, as discussed later, needs not coincide with that used for static breakdown, namely, the establishment of a self-sustaining discharge.

The time to breakdown, i.e., the observational time lag, consists of two portions: the statistical time lag (the time elapsed from the application of the voltage to the gap to the appearance of a breakdown initiating electron) and the formative time lag (the time it takes the space charge to grow and cause breakdown). The formative time is of the order of an electron transit time or less and may not correspond to the bridging of the gap by a weakly conducting channel. Because of this last point, the formative time in this context may differ from the defined for $V \geq V_s$.

Since the observational time lag may be as short as a few nanoseconds, it is necessary for the risetime of the applied voltage to be a nanosecond or less. To achieve this goal, coaxial lines are used to generate the incident pulses. A diagram of the experimental set-up in our laboratory is shown in Figs. 3a and 3b. The pulse applied to the gap is shown in Fig. 4.

CLASSIFICATION OF EXPERIMENTS

The objective of these investigations is to elucidate the processes associated with the statistical and formative time lags and the dependence of these times on the gap parameters.

The data obtained from the experiments consists of traces of the voltage across the gap, the current at the load (see Figs. 2 and 7), and optical records taken with streak and framing cameras, and photomultiplier tubes (see Figs. 13 and 14). A general discussion of various diagnostic techniques is given by Waters (this ASI). See also Koppitz (1971), Mesyats et al. (1972), and Stritzke et al. (1977) for specific applications to the regime being discussed here. Time lag information is obtained from electrical measurements, whereas the optical records help to determine the state of the gas.

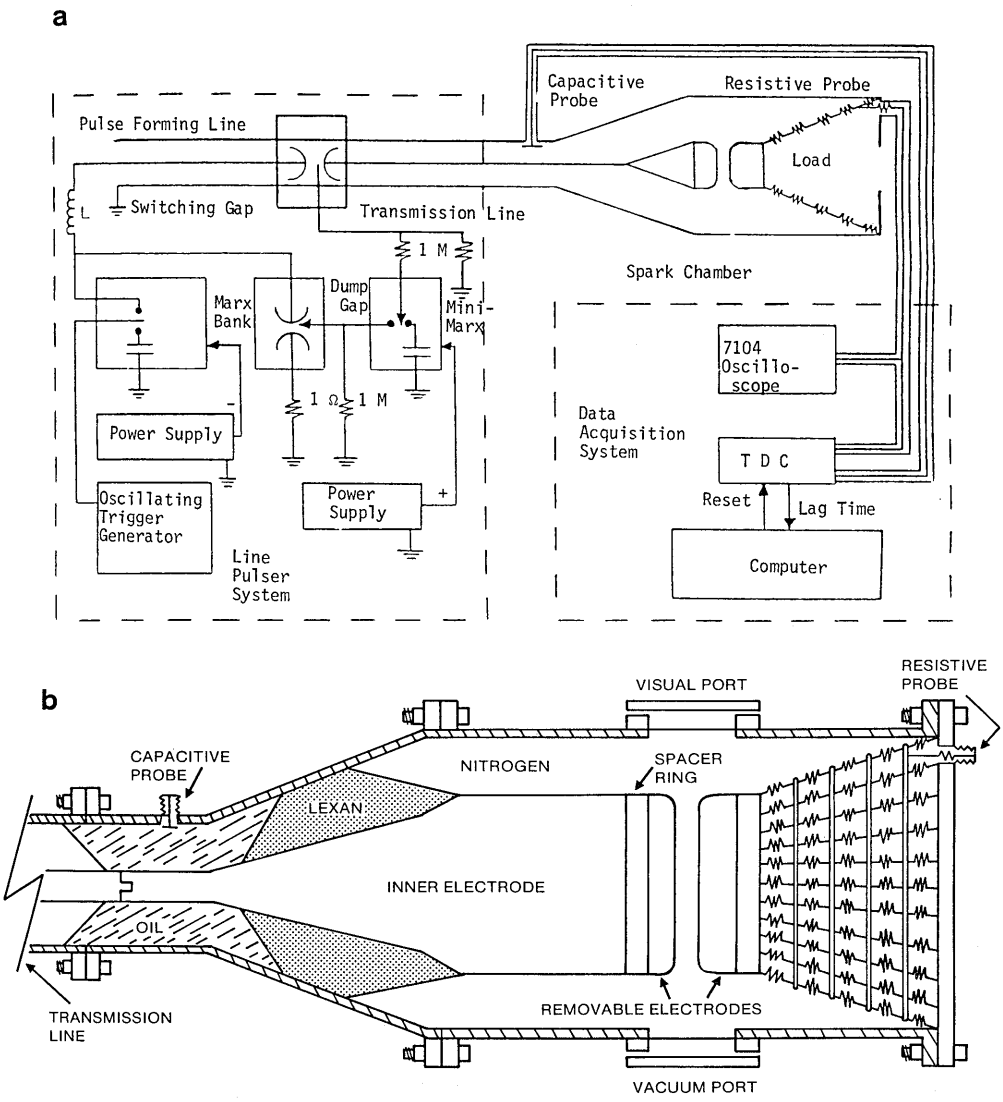

Fig. 3. a) Experimental arrangement b) Spark Chamber.

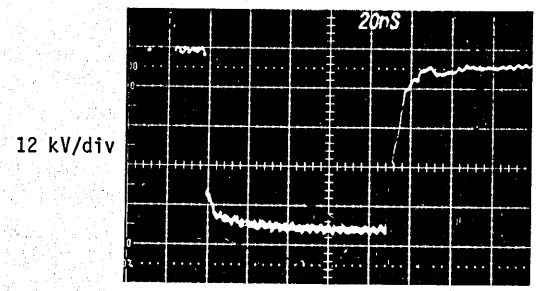

Fig. 4. Incident Nanosecond Pulse.

Using the set-up described in the previous section, two types of experiments can be carried out, identified by whether or not an initial space charge is introduced in the gap prior to the application of the voltage pulse to the gap.

Although there are a number of ways of introducing the initial space charge in the gap (by laser irradiation, electron beam, etc.), the one most commonly used is by irradiation of the cathode with the U-V generated by a short spark (see Fig. 1).

The experiments without externally supplied electrons provide information on the statistical and formative time lags, whereas those with external electron supply, by defacto, completely eliminate the statistical time lag; that is, electrons are already present at the time the voltage pulse arrives at the gap. The physical appearance of the gap during the development of breakdown for U-V irradiated experiments is markedly different depending on whether or not the irradiation is uniformly distributed over the surface of the cathode. Optical records show that when the illumination is uniform, the ionized channel in the gap is broad [Koppitz (1971, 1973), Koppitz and Stuhm (1976)]; whereas in nonuniform illumination, it may be broad or constricted depending on the gas parameters and overvoltage [Vorob'ev and Iskol'dskie (1967), Mesyats et al. (1972), Bichkov et al. (1973), Bayles et al. (1975)]. The length of the formative time lag for U-V irradiated experiments has been found to depend on the initial number of photoelectrons present at the cathode. As a result, the experiments have been labeled as "single electron initiated" and "multiple electron initiated," depending on the initial number of electrons [Kremnev and Mesyats (1971)].

In the following section, results obtained under a variety of experimental conditions will be discussed.

EXPERIMENTAL RESULTS

Electrical measurements of either the voltage across the gap or the current at the load as a function of overvoltage and gap parameters have been made by a number of workers: Rogowski (1928), Fletcher (1949), Nesterikhin et al. (1964), Mesyats and Bychkov (1968), Mesyats et al. (1969), Korshunov et al. (1970), Levinson and Kunhardt (1981). The early measurements of Rogowski are in part responsible for the controversy over the processes contributing to voltage collapse for pd > 200 torr-cm (see Llewellyn-Jones, this ASI).

From these electrical measurements, it is possible to measure the length of the statistical and formative time lags and their probability distribution. These measurements are used to support conclusions drawn from theoretical models. It should be noted that agreement between this data and the model is a necessary but not a sufficient condition to justify the validity of the model and that other means for justification must also be used. I will now discuss results from three different experiments which cover the conditions described in the previous section. First, are experiments in which no U-V illumination is used. Second, those experiments carried out using U-V irradiation nonuniformly distributed over the cathode area, and finally experiments with uniform irradiation over the whole cathode surface leading to a broad channel discharge. The experimental procedures for these experiments are very similar. Referring to Figs. 3a and 3b (the experimental set-up shown is typical of overvolted gap experiments), a coaxial cable is charged to the desired voltage, and a voltage pulse is formed when the output gap of the generator is shorted. This pulse travels along a coaxial line and is incident on the test gap. The difference between the three experiments to be discussed lies in the intensity and distribution of the U-V irradiation prior to the arrival of the voltage pulse to the gap.

In the first experiment to be discussed, there is no U-V irradiation. Figure 5 is a trace of the current at the load from Levinson and Kunhardt (1981). The first small negative spike corresponds to the arrival of the incident pulse to the gap. After a short time, the insulating properties of the gap breakdown, generating a fast rising current pulse at the load. The observational delay corresponds to the time interval from the initial spike to the time the current is observed to rise. To measure this time we have used the data acquisition system shown in Fig. 3a. The initial spike is used to turn on a time to digital converter (TDC), and the current pulse generated by the breakdown is used to stop it. The time resolution of the system is 100 ps. With this technique, the probability distribution for the observational delay were determined for a number of experimental conditions. For each

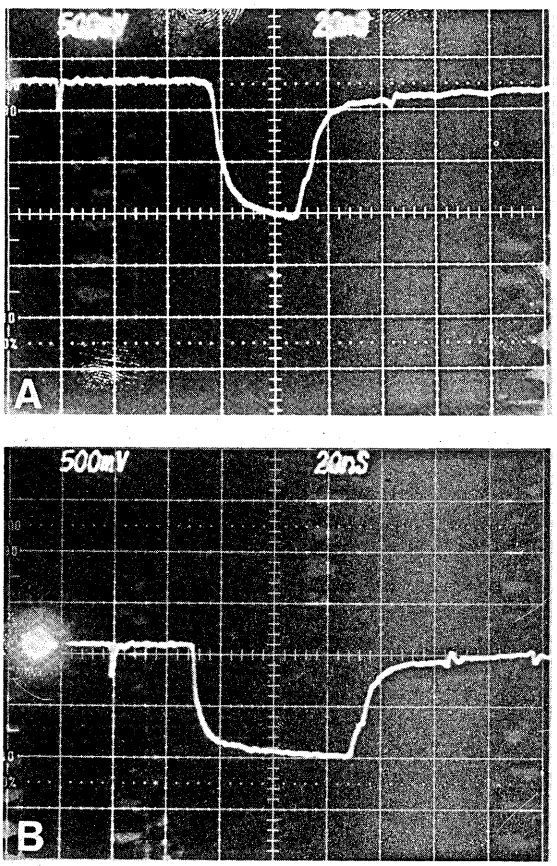

Fig. 5. Current waveforms detected at the load: a) Parameters: gas: nitrogen; pressure: 950 Torr; gap width: 2 cm; incident voltage: 140 kV, b) Parameters: gas: nitrogen; pressure: 1350 Torr; gap width: 1 cm; incident voltage: 110 kV.

condition, 3,000 points were used to construct the distribution. Histograms of the distribution are shown in Figs. 6 and 7. From these histograms, information on the electron emission properties of the cathode and the formative time can be obtained. In Fig. 6, the histograms, obtained using brass and amorphous graphite cathodes, are shown.

The distribution for graphite is strikingly narrower for the same parameter setting. This was also true when graphite was compared to other cathode materials used: aluminum and copper. Assuming that the initial electron leading to breakdown is generated

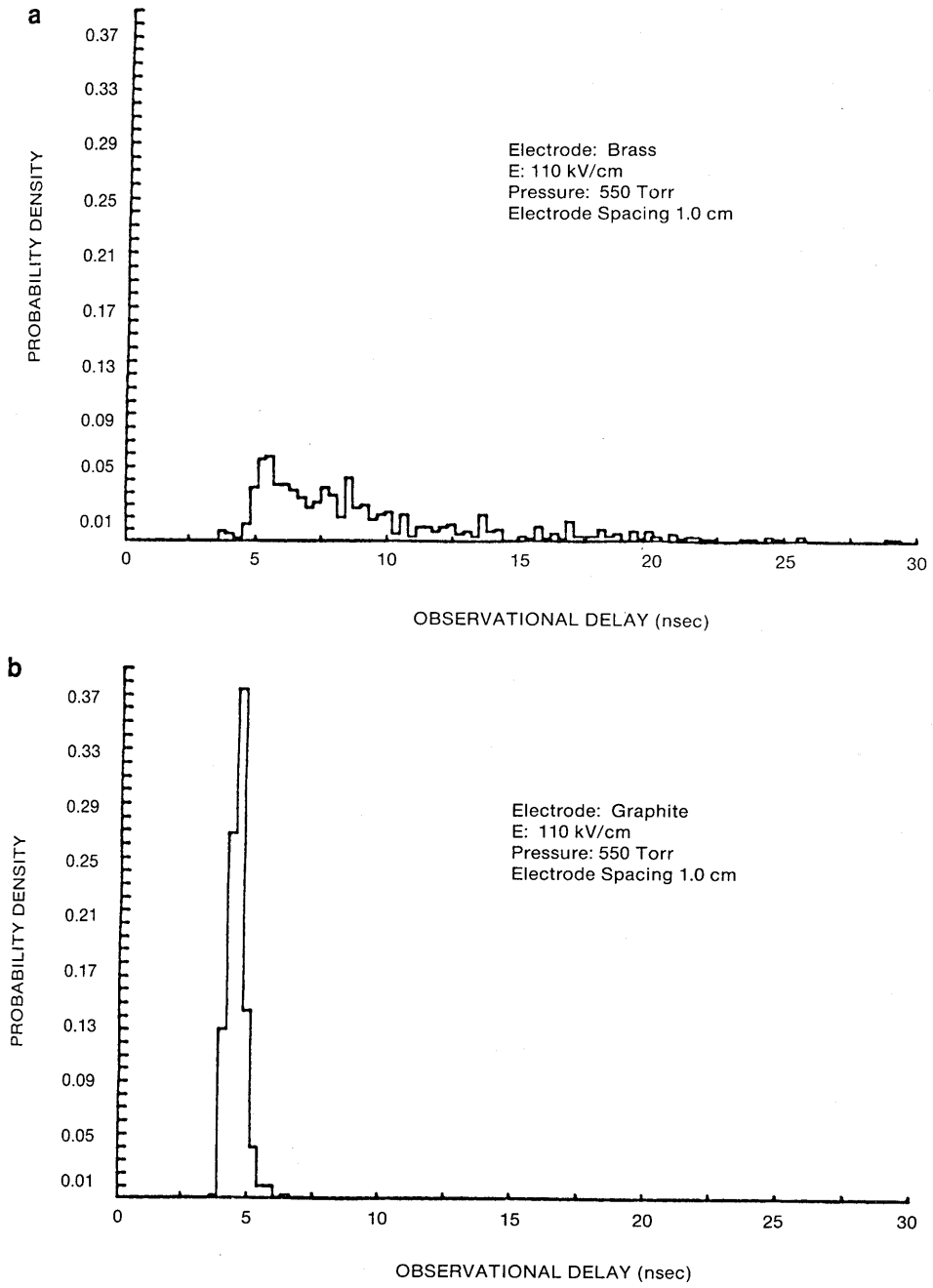

Fig. 6. Histograms of observational delay time: a) Brass, b) Graphite.

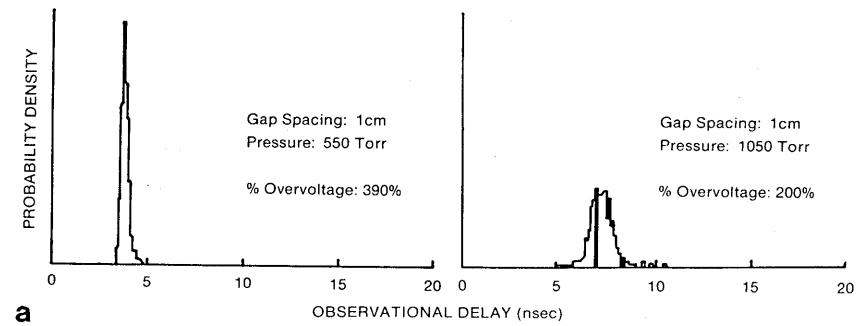
PROBABILITY DENSITY
Gap Spacing: 1cm
Pressure: 550 Torr
% Overvoltage: 390%
Gap Spacing: 1cm
Pressure: 1050 Torr
% Overvoltage: 200%
0 5 10 15 20
OBSERVATIONAL DELAY (nsec)

a

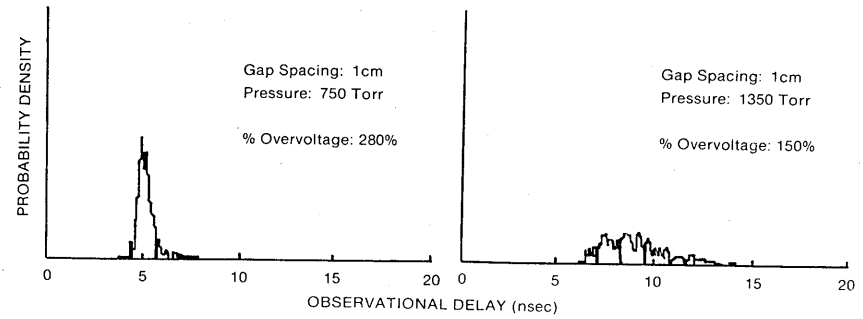
PROBABILITY DENSITY
Gap Spacing: 1cm
Pressure: 750 Torr
% Overvoltage: 280%
Gap Spacing: 1cm
Pressure: 1350 Torr
% Overvoltage: 150%
0 5 10 15 20
OBSERVATIONAL DELAY (nsec)

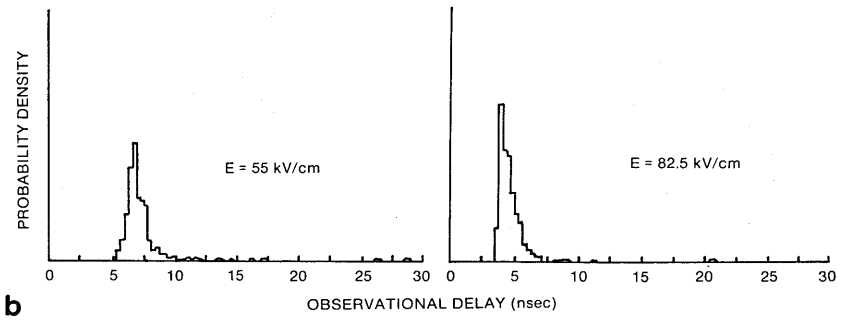
PROBABILITY DENSITY
E = 55 kV/cm
E = 82.5 kV/cm
0 5 10 15 20 25 30
OBSERVATIONAL DELAY (nsec)

b

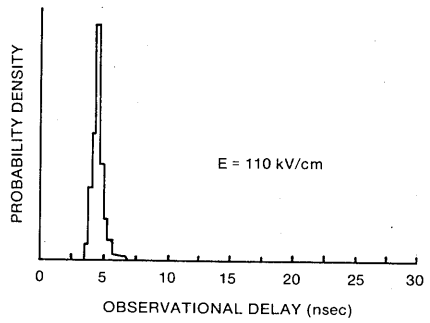
PROBABILITY DENSITY
E = 110 kV/cm
0 5 10 15 20 25 30
OBSERVATIONAL DELAY (nsec)

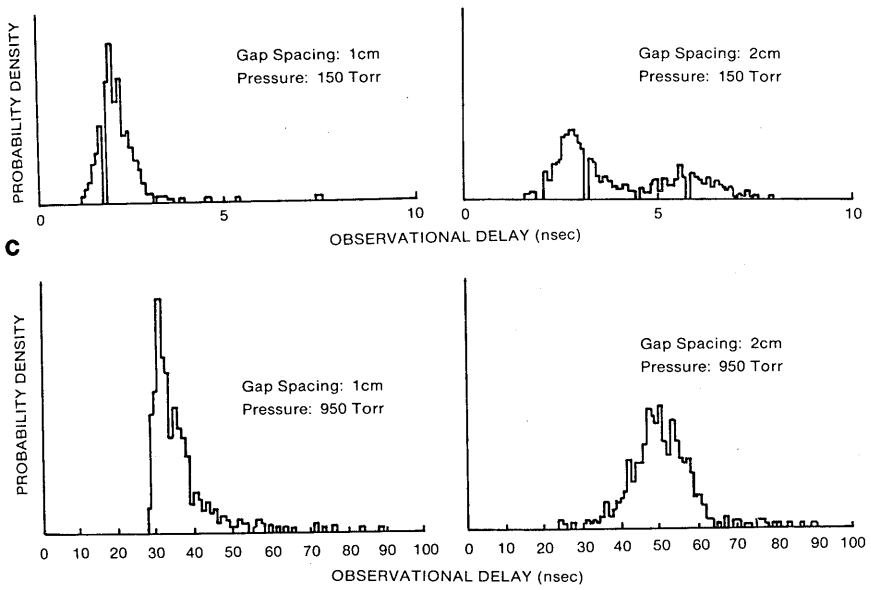

Fig. 7. a) Histograms of observational delay time for various overvoltage conditions. Graphite electrodes. b) Histograms of observational delay time for various electric field strengths and fixed values of pressure (550 Torr N_2). Graphite electrodes. c) Histograms of observational delay time for two values of gap spacing 1 cm and 2 cm. Graphite electrodes.

at the cathode and using a simple stochastic model, the cummulative probability distribution is found to be [Wilson (1936)]:

$$P_c(t) = 1 - e^{-\lambda(t-t_f)} \qquad t \geq t_f$$

$$= 0 \qquad t \leq t_f \qquad (1)$$

where P_c is the probability for having a delay time of t or greater, λ is the "apparent" emission rate and t_f is the formative time which is assumed to be deterministic. The reason the emission rate is referred to as "apparent" is that the actual emission rate may be higher, since a number of electrons may scatter back into the cathode due to the presence of the gas. Histograms obtained using graphite electrodes for a number of experimental conditions (i.e., overvoltage, pressure, gap separation) are shown in Figs. 7a, b, c. Equation (1) can be used to approximately describe the experimental data. The parameter λ is chosen by using a least squares criteria to fit Eq. (1) to the experimental results for the cummulative

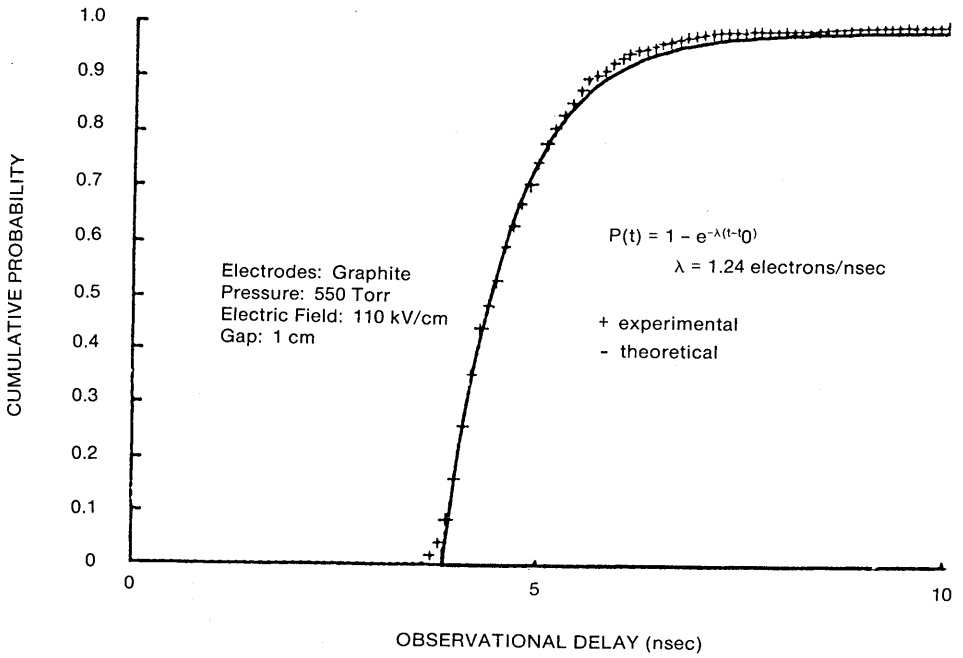

Fig. 8. Cumulative probability density

distribution. An example of a particular cummulative distribution and associated curve using Eq. (1) is shown in Fig. 8. Note that there is good agreement except for very short times. For these times, the error introduced by assuming that the formative time is deterministic is significant. The emission rate obtained from this procedure is $\lambda = 1.24$ electrons/nsec.

For all experiments, the cathode surfaces were thoroughly polished. The state of the surface of the cathode prior to and during the experiments influences the emission rate. To examine this effect, a glow discharge was applied to the three types of electrodes for varying durations prior to the time lag experiments in an effort to "clean" the cathode surface. Figure 9 is a plot of the "apparent" emission rate versus time of duration of glow discharge. Note that the exposure time had virtually no effect on the graphite electrode data. No correlation could be found for the aluminum electrode. This is not surprising due to the presence of an oxide layer on the electrode. The effect of pressure is shown in Fig. 10. Note that for a fixed electric field there is considerable deviation in λ with pressure. Since the emission rate is primarily the result of cathode emission (which is related to the electric field), this behavior is attributed to gas-related phenomena, i.e., electron back-scattering into the cathode, rather than change

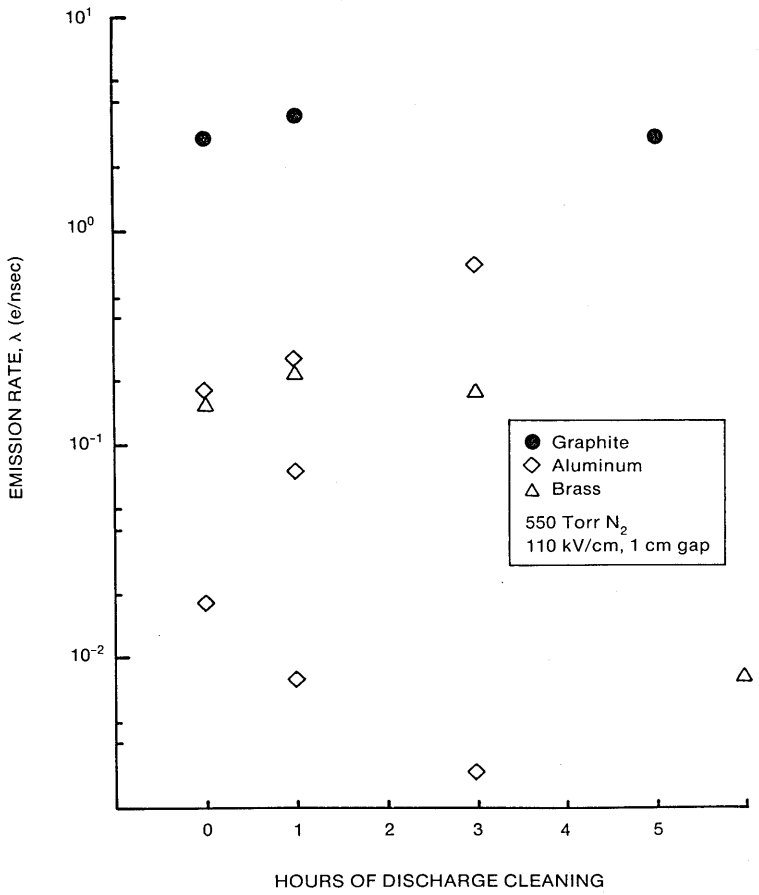

Fig. 9. "Apparent" electron emission rates versus electrode condition.

in the emission rate of the cathode, the "intrinsic" emission rate. A change in the field tended to increase the emission rate as expected. Electrode separation had no effect on the apparent emission rate. This tends to reinforce the assumption that electrons are initiated at the cathode rather than at the interelectrode volume.

In all cases, the emission rate from graphite was an order of magnitude higher. Surface analysis of the electrodes before the experiments show a very smooth cathode surface (the electrodes were carefully polished). Subsequent analysis after a single breakdown shows that a large number of micro-protrusions appear on the surface. This appearance has been attributed to condensation of the carbon

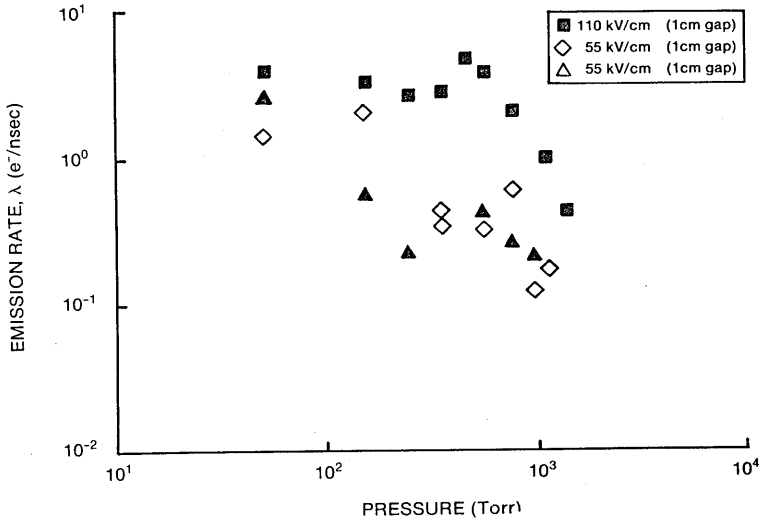

Fig. 10. "Apparent" electron emission rates versus pressure.

vapor created by the spark (carbon sublimates). Thus, irrespective of the degree of polishing, the cathode surface contains a large number of centers, after a single spark, from which field emission is favored. This finding may explain the high rates observed.

From the histograms in Figs. 6 and 7, it is possible to obtain the formative time. This corresponds to the minimum time observed in the delay data. The error bar in this measurement is determined by the statistics of the formative time. In this experimental regime the variance is ~0.5 nsec. [Korshunov et al. (1970)]. The minimum time is plotted in Fig. 11 for a number of experimental conditions. These times do not agree with times obtained from the streamer criteria relation [Raether (1964)]. Possible reasons for this disagreement are discussed later in the paper.

Using a set-up similar to that in Fig. 3, Mesyats et al. (1969) carried out experiments in which the cathode was illuminated prior to the arrival of the voltage pulse to the gap, thus eliminating the statistical time. The formative time is directly obtained from measurements of the time for voltage collapse. When the illumination intensity was low, the times measured did not agree with those obtained by Fletcher (1949). Fletcher's results are in agreement with the streamer criteria and have been used as support for it. However, for high intensity illumination (i.e., initial number of electrons ~10^4) the time lags observed did agree with Fletcher's results. Mesyats et al. concluded that for "single electron initiation" (i.e., low illumination intensity) the voltage collapse is due to space charge motion in the gap. This had been

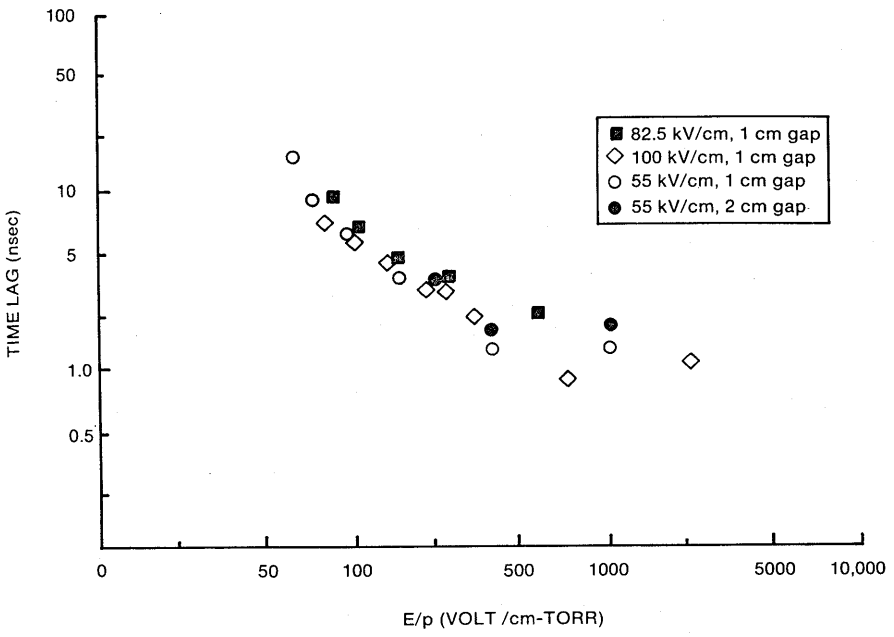

Fig. 11. Minimum observed delay versus overvoltage.

suggested earlier by Dickey (1952) to explain Fletcher's results (see next section).

For the high intensity results, Kremnev and Mesyats (1971) proposed a model in which a large number of avalanches are initiated at the cathode by photoelectric emission. These avalanches reach a stage of growth after which electron multiplication stops. A new avalanche develops from the head of each subsequently retarded avalanche. Thus, avalanche chains propagate across the gap. Subsequent chains are produced via the photoelectric effect. Voltage collapse is due to a growth in current due to these chains.

In Fig. 12, the formative times measured by a number of workers are shown as a function of E/p. The results of Mesyats et al. are for single electron initiation. The correction on the streamer theory results accounts for the finite propagation speed of the streamer taken to be its maximum possible value, i.e., the speed of light. It should be noted that there are significant differences in the width of the gap for all cases. Our results are closer to Mesyats than to the rest. We expect to have single electron initiation in our experiments.

If the cathode surface is uniformly illuminated with very high intensity U-V so that the number of primary electrons is very high

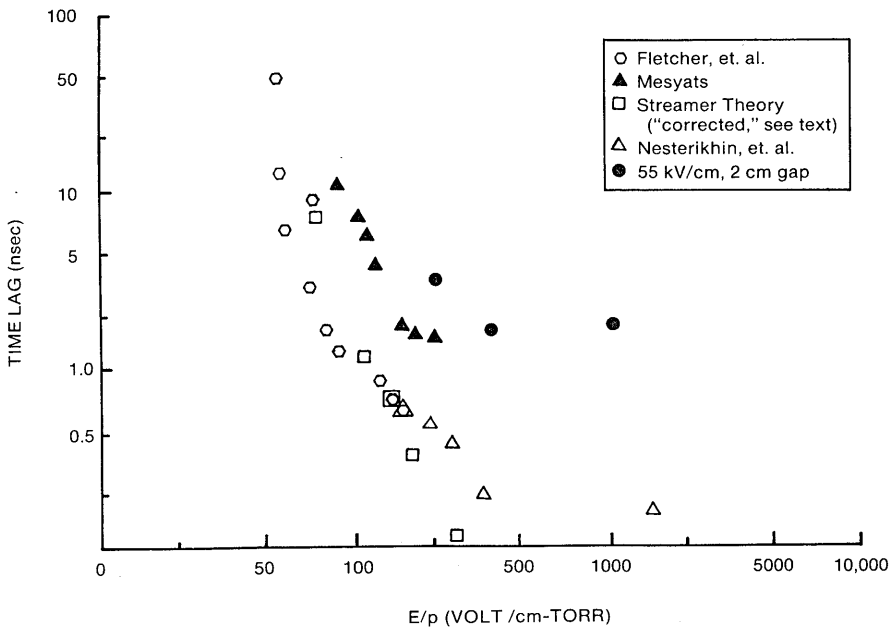

Fig. 12. Minimum time lags versus E/p from various sources.

($\sim 10^8$), optical records of the breakdown show that a broad luminous front develops and moves across towards the anode. Koppitz (1971, 1973) and Koppitz and Stuhm (1977) investigated these large cross-section, overvolted breakdowns using optical diagnostic techniques (streak and shutter photography). The broad character of the ionized channel is shown in Fig. 13b. In Fig. 13a the narrow channel characteristic of lower nonuniform intensities (including no illumination) is shown. The luminous front moving towards the anode is observed to have two phases characterized by different propagation speeds. A streak photograph taken by Koppitz (1973) is shown in Fig. 14. He suggested that the slow speed phase (speeds $\approx$ 1.5 times the electron drift speed) may be explained by field distortion. This phase is labeled a_1 in the schematic picture to the right of the streak photograph in Fig. 14. In the fast phase (labeled a_2 in Fig. 14), propagation speed may be ten times greater than the drift speed. To explain this speed, it is necessary to introduce a far-reaching ionization mechanism such as photoionization.

Because of the broad character of the ionization front, its development may be described using a one-dimensional mode. A number of computational models have been developed: Davies et al. (1971, 1977), Kline (1974), and Yoshida and Tagashira (1976). In these models, a varying number of assumptions are made in order to reproduce the experimental results. The agreements are satisfactory.

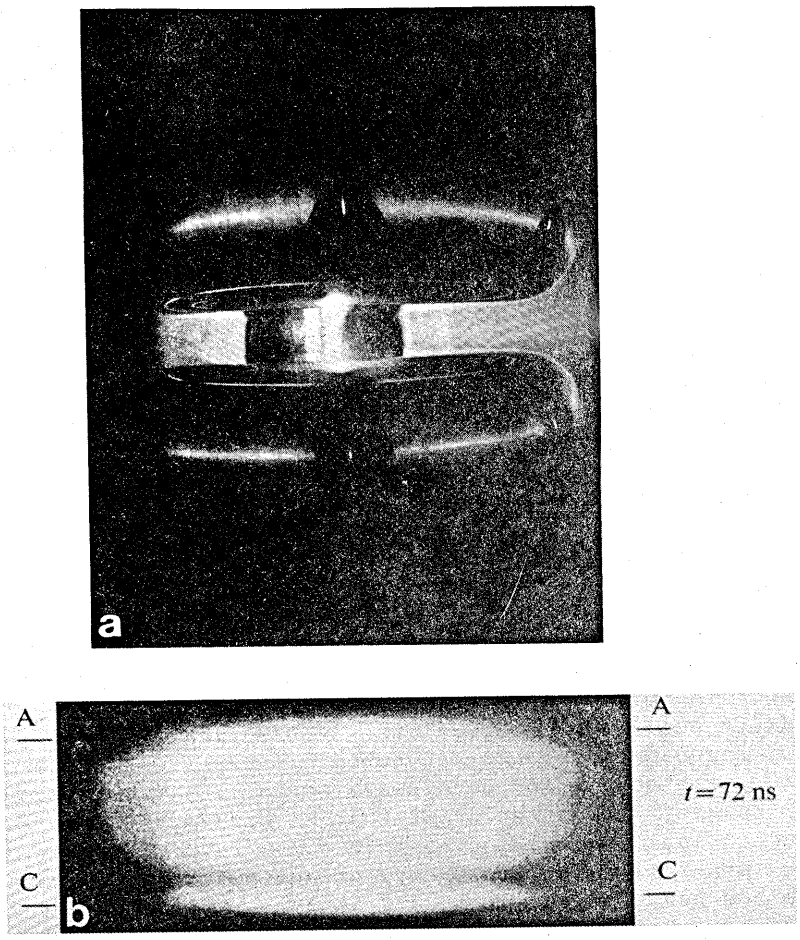

Fig. 13. Influence of U-V irradiation on spatial characteristics of discharge. a) No radiation, b) U-V irradiated [Koppitz (1973)].

However, the assumptions among the models are not uniform so that there are no definite answers as to what are the important processes involved.

THEORETICAL MODELS

A number of models have been proposed to explain the short breakdown times that have been experimentally obtained and the spatial properties of the ionization channel. A review of these models is given by Kunhardt (1980). The first such model is the

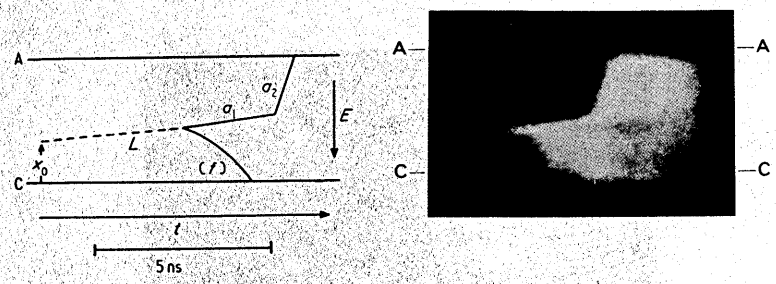

Fig. 14. Streak records of broad discharge [Koppitz (1973)].

streamer model introduced by Raether (1964), Meek (1940), and Loeb (1939). In this model, an avalanche generated by a single electron reaches a critical stage (determined by the total number of electrons in the avalanche) and transforms into a fastmoving ionization front due to photoionization of the gas ahead of the front. From this model, the time to breakdown of a gap is given by [Raether (1964)]:

$$t_{ob} = \frac{\ln N_{cr}}{\alpha V_d} \tag{2}$$

where N_{cr} is the number of electrons in the avalanche at the critical stage, α is the Townsend primary ionization coefficient and V_d is the drift velocity. As mentioned in the previous section, Fletcher (1949) found good agreement between his experimental measurements and the breakdown times obtained from Eq. (2) (see Fig. 12). However, Dickey(1952) pointed out that a voltage collapse may also be due to space-charge motion in the gap inducing a current in the external circuit. This current generates a voltage at the load, and since the supply voltage is constant, the voltage across the gap collapses. Using a transmission line model for the gap region as shown in Fig. 15, the voltage V_t is found to satisfy the equation:

$$C \frac{dV_t}{dt} + \frac{V_o}{z} V_t = I_s + C \frac{dv_i}{dt} \tag{3}$$

where C = capacitance of the gap

Y_o = characteristic admittance of line

V_i = incident pulse

and I_s is a current source due to the motion of electrons in the gap (the ions are assumed to remain stationary in these time scales) and is given by:

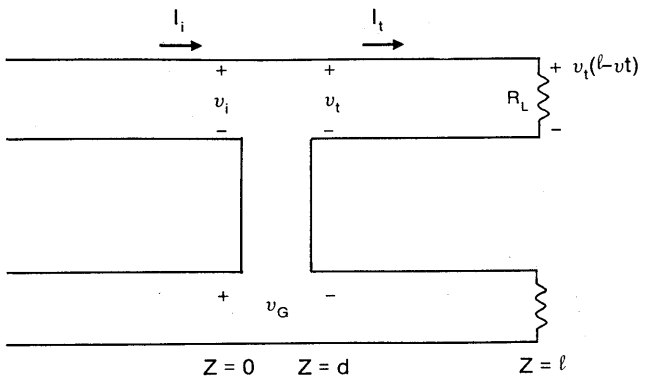

Fig. 15. A Transmission Line Model.

$$I_s = \frac{eV_d N_o}{2\delta} \; e^{\int_o^t \alpha v_d dt} \tag{4}$$

where

$e \equiv$ electronic charge

$N_o \equiv$ initial number of electrons

$\delta \equiv$ gap width.

The general solution of Eq. (3) is:

$$V_t(t) = \frac{1}{2C} \int_o^t I_s(t-\tau) e^{-\tau/ZRC} \frac{}{dx} - \frac{1}{2RC} \int_o^t V_i(t-\tau) e^{-\tau/ZRC} dx + V_i(t) \tag{5}$$

This voltage will appear across the load delayed by an amount equal to the transit time to the load. The shape will be the same. If α and V_d are assume constants, Eq. (5) yields:

$$V_t(t) = \frac{e\, V_d N_o}{2\delta C\, (\alpha V_d + \frac{1}{2}RC)} \left[e^{\alpha V_d t} - e^{-t/ZRC}\right] + e^{-t/ZRC}. \tag{6}$$

The load current is $V_t(t)/R_L$. A sketch of this current is given in Fig. 2b. Note that for this model, voltage collapse occurs before the electrons have reached the anode. Thus, what is meant by breakdown takes on a different context than in the case of static breakdown.

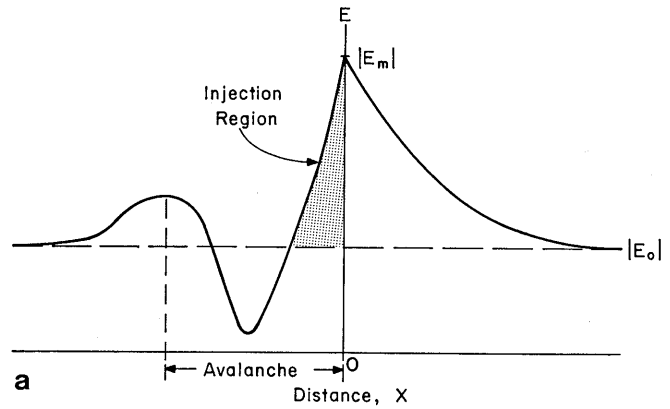
E
|Em|
Injection
Region
|Eo|
Avalanche
0
Distance, X
a

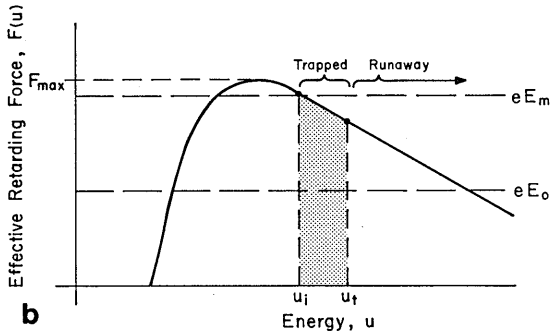
Effective Retarding Force, F(u)
Fmax
Trapped
Runaway
eEm
eEo
ui
ut
Energy, u
b

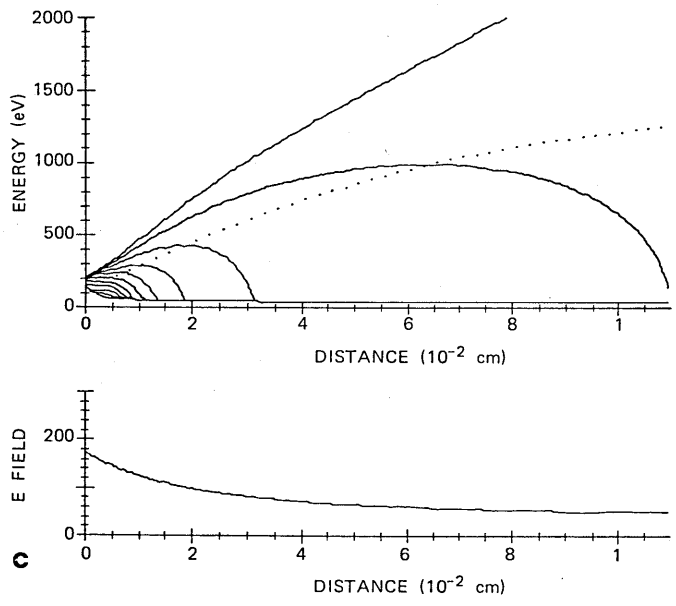
2000
1500
1000
500
0
ENERGY (eV)
0
2
4
6
8
1
DISTANCE (10-2 cm)
200
0
E FIELD
0
2
4
6
8
1
DISTANCE (10-2 cm)
c

As mentioned in the previous section, Mesyats et al. (1972) found that they were able to explain their results using this model for the case of single electron initiation. For conditions in which $N_o \simeq 10^4$, they introduced the avalanche chain model [Kremnev and Mesyats (1971)].

Experiments similar to those Fletcher (1949) were carried out by Felsenthal and Proud (1965). To explain the observed breakdown delay times they used a modified pulsed-microwave breakdown theory with very satisfactory results. Lozanskii (1976) quantified the streamer model by proposing a mechanism for electron generation ahead of the avalanche. This was an ill-defined issue in the streamer theory. He proposed that associative ionization of atoms excited by photons of energy lower than that required to ionize are responsible for the formation and propagation of the streamer. Assuming a Lorentzian profile for the spectral line of interest, he obtained an expression for the absorption coefficient of the photons. Because of the finite line width, the off-resonant photons can escape the avalanche and excite atoms just ahead of it. He then estimated the number of electrons that will be produced via the chemical reaction:

$$A^* + B \longrightarrow AB^+ + e^-$$

where A* is an excited atom or molecule and B is an atom or molecule in the ground state. The cross section for this reaction may be large. In helium, for example, it is of the order of 10^{-15} cm^2. The number of electrons produced ahead of an avalanche via this process is sufficient to create and maintain a streamer. However, the occurrence of this (or any other process) has not been confirmed experimentally.

Fig. 16. a) Sketch of Axial Electric Field in Avalanche Region. b) Retarding Force versus electrons energy [Kunhardt and Byszewski (1980)]. c) Electron energy versus distance from avalanche also from Kunhardt and Byszewski (1980). Avalanche Radius, R_e = 0.05 cm; External E Field, E_o = 42. kV/cm; Gas = Nitrogen; Pressure = 750 Torr; Minimum injection energy, U_i = 112.6 eV; E_m = 175.1 kV/cm.

Recently, Kunhardt and Byszewski (1980) introduced a model for highly overvolted breakdown. In this model, the energy distribution function for electrons in the advancing avalanche is assumed to have two components: fast electrons and slow (thermal) electrons. The fast electrons can "run away" from the avalanche. This happens because the effective retarding force on an electron moving through a neutral gas decreases with increasing velocity in the case of electrons possessing sufficiently high energy (i.e., $u \gtrsim 3\text{-}5_i$, where i is the ionization energy). The energy threshold for these runaway electrons is determined by the electric field strength and the pressure and properties of the gas (Fig. 16a). Once these fast electrons leave the avalanche, most of them no longer meet the runaway condition and become "trapped" because they enter a region of decreasing field ahead of the avalanche, and the energy they gain from the field along their trajectory is not enough to overcome the losses (Fig. 16b). The "trapping" distance of these electrons is a function of their initial energy (Fig. 16c). Thus, these "seed" electrons, which are continuously "emitted" from the avalanche, multiply at various distances from the parent avalanche rapidly extending the avalanche space charge towards the anode. On the cathode side, the photoelectric effect is assumed to be the primary mechanism for generating secondary electrons which are subsequently accelerated towards the high-field region of the parent avalanche.

The most important concept associated with an avalanche is that of the nature of the electron distribution function. To understand the development of avalanches (and for that matter, breakdown) when the space charge effects are important, we must make an effort to obtain the distribution under these conditions.

REFERENCES

Bayle, M., Bayle, P., and Crokaert, M., 1975, J. Phys. D, 8:2181.
Bychkov, Y. K., Korolev, Y. D., and Gavrilyuk, P. A., 1973, Sov. Phys. Tech. Phys., 17:1337.
Davies, A. J. Davies, C. S., and Evans, C. J., 1971, Proc. Inst. Elec. Eng., 124:179.
Dickey, F. R., Jr., 1952, J. Appl. Phys., 23:1336.
Fletcher, R. C., 1949, Phys. Rev., 76:1501.
Felsenthal, P. and Proud, J. M., 1965, Phys. Rev. A, 139:1796.
Kline, L. E., 1974, J. Appl. Phys., 45:2046
Kunhardt, E. E. and Byszewski, W. W., 1980, Phys. Rev. A., 21:2069.
Kunhardt, E. E., 1980, IEEE Trans. Plasma Science, PS-8:130.
Kremnev, V. V. and Mesyats, G. A., 1971, Prk. Mek. i Tek. Fiz., 1:40.
Koppitz, J., 1971, Z. Naturforsch., 26a:700.
Koppitz, J., 1973, J. Phys. D, 6:1494.
Koppitz, J. and Stuhm, K., 1977, Appl. Phys., 12:23.
Korshunov, G. S., Rudenko, N. S., and Tsvetkov, V. I., 1970, Sov. Phys. Tech. Phys., 14:1074.
Levinson, S. and Kunhardt, E. E., 1981, in: "Digest of Technical Papers, 3rd International Pulsed Power Conference, Albuquerque, NM," T. Martin and A. Guenther, eds., p. 226.
Loeb, L. B., 1939, "Fundamental Processes of Electrical Discharges in Gases," Wiley, New York.
Lozanskii, E.D., 1976, Sov. Phys.-USP., 18:893.
Mesyats, G. A., Byrchkov, Y. I., and Iskol'kskii, A. I., 1969, Sov. Phys. Tech. Phys., 13:1051.
Mesyats, G. A., Bychkov, Y. I., and Kremnev, V. V., 1972, Usp. Fiz. Nauk., 107:201.
Meed, J. M., 1940, Phys. Rev., 57:722.
Morgan, C. G. and Harcombe, D., 1953, Proc. Phys. Soc. B, 66:665.
Rogowski, W. 1928, Arch. Electrotech., 20:99.
Raether, H., 1964, "Electron Avalanches and Breakdown in Gases," Butterworth, London.
Stritzke, P., Sanders, I., and Raether, H., 1977, Sov. Phys. Tech. Phys., 10:2285.
Vorob'ev, V. V. and Iskol'dskii, A. M., 1967, Sov. Phys. Tech. Phys., 11:1560.
Wilson, R. R., 1936, Phys. Rev., 50:1082.
Yoshida, K., and Tagashira, H., 1976, J. Phys. D, 9:491.

PHYSICAL MODELS OF LONG AIR GAP BREAKDOWN PROCESSES

I. Gallimberti

Inst. di Elettronica
Via Gradenigo 6A
Universitá di Padova
Padova, Italy

INTRODUCTION

The equations for the conservation of mass, momentum and energy are the starting point for the formulation of physical models of the breakdown processes in long air gaps. Separate equations must be written for each of the charged, ground state neutral, and excited neutral species present in the developing discharge. The system of equations can be completed by adding field equations. Since the discharge processes are usually two (or three) dimensional, the resulting partial differential equations depend on time and two or three spatial coordinates. Needless to say, the resulting general set of equations becomes enormous and impossible to solve, even with state-of-the-art numerical techniques. To make progress, various simplifications have been made based on the experimental observations of long air gap breakdown which are described in the next two sections. Some of the models that have been developed are also described in the following sections along with representative model predictions. Some of these models are described in more detail in a previous review (Gallimberti, 1979) which also gives an extensive list of references to previous work and lists the sources of physical data which are required as input to the various models.

COLD DISCHARGE MODELS (CORONAS)

The first corona and the leader coronas are "cold" discharges, in the sense that the gas is not significantly heated as shown in the experimental results, particularly spectroscopic and strioscopic measurements. Thus it can be assumed that the neutral particles are in thermodynamic equilibrium at the ambient temperature and

that the pressure is constant in space and time. Thus the density, n, average velocity, $\bar{v}$, and temperature, T of the neutral particles may be assumed to be constant in space and time. Subsequently, subscripted variables, n_j, v_j, and T_j, will be used to denote those variables associated with species j (e ≡ electrons, + ≡ positive ions, - ≡ negative ions, n ≡ neutrals). In particular cases, it may also be of interest to calculate the population of the excited states even if their density is much lower than the total gas density. In this case, $\bar{v}_n = 0$ may still be assumed but the source term $\dot{n}_n \neq 0$. The variation of the local density can then be calculated with the mass conservation equation $dn_n/dt = \dot{n}_n$. The charged particles move under the action of the electric field. The experimental data show that the streamer formation times are too short for an appreciable drift of the ions, but long enough for the establishment of "swarm" conditions for the electrons. The equations of momentum and energy conservation become for ions:

$$\bar{v}_i = 0 \qquad (1)$$

$$T_i = T_n$$

and for electrons:

$$\bar{v}_e = \mu_e \bar{E} - \frac{1}{n_e} \nabla\cdot(n_e D_e) \qquad (2)$$

$$T_e = F_e(E/N_n)$$

where μ_e is the electron mobility and D_e is the electron diffusion coefficient. In this case we can use a model consisting of continuity equations for electrons, negative ions, and positive ions together with Poisson's equation:

$$\frac{\partial n_e}{\partial t} + \nabla\cdot(n_e \mu_e \bar{E}) - D_e \nabla^2 n_e = (\alpha - \eta) n_e \mu_e \bar{E} + n_e^*$$

$$\frac{\partial n_-}{\partial t} = \eta n_e \mu_e \bar{E} \qquad (3)$$

$$\frac{\partial n_t}{\partial t} = \alpha n_e \mu_e \bar{E} + n_e^*$$

$$\nabla\cdot\bar{E} = \frac{(n_e + n_- - n_+)e}{\varepsilon_o}$$

where n_e^* represents the photoionization generation term which is included based on experimental evidence. The other source terms are represented by the ionization coefficient, α, and the attachment coefficient, η.

The solution of Eq. (3) is hindered because of two factors: the complexity and nonlinearity of n_e^*, and the distortion of the geometrical field (nonuniform but constant in time) due to the highly concentrated space charge that develops.

The experimental results support the original "streamer theory" proposed by Loeb and Meek (1947) and Raether (1964). The streamer tip (active region) is assumed to be the front of a "space charge wave", where positive ions and excited molecules are highly concentrated. A schematic representation of the streamer is shown in Fig. 1a. Photoionization produces secondary electrons ahead of the streamer which, in turn, produce secondary avalanches. These avalanches feed into the streamer tip. The total field at the streamer tip is equal to the sum of the applied field and the space charge field. If this field is high enough, the avalanche electrons neutralize the space charge and advance the space charge further into the gap.

In air at atmospheric pressure, the active region is limited by a boundary of 26 kV/cm ($\alpha = \eta$). In low applied field, the streamer may still advance because of its own field (Dawson-Winn: 10^8 ions within a sphere of 30 μm radius are self-propagating). Gallimberti (1979) has shown that it is possible to bypass the problems of solution of the system (3) with a single equivalent avalanche model as shown schematically in Fig. 1b. The field in the active region is calculated as

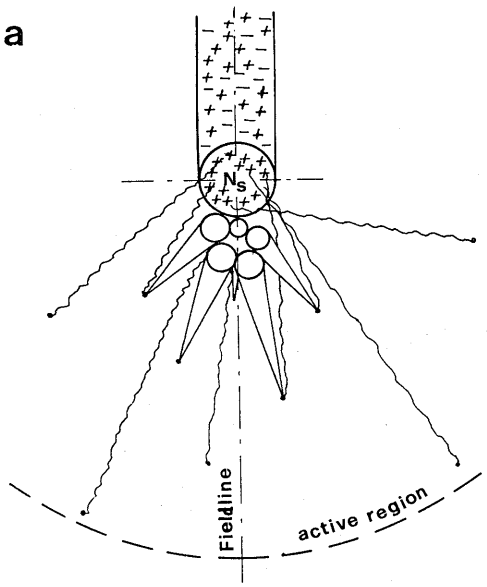

Fig. 1a. Schematic representation of the streamer active region.

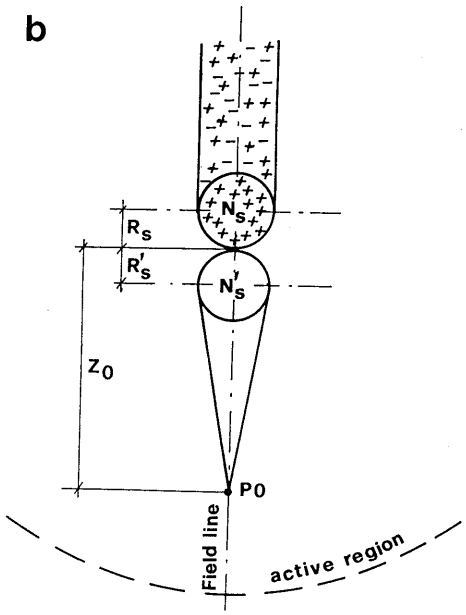

Fig. 1b. The equivalent avalanche.

$$\bar{E} = E_g + \frac{N_s e}{4\pi\varepsilon_o (Z_o + R_s)^2} \tag{4}$$

where E_g is the applied field, N_s is the number of charges in the avalanche head of radius R_s, and the starting point Z_o of the equivalent avalanche is calculated with an energy balance condition. In the series of avalanches developing in the active region, the energy gained from the applied field, W_g, by the drifting electrons is accounted for by: 1) W_e, which is the energy lost in collisions with the gas molecules (ionization, attachment, scattering, etc.) and the electron thermal energy: and 2) ΔW_p, which is stored as potential energy in the streamer tip. The energy balance equation

$$W_e = W_g + \Delta W_{pot} \tag{5}$$

must be satisfied, and is used to define the starting point of the equivalent avalanche. W_e includes losses due to ionization, attachment, vibrational and electronic excitation, dissociation, elastic scattering and variations of kinetic energy along the avalanche path; W_{pot} includes the potential energy because of the concentration of charges and their position in the applied field. The avalanche development is calculated with the three continuity equations (3), where $n_e^* = 0$. The propagation is built up by a series of subsequent steps: in high E_g, the charge in the streamer tip increases

(because the energy gains exceed the losses); the opposite occurs in low E_g. The propagation occurs at expense of W_{pot} (see Fig. 2). The propagation stops when N_s becomes too low to sustain the space charge, Eq. (4), and hence the tip advancement.

Examples of the comparison between experimental and calculated results are given in Figs. 3 and 4. This model applies quite well to the first corona, where the applied field E_g is well defined and easily computed. In the case of the leader corona the space charge in the gap makes the calculation much more complex.

HOT DISCHARGE (LEADER CHANNEL)

In the leader channel the charged particle flux heats the gas giving rise to complex thermodynamic and hydrodynamic phenonema. The leader channel is a "hot" discharge in this sense, in contrast with the corona streamers. This "hot" discharge picture of the leader channel is supported by the spectroscopic and strioscopic evidence described in (Gallimberti, 1979) and (Les Renardières Group, 1981).

As a first simplification in developing a leader model, we can assume cylindrical symmetry and neglect axial variations in the leader properties. The axial uniformity assumption is justified by the fact that the leader diameter is such smaller than the leader length. Therefore the longitudinal derivatives are always negligible compared with the radial derivatives. With these assumptions all particles but electrons have radially directed average velocities. The nonzero axial component of the electron average velocity is the

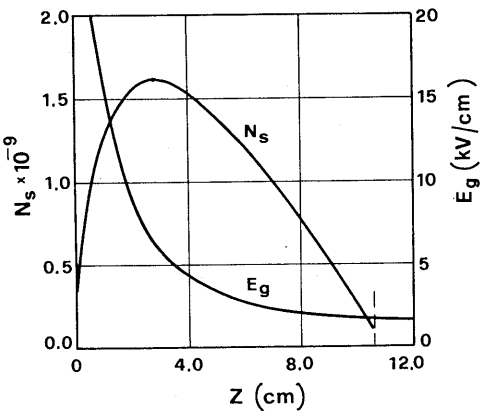

Fig. 2. The variation of the number of positive ions in the tip N_s and applied field distribution E_g along the streamer path (same conditions as Fig. 3).

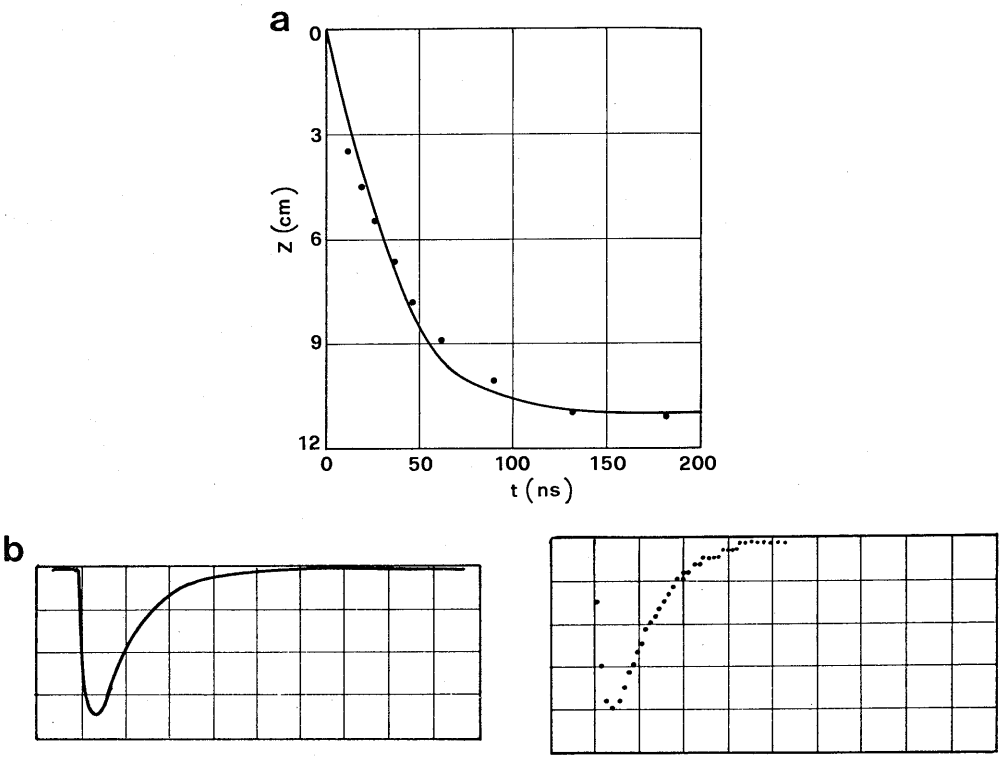

Fig. 3. (a) The variation of the streamer length with time. The solid line represents the computed values; the points are experimental results; (b) Experimental and computed current oscillograms.

source of the input power to the leader channel.

Three types of models have been proposed to study leader channels and similar situations. These three models differ primarily in the number of energy reservoirs that they include. They are described below in order of increasing complexity.

Local Thermodynamic Equilibrium Models

In this model the particles are considered as an assembly where the population repartition is given by the Boltzmann law; $T_j = T$ and $v_j = V$ are the same for all the particles and N is the total population density. The conservation equations for the assembly are obtained by adding the single equations over all types of particles which constitute the assembly.

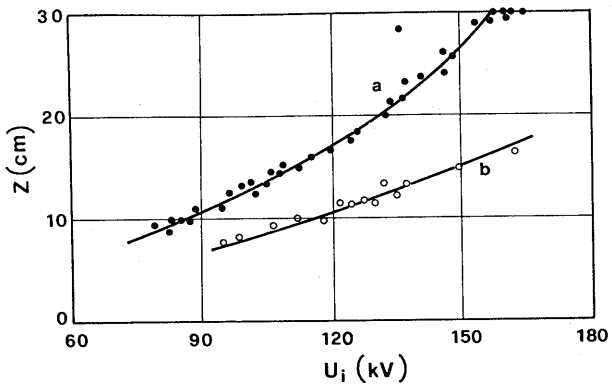

Fig. 4. The streamer length as a function of the inception voltage for gap lengths of 30 cm (curve a) and 150 cm (curve b); the solid lines represent computed values; the points are experimental results (Square-cut rod of 1 cm radius).

$$\frac{\partial N}{\partial t} + \frac{1}{r}\frac{\partial}{\partial r}(r\,NV) = 0$$

$$\frac{\partial}{\partial t}(NV) + \frac{1}{r}\frac{\partial}{\partial r}(rNV^2) + \frac{1}{m}\frac{\partial P}{\partial r} = 0 \qquad (6)$$

$$\frac{\partial}{\partial t}\left[N\left(\frac{3}{2}kT + \varepsilon\right)\right] + \frac{1}{r}\frac{\partial}{\partial r}\left[rNV\left(\frac{3}{2}kT + \varepsilon\right)\right]$$

$$+ \frac{P}{r}\frac{\partial}{\partial r}(rV) - \frac{\lambda}{r}\frac{\partial}{\partial r}\left(r\frac{\partial T}{\partial r}\right) = j_e E_z$$

where T is the thermal conductivity, and p and ε are "state functions" which depend only on temperature and density. For example,

$$p = kNT;\quad \varepsilon = \frac{1}{m}\frac{kT}{\gamma - 1}\ . \qquad (7)$$

The density of free electrons is calculated according to the Saha equation (particular case of the Boltzmann equation for the ionized levels):

$$\frac{n_e^2}{N} = 2\frac{g_+}{g}\left(\frac{2\pi m_e kT}{h^2}\right)\exp\left(\frac{\varepsilon_e}{kT}\right) \qquad (8)$$

where g_+ and g are the multiplicity of the ion and molecule ground states and ε_e the ionization energy (for gas mixtures average values can be used).

The electron velocity components are:

$$v_{et} = V \; ; \; v_{ez} = \mu_e E_z \; .$$

This type of model has been used by Rogoff (1972) for the simulation of the glow-at-arc transition and by Brambilla (1978) for high current leaders; it gives satisfactory agreement with experimental observation only for high currents, temperatures, and electron densities. Therefore, it can be applied to the last stages of the final jump and to the arc formation in the experimental results of Gallimberti, Hartmann, and Marode (1977) which show that thermalization of the leader occurs only when the final jump is almost completed.

The Temperature Models

In the two temperature models the neutral particles are still considered as an assembly, where the population repartition is given by the Boltzmann law at the gas temperature, $T_n = T$; but the electrons are not assumed to be in equilibrium. The electric field E_z gives the electrons a higher temperature T_e. If the electron density $n_e << N$, the behavior of the gas particles can be still represented by the Eqs. (6) and (7).

The electron density must be calculated with the continuity equation. The generation term $\dot{n}_e$ includes ionization and recombination only because the calculated thermal detachment rate exceeds the attachment rate for temperatures between 1000 and 2000°K as shown in Fig. 5. Thus the effect of attachment is cancelled. Photoionization is negligible. The continuity equation becomes, therefore:

$$\frac{\partial n_e}{\partial t} + \frac{1}{r} \frac{\partial}{\partial r} (r \, n_e \, v_{ez}) = \alpha \, n_e \, \mu_e \, E_z - a_e \, \mu_e^2 \qquad (9)$$

where a_e is the electron-ion recombination coefficient.

The electron velocity component in the axial direction is $v_{ez} = \mu_e E_z$.

The electron radial component derives from the combination of the neutral transport V, plus the ambipolar diffusion. The latter can be derived by eliminating the field from the equations for electrons and positive ions under the conditions of ambipolar diffusion ($n_e = N_+$; $v_{er} = v_{+r}$)

$$v_{er} = V - \frac{1}{M_e} D_+ \left(1 + \frac{T_e}{T}\right) \frac{\partial n_e}{\partial r} \; . \qquad (10)$$

The model can be applied only on relatively long time scales because it assumes implicitly that all the energy which is trans-

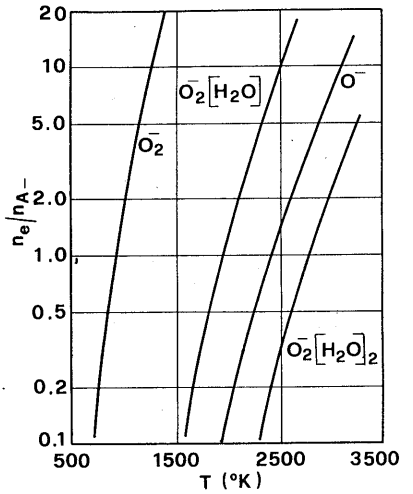

Fig. 5. Thermal detachment degree of negative ions in air at atmospheric pressure as a function of the temperature (the ion temperature and the gas temperature are assumed in equilibrium).

ferred from the electrons to the neutral molecules in all kinds of elastic and inelastic collisions is relaxed in the form of thermal energy on a time scale which is short compared with the time scale of interest. This assumption is not valid for the leader channel because: (1) most of the input energy goes to vibrational excitation in the relevant E/N range of 10^{-16} to 10^{-15} Vcm^2, as shown in Fig. 6, and (2) the vibrational relaxation times are strongly temperature dependent and comparable to the leader development time as shown in Fig. 7. The two-temperature model can be applied to the special case of the relatively slow variation of a well developed, hot leader channel because the vibrational relaxation time decreases to a few μs for $T \simeq 4000°K$ (see Fig. 7). The two-temperature model can also be applied to model μs time scale variations in the earlier stages of leader development by assuming that the input energy that goes into vibrational excitation does not contribute to gas heating.

The model can, therefore, represent the evolution of the leader channel, when short current pulses flow along it; and the radial profiles of pressure, density, and temperature can be calculated as functions of time. Figure 8 shows the development of a sonic pressure wave, generated around the leader channel by a current pulse of about 8A. The expansion velocity is in good agreement with the strioscopic measurements as shown in Fig. 9.

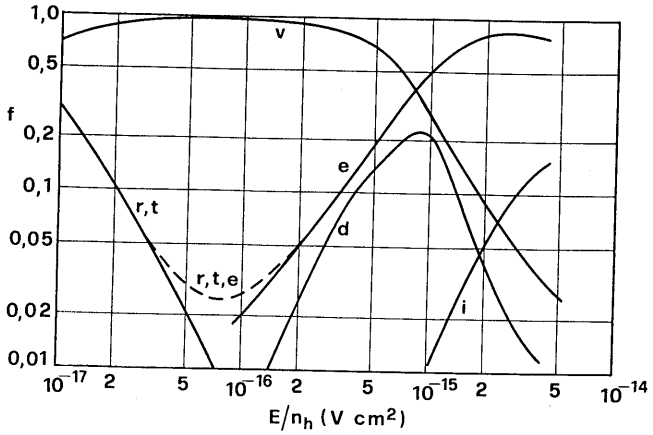

Fig. 6. The repartition of the electron energy transferred to neutral molecules in the different forms of internal energy against the reduced field (t-translation, r-rotation, v-vibration, e-electronic excitation, d-dissociation, i-ionization).

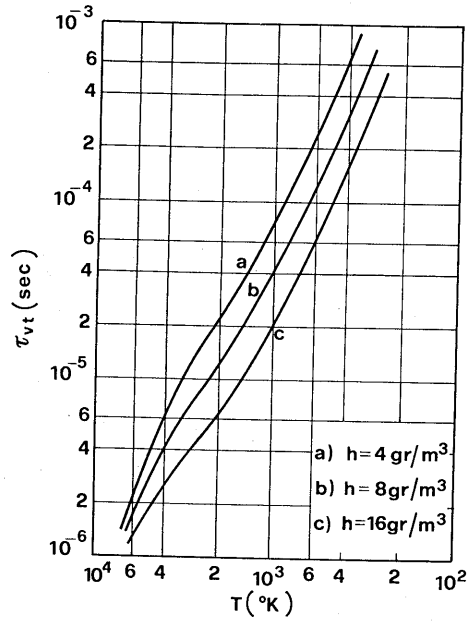

Fig. 7. Equivalent time constant for vibrational relaxation in air at atmospheric pressure as a function of the temperature for different values of absolute humidity.

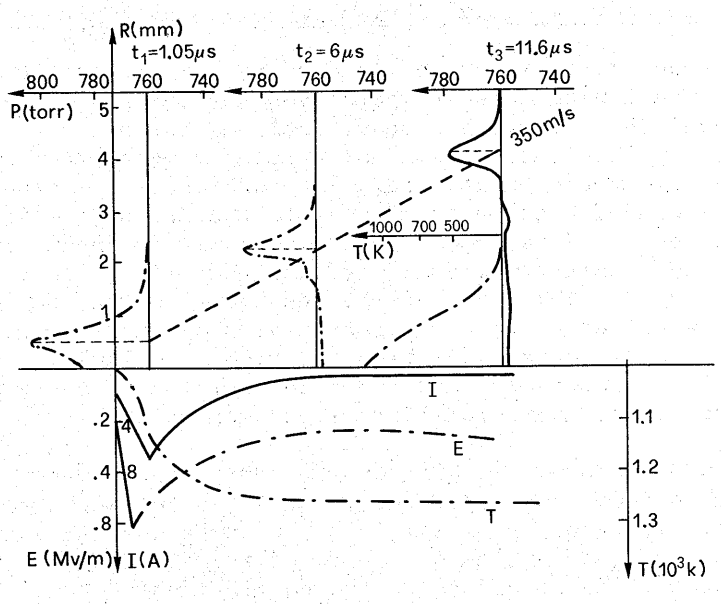

Fig. 8. a) Calculated diagram showing the field E and neutral temperature T variations with the current impulse I(t). b) Calculated diagram showing, at different instants t, the radial profile of the pressure P and the speed of the pressure wave. The temperature profile at t = 11.6 μs is also given.

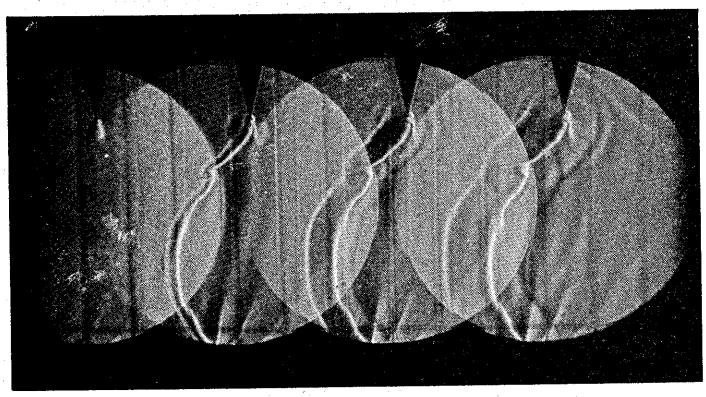

Fig. 9. Typical striogram showing the leader-channel expansion (negative polarity).

Nonlocal, Thermodynamic Equilibrium (Three-Temperature) Models

A more accurate picture of leader development can be obtained by using a model with three temperatures (or energy reservoirs). In this model the thermal reservoir includes the direct energy input from elastic collisions as well as the energy which goes into rotational and electronic excitation. The rotational and electronic energy is included because it relaxes to thermal energy in a time < 1 μs. A second vibrational energy reservoir is included because the vibrational-to-thermal-energy relaxation time is long, as previously discussed. The third energy reservoir is the chemical energy one which is filled by electron impact dissociation and relaxes through recombination-dissociation reactions. Calculated time constants for O_2 dissociation are shown in Fig. 10. The energy flows in the three-temperature model are shown schematically in Fig. 11.

A complete system of equations for this three-temperature model includes mass, momentum, and energy equations for each type of particle, i.e. electrons, positive ions, and neutrals in radial coordinates. Because this system of equations is very complex, the model has been simplified according to the conclusions of Braginskii (1958). The leader channel is assumed by a thin dense shell; P_j, n_j, T_j are assumed constant over the cross section with variations concentrated in the shell. In the core the radial derivatives disappear, and the mass conservation equations can be integrated from the center to the radius a giving:

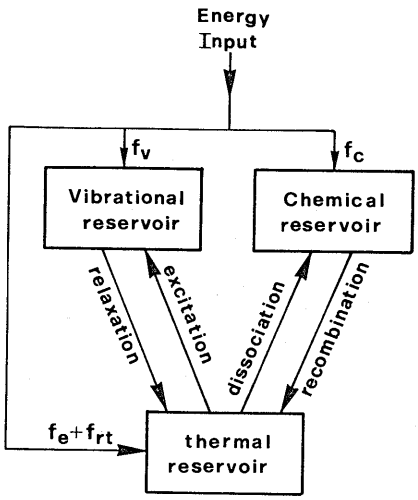

Fig. 10. The equivalent time constant for oxygen dissociation in atmospheric air as a function of the gas temperature and the dissociation degree.

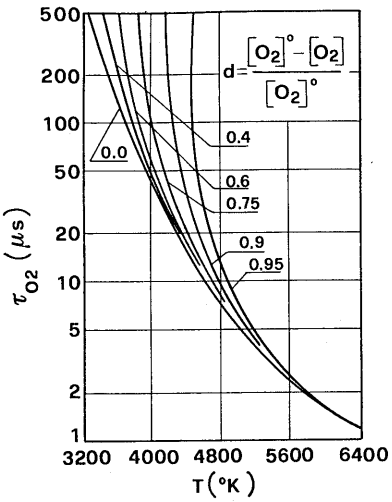

Fig. 11. Schematic flow-chart of the energy exchanges between the different forms of internal energy, under the conditions appropriate for the leader channel.

$$\frac{dN_e}{dt} = \frac{dN_+}{dt} = \dot{N}_e$$

$$\frac{dN_n}{dt} = -\dot{N}_e + \dot{N}_d \quad . \tag{11}$$

The N_j represents the total number of particles of j type within the radius a, per unit leader length; $\dot{N}_d$ represents the corresponding rate of dissociation with the assumption that each dissociated molecule produces two fragments.

The three momentum equations can be added together so that the collision term vanishes. If it is assumed that the average expansion velocity $\langle\dot{Q}\rangle$ is the same for all the particles, the resultant equation becomes

$$\frac{d}{dt}\left[(N_e m_e + N_+ m_+ + N_n M_m \langle Q\rangle\right] = 2\pi a \left[\langle p_c\rangle - \langle p_s\rangle\right] \tag{12}$$

where $\langle p_c\rangle$ and $\langle p_s\rangle$ are the average pressures in the core and the shell.

The three conservation equations for the three energy reservoirs become

$$\frac{d}{dt}[NC_v^* T] + P\frac{d}{dt}(\Pi a^2) = (f_{rt}+f_e)J_e E_z + \frac{W_v(T_v) - W_v(T)}{\tau_{vt}} - \frac{N_{o_2} D_T^\circ}{\tau_{o_2}}, \tag{13a}$$

$$\frac{d}{dt}[W_v(T_v)] = f_r J_e E_z - \frac{W_v(T_v) - W_v(T)}{\tau_{vt}}, \quad \text{and} \tag{13b}$$

$$\frac{d}{dt}[N_{oz} D_T^\circ] = f_r J_e E_z - \frac{N_{oz} D_T^\circ}{\tau_{oz}} \tag{13c}$$

where C_v^* is the partial specific heat at constant volume including only the translational, rotational, and electronic components of internal energy; $W_v(T_v)$ is the total vibrational energy of a unit-length channel section at temperature T_v; and D_T° is the dissociation heat at temperature T.

The equation system has to be completed with the state equation

$$\Pi a^2 \langle p_c \rangle = N_e kT_e + N_+ kT_+ + N_n kT, \tag{14}$$

and the classical Rankine-Hugomet formulae for the shock wave out of the shell by the core "piston":

$$\langle p_s \rangle = [1 + \frac{2\gamma}{+1}(M^2 - 1)]p_o$$

$$M = \frac{\gamma + 1}{4}\frac{\langle \dot{a} \rangle}{C_o}\left[1 + \sqrt{\left(\frac{4}{\gamma+1}\frac{C_o}{\langle \dot{a} \rangle}\right)^2 + 1}\right] \tag{15}$$

where C_o and p_o are the sound speed and the pressure in the undisturbed gas and M is the Mach-number.

The ionization rate is calculated by integrating in the core Eq. (9)

$$\frac{\partial N_e}{\partial t} = \alpha \mu_e N_e E_z - N_e \frac{N_+}{\pi_a 2} Q_e \tag{16}$$

while current, field, and electron density are related by a simple resistive-conduction relation

$$E_z = \frac{I}{e\,\mu_e N_e}. \tag{17}$$

Results obtained using the model described by Eqs. (12) to (17) are shown in Figs. 12 to 18. The first three figures show the leader-channel development for a constant current of 0.6A. The time t = 0 corresponds to the time at which the leader section is

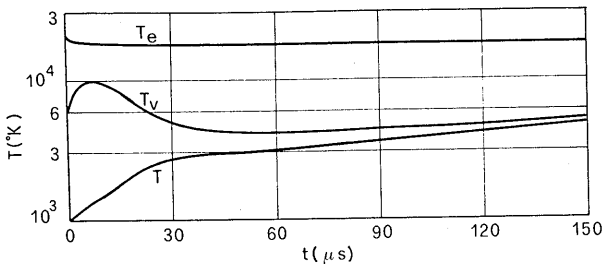

Fig. 12. The temperatures T, T_v, and T_e in the leader channel as functions of time.

formed. Two successive phases can be seen in the evolution of the channel conditions. In the first one, the gas temperature and the leader radius increase rapidly, while the gas number density, the electron concentration, and the electric field decrease at about the same rate. The vibrational temperature increases up to a point where the relaxation time constant τ_v becomes short enough for the output rate from the vibrational reservoir to exceed the input rate. Then T_v decreases as the vibrational energy is relaxed in the thermal reservoir. In this phase the rate of thermal energy input is high because of both the relatively high electric field and the large contribution of the vibrational relaxation. In the second phase, the rate of variation becomes much slower because of the decrease of the power input to the thermal reservoir. The expansion velocity is correspondingly high in the first phase and decreases in the second. It is always much smaller than the sound speed, confirming the assumption of an acoustic expansion in pressure equilibrium. E/N remains approximately constant throughout the channel development because E and N decrease at about the same rate.

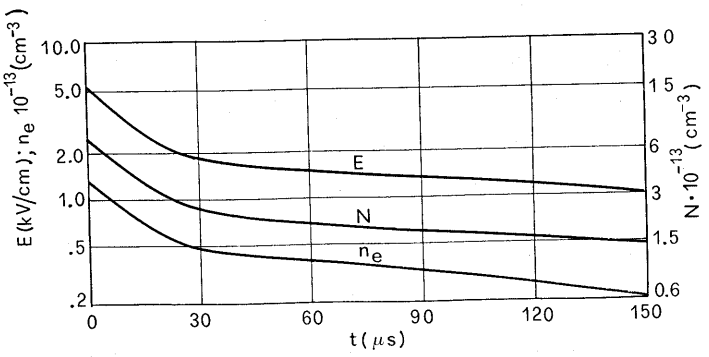

Fig. 13. The electron and gas densities (n_e and N) and the electric field E in the leader channel as functions of time.

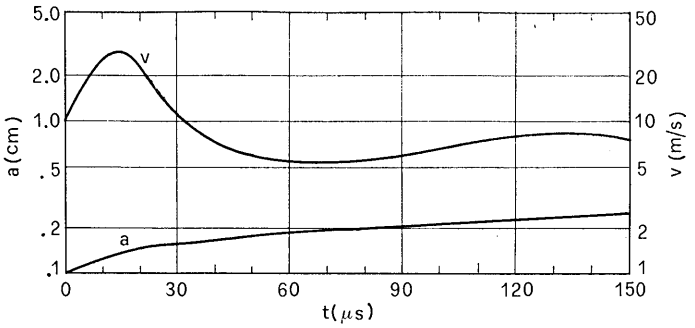

Fig. 14. The radius a and the velocity of expansion v of the leader channel as functions of time.

Figure 15 to 18 show the calculated leader development when the experimentally measured current shown in Fig. 15 is assumed. E/N again remains approximately constant in this case, and all of the calculated variables except the electron density are rather insensitive to the sharp peaks in the driving current.

These results indicate that the leader has "almost stable" internal conditions. Gallimberti (1979) has shown from Eqs. (11), (16) and (17) that the reduced field E/N, the electron temperature T_e, the channel conductivity σ, and ionization degree i are only functions of the leader current as shown in Fig. 19. E/N and T_e

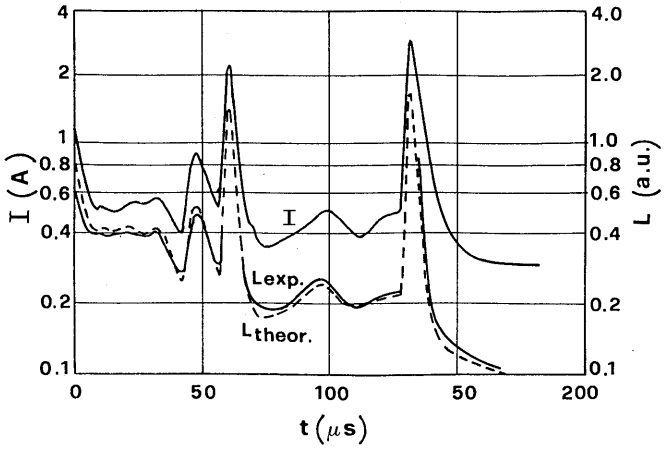

Fig. 15. Experimental current oscillogram I (10 m. cone-plane gap, 500/10,000 μs wave), and experimental and computed light emission from a section of leader channel.

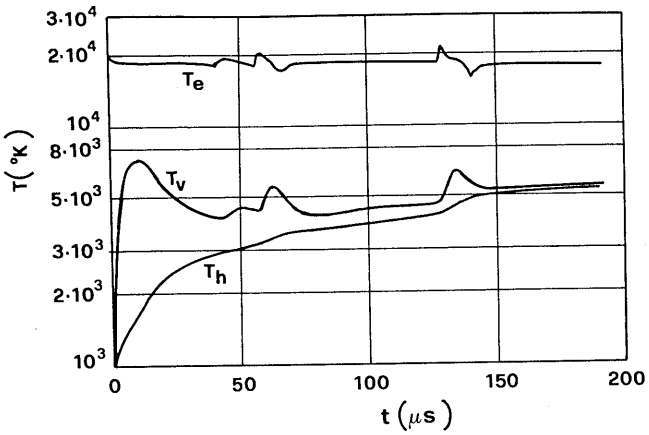

Fig. 16. The computed variations of gas temperature T_h, vibrational temperature T_v, and electron temperature T_e, for the experimental current input of Fig. 15.

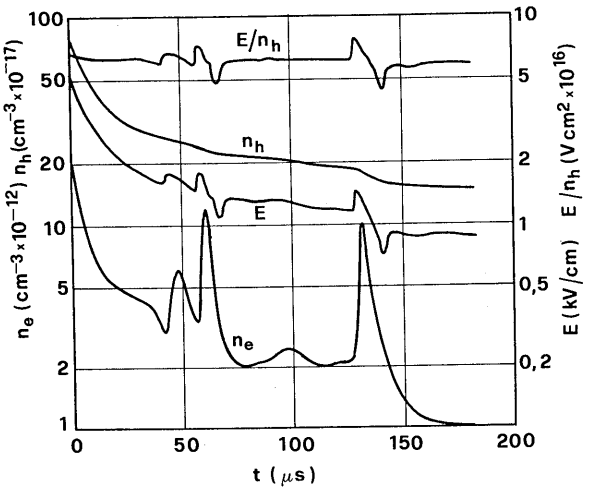

Fig. 17. The computed variations of the gas and electron densities (n_e and n_h respectively), for the experimental current of Fig. 15.

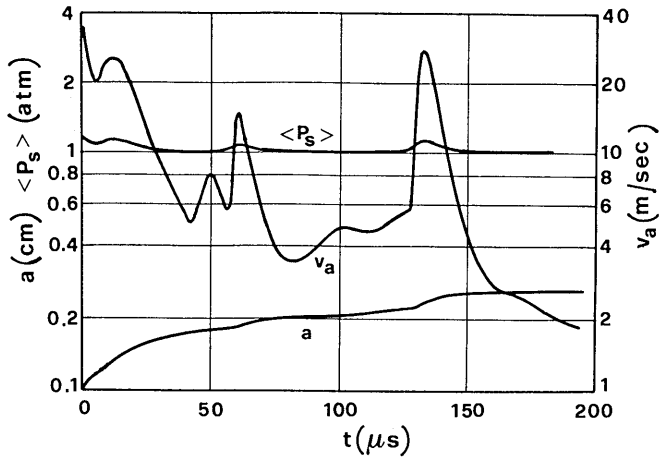

Fig. 18. The computed variations of the channel radius a, of the shell overpressure $\langle p_s \rangle$, and of the expansion velocity v_a, for the experimental current input of Fig. 15.

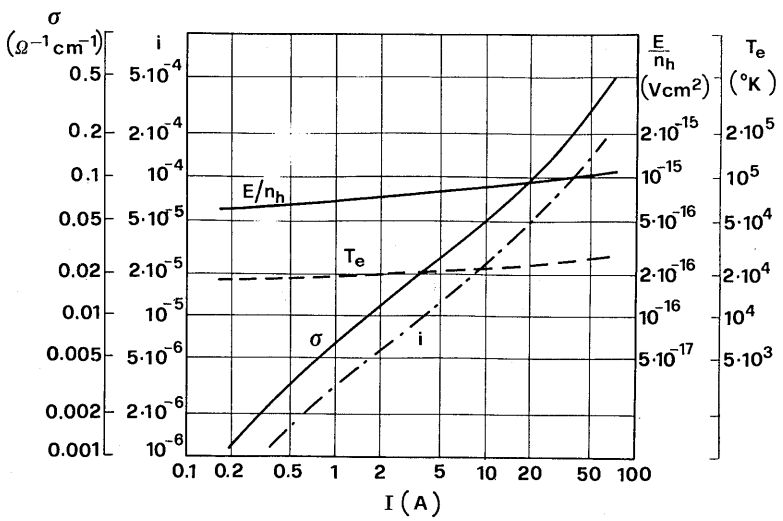

Fig. 19. Quasi-equilibrium characteristics of the leader channel as functions of the input current ($N_h = 2.5 \times 10^{17}$ cm^{-1}).

remain almost constant over a large range of current values. Under rapid transient conditions, these parameters can change slightly with respect to the "quasi-stationary" values, but the equilibrium is rapidly reestablished by the strong feedback reaction because of the short time constant in the equilibrium between ionization and recombination. This feedback loop is shown schematically in Fig. 20.

LEADER PROPAGATION

The leader head advances in the preionized region created in front of it by the leader corona. The region around the leader head is a transition region where a change from the corona to the leader conditions occurs. The corona region adjacent to the advancing leader is a "passive region" with characteristics very similar to the characteristics of a glow discharge. Gallimberti et al. (1977) have shown that this region is almost neutral, with a low electron concentration and high positive and negative ion concentrations. The resulting conductivity is relatively low. This passive region of the corona streamers is quite different from the active streamer region discussed above. The positive corona and positive leader are compared in Table I.

Several models have been proposed to explain the corona-to-leader transition and the resulting propagation of the leader. Alexandrov (1966) has proposed a model where the energy input in the transition region increases the temperature to a sufficiently high value that LTE is reached and thermal ionization occurs. This is consistent with the change in conductivity between corona glow and leader channel. However, many experimental results on leader conditions contradict this hypothesis, and there is doubt that LTE can be established within the time available and with a relatively low electron density.

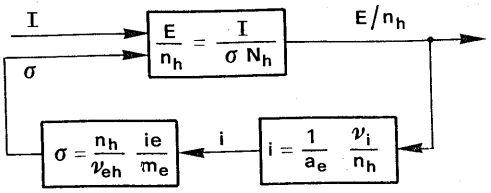

Fig. 20. Block diagram of the relations between leader current, reduced field and conductivity.

Table 1. Positive corona and positive leader properties and physical phenomena.

POSITIVE CORONA	POSITIVE LEADER
Electrodynamic nonequilibrium: ionization, attachment, photoionization.	Electrodynamic quasi-equilibrium; ionization balanced by recombination.
Space-charge effects important	Space-charge effects negligible; normal conduction.
Thermo-hydrodynamic phenomena negligible	Thermo-hydrodynamic phenomena important; three energy reservoirs.
Low conductivity	High conductivity
Self-sustained propagation	Slow axial variation - rapid radial variation.

A second model proposed by Kekez and Savic (1974) represents the leader advancement as the propagation of a hypersonic shock wave. They consider a parbolic leader profile near the tip of very small radius. A very rapid thermalization of free electrons from the leader corona raises the temperature in the small volume tip to extremely high values, of the order of 10^6°K. The very strong shockwave velocity (punctual explosion) then constitutes the leader-advancement velocity. However, the high temperature necessary to produce the punctual explosion, and the relatively high density of free electrons in the leader corona glow seem to be in contrast with the experimental results.

In a third model, suggested by the author, the leader tip represents a boundary at which the negative ions present in the corona glow became subject to thermal detachment. A gas temperature in the range 1000-2000°K is required for this process. The large difference of mobility between electrons and ions determines the transition in conductivity between corona glow and leader channel.

The large difference in conductivity makes the leader surface almost an equipotential surface. If it is assumed to be a slender paraboloid, the field and equipotential lines can be traced together with the lines of constant energy input. Calculated results are shown in Fig. 21.

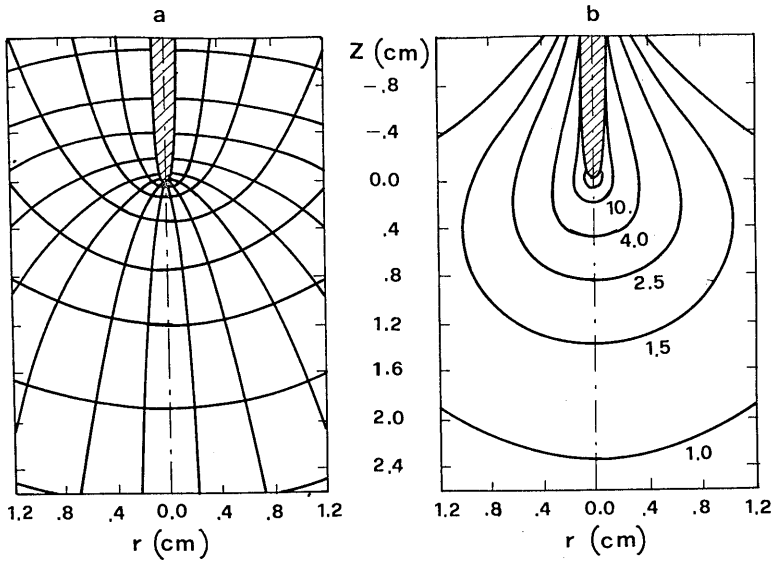

Fig. 21. Schematic representation of the leader head transition region: a) field and current lines; b) lines of constant power input.

The maximum of power input is concentrated in a small region around the tip. If the temperature in this region is increased above the critical value of thermal attachment, a new leader section is built up in a more advanced position.

We will assume a reference frame having a constant velocity, $\bar{v}_L$, along the leader axis, with respect to the laboratory frame and assume that there exists a steady state solution, which represents the stable propagation of the transition region in the form of nondamped wave. In the earlier discussion, we saw that the system of equations for neutral particles (divided into subsets, thermalized and vibrationally excited particles), can be written in the form of Eq. 18, where $\bar{J}_e$ and $\bar{E}$ are calculated for the parabolidical current field of Fig. 21.

If the temperature equations are integrated along the axis of the transition region, from a point of T = 300°K to the leader tip, it is possible to calculate the temperature increase along the transition region ΔT_L.

$$\nabla\cdot[N_n(\bar{V} - \bar{v}_L)] = 0$$

$$\nabla\cdot[N_n M(\bar{V} - \bar{v}_L)\ (\bar{V} - \bar{v}_L)] + \nabla p = 0$$

$$\nabla\cdot[N_n c_p^* T(\bar{V} - \bar{v}_L)] = (f_{rt} + f_e)\bar{J}_e\bar{E} + \frac{w_v(T_v) - w_v(T)}{\tau_{vt}} \qquad (18)$$

$$\nabla\cdot[W_v(T_v)(\bar{V} - \bar{v}_L)] = f_v\bar{J}_e\bar{E} - \frac{w_v(T_v) - w_v(T)}{\tau_{vt}}$$

$$P = N_n kT$$

If it is assumed that ΔT_L is high enough to produce thermal detachment of negative ions (e.g., $\Delta T_L = 1500°K$), the steady state propagation velocity can be calculated giving:

$$v_L = \left[f_{rt} + f_e + f_v \frac{\langle\tau_L/\tau_{vt}\rangle}{1 + \tau_L/\tau_{vt}} \frac{2}{7kN_n\Delta T_L}\right] \int_{z_o}^{\rho/2} J_e E_z dz. \qquad (19)$$

where the interval is extended over the transition region and ρ is the tip curvature radius, and $\langle\tau_L/\tau_{vt}\rangle$ is the average value of the ratio between the leader transit-time across the transition region and the vibrational relaxation time. The term in square brackets represents the fraction of the total energy which is relaxed in the transition region during the transit time.

v_L represents the frame velocity which is consistent with the self-similarity of the "leader-wave" during its propagation.

For the parabolodical current field of Fig. 21, the energy input is:

$$\int_{z_o}^{\rho/2} J_e E_z dz = \frac{-U_{Lt}\ I_L}{\ell n[\sqrt{\rho/2H}]} \frac{2}{\Pi^2\eta_o^2}\left[\frac{1}{\rho^2} - \frac{1}{4z_o^2}\right] \qquad (20)$$

where U_{Lt} is the leader tip potential, I_L the current, η_o the parabolic coordinate corresponding to the radial extension of the corona glow, and H the distance of the leader tip from the plane electrode.

Equations (19) and (20) combined show that the leader velocity is proportional to the total current

$$v_L = \frac{1}{q} I_L. \qquad (21)$$

The proportionality factor q is expressed by

$$q = -\left[f_{rt} + F_e + f_v \frac{\langle \tau_L/\tau_{vt} \rangle}{1 + \langle \tau_L/\tau_{vt} \rangle}\right]^{-1} \frac{7KN_n\Delta T_L}{4U_{Lt}} \Pi^2 \eta_o^2 \rho^2 \cdot \ell n[\sqrt{S/2H}] \; ; \qquad (22)$$

q represents the average charge necessary for the unit length advancement of the leader channel.

This model predicts many of the experimentally observed features of leader propagation including:

- Advancement velocity is proportional to current I_L.
- Charge per unit length is constant for given atmospheric condition and voltage shape.
- q decreases with humidity because τ_{vt} decreases.
- q depends on the waveshape because U_{Lt} depends on waveshape (see Fig. 22).
- The leader advancement depends on the ionization activity in the leader corona front which injects the current I_L in the transition region.

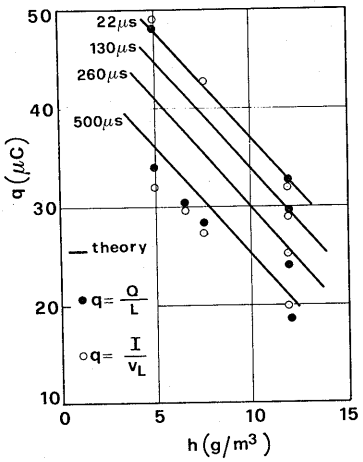

Fig. 22. Comparison between computed and experimental values of the q per unit leader length, for different wavefront durations and humidities.

- The instabilities in this ionization activity produce velocity fluctuations, sharp elongations (restrikes), and eventually the leader arrest.

The formation of the leader channel occurs at the root of the first corona, when the critical conditions for thermal detachment are reached and the stable propagation mechanism can start.

A single strong corona may be enough to create such conditions with large curvature electrodes. The leader is formed immediately after the corona pulse. Electrodes with a smaller radius of curvature give smaller corona currents, and the critical conditions may not be reached for some μs during which the vibrational energy is relaxed in the corona stem, enhancing its temperature. Corona photographs and current and electric field waveforms are shown in Fig. 23 for an electrode with a large radius of curvature and in Fig. 24 for an electrode with a small radius of curvature.

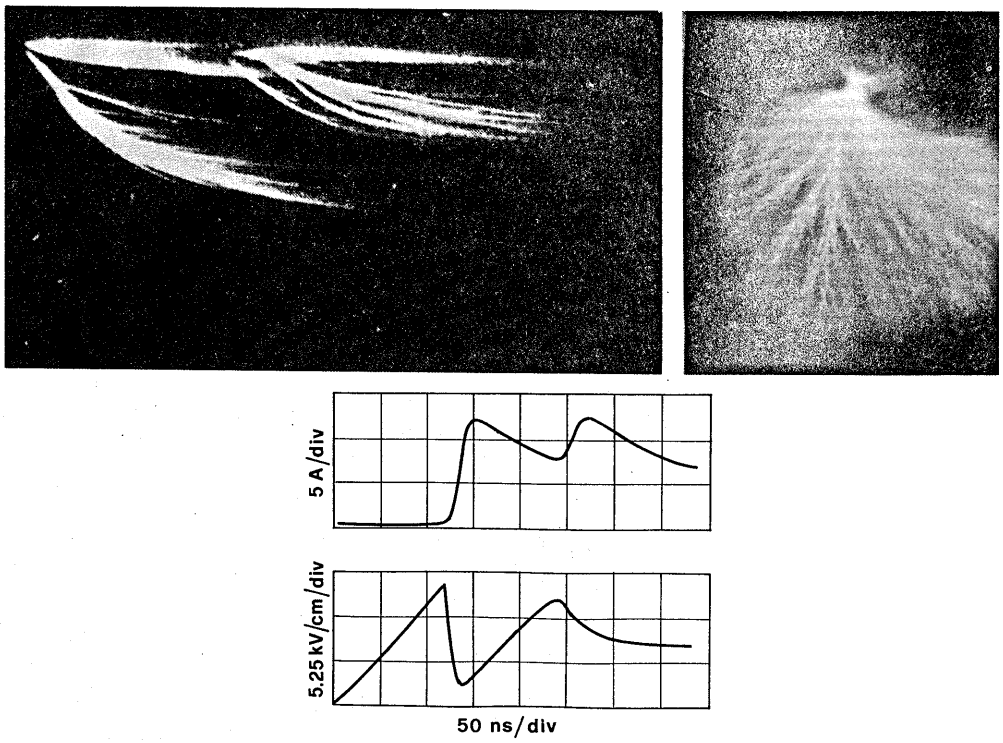

Fig. 23. The first and second corona pulses for large curvature radii: (a) and (b) streak and static photos; (c) current in the anode; (d) electric field on the anode surface.

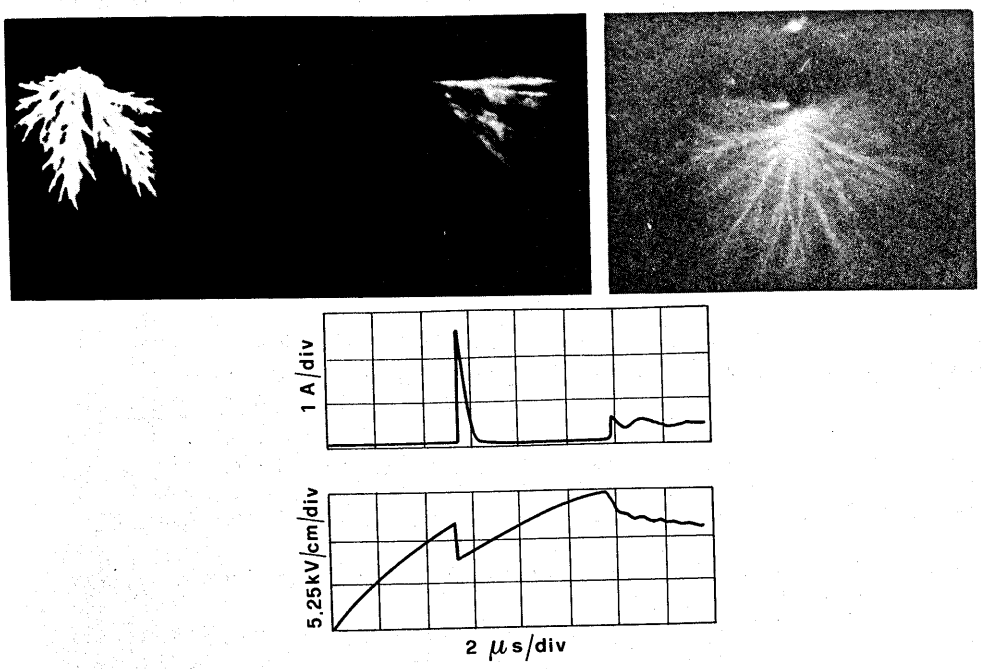

Fig. 24. The first and second corona pulses for small curvature radii: (a) and (b) streak and static photos; (c) current in the anode; (d) electric field on the anode surface.

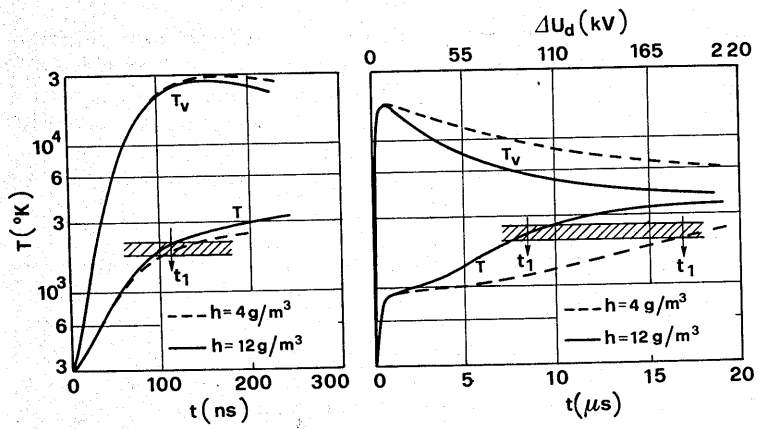

Fig. 25. The computed temperatures T_h and T_v in the stem, for the conditions of Fig. 23. The dashed area represents the critical temperature range: the second corona inception time T_1 is indicated.

The corresponding calculated vibrational and thermal reservoir temperature are shown for both cases in Fig. 25. With electrodes with very small curvature radii, many subsequent coronas may be necessary for leader inception.

REFERENCES

Aleksandrov, G. N., 1966, Sov. Phys. Tech. Phys., 10:949.
Brambilla, R. A., 1978, "Proceedings, 5th International Conference on Gas Discharges, Liverpool," IEE Conf. Publ. No. 165., p. 104.
Braginskii, S. I., 1958, Sov. Phys.-JETP, 34:1068.
Gallimberti, I., 1979, J. Phys. (Paris), 40:C7-C193.
Gallimberti, I., Hartmann, G., and Marode, E., 1977, Electra, 53:123.
Kekez, M. M. and Savic, P., 1974, J. Phys. D, 7:620.
Les Renardières Group, 1981, Electra, 74:176.
Loeb, L. B. and Meek, J. M., 1947, "Mechanism of the Electric Spark," Stanford Univ. Press, Stanford.
Raether, H., 1964, "Electron Avalanches and Breakdown in Gases," Butterworth, London.
Rogoff, G., 1972, Phys. Fluids, 15:1931.

ACKNOWLEDGEMENT

I would like to thank L.E. Kline, Westinghouse R&D Center, Pittsburgh, PA, for delivering this paper at Les Arcs and for preparing the manuscript.

SPARK-OVER CHARACTERISTICS OF LONG GAPS

G. Baldo
Instituto di Electrotecnica ed Elettronica
Via Gradenigo 6A
Universitá di Padova
Padova, Italy

INTRODUCTION

The continuing demand for electrical energy requires a continual increase in the power to be transmitted. Because overhead lines remain the best solution for power transmission, at least for the next few decades, it will be necessary to increase their transport capability by raising rated voltages rather than by indiscriminately increasing their number. Apart from economical considerations, this fact also derives from the need both for better use of territory and the reduction in the effect of overhead lines on the environment. This fact can be quantified in Fig. 1. In Fig. 1a the section of solid surrounding the line represents transmissible power at various voltages; the base width of the solid represents the right-of-way; Fig. 1b shows a comparison between width of the right-of-way necessary to transmit the same power at 420 kV and 1050 kV. It is clear that transmissible power, per unit of right-of-way, increases notably with voltage.

Higher voltage levels obviously need larger insulating distances. Because the dielectric strength of long-air insulations does not increase linearly with clearances, and insulation costs increasingly weigh on the total cost of a transmission system as the voltage is raised, insulation design must be improved by increasing the knowledge about the physical mechanism of breakdown of long gaps. This may also help in optimizing the number and procedure of full-scale tests, which require large, very expensive laboratories.

For this reason the study of breakdown processes in long gaps, has greatly intensified over the last twenty years. The results obtained up to now are quite satisfactory for many applications.

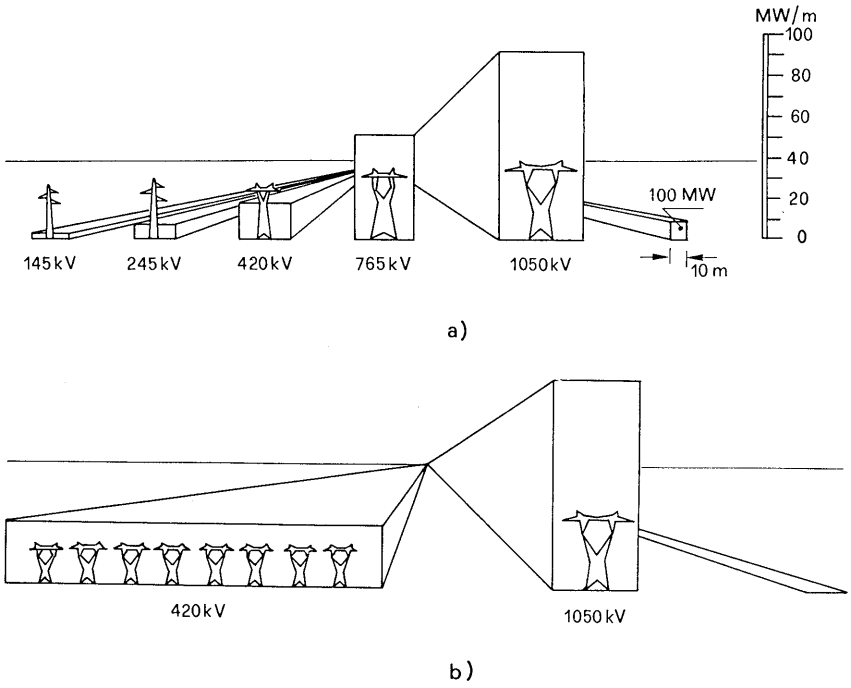

Fig. 1. a) Transmissible power and land occupation of transmission lines. b) Number of 420 kV lines required to carry the same power of a 1050 kV line (ENEL, 1978).

They supply a complete and detailed description of various discharge phases, provide an interpretation of their physical structure, and have led to the development of more refined semiempirical models which can be usefully applied in engineering.

The subject of this short paper will be a general description of the behavior of long air gaps with the aim of presenting the main problems and of introducing the terminology normally used. Review papers which are more complete may be found in the literature (Waters, 1978; Jones and Waters, 1978; and Gallimberti, 1979). The results which will be presented here mainly refer to the work performed by the Les Renardières Group in the last ten years (1972, 1973, 1977, 1981).

BREAKDOWN CHARACTERISTICS

Due to long insulating distances in h.v. transmission systems, the electric field distribution in the gaps is largely nonuniform,

with the degree of nonuniformity depending both on gap length and electrode size. Two fundamental categories of field distribution can be defined:

- One in which only one part of the gap is highly stressed and which can be schematically represented by a rod-plane gap;

- One in which two parts of the gap are highly stressed and which can be schematically represented by a rod-rod gap.

As the breakdown mechanism depends on the polarity of the highly stressed region, the two types of gap behave in different ways.

When in service, insulation is stressed both by a.c. applied voltage and by transient overvoltages of short duration due to lightning, to faults, or to switching operations. Their impulse shape varies greatly, and for many years they have been simulated with double-exponential impulses, which can easily be obtained in laboratories by using Marx generators. As shown in Fig. 2, this type of impulse is defined by its peak value (U_{cr}), front duration, i.e., time T_{cr} at which the peak value is reached, and tail duration, i.e., time T_2 at which the voltage falls to half U_{cr}. It is completely defined by U_{cr} and T_{cr}/T_2.

With transmission voltages higher than 200 kV, the values of switching surges are a very important factor for external insulation design. Both breakdown phenomena and voltage vary with the front duration of the impulse. Figure 3 shows the 50% breakdown voltage of a rod-plane gap as a function of the front duration in the case of positive applied voltage. The characteristics are U-shaped, and the minimum is more pronounced as gap length is increased. This fact

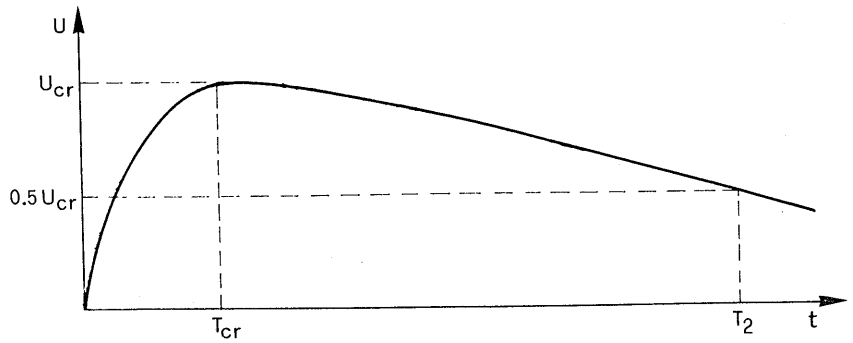

Fig. 2. Double exponential impulse: definition of wave shape parameters. Lightning impulse: $T_{cr} \simeq$ 1-10 μs; switching impulse: $T_{cr} >$ 20-30 μs.

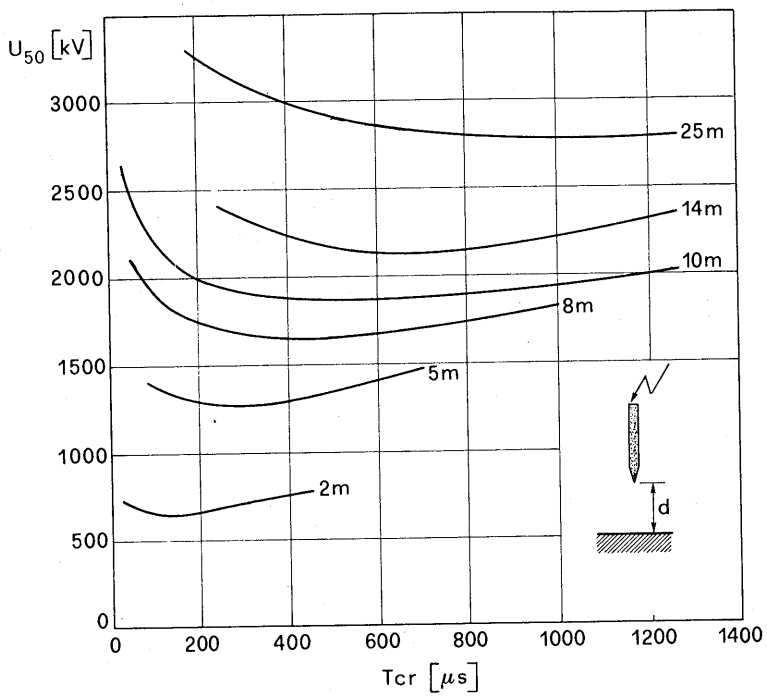

Fig. 3. Fifty percent breakdown voltage of rod-plane gaps as a function of time to crest (Gallet et al., 1975).

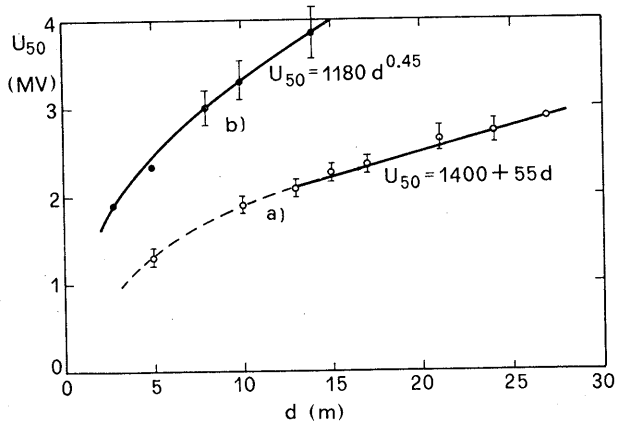

Fig. 4. Minimum breakdown voltage of rod-plane gap as a function of a gap length (Pigini et al., 1979). a) positive polarity; b) negative polarity.

causes a kind of saturation in minimum breakdown voltage as a function of gap length (Fig. 4). It is interesting to note that above a distance of about 15 m, a gap length increase of 1 meter causes an increase in the breakdown voltage of only 55 kV. Figure 4 also shows the same characteristic for negative applied voltage; the curve trend is similar even if the saturation is less pronounced; however, breakdown voltage values for the same gap length are much higher with negative than with positive polarity.

In the case of rod-rod gaps with one earthed electrode, field distribution is not symmetric but depends on the ratio between length H of the earthed rod and gap length d, so that breakdown voltage is a function also of gap geometry for a fixed length (Fig. 5). The two extreme limits correspond to a length of the earthed rod equal to zero, i.e., to the case of rod-plane gaps which have, for a fixed distance d, either minimum or maximum breakdown voltage according to polarity.

Because minimum breakdown voltage for a given length corresponds to the case of a rod-plane gap under positive switching surge, this situation is of major importance from a practical point of view and has been more extensively studied.

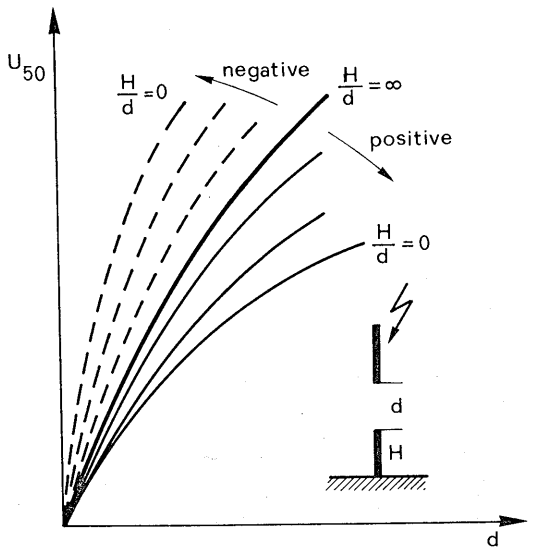

Fig. 5. Fifty percent breakdown voltage versus gap length in rod-rod gap with various electrode geometries.

Before passing to a description of breakdown formation, it is useful to establish when a gap may be considered long, even if a precise definition is not available. Figure 6 shows breakdown voltage as a function of gap length for sphere-plane gaps with different sphere radii, in the case of 120/1800 μs positive applied voltage. For comparison, the two lines with slope 5 and 26 kV/cm give the breakdown voltage respectively of a rod-plane gap under positive lightning impulse and plane-plane gap with uniform field distribution. For gap length d* and sphere ϕ = 15 cm, the breakdown voltage coincides with that of a sharp electrode (ϕ = 0). Ionization phenomena may be observed at voltages higher than U_m even if breakdown occurs at a voltage higher than in the case of a sharp electrode, and the ionization phenomenon cannot occur without causing the gap to break down; not all phases are clearly distinguishable during breakdown formation. Distance d* is usually considered as long only for a 10-cm sphere. For the same behavior with a 50-cm sphere, longer distances are necessary. If the initial ionization phenomenon, the first corona, necessarily causes breakdown to occur, no influence of the impulse shape may be detected. This means that the U-shaped breakdown characteristics of Fig. 3 may only be observed with long gaps.

BREAKDOWN DEVELOPMENT WITH POSITIVE POLARITY

When a voltage of critical time to crest is applied to a rod-plane gap, the phenomenon develops as shown in Fig. 7.

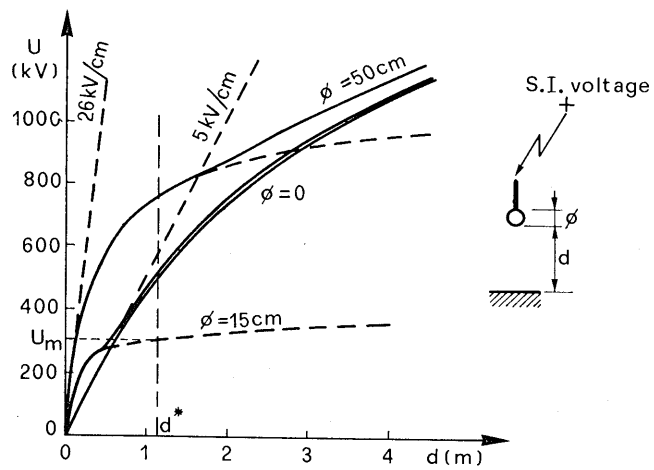

Fig. 6. Fifty percent breakdown voltage versus gap length in sphere-plane gap (Baldo et al., 1979).

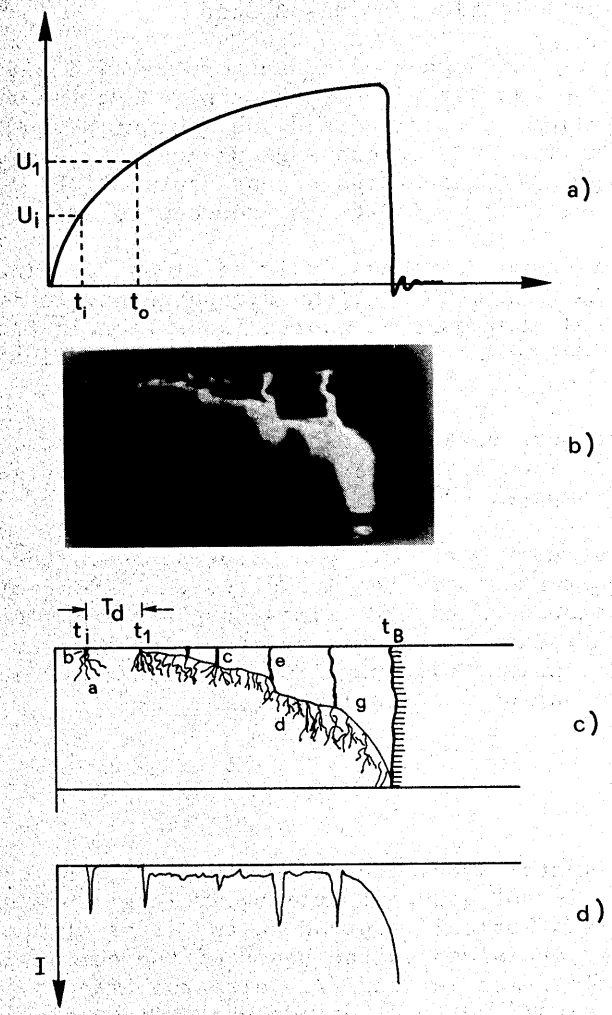

Fig. 7. Long spark development. a) applied voltage; b) streak photograph; c) schematic representation; d) current.

At time t_i when voltage reaches value U_i, depending on electrode geometry, the electric field attains sufficiently high values and the first phase of the process (first corona) occurs. It takes the form of filamentary channels or streamers [(a). in Fig. 7c]. A current pulse with a steep front and total duration of some hundreds of nanoseconds is recorded in the external circuit. At the root of the corona streamers, a short, bright channel, the stem,

is observed [(b). in Fig. 7c]. As a result of corona formation, a net positive charge is injected into the gap, the electric field is reduced, and ionization processes stop.

Depending on the degree of nonuniformity of the field distribution and the rate of rise of the applied voltage, after time interval T_d, called the dark period, at instant t_1, a leader channel (c) develops from the corona stem preceded by a secondary corona discharge. If the radius of curvature of the electrode is large enough, the dark period can be reduced to zero.

The leader channel propagates in an almost continuous way along a tortuous path with a corona discharge developing from its tip (d). Channel luminosity is quite low except in the case of sudden elongations and brightening (e), called reilluminations or restrikes.

Apart from some peaks corresponding to restrikes, the current in the external circuit is almost constant with average values of some tenths of ampere.

When the streamers of the leader corona reach the plane at time t_f, the last phase of the discharge, the final jump, begins (g). Leader velocity increases almost exponentially till instant t_B at which it reaches the plane, and the discharge is completed. Whereas during continuous propagation the leader may stop, this does not happen during the final jump.

First Corona

All experimental conditions being the same, the corona inception voltage U_i is not constant from one voltage application to another but is statistically spread on the front of the voltage. This fact may be explained on the basis of the corona inception mechanism. A field-accelerated free electron creates an avalanche which on its arrival at the electrode has at its head a number of electrons given by

$$n = \exp\left(\int_{r_1}^{r_2} (\alpha-\eta)\, dx\right),$$

where r_1 and r_2 are the starting and final point coordinates and $(\alpha-\eta)$ is the net ionization coefficient. If the avalanche reaches critical size on its arrival at the electrode, a streamer is formed and a corona develops.

At minimum inception voltage, there is only one point P_o (Fig. 8) from which a free electron can successfully initiate such an avalanche. As voltage increases, the region with a high electric field is extended so that a volume can be defined from any point at which an electron can now successfully start such an avalanche. For given electrode geometry, this critical volume V is a function of the applied voltage and time. It can be computed if the impulse shape is known. By combining the production rate of free electrons and the increase of volume V, we can compute the probability of corona inception as a function of voltage as shown in Fig. 9.

The intensity of the first corona, i.e., length of streamer zone and amount of injected charge, is strongly dependent on the divergence of field distribution and, for the same electrode, on the value of the inception voltage. Corona intensity increases both with field and inception voltage.

Leader Inception

As previously stated, after the dark period T_d (Fig. 7), a leader usually develops from the corona stem. This means that after the choking effect of the positive space charge due to corona formation, field distribution changes with time, and field strength in the stem region reaches values high enough to cause new ionization processes. This may have three different causes: increase

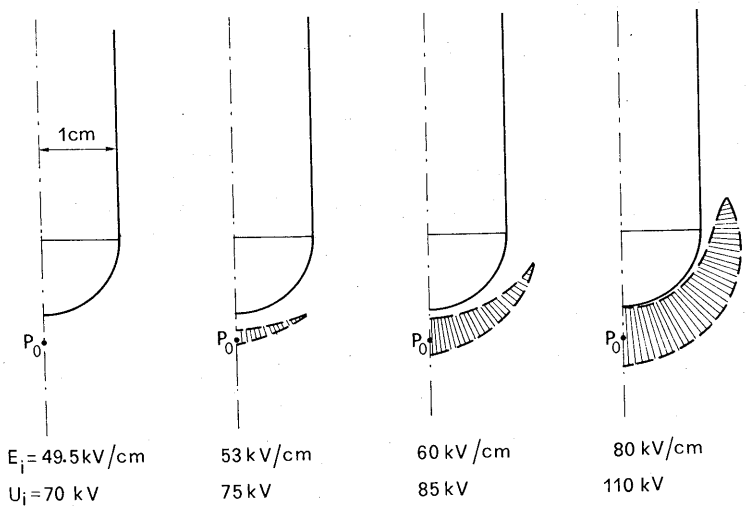

Fig. 8. Critical volume for different applied voltage (Badaloni and Gallimberti, 1972) 30 cm gap. E_i is the electric field at the electrode.

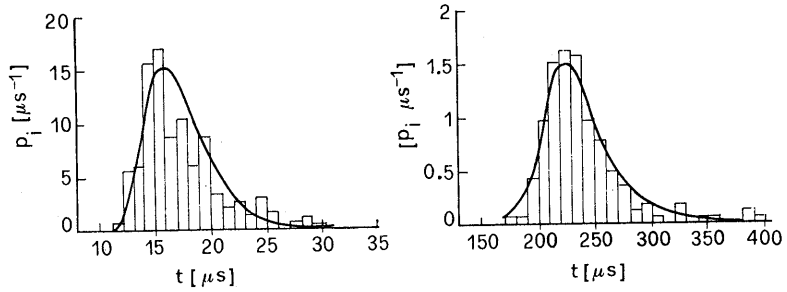

Fig. 9. Experimental and computed distributions of inception probability (Les Renardières Group, 1974). a) 10m gap, cone tip 1 cm curvature radius 500/10000 μs impulse, U_p = 1780 kV; b) 2 m gap, hemispherical tip 30 cm radius 350/10000 μs impulse, U_p = 1000 kV.

of applied voltage, movement of space charge, and increase in stem conductivity, this last cause probably being the most efficient. As discussed by Gallimberti in these proceedings, the gas temperature within the stem may increase because of relaxation of vibrational energy into thermal, causing negative ion detachment (Gallimberti, 1977). Spectroscopic measurements (Hartmann, 1977) have shown that the rotational temperature, which may be assumed as a good estimate of gas temperature, is of the order of 330 K in the corona streamers whereas it is approximately 1200 K in the stem.

It must be noted that for a fixed gap length, voltage U_1, at which the leader starts, remains the same if the curvature radius of the electrode is varied below a critical value. This experimental evidence, which has not been theoretically explained up to now, justifies the negligible influence of electrode size on the breakdown voltage of long gaps and allows this to be calculated on the basis of a semiempirical model (Carrara and Thione, 1976).

Leader Propagation and Characteristics

As shown in Fig. 7, once formed, the leader elongates in an almost continuous way with an axial velocity of about 1.2 - 1.4 cm/μs, less than one-hundredth the streamer velocity. Due to its tortuous path, real leader length is 20-40% longer than axial length, and real leader velocity, determined by three-dimensional analysis, is about 30% higher than axial velocity and shows small fluctuations. An almost constant proportionality exists between real velocity and current (Fig. 10), showing that the charge

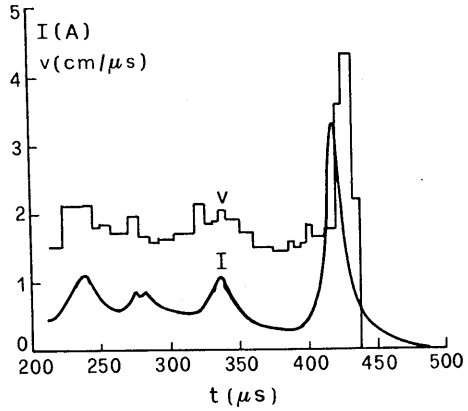

Fig. 10. Simultaneous variations of current and real velocity of the leader (Les Renardières Group, 1977).

injected into the gap per unit leader length is constant at 30-50 μC/m, the value being largely affected by air humidity.

The leader channel, which is preceded by a diffuse bundle of leader corona streamers, is not very bright and may be seen easily in a streak photograph only when restrikes occur. In an image converter frame record (Fig. 11), it appears as a thin luminous channel connecting the corona region to the h.v. electrode and seems to expand in time. Due to the low intensity of the emitted light and the resolution limits of electro-optical systems, it is difficult to estimate the time dependence of its luminous diameter. With time-resolved Schlieren measurements, as shown in Fig. 12, the time variation of the thermal radius of the leader has been obtained (Fig. 13). During leader growth, power is injected into the gap, depending on applied voltage and total current; from their measurement, the energy which is stored or dissipated in the gap may be obtained (Fig. 14). As the ionization and excitation losses in the corona region are small and the radiative power output is negligible, the energy input is essentially stored in two forms: the electrostatic energy W_s of the positive charge distributed in the gap, and the increase of enthalpy ΔW_h of the heated part of the discharge.

As the space charge position during leader growth can be approximately derived from charge and field measurements, W_s and ΔW_h can be separated as shown in Fig. 15. When leader growth is more than a few meters, enthalpy increase becomes the most important part and allows computation of temperature increase in the leader channel up to 7000 K. Apart from the rough simplification used, this value indicates that the overtemperature in the leader

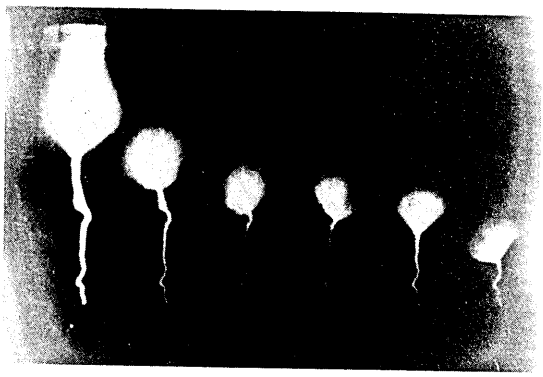

Fig. 11. Successive frames of image-converter picture in a 10 m gap (Leroy et al., 1974).

channel is in a range where thermal ionization and thermodynamic equilibrium cannot be assumed.

Finally, the average field along the leader channel has been estimated from charge and field measurements. As shown in Fig. 16, it decreases with leader length; this means that the local gradient decreases with time, the later sections having a lower gradient than the early ones. Figure 16 indicates that the potential of the leader tip does not vary much during leader development, which is consistent with the uniform velocity and current flow observed. It also justifies the kind of saturation in the sparkover voltage shown in Fig. 4.

Final Jump

The leader corona zone increases as the leader elongates, and when the leader has covered approximately two-thirds of the gap length, the streamers reach the plane (Fig. 17). At this moment the situation in the gap is completely different as the gap is completely bridged by more or less conductive filaments. Leader velocity together with current increases exponentially up to more than 100 cm/μs (Fig. 18) and, as already said, breakdown cannot be avoided.

The situation during the final jump is the same as in the case of breakdown formation with lightning impulse. In this case, in fact, due to the high rate of rise in voltage, subsequent streamer series are formed which reach the plane when the leader has covered only a few centimeters. Almost all the phenomenon develops as a final jump even if, due to the different time scale of the voltage, the leader may stop if the voltage decreases too quickly (Fig. 19).

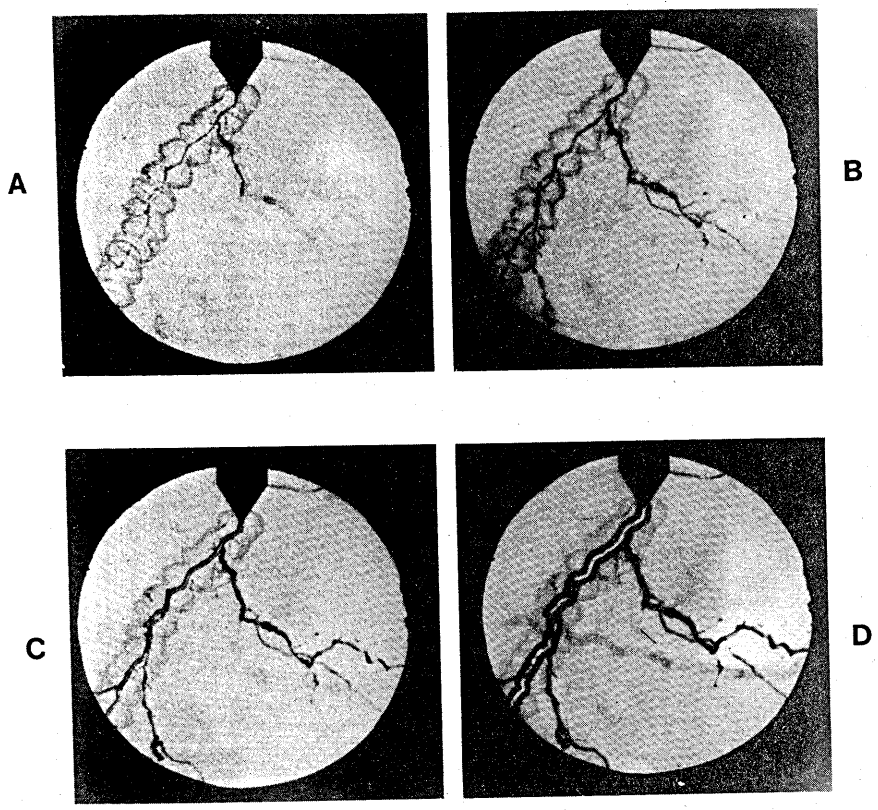

Fig. 12. Schlieren photographs of the leader channel in a 1.5 m gap (Les Renardières Group, 1977). a) t = 5.2 μs; b) t = 8.1 μs; c) t = 15.2 μs; d) t = t_B = 36.5 μs.

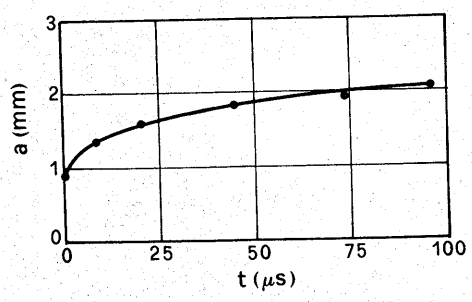

Fig. 13. The variation of leader thermal diameter versus time for a 10 m gap (Gallimberti, 1979).

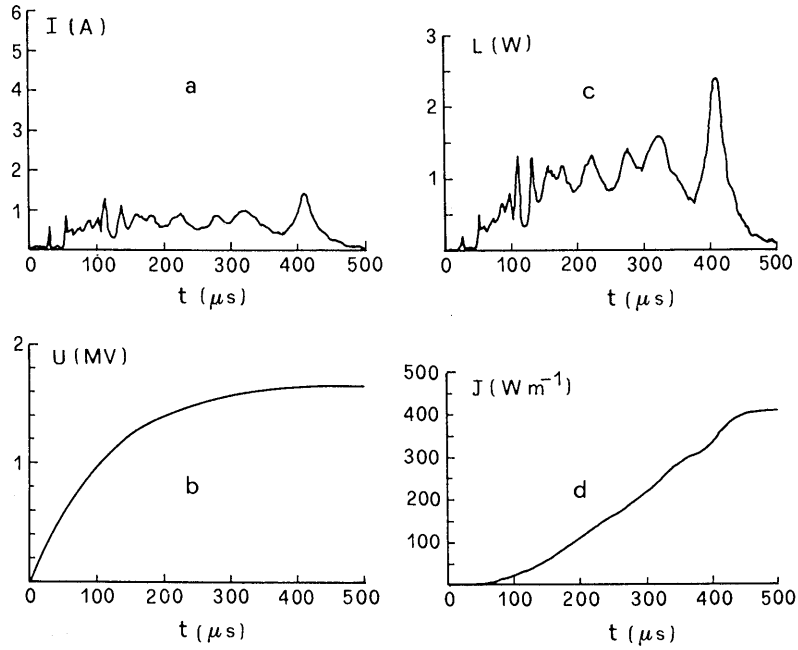

Fig. 14. Current, voltage, power and energy input in the discharge gap (Les Renardières Group, 1977).

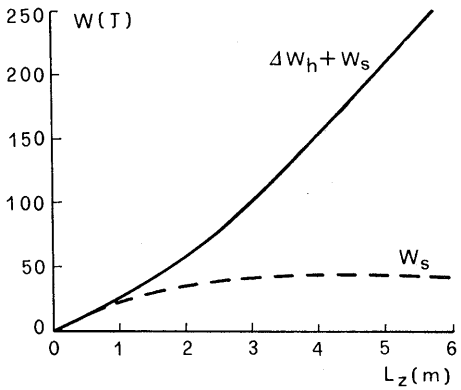

Fig. 15. Energy input (ΔW_h+W_s) and storage (W_s) as a function of axial leader length (Les Renardières Group, 1977) 10 m gap.

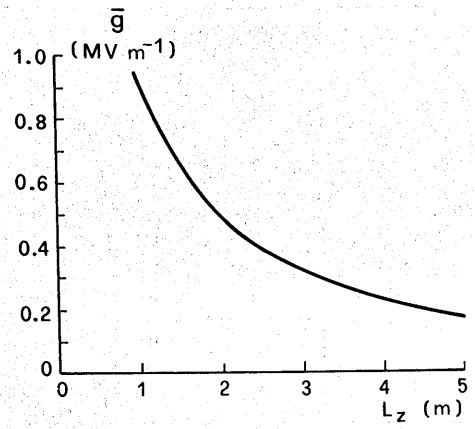

Fig. 16. Derived values of mean leader gradient as a function of axial leader length (Les Renardières Group, 1977) 10 m gap.

BREAKDOWN DEVELOPMENT WITH NEGATIVE POLARITY

Negative polarity breakdown has been studied less than positive because it has higher breakdown voltages (Fig. 4) and greater complexity. However, it is of physical and engineering interest, especially if lightning and "rod-rod" gaps are considered. Even though negative discharge is much more complex, three main phases may also be identified as in the case of positive polarity: corona leader, and final jump. Figure 20 shows an image-converter picture and a simplified sketch of discharge development.

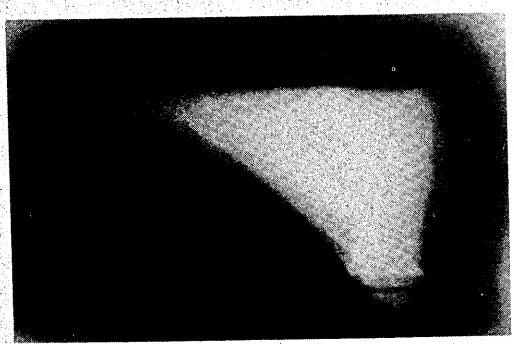

Fig. 17. Arrival of positive streamers at the plane.

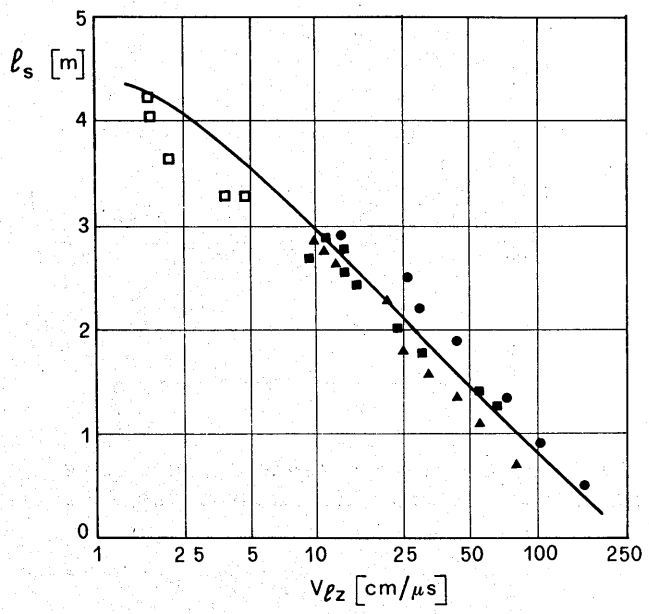

Fig. 18. Length of the unbridged part of the gap as a function of the axial leader velocity (Les Renardières Group, 1973) 10 m gap.

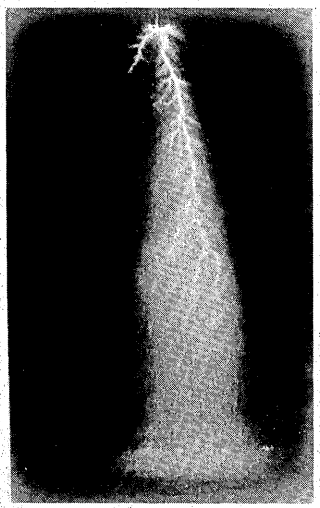

Fig. 19. Static picture of a leader which has stopped 1.5 m gap, 0.9/23 μs impulse.

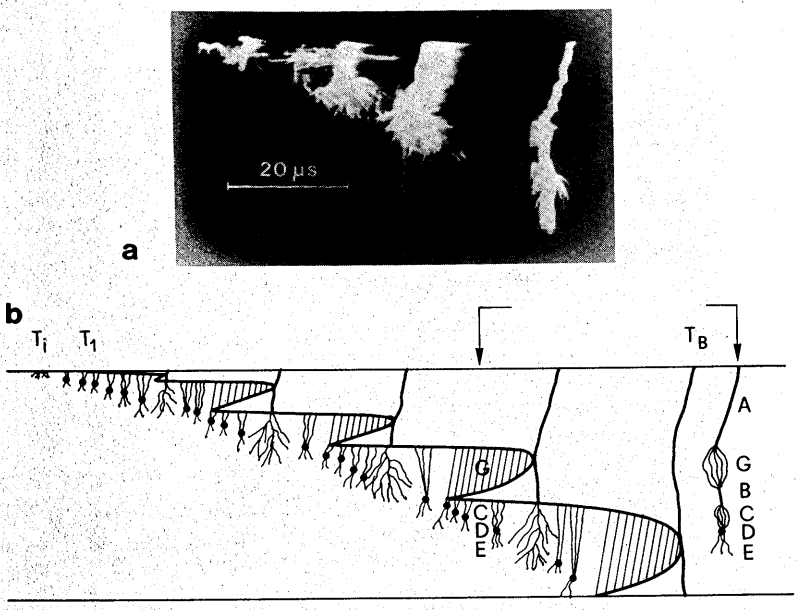

Fig. 20. (a) Image converter picture and (b) simplified sketch of discharge development with negative polarity (Les Renardières Group, 1981) 7 m gap, 60/3000 µs impulse. A negative leader; B space leader; C positive streamers; D space stem; E negative streamers; G positive streamers.

First Corona

When applied voltage reaches a convenient value U_i at instant t_i, a first corona occurs as a burst of streamers developing from the electrode. Inception voltages are approximately the same as in the case of a positive first corona, even if the dispersions of inception characteristics t_i and U_i are normally much smaller. When compared with positive coronas under similar conditions, both streamer length and injected charge are found significantly smaller in negative polarity.

Leader Development

The first corona discharge is followed at time t_1 by a negative leader which appears similar to the positive leader previously described. Propagation direction is largely random and reilluminations with large instantaneous elongations occur. For this reason, it is difficult to define average leader velocity as representative for the advancement of the discharge in the gap. In the continuous

Fig. 21. Image converter record of space leader obtained in a frame mode (Les Renardières Group, 1981). Exp. time: 1 μs; time interval: ~ 5 μs.

phase between reilluminations, velocity is approximately 1 cm/μs with an associate current in the range of 0.5 to 1 A.

The ionized zone which precedes the leader channel has a more complex structure than in positive, polarity. Three different parts may be identified: a luminous nucleus, called a "space stem," at a distance of about 0.5 m ahead of the negative leader tip, and positive and negative streamers propagating from it. This leader-corona system repeats itself regularly in a more advanced position with an equivalent displacement velocity towards the plane of approximately 10 cm/μs.

In the case of long gaps, a new phenomenon may appear. Starting from the space stem, a "space leader" forms which elongates in two opposite directions. The region between the upper tip of the space leader and the negative leader is covered by a glow-like corona (Fig. 21). When this region is bridged, the negative leader, which is now suddenly lengthened, is strongly illuminated and a large corona forms from its new tip. It is this phenomenon which causes the difficulty in defining the average leader velocity mentioned above.

Apart from the complexity of development mechanism, once formed the negative leader may be physically described as a positive one. It presents increasing conductivity as a function of time due to channel expansion. Strioscopic measurements have shown that this expansion mainly occurs with discontinuities associated with reilluminations.

Final Jump

When the negative streamers starting from the space stem reach the plane, a positive leader channel develops from it (Fig.

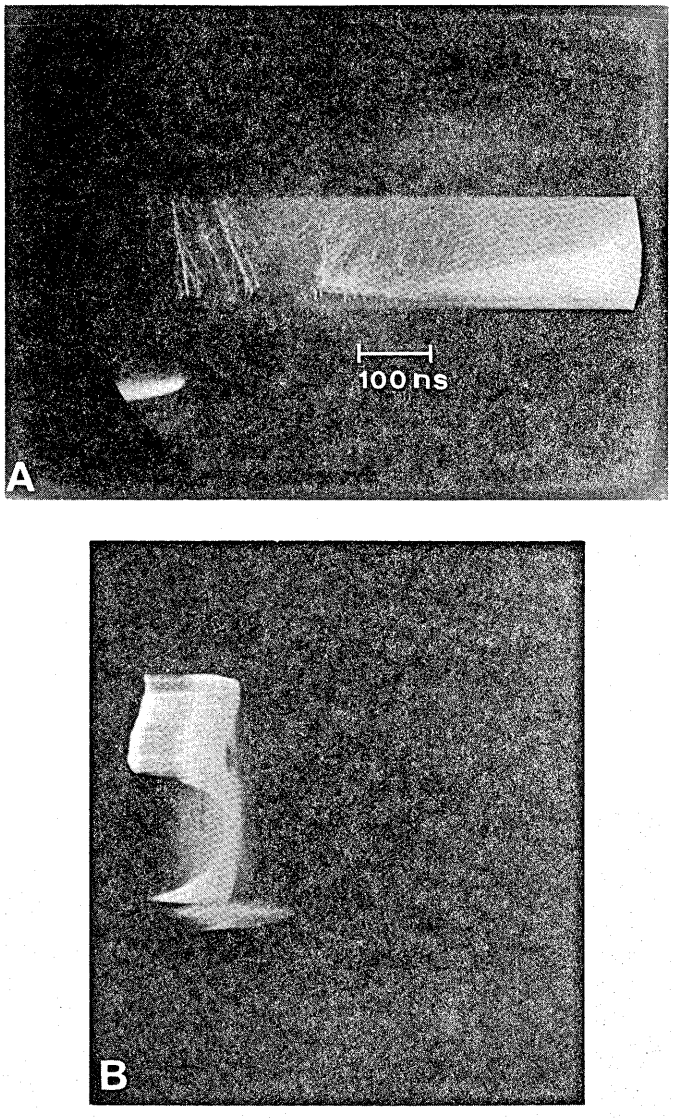

Fig. 22. a) Arrival of negative streamers at the plane and starting of the positive leader; b) negative and positive leaders meet together.

22a). This channel propagates towards the negative leader, both accelerating and meeting to complete breakdown (Fig. 22b).

The formation of a positive leader may be facilitated by the presence of protrusions on the plane which create local field increases and cause a leader to form earlier. Figure 23 shows the effect of a small earthed rod 18 cm long in a 5 m gap. Most discharges terminate on the rod because a positive leader starts from it. When the downcoming negative leader deviates sufficiently from the axis of the gap, a positive leader can still start from the plane but at a distance of more than 1 meter from the rod. This behavior clearly recalls the protective action of a lightning conductor.

CONCLUSIONS

The short description of breakdown formation in long gaps presented here shows the results obtained in the recent years by applying, for the first time, peculiar measuring techniques together with a large number of simultaneous electric and optical measurements.

As it will be shown in other papers, the results allow a much more advanced physical modeling of various phases of discharge. Obviously some points must still be studied carefully; particular effort has to be made in trying to clarify the corona-to-leader transition phase which is of major importance in understanding the whole phenomenon.

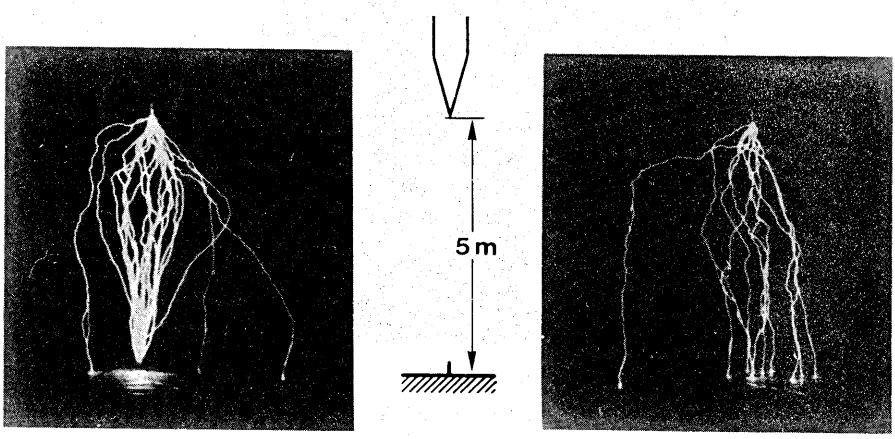

Fig. 23. Still photographs of a series of discharges in a 5 m gap with 18 cm earthed rod (a) and without rod (b) (Les Renardières Group, 1981).

REFERENCES

Badaloni, S. and Gallimberti, I., 1972, Padua University Report, UPee 72/03.

Baldo, G., Marchesi, G., Lalot, J., 1979, in: Proceedings, "Third International Symposium High Voltage Engineering, Milan," Paper 52.19.

Carrara, G. and Thione, L., 1976, IEEE Trans., PAS, 95:512.

Ente Naziouale ped l' Euergia lettrice, 1978, Rassegna Tecnica di Problemi dell'Engergia Electrica, No. 141.

Gallet, G., Leroy, G., Lacey, R., and Kromer, I., 1975, IEEE Trans. PAS., 94:1989.

Gallimberti, I., 1977, in: "Proceedings, World Electrotechnical Conference, Moscow."

Gallimberti, I., 1979, J. Phys. (Paris), 40:C7-193.

Hartmann, G., 1977, PR.D. Thesis, Paris.

Jones, B. and Waters, R. T., 1978, Proc. IEE, 125:1152.

Leroy, G., Simon, M. F., and Liao, T. W., 1974, in: "Proceedings, IEE Summer Power Meeting, Los Angeles," Paper 74 CH 0910-0 PWR, p. 5.

Les Renardières Group, 1972, Electra, 23:53.

Les Renardièrs Group, 1973, Electra, 35:47.

Les Renardières Group, 1977, Electra, 53:31.

Les Renardières Group, 1981, Electra, 74:67.

Pigini, A., Rizzi, G., Brambilla, R., and Garbagnati, E., 1979, "Third International Symposium on H.V. Engineering, Milan," Paper 52.15.

Waters, R. T., 1978, in: "Electrical Breakdown of Gases," 2nd Ed., J. M. Meek and J. D. Craggs, eds., Wiley, New York, p. 385.

A NUMERICAL SOLUTION OF THE BOLTZMANN EQUATION

L. C. Pitchford

Laser Theory Division
Sandia National Labs
Albuquerque, N.M. 87185

INTRODUCTION

The mathematical connection between the microscopic behavior of electrons as described by electron-neutral scattering cross sections and the macroscopic behavior of an electron swarm is through the Boltzmann equation which describes the time-evolution of the electron energy distribution function (EEDF) in phase space. The Boltzmann equation can be solved to yield the EEDF, various integrals over which yield the measurable parameters in a swarm experiment (Huxley and Crompton, 1974). Two preceeding papers describe the mathematical foundation (Skullerud, 1981) and analysis of the Legendre expansion solution of the Boltzmann equation as well as asymptotic forms of the solutions (Allis, 1981). For applications, it is almost always necessary to solve the Boltzmann equation numerically. This article describes some recent work in numerical solution techniques.

The discussion here is limited to the hydrodynamic regime in which measurable swarm parameters are independent of space and time. All changes in the electron numbers density are exponential in time or space. The effects of boundaries are negligible, electron densities are small, and E/N is uniform. This is the regime of interest in most swarm experiments.

In the following sections we discuss the mathematical model describing electron swarm behavior, solution techniques with emphasis on the Galerkin method (Pitchford et al., 1981), applications of the Galerkin method and comparisons with previous techniques in the case of N_2, and comparisons of the numerical

solutions with an analytic solution developed by Long (1979).

MATHEMATICAL MODEL

The form of the Boltzmann equation under discussion here is,

$$\partial f/\partial t + \vec{v} \cdot \vec{\nabla}_r f + \vec{a} \cdot \vec{\nabla}_v f = C(f), \tag{1}$$

where $f = f(\vec{r},\vec{v},t)$ is the EEDF, $\vec{a} = -e\vec{E}/m$ is the acceleration due to the applied electric field which is taken to be in the -z direction, and C is the collision integral. The second and third terms on the left represent a flux in $\vec{r}$ space and a flux in $\vec{v}$ space, respectively.

A complication in solving Eq. (1) is the form of the collision integral. The collision integral represents the rate of change in the number of particles in a volume element centered about $d\vec{v}$ and is the difference between the number scattered in the number scattered out of the element $d\vec{v}$,

$$C(f)d\vec{v} = \int\int_{\vec{V}'\Omega} F(\vec{V}')f(\vec{v}')p d\vec{V}' d\Omega d\vec{v}' - \int\int_{\vec{V}\Omega} F(\vec{V})f(\vec{v})p d\vec{V} d\Omega d\vec{v}, \tag{2}$$

where F and $\vec{V}$ represent the neutral distribution function and velocity, p, is proportional to the scattering cross sections, and the primes represent quantities after the collisions. The integrals are over all molecular velocities and all scattering angles. Discussion of the collision integrals may be found in Allis (1956) and Holstein (1946).

We make the cold gas assumption,

$$\int F(\vec{V})d\vec{V} = N\int \delta(\vec{V})d\vec{V} = N, \tag{3}$$

where N is the neutral density. This assumption is quite accurate for the cases where E/N is such that the electrons gain very little energy in collisions with the neutral particles. After some manipulation, the collision integral may be written as (Holstein, 1946),

$$C(f) = N\int f(\vec{v}')\delta(\vec{v},g(\vec{v}',\vec{v}))p d\Omega - N\, f(\vec{v})p d\Omega. \tag{4}$$

It is only those electrons which start with a velocity $\vec{v}'$ related to $\vec{v}$ through conservation of energy as expressed in the delta functions which can scatter into $d\vec{v}$ after a collision. The collision integral is thus a combination of multiplicative and integral operators, and it is the presence of the integral terms that considerably complicates the solutions.

The transport coefficients are defined as described by Kumar et al. (1978) through recourse to the continuity equation for electrons,

$$\partial m(\vec{r},v)/\partial t = w^{(0)} n(\vec{r},t) - \vec{w}^{(1)} \cdot \vec{\nabla} n(\vec{r},t) + \underline{w}^{(2)} : \vec{\nabla}\vec{\nabla} n(\vec{r},t) + \ldots \qquad (5)$$

where n is the electron density, $w^{(0)}$ is the reaction rate (the ionization or attachment rate), $w^{(1)}$ is the drift velocity, and $\underline{w}^{(2)}$ is the diffusion tensor. Because of the hydrodynamic assumption, these transport coefficients are independent of space and time. Higher order terms in the expansion have not thus far been measured.

Equations for the w's in terms of the EEDF can be derived by use of a density gradient expansion of the EEDF (Skullerud, 1969),

$$f(\vec{r},\vec{v},t) = f^{(0)}(\vec{v}) n(\vec{r},t) - \vec{f}^{(1)} \cdot \vec{\nabla} n(\vec{r},t) + \ldots \qquad (6)$$

This expansion is equivalent to the Fourier expansion treatment of the spatial dependency described by Parker and Lowke (1969). After substitution of Eq. (6) into the Boltzmann equation (1), a hierarchy of equations results,

$$\vec{a} \cdot \vec{\nabla}_v f^{(0)}(\vec{v}) - C[f^{(0)}(\vec{v})] = w^{(0)} f^{(0)}(\vec{v}) = \mathcal{L}[f^{(0)}(\vec{v})]$$

$$\vec{a} \cdot \vec{\nabla}_v \vec{f}^{(1)}(\vec{v}) - C[\vec{f}^{(1)}(\vec{v})] = w^{(0)} \vec{f}^{(1)}(\vec{v}) - (\vec{v}-\vec{w}^{(1)}) f^{(0)}(\vec{v})$$

$$= \mathcal{L}[\vec{f}^{(1)}(\vec{v})] \qquad (7)$$

$$\vdots$$

In what follows we set $w^{(0)} = 0$; i.e., there are no electron number changing processes. The solution techniques outlined in a later section can be applied equally well to the case where $w^{(0)} \neq 0$. Thus, with a unit normalization of the total distribution function, integration of Eq. (7) over velocity then gives,

$$w_z^{(1)} = W = \int v\cos\theta f^{(0)}(\vec{v}) d\vec{v}$$

$$w_{zz}^{(2)} = D_L N = \int v\cos\theta f^{(1,2)}(\vec{v}) d\vec{v}$$

$$w_{xx}^{(2)} = W_{yy}^{(2)} = D_T N = \int v\sin\theta f^{(1,x)}(\vec{v}) d\vec{v} \qquad (8)$$

Knowledge of $f^{(0)}$ and $f^{(1)}$ thus provides all the information required to determine $w^{(0)}$ and $w^{(1)}$. In the absence of particle number changing reactions, these also determine the diffusion tensor. In the presence of ionization or attachment, each of Eqs. (8) will contain an additional term, but the precise formulation of the appropriate transport coefficients for comparison with experiment will depend on the mode of observation (Sakai et al., 1977, Tagashira et al., 1977).

SOLUTION TECHNIQUES

There are two general approaches that have been applied to the solution of the electron Boltzmann equation in the form outlined above: moment methods and integral methods.

By far the most common solution technique has been the moment method, and in particular, a spherical harmonic expansion (or rather a Legendre expansion because of the axial symmetry of the problem) of the angular dependence of the velocity and a truncation after two terms. That is, the EEDF is assumed to be almost spherically symmetric in velocity space. Only terms depending on P_0 (cos θ) and P_1 (cos θ) are retained in the expansion. This so-called two-term expansion technique was pioneered by the work of Allis (1956) and Holstein (1946) and has been used extensively by Phelps and his co-workers and Crompton and his co-workers in the problem of the iterative extraction of cross sections from swarm data. (For a summary of cross sections determined from swarm data through 1973, see Huxley and Crompton (1974).) The criterion for validity of the two-term expansion is usually stated by saying that inelastic cross sections must be small with respect to the elastic cross sections or that the electrons must lose only a small fraction of their energy upon collisions with neutral particles. There are situations where this criterion implies that the two-term approximation is of questionable validity as, for example, in the diatomic or polyatomic molecules where low-energy inelastic channels in rotation or vibration have large cross sections. The two-term solution method is easy to implement and several good computer codes exist for implementation of this technique (Luft, 1975; Morgan, 1979; Rockwood and Greene, 1980). For these reasons and for ease of comparison with previous calculations, it is desirable to use the two-term approximation when possible.

Three-term solutions have been carried out by Makabe and Mori (1979), Ferrari (1975,1977), and by Wilhelm and Winkler (1969). Recently two general multiterm solution techniques have appeared in the literature (Lin et al., 1979; Pitchford et al., 1981). The multiterm solutions have the advantage over the three-term solutions in that the change in the calculated parameters may be studied

as more terms are included in the solution. In that way, it is possible to gain some insight as to the number of terms necessary in the Legendre expansion for solutions to a desired accuracy.

The integral equation approach to the solution of the Boltzmann equation has been suggested by Allis (1981) as preferable to the moment techniques. Kleban and Davis (1977, 1978) used an integral solution method in the calculation of the EEDF and transport coeffients in methane using model cross sections. Questions have been raised as to the accuracy of their solutions in the case of the parallel diffusion coefficient (Lin et al., 1979; Braglia, 1981). Kitamori et al. (1978) performed a direct two-dimensional integration to calculate the EEDF in the case of neon. While these techniques may eventually be preferable to the moment methods, more work must be done to demonstrate that they are computationally competitive.

Monte Carlo techniques offer an alternative to solving the Boltzmann equation and have been used extensively in the simulation of electron swarm behavior. (See, for example, McIntosh, 1974; Braglia, 1977; Reid and Hunter, 1979; Sakamoto et al., 1977.) Monte Carlo simulations may be done very accurately depending on the amount of detail included in the calculations. However, the computational time increases with the amount of detail and such simulations are therefore relatively expensive to perform. They do serve as a valuable check of other methods. The Monte Carlo results quoted in the next sections were performed with a code developed by Ivan Reid (1979).

GALERKIN METHOD

The same computation techniques used to solve Eq. (7) for $f^{(0)}$ can be applied as well to $\vec{f}^{(1)}$. The Galerkin method (Schryer, 1977) will be described for the $f^{(0)}$ equation. We begin by making the usual Legendre expansion,

$$f(\varepsilon,\theta) = \sum_{i=0}^{n-1} f_i(\varepsilon) P_i(\cos\theta). \tag{9}$$

A change of variables has been made at this point to $\varepsilon = \frac{1}{2}mv^2$. The use of the traditional Legendre expansion was retained in the development of the Galerkin method to facilitate comparisons with previous work and because these functions are easy to use in the present context. Moment equations are formed,

$$\int P_j(\cos\theta)\, \mathcal{L}\,[f(\varepsilon,\theta)]\, d\Omega = 0$$

$$\text{for } j = 0,\ldots n-1. \tag{10}$$

The result of these operations is a set of coupled linear differential equations which are three-term recursion relations between any three adjacent expansion coefficients,

$$\frac{eE}{N}\frac{j}{(2j-1)}\left[\varepsilon\frac{df_{j-1}(\varepsilon)}{d\varepsilon}-\frac{(j-1)}{2}f_{j-1}(\varepsilon)\right]+\frac{eE}{N}\frac{(j+1)}{(2j+3)}$$

$$\left[\varepsilon\frac{df_{j+1}(\varepsilon)}{de}+\frac{(j+2)}{2}f_{j+1}(\varepsilon)\right]=-\varepsilon f_j(\varepsilon)Q_T(\varepsilon)+\sum_{k=0}(\varepsilon+\varepsilon_k)$$

$$f_j(\varepsilon+\varepsilon_k)\int P_j(\cos\theta_s)Q_k(\varepsilon+\varepsilon_k,\theta_s)d\Omega. \qquad (11)$$

Here Q_T is the total cross section, ε_k is the energy loss in collisions of the kth kind, k = 0 for elastic scattering, θ_s is the scattering angle, and the sum is over all scattering channels.

In the two-term expansion, inelastic scattering is assumed to be isotropic. The resulting two equations (for j = 0, 1) can be combined into one second-order differential equation for f_0. In the multiterm expansion, the recursion equations must be solved simultaneously.

In order to solve the system of Eqs. (11), a further expansion is made and is illustrated here for one component,

$$f_j(\varepsilon)=\sum_{i=1}^{n}C_iS_i(\varepsilon)+\delta(\varepsilon), \qquad (12)$$

where the S_i's are cubic B-splines (Prenter, 1975; de Boor, 1972) and $\delta(\varepsilon)$ is a small error term. Complications due to the nonlocal terms in Eqs. (11) are eliminated by using expansion (12). Similarly, the derivatives of the splines are known and hence no finite difference or other approximation scheme is necessary to evaluate the derivative terms appearing in Eqs. (11).

For any finite basis set, the error term in Eq. (12) will be nonzero. The error can, however, be forced to have zero projection in the linear space spanned by the basis by requiring that

$$\int S_j(\varepsilon)\,\mathfrak{L}\,[\delta(\varepsilon)d\varepsilon]=0$$

$$\text{for } j=1,\ldots N. \qquad (13)$$

Substitution of Eq. (12) into (11) then gives a set of N linear algebraic equations in the N unknown coefficients, the C_i's. This set of equations may be easily solved by any of a number of readily

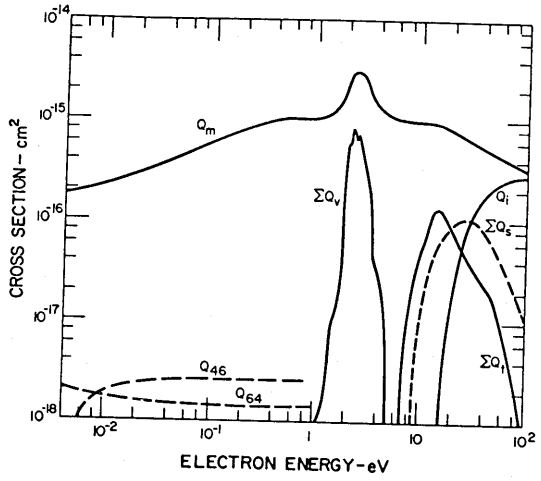

Fig. 1. Electron collision cross section for N_2 used in the multiterm calculations.

available linear system solvers. Extension to the coupled system, Eq. (11), is straightforward.

COMPARISON OF TWO-TERM AND MULTITERM SOLUTIONS

The method outlined above has been applied to the calculation of the EEDF and transport and rate coefficients in N_2 by Pitchford and Phelps (1981a). Results will be shown here for values of E/N up to 200 Td. The cross sections used in the calculations are those of Tachibana and Phelps (1979) and are shown in Fig. 1. These cross sections are assumed to result in isotropic scattering. The momentum transfer cross section shown is therefore equal to the sum of the elastic and inelastic cross sections. The rotational excitation cross sections, an example of which is shown in Fig. 1, were replaced by an effective cross section for a single level (Hake and Phelps, 1967). The vibrational and electronic cross sections are shown in the figure as sums of the individual level excitations. In the calculations, the individual level cross sections were used. Ionization was treated as an energy loss process. Only about 3% of the energy loss at 200 Td goes into ionization.

The computational problem is essentially that of determining the f_i's. Figure 2 shows the result of the first four coefficients in a six-term expansion solution for N_2 at 100 Td. The isotropic component, f_0, is the largest at all energies. The higher order coefficients become comparable with f_0 around 2 eV where the

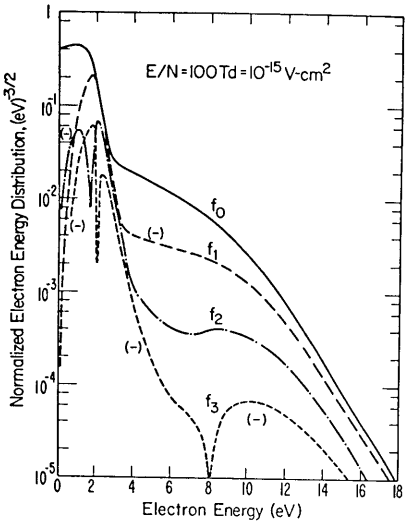

Fig. 2. The first four Legendre coefficients of a six-term solution for the electron energy distribution function in N_2 at 100 Td.

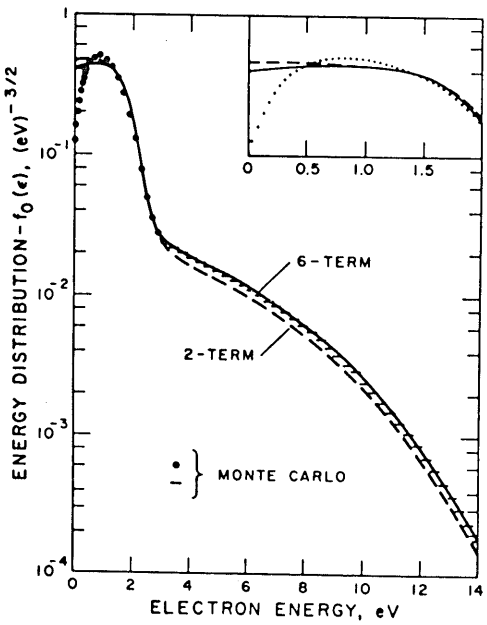

Fig. 3. Comparison of the normalized isotropic component of the distribution function, f_0, calculated using a two-term expansion, a six-term expansion and a Monte Carlo simulation at 100 Td in N_2.

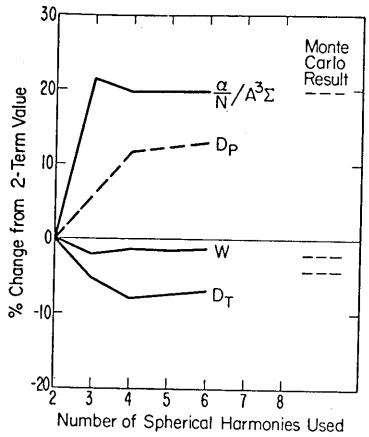

Fig. 4. Changes in the drift velocity, transverse and parallel diffusion coefficients and A-state excitation coefficient with increasing number of Legendre functions in the expansion. The data shown in for N_2 at 100 Td.

vibrational cross sections in N_2 are large. The structure in f_2 and f_3 seems to be correlated with the onset of important inelastic processes.

From Eqs. (7) it can be seen that the calculation of the transport coefficients requires knowledge of only f_0 and f_1. However, because of the coupling of the Eqs. (11), the solution for the lower order coefficients will depend on the higher order ones. Figure 3 shows the results of the calculation of f_0 using a two-term solution, a six-term solution and the Monte Carlo technique. The E/N is the same as for Fig. 2, 100 Td. A four-term solution for the same case yielded values of f_0 very close to the six-term results. It seems that at all energies except near the origin, the six-term result for f_0 has converged even though, as seen in Fig. 2, the higher order coefficients are relatively large.

The variation of the drift velocity, transverse and parallel diffusion coefficients and the electronic excitation coefficient for the $N_2(A^3\Sigma)$ state at 100 Td as a function of the number n of spherical harmonic components used in the calculation is shown in Fig. 4. The two-term values of the drift velocity and transverse diffusion coefficient are larger than the values using $n > 2$. The opposite is true for the A-state excitation coefficient which is illustrative of electronic excitation in general at this E/N. The parallel diffusion coefficient is also lower for the two-term solution than for the $n > 2$ calculations. The increase in the excitation coefficient for the A state is the result of the increase in the tail of f_0, going from two to six terms, as seen in Fig. 3.

The calculated values are seen to converge as the number of terms in the Legendre expansion is increased; beyond four terms there is very little change in the transport and excitation coefficients. The results of a Monte Carlo calculation of the drift velocity, the transverse diffusion coefficient and the A-state excitation coefficient are shown on the right in dashed lines in Fig. 4.

Calculations similar to the one presented in Fig. 4 were carried out over a range of E/N values from 1 to 200 Td and the difference between the two-term result and the six-term values are shown in Fig. 5 as a function of E/N. The same pattern of convergence of the transport and excitation coefficients with increasing n for the seven values of E/N investigated is similar to that shown in Fig. 4. The maximum error in the drift velocities and diffusion coefficients occurs at an E/N of 70 Td, corresponding to the point where a large fraction of the electrons are "seeing" the large ratio of inelastic to elastic cross sections due to the vibrational cross-section peak.

Attempts to correlate the difference between the two-term calculations and the multiterm calculations with an energy-loss parameter defined by experiment have been only partially successful. Figure 6 shows the fractional error in the two-term transverse diffusion coefficient as a function of the ratio of the momentum transfer collision frequency to the energy exchange collision frequency (Frost and Phelps, 1962; Englehart et al., 1964). This ratio is very nearly equal to the ratio of the drift energy to the

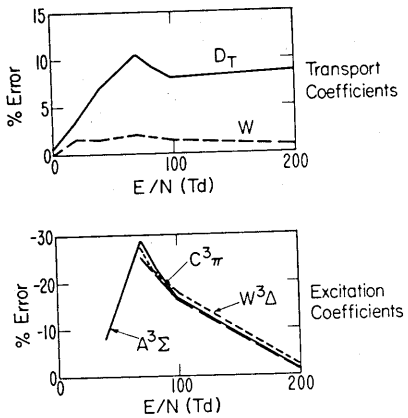

Fig. 5. Error introduced by the two-term approximation compared to the six-term results for drift velocity, transverse diffusion and electronic excitation coefficients as a function of E/N.

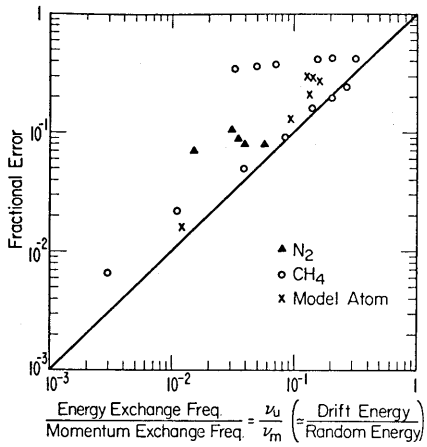

Fig. 6. Error introduced by the two-term approximation as a function of ν_u/ν_m, the ratio of the energy exchange frequency to the momentum exchange frequency.

random energy. The points for CH_4 and the ramp model atom are taken from Pitchford et al. (1981). About all that can be said from this plot is that the error is equal to or larger than the energy loss per collision parameter. Lin et al. (1979) finds an estimate of the error in the transverse diffusion coefficient that falls below the straight line of Fig. 6 by about a factor of two.

One additional feature of the miltiterm formulation is that the effect of anisotropic scattering may be included. Pitchford and Phelps (1978b) have investigated the anisotropic effects in N_2 for E/N from 40 to 1000 Td and find very small effects in the drift velocity and excitation and ionization coefficients. Effects may be larger in the calculated diffusion coefficients.

ANALYTIC SOLUTION FOR HIGH ENERGIES

Long (1979) has obtained a steady-state solution of Eq. (1) for a uniform field and isotropic scattering. He finds that when θ is not near 90^o and ε is above the excitation threshold,

$$f(\varepsilon,\theta) = \frac{Qe}{Q} \frac{\exp(-\varepsilon/kT_f)}{(1-\alpha\cos\theta)} \tag{14}$$

where

$$\alpha = \frac{Qe}{2Q} \ln\left(\frac{1+\alpha}{1-\alpha}\right) \quad . \tag{15}$$

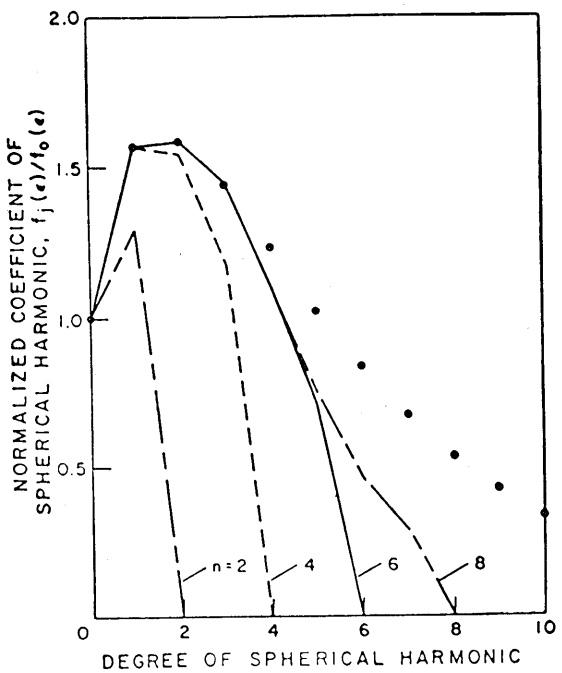

Fig. 7. Comparison of normalized ratios of Legendre coefficients, f_j/f_0 from numerical calculations and results of Long's formula. The model is described in the text.

Q is the total cross section and $kT_f = eE/\alpha NQ$. Qe is the elastic scattering cross section which is assumed independent of energy. The inelastic cross section, Q_k, is a step function which is independent of energy for energies above the threshold. For $Q_k/Qe \ll 1$, $kT_f \to eE/N(3Q_kQ)^{\frac{1}{2}}$ and $f(\vec{v})$ is well represented by a two-term expansion. For $Q_k/Qe > 1$, $\alpha \to 1$ and $f(\vec{v})$ approaches a delta function in the z direction.

Numerical results using the Galerkin method and predictions from Long's model have been made for two cases. The first comparison is for the case $Q_k = Qe$ for which $\alpha = .9575$. The relative values of $f_j(\epsilon)/f_0(\epsilon)$ resulting from a Legendre expansion of the θ dependent portion of Eq. (14) are shown in Fig. 7 as points. The expansion of a delta function in the z-direction would yield a ratio of (2_j+1) for all j. The lines show the ratio calculated with n = 2,4, and 6 for $eE/NQ\epsilon_k = 0.25$ and $\epsilon/\epsilon_k = 1.8$ so that $f_0(\epsilon+\epsilon_k) \ll f_0(\epsilon)$, as required by Long's model. As n is increased from 2 to 8, the lower Legendre components converge to the limiting value given by Long.

A second comparison of the numerical results with Long's predictions was made for the case of N_2. It is convenient to

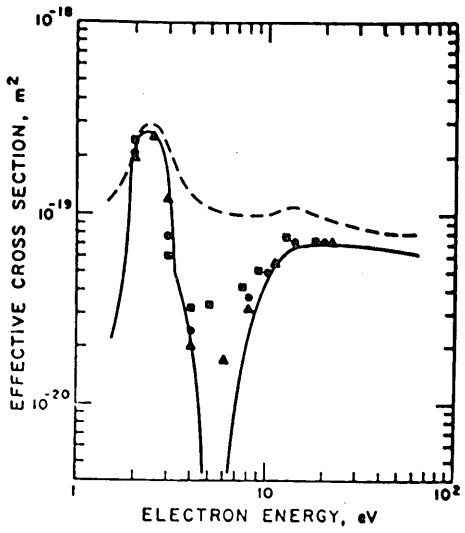

Fig. 8. Comparison of the effective cross sections from the numerical calculations in N_2 at 40 Td (▲), 100 Td (●) and 200 Td (■) with the results from Long's formula. The lower solid line is Long's result for small ratios of inelastic to elastic cross sections, Q_k/Q_e, and the upper dashed line is Long's result for a large ratio, Q_k/Q_e.

describe the distribution function shape with an effective cross section, $Q_f = (E/N)/(kT_f)$. From Eqs. (14) and (15), it can be seen that as $Q_k/Q_e \to 0$, $Q_f \to (3Q_T \sum_k Q_k)^{\frac{1}{2}}$ and as $Q_k/Q_e \to 1$, $Q_f \to Q_T$. These limiting values are shown in Fig. 8 as a function of energy. The calculations of the previous section were used to obtain values of $kT_f^{-1} = -d\ln f_0(\varepsilon)/d\varepsilon$. The values of $(E/N)/(kT_f)$ are shown in Fig. 8 for three values of E/N. The good comparison of the numerical results with Long's formula suggests that Eq. (14) may be used to simplify or improve calculations of the high-energy region of the distribution function.

ELECTRODE EFFECTS

In order to justify the comparison of experimental values of the swarm parameters with those calculated, the hydrodynamic model represented by Eqs. (5) and (8) must be shown to model accurately the experimental situation. Since the hydrodynamic approach taken here cannot take into account the effect of the electrodes present in the experiments, a Monte Carlo simulation was done (Pitchford

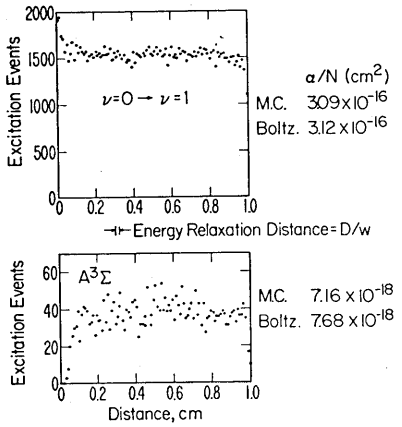

Fig. 9. Monte Carlo calculation of the number of excitation events as a function of drift distance for v = 0 → 1 vibrational excitation and $A^3\Sigma$ electronic excitation in N_2 at 100 Td and a neutral density of 10^{17} cm^{-3}.

and Phelps, 1981a) to determine the effect of the electrodes on the measured values of the swarm parameters.

The Monte Carlo calculations were performed for N_2 using the set of cross sections presented in Fig. 1. The simulation conditions were chosen to approximate the experiments of Tachibana and Phelps (1979), Levron and Phelps (1979) and Urosevic et al. (1980). For this calculation, single electrons were released normal to the cathode with 2 eV start energy. The electrons were allowed to drift through the tube and were absorbed at the cathode and the anode. Upon absorption, a new electron was released with the same start conditions. The simulation continued until the electrons encountered 10^6 collisions with the neutrals. After each collision, a record was kept of the type of collision and the position of the electron in the drift tube when the collision took place. From this record we have plotted the number of excitation events per distance interval as a function of distance as seen in Fig. 9 for the v = 0 → 1 and the $A^3\Sigma$ excitations.

The effect of the cathode and anode can be seen in the figures as a departure from the equilibrium excitation rates. One would expect an energy equilibrium to be established after the distance required for the drift and diffusion currents to become equal, or D/W which for this case is about 0.02 cm. This can be viewed as the characteristic distance to approach equilibrium or the e^{-1} distance to equilibrium and is roughly the distance seen in the figure as necessary to reach the equilibrium rates. The v = 0 → 1 excitation starts out higher than the equilibrium because the

release energy of 2 eV is equal to the energy at which the vibrational excitation cross section is a maximum. Similarly, the $A^3\Sigma$ excitation with a threshold energy of 6.17 eV cannot take place until some electrons have gained enough energy from the field to reach the A-state threshold. These trends in the excitation near the cathode do, of course, depend on the release energy chosen.

The anode effects are independent of the release conditions, provided an equilibrium has been established at some point in the drift region. Here we again see boundary effects on a scale corresponding to the D/W energy relaxation distance. There will be a dificiency of low energy electrons near the anode because of the reduction in the number of back-scattered electrons due to absorption of electrons at the anode.

The excitation coefficients calculated from the Boltzmann code and those from the Monte Carlo simulation are compared on the right of the figures. The agreement is good for the $v = 0 \rightarrow 1$ transition and only fair for the A-state excitation. However, when excitation events near the boundaries (0.1 cm on either end) are excluded, the agreement between Boltzmann and Monte Carlo rates agree to within 0.5%. We conclude from this excellent agreement that the Boltzmann treatment is valid in real experimental situations where boundaries are present and that the most accurate comparisons between the Boltzmann calculations and the excitation experiments will be for those experiments which focus on the center of the drift region rather than the entire drift distance.

CONCLUSIONS

Numerical techniques for solving the electron Boltzmann equation have been discussed with emphasis on a recently developed multiterm Legendre expansion solution technique. Applications of the technique have been shown in N_2 at E/N values low enough that ionization may be treated as an energy loss only. The cross sections used were from Tachibana and Phelps (1979). We have seen that use of the traditional two-term expansion results in errors of 1%, 5%, and 30% for the drift velocity, transverse diffusion coefficient and the electronic excitation coefficients, respectively, at 70 Td, with smaller errors resulting at other values of E/N. A Monte Carlo simulation at 100 Td showed that electrode effects were negligible for the conditions of recent measurements of electronic excitation coefficients in N_2. Comparisons of the numerical results with the high-energy analytic solution of Long and with Monte Carlo calculations support the validity of the multiterm calculations when the inelastic cross sections are large. We conclude that for low E/N, transport and excitation coefficients may be calculated as accurately as required for cross-section determination from swarm data.

Solutions of the Boltzmann equation are required for a variety of applications. The demanded accuracy of the solution technique depends to a large extent on the application. For the iterative extraction of cross sections from swarm data for comparison with beam cross sections, a very accurate solution is required, and errors introduced by the two-term approximation must be considered. If, however, cross sections derived from a two-term analysis of swarm experiments are available and swarm parameters are desired, then it is the two-term approximation that should be used for consistency in reconstructing swarm parameters. Gas mixtures present different problems. Given two-term derived cross sections for separately Ar and CH_4, for example, there is no assurance that a two-term code will accurately predict swarm parameters in an Ar-CH_4 mixture.

Electron number-changing processes, i.e., ionization and attachment, have been included in multiterm calculations (Pitchford and Phelps, 1981b) and in some of the two-term codes (Morgan, 1979 and Rockwood and Greene, 1980). Problems relating to the precise definitions of the transport coefficients in the presence of ionization have been discussed by Tagashira (1976). The multiterm formulation relies on the hydrodynamic assumption. The next effort in numerical solutions techniques will probably be a relaxation of the hydrodynamic assumption.

REFERENCES

Allis, W. P., 1956, Handb. Phys., 21:383.
Braglia, G. L., 1977, Physica (Utrecht), 92C:91.
Braglia, G. L., 1981, J. Chem. Phys., 74:2990.
DeBoor, C. J., 1971, J. Approx. Theory, 6:50.
Englehardt, A. G., Phelps, A. V., and Risk, C. G., 1964, Phys. Rev. A, 135:1566.
Ferrari, L., 1975, Physica (Utrecht), 81A:276.
Ferrari, L., 1977, Physica (Utrecht), 85C:161.
Frost, L. S. and Phelps, A. V., 1962, Phys. Rev., 127:1621.
Hake, R. D., Jr. and Phelps, A. V., 1967, Phys. Rev., 158:70.
Holstein, T., 1946, Phys. Rev., 70:367.
Huxley, L. E. H. and Crompton, R. W., 1974, "The Diffusion and Drift of Electrons in Gases," Wiley, New York.
Kitamori, K., Tagashira, H., and Sakai, Y., 1978, J. Phys. D, 11:283.
Kleban, P. and Davis, H. T., 1977, Phys. Rev. Lett., 39:456.
Kleban, P. and Davis, H. T., 1978, J. Chem. Phys., 68:2999.
Kumar, K., Skullerud, H. R., and Robson, R. E., 1980, Aust. J. Phys., 33:343.
Levron, D. and Phelps, A. V., 1979, Bull. Am. Phys. Soc., 24:129.
Lin, S. L., Robson, R. E., and Mason, E. A., 1979, J. Chem. Phys., 71:3483.

Long, W. H., Jr., 1979, Air Force Aero Propulsion Laboratory Report, AFAPL-TR-79-2038 (unpublished).
Luft, P. E., 1975, JILA Information Center Report No. 14, Boulder, Co.
Makabe, T. and Mori, T. J., 1979, J. Phys. (Paris) Colloq., 40:43.
McIntosh, A. I., 1974, Aust. J. Phys., 27:59.
Morgan, W. L., 1979, JILA Information Center Report No. 19, Boulder, Co.
Parker, J. H., Jr. and Lowke, J. J., 1969, Phys. Rev., 181:290.
Pitchford, L. C., O'Neil, S. V., and Rumble, J. R., Jr., 1981, Phys. Rev. A, 23:294.
Pitchford, L. C. and Phelps, A. V., 1982a, Phys. Rev. A, 25:540.
Pitchford, L. C. and Phelps, A. V., 1982b, to be published.
Prenter, P., 1975, "Splines and Variational Methods," Wiley, New York.
Reid, I. D. and Hunter, S. R., 1979, Aust. J. Phys., 32:255.
Reid, I. D., 1979, Aust. J. Phys., 32:231.
Rockwood, S. D. and Greene, A. E., 1980, Comp. Phys. Comm., 19:377.
Saelee, H. T. and Lucas, J. J., 1977, J. Phys. D, 10:343.
Sakai, Y., Tagashira, H., and Sakamoto, S., 1977, J. Phys. D, 10:1035.
Schryer, N. L., 1976, Bell Laboratories Computing Science Technical Report No. 52 (unpublished).
Skullerud, H. R., 1969, J. Phys. B, 2:696.
Tachibana, K. and Phelps, A. V., 1979, J. Chem. Phys., 71:3544.
Tagashira, H., Sakai, Y., and Sakamoto, S., 1977, J. Phys. D, 10:1051.
Urošević, V. V., Petrović, Z. Lj., Bozin, J. V., and Zeković, Lj. D., 1980, in: "Proceedings, Symposium on the Physics of Ionized Gases," B. Cŏbić, ed., Boris Kidric Institute, Beograd, p. 88.
Wilhelm, J. and Winkler, R., 1969, Ann. Phys. (Leipzig), 23:28.

THE MICROSCOPIC TREATMENT OF NONEQUILIBRIUM REGIONS IN A WEAKLY IONIZED GAS

P. Segur and M. Yousfi

Centre de Physique Atomique,
Laboratoire Associé au CNRS no. 277
Université Paul Sabatier, 118 route de Narbonne
31062 Toulouse cedex, France

J. P. Boeuf and E. Marode

Laboratorire de Physique des Décharges
Ecole Supérieure d'Electricité
Plateau du Moulon,
91190 Gif-sur-Yvette, France

A. J. Davies and J. G. Evans

Department of Physics,
University College of Swansea
University of Wales,
Swansea, United Kingdom

INTRODUCTION

Macroscopic parameters, such as drift velocity, diffusion, ionization, and attachment coefficients, used to describe the development of a discharge are normally measured in a swarm-type experiment (Huxley and Crompton, 1974). To analyze these experiments, we must assume that the electrons have reached an equilibrium hydrodynamic state so that their behavior after a sufficiently long time is such that the distribution function $f(\vec{r},\vec{v},t,)$ ($\vec{r}$, $\vec{v}$ and t are the position and velocity vectors and the time, respectively) can be considered a function of the density $n(\vec{r},t)$. The transport parameters are then time and position independent (Kumar et al., 1980). In a great number of cases, the equilibrium regime effectively exists, and the preceding hypothesis is perfectly valid. Nevertheless, even if sufficient time has elapsed for the swarm to reach

a stationary state, the condition of equilibrium will not be realized in the neighborhood of the walls, and the theory deduced from the equilibrium hypothesis cannot be applied to describe the nonequilibrium properties of the charged particle swarm in this region. If however, the thickness of the nonequilibrium region is small compared with the dimensions of the equilibrium region, the results obtained with the equilibrium hydrodynamic model may be applied to the whole region with negligible error.

It is possible, however, that equilibrium conditions are never obtained so that appreciable differences can be found between the theoretical predictions and the experimental measurements. This may occur, for example, when the energy gain of the charged particles accelerated by the electric field $\vec{E}$ is not balanced by the energy loss by collisions. In fact, hydrodynamic theory leads to correct results every time the system can be considered infinite — that is, the product N×L (where N is the gas number density and L, a length characteristic of the dimensions of the vessel) is large, or in other words, the free path for all types of collisions λ_T is much smaller than L. When this condition is not satisfied, it will be necessary to apply new methods, such as those described in the present paper, to account for the spatial, or the spatio-temporal, variations of the transport parameters.

In fact, the use of the more accurate methods described here are not only justified for swarm experiments but also for the study of more complex discharges in which, very often, no equilibrium zone is observed. In order for a nonequilibrium region to exist, the transport parameters must vary significantly over distances of the order of a few mean free paths λ_T or in times comparable with ν_T^{-1}, ν_T being the total collision frequency.

This situation is often encountered in electrical discharges, mainly in the cathode region of a glow discharge. We know that in this case (Von Engel, 1965), the spatial dependence of the electric field in the vicinity of the cathode is very strong so that it falls from a high value at the cathode (several hundreds of volts per cm) to a very low value in some tens of mean free paths and then remains nearly consistent until the positive column is reached. The region in which the electric field is small and practically constant is called the "negative glow," and, in general, it extends over a much greater number of free paths than the cathode-fall region.

In the cathode fall the electrons only have relatively few collisions, and, since the spatial variation of the electric field is large over a mean free path, the distribution functions and the macroscopic ionization and transport parameters will be strongly position-dependent. In the negative glow, since E/N is much smaller, the number of collisions will be greatly increased. However, in general, the equilibrium state will not be attained because of the

existence of high energy electrons produced in the cathode fall. The number of such electrons decreases as they penetrate further into the negative glow, and they create low and intermediate energy electrons as they undergo inelastic collisions with the gas molecules.

Thus, we would expect that, at a point in the cathode region where the local value of the field is E, say, the electron energy distribution function would differ appreciably from the distribution that would be obtained for a swarm that is traveling in a constant field E under equilibrium conditions. It follows that this kind of discharge cannot be studied using the same methods as are applicable in the case of equilibrium.

The existence of two regimes corresponding to equilibrium and nonequilibrium is often encountered in other fields of physics, for example, in neutron and radiation transport theory and in the study of electron motion in the solid state. In all these cases, there exist two types of regime: the hydrodynamic equilibrium regime, in general described by diffusion equations and the nonequilibrium regime, which can only be studied by the use of transport equations such as the Boltzmann equation or by the use of simulation methods such as Monte-Carlo computations. However, as we shall see later, these latter "microscopic" methods involve very large computing times. We have thus attempted to replace the microscopic studies by a less accurate but also less time-consuming method which is a modification of the macroscopic simulation methods described by Davies et al., (1980). In these macroscopic simulations, the primary ionization coefficient is related to the local value of the ratio E/N by an expression [see Eq. (90)] and the proposed modifications essentially replace E by an effective field, taking into account the whole field distribution that an electron has encountered. We call this the "Memory Factor" model.

In the second section of this paper, we shall first briefly discuss the major microscopic studies that have already been carried out for the case of nonequilibrium. In the third section, details of the Boltzmann and Monte-Carlo calculations are given, while section four gives typical results obtained using these two methods for steady and varying electric fields. The last section describes the modified macroscopic simulation technique together with some preliminary results.

The investigations described in this work have formed part of the Franco-British Collaborative Research Programme on Gas Discharges. In the main the Boltzmann calculations have been developed in the Centre de Physique Atomique, Université Paul Sabatier, Toulouse, France; the Monte-Carlo simulations in the Laboratoire de Physique des Décharges, Ecole Supérieure d'Electricité, Paris, (LPD) and

the Memory Factor model at LPD and in the Department of Physics, University College of Swansea, Wales.

GENERAL DISCUSSION AND RESUME OF PAST WORK

The Importance of the Nonequilibrium Region

As we mentioned in the introduction, our aim is to develop calculation methods that are able to take into account the effects of nonequilibrium of the electrons in a discharge. The Boltzmann (BE) and Monte-Carlo (MC) methods described in this section are mainly applicable to situations where the number of collisions is relatively small; nevertheless, these methods can be applied in a large number of practical situations. We have already spoken of the cathode-fall and negative-glow regions, and, in the rigorous study of these regions, it is very important to understand the phenomena occurring in the electrode-gas interface, not only at low pressure where the discharge is relatively wide but also at high pressure where the discharge has a filamentary structure. In this case, it has been shown (Marode, 1975) that globally the discharge has the same structure as a glow discharge — in experiments, when the cathode streamer arrives at the cathode, both cathode-fall and negative glow regions being established. Subsequently, by a mechanism that is not well understood, the discharge interacts with the electrode forming a hot cathodic spot and evolving to an arc discharge.

The typical structure occurring in the cathode region of a glow discharge appears in many practical situations, for example, in plasma display panels, some laser discharges, and discharges used for the treatment of surfaces. In each case, nonequilibrium phenomena due to charged particle interaction with the electrode surface and with the space-charge field is of great importance. Thus, it is necessary when simulating the cathode region to determine the charged particle densities and to allow for the resulting space-charge distortion of the field.

Another very important application of the methods developed here concerns the problem of gas insulation. In typical industrial configurations, such as gas insulated cables, circuit breakers, etc., the degree of nonuniformity of the electric field distribution is generally small. In the case of concentric cylindrical electrodes, for example, the ratio of the radii of the electrodes is close to unity, which would lead us to hope that it would be fairly straightforward to calculate the discharge parameters using similar methods to those for uniform fields. However, practice shows this is not the case, and there are considerable differences between theory and experiment; in some cases, the measured breakdown voltage is half that predicted theoretically.

This disagreement, which leads to deviations from Paschen's law and which becomes more pronounced as the pressure is increased, arises from several factors: free metallic particles can lead to a decrease in the dielectric strength; the state of the electrode surface can cause local enhancement of the electric field; edge effects can lead to inhomogeneities in the applied electric field due to bad electrode configurations, etc. In all these cases, the perturbing phenomena result in a modification of the applied electric field (homogeneous or quasi-homogeneous) either in the whole interelectrode space or in a very short distance near the surface of the electrodes. Electrode surface microprotusions are of particular interest because their presence leads to a decrease in the breakdown voltage and, even though they are only a few microns in height, the extremely high field in their neighborhood can completely change the properties of the discharge. In the neighborhood of the protusions, the macroscopic ionization parameters vary very rapidly with distance and cannot be related to the corresponding parameters measured under equilibreium conditions. It is clear that any attempt to explain the differences between theory and experiment must take into account the effects of nonequilibrium.

We note the difficulty of such a study, which must be in two dimensions. We must not only choose a simple and realistic form for the shape of the microprotusions, but we must perform the calculations for gas mixtures, which are normally used in high voltage insulation (SF_6, SF_6/N_2, etc.).

Brief Bibliographic Review

As a rule, most of the past work using Boltzmann or Monte-Carlo techniques has been concerned with the equilibrium regime. For example, Itoh and Musha (1960); Sakai et al. (1972); Lucas and Saelee (1975); and Reid and Hunter (1979) have used Monte-Carlo techniques whereas Sakai et al. (1977); Braglia (1980); and Pitchford et al. (1981) have studied methods involving the solution of the Boltzmann equation. The reader will find a complete bibliography on hydrodynamic Boltzmann equation studies in the recent paper of Kumar et al. (1980).

In the case of the study of the nonequilibrium regime, we can once more divide the investigations into those using MC or BE techniques. In all cases, we must be careful to distinguish between constant and varying field situations. The MC studies for a constant field will be described later. A few of the MC studies have attempted to obtain a self-consistent simulation of nonequilibrium electron kinetics by incorporating the effects of space-charge distortion of the applied field (Kline et al., 1972; Swigert and Goldstein, 1967). They respectively consider the temporal growth of electron avalanches (Kline et al., 1972) and the simulation of electron motion in a low pressure plasma diode (Swigert and Goldstein, 1967). The

only MC work on the self-consistent study of the cathode region of a glow discharge has been performed by Boeuf et al. (1980) and Boeuf (1981).

There are also a few nonequilibrium studies of electron kinetics using the Boltzmann equation method. For the case of constant fields, we have the works of Parker et al. (1969); Desloge and Mitchell (1970); Segur and Keller (1977); Segur et al. (1979); and Pareathumby (1979). The varying field situation has been studied by Sockol (1966); Whipple and Parker (1971); Allis (1975); Fournier and Pigache (1976); Long (1979); Segur et al. (1980); Yousfi (1980); and Lalau (1981). Self-consistent BE studies are given in Sockol (1966); Whipple and Parker (1971); Fournier and Pigache (1976); Long (1979); and Lalau (1981). A detailed analysis of the methods used by Whipple and Parker (1971); Allis (1975); and Fournier and Pigache (1976) has been made by Long (1979). We also note that a comparison of the results obtained by Fournier (BE), Marode (MC), and Segur (BE) is to be found in Marode et al. (1979), for the case of a linearly decreasing field.

At the moment, the most comprehensive (BE) study of the cathode region is that of Long (1979). Long's principal advance was to take into account the influence of the motion of the neutral particles on the behavior of the charged particles. He was able to obtain a self-consistent solution but did not give the form of the space-charge field. Furthermore, the motion of the ions is treated using some rough approximations in the macroscopic equations leading to results that disagree with Boeuf (1981) and Lalau (1981). Long has only started the study of the negative glow and his self-consistent solution has been obtained only for low N×L values. His method applies just to discharges in which the anode is very close to the cathode-fall region and the negative-glow is thin. Finally, the method which has been chosen by Long to solve the Boltzmann equation is similar to that developed by Segur and Keller (1977) and leads to very large computing times when the number of discretization points is high. The calculation time is roughly proportional to the square of the number of points. It follows that it is not possible to use this method to study the whole of the glow discharge with a negative glow of normal length.

At the present time no MC or BE study has been devoted to the calculation of transport and ionization parameters in the vicinity of surface microprotusions.

This short bibliographic survey shows that it is clearly necessary to develop further the MC and BE microscopic studies for the treatment of nonequilibrium electron kinetics. However, before considering a self-consistent model in all its generality, it is perhaps necessary to fully develop the nonequilibrium study of

electron kinetics for relatively simple cases such as, for example, a given predetermined electric field distribution. It will then be possible to develop more sophisticated nonequilibrium models and to make a detailed comparison of the power of the MC and BE methods. The aim of the present review is to give a contemporary account of study on this question.

METHODS FOR ANALYZING NONEQUILIBRIUM REGIONS

Physical Basis of the Treatment and Notation

In this section, we will describe the geometrical shape of the system and the simplifying assumptions. For the most part, these are common to the two treatments given and are as follows:

a) The discharge, which has cylindrical symmetry, is set up between two parallel plates and extends radially to infinity (Fig. 1).

b) The gas is weakly ionized; i.e. the electron-electron and other second order collisions are neglected.

c) The mean energy of the electrons is generally much greater than the mean molecular energy, the molecules being at rest.

d) Elastic energy losses are neglected in the BE calculations but taken into account in the MC simulations. This assumption is valid for high values of E/N, particularly in the case of gases with large atomic numbers.

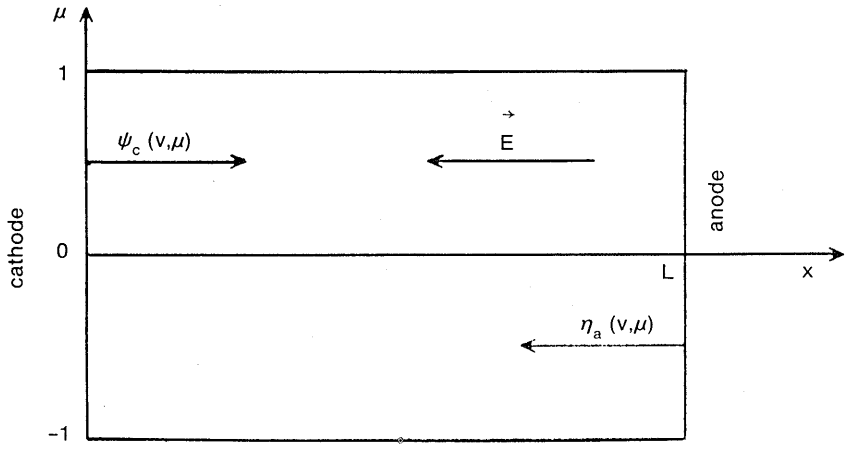

Fig. 1. Geometrical configuration and boundary conditions.

e) Collisions are assumed isotropic with respect to the center of the mass system. The elastic-collision cross section is replaced by the momentum transfer cross section in order to retain consistency with the conventional first order theory (see Braglia, 1970, 1975a, 1975b, 1977). In the Monte-Carlo treatment, we shall also present some results for anisotropic scattering.

f) The electric field E is constant in time, depending only on the x variable (distance from the cathode).

It follows from the first assumption that the distribution function f of the charged particles only depends on three variables: one distance variable and two velocity or energy variables. In the subsequent discussion, the distribution function may be described by the following sets of three independent variables:

(x,v,θ), where x is the distance from the cathode, v the modulus of the velocity, and θ the angle between the velocity vector $\vec{v}$ and the x axis (antiparallel to $\vec{E}$);

(x,ε,μ), where $\varepsilon = m\,v^2/2$ is the kinetic energy, $\mu = \cos\theta$;

(w,r,μ), where w is the total energy and $r = 2\sqrt{\varepsilon}$; and

$(w,y.h)$, where $y(=r\mu)$ is related to the longitudinal velocity and $h(=r\sqrt{1-\mu^2})$ is related to the radial velocity.

In this three-dimensional phase space, the conservation laws of motion along a free path can be written:

$$w = \varepsilon - |e|\,V(x), \tag{1}$$

$$\varepsilon^* = \varepsilon(1 - \mu^2)\ . \tag{2}$$

The relation (1) above is the total energy conservation law and the relation (2) is related to the radial energy conservation. V(x) is the potential, e the charge of an electron, and ε^* is the radial kinetic energy. These two relations completely define the characteristic electron trajectories in phase space between two collisions. A more detailed study of these trajectories will appear later.

The following definitions now can be made: the elastic momentum transfer, excitation of level k, ionization, and total microscopic cross sections are respectively denoted by $\sigma_{el}(v)$, $\sigma_m(v)$, $\sigma_k(v)$, and $\sigma_T(v)$. The ordinary microscopic differential ionization cross section is $\sigma_{ion}(v,v')$, where v' is the velocity of an electron after an ionizing collision. In the case of the anisotropic scattering treatment for the MC calculations, the differential angular cross

section will be denoted by $\sigma_{el}(v,x)$, where x is the scattering angle in the center of mass system.

The Boltzmann Equation Treatment

The Boltzmann Equation. In a steady-state discharge, the Boltzmann equation, giving the variation of the velocity distribution function $f(\vec{r},\vec{v})$, can be written:

$$\vec{v}\,\frac{\partial f}{\partial \vec{r}} + \vec{\gamma}\,\frac{\partial f}{\partial \vec{v}} = Jf. \tag{3}$$

$\vec{\gamma}$ is the acceleration vector of the external fields. We shall deal with systems without a magnetic field; therefore:

$$\vec{\gamma} = -\frac{|e|\vec{E}}{m}\ . \tag{4}$$

In the relations above, m is the mass of the electron and $\vec{r}$ the position vector. The right hand side of Eq. (3) gives the variation of f per unit of time due to collisions. We may write:

$$Jf = -\nu_T f + \psi f, \tag{5}$$

where $-\nu_T f\ \underline{dr}\cdot\underline{dv}$ gives the number of electrons leaving the element $\underline{dr}\cdot\underline{dv}$ ("out" term). $\psi f\ \underline{dr}\cdot\underline{dv}$ represents the number of electrons that come into $\underline{dr}\cdot\underline{dv}$ element ("in" term).

Taking into account the assumptions made in an earlier section we have:

$$\psi f = \psi_{el}\ f + \psi_{ex}\ f + \psi_{ion}\ f, \tag{6}$$

where the three terms in the right hand side of Eq. (6) are the "out" terms, due to elastic collisions, excitation, and ionization, which can be written:

$$\psi_{el}\ f = \frac{1}{2}N\ v\ \sigma_{el}(v)\phi(x,v), \tag{7}$$

$$\psi_{ex}\ f = \frac{1}{2}N \sum_k \frac{u_k^2}{v}\ \sigma_k(u_k)\phi(x,u_k), \tag{8}$$

$$\psi_{ion}\ f = N \int_{u_{ion}}^{\infty} dv'\ \frac{v'^3}{v^2}\ \sigma_{ion}(v',v)\phi(x,v'). \tag{9}$$

We have set:

$$u_k^2 = v^2 + 2\,\varepsilon_k/m, \tag{10}$$

$$u_{ion}^2 = v^2 + 2\,\varepsilon_{ion}/m, \tag{11}$$

$$\phi(x,v) = \int_{-1}^{+1} d\mu\; f(x,v,\mu), \tag{12}$$

where ε_k and ε_{ion} are the excitation energies of level k (for transition from the ground state) and the ionization energy, respectively. The ϕ function is twice the isotropic part of the distribution function f. Taking into account the assumptions mentioned earlier, the Boltzmann equation takes the form:

$$v\mu\,\frac{\partial f}{\partial x} + \frac{|e|E}{m}\cdot\left(\mu\,\frac{\partial f}{\partial v} + \frac{1-\mu^2}{v}\cdot\frac{\partial f}{\partial \mu}\right) = -\,\nu_T\, f + \psi f. \tag{13}$$

The method of solution of this equation is based on the study of the motion of electrons acted upon by the electric field, in the absence of collisions.

If electrons do not undergo collisions, the right-hand side of Eq. (13) vanishes and f is constant along the trajectories defined by the relations (1) and (2).

Let us notice now that Eq. (2) may be written:

$$(w + |e|V(x))\cdot(1 - \mu^2) = w + |e|V(x^*). \tag{14}$$

Here x^* is the abscissa where μ is zero. From Eq. (14) it follows that:

$$\mu^2 = 1 - \frac{w + |e|V(x^*)}{w + |e|V(x)}\quad . \tag{15}$$

If the electric field E is constant, V(x) = Ex, and the relation above takes the simple form:

$$\mu^2 = 1 - \frac{x^* - x_o}{x - x_o}\quad . \tag{16}$$

x_o is the abscissa of the zero kinetic energy point. From Eq. (1) we have:

$$w = - |e| E x_o .$$

We shall see later the results that we may deduce from the relation in Eq. (16).

Let us introduce now the new variables:

$$w = \frac{1}{2} mv^2 - |e|V(x); \tag{17}$$

$$r = \sqrt{2m}\ v. \tag{18}$$

Equation 13 becomes:

$$\mu \frac{\partial f}{\partial r} + \frac{1 - \mu^2}{r} \cdot \frac{\partial f}{\partial \mu} = - \alpha_T f + Sf, \tag{19}$$

with:

$$\alpha_T = N \frac{r\, \sigma_T(r)}{2\, E(x)} , \tag{20}$$

$$Sf = S_{el}f + S_{ex}f + S_{ion}f , \tag{21}$$

$$S_{el}f = N \frac{1}{2} \cdot \frac{r\, \sigma_{el}(r)}{2\, E\,(x)} \cdot \phi(w,r) , \tag{22}$$

$$S_{ex}f = N \frac{1}{2} \cdot \frac{r^2 + 4\, \varepsilon_k}{r} \cdot \frac{\sigma_k(\sqrt{r^2 + 4\, \varepsilon_k})}{2\, E(x)} \cdot \phi(w+\varepsilon_k,r), \tag{23}$$

$$S_{ion}f = N \int_{w+\varepsilon_{ion}}^{\infty} dw' \frac{[w' + |e|V(x)]}{[w + |e|V(x)]} \frac{\sigma_{ion}(w',r)}{2\, E(x)} \phi(w',r) \tag{24}$$

We are using the same notations as above, but it is clear that the functions f, ϕ, σ_{el}, σ_k and σ_{ion} in Eqs. (19) through (24) are distinct from the corresponding ones in Eqs. (3) through (12). More precisely, f now depends on w, r and μ. We also still write V(x) or E(x) but note that x is now a function of w and r through the relations in Eqs. (17) and (18). It is to be noted that α_T has the dimensions of the square root of energy.

Motion of Electrons in the Phase Space. Equation (19) looks like the neutron transport or radiative transfer equation in a spherical geometry. The only difference is found in the excitation or ionization operators of the "out" term. In the (r,μ) space, Eq. (19) describes the motion of particles free of external strengths that undergo some collisions with a total cross section α_T. Between two collisions, the particles move along a straight line.

Let us also notice that Eq. (19) is the projection of Eq. (13) on the characteristic of constant total energy w. It follows that, if an electron starts from the cathode with an initial energy, ε_o — its total energy, $w = \varepsilon_o$ — it moves, while it does not undergo collisions in the (r,μ) plane of total constant energy (see Fig. 2). If this electron undergoes elastic collisions in agreement with the relation (22), it always moves in the (r,μ) plane because elastic collisions involve here only rotation of the velocity vector. Each inelastic collision (excitation, ionization, etc.) produces an energy loss for the electron, so that it leaves the initial constant energy plane.

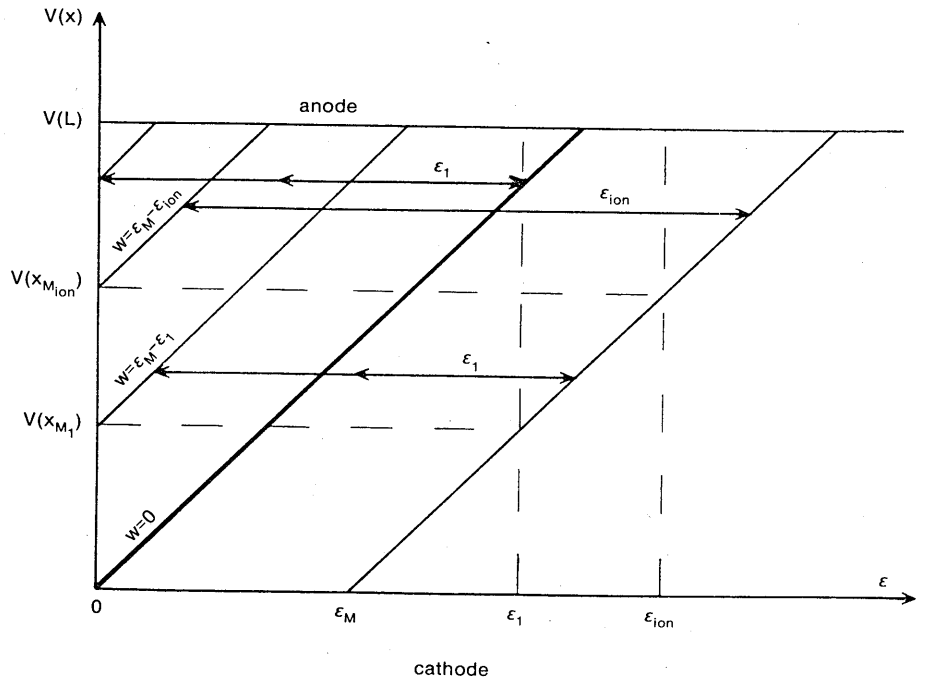

Fig. 2. Motion of electrons between the characteristics of constant total energy in the $(\varepsilon, V(x))$ plane.

If we assume that electrons have a low maximum energy of emission, ε_M, at the cathode (which is a good hypothesis because the energy spectra of photoelectrons emitted by the cathode is narrow), the previous comments allow us to draw the electron path in phase space, generated by the potential V(x) and the kinetic energy ε (Fig. 2).

The electron emitted by the cathode with an energy ε_M moves before undergoing inelastic collisions in the plane related to the total energy, W_M. The intersection of this plane with the $[\varepsilon, V(x)]$ plane is the straight line defined by Eq. (1).

If ε_M is greater than the first excitation threshold ε_1 of the molecules, the electron can undergo an inelastic collision just after leaving the cathode. On the other hand, if ε_M is lower than ε_1 the electron must travel a length x_{M_1} defined by:

$$|e|V(x_{M_1}) = \varepsilon_1 - \varepsilon_M ,$$

before being able to lose some energy by an inelastic collision. In this case, the abscissa, $V(x_{M_1})$, on the V(x) axis gives the origin of the characteristic related to the total energy, $\varepsilon_M - \varepsilon_1$. This characteristic is associated with the electrons which have undergone only one inelastic collision relative to the first excitation level.

In the same way, the electrons of total energy, W_M, are only able to ionize after a length defined by:

$$|e|V(x_{M_{ion}}) = \varepsilon_{ion} - \varepsilon_M .$$

They then move on the characteristic related to the total energy $\varepsilon_M - \varepsilon_{ion}$. The electrons located on these two new characteristic lines will lose some energy after traveling a sufficiently long way and will then move along some new characteristics, and so on.

We notice that the electrons emitted from the cathode move in phase space in a band located between the characteristics corresponding to total energies zero and W_M. Before the electrons reach the distance $x_{M_{ion}}$, the energy distribution has two peaks: 1) a high energy peak populated by electrons directly emitted from the cathode which have undergone no collision, and 2) a low energy peak populated by the first electrons which have made inelastic collisions. The lower bound of this peak is zero and the upper bound is equal to $\varepsilon_M - \varepsilon_1 + |e|V(x)$. When the distance traveled by the electrons is greater than $x_{M_{ion}}$, the part of the low energy peak that is created by excitation is masked for all the energies below

$\varepsilon_M - \varepsilon_{ion} + |e|V(x)$ by the electrons produced by ionization. The part due to excitation only appears for characteristics with total energies between $\varepsilon_M - \varepsilon_{ion}$ and $\varepsilon_M - \varepsilon_1$.

All the electrons emitted directly from the cathode are such that $w \geq 0$. On the other hand, the electrons which have at least undergone one inelastic collision have a negative total energy.

In the above description, we did not deal with the case where ε_M is larger than ε_1, since all the calculations were made in helium so that ε_M is always smaller than ε_1.

The Integral Form of the Boltzmann Equation. The above analysis of electron motion in the phase space $[\varepsilon, V(x)]$, shows us the line to take to determine the distribution function $f(w,r,\mu)$. As we have seen, electrons travel from the total energy characteristic W_M, which gives the maximum energy of electrons in the discharge, towards the lower energy characteristics. The last characteristic, defined by $W_L = -|e|V(L)$ where L is the gap length, becomes a point.

Initially, the electrons will fill the phase-space region located between the characteristics $W = 0$ and $W = W_M$. This region will be called zone I, and it is set up by electrons emitted from the cathode or the anode. The other phase-space region filled by electrons is located below the characteristic where total energy is lower than $\varepsilon_M - \varepsilon_1$. In this region, electrons have a negative total energy, and we shall call this region zone II.

Along a total energy characteristic line, the distribution function f obeys Eq. (19). In zone I, Eq. (19) takes the form (since there is no inelastic "in" term):

$$\mu \frac{\partial f^I}{\partial r} + \frac{1 - \mu^2}{r} \cdot \frac{\partial f^I}{\partial \mu} = - \alpha_T f^I + N \frac{1}{2} \frac{r \sigma_{el}(r)}{2 E(x)} \phi^I(w,r); \quad (25)$$

f^I is the value of f in the zone I. In this region, electrons come only from the walls of the vessel. To Eq. (25) we must add the appropriate boundary conditions taking into account the emission or reflection of electrons from the cathode or anode. We set (see Fig. 1):

$$\begin{aligned} f(0,v,\mu) &= R_c(v) f(0,v,-\mu) + \psi_c(v,\mu) \ , \ \mu \geq 0 \\ f(L,v,\mu) &= R_a(v) f_L(L,v,-\mu) + \eta_a(v,\mu), \ \mu < 0 \ . \end{aligned} \quad (26)$$

In these relations, ψ_c and η_a are the distributions of electrons emitted from the cathode and the anode, and $R_c(v)$ and $R_a(v)$ are the corresponding reflection coefficients. We assume that R_c and

R_a are independent of v. Along a characteristic line w, we have:

$$f^I(w,r_o,\mu) = R_c f^I(w,r_o,-\mu) + \psi_c(w,\mu) \quad , \quad \mu \geq 0$$
$$f^I(w,r_L,\mu) = R_a f^I(w,r_L,-\mu) + \eta_a(w,\mu) \quad , \quad \mu < 0 \quad , \tag{27}$$

where $r_o = 2\sqrt{w}$ and $r_L = 2\sqrt{w + |e|V(L)}$.

In the zone II, Eq. (19) is unchanged: i.e.,

$$\mu \frac{\partial f^{II}}{\partial r} + \frac{1 - \mu^2}{r} \cdot \frac{\partial f^{II}}{\partial \mu} = - \alpha_T f^{II} + N \frac{1}{2} \frac{r\, \sigma_{el}(r)}{2\, E(x)} \phi^{II}(w,r) + S_{in}\, f, \tag{28}$$

with

$$S_{in}\, f = S_{ex}\, f + S_{ion}\, f. \tag{28a}$$

Here f^{II} is the value of f in zone II. $S_{in}f$ is a known source term in which f has been calculated along some higher total energy characteristics. For example, if the inequality $\varepsilon_M < 2\,\varepsilon_1 + \varepsilon_{ion}$ holds, we can see that:

$$S_{in}f = S_{in}f^I$$

for the electron group located between the characteristics $w = -\varepsilon_{ion}$ and $w = \varepsilon_M - \varepsilon_1$. If w is lower than $-\varepsilon_{ion}$, $S_{in}f$ is a function of f^I and f^{II}, i.e., of the distribution functions belonging to zone I and II but obtained on the characteristics lines with total energy higher or equal to $w + \varepsilon_1$.

Electrons in zone II cannot reach the cathode but turn back at the point where they have zero kinetic energy. Here we must write the continuity conditions:

$$f^{II}(x_o,0,\mu) = f^{II}(x_o,0,-\mu) \quad , \quad \mu = 1 \quad ,$$

or

$$f^{II}(w,0,\mu) = f^{II}(w,0,-\mu) \quad , \quad \mu = 1,$$

with $w = -|e|V(x_o)$.

As in the zone I case, we have at the anode:

$$f^{II}(w,r_L,\mu) = R_a f^{II}(w,r_L,-\mu) + \eta_a(w,\mu) \quad , \quad \mu < 0. \tag{29}$$

Equations (25) and (28) can now be integrated, transforming the variables as follows:

$$\begin{aligned} y &= r\,\mu \\ h &= r\sqrt{1-\mu^2} \quad . \end{aligned} \tag{30}$$

Using the relations (30), the rectangular region of Fig. 3, in which the characteristics are curvilinear with:

$$\mu^2 = 1 - \frac{r_*^2}{r^2} \quad , \tag{31}$$

and

$$r_* = 2\sqrt{w + |e|V(x^*)} \quad , \tag{31a}$$

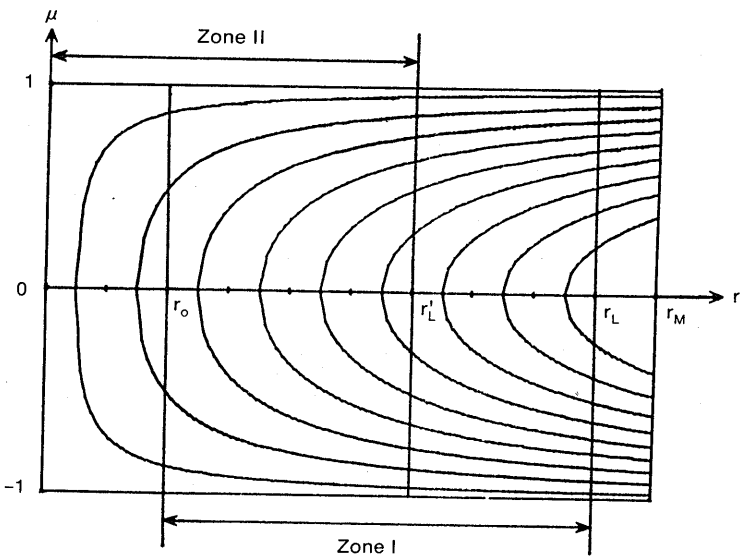

Fig. 3. Motion of electrons in the (r,μ) plane. The trajectories are curvilinear. $r_M = 2\sqrt{w_M + |e|V(L)}$. In the zone I, $r_o = 2\sqrt{w}$ and $r_L = 2\sqrt{w + |e|V(L)}$. In the zone II, $r_o = 0$ and $r'_L = 2\sqrt{|e|[V(L) - V(x_o)]}$.

becomes the circular region of Fig. 4 in which the characteristics are straight lines parallel to the Oy axis. The cathode and anode are now the spherical shells with radii r_o and r_L, respectively. In zone II, r_o obviously vanishes. It follows that we need only carry out the calculations in zone I with relations valid in zone II obtained by putting $r_o = 0$.

Once integrated, Eqs. (25) and (28) become:

a) $0 \leq h \leq r_o$; $\quad -1 \leq \mu \leq -\mu_o(r)$

$$f^{I,II}(w,r,\mu) = \int_r^{r_L} \frac{dr'r'Q(w,r')}{y^1} e^{-\tilde{\alpha}_T(y_<,y_>)} + f_a^< e^{-\tilde{\alpha}_T(y,y_L)} \tag{32}$$

$$f_a^< = \frac{1}{1 - R_a R_c e^{-2\tilde{\alpha}_T(y_o,y_L)}} \{R_a \int_{r_o}^{r_L} \frac{dr'r'Q(w,r')}{y^1} e^{-\tilde{\alpha}_T(y',y_L)} \tag{33}$$

$$\times(1 + R_c e^{-2\tilde{\alpha}_T(y_o,y')}) + R_a \psi_c(w,\mu_c) e^{-\tilde{\alpha}_T(y_o,y_L)} + \eta_a(w,\mu_a)\}$$

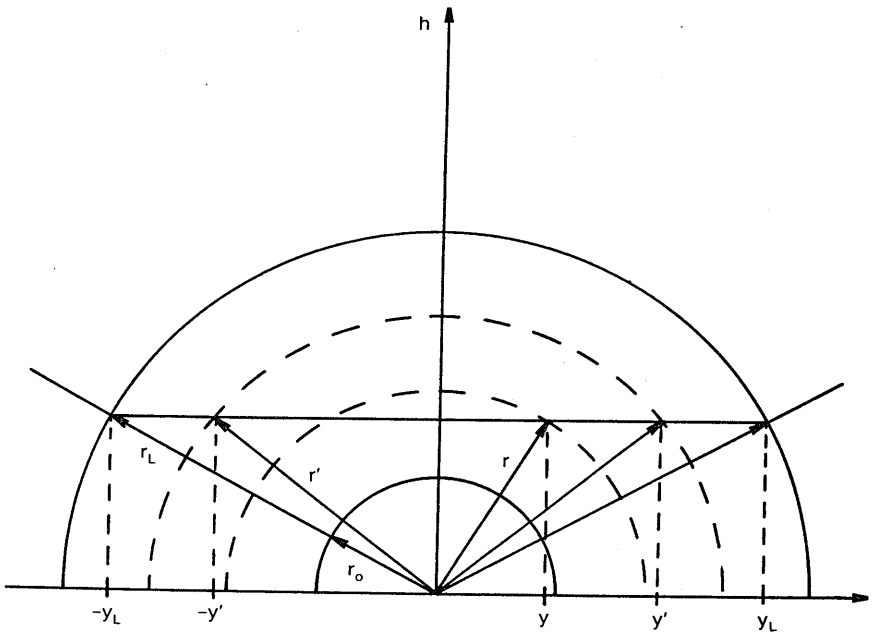

Fig. 4. Motion of electrons in the (y, h) plane. The trajectories are straight lines.

b) $r_o \leq h \leq r_L$; $-\mu_o(r) \leq \mu \leq 0$

$$f^{I,II}(w,r,\mu) = \int_r^{r_L} \frac{dr'r'Q(w,r')}{y^1} e^{-\tilde{\alpha}_T(y_<,y_>)} + f_a^> e^{-\tilde{\alpha}_T(y,y_L)} \tag{34}$$

$$f_a^> = \frac{1}{1 - R_a e^{-2\tilde{\alpha}_T(0,y_L)}} \{R_a \int_h^{r_L} \frac{dr'r'Q(w,r')}{y^1} (e^{-\tilde{\alpha}_T(y',y_L)}$$

$$+ e^{-\tilde{\alpha}_T(-y',y_L)}) + \eta_a(w,\mu_a)\} \tag{35}$$

c) $0 \leq h \leq r_o$; $\mu_o(r) \leq \mu \leq 1$

$$f^{I,II}(w,r,\mu) = \int_{r_o}^{r} \frac{dr'r'Q(w,r')}{y^1} e^{-\tilde{\alpha}_T(y_<,y_>)} + f_c e^{-\tilde{\alpha}_T(y_o,y)} \tag{36}$$

$$f_c = \frac{1}{1 - R_a R_c e^{-2\tilde{\alpha}_T(y_o,y_L)}} \{R_c \int_{r_o}^{r_L} \frac{dr'r'Q(w,r')}{y^1} e^{-\tilde{\alpha}_T(y_o,y)}$$

$$\times(1 + R_a e^{-2\tilde{\alpha}_T(y',y_L)}) + R_c\eta_a(w,\mu_a)e^{-\tilde{\alpha}_T(y_o,y_L)} + \psi_c(w,\mu_c)\} \tag{37}$$

d) $r_o \leq h \leq r_L$; $0 \leq \mu \leq \mu_o(r)$

$$f^{I,II}(w,r,\mu) = \int_h^{r} \frac{dr'r'Q(w,r')}{y'} e^{-\tilde{\alpha}_T(y_<,y_>)}$$

$$+ \int_h^{k} \frac{dr'r'Q(w,r')}{y'} e^{-\tilde{\alpha}_T(-y_<,y_>)} + f_a^> e^{-\tilde{\alpha}_T(y,y_L)} \tag{38}$$

In the relations (32) to (38), the variables y and y ' are positive. We then have (see Fig. 4):

$$y = r|\mu| \tag{39}$$

$$y' = [r'^2 - r^2(1 - \mu^2)]^{1/2} \tag{40}$$

$$y_L = [r_L^2 - r^2(1 - \mu^2)]^{1/2} \tag{41}$$

$$y_o = r_o^2 - r^2(1 - \mu^2)^{1/2} \tag{42}$$

$$y_{\leq} = \min (y, y') \tag{43}$$

$$y_{\geq} = \max (y, y') \tag{44}$$

$$\tilde{\alpha}_T(y_a, y_b) = \int_{y_a}^{y_b} d\xi \, \alpha_T[(\xi^2 + h^2)^{1/2}] \tag{45}$$

$$\mu_c^2 = 1 - \frac{r^2}{r_o^2}(1 - \mu^2) \quad , \mu_c \geq 0 \tag{46}$$

$$\mu_a^2 = 1 - \frac{r^2}{r_L^2}(1 - \mu^2) \quad , \mu_a \leq 0 \tag{47}$$

$$\mu_o(r) = 1 - \frac{r_o^2}{r^2} . \tag{48}$$

Let us note that the function $e^{-\tilde{\alpha}_T(y_a, y_b)}$ is the probability that an electron makes no collision between y_a and y_b.

The source term, Q(w,r), used above has a different form depending upon the zone.

In zone I:

$$Q(w,r) = N \frac{1}{2} \cdot \frac{r \, \sigma_{el}(r)}{2 \, E(x)} \, \phi^I(w,r) . \tag{49}$$

In zone II:

$$Q(w,r) = N\frac{1}{2}\frac{r\,\sigma_{el}(r)}{2\,E(x)}\,\phi^{II}(w,r)$$

$$+ N\frac{1}{2}\sum_{k}\frac{r^2+4\varepsilon_k}{r}\cdot\frac{\sigma_k(\sqrt{r^2+4\varepsilon_k})}{2\,E(x)}\,\phi^{I,II}(w+\varepsilon_k,r)$$

$$+ N\int_{w+\varepsilon_{ion}}^{-\varepsilon_{ion}} dw'\,\frac{[w'+|e|V(x)]}{[w+|e|V(x)]}\,\frac{\sigma_{ion}(w',r)}{2\,E(x)}\,\phi^{II}(w',r) \qquad (50)$$

$$+ N\int_{o}^{w_M} dw\;\;\frac{[w'+|e|V(x)]}{[w+|e|V(x)]}\;\;\frac{\sigma_{ion}(w',r)}{2\,E(x)}\,\phi^{I}(w',r).$$

In the relation (50) above, $\phi^{I,II}$ equals ϕ^{I} when $w > -\varepsilon_{ion}$ and equals ϕ^{II} in all other cases.

The source term, $Q(w,r)$, is a linear function of $\phi^{I}(w,r)$ (or $\phi^{II}(w,r)$), and we may obtain an integral equation for $\phi^{I}(w,r)$ (or $\phi^{II}(w,r)$) by integrating with respect to μ the relations (32), (34), (36) and (38). We then have in zone I:

$$\phi^{I}(w,r) = \int_{r_o}^{r_L} dr'\;\alpha_{el}(r')H(w,r',r)\phi\;(w,r') \qquad (51)$$

$$+ G_c(w,r) + F_a(w,r) + E_a(w,r)$$

and in zone II:

$$\phi^{II}(w,r) = \int_{o}^{r_L} dr'\;\alpha_{el}(r')H(w,r',r)\phi^{II}(w,r') \qquad (52)$$

$$+ \int_{o}^{r_L} dr'\;H(w,r',r)S_{in}f + E_a^{o}(w,r).$$

In the equations above, we have set:

$$H(w,r',r) = \frac{1}{2}\frac{r'}{r}\Bigg\{ \int_o^{r_o} \frac{dh\ h}{y\ y'}\ e^{-\tilde{\alpha}_T(y_<,y_>)} \times \frac{(1 + R_c\, e^{-2\tilde{\alpha}_T(y_o,y')})(1 + R_a\, e^{-2\tilde{\alpha}_T(y,y_L)})}{1 - R_a R_c\, e^{-2\tilde{\alpha}_T(y_o,y_L)}} \tag{53}$$

$$+ \int_{r_o}^{r_<} \frac{dh\ h}{y\ y'} \left(e^{-\tilde{\alpha}_T(y_<,y_>)} + e^{-\tilde{\alpha}_T(-y_<,y_>)}\right) \cdot \frac{(1+R_a e^{-2\tilde{\alpha}_T(y,y_L)})}{1-R_a e^{-2\tilde{\alpha}_T(0,y_L)}}$$

$$r_< = \min(r,r') \tag{54}$$

$$\alpha_{el} = N\frac{r\,\sigma_{el}(r)}{2\,E(x)} \tag{55}$$

$$G_{cc}(w,r) = \int_o^{r_o} \frac{dh\ h}{r\ y}\ e^{-\tilde{\alpha}_T(y_o,y)}\ \psi_c(w,\mu_c)\ \frac{1}{1 - R_a R_c\, e^{-2\tilde{\alpha}_T(y_o,y_L)}} \tag{56}$$

$$G_{ca}(w,r) = R_a \int_o^{r_o} \frac{dh\ h}{r\ y}\ e^{-\tilde{\alpha}_T(y_o,y_L)}\ e^{-\tilde{\alpha}_T(y,y_L)}\ \psi_c(w,\mu_c) \times \frac{1}{1 - R_a R_c\, e^{-2\tilde{\alpha}_T(y_o,y_L)}} \tag{57}$$

$$G_c(w,r) = G_{cc}(w,r) + G_{ca}(w,r) \tag{58}$$

$$F_{aa}(w,r) = \int_o^{r_o} \frac{dh\ h}{r\ y}\ e^{-\tilde{\alpha}_T(y,y_L)}\ \eta_a(w,\mu_a)\ \frac{1}{1 - R_a R_c\, e^{-2\tilde{\alpha}_T(y_o,y_L)}} \tag{59}$$

$$F_{ac}(w,r) = R_c \int_o^{r_o} \frac{dh\ h}{r\ y}\, e^{-\tilde{\alpha}_T(y_o,y_L)}\, e^{-\tilde{\alpha}_T(y_o,y)} \times \frac{1}{1 - R_a R_c\, e^{-2\tilde{\alpha}_T(y_o,y_L)}} \tag{60}$$

$$F_a(w,r) = F_{aa}(w,r) + F_{ac}(w,r) \tag{61}$$

$$E_a^{<}(w,r) = \int_{r_o}^{r} \frac{dh\ h}{r\ y} \cdot \frac{e^{-\tilde{\alpha}_T(-y_L,y)}}{1 - R_a\, e^{-2\tilde{\alpha}_T(0,y_L)}}\, \eta_a(w,\mu_a) \tag{62}$$

$$E_a^{<}(w,r) = \int_{r_o}^{r} \frac{dh\ h}{r\ y} \cdot \frac{e^{-\tilde{\alpha}_T(y,y_L)}}{1 - R_a\, e^{-2\tilde{\alpha}_T(0,y_L)}}\, \eta_a(w,\mu_a) \tag{63}$$

$$E_a(w,r) = E_a^{>}(w,r) + E_a^{<}(w,r) \tag{64}$$

In Eq. 52, $E_a^o(w,r)$ is the value of $E_a(w,r)$ for $r_o = 0$.

The two equations (51) and (52) are Fredholm integral equations of the second kind.

Each term in these equations has a precise physical meaning. The first term on the right hand side of (51) and (52) gives the part of ϕ^I coming from the "out" elastic term. In this way, if there are $\phi^{I,II}(w,r')dr'$ electrons with a total energy w in dr', they will give $\alpha_{el}(r')H(w,r',r)\ \phi^{I,II}(w,r')\ dr'dr$ electrons in the interval dr (Fig. 5).

The function, $G_{cc}(w,r)$, is the distribution of the electrons coming directly from the cathode. If these electrons are reflected by the anode, their distribution function is $G_{ca}(w,r)$ (Fig. 5). The distribution of electrons emitted by the anode is given by $F_a(w,r)$ and $E_a(w,r)$. $F_{aa}(w,r)$ and $E_a^{>}(w,r)$ are related to those electrons emitted by the anode but not reflected at the cathode nor turned back in the gap.

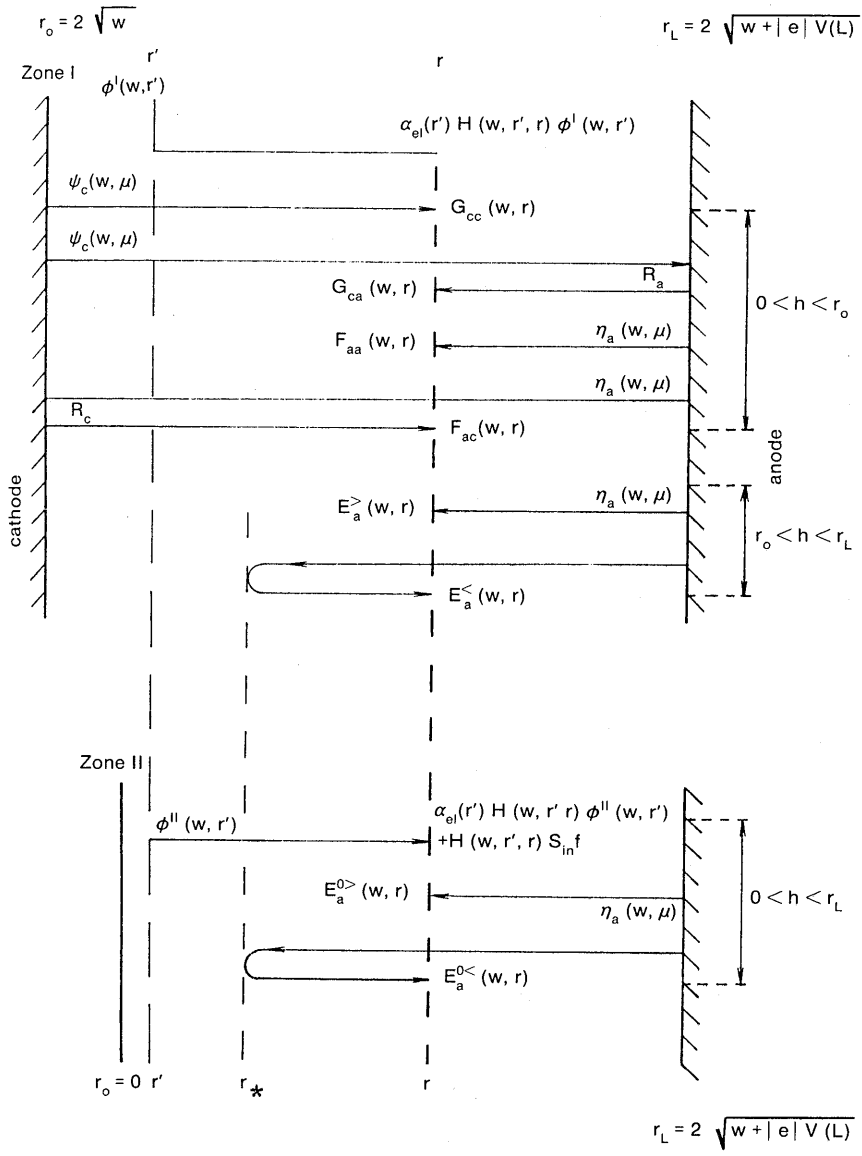

Fig. 5. Physical meaning of the various terms in Eqs. (51) and (52).

$F_{ac}(w,r)$ is the distribution of those electrons emitted by the anode which have been reflected at the cathode. Finally, $E_a^<(w,r)$ is the distribution corresponding to the electrons, also emitted by the anode, which have turned back in the gap (Fig. 5).

To conclude, we notice that in zone I, the distribution function $F^I(w,r,\mu)$, has a discontinuity on both sides of the $\mu_o(r)$ curve. This discontinuity comes from electrons emitted by the cathode. It could be suppressed with a convenient choice of the function $\psi_c(w,\mu)$ (Grosswald, 1961).

A Numerical Solution of the Boltzmann Equation. In the previous section, the Boltzmann equations (25) and (28) have been transformed into the integral forms (51) and (52); i.e., the problem of the solution of an integrodifferential equation has been reduced to the solution of an integral equation. Except in some special cases, equations, such as Eq. (51) and Eq. (52), cannot be exactly solved by analytical means. We are then forced to choose a numerical method of solution.

The main difficulty in that case comes from the singularity in the kernel $H(w,r',r)$ when r' equals r. Many methods can be found in the literature to overcome this drawback (Baker, 1977). Taking into account the physical situation, we have chosen the generalized collision probability method developed by Sanchez (1978) and Ligou (1973) in neutron transport theory.

First of all, the integration range is partitioned into N_d spherical shells so that:

$$V = [r_o, r_L] = \bigcup_{i=1}^{i=N_d} V_i \quad ; \qquad V_i = [r_i, r_{i+1}] \ . \tag{65}$$

In each shell V_i, the function $\phi(w,r)$ is approximated by a linear combination of functions:

$$\phi(w,r) = \sum_{k=1}^{A_i} a_k^i(w)\phi_k^i(r) \quad ; \quad r \in V_i \tag{66}$$

where the functions $\phi_k^i(r)$ are linearly independent in V_i.

If, for example, we put Eq. (66) into Eq. (51), it becomes:

$$\phi^I(w,r) = \sum_{k=1}^{A_i} a_k^{iI}(w)\phi_k^i(r)$$

$$= \sum_{j=1}^{N_d}\sum_{k=1}^{A_i} a_k^{jI}(w)\left|\alpha_{el}(r')H(w,r',r)\right|\phi_k^j(r') \geq \qquad (67)$$

$$+ G_c(w,r) + F_a(w,r) + E_a(w,r),$$

where:

$$r \in V_i \qquad\qquad r' \in V_j$$

and

$$\left|\alpha_{el}(r')H(w,r',r)\right|\phi_k^j(r')> = \int_{r_j}^{r_{j+1}} dr'\alpha_{el}(r')H(w,r',r)\phi_k^j(r'). \qquad (68)$$

The trouble, due to the singularity in $H(w,r',r)$, can then be overcome by a suitable choice of $\phi_k^j(r')$.

The function $\phi^I(w,r)$ will be known after the calculation of the coefficients $a_k^j(w)$. In order to do this, it is necessary to write

$$\sum_{i=1}^{N_d} A_i$$

equations (67). A_i points are chosen in each shell $V_i(r_i^s,\ s = 1, \ldots, A_i)$ and one writes an equation of the form (67) for each point. It follows that:

$$\phi^I(r_i^s) = \sum_{k=1}^{A_j} a_k^{jI}(w)\phi_k^i(r_i^s)$$

$$= \sum_{j=1}^{N_d}\sum_{k=1}^{A_j} P_{ij}^{sk}(w)a_k^{jI}(w) + G_c(w,r_i^s) \qquad (69)$$

$$+ F_a(w,r_i^s) + E_a(w,r_i^s),$$

with

$$s = 1,\ldots,A_i \quad ; \quad i = 1,\ldots, N_d,$$

and

$$P_{ij}^{sk}(w) = |\alpha_{el}(r')H(w,r',r_i^s)|\phi_k^j(r')> \quad . \tag{70}$$

Solving this linear system of order

$$\sum_{i=1}^{N_d} A_i$$

gives the $a_k^{iI}(w)$. Usually, the functions $\phi_k^j(r)$ are Legendre polynomials of order k. To keep the method tractable from a numerical point of view, it is assumed that the shells V_i are homogeneous, that is:

$$\alpha_T(r) = \text{cste} \quad ; \quad r \in V_j \tag{71a}$$

$$\alpha_{el}(r) = \text{cste} \quad ; \quad r \in V_j \tag{71b}$$

The r' integration in the calculation of the coefficients $P_{ij}^{sk}(w)$ is handled analytically. However, the h intergration must be carried out numerically.

Obviously $\alpha_T(r)$ or $\alpha_{el}(r)$ are not constant. If the electric field is quickly varying, they will strongly depend on x. It is then possible, depending upon the values of α_T, to distinguish two situations:

a) the case of a strong electric field which may or may not depend on x : $\alpha_T(r)$ is weak and $\tilde{\alpha}_T$ strong, and

b) the case of a low electric field: $\alpha_T(r)$ is strong and $\tilde{\alpha}_T$ is weak.

In the first case, the particles undergo few collisions along the characteristic w and are strongly accelerated by the electric field. In the second case, the number of collisions is very large. The first case is connected, for example, to the cathode fall, the second to the negative glow.

To treat the first situation, it will be necessary to choose small shells V_i so that α_T may be assumed to be constant for each. Furthermore, the electrons will undergo a small number of collisions in each shell. In the negative glow, since the field is slowly varying, the shell size, in which α_T is assumed to be constant, can be larger but the electrons will undergo a large number of collisions.

However, in the present work, we shall choose very small shells, and because the distribution function is slowly varying for each, we do not need to assume a sophisticated approximation for $\phi(w,r)$. In all the following, $\phi(w,r)$ will be assumed constant in each shell, so that $\phi_k^j(r)$ and A_i equal unity. Equation (69) is then written:

$$\phi_i^I(w) = \frac{1}{2} \sum_{j=1}^{j=N_d} P_{ij}^I(w)[\phi_j^I(w) + \phi_{j+1}^I(w)] + G_c(w,r_i) + F_a(w,r_i) + E_a(w,r_j), \tag{72}$$

with

1) $i \leq j$

$$P_{ij}^I(w) = \frac{\alpha_{el,j}}{2\,\alpha_{T,j}} \left\{ \int_o^{r_o} \frac{dh\ h}{r_i y_i} (\theta_i^{-1} + R_c\theta_j)\cdot(\theta_j - \theta_{j+1}) \frac{(1 + R_a \frac{\theta_L^2}{\theta_i^2})}{(1 - R_a R_c \theta_L^2)} \right.$$

$$\left. + \int_{r_o}^{r_i} \frac{dh\ h}{r_i y_i} (\theta_i^{-1} + \theta_i)\cdot(\theta_j - \theta_{j+1})\cdot \frac{(1 + R_a \frac{\theta_L^2}{\theta_1^2})}{(1 - R_a\,\theta_L^2)} \right\}. \tag{73}$$

2) $i > j$

$$P_{ij}^I(w) = \frac{\alpha_{el,j}}{2\,\alpha_{T,j}} \left\{ \int_o^{r_o} \frac{dh\ h}{r_i y_i} \theta_i(\theta_{j+1}^{-1} - \theta_j^{-1} + \theta_j - \theta_{j+1})\cdot \frac{(1 - R_a \frac{\theta_L^2}{\theta_i^2})}{(1 - R_a R_c \theta_L^2)} \right.$$

$$+ \int_{r_o}^{r_j} \frac{dh\ h}{r_i y_i} \theta_i(\theta_{j+1}^{-1} - \theta_j^{-1} + \theta_j - \theta_{j+1})\cdot \frac{(1 + R_a \frac{\theta_L^2}{\theta_i^2})}{(1 - R_a\,\theta_L^2)}$$

$$\left. + \int_{r_j}^{r_{j+1}} \frac{dh\ h}{r_i y_i} \theta_{j+1}^{-1} - \theta_{j+1}) \cdot \frac{(1 + R_a \frac{\theta_L^2}{\theta_i^2})}{(1 - R_a\,\theta_L^2)} \right\}$$

In this case:

$$\alpha_{T,i} = \alpha_T(r_i) \quad ; \quad \alpha_{el,i} = \alpha_{el}(r_i) \tag{74}$$

$$\theta_i = \exp - \int_o^{y_i(h)} \alpha_T[(\xi^2 + h^2)^{1/2}]d\xi$$

$$= \exp - \sum_{k=\ell}^{k=i-1} y_k(h)(\alpha_{T,k+1} - \alpha_{T,k}) + y_i(h)\ \alpha_{T,i}\ \} \qquad (75)$$

$$h \in V_\ell \ ; \qquad y_k^2(h) = r_k^2 - h^2.$$

In zone II,

$$\phi_i^{II}(w) = \frac{1}{2} \sum_{j=1}^{j=N_d(w)} P_{ij}^{II}(w)[\phi_j^{II}(w) + \phi_{j+1}^{II}(w)]$$

$$+ \frac{1}{2} \sum_{j=1}^{j=N_d(w)} P_{ij}^{II}(w)\ \alpha_{el,j}^{-1}(S_{in}F_j + S_{in}F_{j+1}) \qquad (76)$$

$$+ E_a^o(w,r_i).$$

To calculate $P_{ij}(w)$ in zone II, r_o is put equal to zero in the relations (73). The number of shells is now a function of w, because the length of the characteristics decreases with w.

Equations (74) and (76) are the two linear systems that allow us to calculate the isotropic part of the distribution function. Their main matrix is U(w), whose elements are written:

$$U_{i,j} = \delta_{i,j} - [P_{i,j}(1 - \delta_{N_{d+1},j}) + P_{i,j-1}(1 - \delta_{1,j})] \qquad (77)$$

$$i = 1, \ldots, N_d + 1 \ ; \quad j = 1, \ldots, N_d + 1$$

is diagonally dominant. The systems of Eq. (72) and Eq. (76) are well behaved and can easily be solved numerically.

In the case of a constant uniform field, the relation (16) suggests that the variation of the cosine μ between the electrodes depends only on the differences $x^* - x_o$ and $x - x_o$. It follows that the characteristic lines defined by the relations (1) and (16) belong to the region given in Fig. 3, which is located between the points $x = 0$ and $x = w_M/|e|E$. In (r,μ) space this region becomes a disk of radius $r_M = 2\sqrt{w_M + |e|V(L)}$. In zone I, the particles are located

between the spherical shells of radius $r_o = 2\sqrt{w}$ and $r_L = 2\sqrt{w + |e|V(L)}$. In zone II, they are inside the sphere of radius $r_L' = 2\sqrt{w + e\,V(L)}$.

The main consequence, from a numerical point of view, is that the probability coefficients, $P_{ij}(w)$, need to be calculated only once in the whole sphere of radius r_M and used in zone I or zone II depending on the values of r_o and r_L. In this case, this property considerably decreases the computation time.

That the integral equations only depend on the isotropic part of the distribution function comes from our isotropic assumption for the scattering cross section. If, for example, the scattering cross section had been assumed to be linearly anisotropic, two integral equations would be obtained for the isotropic and the first anisotropic parts, respectively.

In the present case, a knowledge of the isotropic part of the distribution function completely solves the problem. The first anisotropic part could be obtained by integrating with respect to μ the relations (32) to (38) after multiplication by μ. Alternatively, since the first anisotropic part is needed only in the calculation of the drift velocity, we may first obtain its cathode value by integrating Eq. (32) and Eq. (36). The drift velocity in the whole gap is then calculated with the help of the continuity equation.

In conclusion, it is to be noted that the methods of solution of the Boltzmann equation carried out by Fournier and Pigache (1976) and Long (1979) are based on the integrodifferential form (13). The integral methods lead generally to shorter computing times than integrodifferential methods and are more stable numerically. Furthermore, the integral methods allow a better understanding of the physical problem.

The Monte-Carlo Simulation

Previous Monte-Carlo Calculations. The Monte-Carlo simulation of the electron swarm behavior in a neutral background gas consists in determining the trajectories of a great number of electrons emitted at the cathode or created in the gap by ionization. The classical equations of motion are employed between collisions, while the free path lengths, the nature of collisions, and the change of velocity during a collision are choosen from the total and differential collision cross-sections by a stochastic method. This approach, which is closely related to free path methods in transport theory, is fully equivalent to a Boltzmann equation approach. The main drawback of the Monte-Carlo approach is that the simulation requires considerable computer time. However, in spite of this limitation, (which seems less and less serious with the in-

creasing speed of modern computers), a number of advantages make this method very powerful. Some of these advantages are the simplicity of the method, the case of incorporating any type of boundary condition, and the fact that this approach is very closely related to the physical situation. (The simulation could be classified as experimental rather than theoretical.)

The MC simulation method was used for the first time in discharge physics by Yarnold (1945, 1946). Only elastic collisions were taken into account, and the energy dependence of the mean free path was neglected in this work.

The determination of the free path length in a Monte-Carlo simulation is generally not easy. If r is a random number uniformly weighted on the interval (0,1), the time interval (which is considered as a random variable) between two successive collisions is the solution of the equation:

$$\mathrm{Log}\,\frac{1}{1-r} = \int_0^{\Delta t} \nu_T[\varepsilon(t)]\,dt \ , \tag{78}$$

where $\nu_T(\varepsilon) = N\sigma_T(\varepsilon)v$ is the total collision frequency. Because the total cross section σ_T is a complicated function of the kinetic energy, Eq. (78) cannot be solved without a numerical integration--the use of a model gas with simple collision cross sections (Braglia, 1977) can make the analytical integration of Eq. (78) very easy. Itoh and Musha (1960) improved the simulation of Yarnold (1945, 1946) with an attempt to take into account the energy dependence of the free path distributions. In their method, whether or not a collision between an electron and a gas atom occurs is decided by generating a random number at every path length equal to one-tenth of the mean electron free path. The same technique is used by Sakai et al. (1972, 1977) and by Lucas and Saelee (1975).

The calculations of Itoh and Musha (1960) used the ergodic hypothesis; i.e., it was assumed that the mean behavior of a single electron sampled a large number of times was the same as the mean behavior of all the electrons at any time. This assumption was criticized by Thomas and Thomas (1969) because it is equivalent to neglecting the influence of ionization and attachment on the diffusion terms in the Boltzmann equation. Therefore, this procedure is not valid within a gas discharge when ionization (or attachment) is important. Thomas and Thomas (1969) improved the model of Itoh and Musha (1960) by simulating the behavior of a great number of avalanches growing between plane-parallel electrodes.

The problem of the determination of the path length was drastically simplified by the use of the so-called "null collision technique," introduced by Skullerud (1968) in gaseous swarms. This

technique, described by Lin and Bardsley (1977), was used by Boardman et al. (1968) in solid state physics, and by Woodcock et al. (1965), Miller (1967), and Carter et al. (1972) in neutron transport physics. The null collision technique consists of introducing a fictitious collision, called a null collision, which does not change the electron velocity, and whose cross section is chosen so that the new collision frequency ν^1, including the null collision, remains constant along a free path. Equation (78) then becomes

$$\Delta t = \nu'^{-1} \text{ Log } \frac{1}{1 - r}$$

and the time interval between two successive collisions can therefore be obtained without any approximation or numerical integration. An extension of this null collision technique for the case of spatially varying electric fields is described later.

Tran Ngoc et al. (1977) dealt with the problem of swarm behavior in a nonuniform electric field with a one-dimensional Monte-Carlo simulation assuming only forward scattering. In spite of this drastic assumption, significant qualitative results were obtained. Since the electron trajectories between collisions are not simple for a nonuniform field, the equation of motion must be integrated generally. A method which avoids any numerical integration is presented later.

Description of the Method. The MC technique which will be described in this section simulates the steady state discharge produced by a continuous flux of electrons emitted at the cathode.

The simulation is not self-consistent (electrostatic field spatial variations are imposed). The basic hypotheses of the model are described earlier. These hypotheses are the same as those adopted in the Boltzmann approach except for the following points:

1) Elastic collision losses are taken into account in the MC approach, although neutral species are assumed to be at rest.

2) As in the Boltzmann approach, isotropic angular scattering is assumed (the elastic cross section replaced by the momentum transfer cross section), but some results will be presented for anisotropic scattering, which can easily be taken into account in a MC approach.

Under a nonuniform electrostatic field, the electron trajectories are not as simple as in the uniform field case, and the equations of motion must be integrated along the free path. In order to avoid these numerical integrations, which increase the computation time and introduce numerical errors, a method enabling the distribution functions for a steady state situation to be calculated without

any integration is described in the following section. The method of determining the random variables associated with a collision (position, nature, change of energy, and angular scattering) is also presented below where the notations defined earlier are used.

1) Distribution Functions: The simulation of a steady-state experiment should be carried out by following the motion of initial electrons continuously generated at the cathode for a time long enough to get stationary swarm properties. Since this method involves a very large computation time, another approach must be adopted.

Let us consider an avalanche started by one electron at the cathode at time t_o, and let $p(x,\varepsilon,\mu,t-t_o)$ be the probability density per unit time of finding an electron at time t in the element $\{(x,x+\Delta x), (\varepsilon,\varepsilon+\Delta x), (\mu,\mu+\Delta\mu)\}$ of phase space.

The steady-state distribution function $f(x,\varepsilon,\mu)$ can be obtained by adding the contributions of successive avalanches, started at different times t_o with t_o, varying continuously from $-\infty$ to the time t; i.e.:

$$f(x,\varepsilon,\mu) = \phi_{eo}\, S_c \int_{-\infty}^{t} p(x,\varepsilon,\mu,t-t_o)dt_o, \tag{79}$$

which is equivalent to:

$$f(x,\varepsilon,\mu) = \phi_{eo}\, S_c \int_{o}^{\infty} p(x,\varepsilon,\mu,\zeta)d\zeta, \tag{80}$$

where ϕ_{eo} is the electron flux at the cathode and S_c the area of its emission.

From the definition of $p(x,\varepsilon,\mu,\tau)$, the integral which appears on the right-hand side of Eq. (80) can be thought as the sum of the times spent by each of the electrons in crossing the unit volume around (x,ε,μ) in phase space.

This sum can be approximated by simulating the development of an avalanche started at the cathode by a great number N_o of electrons. The time $\Delta t_i(x,\varepsilon,\mu)$, during which the phase space coordinates of the i^{th} electron lie in the element $\{(x,x+\Delta x), (\varepsilon,\varepsilon+\Delta\varepsilon), (\mu,\mu+\Delta\mu)\}$, is recorded, and the distribution function is then given by:

$$f(x,\varepsilon,\mu) = \frac{\phi_{eo}\, S_c}{N_o} \sum_{i=1}^{M_i(N_o)} \frac{\Delta t_i(x,\varepsilon,\mu)}{\Delta x\, \Delta\varepsilon\, \Delta\mu}, \tag{81}$$

where M_i is the total number of electrons.

This method, which has been generally adopted (Sakai et al., 1972; Sakai et al., 1977; Lin and Bardsley, 1977) depends upon knowledge of the time variations of the phase space coordinates of the electrons and then an integration of the equations of motion. Because we are dealing with the case of nonuniform fields, this approach leads to numerical integrations. They can be avoided only by calculating the steady-state flux distribution function Φ.

Let $\Phi(x,\varepsilon,\mu)\ \Delta\varepsilon\ \Delta\mu\ \Delta t$ be the number of electrons crossing the plane x = const. during the time interval Δt in the element $\Delta\varepsilon \cdot \Delta\mu$ around (ε,μ). f is linked to Φ by:

$$f(x,\varepsilon,\mu) = \frac{\Phi(x,\varepsilon,\mu)}{v|\mu|} \quad . \tag{82}$$

It is easy to see that $\Phi(x,\varepsilon,\mu)$ can be approximated similarly by:

$$\Phi(x,\varepsilon,\mu) = \frac{\phi_{eo}\ S_c}{N_o} \sum_{i=1}^{M_i(N_o)} \frac{\Delta n_i(\varepsilon,\mu)}{\Delta\varepsilon\ \Delta\mu} \quad , \tag{83}$$

where $\Delta n_i(\varepsilon,\mu)$ is the number of times the i^{th} electron has crossed the plane x in $\Delta\varepsilon\ \Delta\mu$ around (ε,μ).

Clearly, the calculation of Φ is much simpler than that of f. Φ can be obtained simply by recording the total number of times that each plane x has been crossed by an electron of the avalanche in each cell $\{(\varepsilon,\varepsilon+\Delta\varepsilon),\ (\mu,\mu+\Delta\mu)\}$ of the space phase. Thus, no numerical integration of the motion equation is needed, and the distribution function f is deduced from Φ with the help of Eq. (82).

2) Determination of the Collisions Parameters. The gap length is divided into intervals $(x_i,\ x_i\ \Delta x)$, where Δx is a constant step of the order of magnitude of the mean free path. In each of these intervals, the spatial variations of the electrostatic field E is assumed to be linear. As mentioned later, the position and nature of the collisions and the velocity change during a collision are stochastically determined by the use of sequences of random numbers uniformly weighted on the interval (0,1).

The abscissa of a collision is generally deduced from a stochastic determination of the time interval between two collisions. This method involves the integration of the motion equations.

A simpler way is first to determine the variation of kinetic energy between two collisions by using the conservation laws (1) and (2). The abscissa of the next collision can be easily deduced from (1). Let ε_a be the kinetic energy just after a collision (at point x_a) or at a mesh point.

Using (2), Eq. (78) can be written:

$$\text{Log}\,\frac{1}{1-t} = \text{sg}\int_{\varepsilon_a}^{\varepsilon_c} \frac{N\,\sigma_T(\varepsilon)}{E(x)} \cdot \frac{\sqrt{\varepsilon}}{\sqrt{\varepsilon-\varepsilon^*}}\,d\varepsilon\ , \tag{84}$$

where sg = 1 if $\mu > 0$ and sg = -1 if $\mu < 0$.

Since the trajectory between collisions is situated in a plane parallel to the x axis, the following changes of variable have been used:

$$vdt = \frac{dx}{\mu(x)} = -\frac{d\varepsilon}{E(x)\mu(\varepsilon)} = \text{sg} \cdot \frac{d\varepsilon}{E(x)} \cdot \frac{\sqrt{\varepsilon}}{\sqrt{\varepsilon-\varepsilon^*}}\ . \tag{85}$$

ε_c may be deduced from Eq. (84). The use of a null collision technique drastically simplifies the calculation of ε_c and avoids any approximation or numerical integration.

Let M_i be an upper bound of:

$$\frac{N\,\sigma_T(\varepsilon)\sqrt{\varepsilon}}{E(x)} \tag{86}$$

in the interval $(x_i,\ x_i + \Delta x)$, and let us introduce a fictitious process which will be called a null collision; this process will be defined by the conditions:

a) The electron velocity does not change during a null collision.

b) The null collision cross section $\sigma_{null}(\varepsilon)$ is chosen such that:

$$\frac{N\,\sigma'_T(\varepsilon)\sqrt{\varepsilon}}{E(x)}\ , \tag{87}$$

where $\sigma'_T(\varepsilon) = \sigma_T(\varepsilon) + \sigma_{null}$, the new total cross section, remains constant and equal to M_i within the interval $(x_i, x_i, \Delta x)$.

Thus:

$$\sigma_{null}(\varepsilon) = M_i\,\frac{E(x)}{\sqrt{\varepsilon}} - \sigma_T(\varepsilon) \tag{88}$$

In the interval $(x_i, x_i+\Delta x)$, Eq. (84) becomes:

$$\text{Log}\,\frac{1}{1-r} = sq \cdot M_i \cdot 2\,\{(\varepsilon_c - \varepsilon^*)^{1/2} - (\varepsilon_a - \varepsilon^*)^{1/2}\}. \quad (89)$$

The kinetic energy ε_c just before the collision can then be deduced from Eq. (89) (if the collision does not occur in the interval $(x_i, x_i + \Delta x)$, i.e., if ε_c does not fall in the corresponding interval $\varepsilon_i(x_i)$, $\varepsilon_{i+1}(x_{i+1})$, a similar procedure is used in the following interval). Having determined ε_c, the abscissa x_c of the collision is given by Eq. (1). Since the field is assumed to vary linearly in each interval, x can be easily expressed as a function of ε.

The nature of the collision is determined by comparing the probability of occurrence of each type of collision with a random number uniformly weighted on (0,1). If a null collision occurs, the next collision is determined without any change in the electron velocity.

In the other cases, the scattering angle and repartition of energy are stochastically determined in agreement with the differential angular cross sections. In the case of ionization, the repartition of energy between the two emerging electrons is similarly obtained by the use of differential ionization cross sections.

Let us note that the expression (86) above is exactly equal to the parameter α_T used in the BE method.

ANALYSIS OF SOME NONEQUILIBRIUM SITUATIONS

The calculations described in this section have been made for helium at a pressure of 1 torr. The cross sections used come from Alkhazov (1970) for the total and differential ionization cross sections and from Labahn and Callaway (1970) for the elastic and excitation cross sections. Full details of these cross sections can be found in Boeuf (1981), Boeuf and Marode (1982).

In the following, whenever it is possible we shall compare the results of the BE and MC methods.

Results for the Case of a Constant Field

In the case of a constant field, the results will depend only on the ratio E/N (or E/P) and on the product N×L (P×L). We have usually chosen the values E/P = 100 V cm^{-1} $torr^{-1}$ (E/N = 282 Td) and P×L = 2 torr×cm so that an equilibrium regime can be attained between the electrodes. The speed distribution of the electrons

emitted by the cathode is flat and extends over the range 4 to 5 eV. Electrons are not emitted by the anode ($\eta_a(w,\mu) = 0$), but they can be reflected by it, with a reflection coefficient R_a introduced earlier.

The spatial variations of the reduced density of the electrons given by the BE calculations are plotted in Fig. 6. The density initially decreases in the neighborhood of the cathode because the current is constant. When the electrons have traveled a sufficiently long distance from the cathode, they can ionize the gas and, as a result, density may increase. However, it is seen that this behavior is modified by the anode and depends upon the value of the reflection coefficient. If $R_a = 0$, the anode is perfectly absorbing, and the density decreases. This decreasing electron density is due to the absence of back-scattered electrons, which implies a high mean energy near the anode. We can see that this effect is reduced when R_a is increased.

In Fig. 7 the variation of the electron density for different values of the product P×L is shown. It is clear that the form of the variation of electron density is not modified if the electrons are far enough away from the anode.

In Figs. 8 and 9, we have plotted the variation of the convective drift velocity and the mean energy of the electrons. The non-equilibrium regions near the cathode and the anode are clearly seen. In the neighborhood of the cathode, the two curves increase since the electrons gain energy from the electric field and then oscillate before reaching equilibrium values. (We note, however, that equilibrium is fully realized only for the drift velocity).

These oscillations are due to the relative numbers of high and low energy electrons in different parts of the discharge.

In the neighborhood of the anode, both the drift velocity and the mean energy increase in order to maintain the growth of the current near the anode (Sakai, 1972).

The spatial variation of α can be seen in Fig. 10. The three regions found in Figs. 8 and 9 exist here also. However, α is zero near the cathode and begins to grow only after the electrons have traveled a distance sufficient for their energy to be higher than the ionization threshold. The quasiequilibrium value of α which we obtain is in very good agreement with the latest experimental measurements of α in helium (Lakshminarasimha et. al. 1975).

We report that for all the above results very good agreement is obtained between the BE and MC computations. In the case of MC calculations, there is a little discrepency concerning the results obtained with isotropic or anisotropic angular differential cross sections.

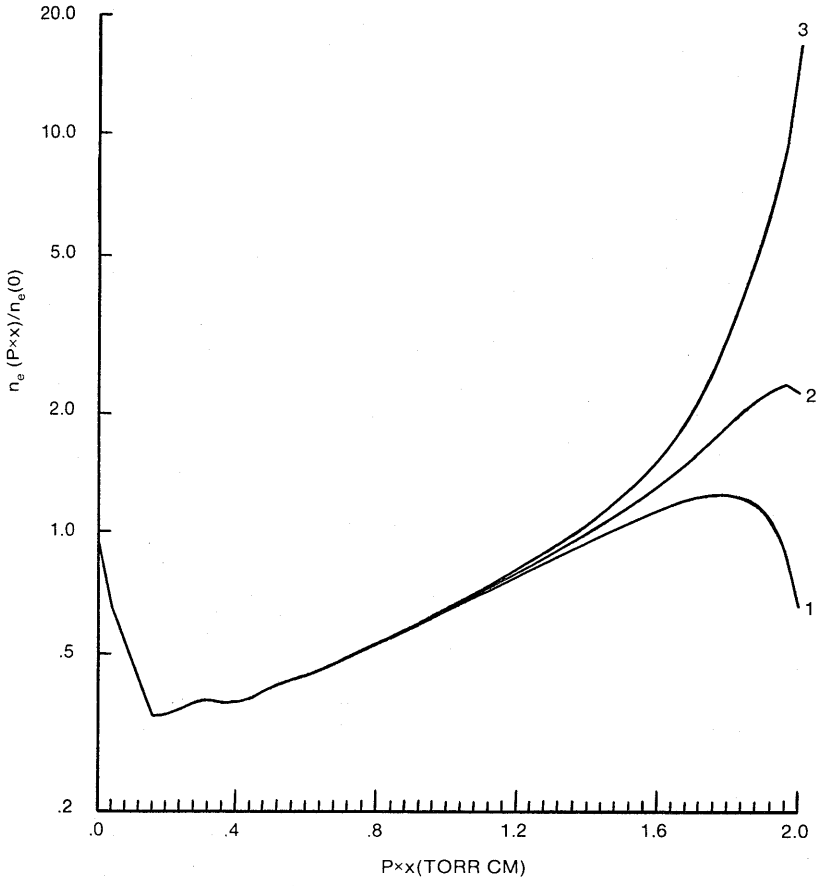

Fig. 6. Spatial variation of the reduced electron density for different values of the reflection coefficient at the anode E/P = 100 V cm^{-1} $torr^{-1}$ 1 - R_a = 0; 2 - R_a = 0.5; 3 - R_a = 0.99. BE calculations.

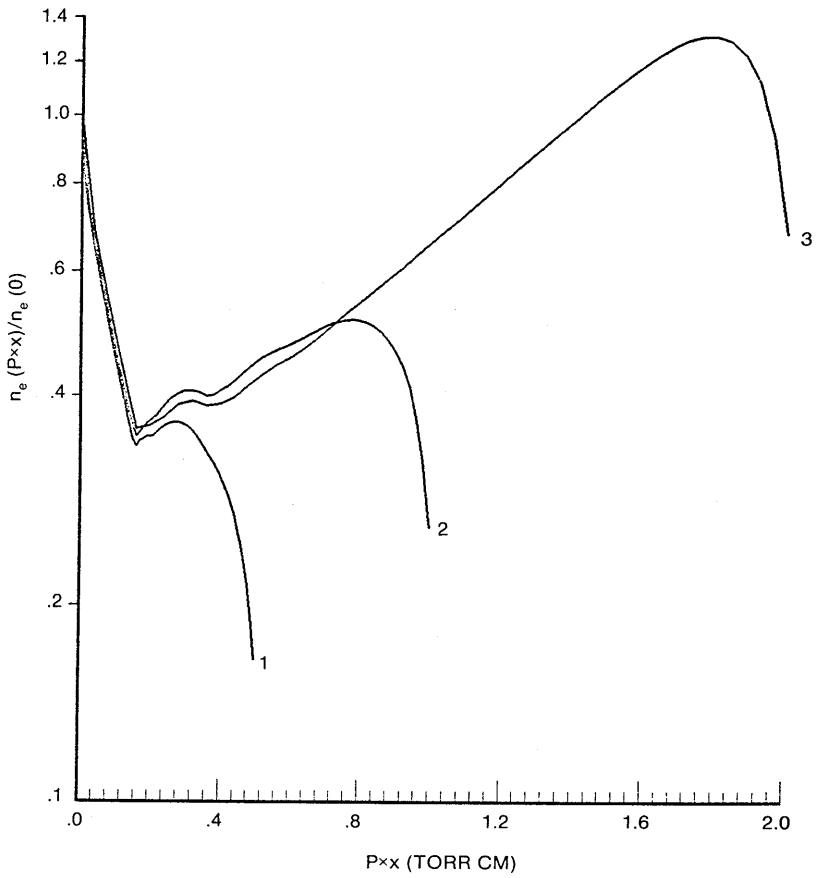

Fig. 7. Spatial variation of the reduced electron density for different values of the gap length. E/P = 100 V cm^{-1} $torr^{-1}$ 1 - P.L = 0.5 torr.cm; 2 - P.L = 1 torr.cm; 3 - P.L = 2 torr.cm. BE calculations.

The spatial variation of the normalized energy distribution function is shown in Fig. 11. It is clear that for points sufficiently distant from both electrodes, the normalized distribution function depends no more on the position, and equilibrium is almost attained (see Fig. 12). In the nonequilibrium region in the vicinity of the cathode, the distribution function is made up of several groups of high and low energy electrons coming from the combined action, on electrons emitted from the cathode, of the electric field and inelastic collisions (see Fig. 13).

In Fig. 14 the angular distribution function related to the energy distribution function given in Fig. 12 is shown. The anisotropy of electrons grows with energy in a monotonic way.

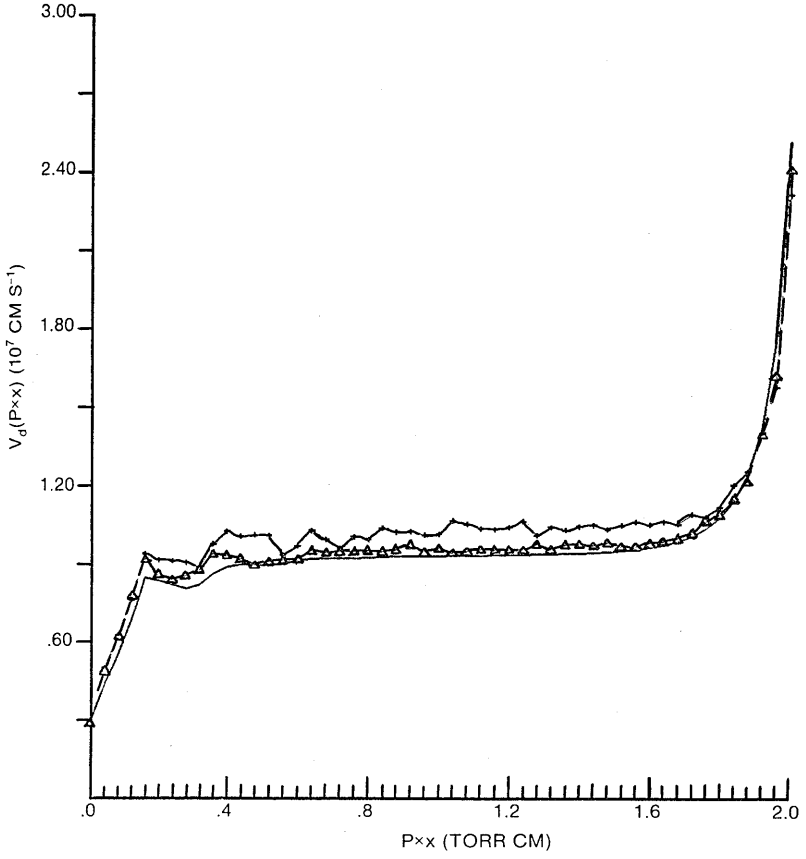

Fig. 8. Spatial variation of the convective drift velocity V_d. $\vec{V}_d = \int \vec{v} \frac{f(x, \vec{v})}{n_e} \underline{dv}$ E/P = 100 V.cm^{-1}.torr^{-1}; — BE calculations; +–+ MC simulations (anisotropic case); Δ_Δ MC simulations (isotropic case).

The total angular distribution function, defined by

$$f(x,\mu) = \int_o^\infty f(x,v,\mu)v^2 dv \ ,$$

is plotted in Fig. 15. The evolution in space of the anisotropy of electrons must be related to the spatial variation of the drift velocity (Fig. 8). For example, we see that electrons are directed forward at the anode corresponding to the growth of the drift velocity.

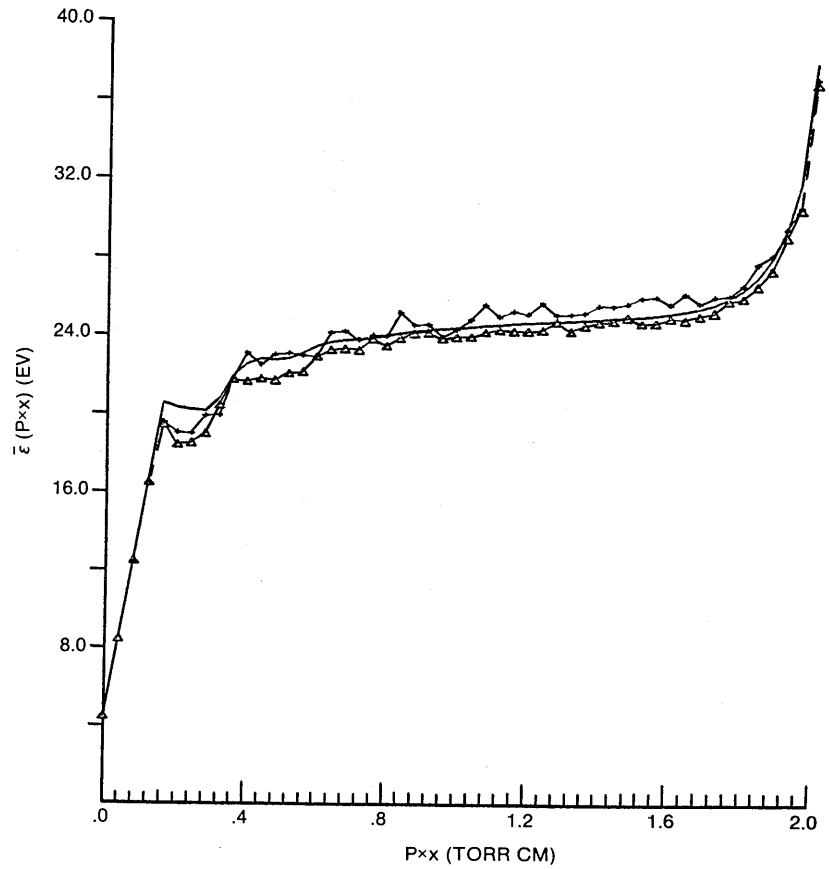

Fig. 9. Spatial variation of the electron mean energy. E/P = 100 V.cm^{-1} torr^{-1}. Notations same as in Fig. 8.

Results in the Case of a Spatially Varying Field

The results which will be discussed in this section are related to the field distribution shown in Fig. 16. This field distribution roughly approaches the case of a normal glow discharge in helium (Davies, 1981). The values of the voltage V, the product P×L, the length of the negative glow L_g, and the field in the negative glow E_g, used in the calculations are given in the caption to Fig. 16.

In Fig. 17, which gives the spatial variation of the reduced density, we may see that the form of the density variation in the case of the constant field is roughly maintained with a decreasing part near the cathode, followed by an increasing one and another decreasing one near the anode. However, this last decreasing part is much more pronounced than for the constant-field case.

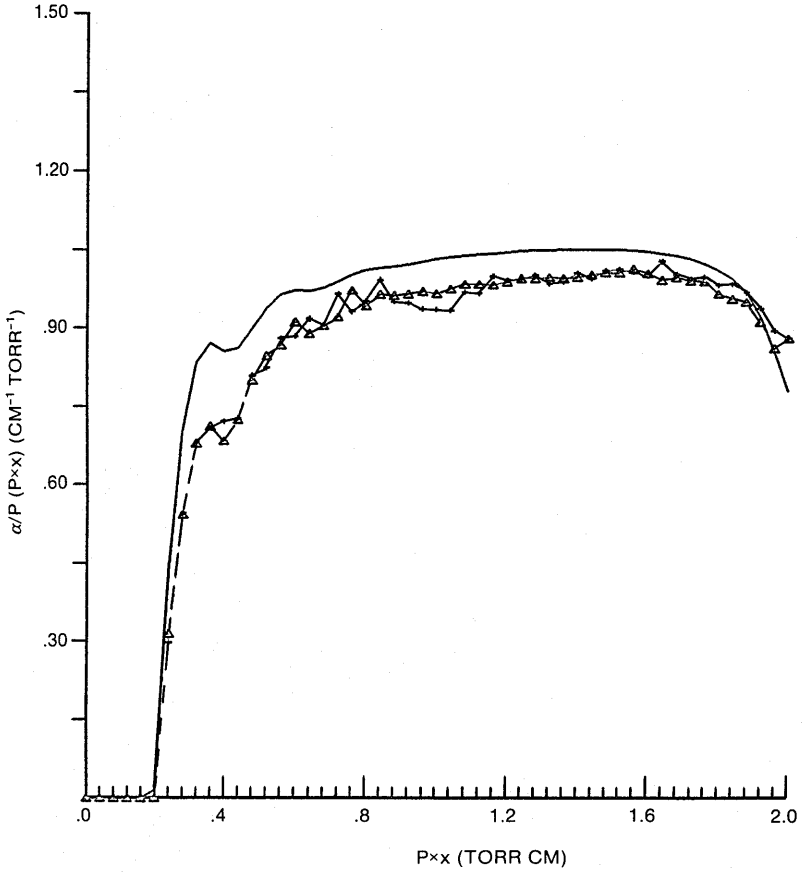

Fig. 10. Spatial variation of the Townsend Ionization Coefficient. $E/P = 100\ V.cm^{-1}\ torr^{-1}$. Notations same as in Fig. 8.

The form of the convective drift velocities and the mean energies are now very different, (Figs. 18 and 19), and equilibrium is not reached. A maximum in the two curves can be seen near the cathode, which is clearly related to the position corresponding roughly to the maximum of the ratio $E/N \times \bar{\nu}_T^{-1}$, where $\bar{\nu}_T$ is the mean value of ν_T and depends on position. It is clear that a maximum in $E/N\ \bar{\nu}_T^{-1}$ can be obtained when the acceleration of the electrons by the electric field and the losses of energy by the collisions have optimal values: the action of the field must not be too low and the losses of energy by collisions not too strong. These two curves decrease with the field until the negative glow is reached; then they grow again in the neighborhood of the anode in the same way as in the constant field.

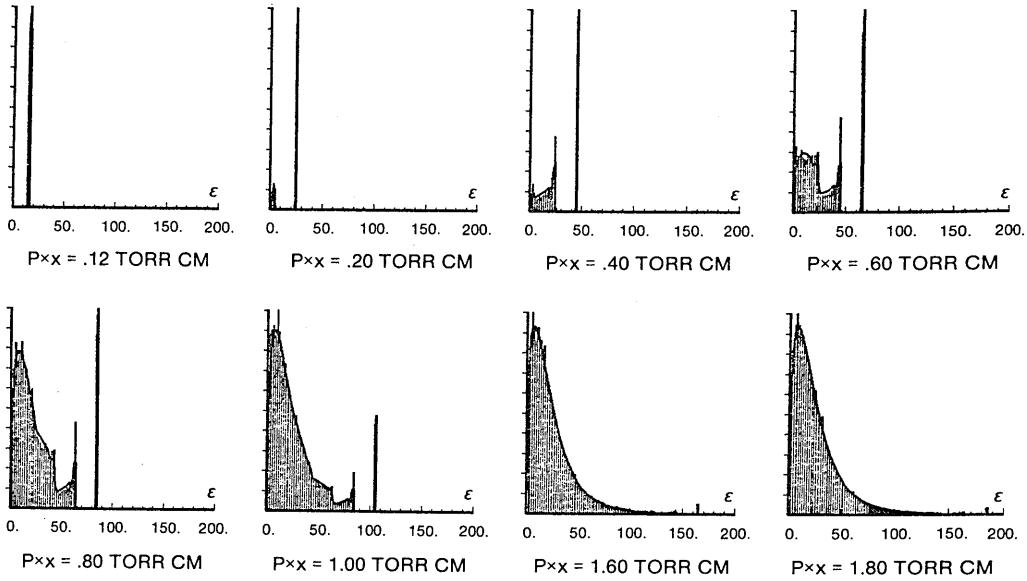

Fig. 11. Electron energy distribution functions for different values of the position. E/P = 100 V.cm^{-1} torr^{-1}. —— BE calculations; histograms, MC simulations. The curves are not normalized and the electron energies are expressed in eV.

The variation of α with position is shown in Fig. 20, where increasing and decreasing regions can again be seen. The same variation of α is found in the next section from the Memory Factor model and a comparison is also made with the MC simulations.

The MC or BE calculations allow us to obtain also the spatial variation of the rate of production of excited species (Fig. 21). In this way, we are able to calculate the spatial variation of the light emitted from the cathode region. We have chosen the 5.016 nm (green) line of helium, known to be one of the most intensive lines in such situations. Calculations have been made by solving a kinetic scheme taking into account the populating and depopulating of level 3^1P by upper and lower levels (Yousfi, 1980). We see that the variation of the light emission from the 5.016 nm line (Fig. 22) has globally the same form as α (Fig. 20), but the maximum of the light emitted is shifted towards the negative glow. This result shows, in fact, that the negative glow begins slightly before the minimum of the field is reached.

Figures 23 and 24 show the variation of the energy distribution functions obtained by the MC method. In Fig. 24, the overall structure of the cathode region is clearly seen with high energy electrons in the neighborhood of the cathode and low energy electrons

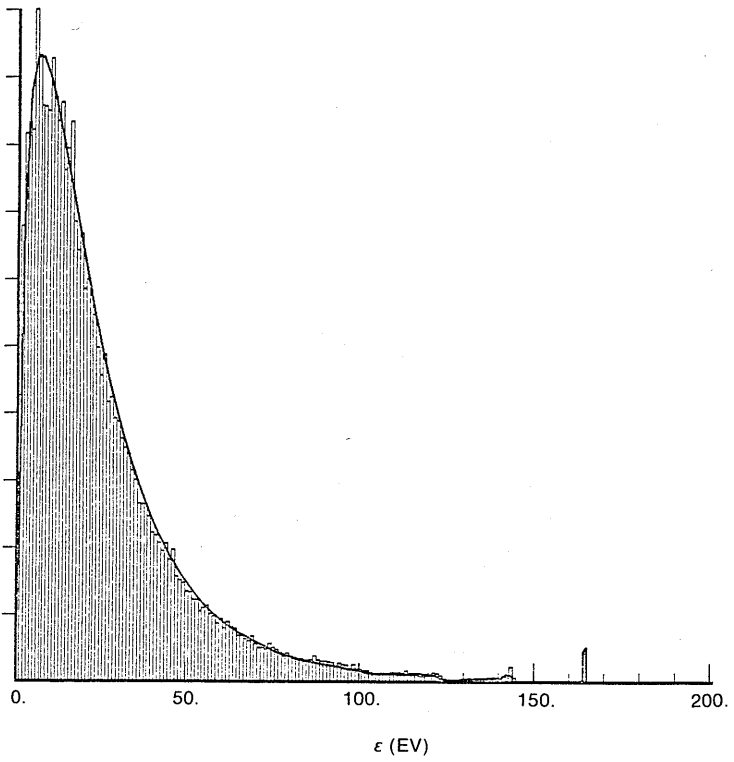

Fig. 12. Electron energy distribution function close to equilibrium for P_x = 1.8 torr.cm. E/P = 100 V.cm^{-1}. torr^{-1}, BE calculations; histograms, MC simulations. Arbitrary units.

at the anode. The angular distribution function is plotted in Fig. 25 and Fig. 26 for two different values of the position. In the first case, for P×x = 0.57 cm torr, a discontinuity in the angular variation of the distribution is seen in the high energy part. This discontinuity is due to the presence of electrons emitted from the cathode. In the same way with constant-field, the angular distribution is more isotropic at low energy.

Last, we note that the results obtained in this section with BE and MC methods are not so close as in the constant-field case. However, the general forms are similar.

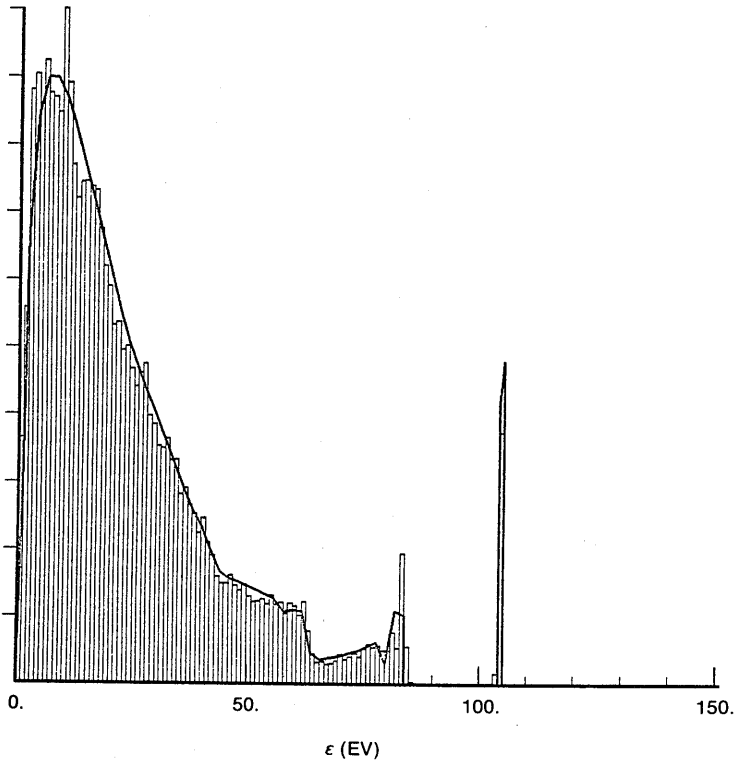

Fig. 13. Electron energy distribution function far from equilibrium for Px = 1 torr.cm. E/P = 100 V.cm^{-1}. torr^{-1}, BE calculations; histograms, MC simulations. Arbitrary units.

A MACROSCOPIC SIMULATION MODEL FOR THE NONEQUILIBRIUM REGIME

Introduction

The macroscopic simulation studies of discharge development (see, for example, Ward, 1962 or Davies, 1981) are based on the use of macroscopic ionization and transport parameters, such as the Townsend Primary Ionization Coefficient, α, and the electron and ion drift velocities, deduced from experimental or theoretical studies of electron or ion swarms in equilibrium. In regions, such as the cathode-fall or in the vicinity of a microprotusion, the spatial variation of the macroscopic coefficients cannot be simply taken from the equilibrium results (Tran Ngoc et al., 1977; Long, 1979). In addition, even though the field is low in the negative glow region, it is not possible to use equilibrium values for the ionization coefficients and drift velocities because, as we have already mentioned, there are many high-energy electrons produced in the cathode fall which reach the negative glow region and give

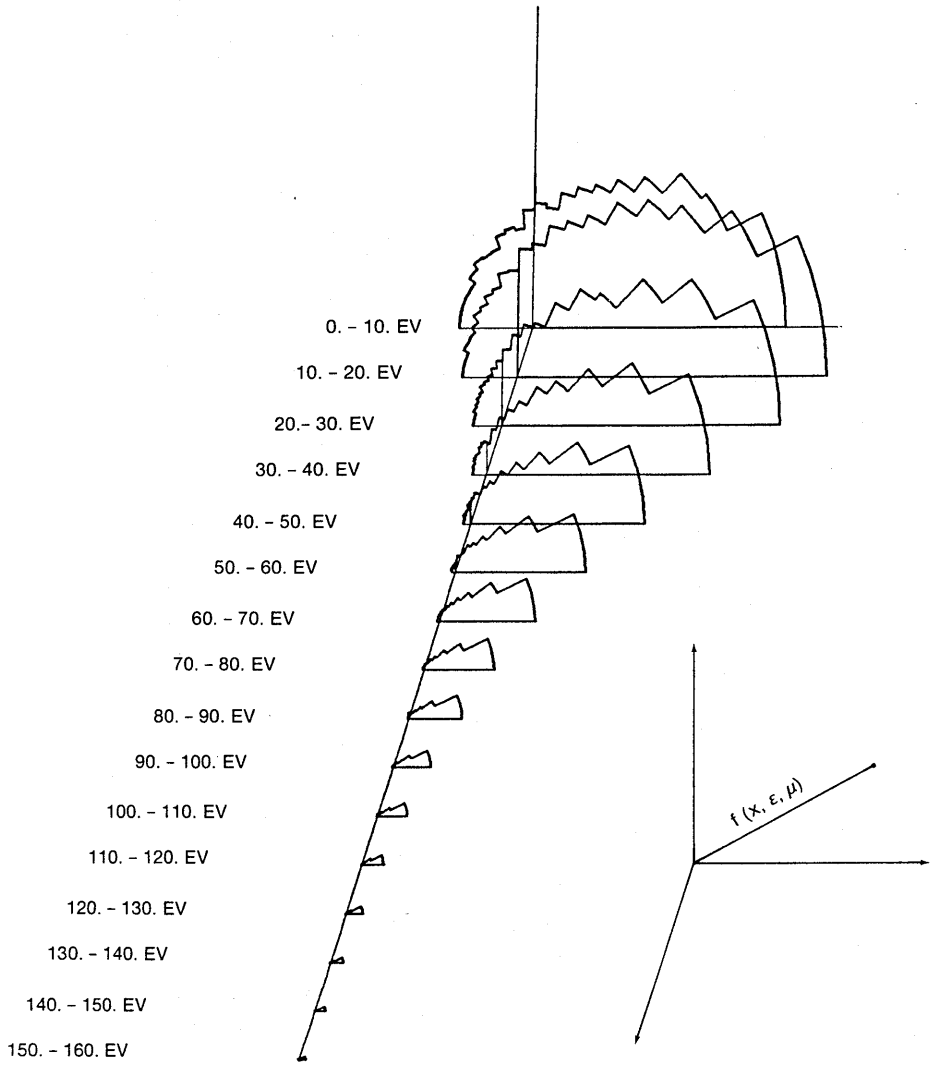

Fig. 14. Angular electron distribution functions for different values of the energy. E/P = 100 V.cm^{-1}. torr^{-1}. Px = 1.8 torr.cm. MC simulations. Arbitrary units.

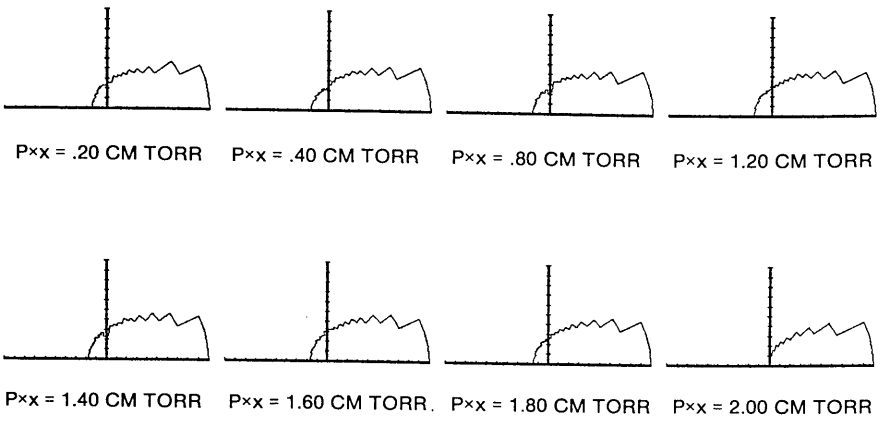

Fig. 15. Total angular distribution functions for different values of the position. E/P = 100 V.cm^{-1}, torr^{-1}. MC simulations (the curves are not normalized).

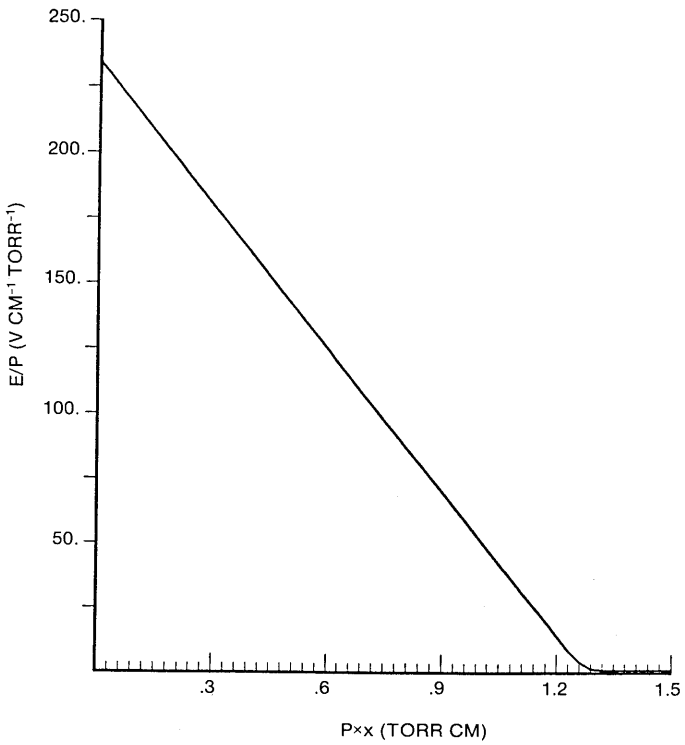

Fig. 16. Spatial variation of the electric field which has been assumed in the cathode region of a glow discharge. V = 150 volts; P L = 1.5 torr.cm; Eg = 1 volt.torr^{-1}.cm^{-1}; P Lg = 0.2 torr. cm.

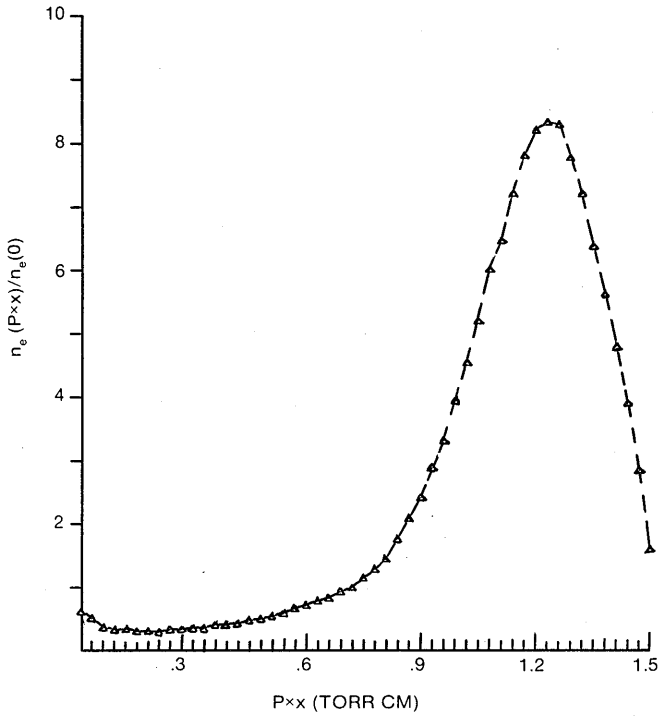

Fig. 17. Spatial variation of the reduced electron density in the cathode region. MC simulations.

effective ionization coefficients and drift velocities much greater than those expected from equilibrium studies.

In a nonequilibrium situation, the Primary Townsend Coefficient, $\alpha(x)$, at a point between the electrodes is not dependent uniquely on the local value of the electric field but on the entire distribution of the electric field between the cathode and the point under consideration. In the following we present a tentative method for modifying the macroscopic simulation method to allow for the "memory" which an electron will have for the field distribution that it has encountered during its motion. Also, we will make a comparison between the predictions of this method and the results of the Monte-Carlo calculations in helium described earlier.

Equilibrium Waves of the Primary Ionization Coefficient

In the case of equilibrium, the value of the Townsend Primary Ionization Coefficient in the rare gases may be related to the electric field (over a restricted range) by an expression of the form

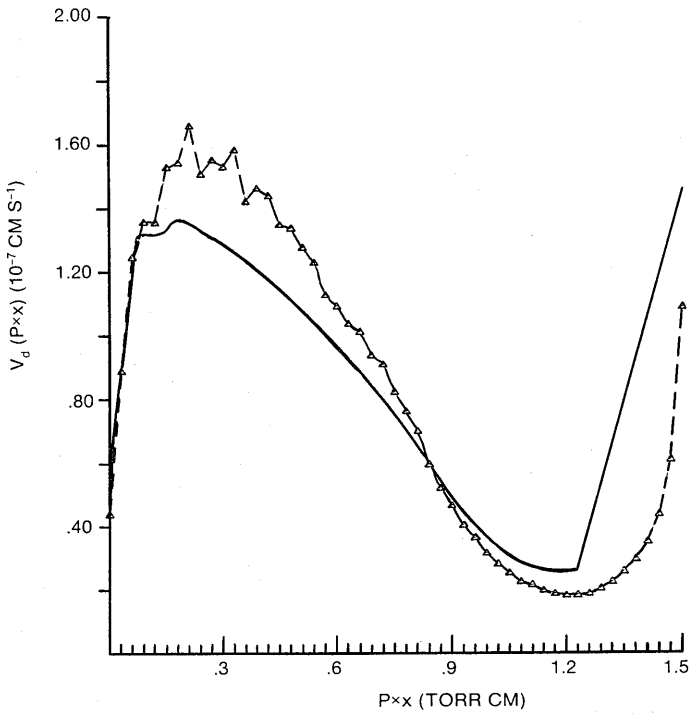

Fig. 18. Spatial variation of the convective drift velocity in the cathode region. ___, BE calculations; Δ__Δ MC simulations.

$$\alpha(E/P) = APexp(-B/(E/P)^r). \qquad (90)$$

In the case of helium, many different values of the coefficients A and B have been proposed by different authors with r generally taken to be 1/2. Ward (1962) has proposed the following values of A and B (E is expressed in $V.cm^{-1}$ and P in torr):

$$A = 4.4 \qquad B = 14.0 .$$

The experimental results of Chanin and Rork (1964) are well represented by Eq. (90) for

$$A = 6.5 \quad \text{and} \quad B = 16.4$$

Last, the results of Lakshminarasimha and Lucas (1975) can be approximated by

$$A = 3.2 \quad \text{and} \quad B = 12.9 \quad \text{for} \quad 20 < E/p < 80.$$

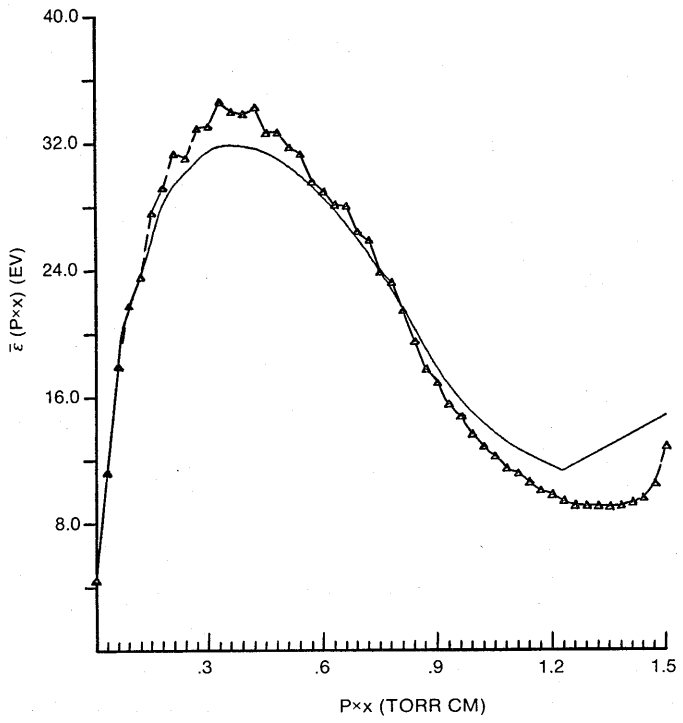

Fig. 19. Spatial variation of the electron mean energy in the cathode region. ___, BE calculations; Δ__Δ MC simulations.

We note, equally, that Badareu (1965) proposes the values r = 1, with

A = 3 and B = 34.

On the other hand, the results obtained for a uniform field by the Monte-Carlo method described earlier lead to an expression of the type (90), with r = 1/2 and

A = 3.6 and B = 12.9 for $20 < E/p < 200$;

it thus agrees best with the recent results of Lakshminarasimha and Lucas (1975).

For values of E/p greater than 200 $V.cm^{-1}.torr^{-1}$ it seems that, given both the Monte-Carlo and Boltzmann results, an equilibrium distribution does not exist and that $\alpha(E/p)$ will attain a steady-state value less than that given by expression (90) with A = 3.6

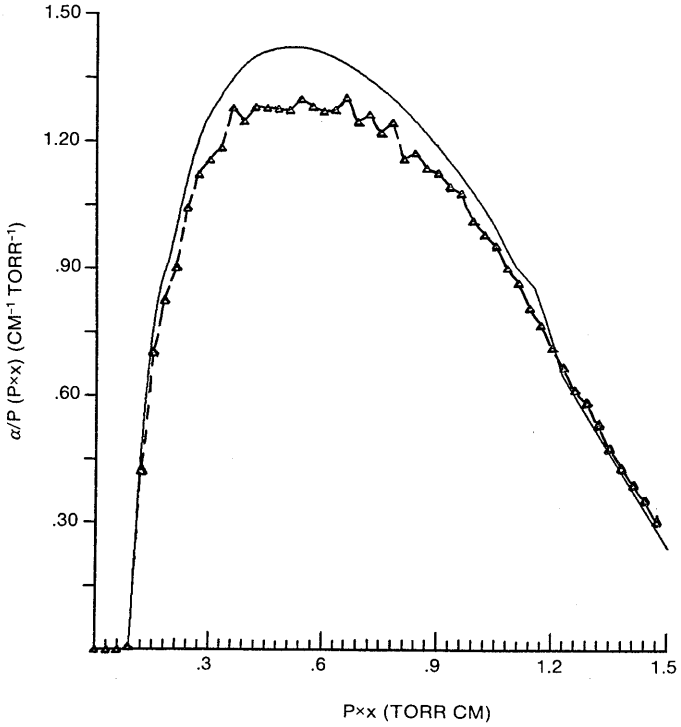

Fig. 20. Spatial variation of the Townsend Ionization Coefficient in the cathode region. ___, BE calculations; Δ__Δ MC simulations.

and B = 12.9. In the following we have limited our attention to the domain 20 < E/p < 200, with A and B equal to these values.

The Nonequilibrium Regime. The Memory Factor

As we have mentioned, the aim of this study is to take into account the "memory" that an electron has of the field distribution it has traversed during its motion. We attempt to describe the spatial variation of α in a nonequilibrium situation by an expression still of the form (90) but with the local value E of the field replaced by an effective field $E_{eff}(x)$ which takes into account the variation of the actual field in the interval (0,x) through an expression of the form

$$E_{eff} = \int_0^x E(y)\Phi(x-y)dy. \qquad (91)$$

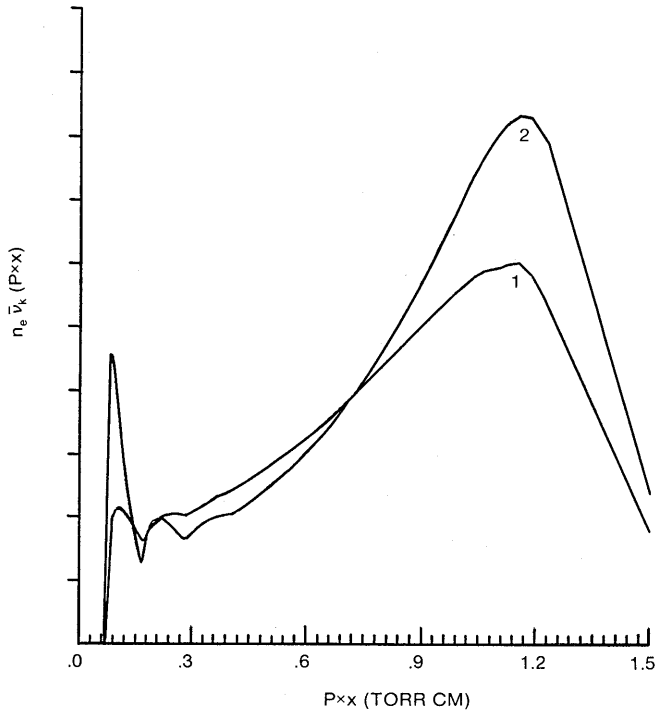

Fig. 21. Rate of production of metastable species in the cathode region. BE calculations. 1 - excitation of the 2^3S state; 2 - excitation of the 2^1S state. Arbitrary units.

Here the function Φ satisfies the condition

$$\lim_{x\to\infty} \int_0^x \Phi(x-y)dy = 1, \qquad (92)$$

which ensures that, for the case of a constant uniform field E,

$$\lim_{x\to\infty} E_{eff} = E.$$

The form of the "Memory Factor" function Φ has been determined from greatly simplified physical considerations, and a great number of the Monte-Carlo simulations have permitted the determination of an analytic optimum expression for Φ giving values of $\alpha(x)$, calculated with the aid of (90) and (91), which give best agreement with the Monte-Carlo Results.

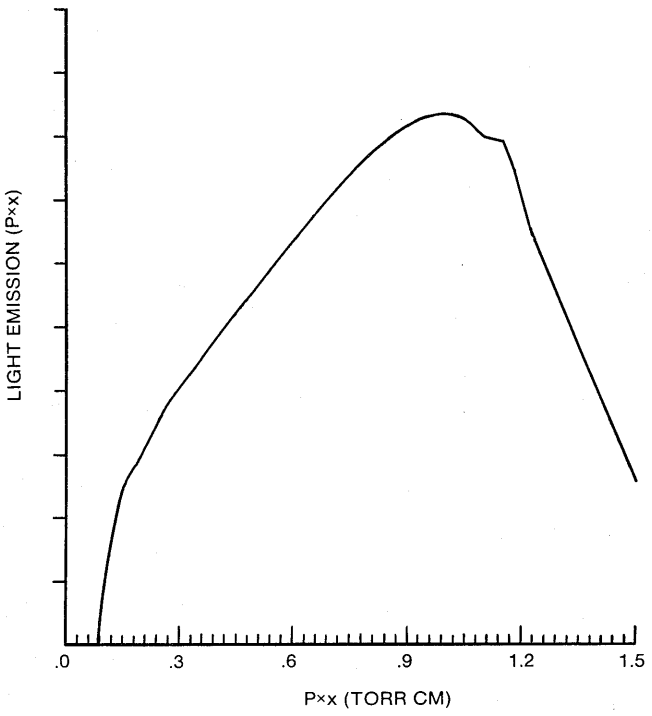

Fig. 22. Spatial variation of the light emission from the 5.016 nm green line of Helium. BE calculations. Arbitrary units.

The function Φ must first increase and then decrease; in effect, the rising part of the curve will correspond to the time-lag effect where electrons do not respond immediately to any field change. The decaying part of the curve represents the diminishing memory that an electron has of the field at a point the further away it is from that point. In practice the expression,

$$\Phi(x) = \frac{\lambda}{2} e^{-x/\lambda}(1 - e^{-x/\lambda}), \tag{93}$$

gives good agreement between the values of $\alpha(x)$ calculated by the Monte-Carlo method and the values deduced using the concept of an effective field. These results are summarized in the following section.

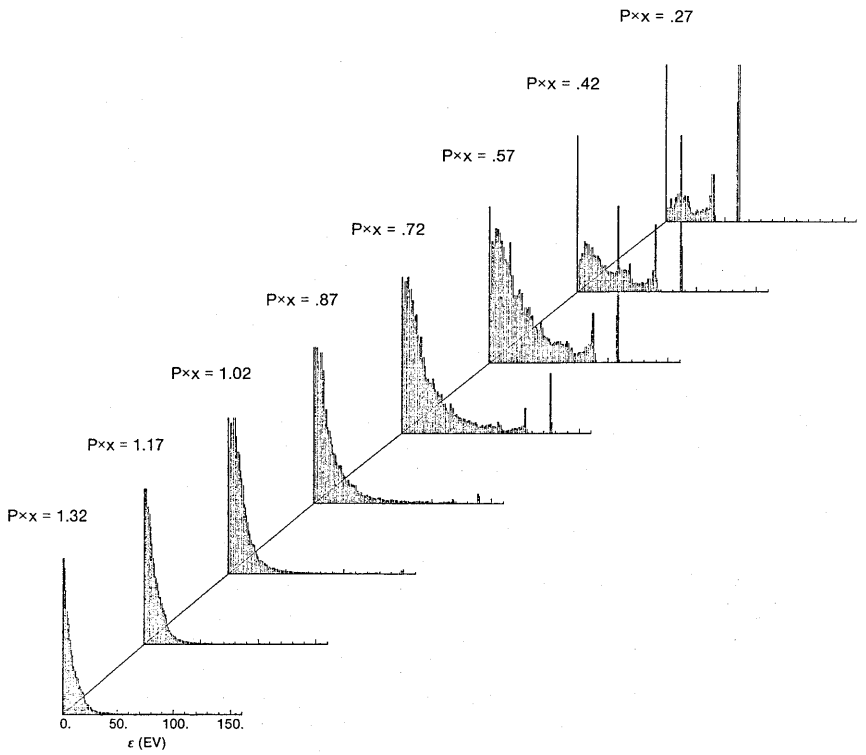

Fig. 23. Electron energy distribution functions for different values of the position in the cathode region. MC simulations (the curves are not normalized).

Comparison of the Memory Factor Model with the Monte-Carlo Simulations

In order to test the Memory Factor model, a comparison was made between the predictions of this model and the results of the Monte-Carlo simulations for the case of helium at a pressure of 1 torr. Good agreement was obtained between the two methods, provided the parameter λ in Eq. (93) was given the value 0.15 cm.

Figure 27 compares the values of the primary ionization coefficient for the case of a constant electric field E of 150 V cm^{-1}. We see that the values of α are in good agreement (tending to the same steady-state value at large Px), except in the initial transition region near the cathode where the Monte-Carlo calculations show that no ionizations can occur until the electrons have attained

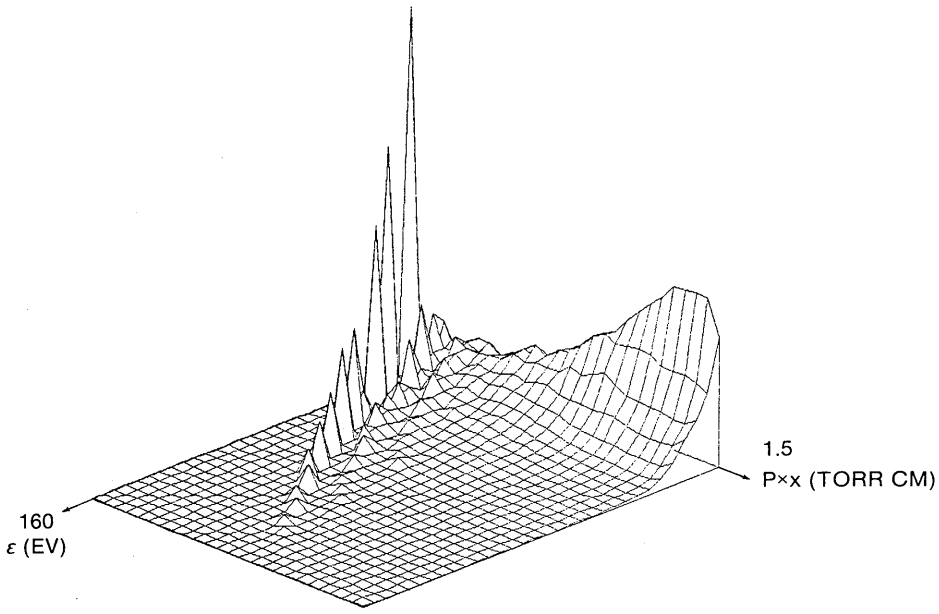

Fig. 24. Variation of the energy distribution function in the cathode region. Arbitrary units.

at least the ionization threshold. The Memory Factor model is at present being modified to take into account this initial transition effect. In the MC computations, the electrons were assumed to leave the cathode (x = 0) with an initial energy of 5 eV. Figure 27 also shows the effective field calculated from Eq. (91).

Figure 28 shows the corresponding results for a constant field of 100 V cm^{-1}, and, once again, we see, that there is good agreement, except in the initial transition region. We also see that the Boltzmann calculations agree well with both the MC and Memory Factor models.

In the study of the cathode-fall region of a discharge, it has been found that, for helium at 1 torr and a current density of order 0.1 mA cm^{-2}, the field distribution in the neighborhood of the cathode is approximately linear, falling from a cathode field in the range 150- 200 V cm^{-1} to practically zero at a distance of about 2 cm from the cathode (see Warren, 1955). Figure 29 shows such a field distribution together with the computed effective field, while Fig. 30 compares the values of α obtained using the MC and Memory Factor methods. Once again, excellent agreement is obtained.

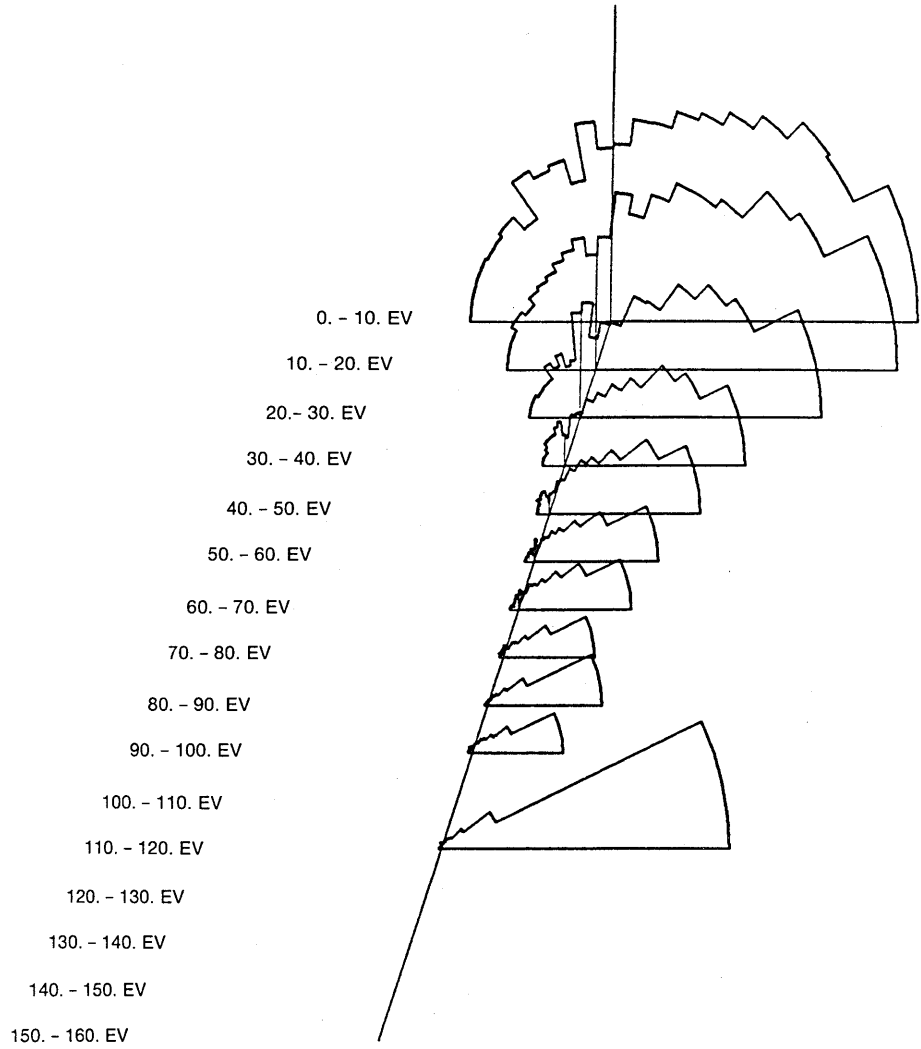

Fig. 25. Angular electron distribution functions for different values of the energy in the cathode region. MC simulations. Px = 0.57 torr. cm. Arbitrary units.

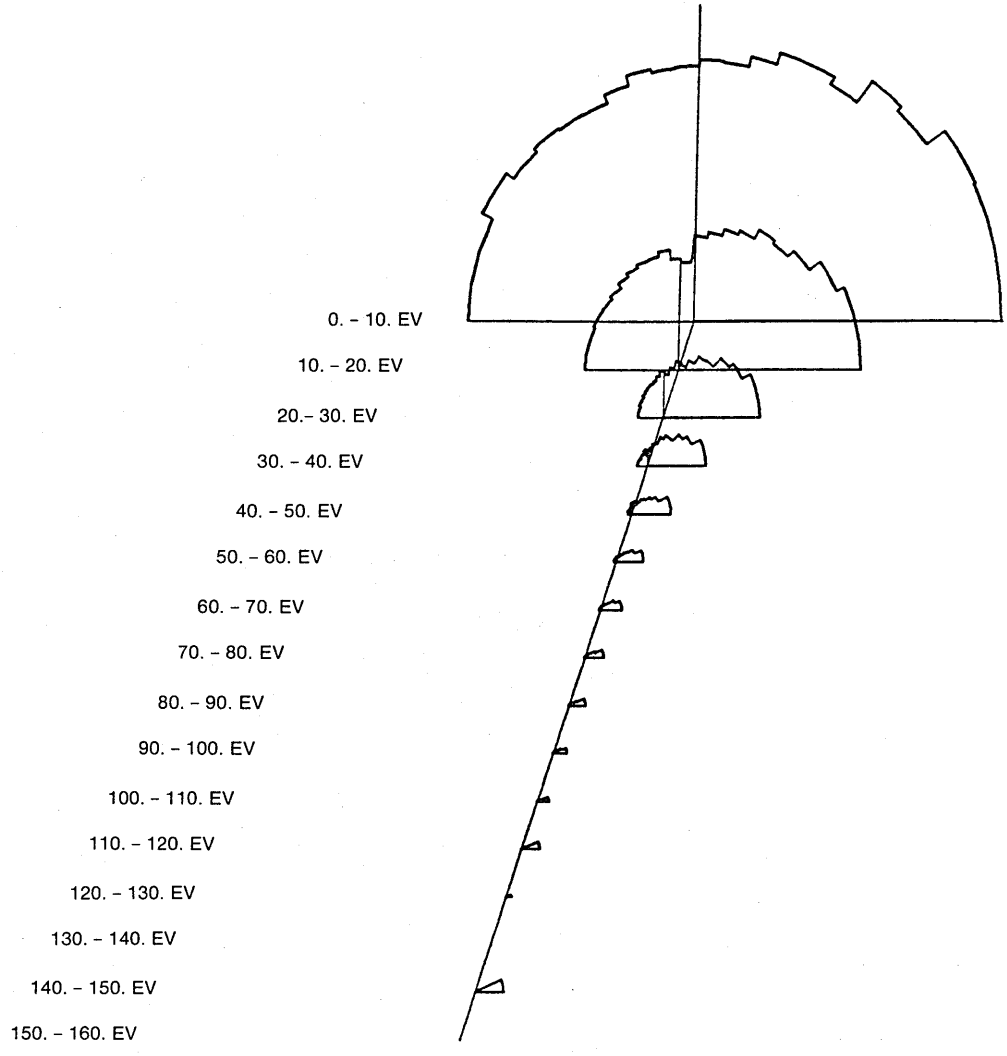

Fig. 26. Angular electron distribution functions for different values of the energy in the cathode region. MC simulations. Px = 0.87 torr.cm. Arbitrary units.

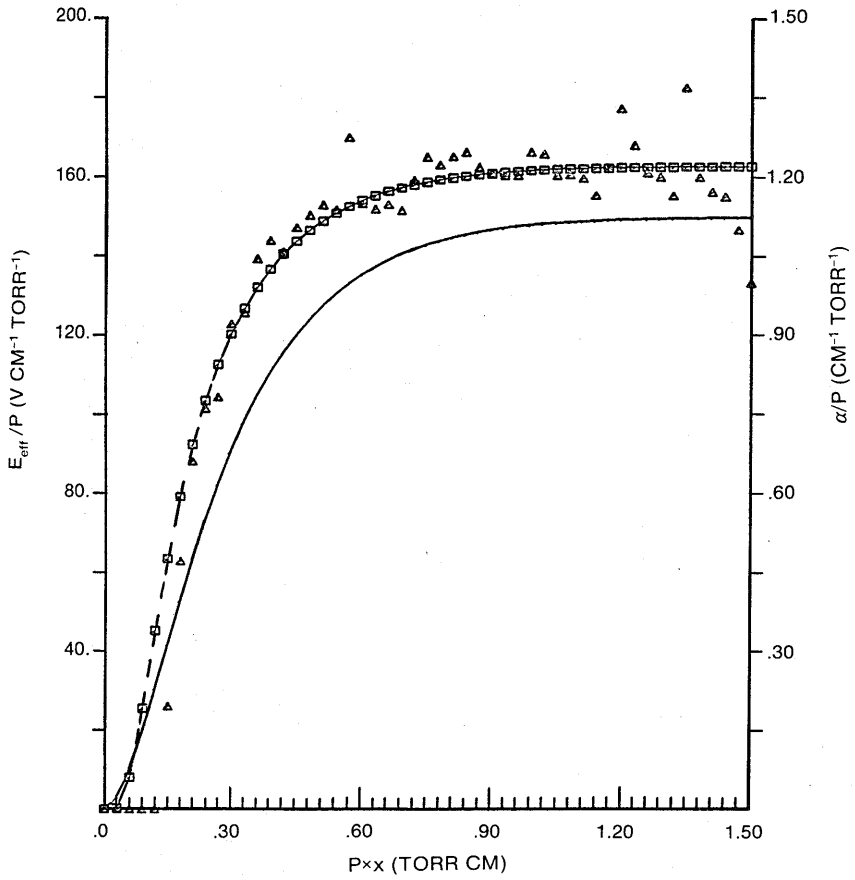

Fig. 27. Spatial variation of the effective field and of the Townsend Ionization Coefficient. Δ__Δ MC simulations; ___ Memory Factor model. E/P = 150 V.cm^{-1} torr^{-1}; P L = 1.5 torr.cm. ___ Eff/p.

It is hoped that the Memory Factor model will be valid at any point in the discharge space where there is a quickly varying field and not only in the cathode-fall region. In order to test this, the calculations were repeated for the cyclically varying field shown in Fig. 31 where we have also plotted the effective field E_{eff}. Figure 32 shows the corresponding values of the primary ionization coefficient, and we see that, even in this extreme case, the Memory Factor model successfully predicts values that closely follow the cyclically varying values found in the MC simulations.

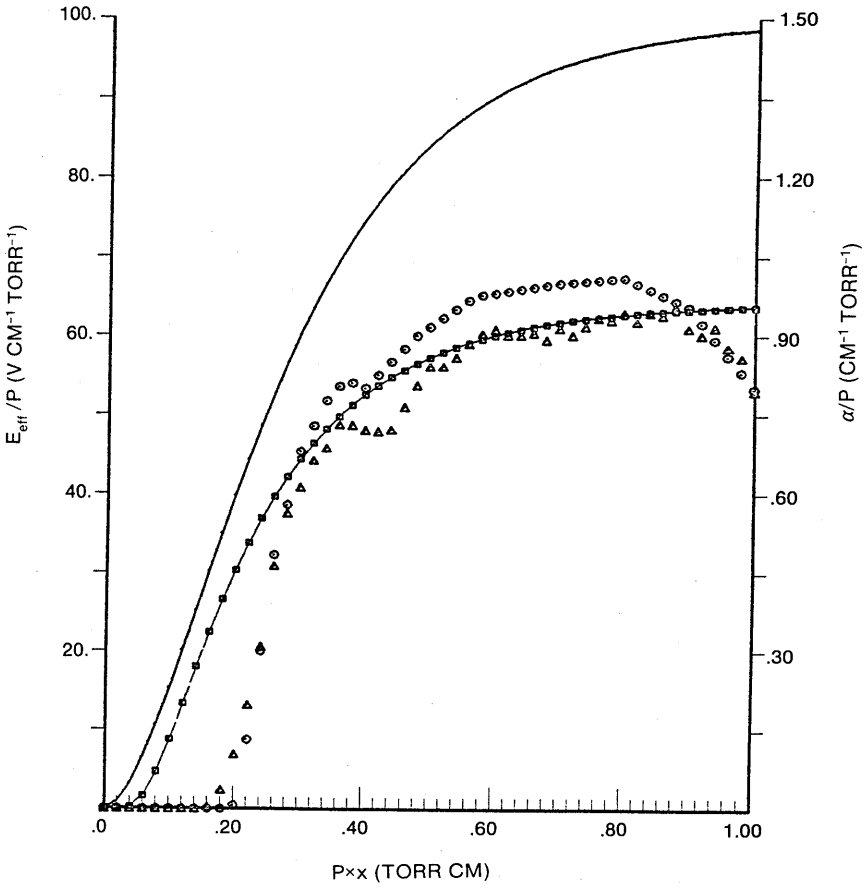

Fig. 28. Spatial variation of the effective field and of the Townsend Ionization Coefficient. Δ__Δ MC simulations; o__o, BE calculations; □__□ Memory Factor model. E/P = 100 V. cm^{-1} torr^{-1}; P L = 1 torr.cm. ___ E_{eff}/p.

At the present time, the Memory Factor model is being incorporated into a macroscopic simulation method (Davies et al., 1980) used to analyze the experimental measurements of cathode-fall characteristics made in helium by Warren (1955), and it is hoped that the results of this analysis will be published shortly (Boeuf et al., 1982).

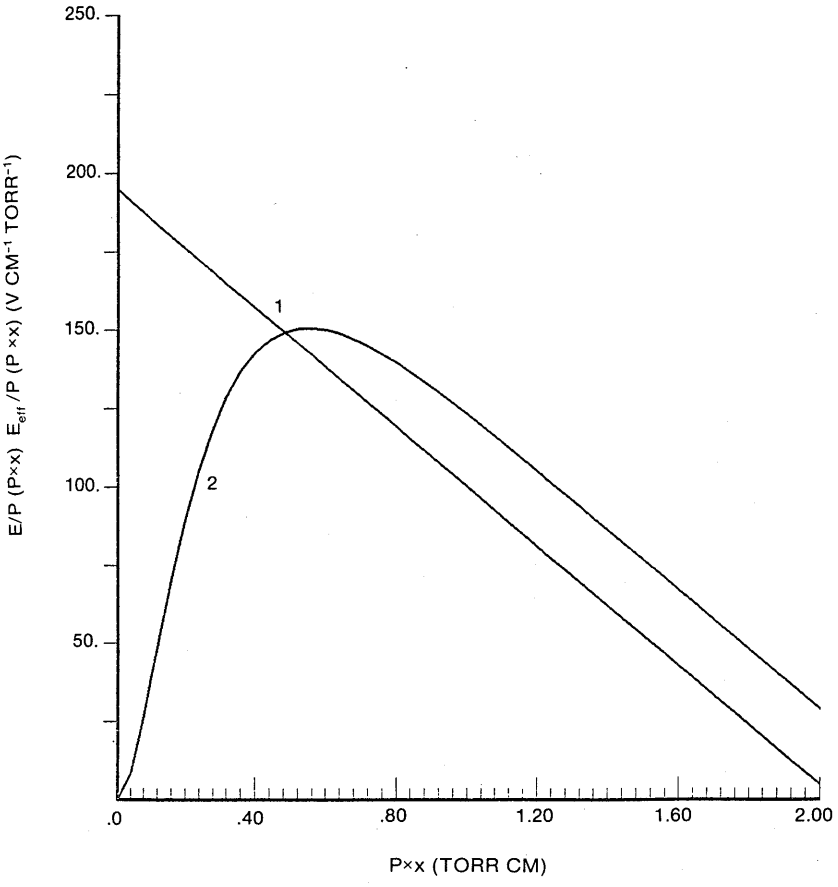

Fig. 29. Linear-decreasing field and the corresponding spatial variation of the effective field E_{eff}. P L = 2 torr.cm. 1 - E/P(Px); 2 - E_{eff}/P (Px).

CONCLUSIONS

In the present work, we have described the main principles of the techniques that may be used to undertake a microscopic study of the nonequilibrium regime. We have also given a number of results which characterize the behavior of the electrons in the case of a steady-state discharge in helium. In addition, we have laid the foundation for a new macroscopic theory adapted for the study of nonequilibrium situations and have compared the results obtained in this case with the Monte-Carlo microscopic studies.

In the case of a constant electric field, microscopic studies show that there are two nonequilibrium regions (near the cathode

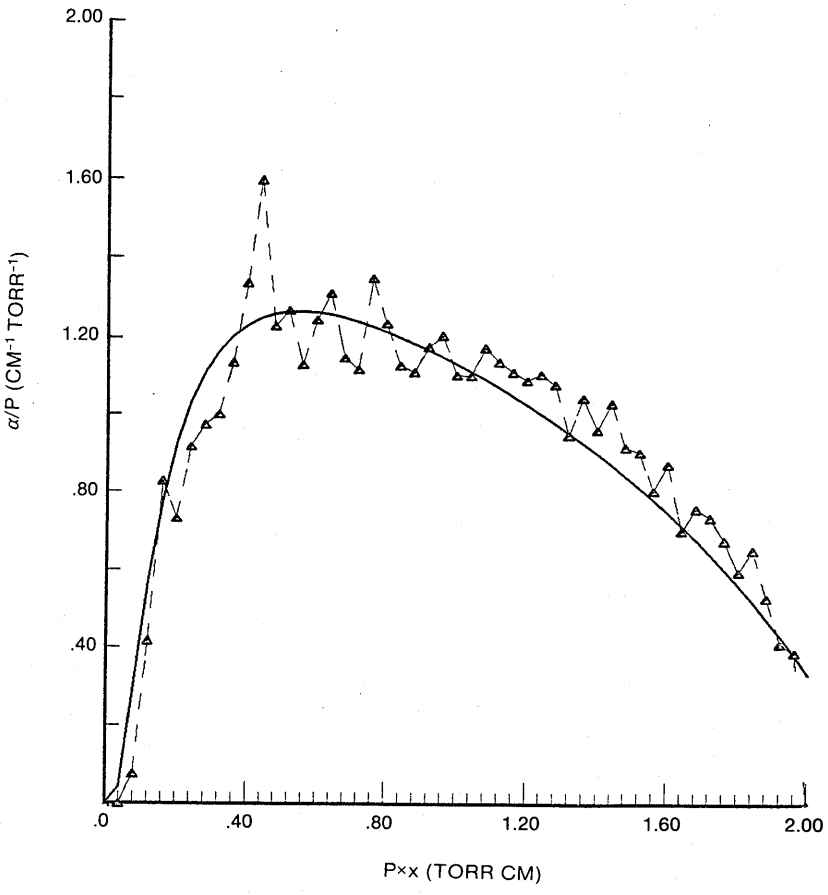

Fig. 30. Spatial variation of the Townsend Ionization Coefficient related to the field given in Fig. 29. Δ__Δ, MC simulations; ___ Memory Factor model.

and anode, respectively), as well as a region where the electrons are in equilibrium with the field, and the macroscopic parameters are constant. It is clear that the ability to ascertain whether an equilibrium zone exists and to determine, for a given transport parameter and a given gas, the distance over which this parameter is constant, is of great importance in the interpretation of swarm experiments. For example, in helium it seems that, for values of E/P greater than or of the order of 200 V cm^{-1} $torr^{-1}$, the ionization coefficient increases indefinitely with distance, and no equilibrium region is established.

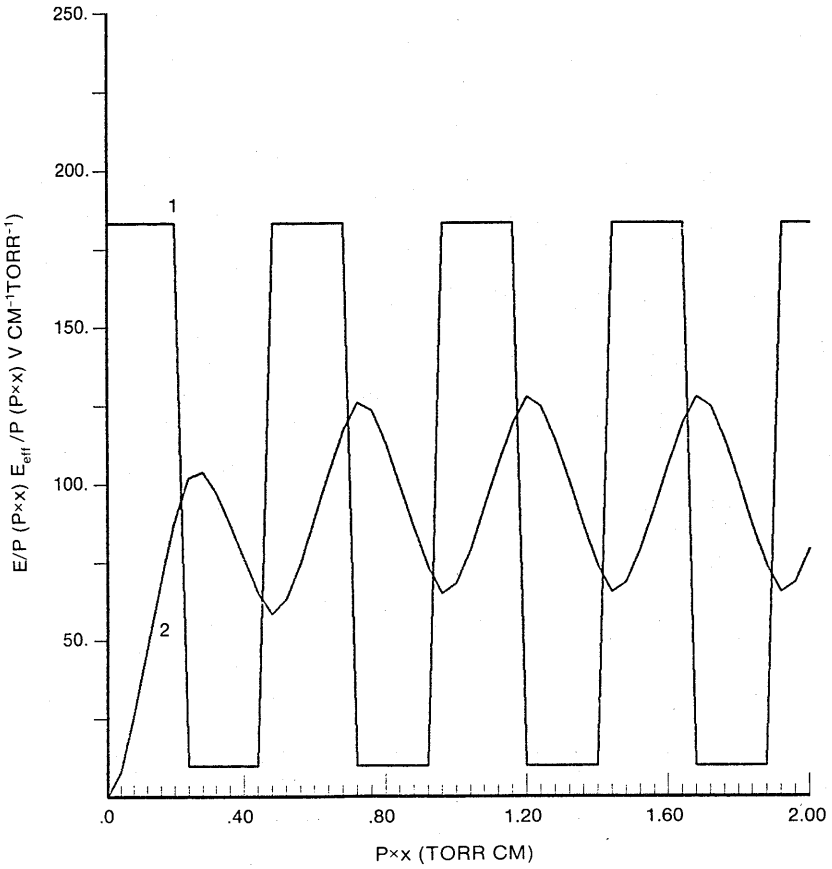

Fig. 31. Cyclically varying electric field and the corresponding spatial variation of the effective field E_{eff}. P L = 2 torr.cm. 1 - E/P (Px); 2 - E_{eff}/P (Px).

The results obtained for the case where the electric field varies with position show that (for the field variations considered) all the macroscopic variables depend strongly upon position and no equilibrium region exists even in the negative glow, where the field is small and practically constant. However, it is clear that the length of the negative glow region which has been chosen in the present study is too short to take into account the real structure of a normal or abnormal glow discharge. In order to avoid excessive computing times, the microscopic study of a glow discharge with a longer negative glow will, at the present time, necessitate modifications to the Boltzmann and Monte-Carlo techniques themselves.

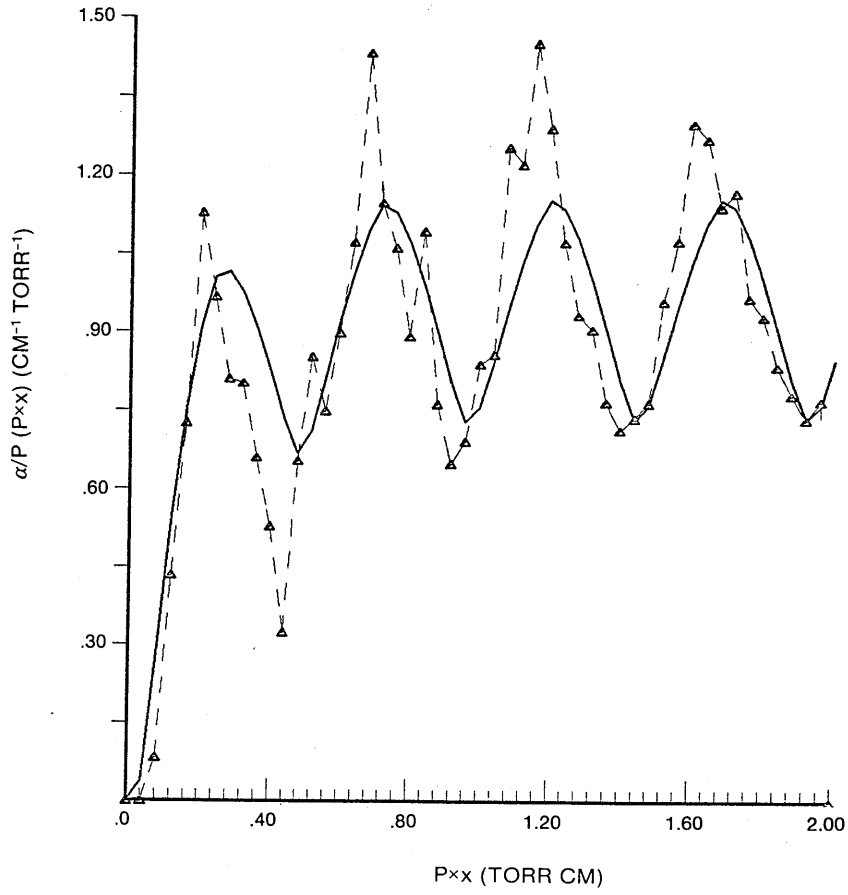

Fig. 32. Spatial variation of the Townsend Ionization Coefficient related to the field given in Fig. 31. Δ__Δ, MC simulations, ___ Memory Factor model.

In the case of the Boltzmann equation method, the necessary modification has already been mentioned and principally involves a more sophisticated expansion of the isotropic part of the distribution function in terms of orthogonal polynomials. In the case of the Monte-Carlo simulations, a number of possible improvements can be envisaged. For example, a modification of the random walk method employed by Englert (1974) can be used in the negative glow.

Improvements are also being sought in the Memory Factor model. These include a modification of the form of the function Φ in order to take into account the initial distribution of electron energies and the existence of an ionization threshold. This should yield more realistic values for the ionization coefficients at low energies.

In addition, solutions of a simplified form of the Boltzmann equation are being investigated in order to relate the parameter λ to the known values of the different collision cross sections.

REFERENCES

Alkhazov, G. D., 1970, Sov. Phys. Tech. Phys., 15: 66.
Allis, W. P., 1975, Rev. Phys. Appl., 10: 97.
Badareu, E. and Popescu, I., 1965, "Gaz Ionisés," Dunod, Paris.
Baker, C. T. H., 1977, "The Numerical Treatment of Integral Equations," Clarendon, Oxford.
Boardman, A. D., Fawcett, W., and Rees, H. D., 1968, Solid State Commun., 6: 305.
Boeuf, J. P., Marode, E., Segur, P., Davies, A. J., and Evans, J. G., 1980, in "Proceedings 6th International Conference on Gas Discharges, Edinburg," IEE Conf. Publ., 189, p. 63.
Boeuf, J. P., 1981, Thèse de Spécialité, No 2967, Université de Paris XI, Orsay.
Boeuf, J. P., Davies, A. J., Evans, J. G., Marode, E., and Segur, P., 1982, to be published.
Boeuf, J. P. and Marode, E., 1982, to be published.
Braglia, G. L., 1970, Nuovo Cimento, B, 70: B. 169.
Braglia, G. L., 1975a, Parma University Reports, IPPR-S-153.
Braglia, G. L., 1975b, Parma University Reports, IPPR-S-162.
Braglia, G. L., 1977, Physica, C, 92: 91.
Braglia, G. L., 1980, Beitr. Plasma. Phys., 20:(3) 147.
Carter, L. L., Cashwell, E. D., and Taylor, W. M., 1972, Nucl. Sci. Eng., 48: 403.
Chanin, L. M. and Rork, G. D., 1964, Phys. Rev., A, 135: 1005.
Davies, A. J., Evans, J. G., Marode, E., and Segur, P., 1980, in: "Proceedings, 6th International Conference on Gas Discharges, Edinburgh," IEE Conf. Publ. 189, p. 59.
Davies, A. J., 1981, in: "Proceedings, 15th International Conference on Phenomena Ionized Gases, Minsk," Invited Papers.
Desloge, E. A. and Mitchell, R. D., 1970, Aust. J. Phys., 23: 497.
Englert, G. W., 1974, Z. Naturforsch., A, 29: 51.
Fournier, G. and Pigache, D., 1976, Bull. Am. Phys. Soc., 21: 174.
Grosswald, E., 1961, J. Math. Mech., 10: 1.
Huxley, L. G. H. and Crompton, R. W., 1974, "The Diffusion and Drift of Electrons in Gases," Wiley, New York.
Itoh, T. and Musha, T., 1960, J. Phys. Soc. Japan, 15: 1675.
Kline, L. E. and Siambis, I. G., 1972, Phys. Rev., A, 5: 794.
Kumar, K., Skullerud, H. R., and Robson, R. E., 1980, Aust. J. Phys., 33: 343.
Labahn, R. W. and Callaway, J., 1970, Phys. Rev., 2: 366.
Lakshminarashimha, C. S., Lucas, J., and Snelson, R. A., 1975, Proc. IEE, 122: 1162.
Lalau F., 1981, Thèse de Spécialité, No 2876, Université de Paris XI.

Ligou, J., 1973, Nucl. Sci. Eng., 50: 135.
Lin, S. L. and Bardsley, J. N., 1977, J. Chem. Phys., 66: (2) 435.
Long, W. H. Jr., 1979, Technical Report, AFAPL-TR, No. 79-3038, Northrop Res. Tech. Cent.
Lucas, J. and Saelee, H. T., 1975, J. Phys. D, 8: 640.
Marode, E., 1975, J. Appl. Phys., 46: 2005.
Marode, E., Tran Ngoc An, Fournier, G., Segur, P., and Pareathumby, S., 1979, Rapport Final Contract D.G.R.S.T. No. 77-7-1918.
Miller, L. B., 1967, Argonne National Laboratory, ANL-7307.
Pareathumby, S., 1979, Thèse de Spécialité, No. 2179, Toulouse.
Parker, J. H. Jr. and Lowke, J. J., 1969, Phys. Rev., 181: 290.
Pitchford, L. C., O'Neil, S. V., and Rumble, J. R. Jr., 1981, Phys. Rev., 23: 294.
Reid, I. D. and Hunter, S. R., 1979, Austr. J. Phys., 32: 255.
Sakai, Y., Tagashira, H., and Sakamoto, S., 1972, J. Phys. B, 5: 1010.
Sakai, Y. Tagashira, H., and Sakamoto, S., 1977, J. Phys. D, 10: 1035.
Sanchez, R., 1974, Rapport CEA No 1793.
Segur, P. Keller, R., 1977, J. Comput. Phys., 24: 43.
Segur, P., Pareathumby, S., Yousfi, M., and Marode, E., 1979, J. Phys., Collo. C7, 40: 599.
Segur, P., Yousfi, M., and Marode, E., 1980, in: "Proceedings, 6th International Conference on Gas Discharges, Edinburgh," IEE Conf. Publ. 189, p. 56.
Skullerud, H. R., 1968, Br. J. Appl. Phys., 1: 1567.
Sockol, P. M., 1966, Nasa TND 3510, Lewis Research Center.
Swigert, P. and Goldstein, M., 1967, Nasa TND 4043, Lewis Research Center.
Thomas, R. W. L. and Thomas, W. R. L., 1969, J. Phys. B, 2: 562.
Tran Ngoc An, Marode, E. and Johnson, P. C., 1977, J. Phys. D, 10: 2317.
Von Engel, A., 1965, "Ionized Gases," Oxford.
Ward, A. L., 1962, J. Appl. Phys., 33: 2789.
Warren, R., 1955, Phys. Rev., 98: 1650.
Whipple, E. C. Jr. and Parker, J. L., 1971, Phys. Fluids, 14:(11) 2368.
Woodcock, E. R., Murphy, T., Hemmings, P. J., and Longworth, T. C., 1965, Argonne National Laboratory, ANL-7050.
Yarnold, G. P., 1945, Philos. Mag., 36: 185.
Yarnold, G. P., 1946, Philos. Mag., 38: 186.
Yousfi, M., 1980, Thèse de Spécialité, No. 2404, Toulouse.

CURRENT RESEARCH TOPICS IN LOW-PRESSURE GLOW DISCHARGES IN RARE GASES AND IN PURE NITROGEN

C. M. Ferreira

Departamento de Física and Centro de Electrodinâmica da Universidade Técnia de Lisboa, Instituto Superior Técnico Av. Rovisco Pais, 1000 Lisboa, Portugal

INTRODUCTION

The present work reports some results of the research in progress concerning the positive column of glow discharges in pure rare gases and in pure nitrogen, at pressures typically below 1 torr and discusses some of the limitations of currently available models for predicting the discharge characteristics and for explaining the kinetics of some important excited atomic and molecular species, such as the metastable ones, in the positive column. The paper is divided into two main sections: the first devoted to the modeling of the positive column in Argon and the second, to the kinetics of the metastable state $N_2(A^3\Sigma^+_u)$ in the positive column of a pure nitrogen glow discharge.

THE POSITIVE COLUMN OF ARGON GLOW DISCHARGES IN LOW-PRESSURE RANGE

A complete, self-consistent, and physically coherent model of the low pressure positive column in rare gases does not seem to exist as yet. Such a model should include a satisfactory theoretical description of the dynamics of charged particles, and of the excitation, ionization and loss processes. It should also yield accurate predications concerning the operating discharge characteristics, the similarity laws and the behavior of the atomic excited species (e.g., radial profiles, density variation with current and pressure) for various operating conditions. Several theories of the positive column have been proposed by a number of authors (Self and Ewald, 1966; Forrest and Franklin, 1966; Ewald et al., 1967; Self, 1967; Ilic, 1973). These cover the experimentally important pressure range between the very low pressure

limit, to which the Tonks-Langmuir (1929) free-fall theory applies, and the high pressure limit, where the classical Schottky's isothermal ambipolar diffusion theory (1924) is commonly used. All these theories provide information about the radial distributions of the plasma density and potential and of the charged particle velocities. In most of them, however, the electrons are assumed to be isothermal and Maxwellian, a critical assumption that can lead to very large errors in the calculated rate coefficients for excitation and ionization by electron impact. These errors, in turn, can result in a poor description of the balance between the production and loss mechanisms both for charged particles and excited atomic species. Moreover, the discharge characteristics and similarity laws result from the balance between collisional ionization of the gas and the loss of electrons and ions to the wall; therefore, the Maxwellian assumption can be largely responsible for the failure of these theories to predict with sufficient accuracy the discharge characteristics and the behavior of the excited species as a function of the experimental parameters, current and pressure. The discrepancies between the results of these theories and the experimental data are particularly significant in the case of the Argon positive column (Ilic, 1973).

The work reported here is an attempt to extend the currently available models of the low pressure positive column to include a non-Maxwellian electron distribution function and to assess the suitability of such an improved version for the prediction of the discharge characteristics. In the present state of this work, the effects of space-charge fields on the electron energy distribution have not yet been included. The form of the distribution is assumed to be independent of radius and to depend only on the ratio E/n_o, where E is the axial electric field and n_o is the neutral gas density. In the following section the distribution is calculated in the range $10^{-16} < E/n_o < 2.10^{-15}$ V cm^2, by solving the Boltzmann equation using analytical methods and appropriate models to describe the experimental Argon cross-section data. Calculated values of excitation and ionization rate coefficients and of electron transport parameters vs. E/n_o are also given and compared to the available experimental data. In the next section, a modified version of current two-moment models (Self and Ewald, 1966) is used to derive the radial profiles of plasma density and potential and the similarity laws E/n_o and $n_e(o)/J$ vs. n_oR. These results are then compared with the experimental data and some limitations of these kinds of theories are briefly discussed on physical grounds.

Calculation of the Electron Distribution Function

The classical first-order expansion of the electron distribution function (assumed here to be spatially homogeneous) in spherical harmonics yields an equation for the isotropic part of the distribution which can be written as:

$$\frac{dG}{du} = \left(\frac{2e}{m}\right)^{\frac{1}{2}} \left\{ \sum_j n_o f(u^+)\, \sigma_j(u^+)\, u^+ - n_o \sigma_x(u)\, f(u)\, u \right\}, \qquad (1)$$

where G is the total flux across the sphere u = const. in velocity space, e and m denote the electron charge and the electron mass, respectively, $\sigma_j(u)$ is the cross section for a particular inelastic process j, $\sigma_x(u) = \Sigma_j \sigma_j(u)$ is the total inelastic cross section, $u = mv^2/2e$ is the electron energy expressed in volts and the superscript + denotes a translation by an amount V_j; i.e., $u^+ = u + V_j$, V_j denoting the threshold for the process j.

The total flux G includes the effects due to the applied electric field, elastic collisions with neutrals and collisions between electrons. Collisions between electrons are not considered for the low-current regime of operation we are interested in, and substituting into Eq. 1 the well-known expressions (Allis, 1956) for the flux due to the field and the elastic collisions, one obtains after some manipulations

$$\frac{d}{du}\left\{ a^2 (1 + 2b\, T_g) \frac{df}{du} + 2bf \right\} = \sigma_x f u - \sum_j \sigma_j(u^+)\, f(u^+)\, u^+, \qquad (2)$$

where:

$$a^2(u) = \frac{1}{3} \left(\frac{E}{n_o}\right)^2 \frac{u}{\sigma_c}, \qquad (3)$$

$$b(u) = \frac{3m}{M} \left(\frac{n_o}{E}\right)^2 \sigma_c^2\, u. \qquad (4)$$

In these expressions σ_c denotes the energy-dependent, momentum transfer cross section, M is the mass of the atom, and T_g is the neutral gas temperature.

In order to derive approximate analytical solutions of Eq. (2), we will consider two energy ranges, $u \geq V_x$ and $0 \leq u \leq V_x$, where V_x denotes the first excitation threshold of the atom ($V_x \sim 11.55$ eV for Argon), the former corresponding to the so-called tail of the distribution and the latter to the body. Moreover, it is obvious that analytical solutions cannot be derived unless one uses some simple models to describe the experimental cross-section data. For Argon, we will use the following approximations:

Momentum transfer cross section:

$\sigma_c(u) \simeq \alpha_c\, u$ for $u \leq V_x$

$\sigma_c(u) \simeq \sigma_c(V_x) \left(\frac{u}{V_x}\right)^{-\frac{1}{2}}$ (i.e., $\nu_c \simeq$ const.) for $u \geq V_x$.

Total inelastic cross section:

Model I: $\sigma_x \sqrt{u} \simeq \alpha\ (u - V_x)$

Model II: $\sigma_x \simeq \alpha'\ \sqrt{u}\ (u - V_x)$.

In the energy range of interest here, the experimental data can be fitted by these simple models within a few percent of error, i.e., and error smaller than the differences between the cross-section data for Argon reported by different authors. Of course, the approximation used for $\sigma_c(u)$ does not take into account the actual behavior of the cross section for energies below the Ramsauer minimum at $u \sim 0.3$ eV. However, in our case most of the electrons have energies in the range of a few volts; therefore the approximation used here is not likely to affect drastically the calculated distribution. Similarly the approximations above for the inelastic cross section deviate considerably from the experimental data for energies above a few tens of electron-volts (typically 30 or 40 eV), but the number of electrons in this high energy region of the tail is vanishingly small and can be assumed to be virtually zero.

It is beyond the scope of this paper to give a detailed account of all the calculations necessary to solve Eq. (2) when the above models are used. Therefore, only the essential steps and results will be mentioned.

Tail of the Distribution. Due to the inelastic collisions, the electrons are withdrawn from the tail and reintroduced in the body, causing the distribution to decrease steeply (more or less, depending on the values of E/n_o) for energies above V_x. For the range of E/n_o values of interest here, typically below 10^{-15}V cm^2, the distribution falls off steeply enough for $u \geq V_x$ so that we can neglect the reintroduced electrons in the tail. Therefore, the equation for the tail is

$$\frac{d}{du}\left\{a^2\ (1 + 2\ b\ T_g)\ \frac{df}{du} + 2\ b\ f\ \right\} - \sigma_x\ f\ u = o. \qquad (5)$$

Solution using model I i.e., $\sigma_x \sqrt{u} = \alpha(u - V_x)$: In this case one obtains the following solution

$$f_t(u) = \frac{C}{\sqrt{u}}\ e^{-(p + p_o)u}\, U\left(-\gamma\ ,\ \frac{1}{2},\ (p_o + 2p)u\right), \qquad (6)$$

where $U(A,B,x)$ is a standard symbol used to identify one of the solutions of the Confluent Hypergeometric equation, C is an arbitrary integration constant, and p_o, p and γ are energy independent

parameters given by:

$$p_o = \frac{2\,b}{1 + 2\,b\,T_g}$$

$$p = \frac{\sqrt{p_o^2 + 4\,q_o\alpha} - p_o}{2} \qquad (7)$$

$$\gamma = \frac{q_o\alpha\,V_x + \frac{3}{4}\,p_o}{p_o + 2\,p} - \frac{1}{4}\,.$$

Here q_o is another constant parameter defined as $q_o = u^{3/2}/a^2\,(1 + 2\,b\,T_g)$. It should be noted that, according to the approximations used, $b(u) = \text{const.}$ and $a(u) \sim u^{3/2}$ in the range $u \geq V_x$.

A detailed numerical analysis of the solutions (6) shows that the effects of the elastic collisions are totally negligible in the tail ($P_o \to o$) in the range of operation here considered. Therefore, the form of the tail is only determined by the competing effects of the field that pushes the electrons up in energy, and of the inelastic collisions that pull them out from the tail.

Solution using model II i.e., $\sigma_x = \alpha'\sqrt{u}(u - V_x)$: When the model II is used and the energy losses by elastic collisions are neglected, one obtains the following solution

$$f_t(u) = C'u^{-3/4}\,\mathrm{Ai}\,\{\delta^{1/3}\,(\frac{u}{V_x} - 1) - \frac{3}{16\delta}\}, \qquad (8)$$

where Ai(x) denotes the Airy function, C' is an arbitrary integration constant and δ is an energy independent parameter given by

$$\delta = \frac{\alpha' V_x^3\,u^{3/2}}{a^2}\,. \qquad (9)$$

We see that the expressions obtained for the solutions are completely different from one model to the other, and it is natural to ask whether such a difference corresponds or not to a distinct form of the tail. In fact, a detailed numerical analysis shows that the differences between the two types of solutions (up to energies of 25 to 30 eV) are always small, in fact, much smaller than the errors which arise from the uncertainties in the published cross-section data. In other words, the question "which model should be used" appears to be quite irrelevant as compared to the question "which cross section should our models try to fit."

This important point will be further discussed below.

The Body of the Distribution. In the body, the electrons do not make inelastic collisions and the equation for the body is

$$\frac{d}{du}\left\{a^2 \ (1 + 2\ b\ T_g)\ \frac{df}{du} + 2\ b\ f\ \right\} = -\ \sum_j \sigma_j(u^+)\ f(u^+)\ u^+. \qquad (10)$$

The term on the right-hand side of this equation represents a source of electrons which is due to the injection of electrons coming from the tail. In principle, this source term can be calculated using the solutions previously derived for the tail, and the equation can be formally integrated. Noting that the total flux G(u) must vanish when $u \to 0$, one obtains the formal solution

$$f_b(u) = f(V_x)\ e^{-W(u)} \left[1 + \int_u^{V_x} \frac{h(u')\ e^{W(u')}}{a^2(u')\ (1 + 2\ b\ T_g)}\ du'\right] \qquad (11)$$

where

$$W(u) = \int_{V_x}^{u} \frac{2\ b}{1 + 2\ b\ T_g}\ du' \ , \qquad (12)$$

$$h(u) = \sum_j h_j(u) = \sum_j \int_{V_j}^{V_j + u} \sigma_j(u')\ \frac{f(u')}{f(V_x)}\ u'\ du' \ , \qquad (13)$$

and $f(V_x)$ denotes the value of f(u) at $u = V_x$.

The factor $f(V_x)\ e^{-W(u)}$ on the right-hand side of Eq. (11) is a solution without reintroduced electrons, i.e., a solution of Eq. (10) when the source term on the right-hand member is set equal to zero. The existence of this source introduces a corrective factor in the solution which is given by the integral term $\int_u^{V_x} (\ )\ du'$.

In general, this corrective factor cannot be calculated analytically unless some approximations are made. The most difficult problem concerns the calculation of the functions $h_j(u)$ which are given by the integrals shown in Eq. (13). The integral functions involve a product $\sigma_j(u)\ f(u)$, i.e., a steeply increasing function of energy times a steeply decreasing one, the result being a function which exhibits a sharp peak at some energy more or less close to the threshold V_j (typically 1 or 2 volts above V_j). This sharp peak can be described by a Delta-function as a first approximation and, in this case, $h_j(u)$ will be represented by a step-function. On physical grounds, this is equivalent to assuming that each inelastic process has an apparent energy threshold situated above

the actual threshold.

With this approximation we have:

$$h_j(u) \simeq o \quad \text{for } u < u_j$$

$$h_j(u) \simeq H_j \quad \text{for } u > u_j \tag{14}$$

where u_j is the energy difference between the apparent and the actual threshold, and H_j is given by

$$H_j = \int_{V_j}^{\infty} \sigma_j(u) \frac{f(u)}{f(V_x)} u \, du. \tag{15}$$

In order to calculate these quantities, H_j, we have used semi-empirical formulas similar to those given by Peterson and Allen (1972) for the cross sections

$$\sigma_j(u) = A_j \left(\frac{V_j}{u}\right)^{\Omega} \left(1 - \frac{V_j}{u}\right)^{\nu}, \tag{16}$$

where Ω, ν and A_j are three parameters that determine the shape and the magnitude of each individual cross section. The integral (15) cannot be calculated using the exact solutions for the tail, i.e., either Eq. (6) or Eq. (8), but we have found that the tail can be fitted up to energies of about 25 to 30 eV, within a few percent of error, by an expression of the type

$$\frac{f(u)}{f(V_x)} = \left(\frac{u}{V_x}\right)^{\beta} e^{-q(u-V_x)}, \tag{17}$$

where $\beta(E/n_o)$ and $q(E/n_o)$ are fitting parameters.

When the expressions (16) and (17) are used, one obtains an analytical expression for H_j which can be written

$$H_j = A_j V_x^2 \left(\frac{V_j}{V_x}\right)^{\beta+2} e^{q(V_x-V_j)} \Gamma(\nu+1) \, U(\nu+1, \beta+3-\Omega, qV_j), \tag{18}$$

where the symbol Γ denotes the Gamma function.

Using the above approximations, the calculation of the solution for the body is now more or less straightforward. In the range of

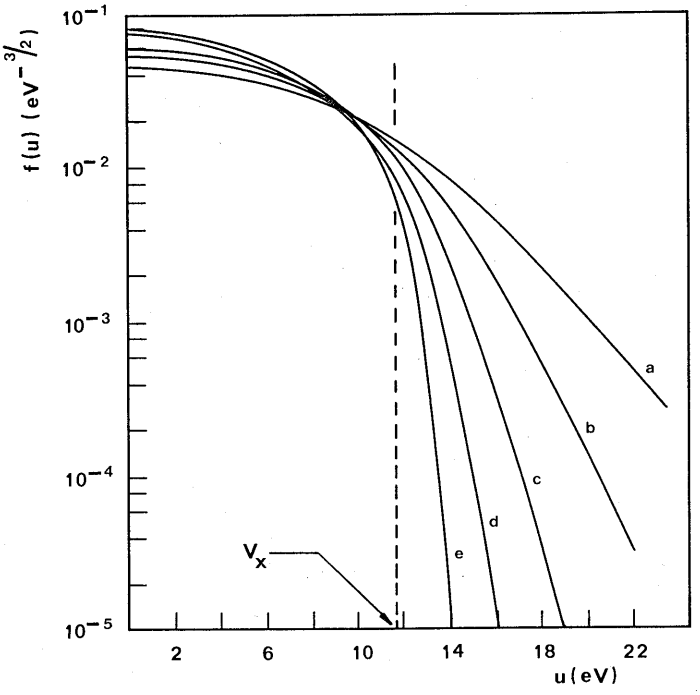

Fig. 1. Calculated electron energy distribution functions, normalized to one electron, for the following values of E/n_o in V cm^2: a) 1.88×10^{-15}; b) 9.40×10^{-16}; c) 4.69×10^{-16}; e) 9.40×10^{-17}.

the parameters of interest here, we have $2bT_g << 1$ and $W(u) < 1$; therefore, the integral term on the right and side of Eq. (11) can be easily calculated expanding the exponential $e^{W(u)}$ in a power series.

The solutions derived for the body and for the tail must be joined at $u = V_x$. It is sufficient to impose that f(u) be continuous in this point, the continuity of its first derivative being automatically satisfied this follows from the continuity of the total flux G(u) . After this has been done we are left only with one arbitrary constant, in this case, the value $f(V_x)$, which is determined by the normalization of the distribution

$$\int_o^\infty f \sqrt{u}\, du = 1 \ . \qquad (19)$$

In Fig. 1, a set of calculated electron distribution functions is given for values of E/n_o in the range from about 10^{-16} to 2.10^{-15} V cm^2. It is seem that the inelastic collisions cause the

distribution to fall off more or less steeply, depending on the values of E/n_o, above the first excitation threshold.

In these calculations the total inelastic cross section used (for determining the values of α and α' for models I and II, respectively) is within 10 to 20% of that measured by Schaper and Scheibner (1969) which is somewhat lower than the cross sections of Eggarter (1975) and of Peterson and Allen (1972). The reason for this choice is related to the problem of the best fit for the calculated to the measured first Townsend coefficient discussed in more detail below.

Electronic Rate Coefficients and Electron Transport Parameters

The electronic rate coefficients are given by:

$$C_j = \langle \sigma_j \, v \rangle = \frac{\sqrt{2e}}{m} \int_{V_j}^{\infty} \sigma_j(u) \, f \, (u) \, u \, du; \tag{20}$$

therefore,

$$C_j = \frac{\sqrt{2e}}{m} f(V_x) \, Hj \tag{21}$$

where the quantities H_j are given by Eq. (18).

In Fig. 2, the calculated rate coefficients for some important excitation processes and for ionization by electron impact are given as a function of the ratio E/n_o. In these calculations, we have used the semiempirical cross sections of Peterson and Allen (1972) for the excitation of the resonant $^3P_1$ and $^1P_1$ states and of the composite forbidden state ($3p^5$, 4p configuration), and the ionization cross section of Rapp and Golden (1965). Unfortunately, detailed and accurate data on the electron impact cross sections of the Argon metastables are not available. For these states ($^3P_0$ and $^3P_2$), we have used the relative excitation cross section measured by Lloyd et al. (1972) which was normalized to the absolute value measured by Pesnelle (1970) at u = 30 eV. This cross section has the same shape as that measured by Borst (1974), but the peak magnitude of the latter is larger by a factor of the order of 2. It should be noted, however, that the measured cross sections for the excitation of these metastable states include the contributions of cascading from higher-lying radiative states, principally from the 4p states. Cross sections for direct excitation of the ^3P_o and $^3P_2$ states are not available as yet.

The calculation of the electron distribution function and of the electronic rate coefficients was made using a number of

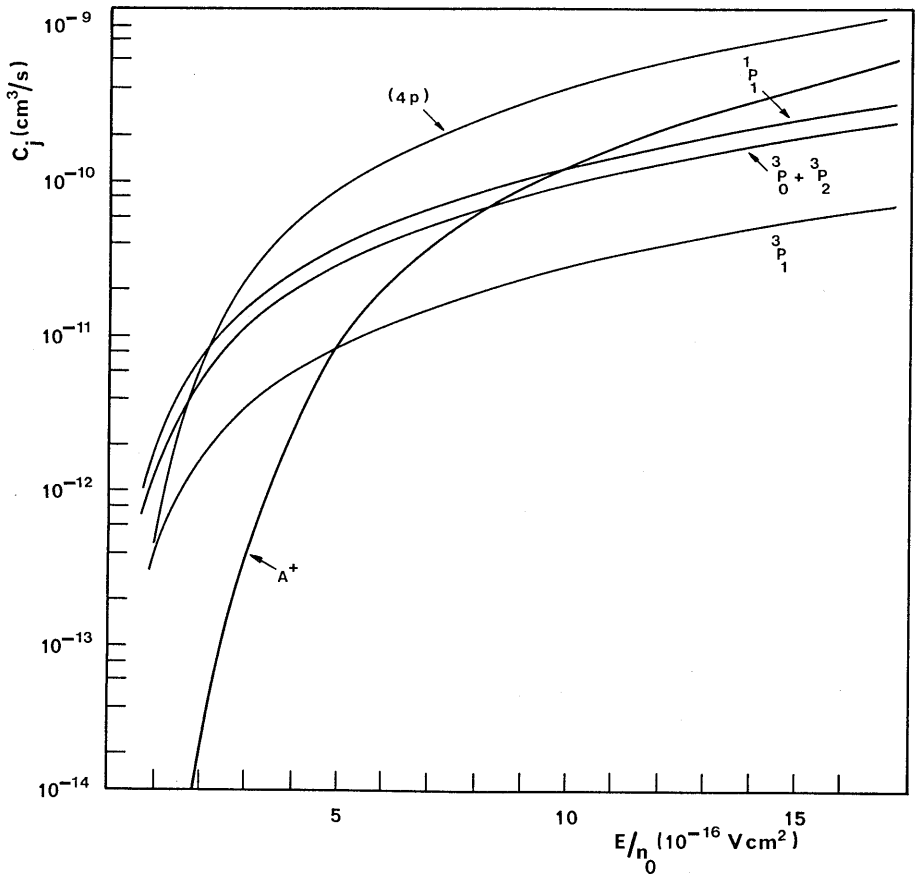

Fig. 2. Energy-averaged electron excitation and ionization rates in argon as a function of E/n_o.

approximations, and it is important at this point to test the accuracy of our results. A convenient and crucial test is the comparison between predicted and measured values of the first Townsend coefficient and of the electron transport parameters. Using approximations similar to those described above, we have calculated the following quantities by analytical methods:

Electron free diffusion coefficient:

$$D_e = < \frac{v^2}{3\nu_c} > = \frac{2e}{3m} \int_o^\infty \frac{u^{3/2}}{\nu_c} f \, du$$

Electron mobility: $\mu_e = -\frac{2}{3}\frac{e}{m}\int_o^\infty \frac{u^{3/2}}{\nu_c}\frac{df}{du}\,du$

Drift velocity: $v_d = \mu_e E$

First Townsend coefficient: $\frac{\alpha^+}{n_o} = \frac{C_I}{v_d}$,

where C_I denotes the rate coefficient for ionization by electron impact.

A detailed presentation of these calculations and analysis of results are beyond the scope of this paper and will be published elsewhere. However, it is interesting to mention some important conclusions, which concern the first Townsend coefficient. We have found that the calculated values of this coefficient are extremely sensitive to the total electron impact excitation cross section. Making small adjustments in the parameter α (cf. model I for the total cross section), we have been able to obtain a very good fit of the predicted to the measured values of α^+/n_o vs E/n_o (Fig. 3). The sensitivity of the results to the values chosen for α has been found to be very large, a change of 50% in α resulting in a change in α^+/n_o, which can reach in some cases one order of magnitude, depending on the values of E/n_o. The reason for this can be easily understood noting that the magnitude of the ionization coefficient C_I is extremely sensitive to the form of the tail of the distribution which in turn is strongly affected by the value of α (for a fixed ratio E/n_o, a change in α results in a change in the parameters p an γ which control the form of the tail according to the expressions (6) and (7) for the model I). The value of α which gives the best fit corresponds to a model cross section which is within 10 to 20% of the measured total excitation cross section of Schaper and Scheibner (1969). Using the cross section data of either Eggarter (1975) or Peterson and Allen (1972) leads to very large decrepancies between predicted and measured values of the first Townsend coefficient as shown in Fig. 3. A similar conclusion was also derived by Jacob and Mangano (1976) who have used a numerical code to solve the Boltzmann equation.

Plasma Density Profiles and Similarity Laws for the Cylindrical Positive Column

The presently available theories of the positive column assume the electrons to be Maxwellian, a poor approximation for the low-current, low-pressure operation conditions in which we are interested. In this paragraph we attempt to introduce some modifications into the theory of Self and Ewald (1966) to account for the non-Maxwellian

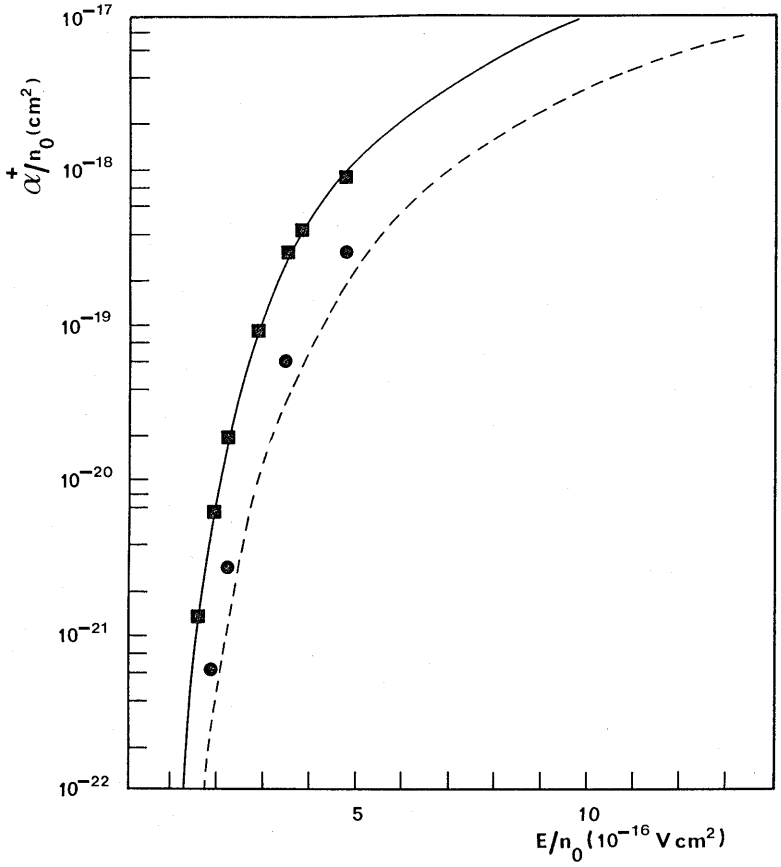

Fig. 3. Experimental and predicted values of the first Townsend coefficient α^+ as a function of E/n_o (—— present result; ■ - experimental data of Golden and Fisher; --- our calculations using Eggarter's cross section; ● - calculated by Jacob and Mangano using Eggarter's cross section)

character of the distribution in order to assess the ability of such a model for predicting the discharge operating characteristics.

We use the following basic equations

$$\nabla \cdot (n \vec{v}) = \nu_I \, n \tag{22}$$

$$n \vec{v} = - D_e \nabla n - n \mu_e \vec{E}_A \tag{23}$$

$$(\vec{v} \cdot \nabla) \vec{v} + \nu_I \vec{v} = \frac{e}{M} \vec{E}_A - \frac{eT_i}{M} \frac{i}{n} \nabla n - \nu_{in} \vec{v} \, , \tag{24}$$

where $n = n_e = n_i$ is the plasma density; $\vec{v} = \vec{v}_e = \vec{v}_i$ is the common average radial velocity of electrons and ions; $\nu_I = n_o C_I$ is the collision frequency for ground state ionization by electron impact; ν_{in} is the collision frequency for momentum transfer between ions and neutrals (including the effects of charge exchange collisions); $\vec{E}_A = -\nabla\phi$ is the radial space charge field; T_i is the ion temperature in volts, here assumed to be radially constant; and the other symbols have the same meaning as before. Eqs. (22) to (24) describe the continuity for both electrons and ions, and the momentum transfer for electrons and for ions, respectively. Eq. (23) was derived on the assumption that the form of the electron distribution function is independent of radius and only determined by the ratio of the axial electric field to the neutral gas density, E/n_o. Therefore, D_e and μ_e are here assumed to be radially constant, the ratio $u_K = D_e/\mu_e$ (which is commonly referred to as the characteristic energy) being only a function of E/n_o. Second and higher order terms in the expansion of the distribution in spherical harmonics were also assumed to be zero, and this is the reason Eq. (23) does not contain nonlinear terms.

Following the methods described in Self and Ewald's paper, we introduce the normalized variables

$$W = \left(\frac{M}{e\,u_K}\right)^{1/2} v \; ; \; S = \left(\frac{M}{e\,u_K}\right)^{1/2} (\nu_{in} + \nu_I)\, r, \tag{25}$$

where r denotes the radial coordinate. The mobility ratio $R = \mu_e/\mu_i$, where $\mu_i = e/M(\nu_{in} + \nu_I)$, is very large for Argon, and taking $R \to \infty$ we obtain, after some simple manipulations, the following system of equations:

$$n(r) = n(o) \exp\left(-\frac{\phi(r)}{u_K}\right) \tag{26}$$

$$1 + \frac{W}{S}\frac{dS}{dW} + W\frac{d}{dW}\log n = A\frac{dS}{dW} \tag{27}$$

$$W\left(1 + \frac{dS}{dW}\right) = -\left(1 + \frac{T_i}{u_K}\right)\frac{d}{dW}\log n \quad , \tag{28}$$

where $A = \nu_I/(\nu_{in} + \nu_I)$ is a parameter which depends only on the ratio E/n_o. In their paper, Self and Ewald derived profiles of the plasma density and potential for different values of A, and they have shown that in the low-pressure ($A \to 1$) and in the high-pressure ($A \to 0$) limits these profiles go over to those predicted by the free-fall and the linear ambipolar diffusion theories, respectively. Moreover, they have shown that the theory leads mathematically to a natural plasma-sheath boundary at a finite radius, given by the

point where the radial velocity equals the isothermal ion sound speed, $e(T_e + T_i)/M^{1/2}$. These conclusions remain valid in our case for a non-Maxwellian energy distribution, provided the electron temperature T_e is replaced by the characteristic energy $u_K = D_e/\mu_e$.

The similarity laws of the positive column can also be derived in a straightforward manner from the equations above. Let us consider first the similarity law E/n_o vs. n_oR. When the ratio E/n_o is fixed at some arbitrary value, the form of the electron energy distribution is automatically defined, and the ionization coefficient C_I, hence the value of A, can be computed. Integrating the system of Eqs. (27) and (28) for $0 < W < 1$ ($W = 1$ corresponds to the plasma-sheath boundary, on the assumption $T_i << u_K$), we obtain the solutions S(W) and n(W), from which the radial profile of density, n(r/R), immediately follows. Because the sheath thickness is negligibly small as compared to the tube radius R, the value of S derived from the computed solution for $W = 1$ must be equal to the value predicted by the Eq. (25) when r is set equal to R. This equality related the values of E/n_o to those of n_oR; therefore it provides the similarity law we were looking for.

Let us consider next the similarity law $n(o)/J$ vs. n_oR, where n(o) is the axial electron density and $J = I/\pi R^2$ denotes the average current density through the section of the column. Neglecting the ion current, we obtain $n(o)/J = n(o)/\langle n\rangle . (ev_d)^{-1}$, where $\langle n\rangle$ denotes the radial average of the electron density and $v_d = \mu_e E$ is the axial electron drift velocity. The average $\langle n\rangle$ can be easily calculated from the profiles and v_d is already known as a function of E/n_o, from the calculations mentioned above. Using the similarity law E/n_o vs. n_oR previously derived, $n(o)/J$ vs. n_oR immediately follows.

Results and Discussion

The plasma density profiles and the similarity laws predicted by the present theoretical model are given in Figs. 4 to 6. Also shown in Figs. 5 and 6 are the experimental data of Klarfeld (1973) and the theoretical results of Ilic (1973), for comparison. In his model, Ilic described the steady state of a cylindrical plasma column by three moment equations, in the plasma approximation, for electrons and ions. The electron distribution function was assumed to be a Maxwellian drifting along the axis of the column with velocity v_d, and the inclusion of the energy transfer equations enabled the radial profiles of the electron and ion temperatures to be also determined. Although this theory is very complete and self-consistent, its predictions are in a very great disagreement with the available experimental data in the case of Argon, as shown in Figs. 5 and 6. It is seen that the present model yields a much better agreement, although we still find significant discrepancies between predicted and experimental values.

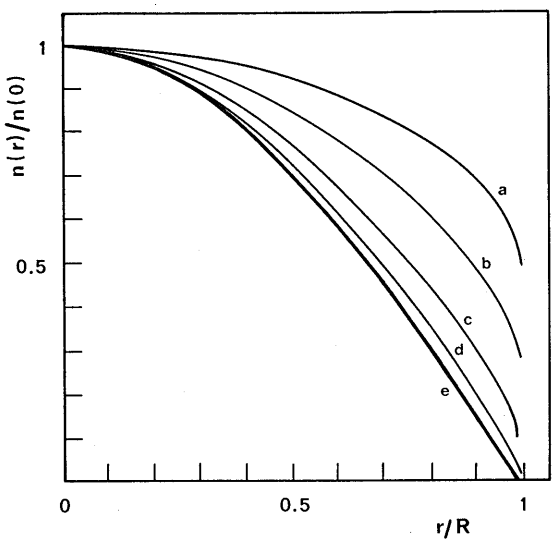

Fig. 4. Calculated plasma density profiles: a) low pressure limit, i.e., $A \to 1$; b) $n_oR = 3.8 \times 10^{15}$ cm^{-2}; c) $n_oR = 1.7 \times 10^{16}$ cm^{-2}; d) $n_oR = 4.6 \times 10^{16}$ cm^{-2}; e) classical Bessel profile of the linear ambipolar diffusion theory.

In order to try to understand the possible reasons for the observed discrepancies, let us briefly discuss on physical grounds some of the assumptions which have been used (for a more extensive discussion the reader is referred, for instance, to Muller and Phelps, 1980). It is well known that the discharge characteristics result from the balance between the creation and the loss of the charged particles. In the low-pressure, low-current discharges considered here the electrons and the ions are lost to the wall at a rate determined by the collisions of the ions with the neutrals and by the effects of space-charge electric fields. At high gas densities, where $\lambda_e/R \ll 1$ and $\lambda_i/R \ll 1$, λ_e and λ_i denote the electron and the ion mean free paths, respectively, the loss of electrons to the wall can be conveniently described in terms of a diffusion coefficient in the two limit cases $\lambda_D/R \ll 1$ and $\lambda_D/R \gg 1$, where λ_D is the electron Debye length. These are the cases of ambipolar and free diffusion, respectively. It is also well known that in the very low pressure limit, where $\lambda_i/R \gg 1$, the ions fall to the wall without making collisions and the loss rate can be accurately predicted in the framework of the so-called free-fall theory. The situation we have been discussing in the present work is intermediate. Typical operation conditions of interest here are $10^{-2} < p < 1$ torr, $10^9 < n_e < 10^{10}$ cm^{-3}, $R \sim 1$ cm; therefore $10^{-3} < \lambda_i/R < 10^{-1}$, $\lambda_D/R < 10^{-2}$ and $10^{-1} < \lambda_e/R < 10$. For these

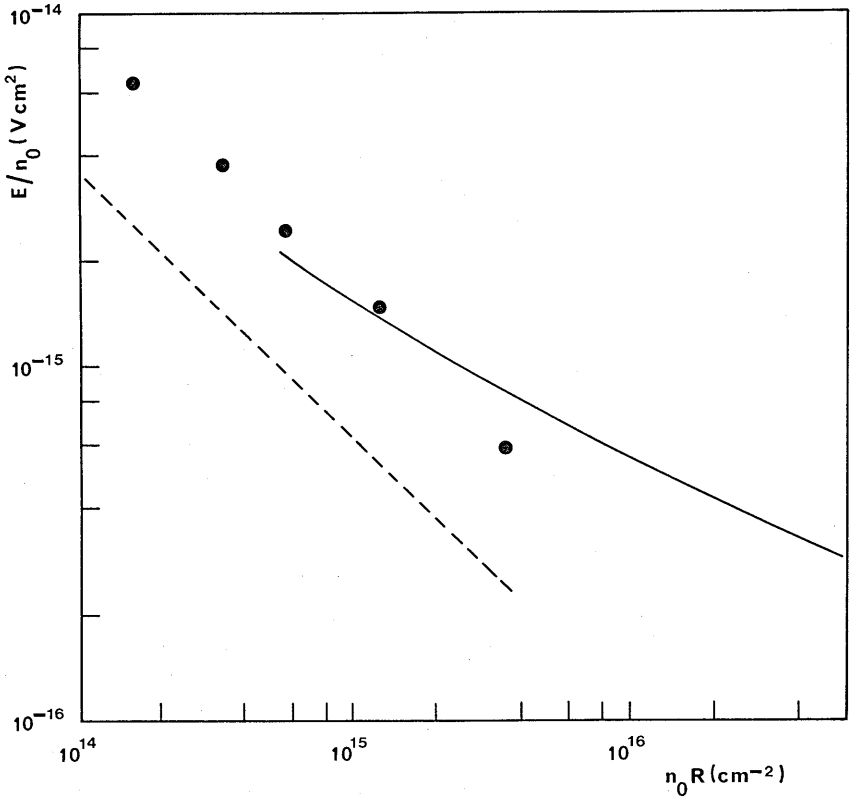

Fig. 5. Comparison of calculated and experimental dependence of E/n_o on n_oR (—— present result; ---- Ilic's calculations; ● - experimental data of Klarfeld).

conditions, it is reasonable to use the plasma neutrality assumption and the hydrodynamic equations for the ions, retaining the nonlinear inertia term as in Eq. (24), although it is known that the assumptions of neutrality and scalar pressure are invalidated near the plasma-sheath boundary. However, the approximations used in the treatment of the electron gas are very crude and physically unsatisfactory. The electrons oscillate more or less freely in the radial space-charge well, and the exchange of kinetic and potential energy is likely to cause just as significant radial variation of the electron energy distribution. Moreover, there should be a preferential loss of high energy electrons to the wall, i.e., of electrons whose kinetic energy is sufficient to escape from the well. Such effects have not been accounted for in the present model, but they are presumingly the most likely source for the observed discrepancies. Therefore, future work on the modeling of low pressure discharges should try to account for these important phenomena.

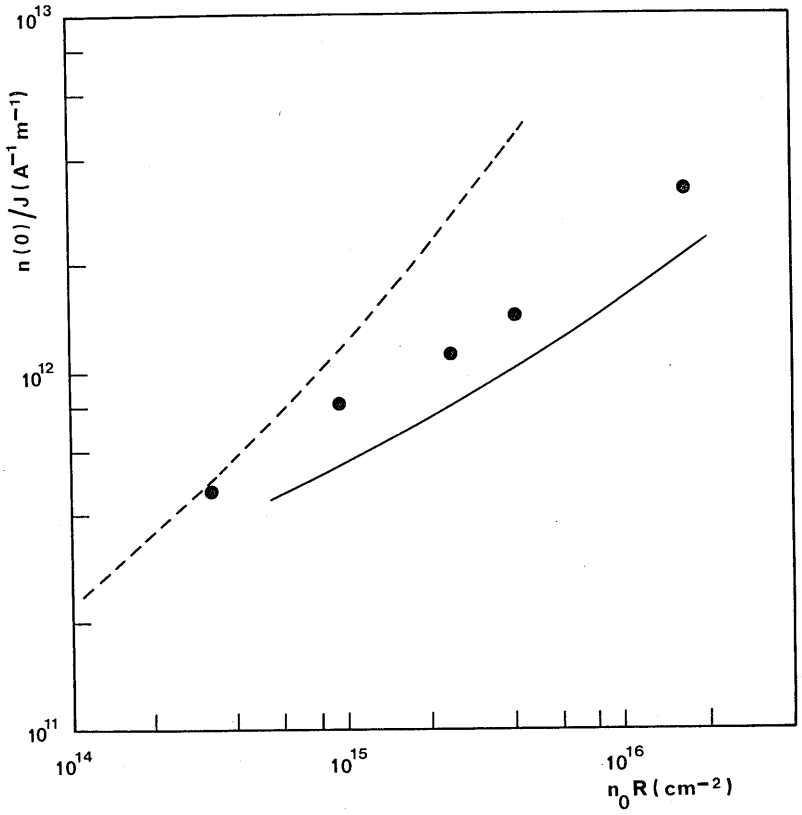

Fig. 6. Comparison of calculated and experimental dependence of $n(o)/J$ on n_oR (notation as in Fig. 5).

POPULATION OF $N_2(A^3\,\Sigma_u^+,\ v)$ METASTABLE STATES IN PURE NITROGEN GLOW DISCHARGES*

The metastable states $N_2(A^3\Sigma_u^+)$ are of great interest in some laser plasmas and plasma chemistry applications. They are also known to play an important role in the chemistry of the upper atmosphere, particularly in the formation of nitrous oxydes in the auroral regions.

In this paragraph, we give a brief account of the experimental

---

*This work has been done in collaboration with G. Cernogora, L. Hochard and M. Touzeau at Laboratoire de Physique de Gaz et des Plasmas, Univ. Paris-Sud, Orsay, France.

$$\xrightarrow{C_x^C} e + N_2\,(C) \text{ followed by } N_2(C) \xrightarrow{h\nu'}$$

$$N_2(B) \xrightarrow{h\nu} N_2(A)$$

Here C_x^A, C_x^B and C_x^C represent the electronic rate coefficients.

Atomic recombination:

$$N(^4S) + N(^4S) + N_2 \xrightarrow{K_s^A} \ldots\ldots \rightarrow N_2(A) + N_2$$

$(K_s^A = 2.4 \times 10^{-33}\ cm^6 s^{-1}$, [20] $)$

b) Loss

Diffusion to the wall ($D_A = 153\ cm^2 s^{-1}$ at p = 1 torr and T = 300 K, [21]).

Electron impact, $e + N_2(A) \xrightarrow{C_A} e +$ unspecified products.

Collisions with ground state dissociated atoms:

$$N_2(A) + N(^4S) \xrightarrow{K_s^P} N_2(x) + N\ (^2P) \quad (K_s^P = 5 \times 10^{-11} cm^3 s^{-1},\ [22])$$

Collisions between metastables:

$$N_2(A) + N_2(A) \xrightarrow{K_A^C} N_2(x) + N_2(C) \quad (K_A^C = 2.6 \times 10^{-10} cm^3 s^{-1},\ [23])$$

$$\xrightarrow{K_A^B} N_2(x) + N_2(B) \quad (K_A^B = 1.1 \times 10^{-9} cm^3 s^{-1},\ [23])$$

Taking into account these processes and assuming as a first approximation that the radial distribution of the metastables is approximately that corresponding to the fundamental diffusion mode, we can give the overall population in the $N_2(A)$ electronic state by:

$$n_A \simeq \frac{n_x (n_e C^A + n_s^2 K_s^A)}{\left(\frac{2.4}{R}\right)^2 D_A + n_e D_A + n_s K_s^P + n_A (K_A^C + K_A^B)}\ ,$$

where $C^A = C_x^A + C_x^B + C_x^C$; n represents a density, and the subscripts

and theoretical research in progress concerning the kinetics of $N_2(A)$ species in low-pressure nitrogen glow discharges. For more detailed information, the reader is referred to Cernogora et al. (1981).

The concentration of the $N_2(A, 0 \leq v \leq 5)$ states in a 2 cm i.d., 50 cm long, pyrex discharge tube has been measured by an optical absorption technique, for pressures ranging from 0.1 to 2 torr and values of discharge current up to about 100 mA. The experimental arrangement is schematically represented in Fig. 7. The light emitted by the optical source (another pure nitrogen glow discharge in a 7 mm i.d., 50 cm long pyrex tube) is divided by a semireflective mirror into two beams which are modulated in opposition of phase by a mechanical chopper. The beam 1 passes through the discharge tube where it is partially absorbed. A second semireflective mirror adds up the two beams which are then focussed at the entrance slit of a monochromator. This apparatus has enabled us to measure the absorption of the first positive system bands down to values as low as 0.1%. The concentration of the $N_2(A,v)$ states has been calculated from the measured absorption with the help of a computer program which accounts for the detailed structure of the band spectra and for the effects of the monochromator's instrumental function.

The concentration of the $N_2(A, v = 0)$ level is given in Fig. 8 as a function of the discharge current for different values of the gas pressure. A maximum concentration of about 1.4×10^{12} cm^{-3} was obtained, the corresponding value for the absorption being of the order of 2%. Similar measurements have been done for the $v = 1 - 5$ levels, and a report is now in preparation which gives a detailed account of the results obtained.

A simple kinetic model has also been derived which attempts to give a physical interpretation of the experimental data. In this model, we take into account the most likely mechanisms that contribute to the formation and destruction of the $N_2(A)$ states in our discharge conditions. These mechanisms are listed below:

a) Creation

Ground state excitation by electron impact:

$$e + N_2(x) \xrightarrow{C_x^A} e + N_2\ (A)$$

$$\xrightarrow{C_x^A} e + N_2\ (B) \text{ followed by } N_2(B) \xrightarrow{h\nu} N_2(A)$$

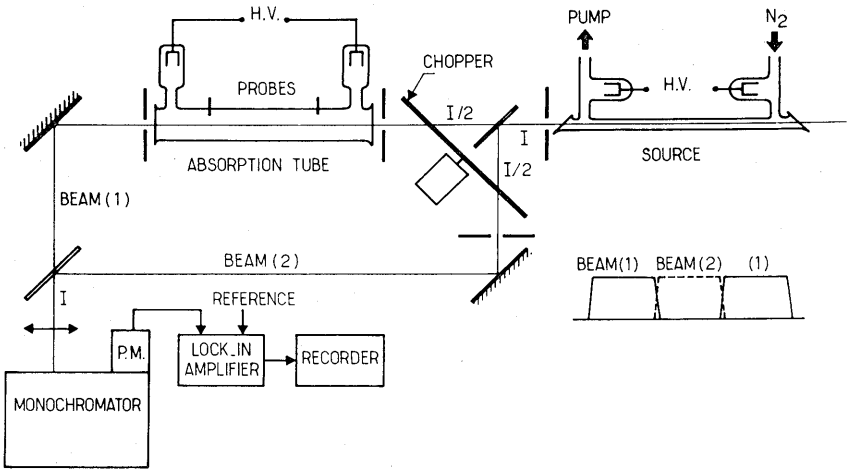

Fig. 7. Schematic diagram of the experimental arrangement used for measuring the concentration of the $N_2(A,v)$ metastable states in a glow discharge.

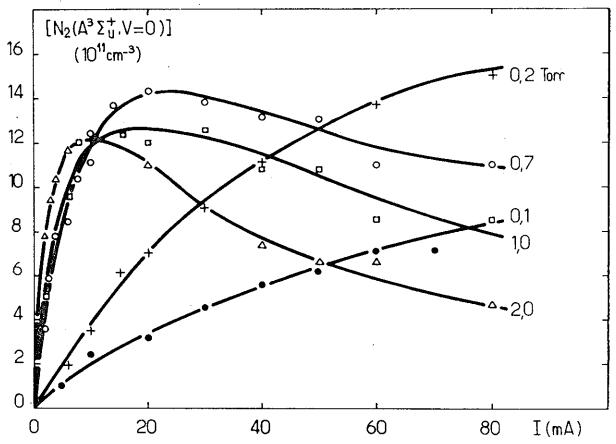

Fig. 8. Concentration of the $N_2(A,v=o)$ state as a function of the discharge current for different pressures.

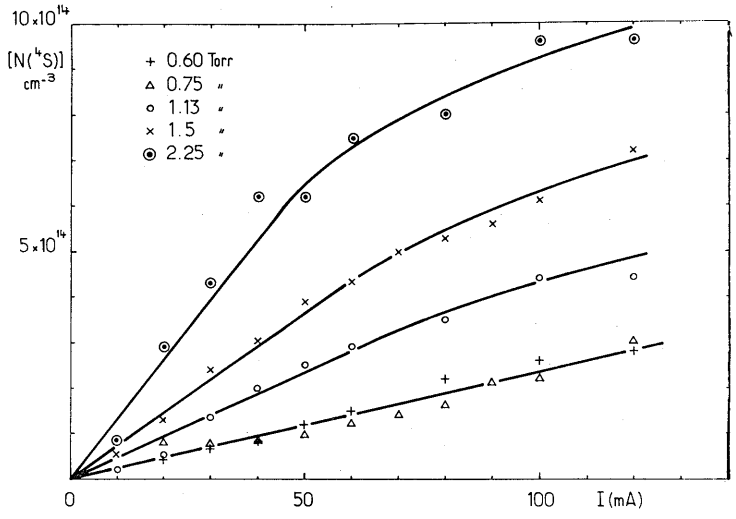

Fig. 9. Concentration of ground state dissociated nitrogen atoms as a function of the discharge current for different pressures.

e, x, A and s refer to electrons, $N_2(x)$, $N_2(A)$ and $N(^4S)$, respectively.

The variation of n_A with the discharge current I and the gas pressure p has been calculated using this equation. The electron density and the concentration of dissociated atoms have been measured as a function of I and p using a microwave cavity and the NO titration method, respectively. Figure 9 gives data obtained for the concentration of $N(^4S)$ vs. I and p. The electronic rate coefficients were calculated as a function of the pressure using C_x^A, C_x^B and C_x^C vs. E/n_x as given by Newman and De Temple (1976) and the similarity law E/n_x vs. n_xR. The latter was calculated from the balance between the collisional ionization of the gas and the loss of charged particles to the wall, and a good agreement with measurements has been found (see Figure 10). In these calculations, the gas temperature was assumed to be 300 K, which is only valid at low currents. In fact, we have found experimental evidence of important gas-heating effects with increasing current from measurements of the wall temperature and of the rotational distribution of the second positive system (0-0) band. Finally, the destruction of $N_2(A)$ by electron impact has been neglected as compared to the destruction by collisions with $N(^4S)$ atoms. In fact, taking into account our measurements, one should have $n_eC_A \ll n_sK_s^p$, unless $C_A > 5 \times 10^{-6}$ cm^3s^{-1}, which is very unlikely.

The results of this simple model are given in Fig. 11 together with the experimental data obtained for the v = 0 level, for

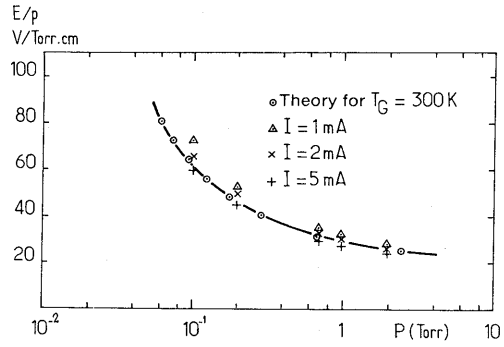

Fig. 10. Comparison of calculated and measured values of the ratio E/p as a function of pressure.

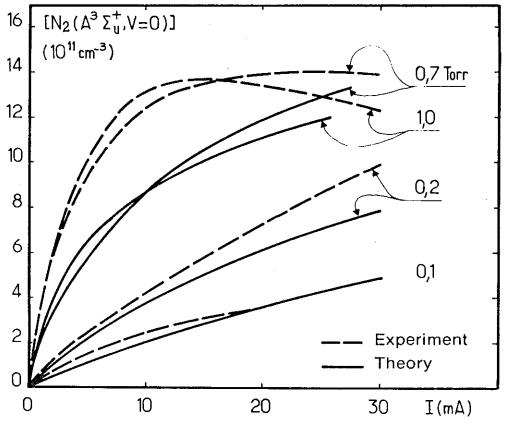

Fig. 11. Comparison of the predicted dependence of the $N_2(A)$ concentration on I and p with the experimental data obtained for the v = 0 level.

comparison. The model predictions are relatively accurate at low pressures and low currents, but serious deviations can be seen to exist when these parameters are increased. The reasons for these discrepancies are not yet well understood, but it is clear that the present model represents but an oversimplification of the real situation. In fact, a physically satisfactory model should include a detailed analysis of the creation and loss mechanisms for each individual $N_2(A, v)$ vibrational level, taking into account the vibrational distribution of the ground state molecules. This distribution is not known for the conditions of a stationary discharge, and it should be calculated together with the electron energy distribution as both distributions are expected to be strongly correlated according to the results of Capitelli and Dilonardo (1978). A detailed analysis of gas heating effects and of the dissociation mechanisms (the destruction of $N_2(A)$ by $N(^4S)$ being very effective) is also necessary.

REFERENCES

Allis, W. P., 1956, Handb. Phys., 21:383.
Becker, K. H., 1972, Faraday Dis. Chem. Soc., 53:35.
Borst, W. L., 1974, Phys. Rev., A, 9:1195.
Capitelli, M. and Dilonardo, M., 1978, Rev. Phys. Appl., 13:115.
Cernogora, G., Hochard, L., Touzeau, M., and Ferreira, C. M., 1981, J. Phys. B, 14:2977.
Eggarter, E., 1975, J. Chem. Phys., 62:833.
Ewald, H. N., Crawford, F. W., and Self, S. A., 1967, J. Appl. Phys., 38:2753.
Forrest, J. R. and Franklin, R. N., 1966, Br. J. Appl. Phys., 17:1061.
Hays, G. N. and Oskam, H. J., 1973, J. Chem. Phys., 59:1507 and J. Chem. Phys., 59:6088.
Ilic, D. B., 1973, J. Appl. Phys., 44:3993.
Jacob, J. H. and Mangano, J. A., 1976, Appl. Phys. Lett., 29:467.
Klarfeld, B., 1941, J. Phys. USSR, 5:155.
Klarfeld, B., 1937, Sov. Phys.-Tech. Phys., 4:44.
Lloyd, C. R., Teubner, P. J. O., Weigold, E., and Hood, S. T., 1972, J. Phys. B, 5:1712.
Muller, C. H. III, and Phelps, A. V., 1980, J. Appl. Phys., 51:6141.
Newman, L. A. and De Temple, T. A., 1976, J. Appl. Phys., 47:1912.
Pesnelle, A., 1970, Thesis 3e Cycle, Univ. of Paris-Sud., Orsay.
Peterson, L. R. and Allen, J. E., Jr., 1972, J. Chem. Phys., 56:6068.
Rapp, D. and Englander-Golden, P., 1965, J. Chem. Phys., 43:1464.
Schaper, M. and Scheibner, H., 1969, Beit. Plasma Phys., 9:45.
Schottky, W., 1924, Phys. Z., 25:635.
Self, S. A. and Ewald, H. N., 1966, Phys. Fluids, 9:2486.
Self, S. A., 1957, Phys. Fluids, 10:1569.
Tonks, L. and Langmuir, I., 1929, Phys. Rev., 34:876.
Young, R. A. and St. John, G. A., 1968, J. Chem. Phys., 48:895.
Zipf, E. C., 1963, J. Chem. Phys., 47:2034.

CONTRIBUTIONS TO CONTINUOUS LEADER CHANNEL DEVELOPMENT

M. M. Kekez and P. Savic

Division of Mechanical Engineering
National Research Council of Canada
Ottawa, Canada K1A 0R6

INTRODUCTION

The continuous propagation of the developing spark channel, known as a "leader" has been studied in considerable depth. Several theories have been proposed to describe the transition region occurring at the leader tip and causing the corona cloud to leader transition. For an overall review and outstanding questions to be tackled see Jones and Waters (1978).

We shall examine the applicability of two such theories, i.e., the hypersonic (detonation) and Volterra model by Kekez and Savic (1974, 1976 and 1980), Kekez et al. (1978) and Savic and Kekez (1980) in the light of our experimental evidence and that of other authors.

Figure 1 depicts the current understanding of the collective processes taking place near the leader tip according to the hypersonic model. The tip is regarded as a hydrodynamic discontinuity. The electric current flowing from the corona cloud across this discontinuity generates the Joule heating at the discontinuity as a result of field intensification at the convex side. This energy is converted into plasma, which is then subjected to rapid expansion in the form of a spherical shock wave. This shock will overtake the incoming electrons, the energy of which will be transferred to the plasma by large cross-section Coulomb collisions, thus further strengthening the shock in the manner of a detonation wave. The net effect is that the leader channel becomes the boundary of a contact surface (thermal channel) partially enveloped by an advancing paraboloidal shock front. At some radial distance downstream from the channel tip, the detonation wave decays into a sound wave.

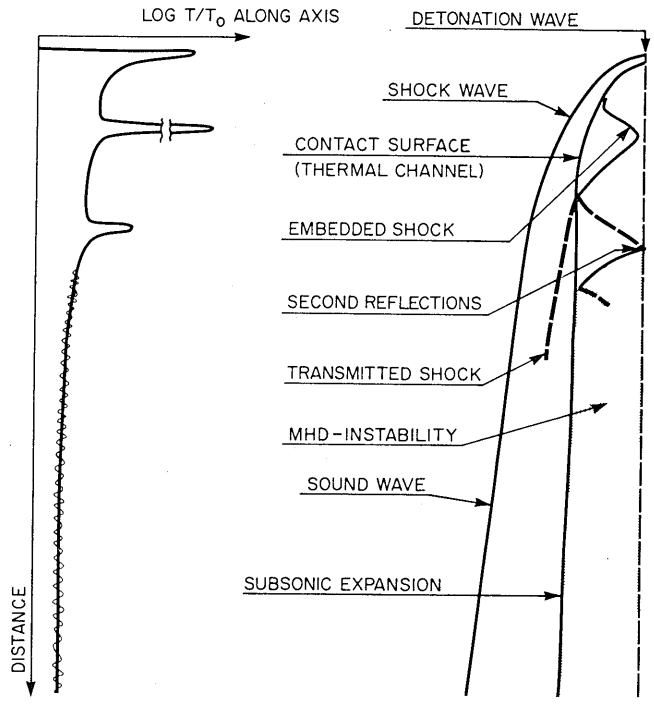

Fig. 1. Shock structure and temperature distribution at the tip of the leader channel.

The present concept of representing the channel as a pressurized gas cylinder subject to a sudden energy release leading to a blast wave leads us to expect that in addition to an outward going paraboloidal shock front near the tip, an inward going (embedded) shock is generated. The latter is the result of overexpansion of the gas caused by an increase in the flow area and subsequent recompression near the axis, where the embedded shock collapses, generating highly luminous spots of very high temperature. The lifetime of this high temperature region is governed by inertial confinement considerations; relatively simple fluid-dynamical reasoning suggests the existence of multiple reflections of the initial embedded shock on the axis and on the contact surface. The phenomenon is further complicated by the presence of the MHD - and other types of instabilities that take place at some distance from the tip. Further downstream, the thermal channel expands with subsonic velocity as a result of ordinary (thermal and electrical) conductivity effects, whereby the pressure inside the channel is almost equal to the outside.

Excellent experimental data of the later phases (subsonic expansion of the thermal channel, presence of sound wave, etc.) were

presented by the Les Renardières Group (1981); in particular, Gibert et al. (p. 193-198) have contributed to the schematic given in Fig. 1.

ESTIMATE OF THE POWER DISSIPATION AROUND THE TIP

An important implication of the hypersonic model is the enormous amount of the Joule power density dissipated at the tip. This can be estimated from simple electrodynamic argument. In Fig. 2 the rough schematic of the leader channel is given. The sphere of radius r_o represents the leader tip, and because the electrical contact between the tip and the corona cloud of radius r_c is taken to be maintained only at the leader head, the leader channel is represented by an insulated conducting rod. We assume that the channel head is immersed into the more or less homogeneous plasma of the corona cloud

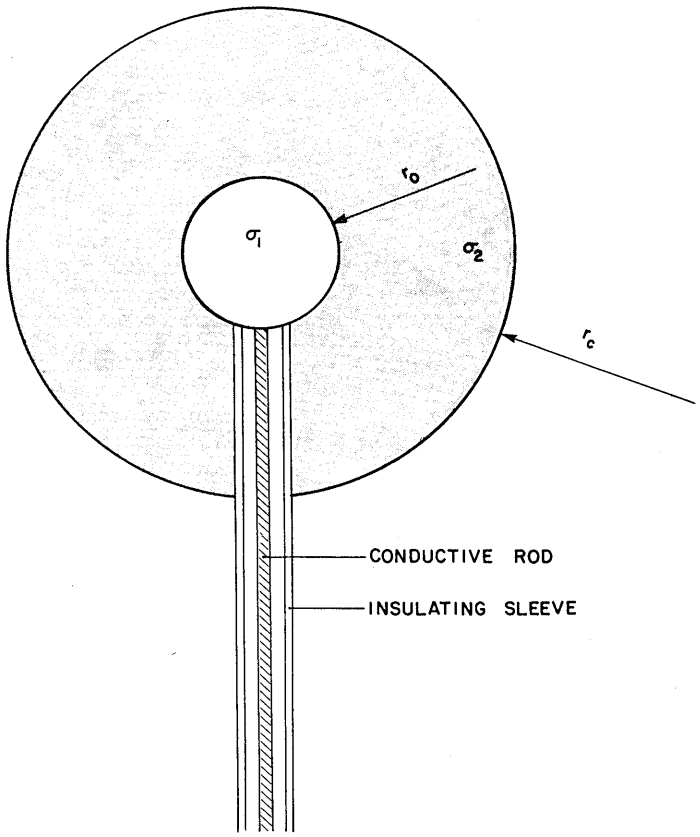

Fig. 2. Schematic of leader channel. Sphere of radius r_o depicts leader tip. r_c is the radius of corona cloud.

with conductivity σ_2. Between these two concentric spheres, the total resistance R is:

$$R = \frac{1}{4\pi\sigma_2}\left(\frac{1}{r_o} - \frac{1}{r_c}\right) . \qquad (1)$$

The experimental value for r_o lies in the range from 1 to 75 μm (See Table III) and for r_c of the order of 1m (Aleksandrov, 1969). Thus $r_c >> r_o$ and $R = (4\pi r_o \sigma_2)^{-1}$. Taking n_2 to be 4×10^{11} electrons/cm^3 (corresponding to $\sigma_2 = 2 \times 10^{-5}$(ohm cm)$^{-1}$), and r_o = 40 μm, we get R = 1 MΩ. If the leader current is 1 Amp, the total Joule heating RI^2 dissipated around the tip is 1 Megawatt. This estimate indicates that if the smaller estimate of r_o is taken, power in the megawatt range can be generated even at the current levels of a few hundred milliamperes. Furthermore, if the corona cloud is not a region of a quasi-uniform plasma but consists of many "streamers" converging towards the inner sphere, and if the conductivity, σ_2 in each streamer is of the same value as above, the total resistance, R, of the streamer-filled corona cloud will be even higher than that of a quasi-uniform corona cloud.

The present concept enables us to estimate the shape of the glow ahead of the leader channel. Assuming that the cold gas before the discharge has a certain low electrical conductivity (for example, if it is pre-ionized), one can plot theoretical lines of constant electrical heating around the tip of the channel. The lines of constant Ohmic dissipation were computed by Kekez and Savic (1976) for the case of the leader channel as a slender half-ellipsoid of revolution sitting on an infinite plane, with the opposite plane electrode infinitely far away. The results are given in Fig. 3a, where the lines are normalized in respect to the value at the infinite plate. Figure 3a clearly exhibits the shielding effect of the spark channel on the field of the top plate, whereby the glow above the channel tip is completely mopped-up. Gallimberti (1977 and 1979) also considers the lines of constant Ohmic heating between the leader channel (depicted by a paraboloid) and a distant plane. The radius of the curvature is 25 μm at the tip, and the (streamer-free) gas ahead of the tip has a constant low conductivity. The results are given in Fig. 3b. Both Figs. 3a and 3b confirm that the greatest concentration of power is near the tip; the region some distance downstream from the tip, where the channel originates is of no importance. In zero order approximation, the shape of the glow at the tip does not depend on the gap length. This is illustrated by high-speed photographs of the leader (Fig. 3c).

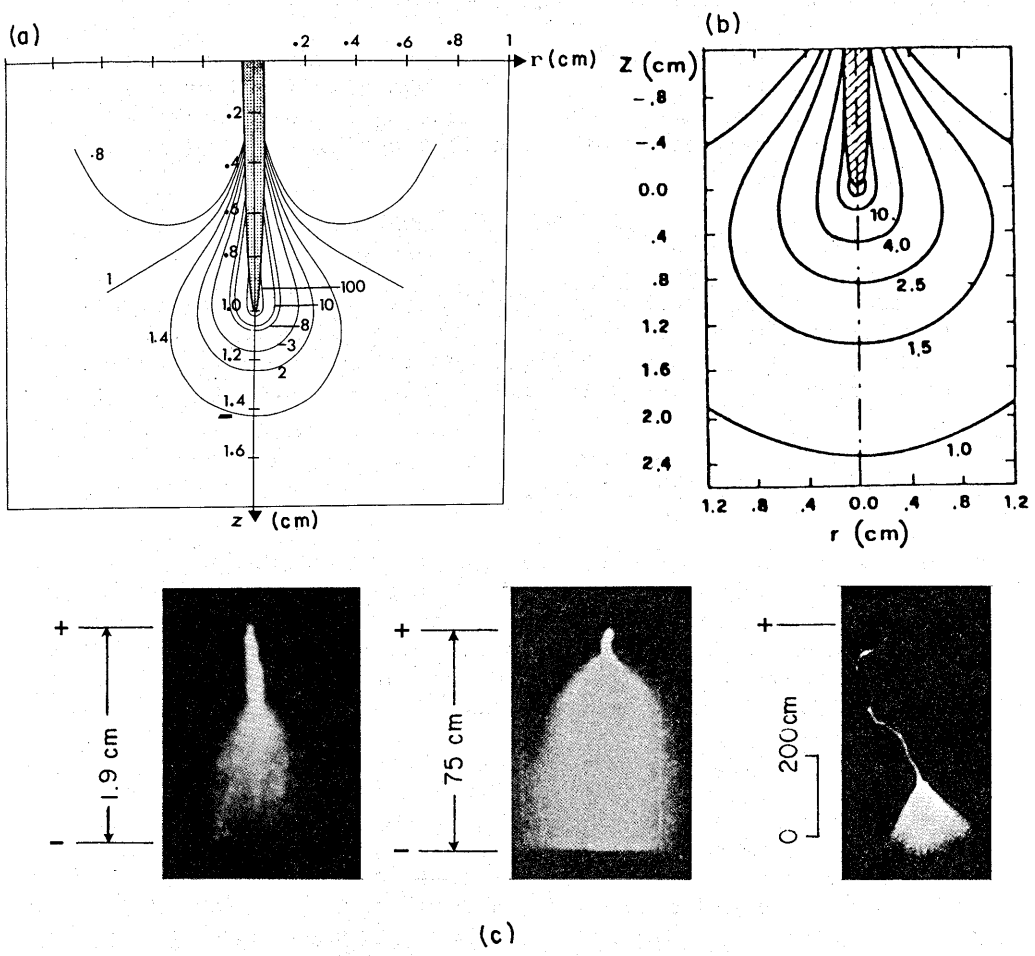

Fig. 3. Lines of constant Ohmic heating around tip of leader channel (shaded area). a) Parallel-plate electrode geometry. Leader approximated by ellipsoid. (Kekez and Savic, 1976. Reproduced by permission of the IEE.) b) Rod-plane geometry. Leader represented by a paraboloid. (Gallimberti, 1979. Reproduced by permission of the Journal de Physique.) c) Experimental results. Left: Shutter photography in H_2: 250 torr pressure, 1.9 cm gap length, plane-plane gap. (Kekez and Savic, 1976. Reproduced by permission of IEE.) Results in a 75 cm rod-plane gap in atmospheric air (Newi, 1973). Reproduced by permission of the author. Right: Shutter picture in a 10 m rod-plane gap in atmospheric air. (Berger et al., 1974. Reproduced by permission of Electricité de France.)

TEMPERATURE EVALUATION AT THE LEADER TIP

The Joule heating taking place in the filamentary channel and causing the glow-to-leader-transition was also considered by Aleksandrov (1966). He assumed that this heating is used entirely to increase the kinetic energy of the gas molecule:

$$\frac{\text{Joule energy}}{\text{unit length}} (\Delta W_J/\Delta \ell) = \frac{\text{kinetic energy}}{\text{unit length}} (\Delta W_k/\Delta \ell) \qquad (2)$$

where $\Delta W_k/\Delta \ell = (z/2)k\Delta T N_o \pi r_o^2$. N_o is the gas number density at N.T.P. (= Loschmidt number), r_o the radius of the filament, k the Boltzmann constant, ΔT the temperature rise, and Z the degree of freedom. (Z = 5 for a "rigid" diatomic molecule). Hence the temperature increase is:

$$\Delta T = (\Delta W_J/\Delta \ell)/((5/2)\ k\ N_o \pi r_o^2) \ . \qquad (2a)$$

The numerical example of Eq. (2a) is given by Aleksandrov for a simple streamer channel. Taking a very large value of the longitudinal gradient along the streamer to be 20 KV/cm, he puts $\Delta W_J/\Delta \ell$ to be equal to 4 J/m (not 4J/cm as stated erroneously by Kekez and Savic, 1981), and with r_o = 500 μm, he obtains ΔT = 5500°K to be the temperature inside the streamer.

If one applies this model to the leader channel, then from the Ohmic dissipation at the tip (Eq. (1)), it is reasonable to interpret ΔW_J in Eq. (2) as approximately equal to the voltage across the discharge, V, times the leader current, I, times the time interval Δt. Because the leader velocity v is $\Delta \ell/\Delta t$, we have $\Delta W_J/\Delta \ell \approx VI/v$ = total power P, divided by the leader velocity, v. Taking P = 1 MW and v = 2 cm/μs, we have ΔW_J = 0.5J/cm. These numbers agree with experimental values at the minimum of the U-curve by Les Renardières group (1977) (see also, Waters, 1981). With $\Delta W_J/\Delta \ell$ = 0.5J/cm, assuming r_o = 40 μm, the Eq. (2a) yields the temperature at the leader tip $\Delta T \approx 10^7$°K. To the left of the U-curve, (the domain of lightning impulses), we find that ΔT will rise even more, since Uman (1971) gives: $\Delta W_J/\Delta \ell$ = 20J/cm for v = 200 cm/μs. Even if the distribution of energy inside the gap proposed by Waters (1981) is considered, the temperature calculated from Eq. (2a) is unrealistically high. At high temperature, the shock will be formed, as rightly pointed out by Aleksandrov, but not included in his model, and the Joule energy will be spent to drive this shock.

The temperature at the tip can be estimated alternatively by assuming that the detonation mechanism is responsible for the development of the spark channel. For a strong detonation (Mach number > 10), we have (Stanyukovich, 1960):

$$\frac{p_f}{\rho_o} = \frac{v^2}{\gamma+1} \tag{3}$$

$$\frac{\rho_f}{\rho_o} = \frac{\gamma+1}{\gamma} \tag{4}$$

where p_f and ρ_f are pressure and density at the shock front, respectively, ρ_o density ahead of the front, γ the effective adiabatic index, and v the detonation speed. Detonation may be thought of as a shock wave followed by a rapid exothermic energy release; this release supports its own shock wave in front of itself which in turn triggers the release. Equations (3) and (4) relate to that part of the detonation front following the so-called von Neumann's pressure spike and the exothermic "reaction" zone.

Substituting Eqs. (3) and (4) into the expression for the specific internal energy at the front, ε,

$$\varepsilon = \frac{p_f}{\rho_f(\gamma-1)} ,$$

we have

$$\varepsilon = \frac{\gamma}{(\gamma^2-1)(\gamma+1)} v^2. \tag{5}$$

Raizer (1965, 1977) has obtained Eq. (5) by a different approach to determine the temperature of a laser spark. In atmospheric air ($\rho_o = 1.29 \times 10^{-3}$ grams/cm^3), the equilibrium parameters of plasma behind the front are given in Table I: temperature, degree of ionization expressed in terms of the average charge of the ions (atoms are assumed to be multiply ionized, so $N_i = N$ and $N_e = ZN_i$, where N_e, N_i and N are numbers of electrons, ions, and original atoms per cm^3), the specific internal energy, ε, and the theoretical detonation velocity, v [obtained from Eq. (5)].

Hence, by observing the speed of propagation (see Table I), information on the discharge characteristics can readily be gathered. Because the velocity of the detonation wave is governed by gas (ion) temperature and not by the electron temperature behind the front, it is important to inquire just how fast and by what mechanism the equilibrium is established.

Table 1. Thermodynamic properties of air.

T (°K)	20,000	30,000	50,000	100,000	250,000	500,000	700,000	1,000,000
ϵ (erg/gram)	$8.03\ 10^{11}$	1.5×10^{12}	3.18×10^{12}	9.24×10^{12}	$3.08\ 10^{13}$	$4.84\ 10^{13}$	$1\ 10^{14}$	$1.52\ 10^{14}$
z	0.24	0.68	1.50	2.65	5	5.2	5.7	6.6
γ	1.175	1.189	1.215	1.225	1.275	1.370	1.318	1.332
v (cm/μs)	0.752	1.069	1.6615	2.898	5.863	8.568	11.38	14.35

IONIZATION AND THERMALIZATION TIME CONSTANTS

Theoretical expressions for ionization of unexcited atoms by electron impact have been given, for example, by Zel'dovich and Raizer (1967, p. 386), where the development of ionization proceeds by electron avalanche. If we assume that the electron temperature is independent of time, then the electron density rises as

$$N_e(t) = N_{eo}\exp(t/\tau_e) \tag{6}$$

where N_{eo} is the initial electron density, and τ_e is given by

$$\tau_e = \frac{1}{\alpha_e N_a} \tag{6a}$$

where

$$\alpha_e = \sigma_e v_e \left(\frac{I}{kT_e} + 2\right)\exp(-I/kT_e). \tag{6b}$$

α_e is the rate constant for ionization from ground level of atoms, v_e is the mean thermal speed of the electrons, σ_e is an average value of the cross section, I is the ionization potential, and N_a is the neutral atom number density.

The growth of electron concentration for moderately low temperature in air is related to the ionization of NO molecules as it has lower ionization potential (9.25ev) than those of all the other constituents of air. Hence, we calculate α_e vs T_e for I = 9.25ev using the cross section given by Zel'dovich and Raizer (1967).

In the detonation model, the incoming electrons (generated by the corona cloud and having a low degree of ionization (i.e., N_{eo} in Eq. (6) may be 10^{11} - 10^{12} electrons/cm^3) are overtaken by the shock. Because of von Neumann's spike, both the neutral and electron gas will be compressed by a factor K equal to $(\gamma+1)/(\gamma-1)$. The compression is of the order of 7-13 (see Table I), and N_a of Eq. (6a) will be increased by this factor. Hence, because of the shock wave, we have a decrease of the time constant τ_e Eq. (6a). The calculated value of τ_e in atmospheric air at von Newmann's spike is given in Fig. 4.

Another point should be made. During compression the neutral gas is being heated. This in turn will lower the ionization potential used in Eq. (6b). Therefore, the above examples of the ionization time constant are rather conservative.

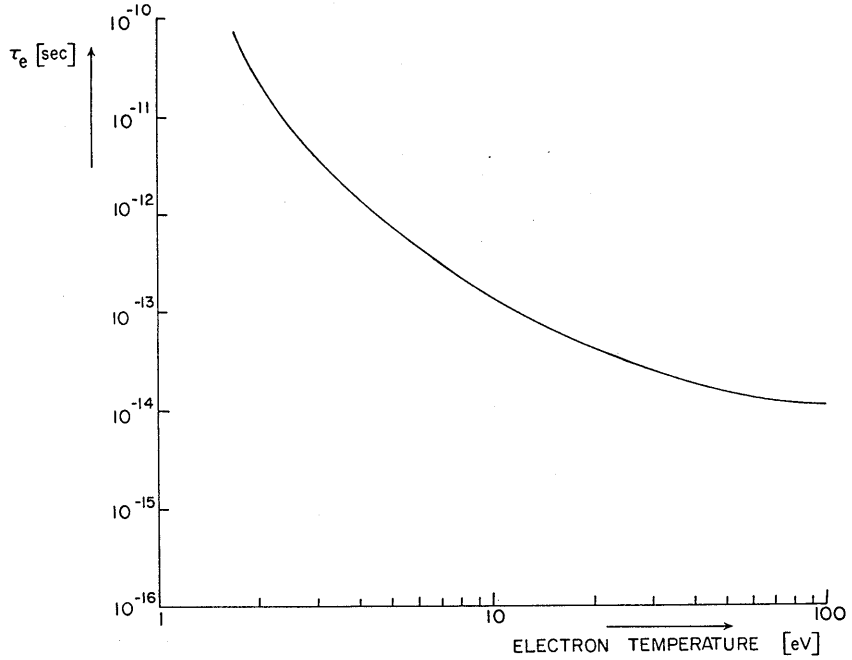

Fig. 4. Calculated ionization time constant, τ_e vs. electron temperature at von Neumann pressure spike.

In addition to the electron multiplication in the rear of the shock, there is a net exchange of thermal energy between electrons and ions. The characteristic time, τ_{ei}, for the energy equipartition through elastic Coulomb collision is identified with the stopping power of the (gradient-free) plasma to an incident-charged particle. Several theoretical studies have been done, notably by Landau, Spitzer and Chandrasekhar leading to identical results in terms of functional relationship for the equipartition time, $\tau_{ei} \sim T_e^{3/2}/N_i$, except for a minor difference in absolute value. (For comparison, see Dougal and Goldstein, 1957).

When density gradients are present in the plasma, as is the case at the shock front, the equipartition of energy takes place also by a hydrodynamic mechanism via the work done by the electron pressure forces on the ion gas because both electrons and ions are coupled strongly by the Coulomb forces. This mechanism was proposed by Raizer (1977, p. 217); an analytical expression will be derived in the following.

Following the classical theory of plasma oscillations any charge separation gives rise to an electric field, described by Poisson's equation:

$$\frac{dE_x}{dx} = -\frac{en_e}{\varepsilon} \tag{7}$$

E_x is the electric field in the x-direction, n_e is a small fluctuating perturbation superimposed on the constant equilibrium value of electron density, $\bar{n}_e$. The electron continuity equation may be linearized to give

$$\frac{\partial n_e}{\partial t} + \bar{n}_e \frac{\partial v_e}{\partial x} = 0 \ . \tag{8}$$

The momentum equation for ions (linearized) is

$$m_i n_i \frac{\partial v_i}{\partial t} = e n_i E_x \ . \tag{9}$$

Hence from Eqs. (7) and (8)

$$\frac{\partial^2 E_x}{\partial x \partial t} = \frac{e\bar{n}_e}{\varepsilon} \cdot \frac{\partial v_e}{\partial x} \ ,$$

or by integrating

$$\frac{\partial E_x}{\partial t} = \frac{e\bar{n}_e}{\varepsilon} v_e \ .$$

Substituting in Eq. (9)

$$\frac{\partial v_i^2}{\partial t^2} = \frac{e^2 n_e}{\varepsilon m_i} v_e = \omega_p^2 v_e \frac{m_e}{m_i} \ , \tag{10}$$

where ω_p is the electron plasma frequency. Assuming v_e to be constant and integrating Eq. (10)

$$v_i = \frac{m_e}{2m_i} \omega_p^2 v_e t^2 .$$

This can be written as

$$\frac{m_i v_i^2}{2} = \frac{m_e v_e^2}{2} \left[\frac{m_e}{4m_i} (t\omega_p)^4 \right] .$$

The ion energy $\frac{m_i v_i^2}{2}$ reaches that of the electron $\frac{m_e v_e^2}{2}$ at time $t = \tau_1$ where

$$\tau_1 = \frac{\sqrt{2}}{\omega_p} \left(\frac{m_i}{m_e} \right)^{1/4} . \tag{11}$$

If one starts with a nonequilibrium plasma, the electrons reach a Maxwellian distribution first in time τ_{ee}, followed by the ions in time, τ_{ii}, and finally the equipartition of energy between electrons and ions in time τ_1. Hence, the total equipartion time, τ_{eq}, is:

$$\tau_{eq} = \tau_{ee} + \tau_{ii} + \tau_1 \tag{12}$$

where τ_{ee} and τ_{ii} are given by Spitzer's formulae. It turns out that in the presence of the steep gradient at the front

$$\tau_{eq} = \tau_{ii} \tag{13}$$

as $\tau_{ii}/\tau_{ee} = (m_i/m_e)^{1/2}$ and $\tau_{ii} >> \tau_1$. With the conditions of Table I and at the detonation front (Eqs. (13) and (14)), the calculated equipartition time of Eq. (13) is given in Fig. 5.

An alternative approach to determine τ_{eq} is to consider Spitzer's electron to ion equipartition time, τ_{ei}, when it is applied to the detonation front conditions (see Fig. 6). Without the front, the electron temperature, T_{eo}, will fall to the final temperature, T_f, and consequently the ion temperature, T_i, will rise from the room value T_1 to T_f, both with the time constant, τ_{ei}. Note that from the definition of τ_{ei}, the ion temperature will rise to 0.632 of T_f in $t = \tau_{eq}$.

At the detonation wave, a jump from A to B (Fig. 6) will occur as a result of the shock compression in the von Neumann spike. After B, the exothermic reaction follows with the time constant τ_{ei}. It can be gathered from Fig. 6, (after some manipulation) that the ion temperature reaches 63.2% of T_f in time, t equal to:

$$t = \tau(1 + \ell n \ \Delta T/\Delta\bar{T}) . \tag{14}$$

From Bartlmä (1975, p. 99), the temperature $\bar{T}_1$, at the point B of the jump is:

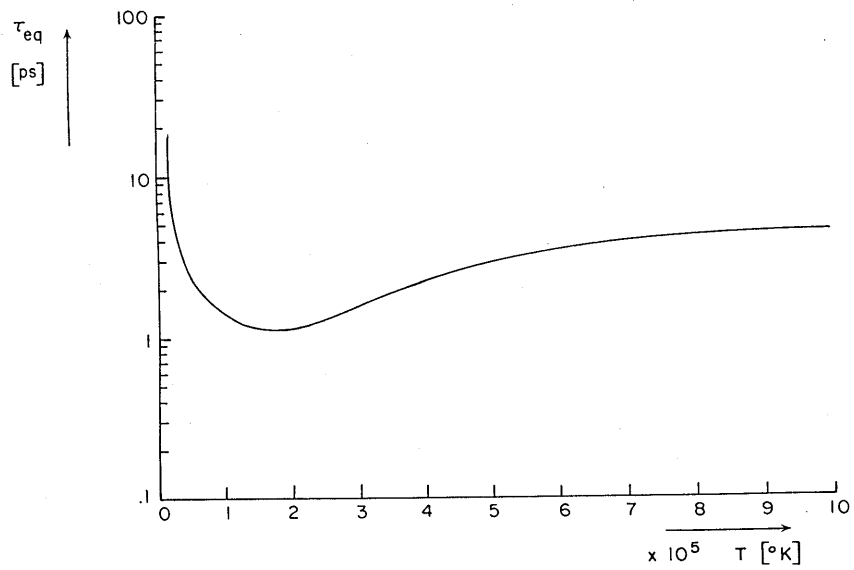

Fig. 5. Calculated equipartition time vs. channel plasma temperature (LTE) at detonation front due to hydrodynamic equilibration mechanism.

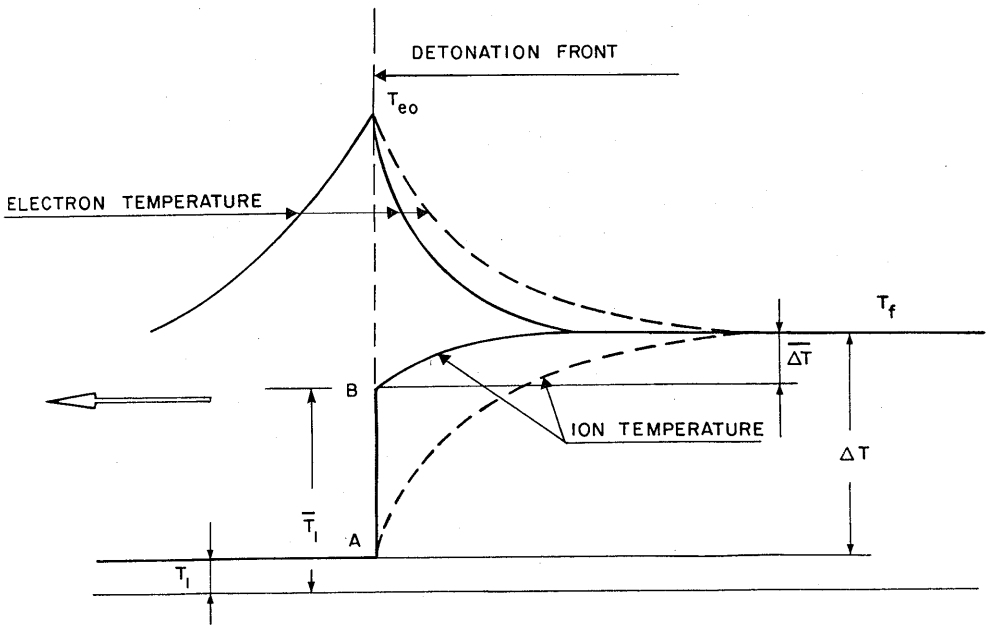

Fig. 6. Schematic of the energy-transfer mechanism with shock (solid line) and without shock (broken line).

$$\bar{T}_1 = 2M^2 T_1(\gamma-1)/(\gamma+1)^2 \quad .$$

M is the Mach number at the Chapman-Jouguet point, and the final temperature, T_f, is

$$T_f = M^2 T_1(\gamma/(\gamma+1))^2 \quad .$$

Hence

$$\Delta T = T_f - T_1 \simeq T_f; \quad \Delta\bar{T} = T_f - \bar{T}_1 \ ,$$

and

$$t = \tau[1-\ell n\gamma/(2-\gamma)] \ . \tag{14a}$$

For an ideal monatomic gas: $\gamma = 5/3$, we have from Eq. (14a) that $t < 0$, implying that the temperature jump from A to B is above 63.2% of T_f. The relevant process during the jump is the ion-ion equilibration of energy; hence we are back to the same result as the one given by Eq. (13): $\tau_{eq} = \tau_{ii}$.

For an ideal diatomic gas: $\gamma = 7/5$, Eq. (14a) suggests that 63.2% of T_f will be reached for $t = 0.153\ \tau_{ei}$. Here τ_{ei} is given by Spitzer's formula.

In summary, we note that in the detonation model, the growth of ionization from the low degree ahead of the shock to a high n_e behind the shock, as well as the energy transfer to heavy particles, is done in the rear of the wave front. The shock front accelerates the ionization built-up by compressing and heating the neutral gas density. This in turn will promote a speeding up of energy exchange via collective hydrodynamic mechanisms and via the presence of the von Newmann spike. The ionization time constant [Eq. (6a)] and the equipartition time constant [i.e., Eq. (15)] are coupled by a positive-feedback loop whereby the lowering of one time constant means a decrease in another one. The thickness of the layer where these two processes take place, Δx, is of the same order of magnitude as the detonation speed (see Table I) multiplied by the time necessary for the reaction to occur: $t = \tau_e + \tau_{eg} \simeq \tau_{eq}$. At $v = 1.069$ cm/μs (see Table I), $T_f = 30000°K$, $T_{eo} \simeq 2T_f = 5.17$ eV (assuming that a small amount of energy is lost in ionization), τ_{eq} from Fig. 5 is equal to 3.5 ps, and we have $\Delta x = 3.7 \times 10^{-6}$ cm.

DERIVATION OF LEADER TIP VELOCITY

To calculate the speed of the leader tip, we will apply the standard detonation (Chapman-Jouguet) theory for reacting gases. We need only to replace the reaction energy by the Joule heat per unit of mass. This is due to the heating of electrons by the high electric field ahead of the channel tip.

Note that Joule heating is also involved in the laser-induced spark. The theory to be presented is that of the laser-supported detonation conceived by Ramsden and Savic (1964), [see also Raizer (1965)], and in many ways is of fairly general validity as it attempts to synthesize both electrical and optical (laser-induced) gas discharges.

The application of the equations of conservation of mass, momentum, and energy to the shock front together with the Chapman-Jouguet requirement leads to a particularly simple expression for the speed of detonation, v, providing that the Joule energy is much larger than the ambient enthalpy of the gas. The speed is

$$v = (2(\gamma^2-1)E/\rho)^{1/2} \tag{15}$$

where γ is the adiabatic index, and E/ρ is the (Joule) energy per unit mass (E = energy density and ρ = mass density). It can be said in favor of Eq. (15) that the velocity is rather insensitive to the detailed processes occurring in the internal structure of the wave front as well as to the detailed front geometry, providing that the diameter is large compared to the front thickness, Δx. On the other hand, the theory of highly curved (filamentary) detonation is not yet fully developed so that it is necessary to search for an alternative approach to supplement Eq. (15).

The discharge of energy into the rear of the shock may also be interpreted as the expansion of a cylindrical piston. Pursuing this "hypersonic analogy" of Chernyi (1961) further, we can regard the leader channel in the rear of the shock as a blunt-nosed cylindrical body, pushing a paraboloidal bow-wave ahead of itself. The energy supporting the shock is then easily re-interpreted in terms of the drag of the body, which can be calculated if we assume a simple nose-shape (e.g., a hemisphere) and apply Rayleigh's pitot tube formula (see Steginsky, 1964). We get:

$$v = \left(\frac{2}{C_d} E/\rho\right)^{1/2} \tag{16}$$

where the drag coefficient, C_d, is given by

$$C_d = \frac{1}{\gamma} \left(\frac{\gamma+1}{2}\right)^{\gamma/(\gamma-1)} \left(\frac{\gamma+1}{2\gamma}\right)^{1/(\gamma-1)} .$$

For $\gamma = 1.4$, $C_d = .92$. For the same E/ρ, the velocity from the drag concept (Eq. (16)) is about 5.7% higher than that from the detonation approach (Eq. (15)).

To determine the velocity in terms of the discharge parameters based on the shock energetics, Eqs. (15) and (16) require knowledge of the electric field distribution around the tip. For a constant electrical conductivity inside the corona cloud, the potential theory can be applied. One of the most suitable geometries is described by the hyperboloidal (rod-plane) model of Aleksandrov (1969). At any given moment, we assume that the hyperboloid of revolution approximates the paraboloidal shock (Eqs. (15) and (16)) at the tip.

If the potential at the tip is ϕ, then the solution of Laplace equation $-\nabla^2\phi = 0$ in prolate ellipsoidal coordinates — is (Moon & Spencer, 1961):

$$\phi = V \frac{\ell n[(1 + \cos\theta)/(1 - \cos\theta)]}{\ell n[(1 + \cos\theta_o)/(1 - \cos\theta_o)]}$$

where η and θ are prolate ellipsoidal coordinates defined by

$$r = a \sin\theta \sinh\eta, \quad z = a \cos\theta \cosh\eta ; \tag{17}$$

r, z are cylindrical coordinates, and a is a length parameter. The hyperboloid is defined by

$$z^2/a^2\cos^2\theta - r^2/a^2\sin^2\theta = 1. \tag{17a}$$

Hence on the center line of the hyperboloid, $\eta = 0$; the electric field becomes

$$\frac{d\phi}{dz} = \frac{2V}{a(1-(z/a)^2)\ell n((1+z_o)/a)/(1-z_o/a))} .$$

For slender hyperboloid, $z_o \tilde{} a$, the field at the tip is

$$\frac{d\phi}{dz} = - \frac{V}{a(1 - z/a)\ell n(1 - z_o/a)} . \tag{18}$$

The Joule energy density is

$$E = \int_{-\infty}^{t_o} \left(\frac{d\phi}{dz}\right)^2 dt$$

where t_o is the time of arrival of the tip at the point under consideration. If the hyperboloid propagates with locally constant velocity, v, every gas particle on the axis in front of the tip gains an energy density given by

$$E = \frac{1}{v} \int_{a+z-z_o}^{\infty} \sigma \left(\frac{d\phi}{dz}\right)^2 da. \tag{19}$$

Putting Eq. (18) into (19) we get

$$E = \sigma V^2 / [v(a-z_o) \ell n^2 (1-z_o/a)] \quad . \tag{19a}$$

Introducing $z = y + \cos\theta$, where y is a shifted length into Eq. (17a), we get the radius of the slender hyperboloid to be:

$$r^2 \simeq 4ay(1 - z_o/a) \quad . \tag{20}$$

The radius of the paraboloidal shock wave predicted by cylindrical blast-wave theory is

$$r = (E_1/\rho)^{1/4} \, F(\gamma) t^{1/2} \tag{21}$$

where E_1 is the energy per unit length, $F(\gamma)$ is a slowly varying function of the adiabatic index, γ, which has a value close to unity and ρ is the density of the gas ahead of the shock. By considering the effect of shock strength and the nature of gas, Steginsky (1964) and Swigart (1960) give the expression for $F(\gamma)$ to third order accuracy in inverse Mach number, and their detailed expression was used by Kekez and Savic (1968) to determine the time of transition, when the shock decays into a sound wave. Here we take $F(\gamma) \simeq 1$.

The theory of high-speed (hypersonic) flow provides a relation between the constant-energy nonsteady similar flow behind the blast wave arising from detonation and steady hypersonic flow about a slender body. Thanks to this hypersonic analogy, it is sufficient in both cases to substitute t in Eq. (21) with y/v. Hence,

$$r = (E_1/\rho)^{1/4} \, (y/v)^{1/2} \quad . \tag{21a}$$

Combining Eqs. (21a) and (20), we get

$$(E_1/\rho)^{1/2}/v = 4(a-z_o),$$

and with Eq. (19a)

$$E = 4\sigma V^2 (E_1/\rho)^{-1/2} \ell n^{-2} [(E_1/\rho)^{1/2}/4va] \ .$$

If A is the cross-sectional area of the leader tip, then $E_1 = AE$. From the Chapman-Jouguet conditions, Eq. (15), we have that the speed of the shock wave surrounding the leader tip, v, is:

$$v = \sqrt{2(\gamma^2-1)} \sqrt[3]{\frac{4\sigma V^2}{\rho A^{1/2} \ell n^2 \lambda}} \qquad (22)$$

where

$$\lambda = \frac{r_o}{4a} \{\pi / [2(\gamma^2 - 1)]\}^{1/2} \ ;$$

r_o is the tip radius and a the gap length. Equation (22) is obtained under the assumption that the Joule energy is added to the heavy particles in the rear of the front where the equilibration time between electron and ion is infinitely short, implying that the diameter of the leader tip, $2r_o$ is larger than the width of the exothermic reaction zone, $\Delta x (2r_o > \Delta x)$. Equation (22) differs slightly from a similar expression which has been presented without derivation by Kekez and Savic (1976). There the Chapman-Jouguet condition was inadvertently used: $v^2 = (\gamma^2-1)E/\rho$ instead of $v^2 = 2(\gamma^2-1)E/\rho$.

It may be of interest to transform Eq. (22) further to faciliate comparison with experiments. If we assume that the electrical contact between the leader channel and the corona cloud is present only at the leader head, using Eq. (1), $\sigma = \sigma_2 = (4\pi r_o R)^{-1}$ and by definition the power, P, is equal to V^2/R, we get

$$v = \sqrt{\frac{2(\gamma^2-1)}{\pi}} \sqrt[3]{\frac{P}{r_o^2 \rho \ \ell n^2 \lambda}} \ ,$$

with

$$\lambda = \frac{r_o}{4a} \sqrt{\frac{\pi}{2(\gamma^2 - 1)}} \ . \qquad (23)$$

If the drag concept presented by Eq. (16) is to be used to replace the detonation theory Eq. (15), it is necessary to exchange the term $2(\gamma^2-1)$ by the term $2/Cd$ in Eqs. (22) and (23). To illustrate these two concepts (Eq. (23)), a numerical example is given in Table II which also attempts to account for the experimental results of the Les Renardières Group (1977) obtained in a 10 m gap in atmospheric air. When the total power was 10^6 watts, they observed a

leader velocity of about 2 cm/μs. We assume two different values for the tip radius: 40 μm and 4 μ.

Note that the expression by Ramsden and Savic (1964) [see also Kekez and Savic (1980)] describes the laser-induced spark via the radiation-supported detonation mechanism:

$$v = \sqrt[3]{\frac{2(\gamma^2 - 1)P}{\pi r_o^2 \rho}} \quad . \tag{24}$$

P is the laser power absorbed in the gas. For other symbols see Eq. (23). Equation (24) is based on a one-dimensional model, while Eq. (23) is the consequence of three-dimensional considerations. The functional relationship between the velocity, v, versus the power, P; the gas density, ρ, and the spark radius, r_o, are the same for both the laser-supported (Eq. 24) and electrically-supported detonation (Eq. 23). The dependence of the gap length, a, in Eq. (23) is very weak as it appears in a logarithmic term.

ESTIMATES OF THE RADIUS AT THE LEADER TIP

From the experimental point of view, the verification of the laser-supported detonation (Eq. (24)) offers an advantage over the electrically supported detonation (Eq. (23)): r_o is a function of the focussing lens. Hence, it is possible to have detonation extending from a nearly full solid angle to a very narrow filament (1.7 μm in diameter) driven by 1 MW laser power (experimental values; see Korobkin and Alcock, (1968)), and to check more easily Eq. (24). In electrical sparks, the value of the channel radius at the tip could be determined as the consequence of the coupling between the

Table II. Theoretical and Experimental Leader Velocities.

Velocity (cm/μs) from:	for r_o = 40 μm	for r_o = 4 μ
detonation model	1.084	4.531
drag concept	1.145	4.789
experiment	2.0 (r_o unknown)	

equations of the shock energetic (Eq. (15) and (16)) and of the field concentration and strength at the tip. While work along this line is still in progress, we will present here the theoretical limits of the leader tip radius, as well as some experimental results.

A lower limit is found if the leader channel is assumed to be filled with highly ionized-hot plasma, and its characteristic dimension must be greater than the Debye length; thus:

$$r > \text{Debye length} = h = 6.9(T/N_e)^{1/2} \quad . \tag{25}$$

T is in °K, N_e in cm^{-3} and h in cm. For example, if $T = 0.91 \times 10^6$°K v of Table I equal 13 cm/μs, and for simplicity take N_e = Loschmidt number, we get h = 0.0129 μm.

First Estimate

The rate of total energy supplied to the leader tip, P_s, goes to drive the shock wave accompanying hot plasma formation and to compensate, e.g., for radiation losses, P_r. The upper limit of the radius can therefore be gathered from the following inequality:

$$P_s \text{ (supplied)} > P_r \text{ (radiated)}. \tag{26}$$

If we suppose that the hot plasma occupies a cylinder at constant temperature, T, surrounded by cold gas, the flux of thermal radiation leaving the frontal surface of the cylinder is [after Raizer (1965)]:

$$S = \frac{1}{2} J r_o \psi \left(\frac{r}{\lambda}\right) f(v_o, v_1) \quad .$$

Here, r_o is the radius of the cylinder, $J = 4\sigma T^4/\ell_1$ the emissivity of the gas, σ the Stefan-Boltzmann constant, ℓ_1 the spectrally averaged radiation mean path, λ the same quantity for cold gas, and ψ and f are slowly varying functions of geometry. We take (after Raizer) $\psi = 0.4$ and $f = 1$. Our (unpublished) work shows that the error in taking the cylinder length d as infinite is negligible provided that $d/r \geq 10$. When T (in °K) is in the interval from 2×10^5 to 10^6 °K, $J = 7 \times 10^{18} (T/5 \times 10^5)$ erg/cm^3 sec for air of atmospheric density. Assuming that the tip can be approximated by a cube with area of $8\pi r^2$, we get P_r (radiated) $= 8\pi r^2 S = 1.6\pi r^3 J$, and from Eq. (26)

$$r_o < [(P_s/(1.6\pi J)]^{1\,3} \quad .$$

For $P_s = 10^6$W, $T = 10^6$ °K, we get $r_o < 52$ μm.

Second Estimate

In the detonation model of leader propagation, the following expression was used:

$$r = (E_l/\rho)^{1/4} F(\gamma) t^{1/2}$$

where E_l is the energy per unit length and may be equated to $\Delta W_j/\Delta \ell = VI/v$ of Eq. (2), t is the time, and we take $F(\gamma) \approx 1$. Equation (21) presupposes LTE. Hence $t = \tau_{eq}$ at the tip. From Fig. 5, we have that in temperature range 3.10^4 to 10^6 °K, $\tau_{eq} < 5$ ps. At atmospheric pressure $\rho = 1.3\ 10^{-3}$ gram/cm^3, and with $E_l = 0.5$ J/cm and $\tau_{eq} \approx 5$ ps, we get from Eq. (21) $r = 5.6$ μm. Note that Eq. (21) can be related to the Debye length (Eq. 25). For Paschen's Law, the minimum breakdown potential is proportional to the pressure (gas density; therefore, $V \approx \rho$). The internal energy of the plasma $\varepsilon \sim v^2$ (Eq. 5) assuming that the adiabatic index, γ, is constant. From thermodynamic tables for air: $\varepsilon \sim T^{1.63}$ (T = temperature). From Eq. (13) $\tau_{eq} \sim T^{3/2}/N_e \sim T^{3/2}/N_i$. Thus, Eq. (21) becomes

$$r = I^{1/4} T^{.046} \cdot \text{Debye length}.$$

The dependence on T is very weak and can be neglected. If the experiment is done at minimum breakdown conditions between parallel plate electrodes where Paschen's law holds, or at conditions along the minimum of U curve for the rod-plane geometry, the current will change less than 1/2 order of magnitude. Thus (Eq. (21) can be approximated as

$$r \approx \text{Debye length}. \qquad (27)$$

An ad hoc assumption that the radius is proportional to the Debye length was used by us (Kekez and Savic, 1976) to explain the experimental findings of Suleebka et al. (1975). Equation (27) offers proof for this assumption.

Third Estimate

For fully developed channels the motion of the gas outside the channel is due to a strong discontinuity (shock wave) with external supply of heat. Braginskii (1958) gives:

$$r = 0.93\ \rho^{-1/6} I^{1/3} t^{1/2}$$

where I is in kamps, t in μs, and r in mm. At atmospheric pressure $\rho = 1.3\ 10^{-3}$ gram/cm^3. Taking as before that the shortest time equals the thermalization time ≈ 5 ps, we find that for 1 Amp $r = 0.6$ μm, and for 10 Amp, $r = 1.4$ μm. Table III summarizes a few experimental findings.

Table III. Estimates of Leader Tip Radius.

Radius (μm)	Method	Comments	Reference
75	1.4×10^6 frame/sec Schlieren system	Initial radius from their Fig. 4 for a few 100 ns shutter pictures.	Kurimoto et al. (1978)
60	Spectroscopy	At 5 ns for completed channel.	Thall (1967)
50-60	App. 10 ns shutter photography	Current density = 10^7 A/cm^2.	Andreev and Sokolov (1966)
20	10-40 ps shutter Schlieren system	Spatial resolution of the system also 20 μm.	Kekez and Savic (1980)
1.25	Crater at electrode	Current through crater, 10 amps	Barreto et al. (1977)
0.75	Crater at electrode	Current through crater, 8 amps	Korlev et al. (1979)

Measurement of the radius is difficult and can be attempted only with sophisticated equipment. To illustrate, we estimate the uncertainty in the measurement due, e.g., to finite exposure time, Δt.

Assuming that the mean velocity in the transverse direction, v_r, is close to the sonic speed — for example, $v_r = 4 \times 10^5$ cm/sec, when the longitudinal (leader) velocity is 10^7 cm/sec — we find the width of the channel after Δt is $r(t) = r_o + v_r \Delta t$. For $\Delta t = 10$ ns, we see that the possible error (uncertainty in measurement) is $v_r \Delta t = 40$ μm. On the other hand, in a parallel-plate configuration, the leader is initiated by a cathode spot following a stage of volume (glow-type) discharge. The size of crater produced at the electrode surface could be related to the high energy density generated at (or imparted to) the surface. In either case, the crater should be related to that of the leader.

Indeed, from the appearance of the electrical breakdown through plexiglass, one finds that the diameter of the individual branches

at the tip is in the micron and submicron range (Kekez and Savic, 1981), suggesting that any suitable experimental system of femtosecond time resolution should also have a submicron spatial resolution.

EXPERIMENTAL SUPPORT

The detonation model suggests that shock waves are already evident when the spark channel is still in the process of formation. This implies that for a small arrested discharge in the laboratory, there should be a "bang" or thunder in large atmospheric discharges even if the leader has failed to bridge the distance from earth to cloud. The observer being some distance from the discharge will probably record only the sound wave, as even a strong wave will degenerate into a weak discontinuity surface, i.e., the sound wave at some distance transverse to the axis of the channel. For example, an advancing paraboloidal sound front surrounding the tip of a self-arrested spark channel has been observed by Berger et al. (1977) and Dastarac (1977). A formula for the time of the transition from hypersonic to sonic motion has been derived by Kekez and Savic (1978). The time-integrated picture of a self-arrested spark channel is shown in Fig. 7, and the radial expansion of the shock wave seen through a Schieren system is given in Fig. 8. The advancing tip has traversed the slit close to the cathode, at the speed of 1.2 cm/μs, when the current through the discharge was a few tens of amperes. With a millimeter spatial resolution, the initial radial shock velocity was about 2200 m/sec + 15%, and the time of hypersonic to sonic transition was about 6 μsec. The gap length was 2.15 cm.

Fig. 7. Time-integrated picture of arrested discharge. Contours of upper electrode (cathode) are made visible by UV source (blob at the bottom) placed beneath the screen (anode). (Kekez and Savic, 1978. Reproduced by permission of IEE.)

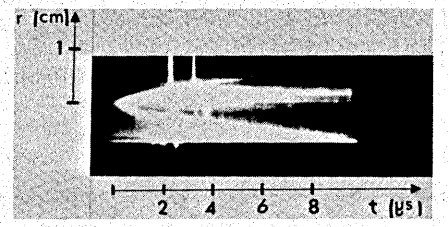

Fig. 8. Radial expansion of shock wave due to developing spark channel (Conditions as in Fig. 7). (Kekez and Savic, 1978. Reproduced by permission of IEE.)

Gibert et al. of the Les Renardières group (1981, p. 193) have carried out similar experiments in 2.18 m gaps. In addition to recording the shock wave of the radial expansion due to the developing spark channel (leader), they have also observed the subsequent shocks due to the current spikes that correspond to the stepped leader motion.

A new stimulus for the study of the radial channel expansion comes from a fusion-related experiment, i.e., a laser-initiated, gas-embedded Z pinch carried out, for example, at Los Alamos (Jones et al. 1981) and Imperial College, London (A. Folkierski, private communication). The Schlieren shadowgraphic technique by Jones et al. using a 3 ns-wide ruby laser pulse shows that the shock wave starts to detach from the contact surface (thermal channel in the Les Renardières terminology or the current-carrying channel is Los Alamos' notation) well within the first 10 ns.

From an experimental point of view, the shock wave in the transverse direction to the axis of the channel is the least difficult to detect, and the experimental evidence now available removes earlier doubt (prior to 1978) that the shock wave can be present and provides an additional impetus towards applying the electrically-driven detonation model to discharge phenomena. Note also that gas dynamic considerations largely dominate the breakdown delay and energy deposition in electrically pumped laser gases [see Savic and Kekez (1977), and Burtsev et al. (1979) and for an overall review, Bychkov et al. (1978)].

In direct support of Eq. (23), the following experimental evidence (Kekez and Savic, 1974) is given. First, for the experiments done in H_2 at 1.9 cm gap, 162 torr gas pressure, and at minimum breakdown voltage applied to a stainless steel electrode of 2-inch diameter, it is observed that for a "clean" electrode the leader is initiated by cathode spots, and that the leader elongation proceeds with constant velocity in the range of 10 - 20% of the total gap length measured from the cathode. However, if the electrode surface is "eroded" by firing a thousand shots, anode spots will be formed

first, resulting in the discharge in which the leader propagates toward the cathode, as if the polarity were reversed. In both cases, the velocity of the anode- or cathode-directed leader was about 3.2 cm/μs. Also in both cases, there was no appreciable change in the shape of glow discharge ahead of the leader. This suggests that the velocity is proportional to Joule heating, hence supporting Eq. (23) and the statements leading to Fig. 3. Note that Joule heating does not depend on the direction of the electric field, implying that the negative leader is physically indistinguishable from the positive one (Waters, 1981).

The second evidence is the observation in Ar of the "radiation overshoot" in self-luminosity of the discharge. This is a thin layer of luminosity close to the shock front created by the tip of the leader; on the shutter photographs it is visible as a crescent-shaped precursor front.

Further check of the the detonation model can be done with the aid of Eq. (23). It states that the velocity increases as $P^{1/3}$ where P is the power delivered to the tip which may be taken to be equal to the total power dissipated in the gap. For constant voltage, Eq. (23) requires that $v \sim I^{1/3}$. These results can be confirmed by the following statistical analysis of a single shot from the Les Renardières group (1977) carried out in a 10 m positive-rod plane gap. Their results are reproduced in Fig. 9a. For the time of interest, the experimental voltage can be considered to have a smooth value (within 16%) in time (J. Jouaire, private communication) and it is similar to that of Les Renardières' Fig. 4.3.1(b).

To obtain an explicit velocity-current relationship from Fig. 9a, for each setment of the velocity vs. time lines, the current variations are plotted for a velocity in this segment, giving a bar of Fig. 9. Using linear regression, (Topping, 1963) curve-fitting is carried out. Points on the left end of each bar, in the center, and on the right end are grouped together. The results are given in Table IV. The best fit in terms of rms deviations is for the points on the left. However, the line-fitting is satisfactory in all three cases as the regression coefficient is > 0.6. Thus, the velocity v vs. the current I, can be expressed as:

$$v = A\, I^{\text{slope}} \quad .$$

Table IV suggests that the experimental slope is close to the theoretical one of 0.333.

Equation (23) can be examined further by considering the results by Baldo et al. (1975). They found that the average current associated with the leader elongation as a function of the overvoltage ratio, V/V_{50} forms a straight line on the linear-linear plot in a

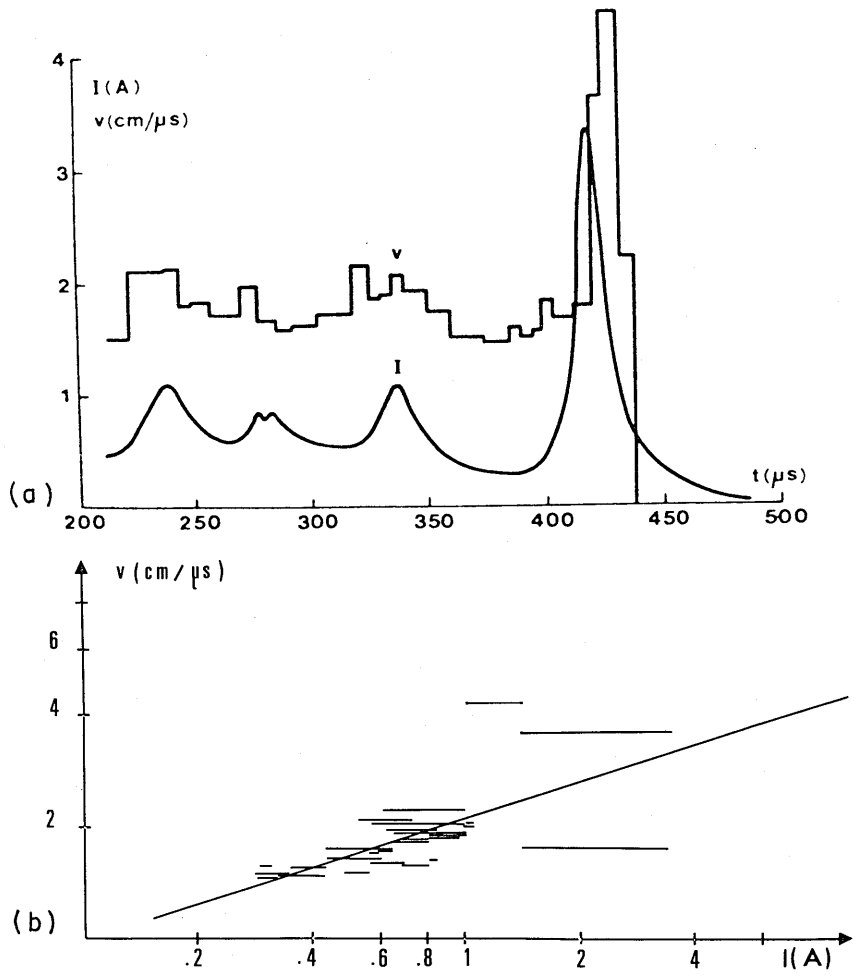

Fig. 9. (a) Current and spark-channel velocity vs. time (Les Renardières Group, 1977. Reproduced by permission of Electra (Cigre).) (b) Log plot of velocity vs. current from Fig. 9a. Line is regression curve for center points (Kekez and Savic, 1978. Reproduced by permission of IEE.)

Table IV. Velocity-Current Relationship: Statistical Analysis.

	Left points	Center points	Right points
Constant A	2.199	2.109	2.003
Slope	0.320	0.326	0.299
Regression Coefficient	0.627	0.690	0.713
Mean Deviation	-1.985	-3.641	-5.177
rms Deviation	22.857%	30.515%	36.103%

given gap. This suggests that the dynamic resistance or the conductivity is constant. Hence from Eq. (23), we find that the theoretical v vs. V/V_{50} law is

$$v \sim V^{2/3} \sim (V/V_{50})^{2/3} \quad .$$

Baldo et al.'s findings are replotted on the log-log graph (Fig. 10), together with a theoretical slope of 2/3. Configuration of the theory appears established, but statistical analysis does not appear feasible, as too few experimental points for a given gap are available. The range of V/V_{50} is also too limited. However, if the effect of the gap length is, for the moment, neglected, analysis such as in Table IV shows that, for all top, center and bottom points of the error bars, the following slopes are obtained respectively: 0.68, 0.61 and 0.54. Work is currently in progress to evaluate some of the experimental findings obtained in the Electricité de France Laboratory. (B. Hutzler, private communication).

Figure 11 shows the experimental rig used to test the hypothesis of the leader tip processes depicted by Fig. 1. It employs the radiation from a mode-locked laser providing a 100 ns long train (25 to 40) of picosecond wide pulses as a light source for a Schlieren study of the developing spark channel. This Schlieren photography permits framing rates in the gigacycle range. The white Schlieren lines on the dark background depict the shock fronts (Fig. 12). Because a small (12.5 μ diameter) wire is used as the knife edge (K in Fig. 11), the Schlieren lines are axis-symmetric.

The spark is formed in a 6 mm gap between a Rogowski-profile cathode and a flat mesh-anode. The potential on C_1 = 570 pF is

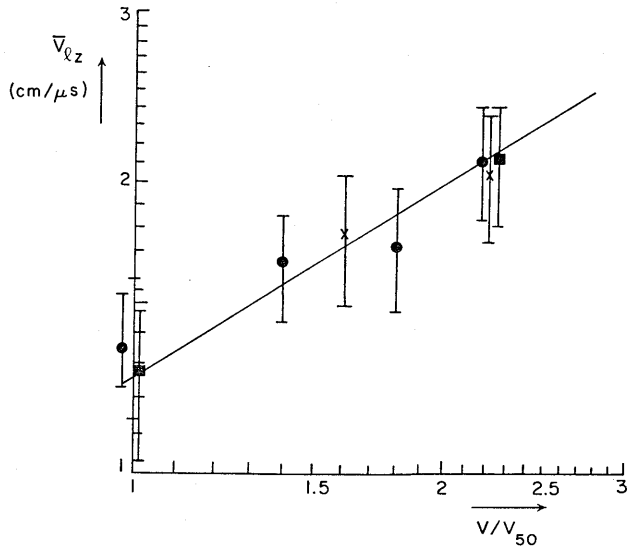

Fig. 10. Log-log plot of axial leader velocity, $\bar{V}_{\ell z}$, vs. overvoltage ratio, V/V_{50}. Experimental points after Baldo et al. (1975). ■ for 4m x 7m and ●, 10m positive rod-plane gaps, with 320/10,000 μs impulses. Straight line indicates theoretical slope of 0.66.

adjusted to be below the breakdown potential (of the total energy per unit length less than 0.5 J/cm) so that with (100 ns long-train) laser pre-ionization, the timelag in the current buildup is also 100 ns. In this manner the laser (pre-ionization) pulse does not interfere with the growth of the spark starting to elongate from the cathode. An average velocity is 13 cm/μs ± 30%.

In Fig. 12 the tip of the leader was recorded at the following distances from the cathode: 2.78 mm, 1.8 mm (not visible) and 0.9 mm (noticeable as a white line in the center). When the channel has bridged, the gap four of the white Schlieren lines that are parallel to the needle-like structure of the developing channel can also be seen. In general, the channel is narrow. For example, at a distance of 0.9 mm, the tip diameter is of the same size as the Schlieren line thickness which is equal to spatial resolution of the system of about 20 μm. However, at the distance of 2.78 mm, we see clear evidence of the diverging cylindrical shock waves surrounding the spark channel in the process of formation. From the expansion in the transverse direction with a velocity of 1 cm/μs and the Hugonoit relation at the shock, the estimate of the temperature of the channel plasma at the tip is made. It was found that the theoretical temperature calculated from the forward speed of the channel tip (see Table I) greatly exceeds that estimated from

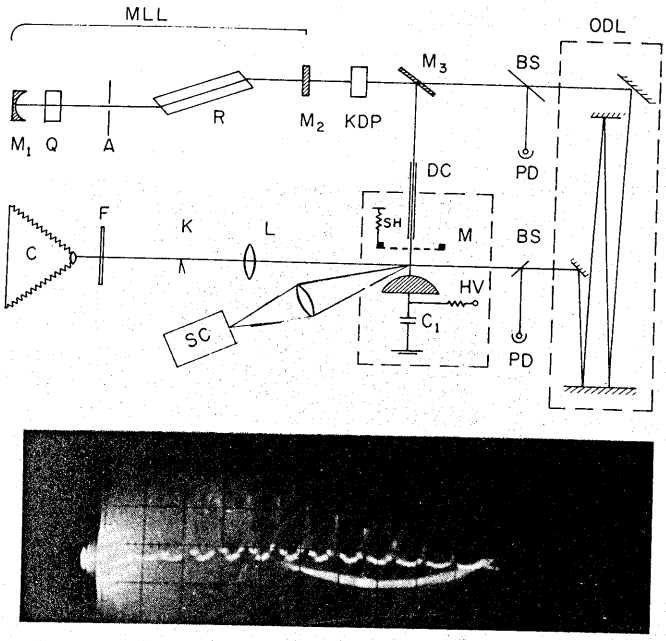

Fig. 11. Experimental setup, MLL, mode-locked laser; KDP, second harmonic generator; BS, beam splitter; ODL, optical delay line; DC, discharge chamber; L, lens; K, knife edge; PD, photodetector; SC, streak camera. Bottom — Pulse train: 10 ns/sq. (Kekez and Savic, 1980. Reproduced by permission of IEE.)

the motion of the radial shock wave. The reason for this is thought to lie in the very rapid expansion from a point of explosions, and with a limited spatial resolution, we were not able to observe the initial Mach number of the transverse motion. In addition, the small scale dimension of the tip will make the plasma optically thin, enabling massive radiation cooling due to the large Z-constituents of air. Both theoretical and experimental work is in progress. There are several alternative models to describe the continuous leader elongation for the speed range 1 to 10 cm/μs considered here. An excellent overall review is given by Marode in this volume. However, we will dwell briefly on the work by Gallimberti (1977 and 1979). Among several assumptions in his work, the following two are essential. He states: a) because of fast evolution, the leader channel can not attain LTE (even for the conditions of Fig. 9a); and b) the Joule heating raises the gas temperature via appropriate relaxation time constant under conditions "similar to low energy punctual explosion".

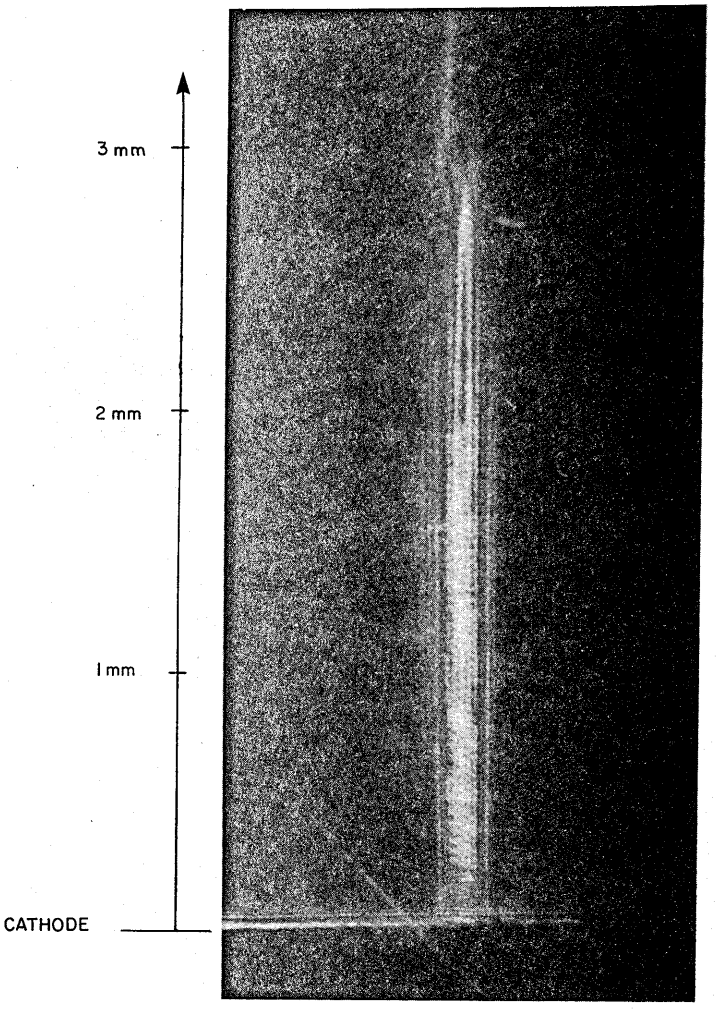

Fig. 12. Schlieren photograph of spark breakdown in atmospheric air. (Kekez and Savic, 1980. Reproduced by permission of IEE.)

It follows from the 2nd law of thermodynamics, that weak detonations are impossible. Clearly, the semiconstant leader velocity requires an application of Chapman-Jouguet hypothesis. Hence, for very short relaxation times, the results of computer experiments by Gallimberti (1977 and 1979) must converge to the results given in this paper as well as to those by Kekez and Savic (1974). But in contrast to our model, he assumes that the average field intensification near the tip is independent of the leader speed. This assumption requires further justification.

VOLTERRA MODEL

In the fast (leader velocity >> 10 cm/μs) or "Volterra" model, the leader tip causes not only strong electron heating in the corona cloud but also electron multiplication. In the Volterra model (Kekez and Savic, 1975 and 1976) the latter process predominates, and we may assume, that the electron concentration near the tip is such a rapidly varying function of position, that the tip can be identified as a travelling discontinuity describing the transition from low to full ionization. The appropriate analytical tool that describes this motion is a Volterra integral equation; hence, the name of the mode. This mechanism should, strictly speaking, be called the "cold" Volterra model (Fig. (13B)). In addition, we propose the "hot" Volterra model, where the dependence of the Townsend coefficient, and drift velocity on temperature is taken into account. The channel tip is here enveloped by a "heat wave," which later steepens into a precursor shock (Fig. 13C).

The Coulomb interaction between electron and ions takes place some distance in the rear of the tip for both the "hot" and "cold" Volterra model. The net effect is the generation of a shock wave.

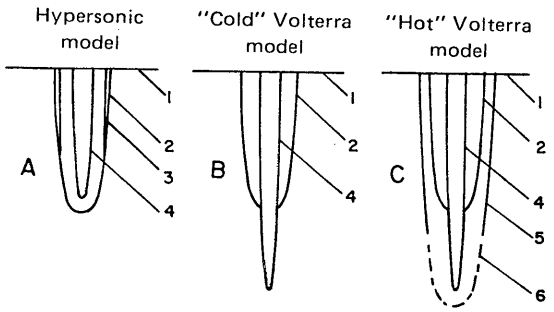

Fig. 13. Schematic of theoretical models (Kekez and Savid, 1976. Reproduced by permission of IEE.) 1. Grounded plate, 2. Equivalent paraboloid (shock), 3. Grounded spheroid, 4. Developing channel (leader), 5. Precursor shock, 6. Heat wave.

As before, we consider the field for the slender hyperboloid (see Eq. 18) geometry

$$\frac{d\phi}{dz} = V/[a(1 - z/a)\ell n(1 - z_o/a)] \equiv E \ .$$

At the high field region ahead of the tip, the electron drift velocity, v_d, and the first Townsend coefficient, α, can be taken (for "cold" Volterra model) as

$$\alpha = pA \exp(-Bp/E)$$
$$v_d = k_1 \sqrt{E/p} \ . \qquad (28)$$

Townsend's theory for the rise in electron density, n, gives

$$n = n_o . \exp(\int \alpha . v_d dt) \ . \qquad (29)$$

We assume that the leader lengthens with constant radius of curvature ($r_o = z_o - a$) at the tip.

If we define the speed of the leader tip's motion as:

$$u(a) = \frac{da}{dt} \ ,$$

then the position of a given electron density, which we identify with the leader tip, will be given by the equation:

$$\frac{n}{n_o} = \int_{a_o}^{z+r_o} \alpha \ v_d \frac{da}{u(a)} = \theta \int_{a_o}^{z+r_o} \frac{\exp\left(-H \frac{a-z}{d} \ell n \frac{a}{r_o}\right)}{\left(\frac{(a-z)}{d} \ell n \frac{a}{r_o}\right)^{1/2} u(a)} da = \text{const} = C. \qquad (30)$$

Here d is the initial gap length, V the gap voltage, $H = Bpd/V$, and $\theta = pAk_1(V/dp)^{1/2}$. To justify the use of the Laplace field equation in front of the leader tip, we have to assume that the real electron density distribution near the tip (Fig. 14) can be replaced by a discontinuous distribution (dashed line).

The foregoing integral equation for the unknown tip velocity u(a) is of the Volterra type and must, in general, be solved numerically. However, if H is large, analytic approximations can be obtained at once when it is realized that the integrand in both cases is negligible, except where a-z is small. The technique is a direct consequence of Watson's lemma and Kelvin's principle of stationary phase (Jeffreys, 1946). The result is:

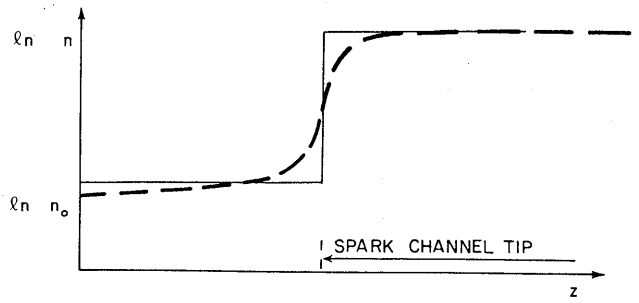

Fig. 14. Schematic of electric density profile: broken line — real distribution; solid line — approximation for the Volterra model.

$$u(a) = \frac{\theta}{C}\sqrt{\frac{\pi}{H}}\;\frac{d}{\ell n\,\frac{a}{r_o}}\left[1 - \mathrm{Erf}\left(\frac{Hr_o}{d}\,\ell n\,\frac{a}{r_o}\right)^{1/2}\right] ,$$

which states that u(a) is proportional to

$$u(a) \sim \text{voltage}/\ell n\; a/r_o \qquad (31)$$

where a is the unbridged gap length. Equation (31) states that the "cold" Volterra speed is a weak function of the gap length, and to some degree similar to Eq. (23). However, note that Eq. (31) defines a pure phase velocity without mass motion (hence no Doppler effect).

CONCLUSIONS

We have briefly described the continuous leader elongation. This work does not treat the stepped-leader phenomenon (Savic et al., 1981) or the unified treatment between the stepped-leader and the Trichel-type electrical discharges (to be published).

The problems that remain can be summarized as follows:

a) What are the precise conditions for the hypersonic to Volterra transition?

b) What is the effect of the finite relaxation times in the hypersonic model in respect to the shape of the shock front onset

and to the initial channel radius at the tip?

c) To what extent does the present understanding of the leader propagation affect technological aspects of UHV system. If the zero-order theory (Kekez and Savic, 1979) suggests the existence of a saturation of the sparkover voltage at large gaps, will further work determine possible "creeping" in the saturation value as the gap rises?

It is a pleasure to acknowledge the interest shown by Mr. R. A. Tyler and Mr. E. H. Dudgeon.

REFERENCES

Aleksandrov, G. N., 1966, Sov. Phys.-Tech. Phys., 10: 948.
Aleksandrov, G. N., 1969, Sov. Phys-Tech. Phys., 14: 560.
Andreev, S. I. and Sokolov, B. M., 1966, Sov. Phys.-Tech. Phys. 10: 1003.
Barreto, E., Jurenko, H., and Reynolds, S. I., 1977, J. Appl. Phys., 48: 4510.
Baldo, G., Gallimberti, I., Carcia, H. N., Hutzler, B., Jouaire, J., and Simon, M. F., 1975, IEEE Trans., PAS-74: 1131.
Bartlmä, F., 1975, "Gasdynamik der Verbrennung," Springer, Vienna.
Berger, G., Boillot, A., Gallet, G., Garcia, H. N., Garry, C., Goldman, M., Hutzler, B., Jouaire, J., Leroy, G., and Simon, M., 1974, R.G.E., 83: 763.
Berger, G., Dastarac, G., and Gibert, A., 1977, in: "Proceedings 13th International Conference on Phenomena in Ionized Gases, Berlin," p. 389.
Braginskii, S. I., 1958, Sov. Phys-JETP, 34: 1068.
Burtsev, V. A., Zelenov, L. A., Kondakov, A. A., Kurunov, R. F., Smirnov, V. G., and Shansky, V. F., 1979, in: "Proceedings 14th International Conference Phenomena Ionized Gases, Grenoble," C7-387.
Bychkov, Yu. I., Korolev, Yu. D., and Mesyats, G. A., 1978, Sov. Phys-Usp., 21: 944.
Chernyi, G. G., 1961, "Introduction to Hypersonic Flow," Academic Press, New York, p. 101.
Dastarac, G., 1977, Dissertation, Université de Pau, France.
Dougal, A. A. and Goldstein, L., 1957, Phys. Rev., 109: 615.
Gallimberti, I., 1977, in: "Proceedings, World Electrotechnical Conference, Moscow," p. 1.
Gallimberti, I., 1979, in: "Proceedings, 14th International Conference on Phenomena in Ionized Gases, Grenoble," Invited Papers, p. C7-193.
Jones, B. and Waters, R. T., 1978, Proc. IEE, 125: (11R) 1152.
Jones, L. A., Finken, K. H., Dangor, A., Kallne, E., and Singer, S., 1981, Appl. Phys. Lett., 38: 522.

Kekez, M. M. and Savic, P., 1974, J. Phys. D, 7: 620, Corrigenda p. 1200.
Kekez, M. M. and Savic, P., 1975, in: "Proceedings 12th International Conference on Phenomena in Ionized Gases, Eindhoven," p. 161.
Kekez, M. M. and Savic, P., 1976, in: "Proceedings, 4th International Conference on Gas Discharges, Swansea," IEE Conf. Publ. No. 143, p. 129.
Kekez, M. M. and Savic, P., 1978, in: "Proceedings, 5th International Conference on Gas Discharges, Liverpool," IEE Conf. Publ. No. 165, p. 336.
Kekez, M. M. and Savic, P., 1979, in: "Proceedings, 14th International Conference on Phenomena in Ionized Gases, Grenoble," p. C7-255.
Kekez, M. M. and Savic, P., 1979, in: "Proceedings, 3rd International Symposium High Voltage Engineering, Milan," p. S1.14.
Kekez, M. M. and Savic, P., 1980, in: "Proceedings, 6th International Conference on Gas Discharges, Edinburgh," IEE Conf. Publ. 189, Vol. 2, p. 220.
Kekez, M. M. and Savic, P., 1980, J. Phys. D, 13: L1167.
Kekez, M. M. and Savic, P., 1981, in: "Proceedings, 15th Internatiional Conference on Phenomena in Ionized Gases, Minsk."
Kekez, M. M., Makomaski, A. H., and Savic, P., 1978, in: "Proceedings, 11th International Symposium on Shock Tube and Shock Wave Research," Univ. of Washington Press, Seattle, p. 602.
Korlev, Yu. D., Kuz'min, B. A., Mesyats, G. A., and Rotshtein, V. P., 1979, Sov. Phys.-Tech. Phys., 24: 236.
Korobkin, V. V. and Alcock, A. J., 1968, Phys. Rev. Letts, 21: 1433.
Kurimoto, A., Farish, O., and Tedford, D. J., 1978, Proc. IEE, 125: 767.
Les Renardières Group, 1975, 1977, Electra, 53: 31.
Les Renardières Group, 1978, 1981, Electra, 74: 70.
Moon, P. and Spencer, D. E., 1961, "Field Theory for Engineers," Van Nostrand, Princeton.
Newi, R., 1973, Dissertation, Braunschweig Universität.
Raizer, Yu. P., 1965, Sov. Phys-JETP, 21: 1009.
Raizer, Y. P., 1977, "Laser-Induced Discharge Phenomena," Consulatants Bureau, New York.
Ramsden, S. A. and Savic, P., 1964, Nature, 203: 1217.
Savic, P., Kekez, M. M., and Lougheed, G. D., 1981, in: "Proceedings, IEEE International Conference on Plasma Science, Santa Fe, N.M.," p. 127.
Savic, P. and Kekez, M. M., 1977, Can. J. Phys., 55: 325.
Savic, P. and Kekez, M. M., 1980, in: "Proceedings, 6th International Conference on Gas Discharges, Edinburgh," IEE Conf. Publ. No. 189, Vol. 1, p. 224.
Stanyukovich, K., 1960, "Unsteady Motion of Continuous Media," Pergamon Press, Oxford, p. 305.
Steginsky, B., 1964, AIAA J., 2: 175.
Suleebka, P., Barrault, M. R., and Craggs, J. D., 1975, J. Phys. D, 8: 2190.
Swigart, R. G., 1960, J. Fluid Mech., 9: 613.

Thall, H., 1967, Z. Naturforsch, 22a: 1068.
Topping, J., 1963, "Errors of Observation and Their Treatment," Chapman & Hall, London.
Uman, M. A., 1971, Proc. IEEE, 59: 457.
Waters, R. T., 1981, Proc. IEE, Pt. A, 128: 319.
Zel'dovich, Ya. B. and Raizer, Yu. P., 1967, "Physics of Shock Waves and High-Temperature Hydrodynamic Phenomena," Academic, New York.

PARTICIPANTS

Allen, J. E.
Department of Engineering Science
University of Oxford
Parks Road, Oxford
OXI 3PJ
England

Allis, W. P.
33 Reservoir St.
Cambridge, MA 02138
USA

Aschwanden, T.
ETH
Swiss Fed. Inst. of Technology
High Voltage Laboratories
Physikstr 3
CH - 8092 Zuerich
Switzerland

Baldo, G.
Instituto di Electrotecnica
ed Elettronica
Via Grademigo 6A
Universita di Padova
Padova
Italy

Bardsley, J. N.
Physics Department
University of Pittsburgh
Pittsburgh, PA 15260
USA

Barrault, M. R.
University of Liverpool
Liverpool L69 3BX
England

Bastien, F.
Laboratoire de Physique
des Decharges
Ecole Superieure d'Electricite
Plateau du Moulon
9110 Gif sur Yvette
France

Bayrakceken, F.
O.D.T.U.
Cevre Muh Bolumu
Ankara
Turkey

Bengston, R. D.
Department of Physics
University of Texas at Austin
Austin, TX 78712
USA

Bicknell, J. A.
University of Manchester
Inst. of Science and Technology
Physics Department
Sackville Street
Manchester M60 1QD
England

Boeuf, J. P.
Laboratoire de Physique
des Decharges
Ecole Superieure d'Electricite
91190 Gif sur Yvette
France

Bradley, L. P.
LLNL
7000 East Avenue
L-464
Livermore, CA 94550

Braithwaite, N. St. J.
Department Engineering Science
Parks Road
Oxford, OXI 3PJ
England

Burgmans, A. L. J.
Philips Research Labs
5600 MD Eindhoven
The Netherlands

Chang, J. S.
McMaster University
Dept. of Engineering Physics
Hamilton, Ontario
Canada L8S 4M1

Christophorou, L. G.
Oak Ridge National Laboratory
Building 4500S, H-158
P.O. Box X
Oak Ridge, TN 37830
USA

Cole, H. R.
1161 West 37th Street
Los Angeles, CA 90007
USA

Conde, C. A. N.
Physics Department
University of Coimbra
3000 Coimbra
Portugal

Danzmann, K.
Institute fur Plasmaphysik
der Universitat Hannover
Callinstr, 38 D-3000
Hannover 1
West Germany

Davidson, H.
DAMA-AR
Washington, D.C. 20310
USA

Desoppere, E.
State University
Rozier 44
B-900
Belgium

DeWitt, R. N.
Code F12
Naval Surface Weapons Center
Dahlgren, VA 22448
USA

Dias, T. T.
Physics Department
University of Coimbra
3000 Coimbra
Portugal

Dorelon, A. A.
Laboratoire de Spectrometrie
BP 53X
38041 Grenoble Cedex
France

Dupuy, J.
Universite de PAU
Laboratoire d'Electricite
Avenue Phillippou
64000 PAU
France

Dutton, J.
University College of Swansea
Singleton Park
Swansea, Glamorgan
SA 2 8PP, England

Ecker, G.
Ruhr-Universitat Bochum
423 Bochum
Universitatsstrasse
Geb. NB7
West Germany

Eliasson, B.
Brown Boveri
Research Center
5405 Baden - Daettwil
Switzerland

Fang, D. Y.
Lehrstuhl fur Technische
Elektrophysik der TUM
Arcisstr. 21
8000 Munchen 2
West Germany

Fernsler, R. F.
Naval Research Laboratory
Code 4770
Washington, D.C. 20375
USA

Ferreira, C. M.
Centro de Electrodinamica
Instituto Superior Tecnico
Av. Rovisco Dais
1000 Lisboa
Portugal

Ferreira, M. de F.
Departamento Fisica
Universidade Coimbra
3000 Coimbra
Portugal

Gayet, P.
Electricite de France
Direction des Etudes et Recherches
B.P. no. 1
77250 Moret/S/Loring
France

Germain, G.
Commissariat a l'Energie Atomiques
Centre d'Etudes Scientifiques
et Techniques D'Aquitaine
Boite Postale no. 2.
Le Barp
33830-Belin-Beliet, France

Goldman, A.
Laboratoire de Physique
des Decharges
Ecole Superieure d'Electricite
Plateau du Moulon
91190 Gif sur Yvette
France

Goldman, M.
Laboratoire de Physique
des Decharges
Ecole Superieure d'Electricite
Plateau du Moulon
9119 Gif sur Yvette
France

Golightly, D.
U.S. Geological Survey
957 National Center
Reston, VA 22092
USA

Gripshover, R. J.
RR2, Box 360 B
King George, VA 22485
USA

Guenther, A.
Chief Scientist (Code CA)
Air Force Weapons Lab
Kirtland AFB, NM 87117
USA

Hackmann, J.
Phys. Inst. II
Der Universitat Dusseldorf
4000 Dusseldorf
Universitatsstrasse 1
West Germany

Hamden, M.
University College of Wales
Department of Physics
Aberystwth SY23 3BZ
United Kingdom

Harjes, C.
Department of Elec. Eng.
Texas Tech University
P.O. Box 4439
Lubbock, TX 79439
USA

Kline, L. E.
1540 Shady Avenue
Pittsburgh, PA 15217
USA

Kristiansen, M.
Plasma and Switching Laboratory
Texas Tech University
P.O. Box 4439
Lubbock, TX 79409
USA

Kunhardt, E. E.
Ionized Gas Laboratory
Texas Tech University
P.O. Box 4439
Lubbock, TX 79409
USA

Lakdawala, V. K.
Department of Elec. Eng.
University of Liverpool
P.O. Box 147
Liverpool, L69 3BX
England

Lawler, J.
Physics Department
University of Wisconsin
Madison, WI 53706
USA

Lea, L. M.
University of Oxford
Dept. of Engineering Science
Parks Road
Oxford, OXI 3 PJ
England

LeNy, R.
Lab. Phys. Exp.
Institut de Physique
Universite de Nantes
2, Rue de la Houssiniere
44072 Nantes
France

Llewellyn-Jones, F. P.
University College of Swansea
Singleton Park
Swansea, Glamorgan
SA 2 8PP, United Kingdom

Leussen, L. H.
Naval Surface Weapons Center
Code F12
Dahlgren, VA 22448
USA

Marec, J.
Laboratoire de Physique
des Plasmas
Universite de Paris Sud
Batiment 212
91405 Orsay
France

Marode, E.
Laboratoire de Physique
des Decharges
Ecole Superieure d'Electricite
Plateau du Moulon
91190 Gif sur Yvette
France

Mentzoni, M.
Physics Department
University of Oslo
Box 1038, Blindern
Norway

Molen, G. M.
Dept. of Electrical Engineering
Old Dominion University
Norfolk, VA 23508
USA

Nolting, E. E.
6142 Camelback Lane
Columbia, MD 21045
USA

Penven, H. Le
Societe Protel
BP7 ZI La Roche de Glun
26600 La Roche de Glun
France

Phelps, A. V.
Campus Box 440
JILA
University of Colorado
Boulder, CO 80309
USA

Pinnekamp, F.
BBC - Research Center
CH 5400 Baden - Daettwil
Switzerland

Pitchford, L.
Division 4211
Sandia National Laboratories
Albuquerque, NM 87117
USA

Plueksawan, W.
Laboratoire de Genie Electrique
U.P.S.
118 Route de Narbonne
31062 Toulousse
France

Pointu, A. M.
Lab Physique des Plasmas
Batiment 212
Univ. de Paris Sud
91405 Orsay
France

Proud, Jr., J. M.
GTE Laboratories, Inc.
40 Sylvan Road
Waltham, MA 02154
USA

Rees, J. A.
Dept. of Electrical Engineering
University of Liverpool
Brownlow Hill, P.O. Box 147
Liverpool, L69 3BX
England

Robledo, A.
Instituto De Investigaciones
Electricas
Div. de Equipos
Shakespear 6
Mexico 5 D.F.

Rodrigo, H.
Dept. of Electrical Engineering
University of Liverpool
P.O. Box 147
Liverpool, L69 3BX
England

Rose, M. F.
Code F-04
Naval Surface Weapons Center
Dahlgren, VA 22448
USA

Savic, P.
National Research Council
Ottawa, Ontario
Canada K1AOR6

Schoenbach, K. H.
Dept. of Electrical Engineering
Texas Tech University
P.O. Box 4439
Lubbock, TX 79409
USA

Schwirzke, F.
Dept. of Physics
Naval Postgraduate School
Monterey, CA 93940
USA

P. Segur
Universite de Paul Sabatieur
118 Route de Narbonne
31062 Toulousse
France

Sigmond, R. S.
Dept. of Physics
University of Trondheim
Norwegian Institute of Tech.
N7034 Trondheim, Norway

Skullerud, H. R.
Electron and Ion Physics Group
Dept. of Physics
University of Trondheim
Norwegian Institute of Tech.
N7034 Trondheim, Norway

Spiga, G.
Via dei Colli, 16
Laboratorio di Ingegneria Nucleare
I - 40136
Bologna
Italy

Szabo, I.
Chemical Center
P.O. Box - 40
S-22007 Lund 7/
Sweden

Tang, T. M.
Dept. of Physics
University of Manchester
Inst. of Science and Tech.
Sackville Street
Manchester M60 1QD, England

Teich, T. H.
Swiss Fed. Inst. of Tech.
ETH, High Voltage Labs
CH - 8092 Zuerich
Switzerland

Thompson, J. E.
College of Engineering
University of South Carolina
Columbia, SC 29208
USA

Tredicce, J.
National Inst. of Optics
Largo Enrico Fermi 6
50125 Florence
Italy

Twiddy, N. D.
University College of Wales
Department of Physics
Aberystwyth SY23 3BZ
United Kingdom

VanBrunt, R. J.
Electro Systems Div., 722
National Bureau of Standards
Washington, D.C. 20234
USA

Vandevender, J. P.
Org 4252
Sandia National Laboratories
P.O. Box 5800
Albuquerque, NM 87185
USA

Vriens, L.
Philips Research Labs, WAG
Eindhoven
The Netherlands

Vitkovitsky, I. M.
10406 Burnt Ember Drive
Silver Spring, MD 20903
USA

Walter, W.
Polytechnic Institute of NY
Microwave Research Institute
Route 110
Farmingdale, NY 11735
USA

Waters, R. T.
Inst. of Science and Technology
University of Wales
Cardiff CF1 3NU
United Kingdom

Williams, F.
Dept. of Electrical Engineering
Texas Tech University
P.O. Box 4439
Lubbock, TX 79409
USA

Wilson, R. M.
Department of Chemistry
University of Durham
South Road
Durham DH1 3LE
England

Wyatt, K.
Apt. D-4
West Gate
Cambridge, MA 02139
USA

INDEX

Associative detachment, see Detachment
Associative ionization, see Ionization
Attachment, 12, 114, 133, 160, 209
  coefficient, 163, 164
  dissociative, 93, 95, 96, 141
  to electronically-excited molecules, 160-162
  to ground state molecules, 141-145
  to "hot" molecules, 148-154
  processes, 133-135
  vertical energy, 138
Auto detachment, see Detachment
Avalanche, 7, 28, 49, 56, 212
  development, 49, 268

B-Splines, 318
Breakdown (see also Overvoltage Breakdown), 1, 2, 15, 43, 207, 258, 265
  nonuniform field, 33-37, 265, 291, 292, 418
    formation
      negative polarity, 305
      positive polarity, 296-305
  uniform field, 3, 23
    extreme conditions, 58, 224
    high fields, 224
    sparking potential (see also Paschen Law) 209, 271, 1, 3, 15
    statistics, 21
    temporal development, 37, 40, 54
    Townsend theory, 208, 209
Breakdown in long gaps, see Breakdown, nonuniform field
Boltzmann equation, 180, 181, 188, 314, 334, 336, 339
  collision operator, 180, 181, 314
  cylindrical coordinates, 188, 204
  high energy solution, 195, 323, 398
  integral form, 344-354
  P_1 approximation 198, 319
    multiterm approximation, 319
  scattering out only, 188-191
  solution methods, 183, 316
    integral methods, 316, 317
    moment methods, 183-186, 191, 315, 316, 319, 397
    numerical solutions, 313, 317, 326, 327, 354-359
  spherical coordinates, 190
  zero order solution, 195

Cathode fall, 332-333, 343
Collision cross sections, 75, 140, 141, 339, 397
  absolute, 79
  attachment, 145, 146, 166
  differential, 77
  elastic, 76, 81
  inelastic, 83, 397
  ionization, 85-87
  measurement techniques, 77, 78, 81, 86
  momentum transfer, 80, 82, 397

total, 318
vibrational, 89
Conservation equations, 271, 272, 406, 407, 429
Continuity equations, 210, 266
Corona, 36, 37, 265, 288, 298, 307
first, 265, 298, 307
negative, 305
positive, 284
streamers, 301

Dark period, 298
Detachment, 12, 209
associative, 96
auto, 135, 136
vertical energy, 137, 138
Dielectrics, 162
Diffuse discharges, 254, 255
Diffusion coefficient, 110-112, 182, 304
ambipolar, 119-121, 296
Diffusion equation, 179
Dissociative attachment, see Attachment
Dissociative recombination, see Recombination
Distribution function, 177
Double exponential impulses, 293
Drift velocity, 110-112, 182
Druyvesteyn distribution, 198

Electron affinity, 137, 138
Electron distribution function, 314, 331, 362, 396, 400
Electron emission rate, 250
apparent, 250
intrinsic, 250
Electronegative gas, 133, 157
Electron runaways, 260
Electron scattering, see Scattering
Electron transport, see Transport
Excitation, 115
electronics, 276, 278, 279
rotational, 276, 278, 279
vibrational, 273, 276, 278, 279
boomerang model, 90
resonant, 89
Excited atoms, 123, 126

Free-free radiation, 116
Free path, 75

Galerkin methods, 313, 317
Gas insulators, 163, 166-172
Glow discharge, 395

High frequency discharge, 65
Hydrodynamic equations, 178, 179
Hydrodynamic regime, 178, 313, 335.

Ion transport, see Transport
Ion-molecule reaction, 97, 118, 121, 209
Ionization, 113
associative, 259
by electron impact, 85-87
by excited atoms, 126
by metastables, 126
by photons, 123
Ionization coefficient, see Townsend...
Ionization current growth, see Prebreakdown...
Ionization time, 427
Isotropic scattering, see Electron scattering

Kanal theory (see also Streamer), 24

LTE, 270
Leader channel, 271, 284, 298, 424
inception, 299
propagation, 283-288, 300, 307, 425, 433-437
velocity-current relation, 443
Leader development, 269, 419
final jump, 302, 308
two-temperature model, 272
three-temperature model, 276
Leader tip
energy balance, 268, 421-423
ohmic dissipation, 422
radius, 437-440
temperature, 424
Legendre expansion of the electron distribution, 191

convergence, 188, 202
Long gaps, 265, 291
rod-plane, 293, 294
rod-rod, 293, 295, 305
Memory factor model, 333, 377-389
Metastables, 123-126, 295, 321, 418
$N_2(A^3\Sigma_u^+)$, 321, 412, 418-425
quenching rates, 412
Monte Carlo methods, 317, 326, 327, 333, 334, 335, 359-374
null collision technique, 360
Multiple electron initiation, see U-V preionization

Negative ions, 139, 154
lifetime, 155, 156
transient, 139
Negative ion resonance, 135
core-excited resonances, 135, 137, 139
nuclear-excited Feshback resonance, 135, 137
shape resonance, 135, 136, 139
Nonequilibrium kinetics, 331, 334, 337-340, 365
Nonuniform field breakdown, see Breakdown

Overvoltage breakdown, 49-54, 226, 241
experiments, 234, 242, 244
influence of space charge, 231, 241
numerical simulations, 232, 233, 235, 255
statistics, 248-250
temporal growth of ionization, 226-229
two-group model, 260

P_1 approximation, see Boltzmann equation
Paschen law, 3, 16, 220-225
range of validity, 220
Phase space, 342
Photoionization, 27, 31, 266, 267
Plasma sheaths, 407
Positive column, 395, 405
Prebreakdown current growth, 28
experimental measurements, 43-48
pulse, 218-220
steady state, 215
numerical simulations with attachment, 74
with space charge, 242
spatial, 73, 208
spatial-temporal, 40-43, 213
statistics, 21
Primary ionization coefficient, see Townsend

Radiation transport (see also Transport), 126
ionizing radiation, 127
resonance excitation, 126
Rate coefficients, 75, 77-79, 110, 326, 327
attachment, see Attachment
excitation, 413
ionization, see Townsend
quenching of Metastables, 412
Recombination, 99, 100
dissociative, 101
radiative, 114
Rotational Excitation, see Excitation

S00-Functions, 191
Scattering
anisotropic, 323, 338
inelastic, 193
isotropic, 318, 338, 362
Secondary coefficient, 8, 14, 208, 209
Secondary ionization processes, 209, 214, 241
Similarity law, 405-408
Single electron initiation, see U-V preionization
Space charge effects, see Overvoltage Breakdown
Space leader, 308
Space stem, 308
Sparking potential, see Breakdown; Paschen Law
Statistical time lag, see Time lag

Streamer, 234, 253, 257, 267
Streamer theory (see also Kanal), 24
Swarms, 177, 313

Thermalization time, 427, 428, 430-434
Time lag, 38, 48, 52, 244
  formative, 52, 244, 247, 253
  observational, 244
  statistical, 244, 247
Townsend primary ionization coefficient, 8, 9, 73, 76, 163, 164, 208, 404
Transport, 110
  electron, 110
  hydrodynamic approximation, 110
  ion, 118, 119, 177
  nonequilibrium effects, 116-118, 325
  radiation, 122
Transport coefficients, 178, 179, 315, 321, 403, 404
  kinetic equations, 181, 183
Two-group model, 53, 260

U-V initiated breakdown, 246
  multiple electron, 246, 254
  single electron, 246, 256